

AD-A268 713 TATION PAGE



Form Approved
OMB No. 0704-0188

age 1 hour per response, including the time for reviewing instructions, searching existing data sources, gathering and maintaining the data needed, and completing and reviewing the collection of information. Send comments regarding this burden or any other aspect of this collection of information, including suggestions for reducing burden, to the Office of Management and Budget, Paperwork Reduction Project (0704-0188), Washington, DC 20503.

1. Agency Use Only (Leave blank).	2. Report Date. 1993	3. Report Type and Dates Covered. Final - Book Editor
4. Title and Subtitle. PE WORKSHOP II Proceedings of the Second Parabolic Equation Workshop		5. Funding Numbers. Program Element No. 0601153N Project No. 3204 Task No. 040 Accession No. DN250057 Work Unit No. 571522103
6. Author(s).		S DTIC ELECTE AUG 20 1993 b D
7. Performing Organization Name(s) and Address(es). Naval Research Laboratory Acoustic Simulation and Tactics Branch Stennis Space Center, MS 39529-5004		8. Performing Organization Report Number. NRL/BE/7181--93-0001
9. Sponsoring/Monitoring Agency Name(s) and Address(es). Office of the Chief of Naval Research 800 N. Quincy St. Arlington, VA 22217-5000		10. Sponsoring/Monitoring Agency Report Number. NRL/BE/7181--93-0001
11. Supplementary Notes. Edited by Stanley A. Chin-Bing, David B. King, James A. Davis, and Richard B. Evans		
12a. Distribution/Availability Statement. Approved for public release; distribution is unlimited.		12b. Distribution Code.
13. Abstract (Maximum 200 words). Perhaps the most important and encouraging results of this PE Workshop were that underwater acoustic parabolic equation (PE) models from both the 6.1 basic research modeling community and the 6.3 Navy operational modeling community were applied to the same set of test problems--each test problem designed to push the PE models to their limits--and each of the two communities' PE models did extremely well, given the requirements and constraints imposed by each community. The PE models developed by the 6.1 basic research modeling community were able to produce results for the test case problems that were benchmark accurate. This is a definite requirement, since the basic research community uses these models to identify, to isolate, and to understand the physical mechanisms involved in underwater acoustic propagation and scattering in highly complex underwater environments. The 6.3 Navy operational community is also interested in accurate model predictions, but the need for computational speed, portability, and the ability to run a computer in the field (micro or desk-top) is also of utmost importance--to the extent that trade-offs among accuracy, speed, and portability must be optimized. The results from this workshop demonstrate that the underwater acoustic PE models used by both modeling communities are performing at their expected levels.		
14. Subject Terms. Underwater acoustics, ocean wave characteristics, environmental technology		15. Number of Pages. 329
		16. Price Code.
17. Security Classification of Report. Unclassified	18. Security Classification of This Page. Unclassified	19. Security Classification of Abstract. Unclassified
		20. Limitation of Abstract. SAR

PE WORKSHOP II
Proceedings of the Second Parabolic Equation Workshop

EDITED BY:

Stanley A. Chin-Bing and David B. King
Naval Research Laboratory
Acoustic Simulation Section, Code 7181
Stennis Space Center, MS 39529-5004

James A. Davis
Planning Systems, Inc.
Two Shaw's Cove
New London, CT 06320

Richard B. Evans
Science Applications International Corp., Inc.
Two Shaw's Cove
New London, CT 06320

PREPARED FOR:

E. D. Chaika
AEAS Program Office
Office of Naval Research
Stennis Space Center, MS 39529

Marshall H. Orr
Ocean Acoustics Program
Office of Naval Research
Arlington, VA 22217-5000

NAVAL RESEARCH LABORATORY
Stennis Space Center, MS 39529-5004

Approved for public release; distribution is unlimited.

93-19345



NAVAL RESEARCH LABORATORY
Captain Paul G. Gaffney II, Commanding Officer

Accession For	
NTIS GRA&I	<input checked="" type="checkbox"/>
DTIC TAB	<input type="checkbox"/>
Unannounced	<input type="checkbox"/>
Justification _____	
By _____	
Distribution/	
Availability Codes	
Avail and/or	
Dist	Special
A-1	

DTIC QUALITY CERTIFIED 3

Preface

At first examination, the results presented at the PE Workshop II and documented in these proceedings are biased! Indeed, the criticism can easily be made that all but a few of the presenters "fine-tuned" their models to get the best answer. After all, they were provided with the available reference solutions several weeks before the workshop was held. Given a thorough knowledge of a model's strengths and limitations, plus a good knowledge of the physics of underwater acoustic propagation, any expert modeler could "tune" his or her model so that it could closely match the reference answers.

We agree with this criticism, for it embodied the precise philosophy we wished to adopt. We sought from the expert modelers the answers to two questions: Using your insight and in-depth knowledge of a particular computer model and the physical situation to be modeled, what is the greatest accuracy that you can attain with this particular model? What techniques, choices of parameters, etc., did you employ in getting the "fine-tuned" answer, and why did you make these choices?

By studying the examples presented in these proceedings, the less-than-expert model user may be better equipped to select an appropriate model for a particular problem and to apply it, as did these experts, so that the best possible answer can be obtained. Understanding the limitations of a model (as well as its capabilities) and fine-tuning it to the problem at hand is what constitutes the "art of model application." Very few underwater acoustic models can be "black-boxed" so that a novice can use the model and always get the best answer for that model. Indeed, even for an expert, many variations of the same problem may be required to obtain a "sensible/meaningful" solution.

A model that one would like to "black-box," namely, Navy Standard PE, was included in this workshop. The modelers who applied Navy Standard PE were expert in its application and limitations, but their application of the model remained within the capability of any knowledgeable user, i.e., with few exceptions, no special modifications or parameter selections were made—just the application of the model. Its performance on the workshop test problems could be considered (1) remarkably "good," considering that it is an applications-operations model (rather than a research model); or (2) remarkably "bad," if one requires precise agreement with the reference solutions—the level of performance is often determined by the expectations of the user.

Selecting a particular model, applying it in a knowledgeable fashion, and interpreting its predictions within the model's domain of validity constitute the "science of model application." Successful underwater acoustic modeling often blends both the science and the art of modeling. We hope that these proceedings will serve the underwater acoustic modeling community by providing a foundation upon which to make knowledgeable choices, and by providing benchmark problems and solutions against which new underwater acoustic models may be tested.

Acknowledgments

The PE Workshop II would not have come about without the efforts of many people. This workshop drew heavily on the experience gained from the first PE workshop (Dr. J. A. Davis planned and hosted that workshop with assistance from Mr. D. White, and Dr. R. C. Cavanagh). The first PE Workshop identified the critical need for accurate range-dependent reference solutions; one value outcome of the first PE Workshop was the development of the benchmark-accurate coupled-mode model, COUPLE. Dr. R. B. Evans used his COUPLE model to provide several reference solutions to the test cases used in the PE Workshop II.

During the Test Case selection phase, Ms. Mona Collins (NRL) supplied many model runs that helped in selecting and fine-tuning the test cases and setting the standard plot scales that were finally used. We thank her for her hard work and patience.

Ms. Faye T. Theriot provided the needed clerical support in a prompt and timely fashion, thus allowing rapid dissemination of material from the workshop organizers to the invited participants.

The experimental acoustic data that accompany Test Case 6 represent the "reference solution" for this case. These data were taken by Mr. Hassan Ali of NRL. We thank him for providing us with this data set.

We thank Mr. Ed Chaika of the ONR AEAS Program office and Dr. Marshall Orr of the ONR Ocean Acoustics Program, both of whom provided the financial support and encouragement for this workshop.

A special acknowledgment is extended to Ms. Jan Lewis of the NRL Public Affairs Office. She handled with great skill the seemingly endless amount of minutia associated with organization, registration, and social functions.

Finally we thank all of the workshop participants whose time, effort, and enthusiastic support really made the workshop a success. We are aware of the magnitude of your contribution—the enormous time and effort spent in making the computer runs, interpreting and graphing the results, presenting and discussing, and then the drudgery of writing the manuscript (an anticlimactic task once the workshop is over), and submitting it within the requested timeframe.

Summary

Perhaps the most important and encouraging results of this PE Workshop were that underwater acoustic parabolic equation (PE) models from both the 6.1 basic research modeling community and the 6.3 Navy operational modeling community were applied to the same set of test problems—each test problem designed to push the PE models to their limits—and each of the two communities' PE models did extremely well, given the requirements and constraints imposed by each community. The PE models developed by the 6.1 basic research modeling community were able to produce results for the test case problems that were benchmark accurate. This is a definite requirement, since the basic research community uses these models to identify, to isolate, and to understand the physical mechanisms involved in underwater acoustic propagation and scattering in highly complex underwater environments. The 6.3 Navy operational community is also interested in accurate model predictions, but the need for computational speed, portability, and the ability to run a computer in the field (micro or desk-top) is also of utmost importance—to the extent that trade-offs among accuracy, speed, and portability must be optimized. The results from this workshop demonstrate that the underwater acoustic PE models used by both modeling communities are performing at their expected levels.

The PE approximation to the elliptic wave equation was first introduced into the underwater acoustic propagation community in 1973 by Hardin and Tappert at a Navy workshop sponsored by the Acoustic Environment Support Detachment (AESD). Following that introduction, other researchers began to use the PE approximation and to extend its limits.

In 1981 a workshop solely devoted to the PE approach to modeling underwater acoustic propagation was sponsored by the Long Range Acoustic Propagation Program, now the ASW Environmental Acoustic Support (AEAS) Program. It was hosted by the Naval Ocean Research and Development Activity, now part of the Naval Research Laboratory (NRL). The objectives of that first PE workshop were threefold:

- provide a forum for those active in theoretical and applied PE model development to exchange ideas, describe their PE models, identify problems or deficiencies in the PE approach, and stimulate new ideas and approaches.
- compare model results for a set of common underwater acoustic problems.
- provide the AEAS program with information on the current state of PE computer models; using this information, make decisions for developing a Navy-supported PE model that could meet the needs of the AEAS program.

The first workshop was a success. The Navy-supported PE model efforts evolved into the present Navy Standard PE model. Although the first PE workshop was sponsored by the Navy's 6.3 Applications Program, the results of that workshop have been extremely useful to both the basic research and the applications communities.

Since the first PE workshop, there has been a virtual explosion of developments in the underwater acoustics PE community, as well as in the supporting technologies of

Summary

computer science and environmental data basing. The synergy among these technologies have produced underwater acoustic calculations that are more accurate and faster than thought possible in 1981.

The progress in underwater propagation modeling, especially in advancing the PE approach, gave impetus for holding a second PE Workshop. It was decided that this PE Workshop II would not be restricted to just the PE technique; the discussion of other innovative techniques would also be encouraged. The workshop was to be highly technical and interactive. Invited participation was restricted to those who would actively participate in the workshop presentations and discussions.

The initial announcement of PE Workshop II was made on 6 September 1990, and suggestions for test cases were solicited from the underwater acoustics community. After assimilating the test case suggestions, a letter was sent on 18 January 1991 defining the test cases that would be used for the workshop. To many, the use of test cases would seem to indicate a competition among the many different PE approaches. Nothing could have been farther from the intention of the workshop organizers. It was their intent to make the results of the workshop as meaningful to the underwater acoustic community as possible. In this spirit the workshop would be noncompetitive, i.e., it would not be a "bake-off" among PE models. The best possible result from each model was the objective. When available, benchmark reference solutions of each test problem were provided to each participant prior to the workshop. A set of reference solutions was forwarded to all invited participants on 23 April 1991. To further enhance a noncompetitive spirit, the participants were encouraged to rework the problems based on what they had learned during the workshop, and then submit their final manuscripts.

The PE Workshop II was divided into two parts. The first part was for presentations by the participants on either the PE approach that they used or some other innovative approach that might be applicable or of interest to the underwater acoustics community. The second part was for comparisons and discussions of the test cases. Each part of the workshop was designed to be very informal. Each test case was introduced and, if available, a reference solution was presented. Then anyone that wished could show their PE model results. All results were compared to each other and to the reference results. This comparison process went smoothly, assisted by the use of a standard plot scale that had been designated for each test case. The test cases were as follows:

- Test Case 1: Lloyd's Mirror – Wide-Angle Propagation
- Test Case 2: Conservation of Energy in Range-Dependent Propagation
- Test Case 3: Range-Dependent Shear Wave Propagation
- Test Case 4: Backscatter from a Waveguide Discontinuity
- Test Case 5: Propagation in Constantly Changing Environment
- Test Case 6: Underwater Acoustic Model Predictions vs. Measured Field Data
- Test Case 7: Long-Range Propagation in a Leaky Surface Duct

The results from the PE Workshop II indicate that present PE models can solve several difficult underwater acoustic problems (e.g., highly range-dependent propagation over shear-supporting ocean bottoms, including backscatter). The models were exercised by experts in acoustic modeling (in most cases, by the model developers). Indications are that many of the models and techniques demonstrated during the workshop can be utilized in operational situations by operators other than the model developers.

Contents

PART 1	PE Workshop II	
	Preface	i
	Acknowledgments	ii
	Summary	iii
	List of Attendees	vii
	Introduction	1
	I Workshop Agenda	5
	II Development of the Test Cases	8
	III Results	13
	IV Summary and Conclusions	22
	References	24
	Appendix A Test Cases: Descriptions and Plotting Formats	25
	Appendix B Reference Solutions to the Test Cases	43
	Appendix C Tappert's Reflections on the Origin of Underwater Acoustic PE	49
PART 2	Test Case Results	57
	Introduction	57
	Test Case 1 Lloyd's Mirror – Wide-Angle Propagation	62
	Test Case 2 Conservation of Energy in Range-Dependent Propagation	68
	Test Case 3 Range-Dependent Shear Wave Propagation	78
	Test Case 4 Backscatter from a Waveguide Discontinuity	87
	Test Case 5 Propagation in Constantly Changing Environment	96
	Test Case 6 Underwater Acoustic Model Predictions vs. Measured Field Data	103
	Test Case 7 Long-Range Propagation in a Leaky Surface Duct	111
	Bibliography	118

Contents

PART 3	Contributed Papers	125
	<i>A Single-Scatter Formalism for Improving PE Calculations in Range-Dependent Media</i> Gary H. Brooke and David J. Thomson	126
	<i>Higher-Order, Energy-Conserving, Two-Way, and Elastic Parabolic Equations</i> Michael D. Collins	145
	<i>The Self-Starter</i> [†] Michael D. Collins	169
	<i>The Navy Standard Parabolic Equation Model, Broadband PE, and PE Workshop II</i> Eleanor S. Holmes and Laurie A. Gainey	175
	<i>PE Workshop II: Test Problem Solutions</i> Finn B. Jensen	214
	<i>Applications of the IFD Model</i> Ding Lee, Martin H. Schultz, William L. Siegmann, Donald F. St. Mary, and George Botseas	228
	<i>FastPE, SlowPE, YourPE, MiPE: What are the Real Issues?</i> Lan Nghiem-Phu, Kevin B. Smith, and Fred D. Tappert	249
	<i>Impedance Bottom Boundary Conditions for the Parabolic-Type Approximations in Underwater Acoustics</i> John S. Papadakis	265
	<i>Coupled Modes for a Rapid Range-Dependent Modeling</i> [†] Michael Porter, Carlo M. Ferla, and Finn B. Jensen	271
	<i>Windowed Transformations and Marching Algorithms for Localized Phase-Space Representations</i> B. Z. Steinberg and J. J. McCoy	282
	<i>PE-Based Spectral Decomposition</i> David J. Thomson	296
	<i>The OPTAMAS System</i> [†] [Editors' Notes]	321
	<i>Bibliography</i>	323

[†] Post-Workshop Contribution – Not Presented at the Workshop

List of Attendees

- Ralph N. Baer** Naval Research Laboratory
Code 7120
4555 Overlook Ave., S.W.
Washington, DC 20375-5320
- Gary H. Brooke** Defence Research Establishment Pacific
FMO Victoria, B. C.
V0S 1B0, Canada
- John A. Campbell, Jr.** Naval Research Laboratory
Code 7183
Stennis Space Center, MS 39529-5004
- John W. Cartmill** Planning Systems, Incorporated
115 Christian Lane
Slidell, LA 70458
- Edward D. Chaika** Office of Naval Research Detachment
Code 124A
Stennis Space Center, MS 39529-5004
- Stanley A. Chin-Bing** Naval Research Laboratory
Code 7181
Stennis Space Center, MS 39529-5004
- Michael D. Collins** Naval Research Laboratory
Code 7124
4555 Overlook Ave., S.W.
Washington, DC 20375-5320
- James A. Davis** Planning Systems, Incorporated
Two Shaws Cove
Suite 200
New London, CT 06320
- Lewis B. Dozier** Science Applications International Corp.
1710 Goodridge Dr.
McLean, VA 22102

Attendees

Richard B. Evans Science Applications International Corp.
Two Shaws Cove
Suite 203
New London, CT 06320

David H. Fabre Planning Systems, Incorporated
115 Christian Lane
Slidell, LA 70458

Lucy C. Fitzgerald Sverdrup Technology
Bldg. 2109
Stennis Space Center, MS 39529

Laurie A. Gainey Science Applications International Corp.
13 Steeple Street
Mashpee, MA 02649

Melanie A. Hebert Planning Systems, Incorporated
115 Christian Lane
Slidell, LA 70458

Eleanor S. Holmes Integrated Performance Decisions
Century Building, Suite 1250
2341 Jefferson Davis Highway
Arlington, VA 22202

Pamela M. Jackson Naval Research Laboratory
Code 7172
Stennis Space Center, MS 39529-5004

Finn B. Jensen SACLANT Undersea Research Centre
Viale San Bartolomeo 400
I-19026,SAN BARTOLOMEO (La Spezia), Italy

William Kesner ALLIANT Techsystems, A.T.C.
1911 Ft. Myer Drive, Suite 601
Arlington, VA 22209

David B. King Naval Research Laboratory
Code 7181
Stennis Space Center, Mississippi 39529-5004

Ding Lee Naval Underwater Warfare Center - New London
Detachment
Code 3122
New London, Connecticut 06320-5594

Attendees

- Walter McBride** Planning Systems, Incorporated
115 Christian Lane
Slidell, LA 70458
- Joseph E. Murphy** University of New Orleans
Department of Physics
Lake Front
New Orleans, LA 70148
- Lan Nghiem-Phu** Mac Systems Corp.
7290 SW 48th Street
Miami, FL 33155
- John S. Papadakis** The Foundation for Research and Technology - Hellas
Institute of Applied & Computational Math.
P.O. Box 1527
Heraklio 711 10
Crete, Greece
- Josette M. Paquin** Neptune
1181 Robert Road
Slidell, LA 70458
- Robert D. Purrington** Tulane University
Department of Physics
New Orleans, LA
- Bruce Z. Steinberg** Catholic University
Department of Electrical Engineering
Washington, D.C. 20064
- Fred D. Tappert** University of Miami/RSMAS
Division of Applied Marine Physics
4600 Rickenbacker Cswy.
Miami, FL 33149-1098
- David J. Thomson** Defence Research Establishment Pacific
FMO Victoria, B. C.
V0S 1B0, Canada
- Henry Weinberg** Naval Underwater Warfare Center - New London
Detachment
Code 3122
New London, Connecticut 06320-5594
- Michael R. Wooten** Planning Systems, Incorporated
115 Christian Lane
Slidell, LA 70458

PART 1 PE WORKSHOP II

***Editors' Note:** These proceedings are divided into three parts. Part 1 gives the historical details of the workshop, the thinking that went into the development of the test cases, the seven test cases as presented to the participants, the agenda that the workshop followed, and representative results for each of the test cases. It is, therefore, the programmatic part of the proceedings with a summary of the results.*

Part 2 gives the results presented for each test case. Part 2 stands alone as a reference source for the underwater acoustics community. Each test case problem is described in detail with an accompanying figure; the primary physical mechanism that is to be modeled is presented with an accompanying rationale. Finally, each of the results presented for that test case is plotted along with a reference solution (when available); noteworthy comments on the results are then offered. Results shown in Part 2 represent predictions from such a cross section of PE models—research models and field operational models—as to render meaningless any attempts at absolute comparisons. And, such comparisons would be contrary to the intent and spirit of the workshop.

Part 3 of the proceedings contains the contributed papers from the workshop participants. It is a most valuable part of the proceedings and should not be neglected in lieu of the results that appear in Part 2. These papers are a valuable adjunct to the results presented in Part 2. They contain the theoretical framework associated with a particular PE model, in-depth discussions of results, and the particulars of how the model was applied to a particular test case problem. In addition, the papers provide the comprehensive list of references associated with a particular PE model. In several cases, the papers represent the first results of a new PE model development-application, e.g., the backscatter capability of the PE model.

INTRODUCTION

The history of the PE application to the underwater acoustics propagation problem began when the approach was introduced to the acoustics community by Hardin and Tappert (1973) at an AESD workshop on non-ray-tracing techniques (Spofford 1973). Following the introduction of the method, a significant amount of work was done by the underwater acoustics community to establish the limits of validity and utility of the model.

PE Workshop II: Part 1

In March 1981 a workshop (Davis et al. 1982) on the PE approach to underwater acoustics propagation was held. The objectives of that workshop were threefold:

- provide a forum for those active in theoretical and applied PE development to exchange ideas, describe their PE computer programs, identify problems or deficiencies in the PE approach, and stimulate new ideas and approaches;
- compare computer results (solutions) for a common set of chosen underwater acoustics problems; and
- provide guidance (via this new information) upon which the AEAS program office could base decisions as to the development of a Navy-supported PE model that could meet the needs of that program.

These objectives were met. Results from the PE workshop were used to define and emphasize the areas in the PE approach where further research was needed. That eventually led to a version of the PE model being selected by the U. S. Navy as a standard range-dependent propagation model.

The first PE Workshop was organized into two parts: the first half of the workshop was devoted to formal presentations on developments and improvements to the PE approach; the second half of the workshop was devoted to the comparison of PE model predictions against a set of four test cases.

Following the first workshop there was a virtual explosion of developments in the field of PE modeling. Great strides were made in extending the areas of applicability of the approach to different environments and conditions. A useful bibliography of these advances in the PE method can be compiled from the references included in the papers in Part 3 of these proceedings.

Because of the large body of work that has been done on the PE method in the past decade it was decided to hold a second workshop. This second PE workshop (PE Workshop II) was jointly sponsored by two divisions of the Office of Naval Research: one responsible for basic research (designated by the U.S. Navy as 6.1) and the other responsible for applied research (designated by the U.S. Navy as 6.3). NRL was invited to host the second workshop.

An organizing group was put together consisting of Stanley A. Chin-Bing and David B. King of NRL; James A. Davis of Planning Systems, Incorporated; and Richard B. Evans of Science Applications International Corporation. This group, in consultation

PE Workshop II: Part 1

with the ONR sponsors, Ed Chaika and Marshall Orr, developed the philosophy of the workshop: the workshop would be highly technical, interactive, and focused. To accomplish this goal, workshop participation was limited to those 6.1 and 6.3 researchers who had actually developed underwater PE models and to those 6.3 researchers who were directly related in the model development and/or improvement of Navy PE operational models.

A further restriction on workshop participation was made by the sponsors' choice of the physical phenomena to be emphasized in this workshop, viz, underwater acoustic propagation and backscatter. The related subject of underwater acoustic rough-surface scattering, incorporated with PE methods, is large enough to warrant a workshop devoted singly to that subject. With the expectation that such a workshop would soon occur, the general topic of underwater acoustic scattering was minimized in this workshop.

The announcement of the workshop was made on 6 September 1990 to the acoustics community at large. The announcement also solicited suggestions as to meaningful test cases that might challenge the state-of-the-art PE models and their developers. After reviewing all suggestions, a letter was sent on 18 January 1991, defining the six test cases that would be studied during the workshop. (These test cases are detailed in Appendix A.)

The use of test cases in a PE workshop environment conjures thoughts of competition among the many different PE approaches. However, this was not to be the situation in PE Workshop II. From the beginning it was planned to make the workshop as meaningful to the underwater acoustics community as possible. In this spirit, the workshop was designed to be noncompetitive, i.e., it would not be a "bake-off" between PE models.

The objective was to obtain the best possible result from each model. Each participant was encouraged to fine-tune their results as much as they desired. It was recognized that no one model would be able to do all of the problems without a significant effort on the part of the developer. With the noncompetitive spirit in mind, benchmark results to several of the test problems were provided to each participant prior to the workshop. Unfortunately, reference solutions were not generated for all of the test cases. The available reference solutions were forwarded to the participants on 23 April 1991.

Since the workshop was meant to be noncompetitive, the model developers were encouraged to go back after the workshop and "fine-tune" their results based on what they

PE Workshop II: Part 1

learned during the workshop. Some of the modelers took advantage of this offer and were able to generate better results after the workshop's conclusion. Other modelers chose not to avail themselves of the opportunity for one reason or another. For example, the custodian of the Navy Standard PE model felt that the model results without the advantage of "fine-tuning" would be more representative of an operational model. Comparison of results at the workshop did identify some deficiencies in the Navy Standard PE model (e.g., in the starting field used by the model). These deficiencies were corrected in the later versions of the model. Test case results from the later version of the Navy Standard PE model are included in these proceedings, since these results now reflect the operational model's capabilities.

The PE Workshop II was organized into two sections. The first section, covering the first day and half of the second day, was devoted to formal presentations of papers. The topics were varied. Participants had been invited to contribute a paper either on some new development in PE modeling or on another innovative approach applicable to underwater acoustic modeling. Authors had been especially encouraged to discuss their models, both in theory and in application. However, they were free to present any material that they felt was germane to the workshop objectives. This unstructured format produced some valuable papers that went beyond the theory-application of a particular model.

Some members of the modeling community were unable to attend due to other commitments, but they still wished to have their work represented in the workshop. In some cases they desired to have a formal paper included in the workshop proceedings; in other cases they wanted the workshop proceedings to include the results of their model's application to the test cases. In all respects, where appropriate, they were accommodated.

I Workshop Agenda

Table 1-1 lists the 14 papers presented at the workshop in the order in which they were given. Unrestricted discussion time was given at the conclusion of each paper so that the chronology indicated in Table 1-1 represents the scheduled time, not the actual time, that a paper was presented and/or concluded.

Manuscripts contributed by the presenters are included in Part 3 of this report. In some cases the authors decided to combine two of their presentations into one paper. In a few cases presentations were given for which the authors did not specifically include that material in their manuscripts. However, all of their important results are included in Part 2 and in their papers in Part 3.

The second part of the workshop was devoted to discussions of the test cases. Each test case was introduced along with the rationale for its selection. If available, a reference solution to the test case was presented which adhered to a specified plot scale. (In the letter that defined the test cases [see Appendix A], a plot scale had been specified for each test case. This information had been provided to each participant prior to the beginning of the workshop.) Thus, anyone who had a solution to a test case problem that they wished to present was asked to overlay their results on the reference solution. (A similar format is followed in Part 2 of this proceedings where each contributor's result is plotted over the reference solution.) This comparison process produced very open discussions and allowed all results to be compared against the reference solution and against one another.

"Reference solutions" were just what the terminology implies; i.e., they were solutions to the test cases provided by the organizing committee and were used as a common reference to compare with the various PE solutions. With the exception of Test Case 1, where an analytic image solution to the Lloyd's Mirror problem was used, all of the reference solutions were numerical solutions obtained from underwater acoustic computer models whose accuracy had been established over many years of peer reviewed applications. As an example, the COUPLE model (Evans 1983) has been accepted as "benchmark accurate" (Felsen 1990; Jensen and Ferla 1990) and it was used where applicable (e.g., Test Cases 2 and 4). Test Case 3 required an accurate solution that included range-dependent shear waves and the SAFE model (Murphy and Chin-Bing 1991) was used to calculate the reference solution.

PE Workshop II: Part 1

Table 1-1. PE Workshop II Agenda

MONDAY, MAY 6, 1991		
1 - 4 PM	REGISTRATION (Holiday Inn, Slidell, LA)	Presenters are in italics
TUESDAY, MAY 7, 1991		
8:30 AM	WELCOME ADDRESSES	<i>E. D. Chaika, James Matthews</i>
9:00 AM	History of PE	Fred D. Tappert
9:30 AM	Application of the IFD Model	Ding Lee
10:00 AM	FEPE and FEPES Benchmark Solutions	Michael D. Collins
10:30 AM	BREAK	
11:00 AM	A Finite-Difference/Split-Step Acoustic PE Code	David J. Thomson
11:30 AM	Finite-Difference Elastic-Acoustic PE Codes for Layered Media	Gary H. Brooke
NOON	LUNCH	
1:00 PM	PE II Workshop Contributions	<i>Finn Jensen, M. Porter, C. Ferla</i>
1:30 PM	FASTPE SLOWPE YOURPE MiPE: What are the Real Issues?	Lan Nghiem-Phu
2:00 PM	Navy Standard PE	<i>Eleanor Holmes, Laurie Gainey</i>
2:30 PM	BREAK	
3:00 PM	Windowed Transformation and Marching Algorithms for Localized Phase-Space Representations	<i>B. Z. Steinberg, J. J. McCoy</i>
3:30 PM	Handling Backscatter by a Marching Program	<i>Ding Lee, Don St. Mary</i>
4:00 PM	Full-Wave 3-D Modeling of Long-Range Oceanic Boundary Reverberation	Fred D. Tappert
5:00 PM	ADJOURN	
7:00 PM	Dinner at Doug's Restaurant (Slidell, LA)	
WEDNESDAY, MAY 8, 1991		
8:30 AM	Impedance Boundary Condition as Applied to PE	John S. Papadakis
9:00 AM	Post-PE Corrections	David J. Thomson
9:30 AM	BREAK	
10:00 AM	Test Case 1 – Comparison of Results, Discussions	Full Audience Participation
11:00 AM	Test Case 2 – Comparison of Results, Discussions	Full Audience Participation
NOON	LUNCH	
1:30 PM	Test Case 3 – Comparison of Results, Discussions	Full Audience Participation
2:30 PM	Test Case 4 – Comparison of Results, Discussions	Full Audience Participation
3:30 PM	Test Case 5 – Comparison of Results, Discussions	Full Audience Participation
4:30 PM	ADJOURN	
THURSDAY, MAY 9, 1991		
8:30 AM	Test Case 6 – Comparison of Results, Discussions	Full Audience Participation
9:30 AM	Ray Methods in Underwater Acoustic Propagation-Scattering	H. Weinberg
10:00 AM	BREAK	
10:30 AM	Test Case 7 – Comparison of Results, Discussions	Full Audience Participation
11:15 AM	Discussions, Workshop Conclusion	
NOON	ADJOURN	

PE Workshop II: Part 1

For Test Case 6 the reference solution was experimental data (Fisher et al. 1989). In a few cases, the participants provided their own test case reference solutions (e.g., the SNAP model was used by Jensen to generate the reference solution for Test Case 7). The reference solutions are given in tabular form in Appendix B.

When available, the reference solutions were provided to each workshop participant prior to commencement of the workshop. Participants were encouraged to use these reference solutions as a guide in preparing their PE solutions.

It should be noted that not all of the models were applied to all of the test case problems (see Tables 1–2 and 1–3 for details). This was expected since each test case problem was designed to test a specific physical mechanism, which until recently, was not included in many PE models. It is a credit to their developers that so many of the PE models did so well on these test case problems.

II Development of the Test Cases

Selection of the test cases was perhaps the most difficult problem faced in organizing the PE Workshop II. The number of underwater acoustic publications involving PE-model development is extensive for the decade of the Eighties as compared with the previous decade. In general the capabilities of PE models have been significantly extended. In the announcement letter the following topics were listed as possible candidates for the test cases:

- wide-angle propagation (a.k.a. high-angle propagation)
- deterministic vs. stochastic propagation
- conservation of energy in the PE model
- full viscoelastic bottom (or equivalent) in the PE model
- pulsed (broadband) propagation; time and arrival structure; Fourier synthesis of frequency domain solutions vs. true time domain solutions
- three-dimensional (3-D vs. $N \times 2$ -D) propagation
- scattering (in-plane and out-of-plane) and backscatter
- very low frequency propagation.

The announcement letter also solicited suggestions for meaningful test cases. The responses were limited, but some very good ideas were offered. The problem then became one of selecting a set of test cases that would cover as many meaningful types of situations as possible. The criteria used in selecting the test cases were as follows:

- Use only a small number of test cases.
- Computer runtimes (and costs) should not be excessive.
- Each test case should test just one type of physical mechanism.
- The test case should involve a new development in PE modeling.

It became apparent that not all of the topics could be covered in a limited set of test cases. Some things had to be eliminated. The first of many difficult decisions made was to eliminate rough boundary scattering problems. It was felt that this would be testing a rough surface scattering algorithm and not necessarily the PE approach. Also it was felt that this topic was so broad in scope as to warrant a workshop in its own right.

PE Workshop II: Part 1

Another area that was difficult to exclude was full 3-D PE underwater-acoustic modeling. After many lengthy discussions and attempts, it was concluded that the detailed description needed for a 3-D underwater acoustic problem—such that the problem would be useful and unambiguous, and would provide a unique test for a specific physical mechanism—was beyond the scope envisioned of this workshop. Simply scattering out-of-plane (i.e., azimuthally off a bathymetric feature) would certainly give a different result than that obtained by an $N \times 2$ -D modeling approach—this had been documented in the literature. However, aside from confirming the obvious, the real issue in this scenario would be how well the PE method could handle scattering from an abrupt environmental feature; this would be a duplication of the issue addressed in Test Case 4. Another environmental situation where 3-D modeling had established a difference from the $N \times 2$ -D techniques was the situation where azimuthal refraction occurs due to changes in the 3-D sound speed field. This would have been a weak phenomenon (unless a front or eddy was involved) and would have required far more early preparation from the workshop organizers and participants than time would allow. (One can readily comprehend the amount of information that would be needed for a 3-D problem by reviewing the data required for the realistic 2-D problem of Test Case 6, shown in Tables A-1, A-2, and A-3 of Appendix A.) Additionally, most of the physical phenomena that would be tested (e.g., energy conservation, sharp refractions) were already included in the other test case problems.

Six test cases were finally developed. This seemed to be the absolute minimum number of cases that would cover the many topics of interest. While the number of test cases seemed excessive (four test cases were used in the first PE workshop), it was realized that only a few of the modelers would try to solve all of the test cases. For example, several participants did not attempt to solve Test Case 3, which involved propagation in elastic media, since their particular model did not include propagation-conversion of shear waves.

Six test cases were distributed to interested parties on 18 January 1991. The test cases selected were as follows:

- Test Case 1: Lloyd's Mirror – Wide-Angle Propagation
- Test Case 2: Conservation of Energy in Range-Dependent Propagation
- Test Case 3: Range-Dependent Shear Wave Propagation
- Test Case 4: Backscatter from a Waveguide Discontinuity
- Test Case 5: Propagation in Constantly Changing Environment
- Test Case 6: Underwater Acoustic Model Predictions vs. Measured Field Data

PE Workshop II: Part 1

The major capabilities that would be tested by this set of test cases are the ability to propagate wide-angle energy, the ability of the model to conserve energy as it goes up and down a slope, the ability to account for shear propagation in elastic media, the ability to handle backscatter from steep (vertical) surfaces, the ability to handle constantly changing environments, and a comparison with measured field data. The information sent to the participants regarding the six test cases is given in Appendix A.

During the course of the workshop discussions, a problem with wide-angle split-step PE's experienced by Finn Jensen and Michael Porter was reexamined. The PE Workshop II organizing committee had not included this problem as a test case problem because the difficulty was peculiar only to some (not all) wide-angle split-step PE models and was not a difficulty to other wide-angle PE models that used finite-difference or finite-element solution techniques. However, in the course of the workshop discussions it became evident that this was indeed an important problem to be considered and, if possible, resolved. Consequently, we have included this problem as:

- Test Case 7: Long-Range Propagation in a Leaky Surface Duct.

The modelers who use a split-step PE solution were requested to further examine Test Case 7 after the workshop had concluded. Relevant post-workshop results on Test Case 7 could be incorporated into their contributed papers. Their responses are included in some of the papers that appear in Part 3 of the workshop proceedings.

Several of the investigators used more than one model to solve the various test cases. Twenty models were used by the modelers. This many models can lead to problems and confusion in labeling different model results. In cases where possible, we maintained the names used by the model developers. There were some cases where liberty was taken and unique names assigned to the models. Sometimes virtually the same model was used by different investigators; to help discriminate between the same model being executed by different investigators, separate names were selected.

Table 1-2 gives an alphabetical listing of the labels used on the plots together with a short discussion of the models. It is not intended to give a complete explanation of the models since adequate information is contained in the literature. Along with each label (model) is the name of the workshop participant who used the model to generate results for the test cases.

Table 1-3 shows the models that were used by participants of the workshop versus the test cases to which the models were applied.

PE Workshop II: Part 1

Table 1-2. Models Used by Workshop Presenters

CU	Steinberg and McCoy's windowed transformation and marching algorithms for localized phase-space representations. Steinberg used it to obtain the solution to Test Case 1.
COUPLE	Richard Evans' coupled mode model; Evans used it to provide several of the reference solutions used during the workshop. It was also used by Finn Jensen (SACLANTCEN) to work Test Case 4.
DREP	Finite-difference PE model developed and used by David Thomson (Defence Research Establishment Pacific (DREP)) to generate solutions to workshop Test Cases 2 through 7. In Test Cases 1 and 7 Thomson used his split-step PE model.
DREPS	The elastic PE model developed and used by Gary Brooke (DREP) to generate solutions to the workshop Test Case 3. It includes shear wave attenuation.
FEPE	The finite-element PE model developed and used by Michael Collins of NRL to generate solutions to the workshop test cases.
FEPES	Collins' elastic version of his FEPE model that includes shear wave propagation and attenuation. Collins used it to provide solutions to Test Case 3.
FEPE ROT	The ROT extension refers to a version of Collins' FEPE where he rotates the coordinate system so that the water-sediment interface can be represented as horizontally flat rather than a sloping bottom. He used this model as a check for Test Case 3.
FEPES ROT	Collins' rotated version of his shear PE (FEPES); he used it as a check for Test Case 3.
IFDPE	The implicit finite-difference PE model developed and used by Ding Lee to generate solutions to the workshop Test Case 3.
IFDPE SAC	IFDPE was also used by Jensen to work some of the cases. To distinguish his results from those reported by Lee, a SAC extension was used.
IMPPE	A version of IFDPE developed and used by John Papadakis. His version replaces the standard "false bottom" method used in IFDPE with an impedance bottom boundary condition.
LOGPE	PE model developed by Berman, Wright, and Baer [Berman, et al. 1989]; it uses a split-step solution technique. In a range-independent environment, its "rays" are identical to the "rays" of the Helmholtz equation. Used by Jensen to get results for Test Case 7.
MIPE	Results generated by Lan Nghiem-Phu with the University of Miami's split-step PE. This model has evolved from the original Hardin and Tappert model developed circa 1972.
NAVY STD PE	Results generated by Eleanor Holmes and Laurie Gainey using the U.S. Navy's standard version of PE. This model uses the split-step algorithm.

PE Workshop II: Part 1

Table 1-2. Models Used by Workshop Presenters (Continued)

NON EC FE	Collins' version of his FEPPE model without the enhancement that "conserves" energy.
OPT	Results generated by Nils Paz using the split-step PE model in the OPTAMAS system.
PAREQ	SACLANTCEN version of PE that uses the split-step algorithm. The label refers to the results generated by Jensen using this model.
REF	REF refers to several different methods of getting a reference solution. For Test Case 1 it is an analytic image solution to the Lloyd's Mirror problem. For Test Cases 2 and 4 the COUPLE model was used. For Test Case 3 the SAFE model was used. For Test Case 6 the reference solution is experimental data.
SNAP	The SNAP (SACLANTCEN Normal Mode Acoustic Propagation) model was used by Jensen to generate the Reference Solution for Case 7.
T-CPE	This label refers to the Thomson-Chapman version of PE used by Jensen.

Table 1-3. Models Used Versus Test Cases

MODELS USED	TEST CASES													
	1	2A	2B	3A	3B	4A	4B	5A	5B	5C	6A	6B	6C	7
CU	X													
Ref.: COUPLE		X	X				X	X						
DREP	X	X	X			X	X	X	X	X	X	X	X	X
DREPS		X	X	X	X	X	X							X
FEPPE	X	X	X				X	X						
FEPES					X	X								
FEPPE ROT					X	X								
FEPES ROT				X	X									
IFDPE	X	X	X	X	X	X	X	X	X	X	X	X	X	X
IFDPE SAC		X	X											X
IMPPE	X	X	X			X	X	X	X	X				
LOGPE														X
MIPE	X	X	X	X	X	X	X	X	X	X	X	X	X	X
NAVY STD PE	X	X	X	X	X	X	X	X	X	X	X	X	X	X
NON EC FE		X	X											
OPT	X	X	X	X	X	X	X	X	X		X	X	X	
PAREQ														X
Ref.: SAFE				X										
Ref.: SNAP														X
T-CPE	X													X

III Results

This section of Part 1 presents an overview of the results from the PE Workshop II. Part 2 of these proceedings is devoted entirely to the workshop results. The reader should therefore consult Part 2 for details of results discussed in this section.

In presenting this overview, the PE models have been categorized into 3 classes. One class represents the "6.1 Basic Research and Development (R&D)" PE models together with the "6.2 Exploratory Development" PE models. Another class represents the "6.3 Applications" PE models. The final class of PE models is composed of the 6.3 "in-the-field" operational PE models. (The general designations of "6.1," "6.2," and "6.3" are used by the Office of Naval Research. While in principle quite distinct, in practice, the same PE model could be used in 6.1, 6.2, and 6.3 research.) As indicated earlier, the primary difference between a 6.3 Applications PE model and the 6.3 "in-the-field" operational PE model is in the constraints imposed on the operational PE model. These constraints are necessary trade-offs between accuracy vs. computational speed vs. portability and compatibility. The OPTAMAS system and the U.S. Navy's Standard PE model were the only bona fide 6.3 "in-the-field" operational PE models used in this workshop. For classification purposes we have chosen some of the PE models as representative of a 6.3 operational PE model. This is due to their similarity with the Navy Standard PE model in their split-step solution techniques. Historical information on the development of the PE method and its evolution into the Navy Standard PE model is given in Appendix C.

This overview of the results adheres to the following format:

- For each of the Test Cases, 1 through 6, 3 representative plots from the PE models' predictions are given.
- These 3 representative plots are from the 3 classes of PE models that were used to obtain solutions to the workshop's test cases; one of the 3 representative plots comes from each of the 3 classes.
- The first set of plots (labeled Fig. 1-x(a), where $x=1,2,\dots,6$) is representative of the R&D PE models' results for Test Case x.
- The second set of plots, Fig. 1-x(b), is representative of the Applications PE models' results for Test Case x.
- The third set of plots, Fig. 1-x(c), is the result from the U.S. Navy's Standard PE model for Test Case x.

PE Workshop II: Part 1

For this overview, Test Case 7 is treated differently than the previous six test cases. Three of the operational PE model's results are shown for this case with different combinations of reference sound speeds and narrow-angle vs. wide-angle propagation options. These three plots in Fig. 1-7 serve to indicate the problems encountered in Test Case 7.

Finally, for this overview, the selection of representative results for each Test Case, 1 through 6, was made on the basis of the best visual agreement with the reference solution. Thus, with the exception of the Navy Standard PE model, no one model's results appear in all of the test cases.

TEST CASE 1 - Lloyd's Mirror – Wide-Angle Propagation

Results shown in Fig. 1-1(a) from the representative R&D PE model indicate that the research-level PE models are able to propagate the acoustic wave at a half-beamwidth approaching 90° . This is an important result since it implies that some PE models are capable of propagating nearly all of the forward propagating acoustic field. In the first PE Workshop (in 1981) the maximum half-beamwidth that could be propagated by the PE models was 40° . Results shown in Fig. 1-1(b) are from a representative operational PE model. The results match the analytic solution to the Lloyd's Mirror

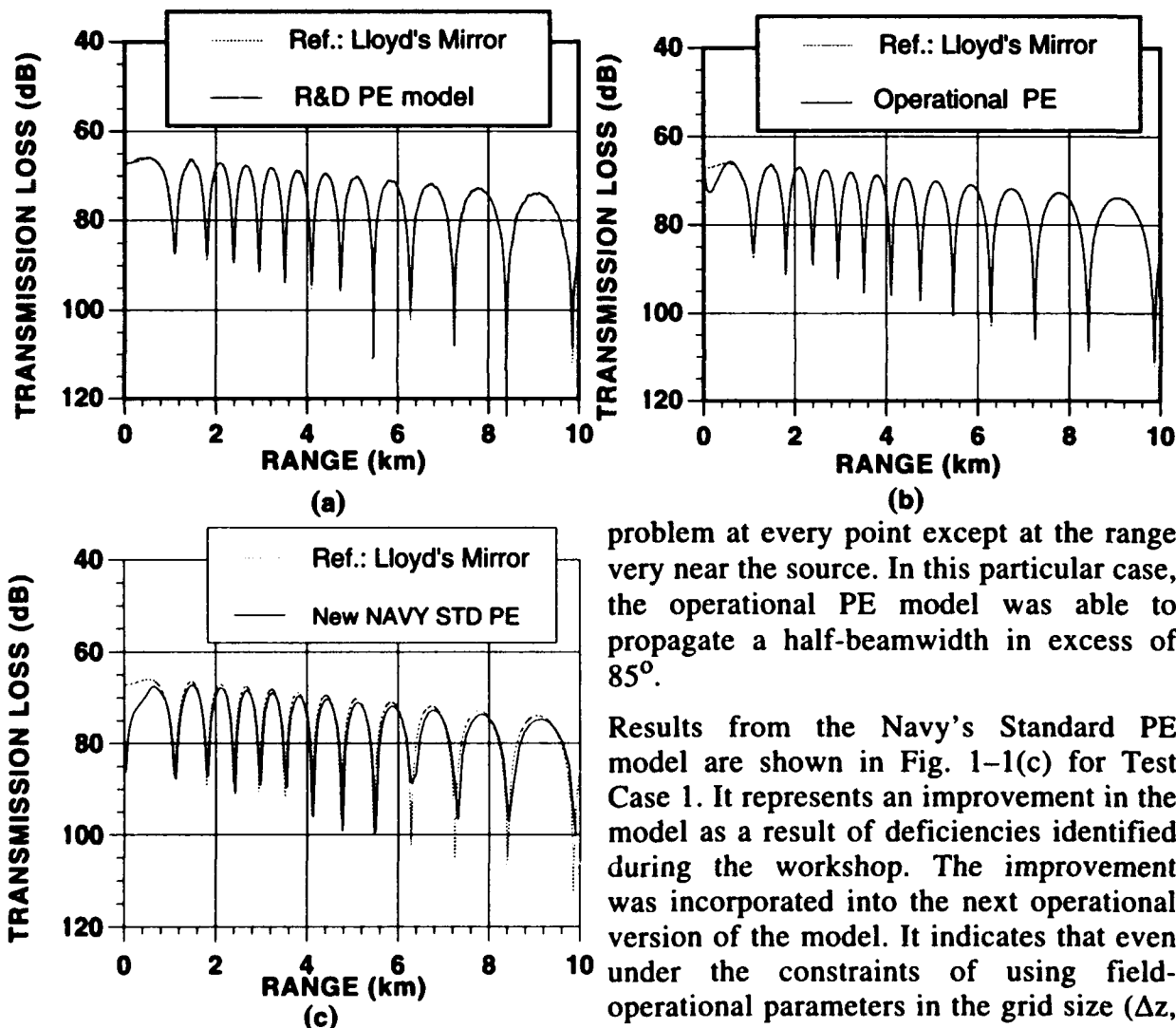


Fig. 1-1. Test Case 1 results from three classes of PE models.

problem at every point except at the range very near the source. In this particular case, the operational PE model was able to propagate a half-beamwidth in excess of 85° .

Results from the Navy's Standard PE model are shown in Fig. 1-1(c) for Test Case 1. It represents an improvement in the model as a result of deficiencies identified during the workshop. The improvement was incorporated into the next operational version of the model. It indicates that even under the constraints of using field-operational parameters in the grid size (Δz , Δr) this model is capable of propagating the acoustic field that is included in a half-beamwidth of greater than 75° .

TEST CASE 2 – Conservation of Energy in Range-Dependent Propagation

This test case required the PE models to propagate the acoustic field upslope in an environment similar to the ASA penetrable lossy wedge benchmark problem. However, this wedge does not intersect the air-water surface. Rather it slopes downward after reaching a height of 25 m from the surface. The physical situation is such that the PE model must propagate three modes upslope, traverse a region at the apex of this upslope-downslope wedge where no modes are propagating, and then propagate downslope where the three modes that were stripped-out going upslope are

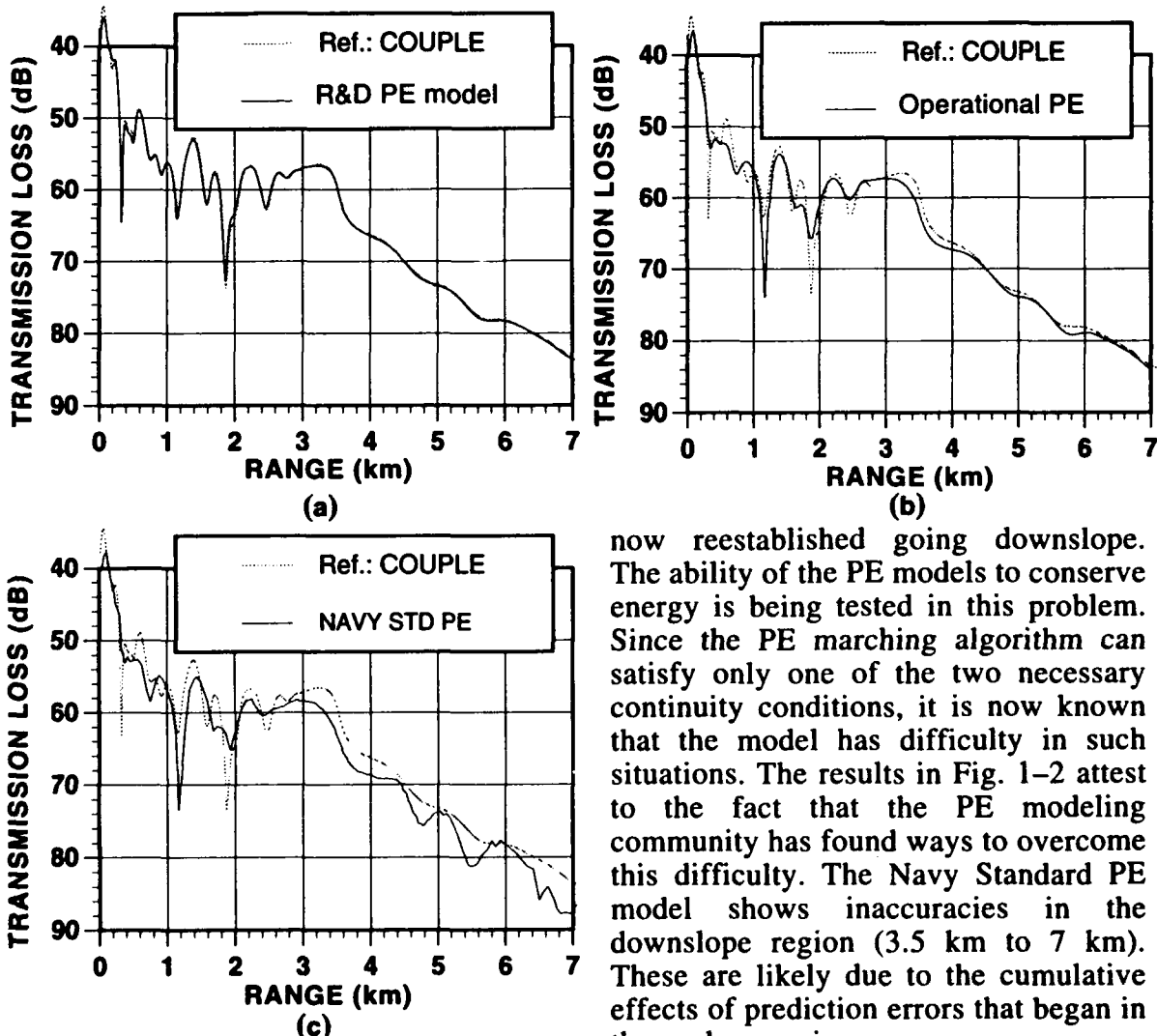


Fig. 1-2. Test Case 2 results from three classes of PE models.

now reestablished going downslope. The ability of the PE models to conserve energy is being tested in this problem. Since the PE marching algorithm can satisfy only one of the two necessary continuity conditions, it is now known that the model has difficulty in such situations. The results in Fig. 1-2 attest to the fact that the PE modeling community has found ways to overcome this difficulty. The Navy Standard PE model shows inaccuracies in the downslope region (3.5 km to 7 km). These are likely due to the cumulative effects of prediction errors that began in the upslope region.

TEST CASE 3 – Range-Dependent Shear Wave Propagation

This test case is just the ASA penetrable lossy wedge benchmark problem with shear wave speed and shear wave attenuation added. Until recently the PE models could only account for shear wave conversion in the ocean bottom by including an “equivalent” attenuation factor. The PE Workshop II was fortunate to have the results from two recently developed shear PE models. These two PE models accurately include range-dependent shear wave conversion as can be seen in Fig. 1-3(a). (The

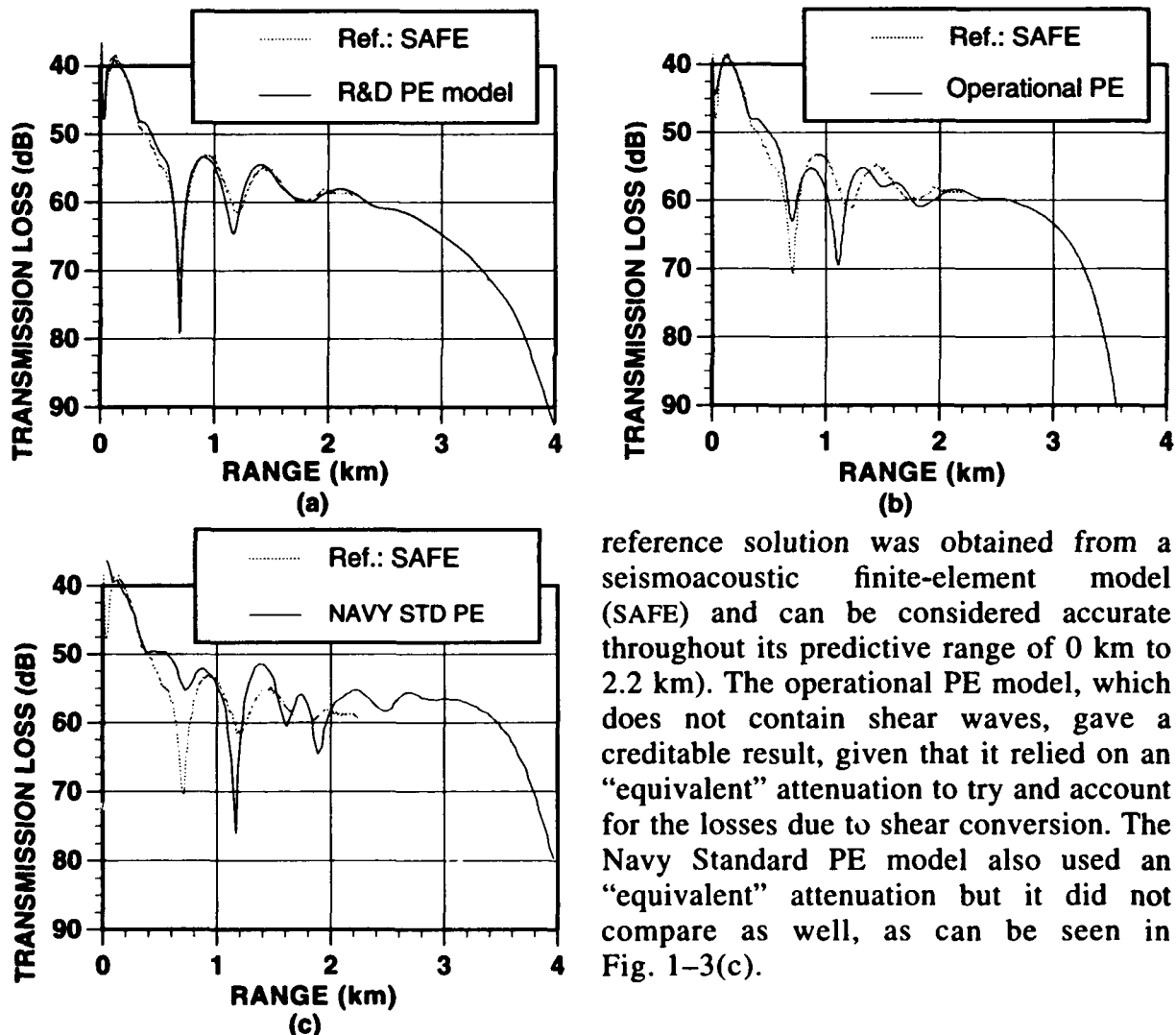


Fig. 1-3. Test Case 3 results from three classes of PE models.

reference solution was obtained from a seismoacoustic finite-element model (SAFE) and can be considered accurate throughout its predictive range of 0 km to 2.2 km). The operational PE model, which does not contain shear waves, gave a creditable result, given that it relied on an “equivalent” attenuation to try and account for the losses due to shear conversion. The Navy Standard PE model also used an “equivalent” attenuation but it did not compare as well, as can be seen in Fig. 1-3(c).

TEST CASE 4 – Backscatter from a Waveguide Discontinuity

This test case required the calculation of backscatter from a step discontinuity in an otherwise flat waveguide floor. The discontinuity begins at range=3 km as is evident from a close scrutiny of the three plots in Fig. 1–4. The “high-frequency” oscillations in the reference curve, between 0 km and 3 km are due to the backscattered field from the step interfering with the forward-propagating field in this 25-Hz continuous wave (cw) example. The reference solution came from the 3-D axially symmetric coupled mode model (COUPLE). The backscattered field (Fig. 1–4(a)) is relatively weak compared to the incident field. For the PE models to calculate the backscattered field

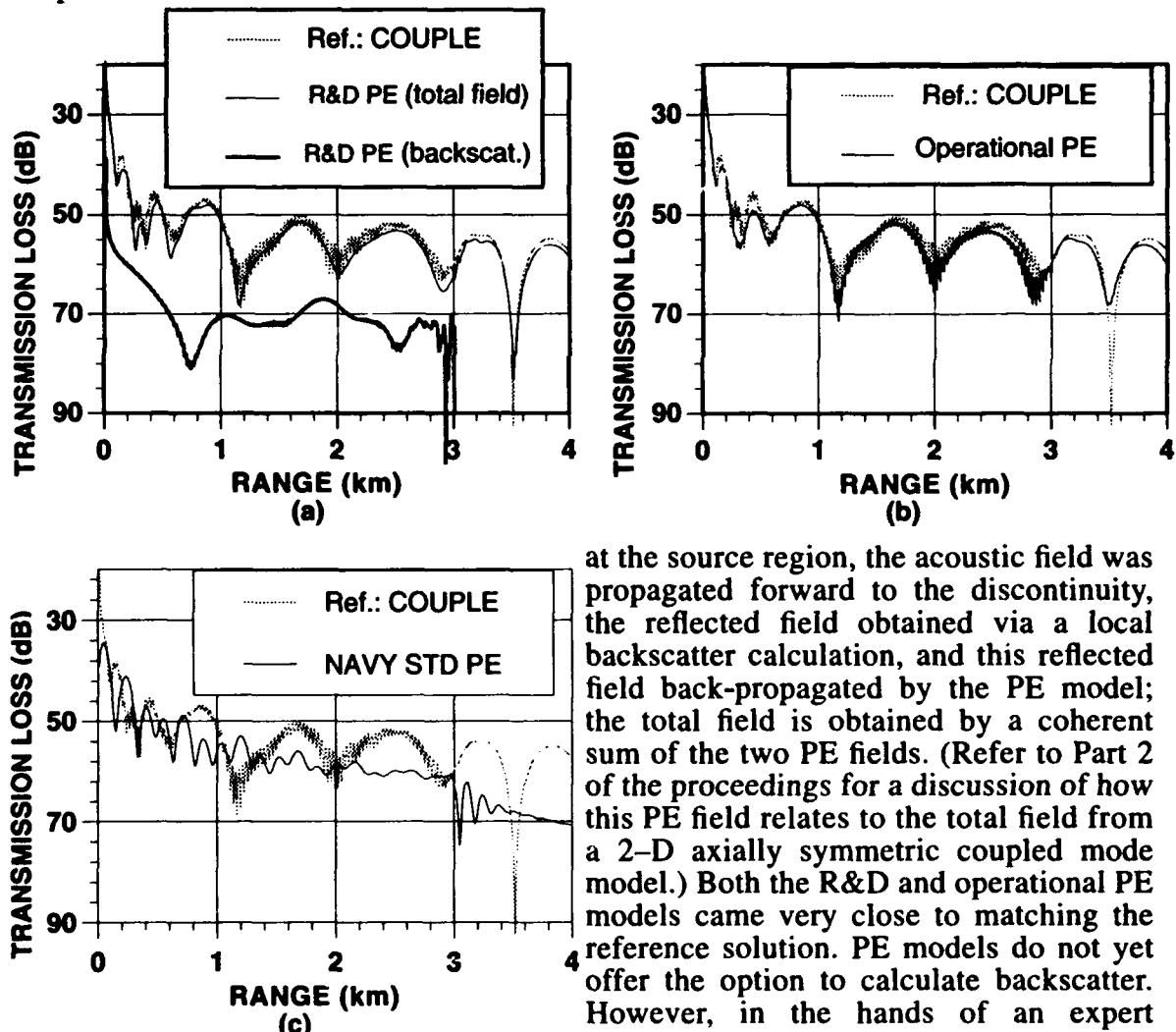


Fig. 1–4. Test Case 4 results from three classes of PE models.

at the source region, the acoustic field was propagated forward to the discontinuity, the reflected field obtained via a local backscatter calculation, and this reflected field back-propagated by the PE model; the total field is obtained by a coherent sum of the two PE fields. (Refer to Part 2 of the proceedings for a discussion of how this PE field relates to the total field from a 2-D axially symmetric coupled mode model.) Both the R&D and operational PE models came very close to matching the reference solution. PE models do not yet offer the option to calculate backscatter. However, in the hands of an expert modeler, the PE models can be used to accurately predict backscatter.

TEST CASE 5 – Propagation in Constantly Changing Environment

This test case involved propagation over a flat ocean bottom that slopes downward (starting at range=0.5 km) and becomes flat again (at range=2.5 km). In the sloping region the rate of variation is different between the continuously changing sound speeds in the water and the corresponding continuously changing bathymetry and sediment depth. The problem is straightforward and requires implementation of a large amount of data to make an accurate prediction. The results shown in Fig. 1-5

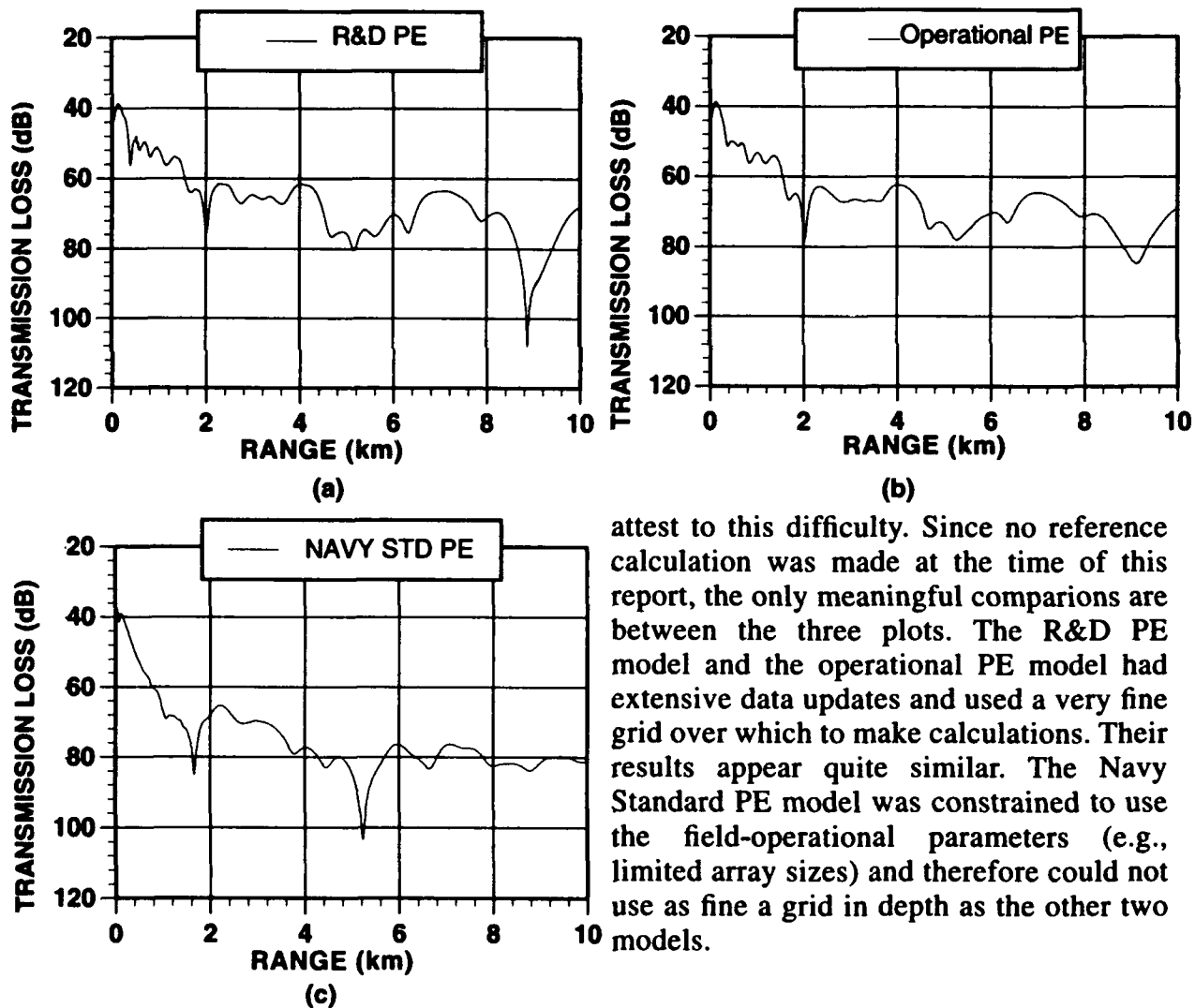


Fig. 1-5. Test Case 5 results from three classes of PE models.

attest to this difficulty. Since no reference calculation was made at the time of this report, the only meaningful comparisons are between the three plots. The R&D PE model and the operational PE model had extensive data updates and used a very fine grid over which to make calculations. Their results appear quite similar. The Navy Standard PE model was constrained to use the field-operational parameters (e.g., limited array sizes) and therefore could not use as fine a grid in depth as the other two models.

TEST CASE 6 – Underwater Acoustic Model Predictions vs. Measured Field Data

This case tested the ability of the various PE models to match acoustic data taken in a region where the environmental and geoacoustic parameters are believed to be well-known. The data track starts in shallow water (200 m) and traverses 100 km to deep water (~4 km). The ocean bottom along the track is sediment overlying a rough shear-supporting subbottom. None of the model predictions agreed with the data but were so consistent in their predictions that the PE Workshop II participants concluded

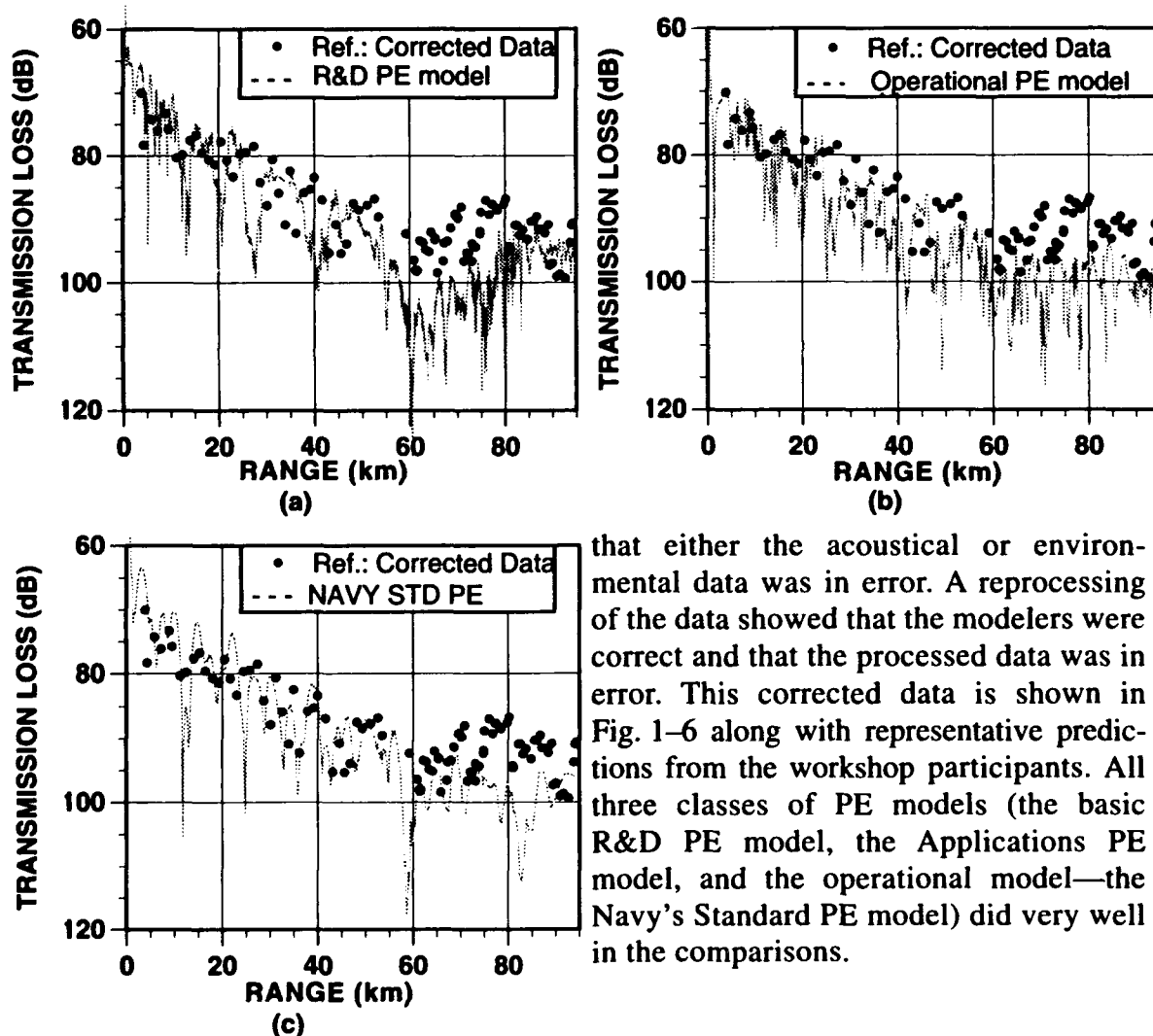


Fig. 1–6. Test Case 6 results from three classes of PE models.

that either the acoustical or environmental data was in error. A reprocessing of the data showed that the modelers were correct and that the processed data was in error. This corrected data is shown in Fig. 1–6 along with representative predictions from the workshop participants. All three classes of PE models (the basic R&D PE model, the Applications PE model, and the operational model—the Navy's Standard PE model) did very well in the comparisons.

TEST CASE 7 – Long-Range Propagation in a Leaky Surface Duct

This test case illustrates that PE models using the split-step solution method together with the Thomson–Chapman (T–C) wide-angle propagation option can give very erroneous results over long ranges when a poor choice of the reference sound speed (C_o) is used. This occurs when a surface duct plus deep upward refracting sound speed profile is present. In Fig. 1–7(a) the operational PE model is using the T–C wide-angle propagation option with $C_o = 1482$ m/s and shows perfect agreement with the reference solution (SNAP SAC).

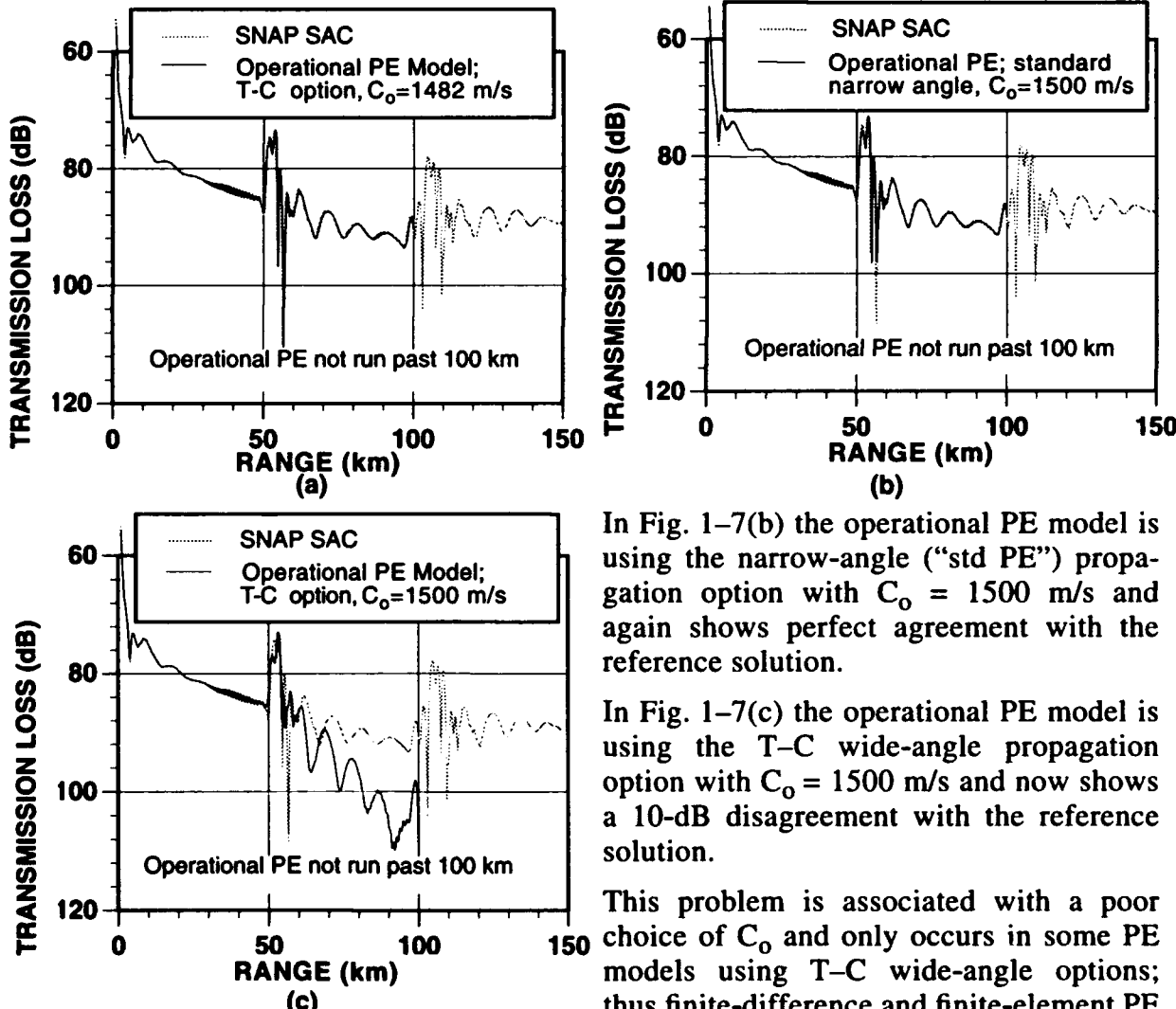


Fig. 1–7. Test Case 7 results from three classes of PE models.

In Fig. 1–7(b) the operational PE model is using the narrow-angle (“std PE”) propagation option with $C_o = 1500$ m/s and again shows perfect agreement with the reference solution.

In Fig. 1–7(c) the operational PE model is using the T–C wide-angle propagation option with $C_o = 1500$ m/s and now shows a 10-dB disagreement with the reference solution.

This problem is associated with a poor choice of C_o and only occurs in some PE models using T–C wide-angle options; thus finite-difference and finite-element PE models are unaffected.

IV Summary and Conclusions

The PE Workshop II provided an avenue to demonstrate the many advances that have occurred in the development of underwater acoustic PE models since the first PE workshop was held in 1981. Both basic research PE models and application-operational PE models were able to account for very wide-angle acoustic propagation; energy conservation in range-dependent propagation; propagation over and through range-dependent, shear-supporting bottoms, including shear attenuations; backscatter from a sharp discontinuity; and propagation in a constantly changing environment. The implications to the underwater acoustic community are that present PE models can be used to accurately simulate underwater acoustic fields in a highly complex ocean environment (e.g., highly range-dependent propagation over shear-supporting ocean bottoms, including backscatter).

The PE models presented at the workshop were exercised by experts in acoustic modeling (in most cases, by the developers of the models). Indications are that many of the models and techniques demonstrated during the workshop can be utilized in 6.3 operational situations by operators other than the model developers.

Perhaps the most important and encouraging result of this workshop is that underwater-acoustic PE models from both the 6.1 basic research modeling community and the 6.3 Navy operational modeling community were applied to the same set of test problems. Each test problem was designed to push the PE models to their limits, and each of the two communities' PE models did extremely well, given the requirements and constraints imposed by each community. The PE models developed by the 6.1 basic research modeling community were able to produce results for the test case problems that were, in most cases, benchmark accurate. This is a definite requirement, since the basic research community uses these models, often in highly complex underwater environments, to identify, isolate, and understand the physical mechanisms involved in underwater acoustic propagation and scattering. The 6.3 Navy operational community is also interested in accurate model predictions, but the need for computational speed, portability, and the ability to run in the field on a field-type computer (micro or desk-top computer) is also of utmost importance; this requires that trade-offs among accuracy, speed, and portability be optimized. The test cases in the PE Workshop II did not address speed and portability, only accuracy. The

PE Workshop II: Part 1

workshop results indicate that some of the operational PE models can be very accurate when not constrained by operational parameters.

A final point of interest from the PE Workshop II: The experimental data set in Test Case 6 constituted one of the more comprehensive acoustic and environmental-geophysical data sets available. When the PE modelers failed to match this data, they questioned not their models' results but rather the data. They were unanimous in their confidence of their models' predictions. This led to a reprocessing of this already twice-processed data, and the subsequent discovery of an error in the processing parameters. The PE models' predictions now compare better with the corrected acoustic data.

In the decade separating the two PE workshops, the underwater acoustic PE models have evolved from a beginning where no two PE models gave the same answer to the point where a poor match between data and model prediction suggests a flaw in the environmental or acoustic data.

References

- Berman, D. H., E. B. Wright, and R. N. Baer (1989), "An optimal PE-type wave equation," *J. Acoust. Soc. Am.* **86**, 228–233.
- Davis, J. A., D. White, and R. C. Cavanagh (1982), "NORDA Parabolic Equation Workshop, 31 March – 3 April 1981," Naval Research Laboratory, Stennis Space Center, MS, U.S.A., NORDA Technical Note 143.
- Evans, R. B. (1983), "A coupled mode solution for acoustic propagation in a waveguide with stepwise depth variations of a penetrable bottom," *J. Acoust. Soc. Am.* **74**, 188–194. See also: R. B. Evans (1986), "COUPLE: A user's manual," Naval Research Laboratory, Stennis Space Center, MS, U.S.A., NORDA Technical Note 332.
- Felsen, L. B. (1990), "Benchmarks: An option for quality assessment," *J. Acoust. Soc. Am.* **87**, 1497–1498.
- Fisher, C. A., H. B. Ali, and M. J. Authement (1989), "A VLF Propagation Experiment off the Coast of Oregon Measurements and Numerical Predictions," Naval Research Laboratory, Stennis Space Center, MS, U.S.A., NORDA Technical Note 418. See also: C. A. Fisher, H. B. Ali, and M. J. Authement, "A VLF propagation experiment off the coast of Oregon: Measurements and numerical predictions," *J. Acoust. Soc. Am. Suppl. 1* **84**, S91 (1988).
- Hardin, R. H., and F. D. Tappert (1973), "Application of the Split-Step Fourier Method to the Numerical Solution of Nonlinear and Variable Coefficient Wave Equations," *SIAM Rev.* **15**, 423.
- Jensen, F. B., and C. M. Ferla (1990), "Numerical solutions of range-dependent benchmark problems in ocean acoustics," *J. Acoust. Soc. Am.* **87**, 1499–1510.
- Murphy, J. E. and S. A. Chin-Bing (1991), "A seismo-acoustic finite element model for underwater acoustic propagation," in *Shear Waves in Marine Sediments*, edited by J. M. Hovem, M. D. Richardson, and R. D. Stoll (Kluwer Press, Amsterdam), pp. 463–470. See also: S. A. Chin-Bing and J. E. Murphy (1993), "Long-Range Ocean Acoustic-Seismic Propagation Modeling Using Hybrid Finite Element and Parabolic Equation Models," in *Computational Acoustics: Scattering, Supercomputing and Propagation*, Vol. 1, edited by R. L. Lau, D. Lee, and A. R. Robinson (Elsevier Publishers, North-Holland, Amsterdam), pp. 105–121.
- Spofford, C. W. (1973), "A Synopsis of the AESD Workshop on Acoustic-Propagation Modeling by Non-Ray Tracing Techniques," Acoustic Environment Support Detachment, Arlington VA, U.S.A., Technical Note 73–05.

Appendix A — Test Cases: Descriptions and Plotting Formats

Appendix A contains the description of each test case problem. Information on Test Cases 1 through 6 (in the form presented below) was sent to the participants several months prior to commencement of the workshop. Included in the descriptions were the sizes of the viewgraph transparencies on which the results of each test case was to be plotted. Test Case 7 was introduced to the participants at the workshop and post-workshop responses solicited for inclusion in the proceedings.

TEST CASES FOR PE WORKSHOP II

TEST CASE 1

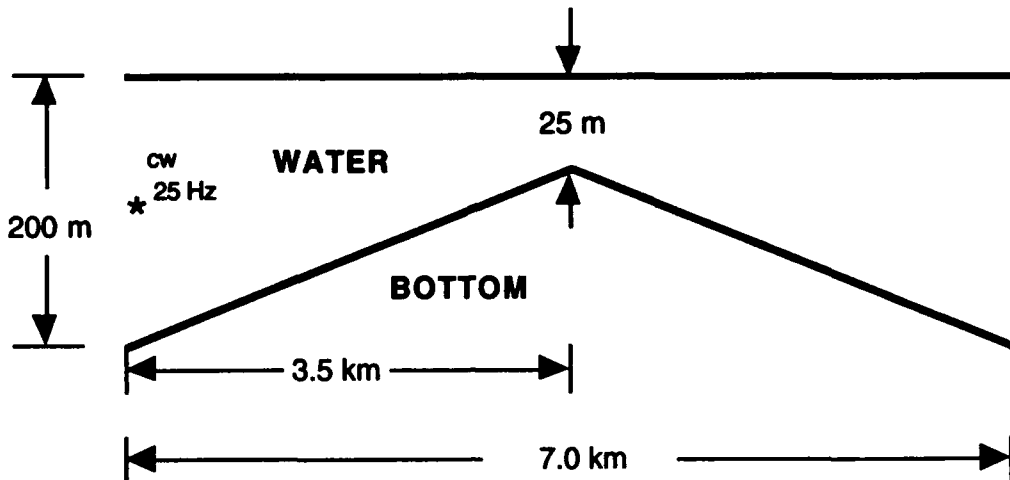
The selection of a starting field can play an important role in the results produced by a PE model. In addition to testing the starting field the geometry of this problem will also test the high angle capability of a model.

The environment is a Lloyd's mirror problem. The fluid is a halfspace with a pressure release surface and a constant sound speed of 1500 m/s. The density is 1.0 g/cm³ with no attenuation. The fixed point depth (source depth) is 350 m with a moving point depth (receiver depth) of 3990 m. The frequency is 40 Hz.

The results from this test case should be in transmission loss (TL) re 1 m versus range in kilometers. The horizontal axis of the plot should be the range, from 0 km to 10 km, with divisions of 1 km/0.9 in. The vertical axis should display the TL (in dB re 1 m) and should be from 30 dB to 100 dB with divisions of 10 dB/0.75 in.

TEST CASE 2

This test case is an upslope-downslope problem that is an extension to the Acoustical Society of America (ASA) benchmark problem. This case is designed to test how well the models conserve energy in a strongly rangedependent environment. The following figure defines the geometry and physical parameters of the problem.



Environmental parameters for Test Case 2.

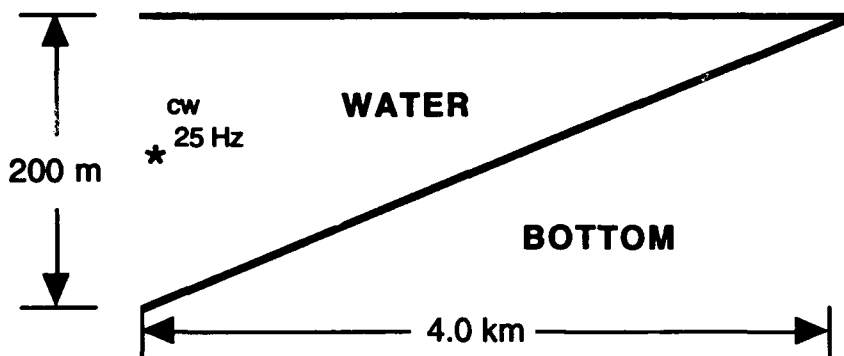
In the water the sound speed is 1500 m/s, the density is 1 g/cm³, and there is no attenuation. In the fluid bottom the sound speed is 1700 m/s, the density is 1.5 g/cm³, and there is an attenuation of 0.5 dB/λ. The frequency is 25 Hz, the fixed point depth (source depth) is 100 m, and the moving point depths (receiver depths) are 20 m and 150 m.

The results for the two different receivers should be presented on separate plots. The range scale should be from 0 to 7 km at 1 km/in. with the transmission loss from 30 to 100 dB with divisions of 10 dB every 0.75 in.

TEST CASE 3

Recently there has been strong interest[†] in extending the capability of underwater acoustic models to include more realistic treatments of the ocean bottom-subbottom, including anelastic media. This case is an adaptation of the ASA Benchmark problem to include an anelastic bottom.

[†]"Special Research Program Bottom/Subbottom Reverberation Science Plan" edited by J. A. Orcutt, Scripps Institution of Oceanography, 1989, for the Office of Naval Research.



Environmental parameters for Test Case 3.

In the water the sound speed is 1500 m/s, the density is 1 g/cm³, and there is no attenuation. In the anelastic bottom the compressional speed is 1700 m/s, the shear speed is 800 m/s, the density is 1.5 g/cm³, both the compressional and shear attenuations are 0.5 dB/λ. The frequency is 25 Hz, the fixed point depth (source depth) is 100 m, and the moving point depths (receiver depths) are 30 m and 150 m.

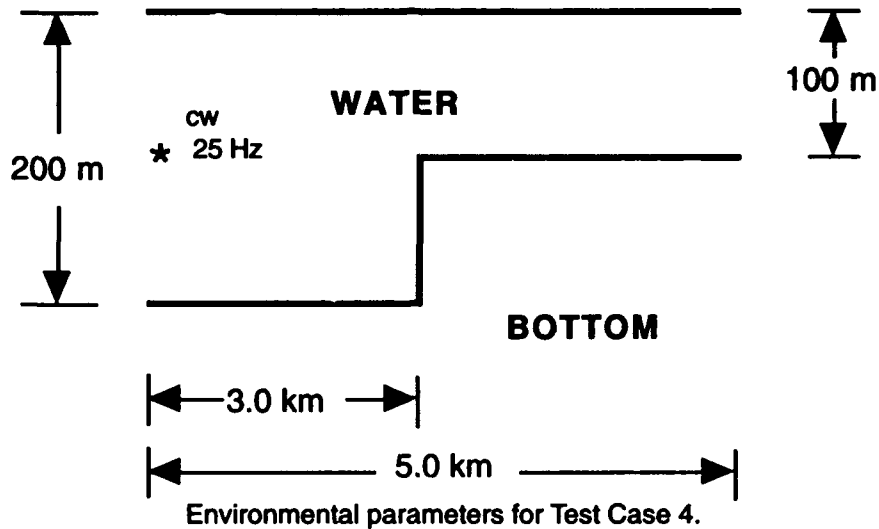
The results for the two different receivers should be presented on separate plots. The plots for this case should be from 0 km to 4 km at 1 km/1.5 inch for the range (horizontal) axis, and from 30 dB to 100 dB with a scale of 10 dB/0.75 in. for the transmission loss (vertical) axis.

TEST CASE 4

This test case is presented to test the ability of different models to handle the problem of backscattered energy.

In the water the sound speed is 1500 m/s, the density is 1 g/cm³, and there is no attenuation. In the fluid bottom the sound speed is 1700 m/s, the density is 1.5 g/cm³, and there is an attenuation of 0.5 dB/λ. The frequency is 25 Hz, the fixed point depth (source depth) is 100 m, and the moving point depths (receiver depths) are 95 m and 150 m.

The results for the two different receivers should be presented on separate plots. The range (horizontal) scale should be from 0 to 5 km at 1 km/in. with the transmission loss (vertical) scale from 30 to 100 dB with divisions of 10 dB every 0.75 in.



TEST CASE 5

This case is designed to test the ability of underwater acoustic propagation codes to handle range variations in the sound speeds in a range-dependent situation.

The bathymetry of this test case has a flat bottom of 200 m depth out to a range of 0.5 km. At that range a downslope section is encountered that drops off 200 m over the next 2,000 m. The bottom then remains flat at 400 m out to the final range of 10,000 m.

The sound speed structure in the water is not a function of depth but does have a dependence on the range. It is a constant 1500 m/s out to a range of 0.5 km. Over the downslope portion of the bathymetry the sound speed varies linearly in range from 1500 m/s to 1540 m/s. At a range of 2.5 km the sound speed remains a constant 1540 m/s out to a range of 10.0 km. The density of the water is 1 g/cm³ and there is no attenuation.

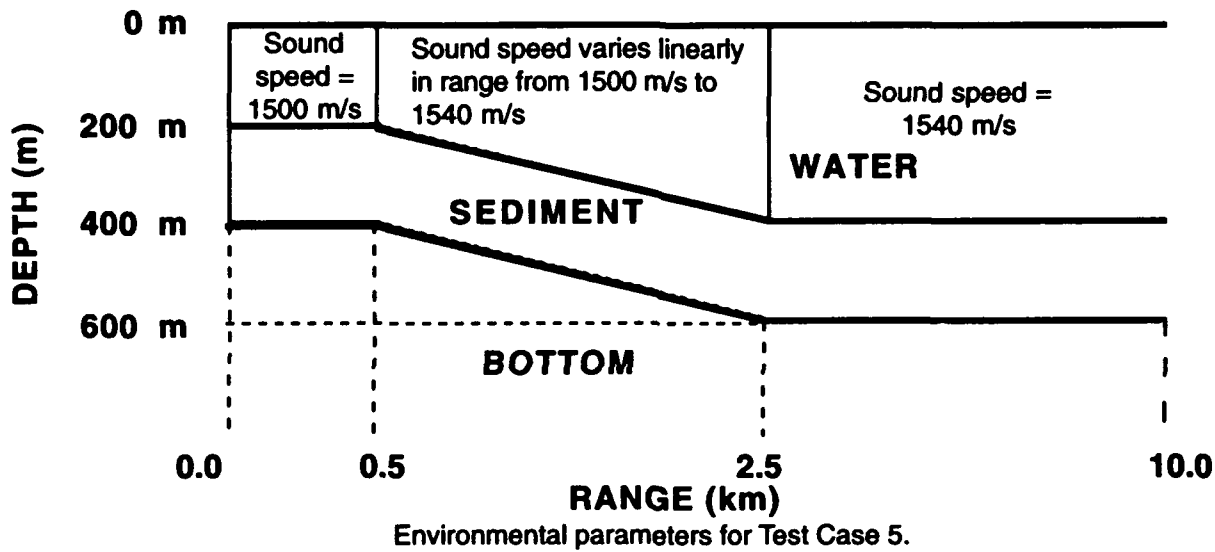
The fluid bottom consists of two layers: the first bottom layer (i.e., the sediment) is a constant 200 m thick and follows the contour of the water/sediment interface; the second bottom layer (i.e., the bottom) is a homogeneous layer of infinite depth. The pertinent physical parameters of these two bottom layers are as follows:

- The sediment sound speed is 1700 m/s, the density is 1.5 g/cm³, and the attenuation is 0.5 dB/λ.
- The bottom sound speed is 1900 m/s, the density is 3.0 g/cm³, and the attenuation is 0.1 dB/λ.

PE Workshop II: Part 1 — Appendix A

The frequency is 25 Hz, the fixed point depth (source depth) is 100 m, and the moving point depths (receiver depths) are 30 m, 150 m and 250 m.

The results for the three different receivers should be presented on separate plots. These plots should be transmission loss, in dB, versus range, in kilometers. The horizontal axis of the plot should be the range, from 0 km to 10 km, with divisions of 1 km/0.9 in. The vertical axis should display the transmission loss (in dB re 1 m) and should be from 60 dB to 130 dB with divisions of 10 dB/0.75 in.



TEST CASE 6

This test case will test the different models against measured field data. The necessary environmental information is provided in the tables below. There were three sound speed profiles measured along the track. The bathymetry is also supplied with the range in kilometers and the depth in meters. A series of range-dependent geoacoustic descriptions are also supplied, where the depths are measured relative to the air /water interface.

The three sound speed profiles are presented in the following tables. Each table is preceded by the initial range of the profile.

The problem parameters to be used are as follows:

- Frequency = 15 Hz
- Fixed Point (Sources) Depths = 88 m, 112 m, and 148 m
- Moving Point (Receiver) Depth = 30 m
- Maximum Range of Calculation = 100 km

PE Workshop II: Part 1 — Appendix A

The plots (one for each source depth) should have a range (horizontal) scale of 0.0 km to 100 km with each 10 km division equal to 0.75 inch. The transmission loss (vertical) axis is in dB re 1 m and should be from 30 dB to 100 dB with divisions of 10 dB/0.75 in.

Editors' Note: The experimental acoustic data that accompanied Test Case 6, and which represents the "reference solution" for this case, was taken by Hassan B. Ali of NRL (Fisher et al. 1989). The geoacoustic ocean-bottom data, compiled by Peter Fleischer of NRL, represented data taken along a seismic line parallel to and within 30 miles of the track over which the acoustic data was taken. The geoacoustic ocean-bottom data compilation was part of the Office of Naval Research's Acoustic Reverberation Special Research Program.

Table A-1. Sound Speed Profiles for Test Case 6
Profile 1 at Range = 0.00 km

Depth (m)	Sound Speed (m/s)						
0.	1506.022	5.	1506.318	10.	1506.614	15.	1502.202
20.	1495.611	25.	1493.545	30.	1491.493	35.	1490.315
40.	1488.301	45.	1487.187	50.	1486.485	55.	1485.437
60.	1485.289	65.	1484.630	70.	1484.677	75.	1483.561
80.	1482.737	85.	1482.261	90.	1481.918	95.	1481.712
100.	1481.555	105.	1481.822	110.	1481.956	115.	1482.079
120.	1482.196	125.	1482.738	130.	1482.723	135.	1482.596
140.	1482.271	145.	1482.296	150.	1481.903	155.	1481.578
160.	1481.571	165.	1481.573	170.	1481.404	175.	1481.367
180.	1481.091	185.	1480.967	190.	1480.912	195.	1480.862
200.	1480.851	205.	1480.923	210.	1480.974	215.	1481.014
220.	1481.063	225.	1481.118	230.	1481.090	235.	1481.124
240.	1481.064	245.	1481.064	250.	1481.042	255.	1481.075
260.	1481.188	265.	1481.215	270.	1481.131	275.	1481.071
280.	1480.886	285.	1480.840	290.	1480.478	295.	1480.914
300.	1480.811	305.	1480.745	310.	1480.683	315.	1480.654
320.	1480.483	325.	1480.337	330.	1480.204	335.	1480.080
340.	1480.012	345.	1479.881	350.	1479.812	355.	1479.806
360.	1479.804	365.	1479.783	370.	1479.726	375.	1479.754
380.	1479.890	385.	1479.786	390.	1479.621	395.	1479.703
400.	1479.717	405.	1479.766	410.	1479.713	415.	1479.651
515.	1479.000	527.	1479.000				

PE Workshop II: Part 1 — Appendix A

Table A-1. Sound Speed Profiles for Test Case 6 (Continued)

Profile 2 at Range = 29.415 km

Depth (m)	Sound Speed (m/s)						
0.	1507.331	5.	1505.019	10.	1502.707	15.	1497.749
20.	1491.660	25.	1488.583	30.	1487.419	35.	1486.231
40.	1485.515	45.	1484.530	50.	1484.153	55.	1484.028
60.	1483.993	65.	1483.809	70.	1483.281	75.	1483.323
80.	1483.123	85.	1482.863	90.	1482.666	95.	1481.924
100.	1481.940	105.	1481.676	110.	1481.778	115.	1482.423
120.	1481.923	125.	1481.753	130.	1481.872	135.	1481.720
140.	1481.677	145.	1481.454	150.	1481.455	155.	1481.426
160.	1481.346	165.	1481.384	170.	1481.290	175.	1481.107
180.	1480.995	185.	1481.022	190.	1480.790	195.	1480.683
200.	1480.632	205.	1480.499	210.	1480.246	215.	1480.133
220.	1480.173	225.	1480.099	230.	1479.915	235.	1479.718
240.	1479.636	245.	1479.585	250.	1479.563	255.	1479.451
260.	1479.365	265.	1478.913	270.	1478.887	275.	1478.780
280.	1478.593	285.	1478.450	290.	1478.477	295.	1478.355
300.	1478.048	305.	1478.023	310.	1478.023	315.	1477.665
320.	1477.547	325.	1477.416	330.	1477.201	335.	1477.134
340.	1476.939	345.	1476.870	350.	1476.903	355.	1476.923
360.	1476.809	365.	1476.786	370.	1476.694	375.	1476.464
380.	1476.346	385.	1476.589	390.	1476.478	395.	1476.814
400.	1477.269	405.	1477.631	410.	1477.666	415.	1477.739
420.	1477.779	425.	1477.809	430.	1477.744	435.	1477.790
440.	1477.828	445.	1477.851	450.	1477.771	455.	1477.813
460.	1477.839	465.	1477.843	470.	1477.837	475.	1477.693
480.	1477.641	485.	1477.680	490.	1477.687	495.	1477.659
500.	1477.683	525.	1476.900	550.	1476.616	575.	1477.078
600.	1477.372	625.	1477.739	650.	1477.995	675.	1478.129
700.	1478.327	750.	1478.841	775.	1479.017	800.	1479.328
825.	1479.552	850.	1479.736	875.	1479.902	900.	1480.127
925.	1480.333	950.	1480.330	975.	1480.592	1000.	1480.602
1100.	1481.446	1200.	1482.158	1300.	1482.986	1400.	1483.890
1500.	1484.961	1600.	1485.871	1959.	1486.506		

PE Workshop II: Part 1 — Appendix A

Table A-1. Sound Speed Profiles for Test Case 6 (Continued)
Profile 3 at Range = 76.556 km

Depth (m)	Sound Speed (m/s)						
0.	1517.191	10.	1505.064	20.	1492.937	30.	1487.920
40.	1485.705	50.	1484.379	60.	1484.078	70.	1483.978
80.	1482.976	90.	1482.394	100.	1481.174	110.	1481.592
120.	1481.793	130.	1481.465	140.	1481.488	150.	1481.396
160.	1481.339	170.	1481.122	180.	1480.959	190.	1480.892
200.	1480.388	210.	1480.202	220.	1479.921	230.	1479.736
240.	1479.643	250.	1479.190	260.	1478.809	270.	1478.561
300.	1477.954	310.	1477.495	320.	1477.879	330.	1477.643
340.	1477.692	350.	1477.434	360.	1477.513	370.	1477.139
380.	1477.470	390.	1477.310	400.	1477.193	410.	1478.001
420.	1477.839	430.	1477.635	440.	1476.783	450.	1476.917
460.	1477.609	470.	1477.031	480.	1477.130	490.	1477.737
500.	1477.886	530.	1477.826	560.	1477.860	590.	1477.819
620.	1478.050	650.	1478.143	680.	1478.475	710.	1478.815
740.	1479.079	770.	1478.416	800.	1478.189	830.	1478.973
860.	1479.113	890.	1479.471	920.	1479.884	950.	1480.106
980.	1480.345	1010.	1480.521	1110.	1481.193	1210.	1482.064
1310.	1482.846	1410.	1483.751	1510.	1484.792	1610.	1485.926
1710.	1487.038	1810.	1488.003	1910.	1489.202	2010.	1490.499
2110.	1491.874	2210.	1493.421	2310.	1494.983	2410.	1496.574
2510.	1498.246	2640.	1499.929				

Table A-2. Bathymetry for Test Case 6

Range (m)	Depth (m)	Range (m)	Depth (m)	Range (m)	Depth (m)
0.00	201.00	3362.00	385.00	10040.00	407.00
15284.00	422.00	18323.00	428.00	20266.00	411.00
23884.00	381.00	25464.00	527.00	29415.00	559.00
30353.00	560.00	35064.00	601.00	40875.00	674.00
42268.00	750.00	46837.00	751.00	50810.00	1038.00
52029.00	979.00	59874.00	1586.00	65524.00	1614.00
69824.00	1713.00	72362.00	1650.00	73968.00	1959.00
74461.00	1892.00	76656.00	1975.00	78364.00	1905.00
79855.00	1702.00	82052.00	1879.00	83148.00	2136.00
85040.00	2627.00	86883.00	2640.00	91132.00	2637.00
93360.00	2490.00	95744.00	2649.00		

PE Workshop II: Part 1 — Appendix A

Table A-3. Geoacoustic Properties for Test Case 6

Depth is measured from the air/water interface. The speed and attenuation are given for the compression wave. The range value (in kilometers) along the track precedes the geoacoustic description.

Range = 0.0 km			
Depth (m)	Speed (m/s)	Density (g/cm ³)	Atten (dB/λ)
201.00	1500.0	2.19	0.12
1757.43	2100.0	2.19	0.27
1760.00	2600.0	2.54	0.10
3700.00	3400.0	2.54	0.09
3708.96	4600.0	2.60	0.06
8000.00	4600.0	2.60	0.06

Range = 3.362 km			
Depth (m)	Speed (m/s)	Density (g/cm ³)	Atten (dB/λ)
385.00	1500.0	2.19	0.12
1811.95	2100.0	2.19	0.27
1815.00	2600.0	2.54	0.10
3580.00	3400.0	2.54	0.09
3584.87	4600.0	2.60	0.06
8000.00	4600.0	2.60	0.06

Range = 10.040 km			
Depth (m)	Speed (m/s)	Density (g/cm ³)	Atten (dB/λ)
407.00	1500.0	2.19	0.12
1867.76	2100.0	2.19	0.27
1870.00	2600.0	2.54	0.10
3325.00	3400.0	2.54	0.09
3331.37	4600.0	2.60	0.06
8000.00	4600.0	2.60	0.06

Range = 15.284 km			
Depth (m)	Speed (m/s)	Density (g/cm ³)	Atten (dB/λ)
422.00	1500.0	2.19	0.12
1736.61	2100.0	2.19	0.27
1740.00	2600.0	2.54	0.10
3179.31	3400.0	2.54	0.09
8000.00	3400.0	2.54	0.09

PE Workshop II: Part 1 — Appendix A

Table A-3. Geoacoustic Properties for Test Case 6 (Continued)

Range = 18.323 km			
Depth (m)	Speed (m/s)	Density (g/cm³)	Atten (dB/λ)
428.00	1500.0	2.19	0.12
1527.55	2100.0	2.19	0.27
1530.00	2600.0	2.54	0.10
3111.79	3400.0	2.54	0.09
8000.00	3400.0	2.54	0.09

Range = 20.266 km			
Depth (m)	Speed (m/s)	Density (g/cm³)	Atten (dB/λ)
411.00	1500.0	2.19	0.12
1361.15	2100.0	2.19	0.27
1365.00	2600.0	2.54	0.10
3074.75	3400.0	2.54	0.09
8000.00	3400.0	2.54	0.09

Range = 23.884 km			
Depth (m)	Speed (m/s)	Density (g/cm³)	Atten (dB/λ)
381.00	1500.0	2.19	0.12
671.12	2100.0	2.19	0.27
675.00	2600.0	2.54	0.10
3021.91	3400.0	2.54	0.09
8000.00	3400.0	2.54	0.09

Range = 26.464 km			
Depth (m)	Speed (m/s)	Density (g/cm³)	Atten (dB/λ)
527.00	1500.0	2.19	0.12
1334.89	2100.0	2.19	0.27
1340.00	2600.0	2.54	0.10
3005.12	3400.0	2.54	0.09
8000.00	3400.0	2.54	0.09

PE Workshop II: Part 1 — Appendix A

Table A-3. Geoacoustic Properties for Test Case 6 (Continued)

Range = 29.415 km			
Depth (m)	Speed (m/s)	Density (g/cm³)	Atten (dB/λ)
559.00	1500.0	2.19	0.12
1439.22	2100.0	2.19	0.27
1445.00	2600.0	2.54	0.10
2979.31	3400.0	2.54	0.09
8000.00	3400.0	2.54	0.09

Range = 30.353 km			
Depth (m)	Speed (m/s)	Density (g/cm³)	Atten (dB/λ)
560.00	1500.0	2.19	0.12
1276.24	2100.0	2.19	0.27
1280.00	2600.0	2.54	0.10
2976.78	3400.0	2.54	0.09
8000.00	3400.0	2.54	0.09

Range = 35.064 km			
Depth (m)	Speed (m/s)	Density (g/cm³)	Atten (dB/λ)
601.00	1500.0	2.19	0.12
994.46	2100.0	2.19	0.27
1000.00	2600.0	2.54	0.10
2984.40	3400.0	2.54	0.09
8000.00	3400.0	2.54	0.09

Range = 40.875 km			
Depth (m)	Speed (m/s)	Density (g/cm³)	Atten (dB/λ)
674.00	1500.0	2.19	0.12
1002.59	2100.0	2.19	0.27
1005.00	2600.0	2.54	0.10
3039.20	3400.0	2.54	0.09
8000.00	3400.0	2.54	0.09

PE Workshop II: Part 1 — Appendix A

Table A-3. Geoacoustic Properties for Test Case 6 (Continued)

Range = 42.268 km			
Depth (m)	Speed (m/s)	Density (g/cm³)	Atten (dB/λ)
750.00	1500.0	2.19	0.12
1454.61	2100.0	2.19	0.27
1460.00	2600.0	2.54	0.10
3061.66	3400.0	2.54	0.09
8000.00	3400.0	2.54	0.09

Range = 46.837 km			
Depth (m)	Speed (m/s)	Density (g/cm³)	Atten (dB/λ)
751.00	1500.0	2.19	0.12
799.01	2100.0	2.19	0.27
805.00	2600.0	2.54	0.10
3151.16	3400.0	2.54	0.09
8000.00	3400.0	2.54	0.09

Range = 50.810 km			
Depth (m)	Speed (m/s)	Density (g/cm³)	Atten (dB/λ)
1038.00	1500.0	2.19	0.12
1509.31	2100.0	2.19	0.27
1515.00	2600.0	2.54	0.10
3251.38	3400.0	2.54	0.09
8000.00	3400.0	2.54	0.09

Range = 52.029 km			
Depth (m)	Speed (m/s)	Density (g/cm³)	Atten (dB/λ)
979.00	1500.0	2.19	0.12
1020.99	2100.0	2.19	0.27
1025.00	2600.0	2.54	0.10
3291.40	3400.0	2.54	0.09
8000.00	3400.0	2.54	0.09

PE Workshop II: Part 1 — Appendix A

Table A-3. Geoacoustic Properties for Test Case 6 (Continued)

Range = 59.874 km			
Depth (m)	Speed (m/s)	Density (g/cm³)	Atten (dB/λ)
1586.00	1500.0	2.19	0.12
2081.44	2100.0	2.19	0.27
2085.00	2600.0	2.54	0.10
3581.72	3400.0	2.54	0.09
8000.00	3400.0	2.54	0.09

Range = 65.524 km			
Depth (m)	Speed (m/s)	Density (g/cm³)	Atten (dB/λ)
1614.00	1500.0	2.19	0.12
1688.34	2100.0	2.19	0.27
1690.00	2600.0	2.54	0.10
3848.86	3400.0	2.54	0.09
8504.21	5100.0	2.70	0.09

Range = 69.824 km			
Depth (m)	Speed (m/s)	Density (g/cm³)	Atten (dB/λ)
1713.00	1500.0	2.19	0.12
2099.88	2100.0	2.19	0.27
2105.00	2600.0	2.54	0.10
4081.08	3400.0	2.54	0.09
8193.83	5100.0	2.70	0.09

Range = 72.362 km			
Depth (m)	Speed (m/s)	Density (g/cm³)	Atten (dB/λ)
1650.00	1500.0	2.19	0.12
1731.42	2100.0	2.19	0.27
1735.00	2600.0	2.54	0.10
4231.64	3400.0	2.54	0.09
8009.84	5100.0	2.70	0.09

PE Workshop II: Part 1 — Appendix A

Table A-3. Geoacoustic Properties for Test Case 6 (Continued)

Range = 73.968 km			
Depth (m)	Speed (m/s)	Density (g/cm³)	Atten (dB/λ)
1959.00	1500.0	2.19	0.12
2201.13	2100.0	2.19	0.27
2205.00	2600.0	2.54	0.10
4335.63	3400.0	2.54	0.09
7889.15	5100.0	2.70	0.09

Range = 74.461 km			
Depth (m)	Speed (m/s)	Density (g/cm³)	Atten (dB/λ)
1892.00	1500.0	2.19	0.12
1932.88	2100.0	2.19	0.27
1935.00	2600.0	2.54	0.10
4366.13	3400.0	2.54	0.09
7854.63	5100.0	2.70	0.09

Range = 76.656 km			
Depth (m)	Speed (m/s)	Density (g/cm³)	Atten (dB/λ)
1975.00	1500.0	2.19	0.12
2229.28	2100.0	2.19	0.27
2235.00	2600.0	2.54	0.10
4512.81	3400.0	2.54	0.09
7693.67	5100.0	2.70	0.09

Range = 78.364 km			
Depth (m)	Speed (m/s)	Density (g/cm³)	Atten (dB/λ)
1905.00	1500.0	2.19	0.12
2176.96	2100.0	2.19	0.27
2180.00	2600.0	2.54	0.10
4633.20	3400.0	2.54	0.09
7567.23	5100.0	2.70	0.09

PE Workshop II: Part 1 — Appendix A

Table A-3. Geoacoustic Properties for Test Case 6 (Continued)

Range = 79.855 km			
Depth (m)	Speed (m/s)	Density (g/cm³)	Atten (dB/λ)
1702.00	1500.0	2.19	0.12
1771.04	2100.0	2.19	0.27
1775.00	2600.0	2.54	0.10
4740.88	3400.0	2.54	0.09
7457.98	5100.0	2.70	0.09

Range = 82.052 km			
Depth (m)	Speed (m/s)	Density (g/cm³)	Atten (dB/λ)
1879.00	1500.0	2.19	0.12
1957.76	2100.0	2.19	0.27
1960.00	2600.0	2.54	0.10
4905.68	3400.0	2.54	0.09
7297.02	5100.0	2.70	0.09

Range = 83.148 km			
Depth (m)	Speed (m/s)	Density (g/cm³)	Atten (dB/λ)
2136.00	1500.0	2.19	0.12
2242.85	2100.0	2.19	0.27
2245.00	2600.0	2.54	0.10
4990.84	3400.0	2.54	0.09
7216.54	5100.0	2.70	0.09

Range = 85.040 km			
Depth (m)	Speed (m/s)	Density (g/cm³)	Atten (dB/λ)
2627.00	1500.0	2.19	0.12
2721.80	2100.0	2.19	0.27
2725.00	2600.0	2.54	0.10
5077.44	3400.0	2.54	0.09
7078.60	5100.0	2.00	0.09

PE Workshop II: Part 1 — Appendix A

Table A-3. Geoacoustic Properties for Test Case 6 (Continued)

Range = 86.883 km			
Depth (m)	Speed (m/s)	Density (g/cm³)	Atten (dB/λ)
2640.00	1500.0	2.19	0.12
3351.10	2100.0	2.19	0.27
3355.00	2600.0	2.54	0.10
5077.44	3400.0	2.54	0.09
6940.63	5100.0	2.70	0.09

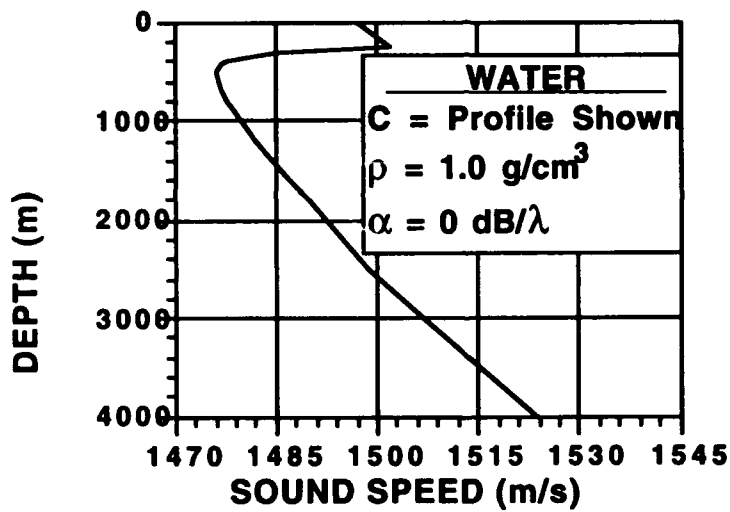
Range = 91.132 km			
Depth (m)	Speed (m/s)	Density (g/cm³)	Atten (dB/λ)
2637.00	1500.0	2.19	0.12
3351.00	2100.0	2.19	0.27
3355.00	2600.0	2.54	0.10
5077.44	3400.0	2.54	0.09
6630.20	5100.0	2.70	0.09

Range = 93.360 km			
Depth (m)	Speed (m/s)	Density (g/cm³)	Atten (dB/λ)
2490.00	1500.0	2.19	0.12
2554.16	2100.0	2.19	0.27
2560.00	2600.0	2.54	0.10
5077.44	3400.0	2.54	0.09
6469.24	5100.0	2.70	0.09

Range = 95.744 km			
Depth (m)	Speed (m/s)	Density (g/cm³)	Atten (dB/λ)
2649.00	1500.0	2.19	0.12
2663.21	2100.0	2.19	0.27
2665.00	2600.0	2.54	0.10
5077.44	3400.0	2.54	0.09
6296.79	5100.0	2.70	0.09

TEST CASE 7

This test case problem was submitted by Finn Jensen. He had observed that some (but not all) wide-angle split-step PE models using the Thomson–Chapman wide-angle approach will overestimate transmission loss (TL) by as much as 20 dB. This overestimation occurs when the PE model is applied to long-range propagation in a leaky surface duct overlying a strong upward-refracting sound speed profile, such as the one shown in the accompanying figure.



BOTTOM PARAMETERS	
$C =$	1523.8 m/s
$\rho =$	1.0 g/cm ³
$\alpha =$	0.1 dB/λ

Environmental parameters for Test Case 7.

The environmental parameters of the problem are also given in the accompanying figure. The source frequency is 80 Hz, the source depth is 25 m, and the receiver depth is 100 m. Note that both the source and the receiver are located in the 250 m deep

PE Workshop II: Part 1 — Appendix A

surface duct. The bottom is a range-independent, lossy fluid halfspace, beginning at a depth of 4 km.

There are 78 propagating models in the water waveguide, one of which is trapped in the surface duct. The first convergence zone (CZ) occurs at ~50 km in range.

The SNAP normal mode model (Jensen and Ferla 1979) was used by Jensen to obtain a reference solution. Since the environment in Test Case 7 is range independent and over a long range (>100 km), a normal mode model should provide an accurate reference solution.

The sound speed profile is given in the following table.

Depth (m)	Sound Speed (m/s)	Depth (m)	Sound Speed (m/s)
0.0	1497.0	1000.0	1480.0
250.0	1502.0	1100.0	1481.0
300.0	1485.0	1180.0	1482.0
375.0	1478.0	1340.0	1484.0
425.0	1477.0	1600.0	1487.0
500.0	1476.0	1800.0	1490.0
600.0	1476.5	2500.0	1498.7
700.0	1477.0	3000.0	1506.8
810.0	1478.0	4000.0	1523.9
900.0	1479.0		

Appendix B — Reference Solutions to the Test Cases

Appendix B contains tabular data from the reference solutions used in the Test Cases. The tabular data represent selected samples from the larger data sets that were used to plot the reference curves, and are sufficient to generate the reference curves used in Test Cases 1, 2, 3A, 4, 6, and 7. This should prove useful to anyone desiring to compare results from other numerical models against the reference solutions used in the PE Workshop II.

CASE 1 – REFERENCE SOLUTION DATA											
Range (km)	TL (dB)	Range (km)	TL (dB)	Range (km)	TL (dB)	Range (km)	TL (dB)	Range (km)	TL (dB)	Range (km)	TL (dB)
0.02	67.17	1.70	72.74	3.38	71.92	5.06	70.26	6.74	71.80	8.42	101.3
0.10	67.08	1.78	83.84	3.46	79.44	5.14	70.42	6.82	72.22	8.50	86.33
0.18	66.90	1.86	77.56	3.54	84.22	5.22	71.70	6.90	73.10	8.58	81.32
0.26	66.65	1.94	70.68	3.62	73.64	5.30	74.42	6.98	74.90	8.66	78.45
0.34	66.39	2.02	67.86	3.70	70.05	5.38	79.88	7.06	77.67	8.74	76.59
0.42	66.15	2.10	67.03	3.78	68.83	5.46	100.21	7.14	82.45	8.82	75.34
0.50	66.02	2.18	67.84	3.86	69.27	5.54	80.81	7.22	94.96	8.90	74.54
0.58	66.06	2.26	70.72	3.94	71.45	5.62	75.24	7.30	87.88	8.98	74.08
0.66	66.37	2.34	78.12	4.02	76.58	5.70	72.58	7.38	80.58	9.06	73.91
0.74	67.06	2.42	82.55	4.10	95.73	5.78	71.31	7.46	77.06	9.14	74.01
0.82	68.32	2.50	72.21	4.18	77.61	5.86	70.99	7.54	74.96	9.22	74.38
0.90	70.50	2.58	68.67	4.26	72.25	5.94	71.51	7.62	73.72	9.30	75.00
0.98	74.43	2.66	67.59	4.34	70.03	6.02	72.91	7.70	73.04	9.38	75.93
1.06	83.28	2.74	68.34	4.42	69.47	6.10	75.49	7.78	72.82	9.46	77.20
1.14	80.55	2.82	71.29	4.50	70.27	6.18	80.20	7.86	73.02	9.54	78.92
1.22	72.85	2.90	79.06	4.58	72.65	6.26	93.03	7.94	73.63	9.62	81.30
1.30	69.17	2.98	82.43	4.66	77.77	6.34	85.24	8.02	74.68	9.70	84.79
1.38	67.24	3.06	72.54	4.74	96.25	6.42	78.17	8.10	76.28	9.78	90.90
1.46	66.52	3.14	69.15	4.82	79.42	6.50	74.88	8.18	78.64	9.86	112.4
1.54	66.93	3.22	68.17	4.90	73.76	6.58	73.03	8.26	82.29	9.94	90.74
1.62	68.70	3.30	68.98	4.98	71.24	6.66	72.10	8.34	89.15		

PE Workshop II: Part 1 — Appendix B

CASE 2 – REFERENCE SOLUTION DATA											
Range (km)	TL (dB)		Range (km)	TL (dB)		Range (km)	TL (dB)		Range (km)	TL (dB)	
	ZR 20m	ZR 150m		ZR 20m	ZR 150m		ZR 20m	ZR 150m		ZR 20m	ZR 150m
0.02	37.94	36.97	1.70	50.59	51.93	3.54	60.67	70.11	5.20	74.82	84.59
0.06	34.46	41.12	1.82	63.95	63.49	3.58	61.99	68.70	5.34	75.22	83.80
0.10	36.56	37.71	1.96	71.82	56.36	3.62	63.01	86.53	5.38	76.53	83.27
0.14	40.13	39.94	1.90	69.87	70.48	3.66	63.78	64.96	5.42	76.01	82.90
0.18	42.34	52.89	1.94	65.80	70.80	3.70	64.37	64.21	5.46	76.41	82.50
0.22	42.63	48.03	1.98	64.66	67.67	3.74	64.82	64.05	5.50	76.84	82.08
0.26	43.08	44.20	2.02	63.40	65.71	3.78	65.19	64.28	5.54	77.20	81.72
0.30	49.40	46.70	2.06	60.86	65.45	3.82	65.47	64.72	5.58	77.47	81.34
0.34	58.65	47.99	2.10	58.62	66.35	3.86	65.71	65.34	5.62	77.70	80.86
0.38	50.55	49.64	2.14	57.42	68.38	3.90	65.93	66.07	5.66	77.92	80.32
0.42	51.30	56.77	2.18	56.93	70.79	3.94	66.11	66.89	5.70	78.04	79.77
0.46	51.51	51.23	2.22	56.73	71.91	3.98	66.24	67.78	5.74	78.06	79.24
0.50	52.41	50.70	2.26	56.71	71.93	4.02	66.41	68.71	5.78	78.09	78.70
0.54	51.11	52.52	2.30	57.20	71.48	4.06	66.58	69.69	5.82	78.09	78.13
0.58	49.02	54.80	2.34	58.29	71.04	4.10	66.73	70.77	5.86	78.10	77.59
0.62	49.25	57.36	2.38	59.82	70.60	4.14	66.90	71.92	5.90	78.08	77.08
0.66	50.80	56.58	2.42	61.70	69.62	4.18	67.05	73.13	5.94	78.08	76.59
0.70	53.27	56.73	2.46	62.89	68.57	4.22	67.31	74.40	5.98	78.14	76.06
0.74	55.40	57.63	2.50	62.14	67.80	4.26	67.55	75.73	6.02	78.24	75.73
0.78	55.65	55.17	2.54	60.28	67.17	4.30	67.86	77.06	6.06	78.36	75.50
0.82	55.32	51.23	2.58	58.72	66.83	4.34	68.22	78.31	6.10	78.47	75.29
0.86	55.86	48.95	2.62	57.82	66.77	4.38	68.57	79.37	6.14	78.61	75.09
0.90	57.42	47.93	2.66	57.57	67.02	4.42	68.95	80.18	6.18	78.79	74.88
0.94	57.45	47.51	2.70	57.83	67.69	4.46	69.40	80.74	6.22	78.99	74.66
0.98	56.38	47.81	2.74	58.23	68.83	4.50	69.84	81.08	6.26	79.17	74.45
1.02	56.18	49.18	2.78	58.36	70.51	4.54	70.25	81.19	6.30	79.35	74.23
1.06	56.89	51.28	2.82	58.03	72.89	4.58	70.70	81.22	6.34	79.58	74.00
1.10	58.77	53.45	2.86	57.61	76.08	4.62	71.14	81.34	6.38	79.78	73.77
1.14	62.04	55.83	2.90	57.39	79.74	4.66	71.51	81.54	6.42	79.97	73.58
1.18	62.07	58.56	2.94	57.30	82.77	4.70	71.85	81.74	6.46	80.15	73.36
1.22	58.92	61.81	2.98	57.17	84.68	4.74	72.20	82.07	6.50	80.34	73.18
1.26	56.46	64.10	3.02	56.99	85.45	4.78	72.47	82.72	6.54	80.57	72.98
1.30	54.77	62.14	3.06	56.84	83.69	4.82	72.84	83.67	6.58	80.80	72.81
1.34	53.47	59.72	3.10	56.72	81.73	4.86	72.81	84.83	6.62	81.01	72.67
1.38	52.74	58.84	3.14	56.63	80.58	4.90	72.99	86.30	6.66	81.21	72.54
1.42	52.92	58.62	3.18	56.56	79.62	4.94	73.09	88.38	6.70	81.46	72.42
1.46	54.14	59.13	3.22	56.53	78.77	4.98	73.14	91.38	6.74	81.77	72.32
1.50	56.38	60.04	3.26	56.54	77.92	5.02	73.25	95.19	6.78	82.07	72.23
1.54	59.30	61.19	3.30	56.60	77.03	5.06	73.41	97.17	6.82	82.32	72.17
1.58	61.88	62.60	3.34	56.75	76.12	5.10	73.54	94.56	6.86	82.58	72.12
1.62	61.02	63.29	3.38	57.02	75.12	5.14	73.68	91.24	6.90	82.88	72.08
1.66	58.65	62.81	3.42	57.46	74.00	5.18	73.91	88.61	6.94	83.19	72.02
1.70	57.49	62.01	3.46	58.12	72.78	5.22	74.20	86.78	6.98	83.44	71.99
1.74	57.84	61.50	3.50	59.12	71.45	5.26	74.49	85.53	7.02	83.52	71.99

PE Workshop II: Part 1 — Appendix B

CASE 3A – REFERENCE SOLUTION DATA															
Range (km)	TL (dB)	Range (km)	TL (dB)	Range (km)	TL (dB)	Range (km)	TL (dB)	Range (km)	TL (dB)	Range (km)	TL (dB)	Range (km)	TL (dB)	Range (km)	TL (dB)
0.000	46.31	0.298	44.81	0.583	55.23	0.843	54.25	1.128	58.28	1.403	55.03	1.693	59.40	1.939	58.10
0.016	44.79	0.296	45.39	0.576	55.41	0.856	54.03	1.136	58.74	1.416	54.98	1.696	59.50	1.976	58.20
0.024	47.27	0.304	46.48	0.584	56.11	0.864	53.85	1.144	59.75	1.424	54.98	1.704	59.50	1.984	58.30
0.032	47.90	0.312	47.00	0.592	56.81	0.872	53.58	1.152	60.05	1.432	54.75	1.712	59.70	1.992	58.40
0.040	47.04	0.320	47.19	0.600	56.94	0.880	53.38	1.160	60.07	1.440	54.52	1.720	59.80	2.000	58.48
0.048	45.82	0.328	47.81	0.608	56.89	0.888	53.42	1.168	60.62	1.448	54.98	1.728	59.80	2.008	58.24
0.056	43.65	0.336	48.66	0.616	57.51	0.896	53.51	1.176	61.41	1.456	55.34	1.736	59.90	2.016	58.50
0.064	41.93	0.344	49.12	0.624	58.61	0.904	53.39	1.184	61.54	1.464	55.18	1.744	59.90	2.024	58.75
0.072	40.98	0.352	49.03	0.632	59.40	0.912	53.17	1.192	61.19	1.472	54.82	1.752	59.80	2.032	58.55
0.080	40.39	0.360	49.13	0.640	59.91	0.920	53.14	1.200	61.21	1.480	55.02	1.760	59.70	2.040	58.35
0.088	39.58	0.368	49.81	0.648	60.68	0.928	53.32	1.208	61.58	1.488	55.35	1.768	59.60	2.048	58.60
0.096	38.98	0.376	50.00	0.656	61.96	0.936	53.35	1.216	61.60	1.496	55.65	1.776	59.70	2.056	58.88
0.100	38.78	0.380	50.01	0.660	62.62	0.940	53.28	1.220	61.43	1.500	55.49	1.780	59.70	2.060	58.66
0.108	38.72	0.388	49.84	0.668	63.94	0.948	53.12	1.228	61.06	1.508	55.19	1.788	59.80	2.068	58.62
0.116	38.74	0.396	49.84	0.676	65.79	0.956	53.19	1.236	60.84	1.516	55.46	1.796	59.90	2.076	58.80
0.124	38.67	0.404	50.16	0.684	68.04	0.964	53.43	1.244	60.71	1.524	56.01	1.804	59.90	2.084	58.86
0.132	38.48	0.412	50.47	0.692	69.37	0.972	53.51	1.252	60.37	1.532	56.18	1.812	59.80	2.092	58.94
0.140	38.49	0.420	50.58	0.700	70.04	0.980	53.47	1.260	59.92	1.540	55.93	1.820	59.80	2.100	58.76
0.148	38.84	0.428	50.72	0.708	70.78	0.988	53.60	1.268	59.39	1.548	56.02	1.828	59.70	2.108	58.70
0.156	39.20	0.436	51.25	0.716	69.68	0.996	53.91	1.276	58.92	1.556	56.55	1.836	59.60	2.116	58.84
0.164	39.34	0.444	51.88	0.724	66.80	1.004	54.08	1.284	58.55	1.564	56.90	1.844	59.80	2.124	58.87
0.172	39.46	0.452	52.13	0.732	64.88	1.012	54.08	1.292	58.29	1.572	56.82	1.852	59.50	2.132	58.73
0.180	39.74	0.460	52.08	0.740	64.19	1.020	54.26	1.300	57.97	1.580	56.84	1.860	59.40	2.140	58.89
0.188	40.17	0.468	52.27	0.748	62.97	1.028	54.74	1.308	57.54	1.588	57.25	1.868	59.30	2.148	58.74
0.196	40.53	0.476	52.77	0.756	61.05	1.036	55.10	1.316	57.18	1.596	57.63	1.876	59.20	2.156	58.72
0.204	40.73	0.484	53.14	0.764	59.75	1.044	55.15	1.324	56.96	1.604	57.69	1.884	59.10	2.164	58.66
0.212	40.99	0.492	53.37	0.772	59.36	1.052	55.32	1.332	56.88	1.612	57.75	1.892	59.00	2.172	58.72
0.220	41.43	0.500	53.68	0.780	58.88	1.060	55.87	1.340	56.60	1.620	58.03	1.900	59.00	2.180	58.80
0.228	41.90	0.508	54.21	0.788	57.77	1.068	56.45	1.348	56.21	1.628	58.24	1.908	58.90	2.188	58.74
0.236	42.15	0.516	54.65	0.796	56.75	1.076	56.66	1.356	55.96	1.636	58.23	1.916	58.80	2.196	58.69
0.244	42.35	0.524	54.78	0.804	56.36	1.084	56.76	1.364	55.93	1.644	58.20	1.924	58.70	2.204	58.86
0.252	42.70	0.532	54.75	0.812	56.22	1.092	57.20	1.372	55.89	1.652	58.35	1.932	58.42	2.212	59.05
0.260	43.27	0.540	54.82	0.820	55.76	1.100	57.85	1.380	55.86	1.660	58.80	1.940	58.13	2.220	59.06
0.268	43.82	0.548	55.02	0.828	55.12	1.108	58.29	1.388	55.38	1.668	59.00	1.948	58.10	2.228	59.07
0.276	44.24	0.556	55.23	0.836	54.69	1.116	58.48	1.396	55.26	1.676	59.20	1.956	58.17	2.236	59.32
0.284	44.41	0.564	55.23	0.844	54.37	1.124	58.21	1.404	55.08	1.684	59.40	1.964	58.10		

PE Workshop II: Part 1 — Appendix B

CASE 4 – REFERENCE SOLUTION DATA											
Range (km)	TL (dB)		Range (km)	TL (dB)		Range (km)	TL (dB)		Range (km)	TL (dB)	
	ZR 95m	ZR 150m		ZR 95m	ZR 150m		ZR 95m	ZR 150m		ZR 95m	ZR 150m
0.01	29.39	36.35	0.99	51.28	50.59	1.95	56.99	56.21	2.91	61.75	55.67
0.03	29.39	36.35	0.99	51.28	50.59	1.95	56.99	56.21	2.91	61.75	55.67
0.05	43.25	40.74	1.01	50.43	48.28	1.97	56.12	55.00	2.93	63.44	57.22
0.07	34.47	43.55	1.03	52.45	47.99	1.99	62.69	56.91	2.95	61.05	59.78
0.09	45.05	47.95	1.05	55.85	49.93	2.01	57.07	56.94	2.97	60.24	59.01
0.11	43.75	37.99	1.07	54.45	47.64	2.03	57.24	57.13	2.99	61.13	59.39
0.13	42.28	41.29	1.09	56.20	48.02	2.05	58.12	59.39	3.01	58.72	58.06
0.15	38.97	41.26	1.11	62.22	50.50	2.07	57.28	59.35	3.03	58.66	54.63
0.17	39.85	46.35	1.13	59.02	48.80	2.09	56.03	59.50	3.05	57.51	54.28
0.19	41.09	49.51	1.15	61.65	50.50	2.11	58.11	62.40	3.07	56.35	55.18
0.21	44.92	49.89	1.17	66.21	52.01	2.13	55.30	61.09	3.09	56.43	55.00
0.23	48.45	52.20	1.19	60.80	49.98	2.15	54.82	61.32	3.11	55.00	56.33
0.25	48.02	47.10	1.21	59.65	52.52	2.17	56.17	54.39	3.13	56.13	57.11
0.27	50.76	44.98	1.23	64.60	53.40	2.19	55.16	63.01	3.17	54.06	57.92
0.29	43.15	47.77	1.25	59.15	51.06	2.21	53.97	61.42	3.21	54.21	59.71
0.31	48.16	45.84	1.27	57.43	53.79	2.23	55.95	62.86	3.23	54.25	60.42
0.33	54.27	46.85	1.29	60.90	53.84	2.25	53.14	52.14	3.27	54.21	52.00
0.35	54.53	52.00	1.31	57.33	51.75	2.27	53.00	59.84	3.29	54.27	62.83
0.37	48.97	49.44	1.33	55.97	54.29	2.29	55.21	61.59	3.33	54.97	54.43
0.39	48.26	56.67	1.35	59.52	53.57	2.31	52.88	61.40	3.35	55.50	65.47
0.41	46.74	58.88	1.37	56.23	51.67	2.33	53.37	58.60	3.37	56.34	69.11
0.43	45.34	61.37	1.39	55.30	53.87	2.35	54.65	60.86	3.39	57.51	66.75
0.45	47.22	54.93	1.41	58.40	52.84	2.37	51.99	60.46	3.43	56.85	68.64
0.47	46.70	54.12	1.43	55.25	51.10	2.39	52.41	57.85	3.45	63.16	69.58
0.49	48.38	49.95	1.45	54.29	52.58	2.41	52.89	52.17	3.47	56.34	70.46
0.51	52.33	46.73	1.47	56.84	51.45	2.43	51.26	60.18	3.49	71.34	71.71
0.53	51.09	48.61	1.49	53.82	50.69	2.45	52.42	58.28	3.51	63.07	73.55
0.55	51.67	45.59	1.51	53.10	52.21	2.47	52.62	64.10	3.53	78.30	75.90
0.57	56.21	46.97	1.53	54.65	51.29	2.49	51.67	59.64	3.55	70.18	77.45
0.59	53.71	48.05	1.55	51.93	51.19	2.51	52.48	58.33	3.57	66.08	78.48
0.61	53.15	46.16	1.57	51.58	52.65	2.53	52.59	64.26	3.59	63.40	79.17
0.63	55.04	48.05	1.59	52.98	51.78	2.55	51.57	59.15	3.63	59.93	78.97
0.65	52.87	49.05	1.61	50.77	52.22	2.57	52.52	59.08	3.65	58.69	77.17
0.67	50.47	47.22	1.63	51.14	54.26	2.59	52.89	64.36	3.67	57.72	74.75
0.69	50.30	50.46	1.65	52.32	53.40	2.61	52.03	59.27	3.69	56.97	72.90
0.71	49.41	50.41	1.67	50.16	54.05	2.63	53.71	58.45	3.73	55.91	71.09
0.73	46.69	48.11	1.69	51.06	55.55	2.65	53.92	62.15	3.75	55.55	70.00
0.75	49.03	51.84	1.71	52.04	54.23	2.67	53.02	57.92	3.77	55.27	68.95
0.77	46.52	51.19	1.73	50.21	54.97	2.69	55.75	57.29	3.79	56.07	69.14
0.79	47.76	49.03	1.75	52.49	56.26	2.71	54.94	61.13	3.81	54.93	67.78
0.81	46.08	52.61	1.77	52.99	55.12	2.73	54.87	57.00	3.83	54.87	67.00
0.83	47.60	51.09	1.79	51.19	55.96	2.75	58.39	57.43	3.85	54.90	67.28
0.85	46.75	50.88	1.81	54.39	56.39	2.77	56.72	60.95	3.87	55.00	66.85
0.87	47.53	55.35	1.83	53.47	55.11	2.79	57.16	56.79	3.89	55.19	66.56
0.89	47.42	52.16	1.85	52.41	55.52	2.81	61.12	57.33	3.93	55.79	66.77
0.91	47.21	50.43	1.87	57.64	55.65	2.83	58.33	61.02	3.95	56.21	66.91
0.93	46.75	53.88	1.89	56.32	55.73	2.85	59.96	56.14	3.99	57.94	66.84
0.95	48.32	50.64	1.91	55.33	55.87	2.87	63.50	57.34	4.01	58.09	67.07

PE Workshop II: Part 1 — Appendix B

CASE 6A – REFERENCE SOLUTION DATA (Source Depth = 88 m)											
Range (km)	TL (dB)	Range (km)	TL (dB)	Range (km)	TL (dB)	Range (km)	TL (dB)	Range (km)	TL (dB)	Range (km)	TL (dB)
1.73	81.73	2.30	83.45	3.19	81.33	4.11	95.33	5.12	82.10	6.13	88.52
4.87	81.73	26.10	85.56	36.09	81.38	47.44	91.26	65.37	93.22	78.45	88.52
5.72	77.03	26.70	75.97	36.62	85.65	47.54	91.47	65.47	88.01	80.20	88.52
8.36	71.72	27.84	76.39	37.13	85.75	47.75	91.47	67.13	96.55	80.93	94.56
10.63	77.03	27.94	76.26	38.18	87.63	49.08	85.63	68.05	83.43	81.06	88.52
12.40	77.03	29.20	82.11	39.50	84.60	50.73	84.90	69.59	89.15	82.57	93.91
13.62	77.65	29.39	82.32	39.70	84.81	51.96	83.86	70.82	88.01	82.68	90.91
14.87	74.21	30.74	88.47	39.91	84.92	52.17	83.86	72.07	85.19	85.92	91.53
16.19	75.15	30.85	88.78	40.01	84.60	53.30	85.00	72.28	95.40	85.56	90.28
17.75	69.17	32.06	85.55	41.14	81.58	54.44	87.82	72.49	85.30	86.69	89.53
19.20	87.65	32.28	85.76	42.48	83.04	54.54	88.13	73.20	93.84	88.35	91.53
19.20	87.65	33.21	83.05	43.53	91.99	60.11	90.41	73.41	94.04	89.27	90.80
20.01	77.85	33.31	83.26	43.63	92.20	61.36	97.91	74.85	91.86	90.11	96.94
20.11	78.17	34.55	82.63	44.67	98.35	61.36	98.02	74.85	92.06	91.66	98.61
21.55	76.19	34.65	82.94	44.88	98.45	61.47	98.22	74.85	92.27	92.79	99.34
22.79	75.04	35.88	81.17	45.90	95.01	61.57	98.02	75.97	86.96	94.12	90.90
24.35	86.81	35.88	81.17	45.90	95.33	62.90	93.64	77.21	87.58	94.32	90.58

CASE 6B – REFERENCE SOLUTION DATA (Source Depth = 112 m)											
Range (km)	TL (dB)	Range (km)	TL (dB)	Range (km)	TL (dB)	Range (km)	TL (dB)	Range (km)	TL (dB)	Range (km)	TL (dB)
3.94	69.99	19.27	81.30	34.96	82.39	49.33	88.44	70.21	89.79	86.19	90.25
4.36	78.25	20.53	77.68	36.25	92.19	51.07	87.70	71.42	96.59	87.16	91.48
5.92	74.20	21.74	80.66	37.85	85.77	52.60	86.78	73.18	96.57	88.52	92.19
7.31	76.05	23.06	83.23	39.18	85.24	53.50	89.54	73.95	94.30	89.48	97.24
9.00	73.24	24.52	79.60	39.96	83.37	59.28	92.27	74.95	88.81	90.98	96.98
9.59	75.72	25.76	79.38	41.61	86.87	60.94	96.38	76.73	89.21	92.75	99.28
11.26	80.24	27.39	78.43	43.18	95.22	62.21	93.38	78.26	88.28	93.85	93.69
12.49	79.72	28.68	84.10	44.62	90.76	63.39	94.81	79.79	87.53		
14.09	77.53	30.12	87.80	44.62	90.76	64.56	92.01	81.01	94.43		
15.32	76.69	31.28	80.56	45.67	95.29	65.87	98.40	82.27	90.91		
16.53	79.47	32.56	85.82	46.87	93.84	67.30	93.74	83.14	92.45		
18.01	80.59	34.04	90.86	48.16	87.42	68.69	91.35	84.92	93.16		

PE Workshop II: Part 1 — Appendix B

CASE 6C – REFERENCE SOLUTION DATA (Source Depth = 148 m)											
Range (km)	TL (dB)	Range (km)	TL (dB)	Range (km)	TL (dB)	Range (km)	TL (dB)	Range (km)	TL (dB)	Range (km)	TL (dB)
4.13	72.47	19.42	79.77	33.50	82.34	48.17	80.53	67.23	83.41	81.92	85.03
6.06	70.42	20.95	78.64	35.55	87.58	49.93	96.10	68.27	100.42	83.60	96.62
7.78	74.84	22.35	75.45	36.58	87.27	50.09	91.07	70.07	103.40	84.53	88.21
9.47	84.19	23.55	79.66	37.84	88.71	52.50	95.28	71.14	98.77	85.93	93.84
10.03	73.40	24.90	73.40	39.57	87.18	54.13	94.15	72.94	101.75	87.18	84.86
11.57	72.78	25.63	80.59	40.18	86.96	59.29	100.62	74.18	101.75	87.72	96.31
13.07	76.27	27.54	84.29	41.22	87.06	60.68	96.21	75.27	98.67	89.01	92.32
14.19	75.66	28.81	79.15	43.52	88.81	61.93	97.44	76.41	92.20	91.22	95.18
15.35	77.20	30.13	84.70	44.22	87.37	63.19	98.77	77.98	92.51	92.57	96.10
16.79	76.79	31.26	84.08	45.92	90.55	64.56	94.36	79.34	94.97	93.25	92.92
18.17	72.47	32.66	81.41	46.88	92.61	66.11	101.03	80.50	96.31		

CASE 7 – REFERENCE SOLUTION DATA											
Range (km)	TL (dB)	Range (km)	TL (dB)	Range (km)	TL (dB)	Range (km)	TL (dB)	Range (km)	TL (dB)	Range (km)	TL (dB)
1.00	55.72	26.00	81.21	51.00	77.89	76.00	91.77	101.00	88.56	126.00	87.09
2.00	67.07	27.00	81.26	52.00	74.56	77.00	91.65	102.00	86.16	127.00	88.09
3.00	71.13	28.00	81.42	53.00	76.22	78.00	90.85	103.00	104.23	128.00	89.48
4.00	78.19	29.00	81.63	54.00	75.39	79.00	90.00	104.00	80.24	129.00	90.61
5.00	72.96	30.00	81.97	56.00	82.34	80.00	89.46	105.00	78.35	130.00	90.55
6.00	74.50	31.00	82.29	56.00	87.21	81.00	89.39	106.00	80.94	131.00	89.62
7.00	75.06	32.00	82.55	57.00	82.70	82.00	89.62	107.00	81.56	132.00	88.41
8.00	74.42	33.00	82.75	58.00	84.74	83.00	90.25	108.00	81.01	133.00	87.55
9.00	74.17	34.00	82.88	59.00	87.02	84.00	91.01	109.00	88.41	134.00	87.16
10.00	75.00	35.00	83.00	60.00	87.70	85.00	91.65	110.00	95.24	135.00	87.27
11.00	76.03	36.00	83.11	61.00	85.13	86.00	91.98	111.00	86.21	136.00	87.87
12.00	76.92	37.00	83.30	62.00	83.80	87.00	91.84	112.00	88.39	137.00	88.74
13.00	77.85	38.00	83.49	63.00	85.03	88.00	91.45	113.00	93.12	138.00	89.53
14.00	78.69	39.00	83.67	64.00	87.25	89.00	91.00	114.00	88.24	139.00	89.85
15.00	78.94	40.00	83.84	65.00	89.12	90.00	90.91	115.00	85.34	140.00	89.58
16.00	78.75	41.00	83.97	66.00	90.70	91.00	90.92	116.00	86.38	141.00	88.97
17.00	78.58	42.00	84.19	67.00	92.03	92.00	91.14	117.00	88.77	142.00	88.42
18.00	78.66	43.00	84.43	68.00	90.57	93.00	91.52	118.00	89.73	143.00	88.35
19.00	78.95	44.00	84.56	69.00	88.56	94.00	91.94	119.00	90.03	144.00	88.52
20.00	79.38	45.00	84.62	70.00	87.55	95.00	92.49	120.00	91.64	145.00	88.84
21.00	79.90	46.00	84.73	71.00	87.31	96.00	93.22	121.00	91.45	146.00	88.97
22.00	80.37	47.00	84.85	72.00	87.42	97.00	93.30	122.00	89.25	147.00	89.26
23.00	80.74	48.00	85.02	73.00	88.07	98.00	90.47	123.00	87.66	148.00	89.46
24.00	80.99	49.00	85.98	74.00	89.29	99.00	88.07	124.00	86.92	149.00	89.39
25.00	81.13	50.00	88.22	75.00	90.77	100.00	90.90	125.00	86.57	150.00	90.37

Appendix C — Tappert's Reflections on the Origin of Underwater Acoustic PE

In 1972 Fred D. Tappert and R. H. Hardin developed the parabolic approximation for underwater acoustic propagation. The records of this underwater acoustic parabolic equation (PE) method are chronicled in a number of publications. An excellent account of this early development, including pertinent references, is given by Tappert¹.

From that point on, their split-step PE method evolved into numerous computer codes. One early version, the AESD PE model², eventually evolved into the Navy Standard PE model (in 1987). The original Tappert version has continued to evolve at the University of Miami. Current versions of it (MIPE and UMPE) were used on the test cases in the PE Workshop II. Along the way, vectorized versions of the Tappert PE method evolved into complete hardware-software computation-display systems (e.g., the PESOGEN system³ (circa 1986), and later the coupling of that system into the OPTAMAS system⁴ (in 1988)).

One of the high points in the PE Workshop II was Fred Tappert's recreation of his initial presentation of the PE method to his colleagues at Bell Laboratories. The workshop's participants viewed with interest the original viewgraphs used by Tappert as he recreated that lecture. The editors felt that this was an opportunity to preserve a bit of history and have thus reproduced those original viewgraphs in this Appendix.

¹F. D. Tappert, "The Parabolic Approximation Method," in *Wave Propagation and Underwater Acoustics*, edited by J. B. Keller and J. S. Papadakis (Springer-Verlag, New York, 1977), Chapter 5, pp. 224-287.

²H. K. Brock, "The AESD parabolic equation model," AESD TN-75-07, Office of Naval Research, Arlington, VA (1975).

³"PESOGEN-II User's Manual Supplement," Version V2.8, Technical Manual TM 03-90, Daubin Systems Corp., Key Biscayne, FL, February 1990.

⁴"OPTAMAS 2.1 User's Guide," Systems Integrated, 8080 Dagget Street, San Diego, CA, September 1990.

(2)

I. Parabolic Equation Method

Reference: V.A. Fock, Electromagnetic Diffraction and Propagation Problems, Prentice-Hall.

Single iteration in cartesian coordinates:



$$\frac{\partial^2 u}{\partial x^2} + \frac{\partial^2 u}{\partial y^2} + k_0^2 n^2(x,y) u = 0$$

$$u = \psi \pm i \phi$$

$$\frac{\partial^2 \psi}{\partial x^2} + 2i\phi \frac{\partial^2 \psi}{\partial xy} + \frac{\partial^2 \psi}{\partial y^2} + k_0^2 (n^2 - 1) \psi = 0$$

Right $\frac{\partial^2 \psi}{\partial x^2}$ equal to zero

$$i \frac{\partial^2 \psi}{\partial y^2} + \frac{1}{k_0^2} \frac{\partial^2 \psi}{\partial x^2} + \frac{1}{k_0^2} [n^2(n^2-1)] \psi = 0$$

(1)

New Developments in Ocean Acoustics

F.D.Tafforeau and R.H.Holland, BTLL

I. Parabolic Equation Method (analytic methods)

II. Split-Step Fourier Algorithm (numerical analysis)

III. Custom Graphical Displaying (computer technique)

(4)

Validity of Approximation

Own derivative - cylindrical coordinate:



1. Configuration of any equation for spherical case

Except any equation:

$$\frac{du}{dr} = \tan \theta \cdot \left(\frac{1}{r^2 \sin^2 \theta} \right) \frac{du}{d\theta}$$

$$\frac{\partial^2 u}{\partial r^2} + \frac{\partial^2 u}{\partial \theta^2} + \frac{1}{r^2} \frac{\partial^2 u}{\partial z^2} + h_0 \nabla^2 (r, \theta) u = 0$$

$$h_0 = \frac{a^2}{r^2}, \quad \nabla^2 = \frac{1}{r^2} + \frac{1}{r^2} \left[\frac{\partial^2}{\partial \theta^2} - \frac{1}{r^2} \left(\frac{\partial^2}{\partial z^2} \right) \right]$$

$$u = \frac{f(r)}{r^2}, \quad f = \text{function}, \quad r = \text{distance}.$$

$$\text{Let } u = \psi(\varepsilon, r, \theta) H_0^{(2)}(k_r r)$$

Neglect $\frac{\partial^2 u}{\partial \theta^2}$ compared to $\frac{\partial^2 u}{\partial r^2}$

Assume $k_r r \ll 1$

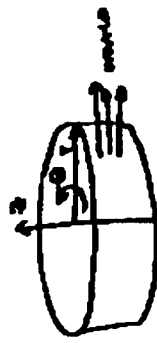
$$\therefore \frac{\partial^2 u}{\partial r^2} + \frac{1}{r^2} \left(\frac{\partial^2 u}{\partial z^2} + \frac{1}{r^2} \frac{\partial^2 u}{\partial \theta^2} \right) + \frac{1}{r^2} [\nabla^2(r, \theta) u] \psi \approx 0$$

$$\delta^2 = \frac{1}{r^2} \ln^2 r$$

$$\text{Thus } \frac{\partial^2 u}{\partial r^2} \approx 1 + \frac{1}{r^2}.$$

(5)

Own derivative - cylindrical coordinate:



Parabolic any equation:

$$\frac{du}{dr} = \frac{1}{r^2} \frac{du}{d\theta}$$

Rectangular any equation:

$$\frac{du}{dr} = \frac{1}{r^2} \frac{du}{d\theta} + \frac{1}{r^2} \frac{du}{dz}$$

$$\frac{du}{dr} + \frac{1}{r^2} \left(\frac{\partial^2 u}{\partial \theta^2} \right) \varphi_{\theta\theta} = \frac{1}{r^2} \frac{\partial^2 u}{\partial z^2}$$

$$\begin{aligned} \text{Parabolic approximation: } & \frac{du}{dr} + \frac{1}{r^2} \left(\frac{\partial^2 u}{\partial \theta^2} + \frac{1}{r^2} \frac{\partial^2 u}{\partial z^2} \right) \varphi_{\theta\theta} \\ u = \text{as } \varphi & = \frac{1}{r} k_r \varphi_{\theta\theta} \end{aligned}$$

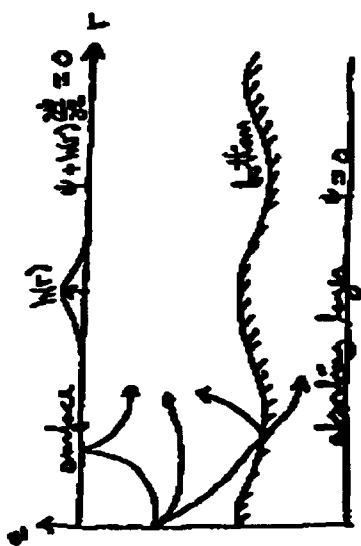
(4)

Main advantages of Parabolic Equation Method.

1. Parabolic equation (wavelike pattern) is easier to solve numerically than elliptic equation (laminar wave pattern).
2. Can handle gradually varying depth, varying and bearing dependent velocity variation.
3. Can easily include depth, varying, and bearing dependent adiabatic drag coefficient.
4. Skimming bottom effects are automatically included.
5. In principle, can handle variable surface height.

(5)

Boundary and Initial Conditions



$$\text{at surface: } \psi + (\kappa r) \frac{d\psi}{dr} = 0$$

Bottom: $\psi = 0$, no reflection

Source: $\psi(0,0)$ specified to be a directed beam, e.g. a wavelength

(1)

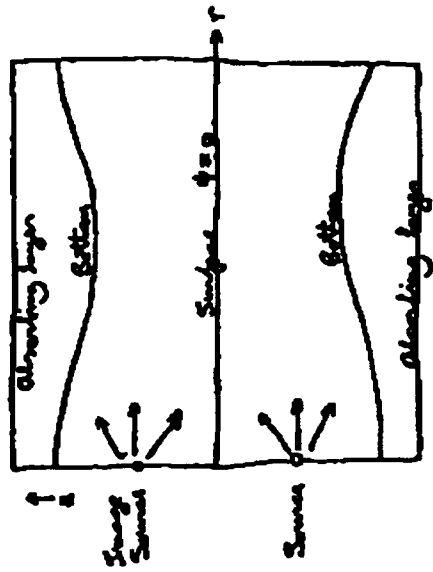
2. Split-Step Fourier Algorithm

$$i \frac{\partial \psi}{\partial r} + \frac{1}{2k} \frac{\partial^2 \psi}{\partial r^2} + \frac{1}{2} [n^2(r, z) - 1] \psi = 0.$$

Method is r :

$$\psi(r+\Delta r, z) = e^{i k \frac{\Delta r}{2} [n^2(r, z) - 1]} e^{i k \frac{\Delta r^2}{2} \frac{\partial^2}{\partial r^2} \psi(r, z)},$$

$$e^{i k \frac{\Delta r}{2} \frac{\partial^2}{\partial r^2} \psi(r, z)} = e^{-\frac{k^2 \Delta r^2}{2}} \left[1 - \frac{k^2 \Delta r^2}{2} \Im \psi(r, z) \right].$$



(2)

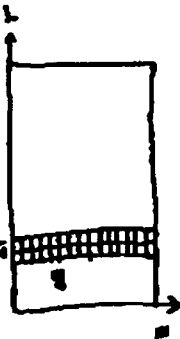
Non-dispersive PEM

1. Limited to small angle of propagation ($\leq 20^\circ$).
2. No large angle scattering.
3. Disentanglement of velocity and density requires careful treatment.
4. Difficultly with source modeling; absolute transmission losses not generally computable.

(10)

III. Conforming Cartesian Meshes

- Form $\Omega(r,z) = 1 + (r, z)^2$ at present range.



- For all e , compute intersections of $\partial_e \cap e$ with sides of rectangle using linear interpolation.
- Connect grid points with straight lines.
- Compute grid with straight lines.
- Solve only last row of b-matrix.

Other advantages

Fast running, very small memory usage.

(1)

Advantages of Eight-Step Fusion Algorithm

- Eigenvalues occurring in \mathbb{R} directions, few points needed.
- Second order accuracy in r , with long step size Δr .
- Non-diagonally scheme, saving memory if no sharing.
- Unconditionally stable.

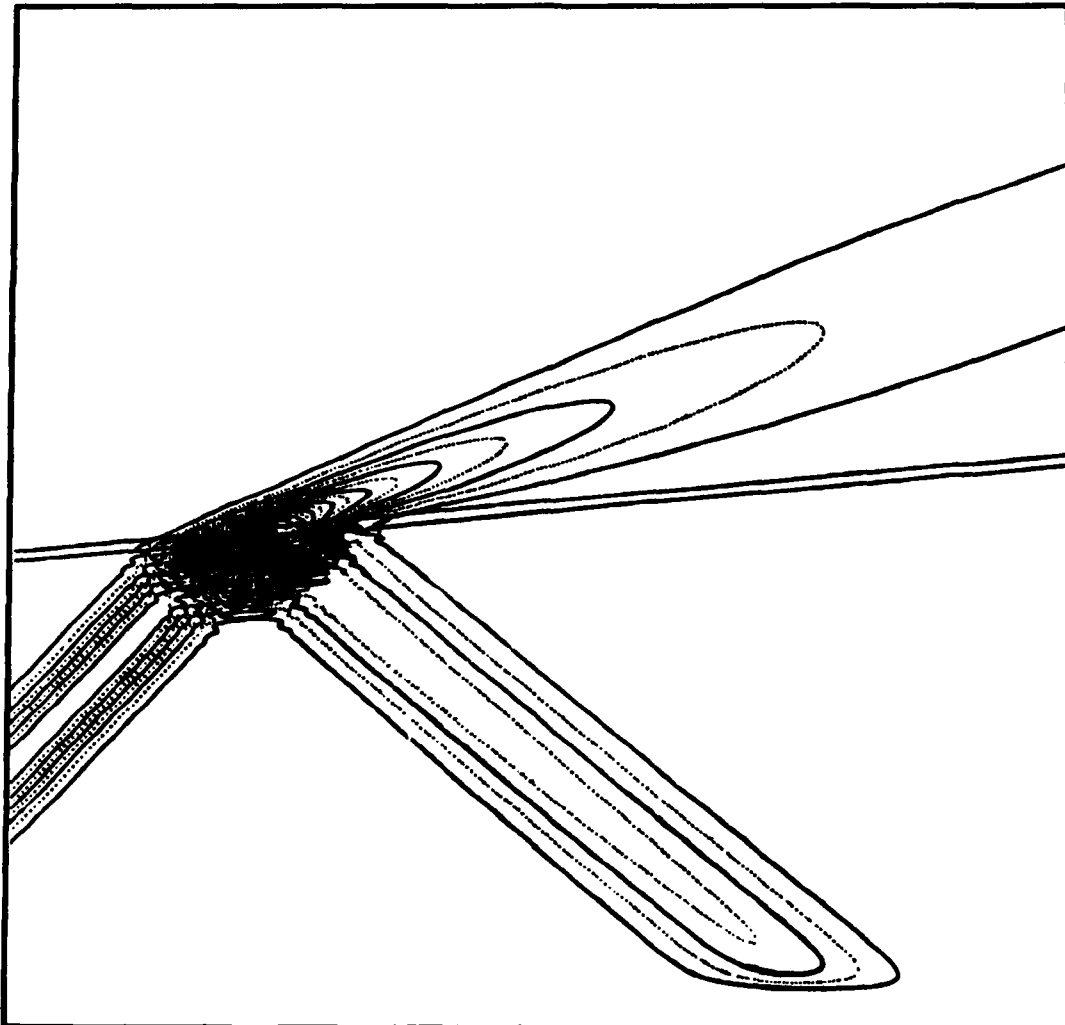
- Relatively easy to implement.
- Computationally efficient and fast-running.

Other disadvantages

- Requires gridline boundary conditions in \mathbb{R} .
- Not use uniform grid, $\Delta r \neq \text{const.}$

PE Workshop II: Part 1 — Appendix C

FRED TAPPERT BOX 35
TIME 19:31:17
DATE 04/26/73
PAGE NO 001



PART 2

TEST CASE RESULTS

INTRODUCTION

This part of the PE Workshop II proceedings contains the solutions to the 7 test case problems posed in the workshop. Part 2 is structured such that for each test case the following format is followed:

- The *objective* of the test case problem is stated.
- Relevant *background* information is presented. The rationale of the test case is discussed in relation to that particular feature of the PE model that is being tested.
- The *test case problem* is posed, accompanied by a figure which illustrates the environmental conditions of the problem.
- The origin of the *reference solution* is discussed.
- Workshop *results* from each PE model that was applied to that test case is plotted together with the reference solution for comparison. This is followed by a brief discussion of the results.
- A *summary* of the findings is given.
- Relevant contributed papers in Part 3 of the workshop proceedings are listed as *further readings*.

Reference Solutions

The reference solutions were obtained from many different sources. In Test Case 1 the reference solution is the analytic solution to the Lloyd's Mirror problem. In Test Case 2 and 4 it was a numerical solution obtained from the coupled mode model, COUPLE (Evans 1983; 1986). In Test Case 3 the reference solution was obtained from the seismoacoustic finite-element model with shear waves, SAFE (Murphy and Chin-Bing 1991; Chin-Bing and Murphy 1993a; 1993b). In Test Case 6 the reference solution was experimental acoustic data (Fisher et al. 1988; 1989) taken in a region where environmental-geophysical conditions and parameters were considered "known." In Test Case 7 the normal mode model, SNAP (Jensen and Ferla 1979), was used to generate the reference solution. In each case, the reference solution was considered the best available solution that could be obtained. Both the COUPLE and the SAFE models give the complete numerical solution to the nonhomogeneous Helmholtz wave equation, i.e., the solution to an elliptic boundary value problem. (The PE solutions

PE Workshop II: Part 2 — Test Case Results

are solutions of a parabolic initial value problem that approximates this elliptic boundary value problem.) Since the SAFE model includes shear wave speeds and shear attenuations, it was used as the reference solution for Test Case 3. Test Case 7 involved long-range propagation of a trapped, leaky mode in a stratified, planar environment; the SNAP model contains all of the significant physics for such a scenario.

Tabular data to the reference solutions are given in Appendix B of Part 1.

Table 2-1. Models Used Versus Test Cases

MODELS USED	TEST CASES													
	1	2A	2B	3A	3B	4A	4B	5A	5B	5C	6A	6B	6C	7
CU	X													
Ref.: COUPLE		X	X			X	X							
DREP	X	X	X			X	X	X	X	X	X	X	X	X
DREPS		X	X	X	X	X	X							X
FEPE	X	X	X			X	X							
FEPES				X	X									
FEPE ROT				X	X									
FEPES ROT				X	X									
IFDPE	X	X	X	X	X	X	X	X	X	X	X	X	X	
IFDPE SAC		X	X											X
IMPPE	X	X	X			X	X	X	X	X				
LOGPE														X
MIPE	X	X	X	X	X	X	X	X	X	X	X	X	X	X
NAVY STD PE	X	X	X	X	X	X	X	X	X	X	X	X	X	X
NON EC FE		X	X											
OPT	X	X	X	X	X	X	X	X	X		X	X	X	X
PAREQ											X			X
Ref.: SAFE				X										
Ref.: SNAP														X
T-CPE	X													X

PE Workshop II: Part 2 — Test Case Results

Table 2–1. Models Used Versus Test Cases (Continued)

MODELS USED	DESCRIPTION OF MODELS AND THE USERS
CU	The Steinberg and McCoy model using Windowed Transformation and Marching Algorithms for Localized Phase-Space Representations.
Ref.: COUPLE	Richard Evans' coupled mode model; used by Evans to obtain reference solutions.
DREP	The finite-difference PE results (Test Cases 2–6) and the split-step PE results (Test Cases 1 and 7) generated by David Thomson.
DREPS	The elastic PE model developed and used by Gary Brooke of DREP. It includes shear wave speeds and shear wave attenuations.
FEPE	Michael Collins' finite-element PE model; used by Collins.
FEPES	A version of Collins' FEPE model that includes shear wave speeds and shear wave attenuations; developed and used by Collins.
FEPE ROT	A version of Collins' FEPE with rotated coordinate system so that the water-bottom interface is horizontal rather than sloping. Collins used it as a check for Test Case 3.
FEPES ROT	A rotated version of Collins' shear code, FEPES, with rotated coordinate system. Collins developed it and used it as a check for Test Case 3.
IFDPE	Wide-angle implicit finite-difference PE model developed and used by Ding Lee.
IFDPE SAC	Ding Lee's IFDPE model used by Finn Jensen (SACLANTCEN).
IMPPE	The IFDPE model used by John Papadakis with his impedance bottom boundary.
LOGPE	Split-step PE model by Berman, Wright, and Baer. In range-independent environments, its "rays" are identical to those of the Helmholtz eq.; used by Finn Jensen.
MIPE; UMPE	The Fred Tappert and Lan Nghiem-Phu University of Miami wide-angle split-step PE models; used by Lan Nghiem-Phu.
NAVY STD PE	The U.S. Navy's standard version of wide-angle split-step PE; used by Eleanor Holmes and Laurie Gainey.
NON EC FE	Collins' FEPE model without its energy conservation enhancement; used by Collins.
OPT	The split-step PE model used in the OPTAMAS system; used by Nils Paz.
PAREQ	The SACLANTCEN version of wide-angle split-step PE; used by Finn Jensen.
Ref: XXX	The model or data that was used to provide a reference solution.
Ref.: SAFE	The Murphy and Chin-Bing finite-element seismoacoustic model with shear wave speed and shear wave attenuation; used as a reference.
Ref.: SNAP	The SACLANTCEN normal mode model; used by Finn Jensen as a reference.
T-CPE	Thomson-Chapman wide-angle version of PE used by Finn Jensen.
XXX SAC	Other models used by F. Jensen; e.g., COUPLE SAC: COUPLE model run by Jensen.

Workshop Models

Table 2-1 gives a list of the models that were applied to each test case. An identifying label (used in these proceedings) is given to each model together with a brief description of the model. Detailed discussions of several of the models and their application(s) are presented by the workshop contributors in Part 3 of these proceedings. Not all of the papers in Part 3 contain adequate references, but in totality, the PE references cited by all the papers in Part 3 form an adequate PE bibliography. That bibliography is given at the ends of Part 2 and Part 3. References cited in Part 2 are also in this bibliography.

Research PE Models and Operational PE Models

The various PE models that were applied to the test cases can be classified into two categories: research and development (R&D) models and (fleet) operational models. The demarcation between the two categories is prominent. Operational PE models are configured to run on a small in-the-field computer (i.e., onboard ships and in naval installations), with selected parameter ranges such that the trade-off between computational speed, accuracy, portability, survivability, and system integration are optimized to fulfill the required mission. Research models have no such constraints and make few, if any trade-offs; their purpose is to faithfully include the required physics and to give highly accurate and reliable answers. Many research PE models now use finite-difference (Lee and McDaniel 1983) and finite-element (Collins 1990b) solutions combined with the full computational capabilities of powerful supercomputers. Thus, it would be expected that the research PE models would give more accurate results than the field-operational PE models.

The demarcation line between the various PE models is not so clear. PE models that are in the operational category were once in the research category. Furthermore, the same PE model may exist in both categories, with the only significant difference contained in the constraints imposed by the operational situation. All of the operational PE models use the split-step solution technique (Hardin and Tappert 1973; Tappert 1977) since it uses FFT's and can do computations more rapidly than other PE solution techniques. The split-step PE models are, therefore, often associated with operational PE models. However, the split-step PE models without the operational constraints are frequently used in basic research (Jensen and Ferla 1990). Thus, in this workshop three categories of PE models are represented: the research PE models, the modified operational PE models with many of their operational parameters changed so that they can give a better answer, and the operational PE models.

PE Workshop II: Part 2 — Test Case Results

The Navy Standard PE model (labeled in these proceedings as "NAVY STD PE"), the University of Miami PE model (labeled as "MIPE"), and the PE model used in the OPTAMAS system (labeled as "OPT") may be classified as operational PE models. These three models have evolved from the original Tappert-Hardin split-step PE formalism (Tappert 1977). Different versions of the split-step PE model are employed in a "field operational mode" to produce NAVY STD PE and the OPTAMAS system. NAVY STD PE is the standard version of PE that is used by the U.S. Navy in operational acoustic calculations. It undergoes frequent official revisions and improvements as determined by the Navy. The MIPE model is an advanced version of Tappert's split-step PE model and also undergoes revisions and improvements as determined by its developers. An earlier version of MIPE forms the basis for the PESOGEN (PE Solution Generation) system; this is a hardware-software combination designed to supply rapid PE calculations and color graphics. OPTAMAS is a proposed tactical prediction system that is based on the PESOGEN system and is now in the implementation phase. The objective of the OPTAMAS system is to provide sensor placement and utilization guidance on a tactical scale. *Editors' Note: Part 3 of these proceedings contains papers on the NAVY STD PE model (Holmes and Gainey), on the MIPE model (N.-Phu, Smith, and Tappert), and on the OPTAMAS system.*

In the PE Workshop II the NAVY STD PE model was run using its operational parameters and its results are fairly representative of "in-the-field" Navy predictions. The OPT model was also run using its set of operational parameters which included several time-saving trade-offs[†]. Its results are representative of the type of PE calculations that would form the basis for "tactical decision aids." The MIPE model users/developers applied knowledgeable (nonoperational) selection of parameters in their use of the model so that its results are representative of what the operational PE model could do if operated in an unconstrained mode and by a knowledgeable user.

Therefore, the PE models' results for the 7 test cases presented in these proceedings span the 3 categories—from research PE models to field-operational PE models, and several configurations in-between.

[†] The custodian of OPTAMAS did not change its operational parameters for the PE Workshop II test case results nor did he change its reference distance to the distance of 1 m as was used by all other workshop contributors. He estimates that the results from OPTAMAS will be approximately 2 dB re 1 m different from the results of the other models in the PE Workshop II.

TEST CASE 1

Lloyd's Mirror – Wide-Angle Propagation

OBJECTIVE Determine the half-beamwidth propagation capability of the PE models. The half-beamwidth propagation capability includes both the wide-angle capability and the angular distribution of energy resulting from the starting field. It is the maximum angle that can be used and still maintain accuracy.

BACKGROUND The Parabolic Equation (PE) model (Hardin and Tappert 1973) that was introduced to the underwater acoustics propagation community in 1973 (Spofford 1973) could accurately include a $17^\circ - 20^\circ$ maximum angle of half-beamwidth propagation. This original version of the split-step PE models has become known as the "Standard PE" approximation.

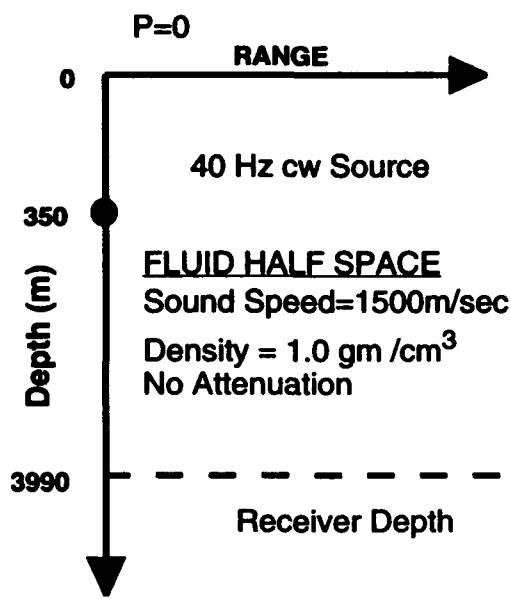
In the early 1980's this maximum angle of half-beamwidth propagation was extended to approximately 40° . The finite-difference PE models accomplished this by using the Claerbout wide-angle approximation (Claerbout 1976; Botseas et al. 1983). The split-step PE models accomplished this by using the Thomson–Chapman wide-angle approximation (Thomson and Chapman 1983).

Currently there are PE model implementations (Collins 1988a; 1988b; 1988c) that come very close to full 90° half-beamwidth propagation. The finite-difference and finite-element PE models employ a high-order Padé approximant to accomplish this wide-angle propagation.

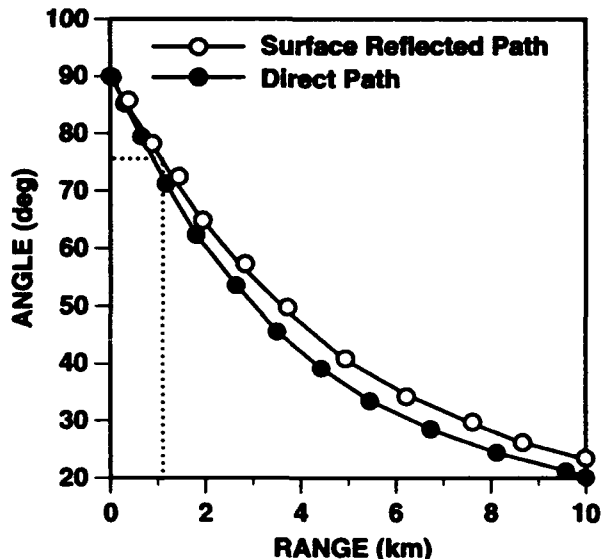
THE TEST CASE PROBLEM To test the capabilities of these wide-angle PE propagation models, a very simple Lloyd's Mirror problem was selected as Test Case 1. The problem consisted of a single fluid layer (half-space) with a pressure-release surface and a constant sound speed of 1500 m/sec. The density is 1.0 g/cm^3 and there is no attenuation. The fixed point depth (source depth) is 350 m with a moving point depth (receiver depth) of 3990 m. The frequency is 40 Hz. Figure 2-1.0(a) gives a schematic drawing of the problem.

Range as a function of maximum launch angle is shown in Fig. 2-1.0(b) for the surface reflected (SR) path and the direct (D) path propagation. It was obtained from the geometry of the source and receiver in Test Case 1. A PE model's wide-angle capability can be established by noting the range where the PE model's prediction starts to agree with the reference solution. The corresponding angle in Fig. 2-1.0(b) is

PE Workshop II: Part 2 — Test Case Results



(a) Lloyd's Mirror Environment—Test of Wide-Angle Propagation



(b) Range vs. Maximum Launch Angle.

Fig. 2-1.0 Environment for Test Case 1.

the maximum angle of propagation for that range. As an example of the usage of Fig. 2-1.0(b), to include all of the pressure field at a range of 1 km from the source (and at a depth of 3990 m) would require a PE model that can include a half-beamwidth propagation in excess of 75°. This is indicated by the dashed lines in Fig. 2-1.0(b).

THE REFERENCE SOLUTION An analytic reference solution was generated for this Lloyd's Mirror problem by using an image solution technique.

RESULTS AND DISCUSSION This problem is a good illustration of the expertise required of the user. A starting field for the PE model must be chosen that represents an acoustic point source in the near-field. The emitted acoustic field near the source should be at least as wide in half-angle as the particular PE model will propagate. The "tried and true" normal mode starting field cannot be used since the problem is a half-space and thus has no trapped modes. The appropriate choice is an image starter.

The analytic reference solution is shown in Figure 2-1.1 along with the PE models' predictions. The vertical axis is transmission loss (in dB re 1 m) and the horizontal axis is range (in kilometers).

PE Workshop II: Part 2 — Test Case Results

All of the PE models used to solved Test Case 1 demonstrated the capability to accurately propagate fields with half-beamwidths of greater than 70° . Impressively some of the R&D PE models were capable of half-beamwidth propagation approaching 90° and the operation-level PE model (NAVY STD PE) was in excess of 75° half-beamwidth propagation.

A closer examination of Fig. 2–1.1 using enlarged plots confined to the first 2 km in range (and not shown here) showed the following details.

- The results for the FEPE model do not show prominently on plot (a) of Fig. 2–1.1 because they lay on the curve of the reference solution (i.e., they are in complete agreement).
- The solution provided by the DREP model, shown in plot (b), reaches agreement with the reference solution at a range of ~ 500 m, implying a $>80^\circ$ capability (see Fig. 2–1.0). The DREP model used in this test case is the Thomson split-step PE model with the Thomson–Chapman wide-angle approximation.
- The SACLANT solution (plot (h)), which for this case is the Thomson–Chapman split-step PE (T-CPE) and run by Finn Jensen, gives a perfect match to the reference solution after ~ 1.5 km, implying a $>65^\circ$ capability.
- Overplots of results from the Navy Standard PE model (NAVY STD PE), the MIPE model, and the PE model used in the OPTAMAS system (OPT) all compare well to the reference solution. These three models have evolved from the original Tappert split-step PE formalism. A visual comparison of the models' results in Fig. 2–1.1 show that except for disagreement in the first ~ 700 m, MIPE matches the reference solution very well. NAVY STD PE shows more loss as well as a range shift in the position of the peaks and nulls. OPT also shows the same range shift problem as NAVY STD PE with the additional feature of the “steps” in the curves. These “steps” are a consequence of the system's requirement to write the results in integer format rather than floating point format. This is done to reduce the amount of computer storage required.
- One comparison that is noteworthy is the two PE models based on the implicit finite-difference method. IFDPE is the original version of the model developed by Ding Lee. The IMPPE is a version of IFDPE that replaces the familiar PE false-bottom treatment with an impedance boundary condition. In principle, when the impedance boundary condition is properly applied, the results from the two models should be virtually identical. The big difference is in the CPU runtime where IMPPE can execute a problem in about half the time of IFDPE since the bottom layers can be replaced with a single impedance layer and thus significantly reduce the depth that must be considered.

- The result from a non-PE model (labeled CU) is also shown in Fig. 2-1.1. A full discussion of the technique behind this model can be found in the paper by Steinberg and McCoy in Part 3. The model's prediction had the right form, but due to an arbitrary source strength, the dB level of the predictions differed from the reference solution by a significant amount. Increasing the loss by a constant value of 32 dB beyond the CU model's predictions produces a quite respectable match with the reference solution (as is shown in plot (i) of Fig. 2-1.1).
- Finally, as a result of the comparisons made at the workshop together with the knowledge gained from this test case problem, the developers-custodians of the NAVY STD PE model have improved the source algorithm to take full advantage of the PE model's capability. The new result for Test Case 1 from this revised version of NAVY STD PE is shown in Fig. 2-1.1(j) and labeled as "New NAVY STD PE." Closer agreement with the reference solution now begins at a range less than 1 km. (Compare this result with the earlier one shown in Fig. 2-1.1(d)). Comparison with the MIPE result in Fig. 2-1.1(c) indicates that the NAVY STD PE model is close to equaling the MIPE result. (The MIPE results could be viewed as the upper limit to what the operationally constrained NAVY STD PE model might achieve.) This improvement in the NAVY STD PE model is a direct result of the PE Workshop II.

Test Case 1 examined the field out to a range of only 10 km. A small phase error as a function of angle could still exist within the results shown in Fig. 2-1.1. Only at much longer ranges would the cumulative effects of such an error be noticeable.

The PE models' wide-angle capabilities with minimum phase errors (shown in Fig. 2-1.1) are valid for the simple homogeneous environment presented in Test Case 1. A test of wide-angle capability with minimum phase error in a strongly refractive environment would be a more difficult problem and the results from Test Case 1 may not be illustrative of the performance of all PE models in such an environment.

SUMMARY All the PE models demonstrated the capability to accurately compute propagation loss for half-beamwidth angles up to $\pm 75^\circ$, or better. The operational PE models exceeded 75° while the R&D models approached full 90° propagation. Test Case 1 has resulted in an improved starting field for the NAVY STD PE model.

FURTHER READINGS IN PART 3 For more in-depth discussions on the use of the wide-angle approximation in the PE models, refer to the papers in Part 3 of these proceedings. The paper, *The Self-Starter* by M. D. Collins, is devoted to starting fields for the PE models. Two papers are devoted to the operational PE models and several of the papers discuss the various research PE models.

PE Workshop II: Part 2 — Test Case Results

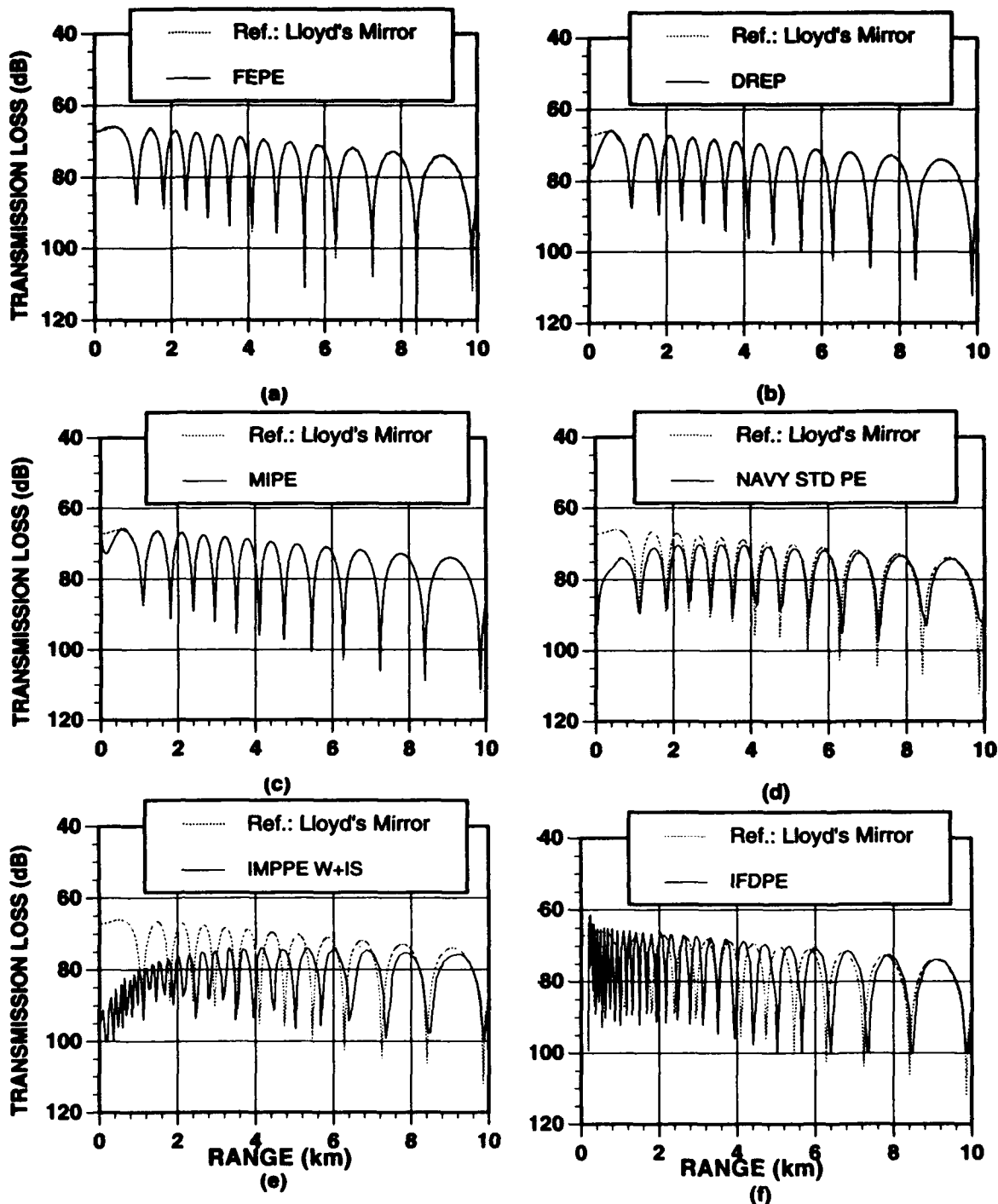


Fig. 2-1.1. Test Case 1 Results

PE Workshop II: Part 2 — Test Case Results

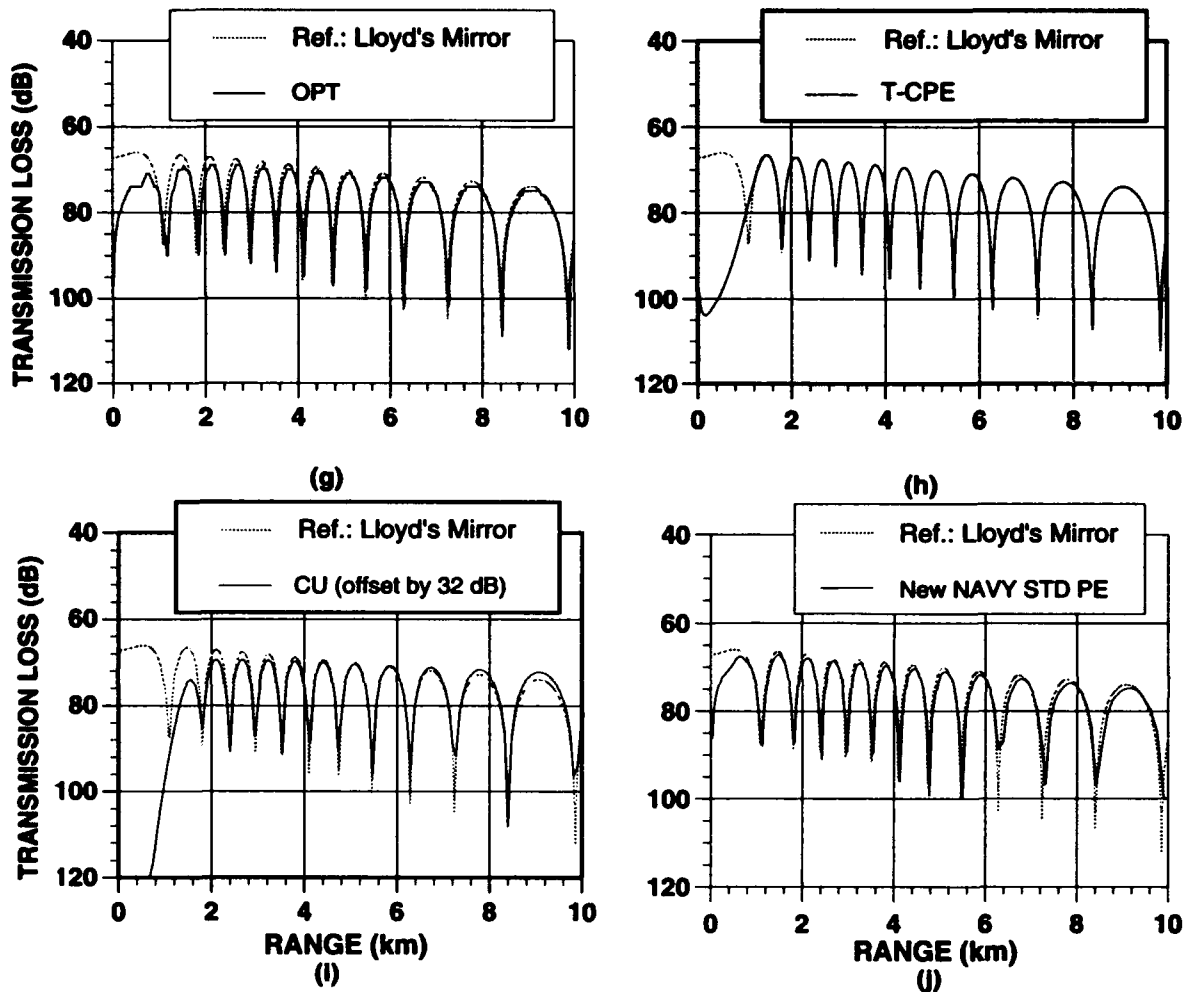


Fig. 2–1.1. Test Case 1 Results (Continued)

TEST CASE 2

Conservation of Energy in Range-Dependent Propagation

OBJECTIVE Test the capability of the PE models to conserve energy in propagating (“marching”) over range-varying bathymetry.

BACKGROUND Matching the boundary conditions in the horizontal direction (as a PE model “marches” in range) requires continuity of the pressure field and of the normal derivative of the pressure field (i.e., continuity of horizontal particle velocity). However, a parabolic equation solution allows only one of these boundary conditions to be satisfied. Experience has shown that the better result is obtained by matching the pressures rather than the velocities.

The consequence of propagating (matching) only the pressure field as a PE model marches in range is seen in range-dependent propagation, where the TL increases too rapidly in going upslope, and decreases too slowly in going downslope. In an upslope-downslope problem, the greatest inaccuracy occurs at the apex while the upslope and downslope errors tend to cancel one another, often producing a reasonably good result after the upslope-downslope propagation has been completed.

Recently an asymptotic correction to the energy conservation problem has been developed. (Collins and Westwood 1991; Porter et al. 1991) The acoustic field computed by the PE model is divided by $(pc)^{1/2}$ (i.e., the square root of the impedance given by the product of density and sound speed) when each environmental change occurs. This dimensionally reduced field is matched at each range-step so that inaccuracies caused by changes in density and sound speed are reduced.

THE TEST CASE PROBLEM This test case is an upslope-downslope propagation problem that is an extension of the Acoustical Society of America’s (ASA) penetrable lossy wedge benchmark problem (Felsen 1990; Jensen and Ferla 1990). This case is designed to test how well the PE models conserve energy in a strongly range-dependent environment. The symmetry of the problem is such as to test the PE models for energy losses (and gains) on the upslope (and downslope) propagation. In Test Case 2 there are initially three trapped modes that propagate upslope. The depth at the shallowest point (25 m deep at a range of 3.5 km) was chosen because at that depth, no trapped modes exist. Thus, 3 trapped modes initially propagate (at range = 0), are stripped-out such that no trapped modes are propagating at range = 3.5 m,

CONSERVATION OF ENERGY IN RANGE-DEPENDENT PROPAGATION

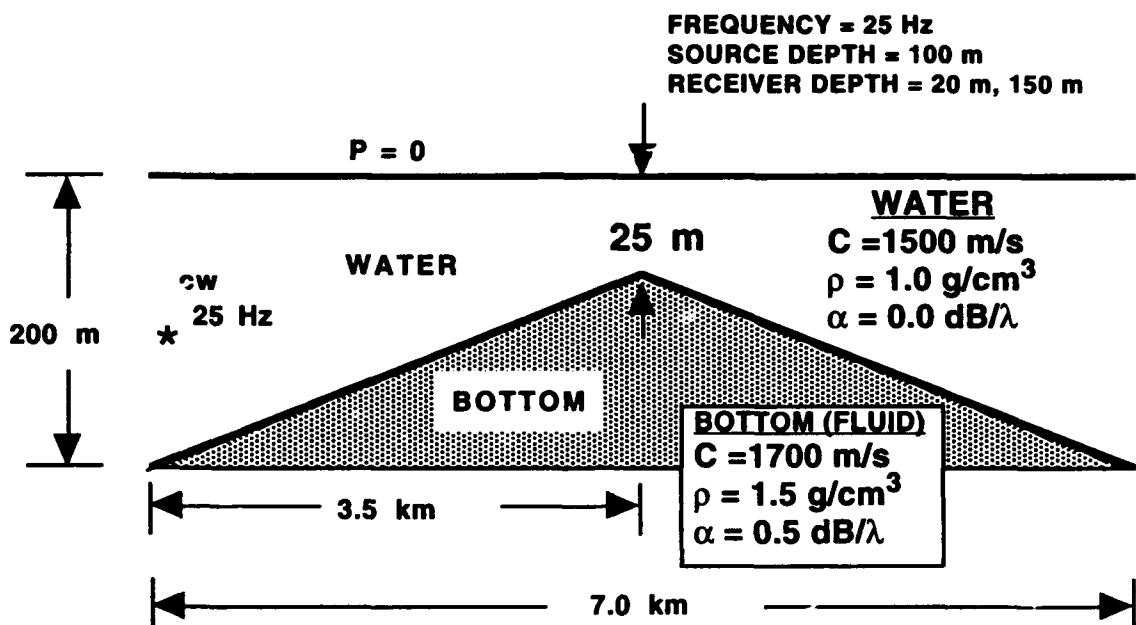


Fig. 2-2.0 Environment for Test Case 2.

and are reestablished in going downslope such that there are again three propagating modes (at range = 7.0 m).

Figure 2-2.0 defines the geometry and physical parameters of the problem. Two moving point (receiver) depths were selected for this test case. The first, at a depth of 20 m, passes just above the highest point of the ridge (by 5 m). The second receiver point, at a depth of 150 m, actually cuts through the ridge.

THE REFERENCE SOLUTION The reference solutions for this test case were generated by Richard B. Evans using his coupled mode model, COUPLE (Evans 1983; 1986). These results are shown in Figures 2-2.1 and 2-2.2 and labeled as "Ref.: COUPLE." The COUPLE model solves the nonhomogeneous Helmholtz equation (for the acoustic pressure due to a point source on the axis) in the 2-D cylindrically symmetric environment whose radial cross section is shown in Fig. 2-2.0. (Implicit in this description is the fact that solving the correct partial differential equation with the

PE Workshop II: Part 2 — Test Case Results

correct boundary conditions yields the unique solution.) COUPLE has been used to provide the “correct numerical solution” at an ASA special session devoted to the benchmark accuracy of ocean acoustic models (Felsen 1990; Jensen and Ferla 1990).

RESULTS AND DISCUSSION Figures 2–2.1 and 2–2.2 indicate that several of the PE models had difficulty propagating up-slope, especially near the apex (at 3.5 km). In the region over the apex and down-slope, only two of the PE models were able to exactly match the reference solutions. (Refer to plots (a) and (b) of Fig. 2–2.1 for the near surface receiver, and plots (a) and (b) of Fig. 2–2.2 for the deeper receiver.) The least restricted of the operational PE models, MIPE, compared favorably to the reference solution (refer to plot (c) of Fig. 2–2.1 for the near-surface receiver and plot (c) of Fig. 2–2.2 for the deeper receiver.) The other operational models (NAVY STD PE and OPT) were constrained to their operational parameters and did not compare as favorably (refer to plots (d) and (g) of Fig. 2–2.1 and plots (d) and (f) of Fig. 2–2.2).

This Test Case produced another revision to the later version of the Navy Standard PE model. (Refer to the discussion in Test Case 1 for a review of the first revision.) In order to handle the shallow-water, sharp-density contrast at the apex of the wedge bottom (at range = 3.5 km), the Navy Standard PE model required a “density transition region length” of one-half of its usual operational value. This smaller value is now included as the default in the later version of the Navy Standard PE model. The plots from NAVY STD PE given in Figs. 2–2.1 and 2–2.2 are from the later version.

A discussion of other observations from Test Case 2 follows:

- The significance of the errors produced by the “violation of conservation of energy” can be illustrated by comparing Figs. 2.2.1(a) and 2.2.1(j) where the FEPE model with the “energy conservation fix” is plotted against a version of FEPE without the correction (labeled as NON EC FEPE). A similar illustration is given in Figs. 2–2.1(k) and 2–2.2(k) where the results from the coupled two-way COUPLE model (which does match both continuity conditions at vertical interfaces) is compared against the uncoupled one-way version of COUPLE (which matches only one continuity condition at vertical interfaces).
- In Fig. 2–2.1(j) the TL is too large in going upslope and too small in going downslope, with the greatest inaccuracy occurring at the apex (at range = 3.5 km), but the errors cancel one another at the base (i.e., at the downslope range of 7.0 km). The upslope-downslope errors thus tend to cancel such that the reference TL and the predicted TL actually coincide after 7.0 km. Such complete cancellation of errors can be expected only in ideally symmetric problems as Test Case 2.

In Figs. 2–2.1(i), and 2–2.2(h), the SACLANT version of IFDPE (referred to here as IFDPE SAC) does not have an “energy conservation fix” and as a result it does not

PE Workshop II: Part 2 — Test Case Results

match the reference solution. The same holds true for the IFDPE results shown in Figs. 2-2.1(f) and 2-2.2(e).

- Results from the FEPE, DREP, and DREPS PE models coincide with the reference solutions for both upper and lower receivers. These PE models use either the reduced pressure field technique or the two-way PE approach.
- The IFDPE SAC predicts ~3 dB more loss at range = 3.5 km than the reference solution indicates for the near surface receiver.
- The results from the two operationally configured split-step PE models (NAVY STD PE and OPT) show a significant error in the region around the apex (in the 2.4 to 4.0 km range). The MIPE model seems to “recover” in the downslope region and gives a reasonable fit to the reference solution. Recall that MIPE and NAVY STD PE essentially use the same solution techniques, but that the NAVY STD PE model is run in an operational mode (with fixed transform sizes) while the advanced version of the MIPE model was used with the best possible choices for parameters and with the knowledge of an expert who could choose the parameters to suit the physical situation. Thus, the comparisons of Navy Standard PE and MIPE are a measure of how well the operational PE model will perform in the field, and how well it might perform in the hands of a very experienced and knowledgeable operator.
- As might be expected, the results obtained from the IMPPE model (Fig. 2-2.1(e) and Fig. 2-2.2(i)) and the IFDPE model (Fig. 2-2.1(f) and Fig. 2-2.2(e)) are identical in their comparison to the reference solutions for both the upper and the lower receivers. (Recall that the IMPPE model is just the IFDPE model with an impedance boundary condition that replaces the customary IFDPE “deep false bottom termination” to the computational grid).
- The effect of the impedance on the “energy conservation” can also be seen in Fig. 2-2.2 where some of the PE models show significant disagreement with the reference solution after the receiver crosses the interface from water into the sediment.

After Test Case 2 was completed, Ed Chaika of the AEAS program office inquired about runtime versus accuracy for the R&D PE models, i.e. would it be possible to use larger range-steps (Δr), larger grid separations (Δz), etc., but maintain accuracy such that the trade-off between runtime and accuracy could be highly favorable. Michael Collins of NRL graciously agreed to provide an example. During one of the workshop breaks he ran Test Case 2A on a VAX 8650 computer, adjusted the Δr and Δz to degrade the accuracy, and recorded the CPU runtimes. Column one of Table 2-2 refers to the particular plot shown in Fig. 2-2.3. Columns two and three give the corresponding Δr and Δz for each plot. Column four gives the runtime in seconds.

PE Workshop II: Part 2 — Test Case Results

Universal criteria for optimum selection of range and depth increments have not been established. The results shown in Table 2-2 are for a simple, short-range problem. Long-range propagation in complicated environments may produce entirely different results. The significance is that some R&D PE models could be used operationally without significantly reducing accuracy. Trade-offs between computational speed, portability, and accuracy are of major concern to the Navy and was one of the motivating factors for this workshop.

Table 2-2. Runtimes vs. Accuracy Parameters for Test Case 2A using FEPE

Figure	Δr (m)	Δz (m)	Runtime (sec)
2-2.3(a)	10	2	12.0
2-2.3(b)	20	4	3.0
2-2.3(c)	40	8	0.8
2-2.3(d)	80	16	0.2

SUMMARY The problems caused by not conserving energy (i.e., by not enforcing both continuity boundary conditions) have been significantly reduced by various methods incorporated into the PE models. Matching the fields after they have been reduced by $(pc)^{1/2}$ is one successful method. The two-way PE approach is another method which has proven successful. However, the difficulty still exists and is inherent in the PE marching method. Trade-offs in accuracy vs. runtimes can be made such that some PE models can give acceptable accuracy while performing at operational speed.

FURTHER READINGS IN PART 3 The reduced pressure field technique is discussed in the paper by Collins. The two-way PE method is discussed in the paper by Brooke and Thomson. Pertinent discussions on the energy conservation problem in the PE model can be found in several other papers in Part 3 of these proceedings.

- Brooke, Gary H., and David J. Thomson, "A Single-Scatter Formalism for Improving PE Calculations in Range-Dependent Media."
- Collins, Michael D., "Higher-Order, Energy-Conserving, Two-Way, and Elastic Parabolic Equations."
- Holmes, Eleanor S., and Laurie A. Gainey, "The Navy Standard Parabolic Equation Model, Broadband PE, and PE Workshop II."
- Jensen, Finn B., "PE Workshop II: Test Problem Solutions."
- Nghiem-Phu, Lan, Kevin B. Smith, and Fred D. Tappert, "FastPE, SlowPE, YourPE, MiPE: What are the Real Issues?"

PE Workshop II: Part 2 — Test Case Results

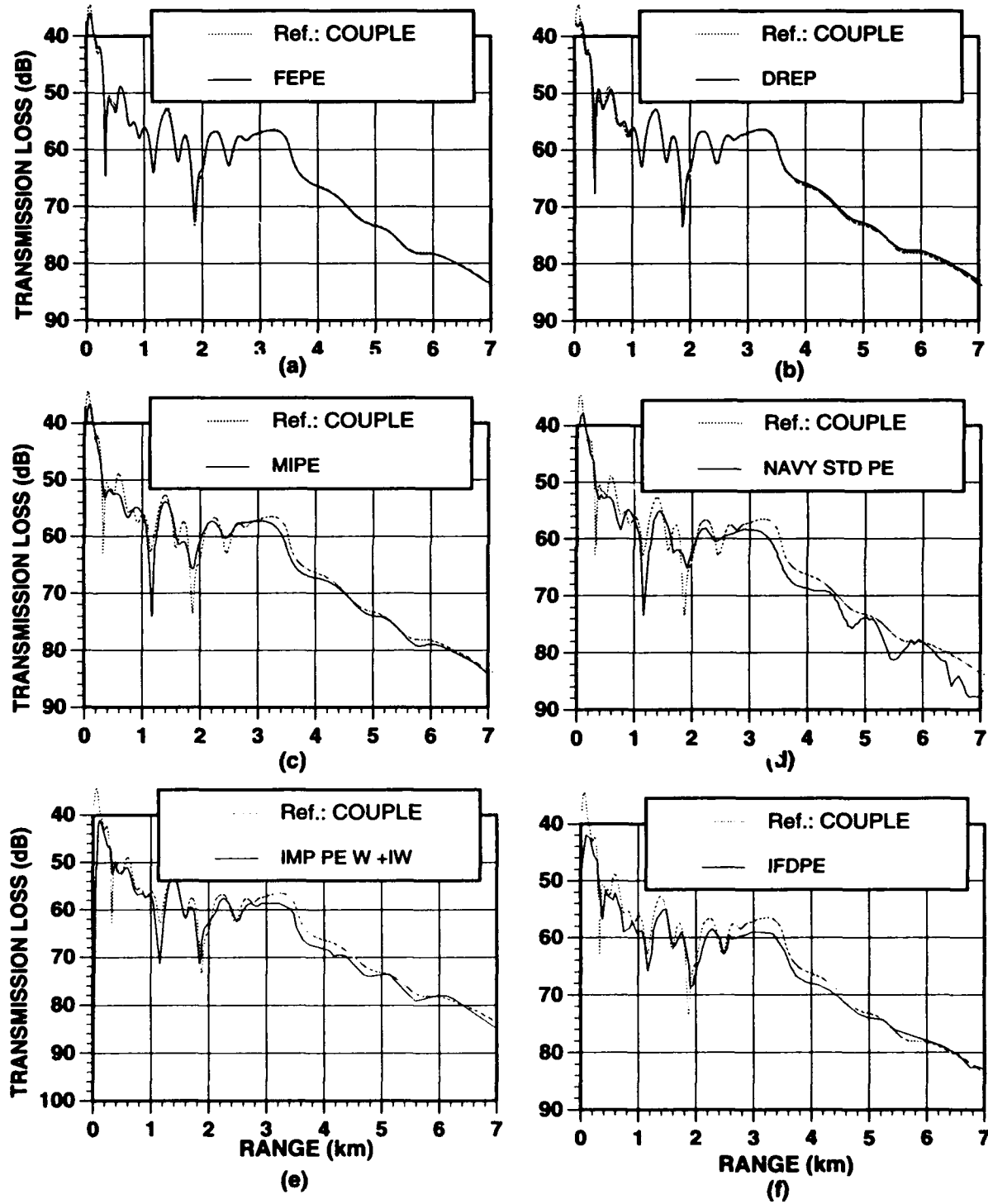


Fig. 2-2.1. Test Case 2A Results

PE Workshop II: Part 2 — Test Case Results

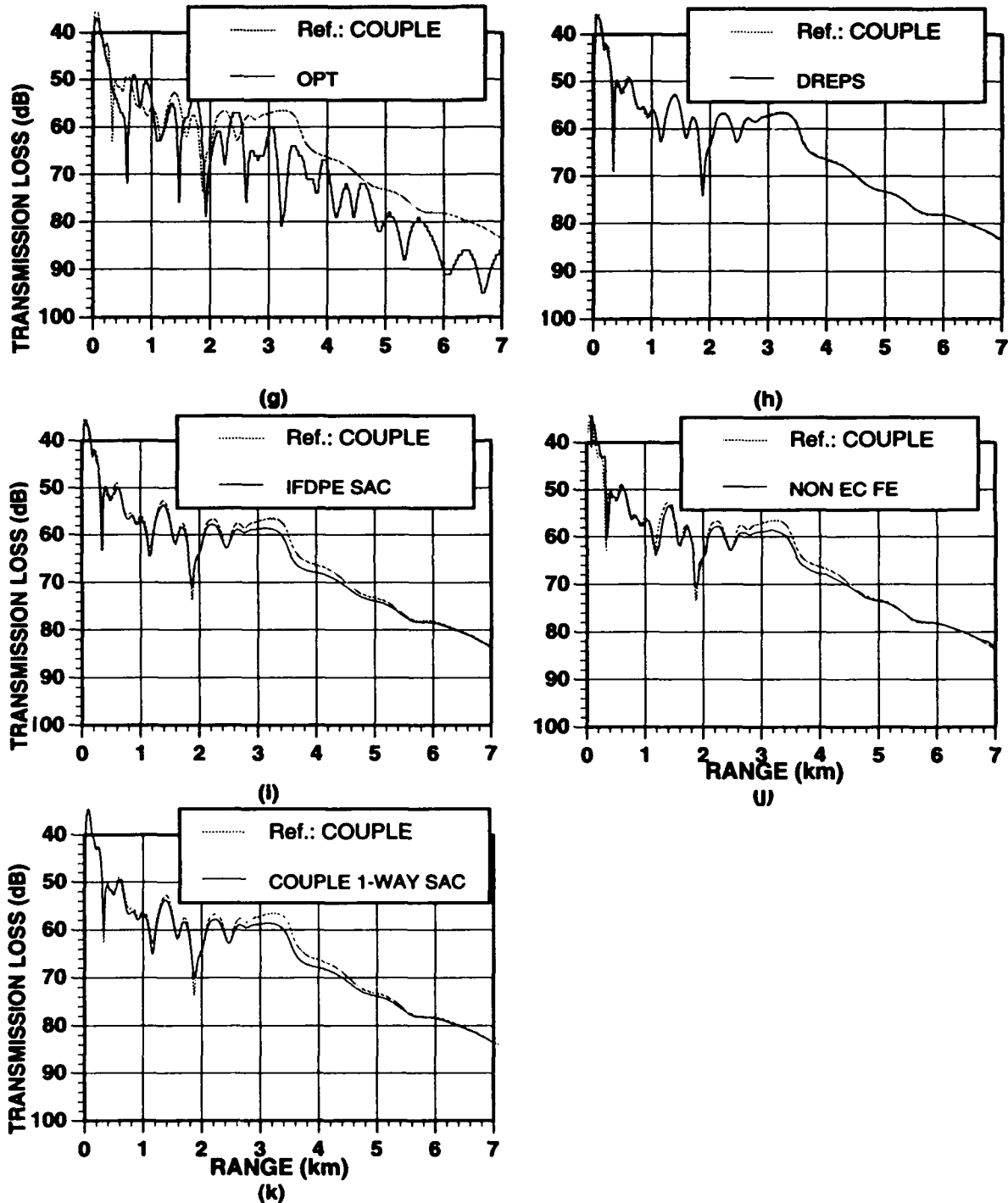


Fig. 2-2.1. Test Case 2A Results (Continued)

PE Workshop II: Part 2 — Test Case Results

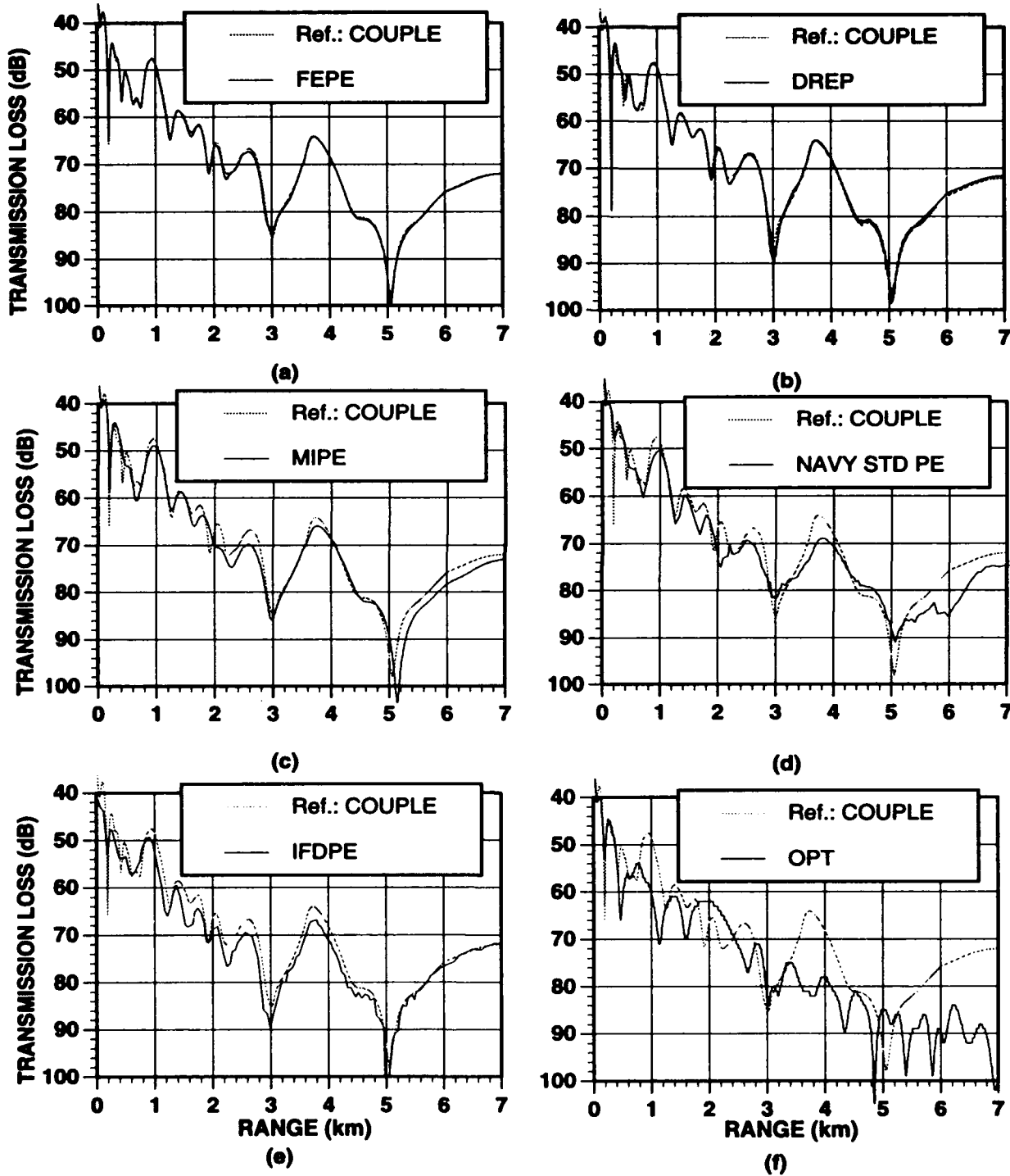


Fig. 2-2.2. Test Case 2B Results

PE Workshop II: Part 2 — Test Case Results

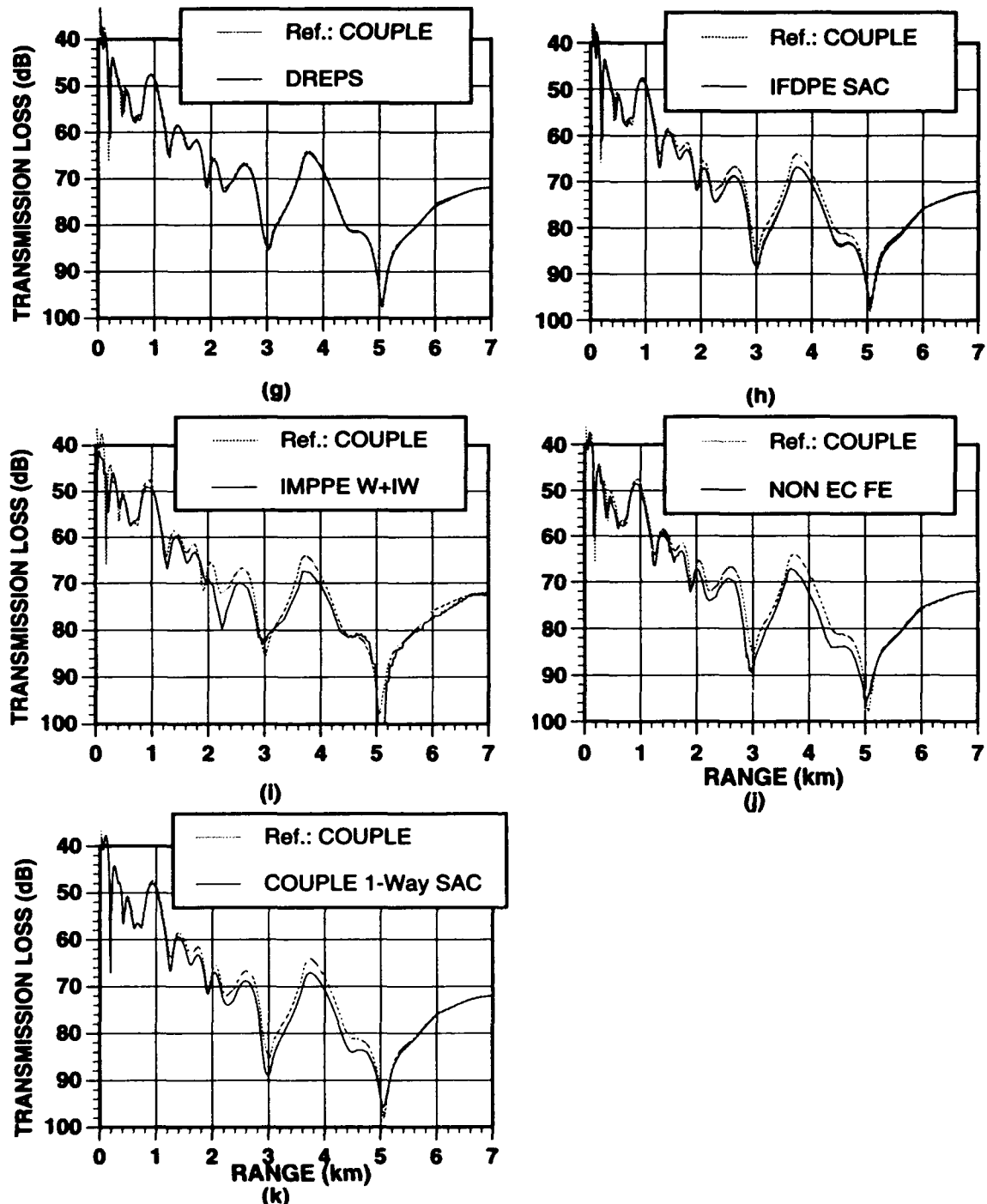


Fig. 2-2.2. Test Case 2B Results (Continued)

PE Workshop II: Part 2 — Test Case Results

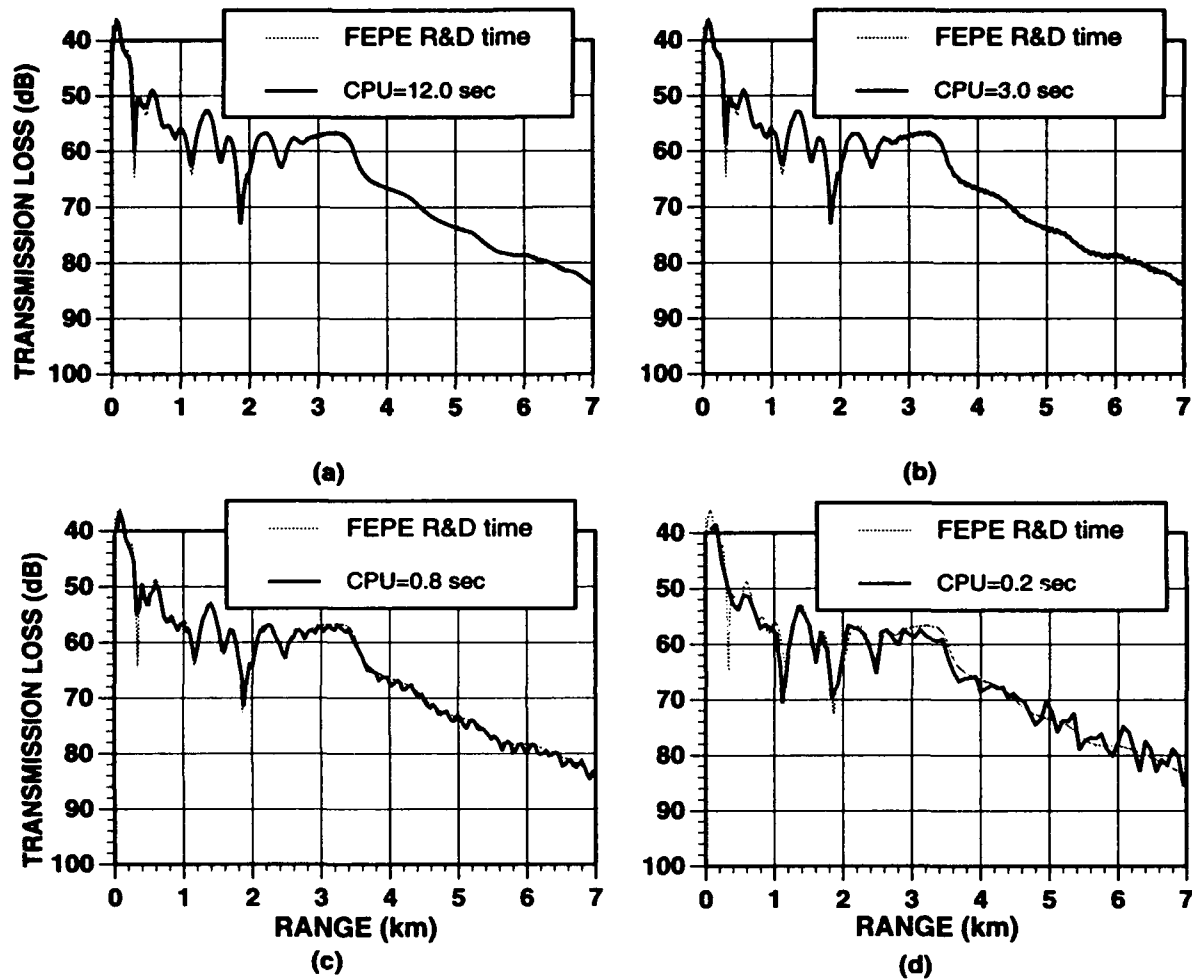


Fig. 2-2.3. Test Case 2A Results Speed vs. Accuracy

TEST CASE 3

Range-Dependent Shear Wave Propagation

OBJECTIVE Test the ability of PE models to accurately propagate the water-borne acoustic field over a range-dependent, lossy, ocean bottom with anelastic[†] properties (i.e., with shear wave speeds and shear wave attenuations).

BACKGROUND Recently, there has been strong interest in extending underwater acoustic models to include more realistic treatments of the ocean bottom, including anelastic media. There are very few ocean acoustic PE models that include either elastic or anelastic propagation. Until recently, those PE models that were applied in anelastic ocean-bottom regions treated the shear waves as an additional loss mechanism. There is both reason and experience to suggest that this is a viable alternative to actually incorporating anelasticity in the PE model. The reasoning goes as follows: When a water-borne acoustic (compressional) wave penetrates the ocean bottom, it can be partially converted into shear wave propagation which is then attenuated. Reverse conversion (ocean-bottom shear waves into water-borne compressional waves) can be relatively weak. Additionally, interface (Scholte) wave propagation along the shear-supporting water-bottom interface is evanescent and not easily detectable at vertical distances from the interface that are beyond a few wavelengths. All of this is generally true in forward propagation which is the type of propagation that underwater acoustic PE models are designed to handle. In some cases ocean acoustic propagation over ocean-bottoms that include shear waves and shear wave attenuations can be accurately represented as an additional loss factor in PE models that do not explicitly include shear waves. This, however, has not been universally verified. Furthermore, the effects of ocean-bottom shear waves on reverberation (acoustic backscatter) have not been quantified. Since backscattered acoustic fields are weak in magnitude, the loss due to shear conversion could be a significant factor.

THE TEST CASE PROBLEM With such motivation and the fortuitous occurrence that two anelastic PE models had recently been developed, Test Case 3 evolved. Test Case 3 is designed to test the ability of PE models to include lossy, anelastic media

[†] The American Geological Institute's *Glossary of Geology* defines *anelasticity* as the effect of attenuation of a seismic wave; it is symbolized by Q. 1/Q is the specific attenuation factor or specific dissipation function; it is the relative energy loss per cycle.

PE Workshop II: Part 2 — Test Case Results

effects. It uses the basic geometry of the ASA penetrable, lossy, wedge benchmark problem (Jensen and Ferla 1990). The only addition is the inclusion of shear wave speed and shear wave attenuation in the bottom.

The environment for this test case is shown in Fig. 2–3.0. In the water the sound speed is 1500 m/s, the density is 1 g/cm³, and there is no attenuation. In the anelastic bottom the compressional speed is 1700 m/s, the shear speed is 800 m/s, the density is 1.5 g/cm³, and both the compressional wave and shear wave attenuations are 0.5 dB/λ. The frequency is 25 Hz, the fixed point depth (source depth) is 100 m, and the moving point depths (receiver depths) are 30 m and 150 m.

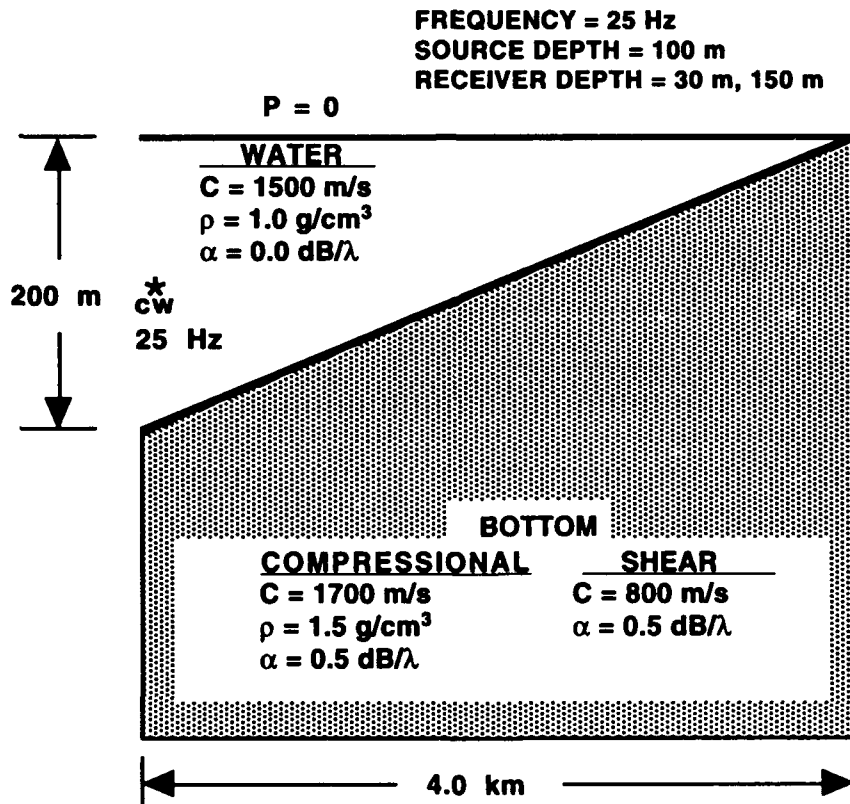


Fig. 2–3.0 Environment for Test Case 3.

THE REFERENCE SOLUTION The reference solution for this problem was generated by Stanley A. Chin-Bing using the SAFE model (Murphy and Chin-Bing

PE Workshop II: Part 2 — Test Case Results

1991; Chin-Bing and Murphy 1993a; 1993b). The SAFE model, like the COUPLE model, solves the nonhomogeneous Helmholtz equation for a 2-D axisymmetric environment; however, the SAFE model also accurately includes shear waves and shear wave attenuations. The SAFE model uses the finite-element solution method and provides accurate numerical predictions for 2-D range-dependent ocean and ocean-bottom seismoacoustic propagation and scattering. It has been accurately validated against the SAFARI model in range-independent shear-supporting scenarios (including Scholte interface wave interference) and against the COUPLE model in nonshear range-dependent scenarios. The SAFE model can accept any type of starting field as its initial boundary condition. A point source was used for this test case. Difficulty in obtaining sufficient computer memory precluded having the result for Test Case 3A in time for the workshop and for Test Case 3B prior to this report.

RESULTS AND DISCUSSION Figure 2–3.1 shows the reference solution together with results from each of the PE models that were applied to this test case.

The following is noted in regard to Test Case 3:

- There were two PE models that accurately propagated and converted shear wave energy: the FEPES model developed by Collins and the DREPS model developed by Brooke. Figure 2–3.1 shows that each of these PE models compares well with the reference solution and with each other. In Fig. 2–3.1(a) the FEPES model compares very well with the reference solution (from the SAFE model) and in Fig. 2–3.1(g) the DREPS model compares equally well with the reference solution. A direct comparison between FEPES and DREPS, shown in Fig. 2–3.1(i), indicates that the only two PE with shear models give nearly identical results for Test Case 3A. Such agreement among these three models (i.e., the two PE models and the reference model), with different solution techniques, gives confidence that the actual numerical solution to Test Case 3A has been obtained. While no reference solution to the deep receiver was provided, the FEPES and DREPS results for the deep receiver (shown in Figs. 2–3.2(a) and 2–3.2(b), respectively), compare favorably to each other, as is seen in Fig. 2–3.2(i).
- Results from three split-step models (NAVY STD PE, MIPE, and OPT) were also submitted for this test case. Each of these models treat shear waves as an added loss mechanism. Thus, if shear wave conversion is a significant factor in this propagation, treating the conversion just as an added loss would produce results different from that predicted by a model that accurately propagates anelastic energy. This is especially true for the deep receiver which is actually in the bottom for a large portion of the track. For the shallow receiver, MIPE gives a credible match to the reference solution, as is shown in Fig. 2–3.1(d). In the vicinity where the receiver crosses the water

sediment interface (~3.4 km) the MIPE curve begins to fall off too rapidly as compared with FEPES and DREPS. This excessive fall-off is even more evident in Fig. 2-3.2(c) for the deep receiver. NAVY STD PE seems to have underestimated the amount of loss that needs to be attributed to the shear mechanism since it shows less loss (in Figs. 2-3.1(d) and 2-3.2(e) for the shallow and deep receivers, respectively) than the other models. The OPT model appears to have made better use of the “effective shear loss” concept in that it gives a reasonable fit (in Fig. 2-3.1(f)) to the reference solution for the shallow receiver and a fair fit to the FEPES and DREPS results for the deep receiver (comparing Fig. 2-3.2(f) to Figs. 2-3.2(a) and 2-3.2(b), respectively).

- The approximation that shear waves can be treated as a simple loss mechanism breaks down when anelastic propagation becomes a very significant contributing factor. This is evident in Figure 2-3.2 which shows the results for the deep receiver.
- In Test Case 2 the “violation of conservation of energy” was due to only one continuity condition being matched by the marching solution PE models. This difficulty was resolved by employing an asymptotic correction whereby the marching acoustic field was divided by $(pc)^{1/2}$ when an environmental change occurred. This energy conserving method was used in the FEPE model (as compared with the NON EC FE model which is the FEPE model *without* this adjustment to the field). Another way of getting an improvement in results was to rotate the coordinate system such that the incline of the wedge “appeared” to the PE model as a flat, horizontal water-bottom interface. Then the problem appears as a horizontally stratified scenario and PE models have been shown to give very good results in such cases. Such an attempt was made in Test Case 3 to see if any improvement could be obtained by using a rotated environment; the FEPE ROT model is the FEPE model with the rotated environment and the FEPES ROT model is the FEPES model with the rotated environment. Comparisons of FEPE ROT and FEPES ROT with the reference solution (shown in Figs. 2-3.1(b) and 2-3.1(c) respectively) indicate that a rotation of the coordinate system does not affect (improve) the results. FEPE ROT still produces the nonshear, ASA penetrable lossy wedge benchmark solution and FEPES ROT still produces the FEPES result—these results are also observed in Figs. 2-3.2(g) and 2-3.2(h), respectively, when compared to Fig. 2-3.2(a) for the deep receiver in Test Case 2B. All of this suggest that failing to match both continuity conditions while marching out in range is not the primary reason for the differences between the shear PE models and the nonshear PE models in this test case. Rather, the differences can be attributed to not including the shear wave speeds and attenuations.

PE Workshop II: Part 2 — Test Case Results

- The results from the IFDPE model are shown in Fig. 2–3.2(h) for the shallow receiver and in Fig. 2–3.2(e) for the deep receiver. Since IFDPE does not include shear wave speeds and shear wave attenuations, and Ding Lee did not try to include an “effective shear loss,” the results for the IFDPE model for the shallow and deep receivers (Figs. 2–3.1(h) and 2–3.2(e), respectively) are the same as those for the ASA penetrable, lossy, benchmark wedge problem.

SUMMARY Two recently developed PE with shear models have demonstrated a high degree of accuracy when their results are compared to the reference solution and to each other. Nonshear PE models have demonstrated that an “effective shear loss” can be used to obtain an “acceptable” result to Test Case 3. Competing and complicated physical mechanisms, viz backscatter and nonconservation of energy, were shown not to be contributing factors in Test Case 3; thus, the results presented are a measure of how well the PE models can account for shear wave speeds and shear attenuations in a range-dependent scenario.

FURTHER READINGS IN PART 3 For more in-depth discussions on shear effects in PE models, refer to the following papers in Part 3 of these proceedings:

- Collins, Michael D., “Higher-Order, Energy-Conserving, Two-Way, and Elastic Parabolic Equations.”
- Holmes, Eleanor S., and Laurie A. Gainey, “The Navy Standard Parabolic Equation Model, Broadband PE, and PE Workshop II.”
- Jensen, Finn B., “PE Workshop II: Test Problem Solutions.”
- Lee, Ding, Martin H. Schultz, William L. Siegmann, Donald F. St. Mary, and George Botseas, “Applications of the IFD Model.”
- Nghiem-Phu, Lan, Kevin B. Smith, and Fred D. Tappert, “FastPE, SlowPE, YourPE, MiPE: What are the Real Issues?”
- Papadakis, John S., “Impedance Bottom Boundary Conditions for the Parabolic-Type Approximations in Underwater Acoustics.”

PE Workshop II: Part 2 — Test Case Results

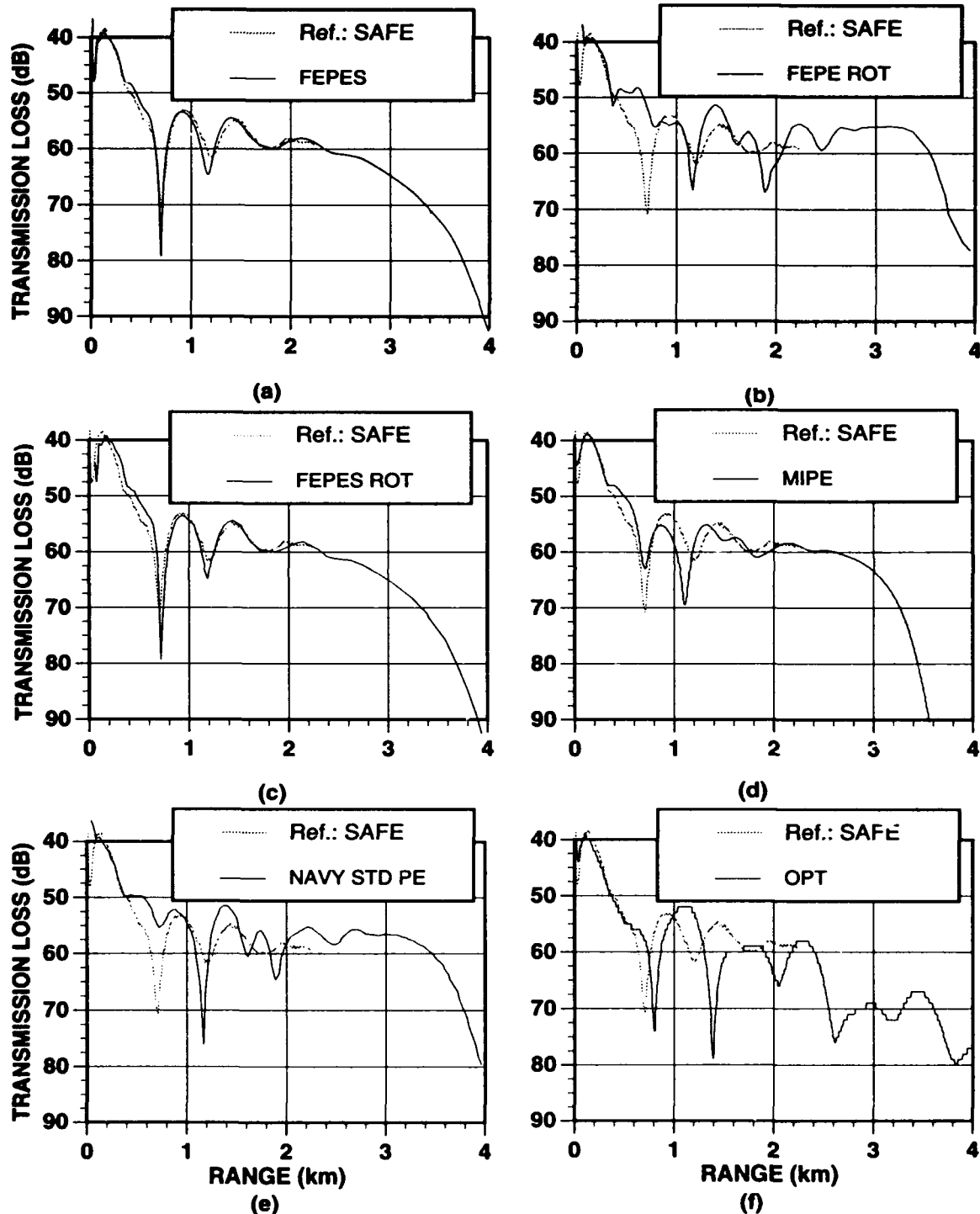


Fig. 2-3.1. Test Case 3A Results

PE Workshop II: Part 2 — Test Case Results

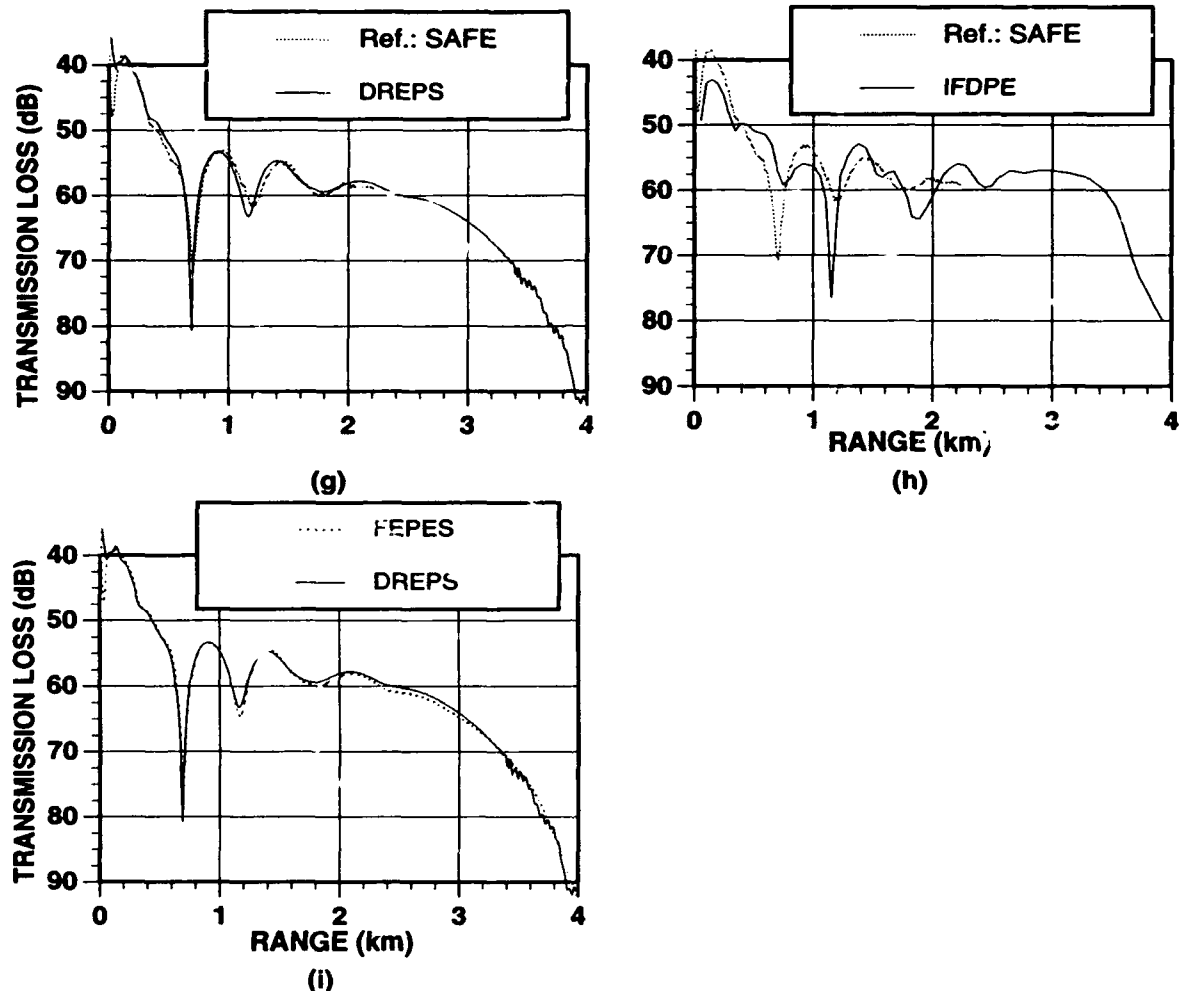


Fig. 2–3.1. Test Case 3A Results (Continued)

PE Workshop II: Part 2 — Test Case Results

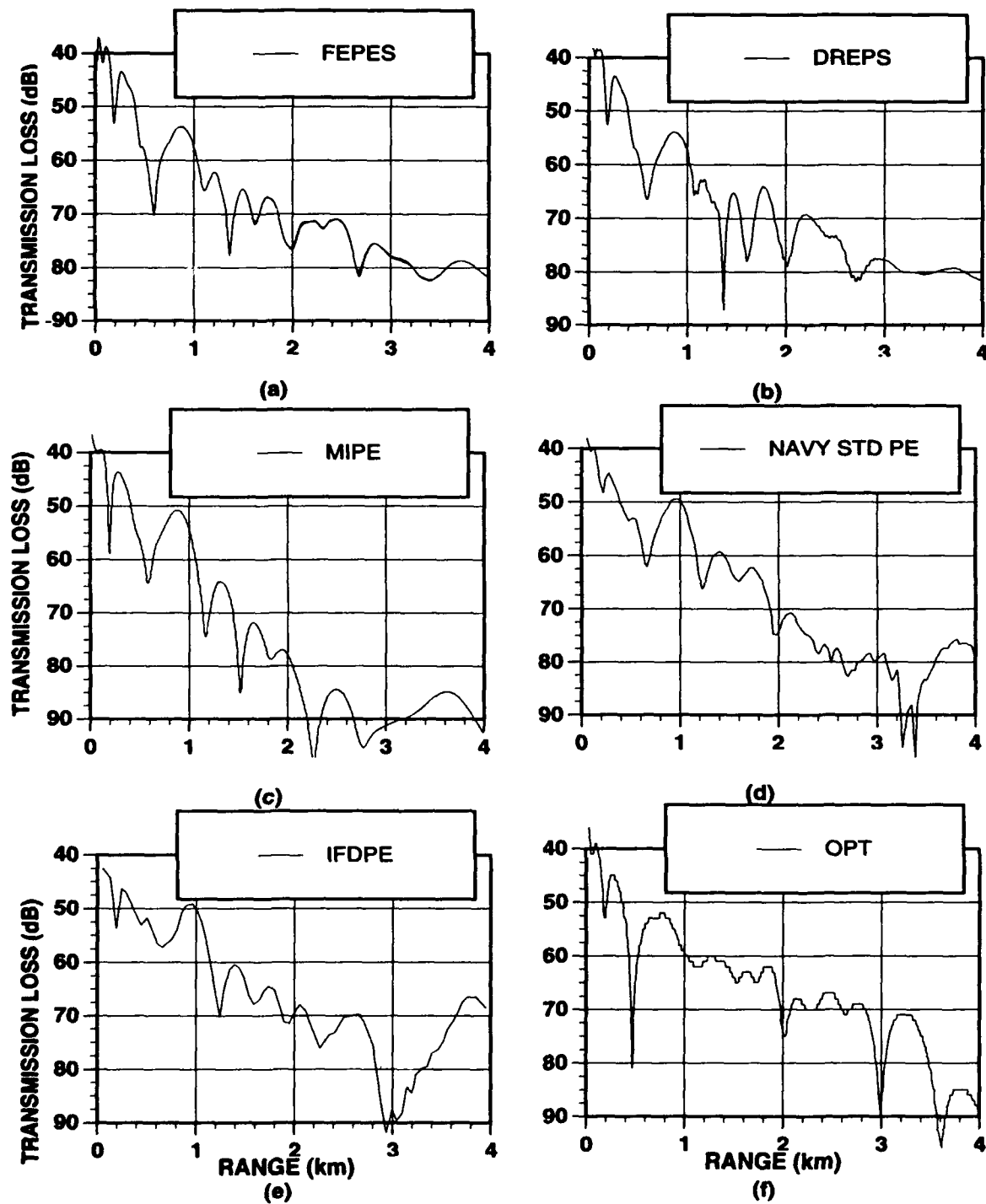


Fig. 2-3.2. Test Case 3B Results

PE Workshop II: Part 2 — Test Case Results

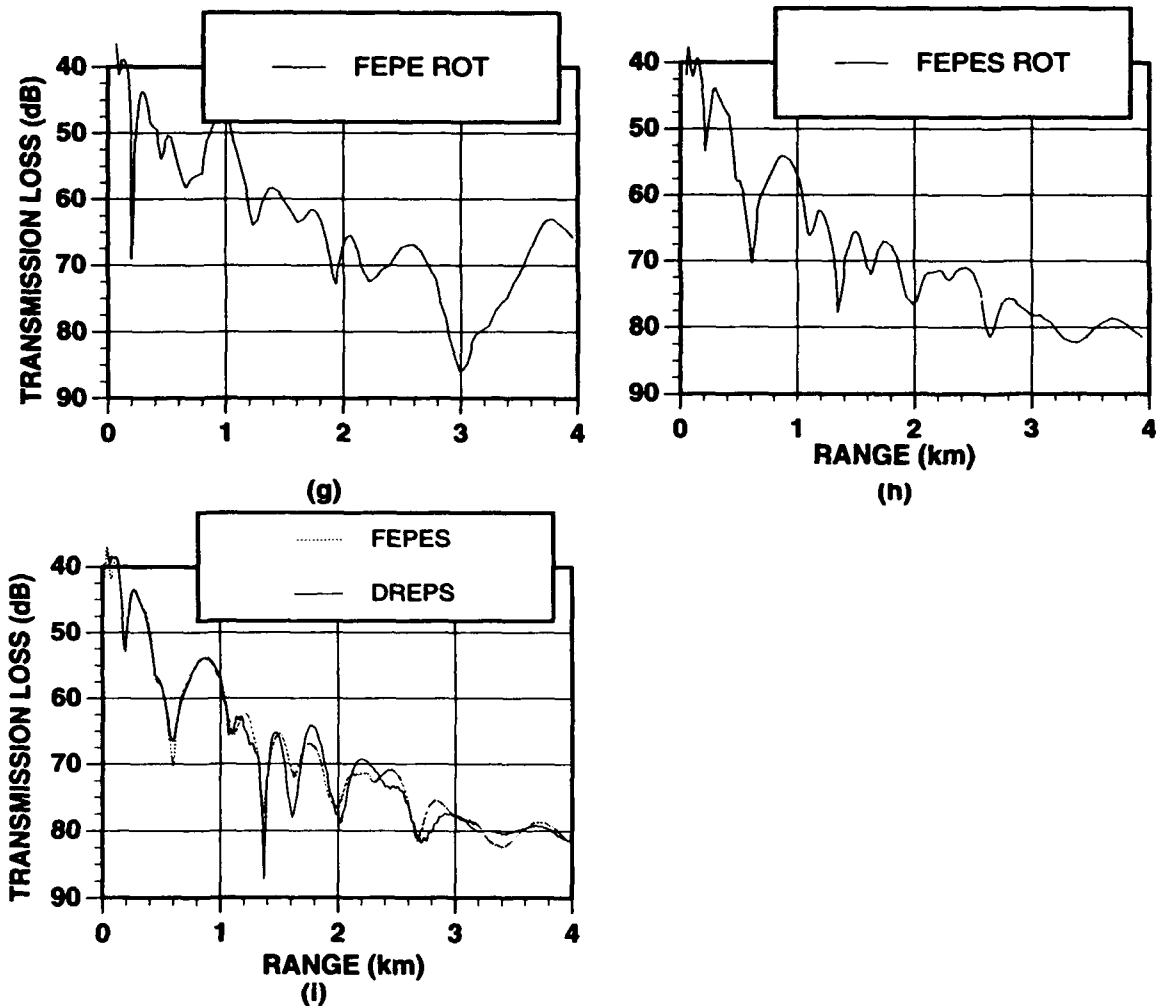


Fig. 2-3.2. Test Case 3B Results (Continued)

TEST CASE 4

Backscatter from a Waveguide Discontinuity

OBJECTIVE Test the ability of the different PE models to accurately calculate the backscattered acoustic field.

BACKGROUND In their general configurations PE models propagate the field only in one direction (forward) and thus do not include backscatter. However, PE models can be used to account for backscatter in a straightforward fashion. One method is to propagate the field to the scatterer via the PE model, modify the field by the appropriate reflection coefficient, and propagate the modified (scattered) field in the backward direction. The two resulting fields could then be added together if the total cw field was desired. In most cases, it is the back-propagated field alone that is sought.

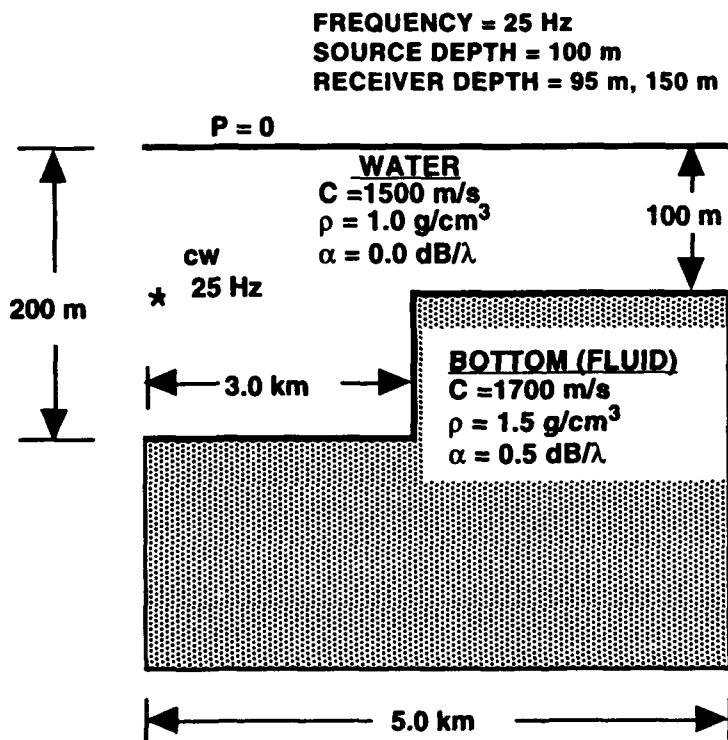


Fig. 2-4.0 Environment for Test Case 4.

PE Workshop II: Part 2 — Test Case Results

THE TEST CASE PROBLEM The environment to Test Case 4 is shown in Fig. 2-4.0. In the water column the sound speed is 1500 m/s, the density is 1 g/cm³, and there is no attenuation. In the fluid bottom the sound speed is 1700 m/s, the density is 1.5 g/cm³, and the attenuation is 0.5 dB/λ. The frequency of the point source is 25 Hz, the fixed point depth (source depth) is 100 m, and the moving point depths (receiver depths) are 95 m and 150 m.

THE REFERENCE SOLUTION The reference solution was produced by the COUPLE model. As discussed in Test Case 2, the COUPLE model solves the nonhomogeneous Helmholtz equation (for the acoustic pressure due to a point source on the axis) in the 2-D cylindrically symmetric environment whose radial cross section is shown in Fig. 2-4.0.

RESULTS AND DISCUSSION The reference solution and the PE models' results are shown for the shallow receiver in Fig. 2-4.2 and for the deep receiver in Fig. 2-4.3.

When backscatter is present the COUPLE model solution includes the backscattered and multiple scattered components. This is generally not the case for the PE models. Careful and thoughtful comparisons must be made between the reference solution and the PE solutions. The following discussion with the illustrations given in Fig. 2-4.1 should help to grasp the fundamental differences.

Figure 2-4.1 shows schematic diagrams depicting the outgoing acoustic field from a point source located on the vertical axis. The resulting backscattered field comes from the *step* discontinuity in the seafloor. Figure 2-4.1(a) shows the scenario that would apply to a PE model and Fig. 2-4.1(b) shows the scenario that would apply to 2-D axisymmetric models such as COUPLE. In Fig. 2-4.1(a) the PE model propagates the uncoupled outgoing field to the step region in the seafloor. Backscatter is calculated based on the single scatter approximation that locally matches pressure and velocity. The scattered field from the step seafloor is then back-propagated by the PE model (often using reciprocity). These are two separate applications of the PE model and each application produces a one-way propagating field.

A similar scenario would be modeled differently by 2-D axisymmetric acoustic and seismoacoustic models, such as COUPLE and SAFE. These models solve the nonhomogeneous Helmholtz equation with correct boundary conditions. They globally match pressure and velocity and consequently allow for multiple scattering. The outgoing, backscattered, and multiple scattered fields are coupled together and cannot be readily separated. These models actually model the scenario shown in Fig. 2-4.1(b) so that the 2-D backscattered fields at all azimuthal angles are "focussed"

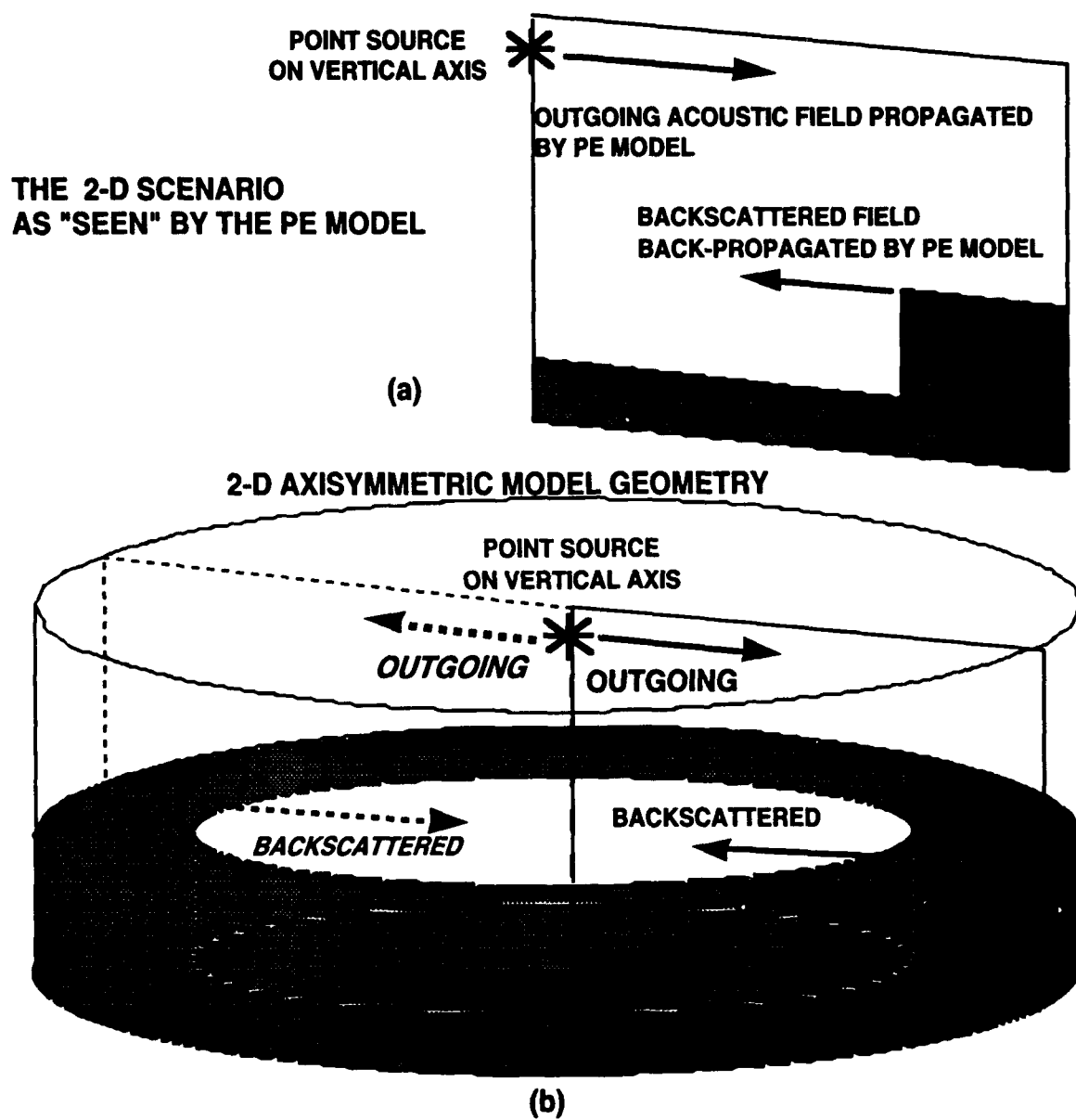


Fig. 2–4.1 2-D Axisymmetric Environment. Schematic diagrams depicting the outgoing acoustic field from a point source (located on the vertical axis) and the resulting backscattered field from the step discontinuity in the seafloor—as modeled by a PE model (shown in (a)), and by a 2-D axisymmetric model such as COUPLE (shown in (b)).

PE Workshop II: Part 2 — Test Case Results

onto the vertical axis located at the origin. (There are ways to obviate this situation and obtain one-way fields (outgoing and incoming waves) using these models. Note however, that in a range-dependent case the one-way "field" or one-way "wave" obtained from models such as COUPLE and SAFE does not necessarily correspond to the total one-way propagating energy—a point better left to the literature (Sluijter 1970).)

It should be noted that the 2-D axisymmetric geometry shown in Fig. 2-4.1(b) is not the physical situation that usually exists in underwater acoustics; the situation that does generally occur is represented by Fig. 2-4.1(a). Since PE models give an uncoupled, one-way range-dependent solution, they can straightforwardly be used to solve the physical situations represented in Fig. 2-4.1.

- Collins used his FEPE model to model a horizontal line-source thus avoiding any confusion caused by the 2-D axisymmetric interpretation of the test problem. He also provided the corresponding reference solution using the COUPLE model with a horizontal line-source (designated as "COUPLE-L" in Fig. 2-4.2). (The remaining participants used the point source assumption. Thus, Collins' results are approximately 30 dB above their reference solutions since the line-source assumption does not reproduce the cylindrical spreading exhibited in the 2-D axisymmetric point-source COUPLE model.)
- Jensen provided one-way reference results using a point source and the single-scatter approximation in the COUPLE model. (All designations "(out)" refer to the field propagating out—away from the source; all designations "(back)" refer to the backscattered field propagating back—toward the source. Thus, the Jensen plot of the one-way field propagating out (from the point source) is designated as "COUPLE SAC (out)" and the field propagating back (toward the source) is designated as "COUPLE SAC (back)." "COUPLE SAC (two-way)" refers to the total field—coupled outgoing and backscattered fields—as calculated by Jensen using the COUPLE model.)
- The DREP PE solution, which uses the single scatter approximation, matches the reference solution, even in the calculation of the incoming waves. The single-scatter approximation is apparently a simple way to eliminate the standing waves in the basin which occur because of multiple scattering from the 2-D axisymmetric step discontinuity.
- The MIPE operational PE model also matches the reference solution, indicating that split-step PE models can also be used to accurately predict the backscattered field.

- The NAVY STD PE model is not operationally configured to include backscatter. Thus, the NAVY STD PE results shown for Test Case 4 are the result of ingenious application by its custodians.
- Because of the various ways of computing and displaying the backscattered fields and the total fields, a review of the appropriate papers given in Part 3 is highly recommended before attempting to compare results given in Figs. 2-4.2 and 2-4.3 for the various PE models.

SUMMARY Prior to this workshop the ocean acoustics PE models were virtually never used for backscatter calculations. However, the results shown in Test Case 4 indicate that the PE models can be used to provide accurate calculations of backscatter.

The methods employed to obtain these accurate backscatter calculations were originated by the expert users rather than being a feature included in the PE models—thus, the average user can not expect to simply run a PE model and obtain backscatter calculations. The technique employed by the workshop contributors could be described as a “multiple forward propagation, localized single backscatter” approach. It fits well into the PE marching scheme and will undoubtedly become a part of future PE model development.

FURTHER READINGS IN PART 3 For more in-depth discussions on how to include backscatter effects into PE models, refer to the following papers in Part 3 of these proceedings:

- Brooke, Gary H., and David J. Thomson, “A Single-Scatter Formalism for Improving PE Calculations in Range-Dependent Media.”
- Collins, Michael D., “Higher-Order, Energy-Conserving, Two-Way, and Elastic Parabolic Equations.”
- Holmes, Eleanor S., and Laurie A. Gainey, “The Navy Standard Parabolic Equation Model, Broadband PE, and PE Workshop II.”
- Jensen, Finn B., “PE Workshop II: Test Problem Solutions.”
- Lee, Ding, Martin H. Schultz, William L. Siegmann, Donald F. St. Mary, and George Botseas, “Applications of the IFD Model.”
- Nghiem-Phu, Lan, Kevin B. Smith, and Fred D. Tappert, “FastPE, SlowPE, YourPE, MiPE: What are the Real Issues?”

PE Workshop II: Part 2 — Test Case Results

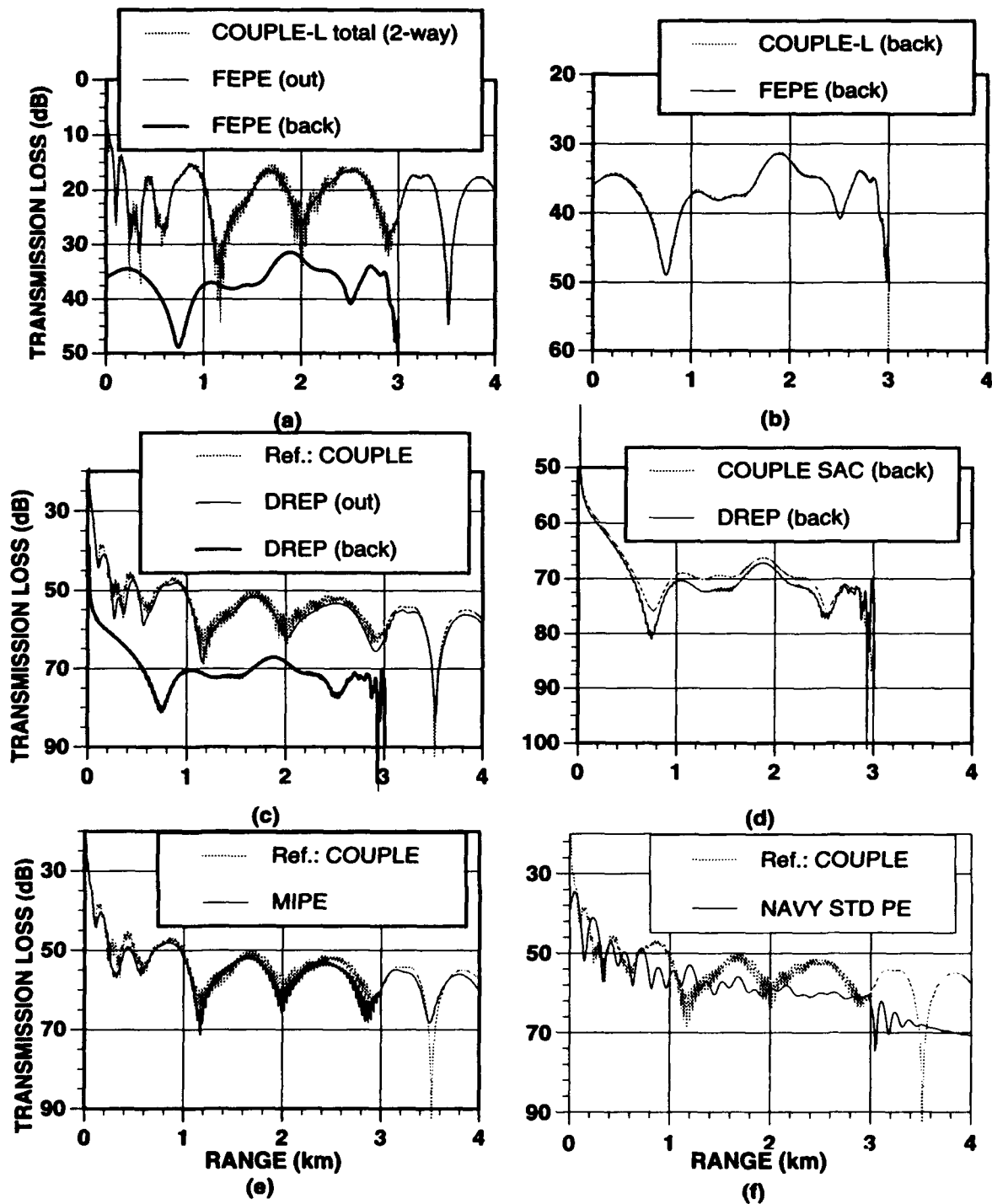


Fig. 2-4.2. Test Case 4A Results

PE Workshop II: Part 2 — Test Case Results

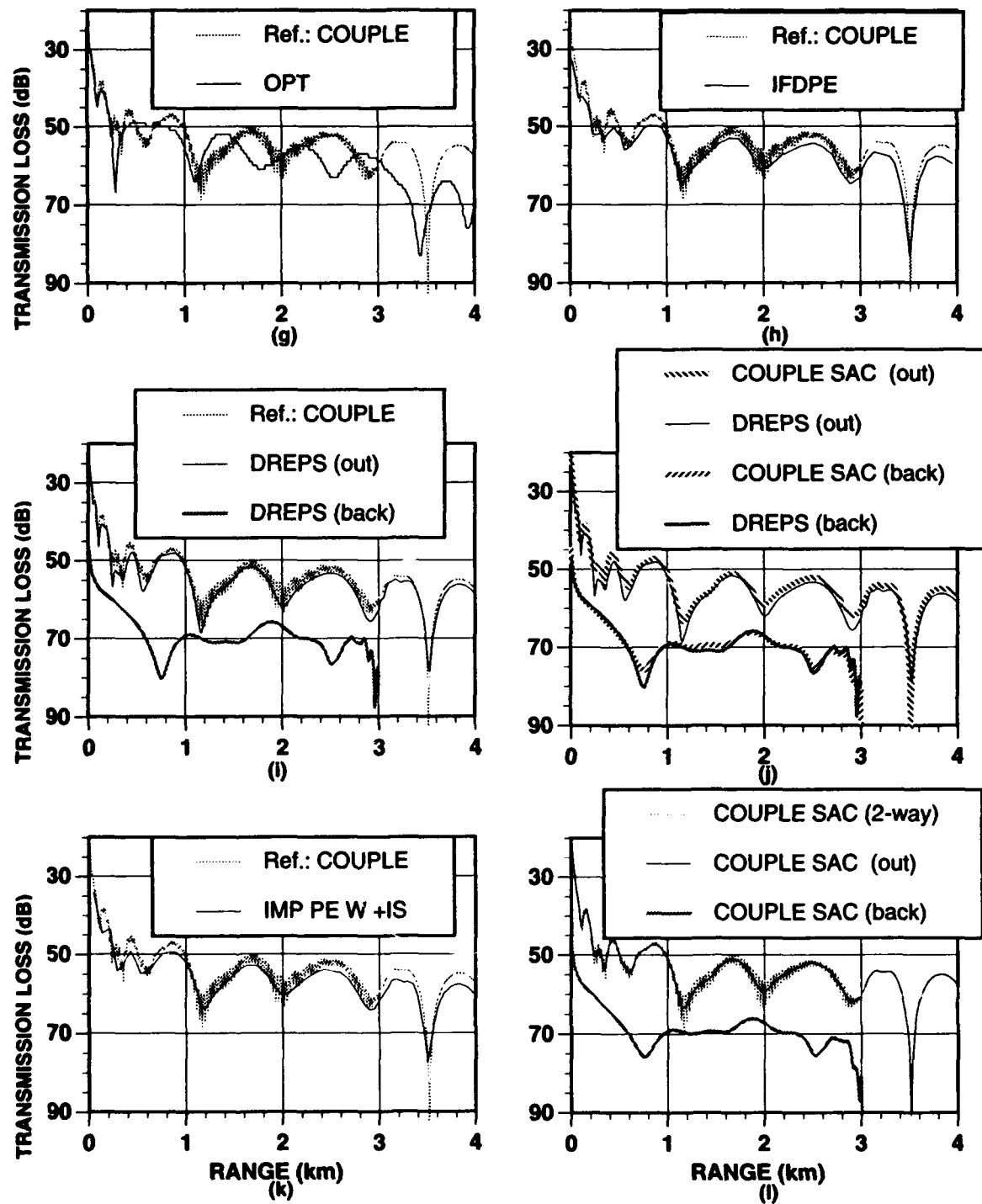


Fig. 2-4.2. Test Case 4A Results (Continued)

PE Workshop II: Part 2 — Test Case Results

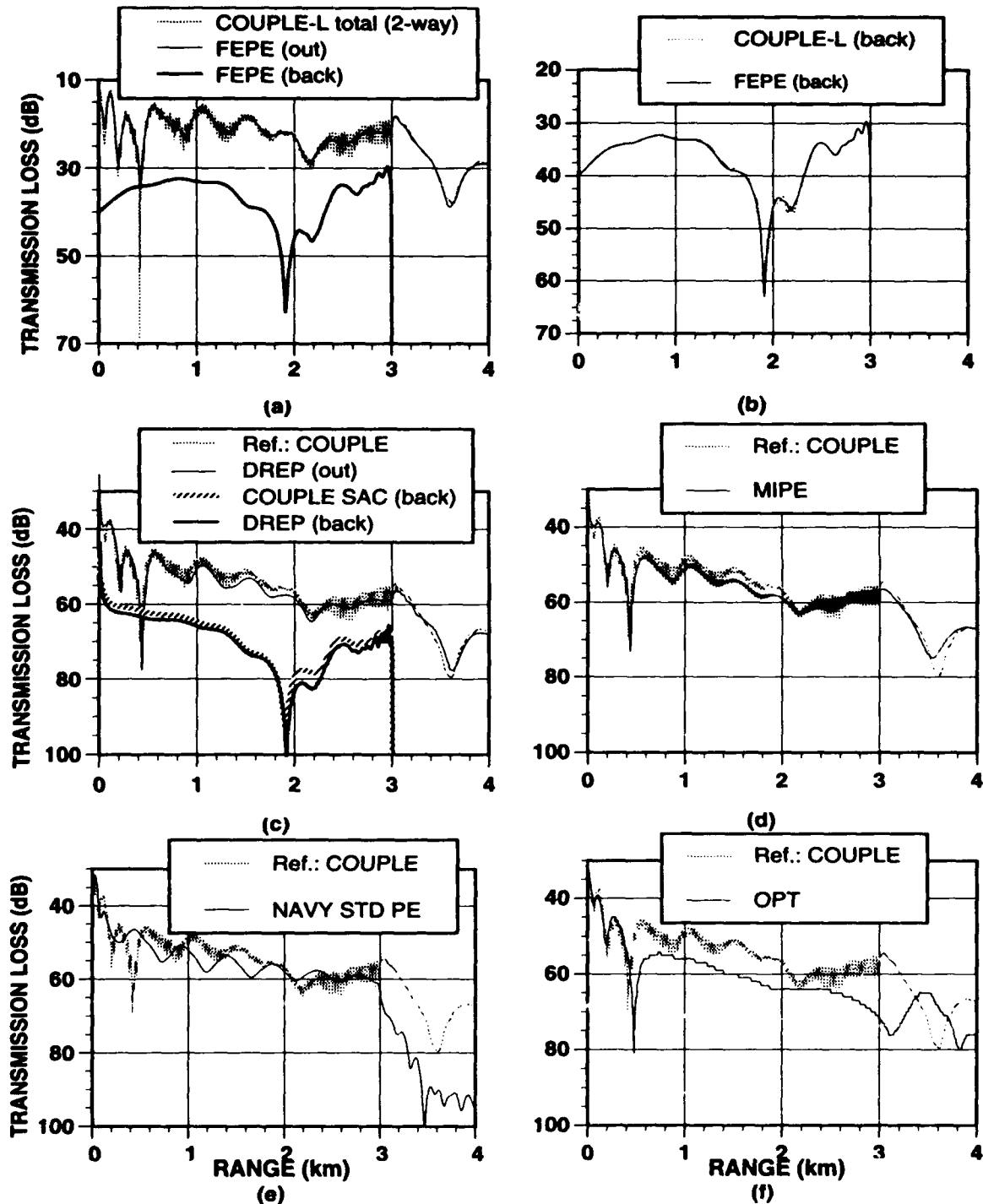


Fig. 2-4.3. Test Case 4B Results

PE Workshop II: Part 2 — Test Case Results

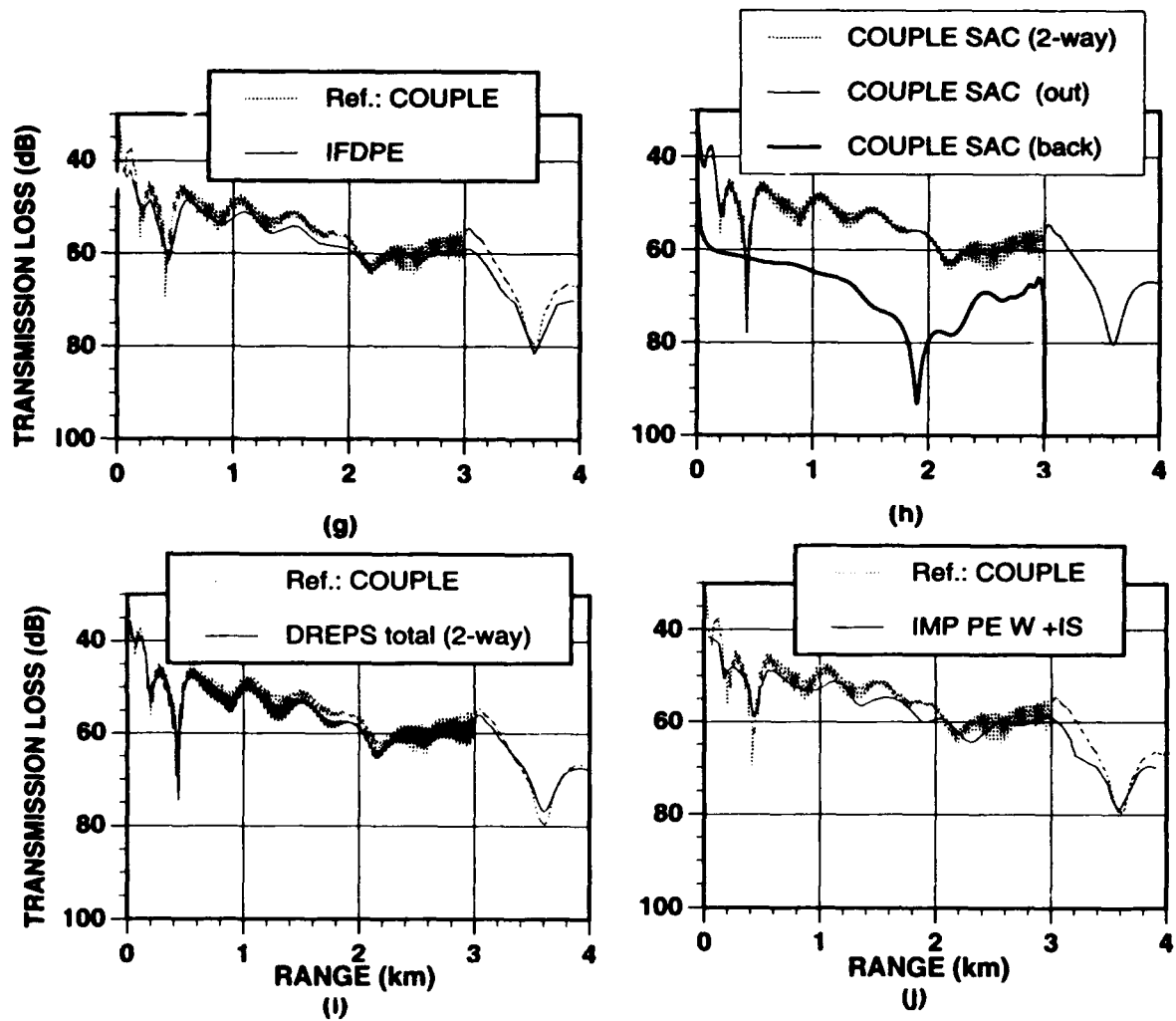


Fig. 2-4.3. Test Case 4B Results (Continued)

TEST CASE 5

Propagation in a Constantly Changing Environment

OBJECTIVE Accurately propagate the acoustic field through a region of constantly changing environmental parameters.

BACKGROUND This test case is designed to test the ability of underwater PE propagation models (and model users) in handling a water-borne sound speed that varies linearly in range while the bathymetry and sediment layer depths also vary linearly in range. Variations in the water-borne sound speed over a 2-km range (from 0.5 km to 2.5 km) rise linearly from 1500 m/s to 1540 m/s (i.e., a slope of $+1.14576^\circ$) while variations in the ocean-bottom depth and sediment layer thickness fall linearly from 200 m to 400 m, and 400 m to 600 m, respectively, over the same 2-km range (i.e., a slope of -5.71059° for each). Thus the rate of variation is different between the continually changing sound speeds and the corresponding continually changing bathymetry and sediment depths.

Ideally any PE model would be given a new sound speed profile and precise bathymetric depth for each range step (Δr) it makes, and it would take small enough steps so as to properly include the linearly varying effects of sound speed and bathymetry; the model would also use a grid sufficiently small in depth (i.e., the distance (Δz) between nodes) so as to properly include the linearly varying effects.

This test case required some ingenuity on the part of some of the model users since inclusion of the continuously changing environment into their models was not a trivial task—most, if not all, of the basic R&D PE models do not access data bases or data base generators; the user generally enters data into the model via a user-created input file. This input method is usually sufficient for the study of research oriented problems where the choice of a pertinent, but simple, environment allows isolation and understanding of the physical mechanisms. However, in a realistic ocean acoustics scenario, the situation posed in Test Case 5 is more likely to be encountered.

THE TEST CASE PROBLEM The environmental parameters for Test Case 5 are given in Fig. 2-5.0. The sound speeds, bathymetries, and sediment layer depths are constant in the regions before and after the linearly varying region. The total ocean bottom consists of two layers: the first bottom layer (i.e., the sediment) is a constant 200 m thick and parallels the contour of the water/sediment interface; the second

PE Workshop II: Part 2 — Test Case Results

bottom layer (i.e., the subbottom) is a homogeneous fluid half-space. The pertinent physical parameters of these two bottom layers are constant throughout the entire range of 10 km and are as follows: the sediment layer sound speed is 1700 m/s, the density is 1.5 g/cm³, and the attenuation is 0.5 dB/λ; the subbottom fluid half-space has a sound speed of 1900 m/s, the density is 3.0 g/cm³, and the attenuation is 0.1 dB/λ. The sound speed structure in the water is a constant 1500 m/s out to a range of 0.5 km and remains a constant 1540 m/s from 2.5 km out to a range of 10.0 km. Throughout the 10 km range the density of the water is 1 g/cm³ with no attenuation. The frequency is 25 Hz, the fixed point depth (source depth) is 100 m, and the moving point depths (receiver depths) are 30 m, 150 m and 250 m.

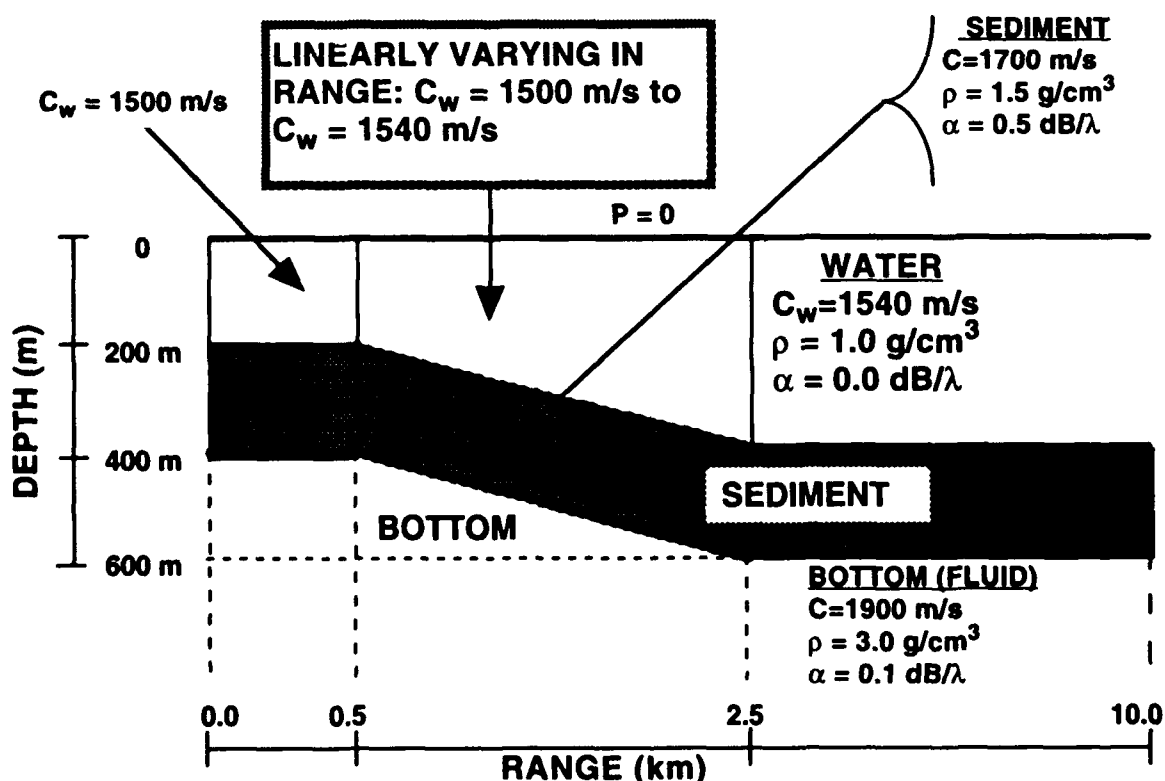


Fig. 2-5.0 Environment for Test Case 5.

THE REFERENCE SOLUTION Test Case 5 proved to be a formidable challenge to both the contributors and the PE Workshop II organizing committee. The COUPLE model solves only a two-layer problem and therefore could not be used to obtain a reference solution. There are some finite-element models (including the SAFE model) that can adjust the nodes on its grid to lie along the constantly varying bathymetries and include different environmental and acoustic parameter values at each of its nodes. The entry of such a volume of data is not trivial for either the PE models or the finite-element model that was to be used to provide the reference solution. Time constraints prior to and following the workshop prevented the generation and validation of a reference solution.

RESULTS AND DISCUSSION Model results for this test case were submitted from three of the finite-difference PE models (DREP, IFDPE, and IMPPE models) and three of the split-step PE models (NAVY STD PE, MIPE, and OPT). Results for the three receiver depths, 30 m, 150 m, and 250 m are shown in Figs. 2-5.1, 2-5.2, and 2-5.3, respectively.

A visual comparison of the plots in Figs. 2-5.1, 2-5.2, and 2-5.3 indicate that some differences exist between the PE models' predictions, in particular between the collective predictions of the R&D models and the operational PE models. This could be due to a number of reasons:

- The choice of optimum grid size (Δr , Δz) is important so that the sloping water-sediment and sediment-bottom interfaces are adequately represented. In the case of the MIPE model, the workshop contributor refined the PE grid until he had achieved a stable solution. He then maintained that grid size while he varied the "mixing lengths" that are used to smoothly join the index of refraction and density discontinuities. He used this approach on all of the test cases. But, in the case of Test Cases 5 and 6, he wrote a special code to handle the extra layers and additional mixing length. These additions apparently were beneficial judging from the similarity in the MIPE results with the R&D models' results.
- As noted, the selection of the mixing length is very important in the split-step PE models. The NAVY STD PE and OPT models were run under operational conditions and did not have the extra layers and mixing length that the MIPE model had.
- The method of interpolating between the sound speed profiles can be very important. The NAVY STD PE model was given new interpolated data at each range step taken. This interpolated data was generated by a program that performs triangular interpolation between profiles. These interpolated profiles were then used in the Navy Standard PE model's alternate sound speed file to provide updated data at each range step taken by the model. This is different from the way the OPTAMAS system

interpolates between sound speed profiles. OPT uses a linear interpolation of sound speed profiles, both in range and depth. This has the advantage of no discontinuities in the sound speed profile, but is not always the best way to interpolate.

- Many operational PE models use data obtained from a massive data base and data base generator; the PE model then automatically accesses this data base according to predetermined rules that make trade-offs between maximum grid (or transform) size, required accuracy, runtime, etc. This allows ease of application and operation but suffers from the rigid methodology (constraints) imposed on the operational models' access to new data. Thus, in a constantly changing environment such as that defined in Test Case 5, operational constraints on the PE model can limit the amount of data allowed to the PE model, resulting in significant errors in the model's predictions.
- R&D PE models usually have no data bases from which to extract environmental data. The data files used by these PE models are generally created by the user, employing a "hands-on" approach. Therefore, continual updating of data requires that the user write a data generator for his model or build a massive data file. There is obvious reluctance to do either, and this is reflected in the fact that, although this was the one test case problem that all of the participants might have solved, only about half of the workshop participants chose to work this problem.

SUMMARY Accurate physics, stable numerical algorithms, and fast computational speed do not guarantee reliable PE model predictions. Accurate environmental data bases must exist, and a methodology established for efficiently transferring and using this data in the model so that the environment is neither undersampled (which will result in erroneous predictions) or oversampled (which will result in wasted computational resources).

The results from those contributors that did work Test Case 5 are in fair agreement. The Navy Standard PE model seems to have deviated the most in its predictions and the MIPE model tends to follow the trend set by the R&D models. Apparently a major item for discussion in the near future will be the high resolution of the environmental data required by the acoustic models, and the consequences (expressed quantitatively) of not having such high resolution environmental data.

FURTHER READINGS IN PART 3 The following two papers on the operational models discuss some of the parameters sizes used in this test case:

- Holmes, Eleanor S., and Laurie A. Gainey, "The Navy Standard Parabolic Equation Model, Broadband PE, and PE Workshop II."
- Nghiem-Phu, Lan, Kevin B. Smith, and Fred D. Tappert, "FastPE, SlowPE, YourPE, MiPE: What are the Real Issues?"

PE Workshop II: Part 2 — Test Case Results

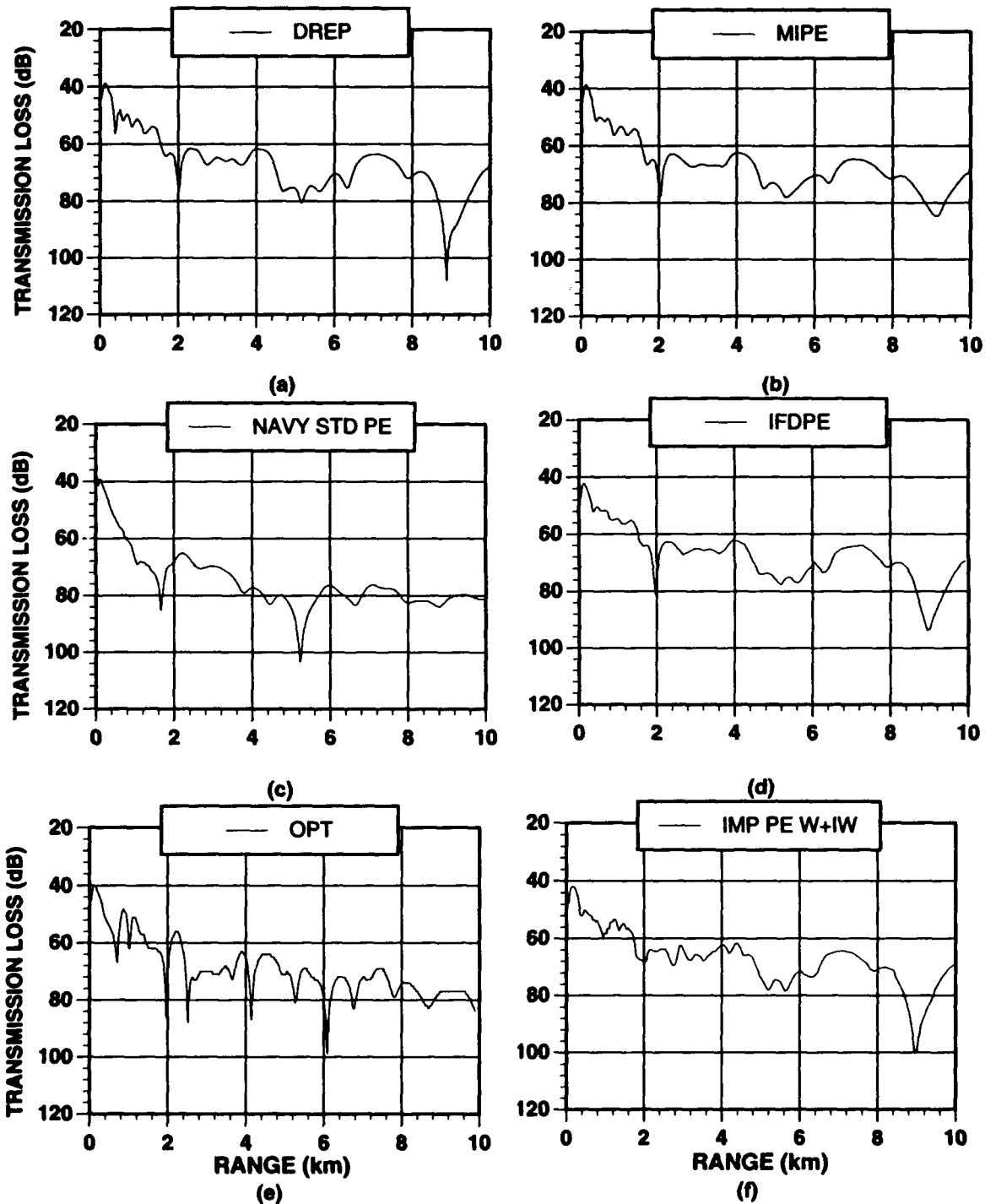


Fig. 2-5.1. Test Case 5A Results

PE Workshop II: Part 2 — Test Case Results

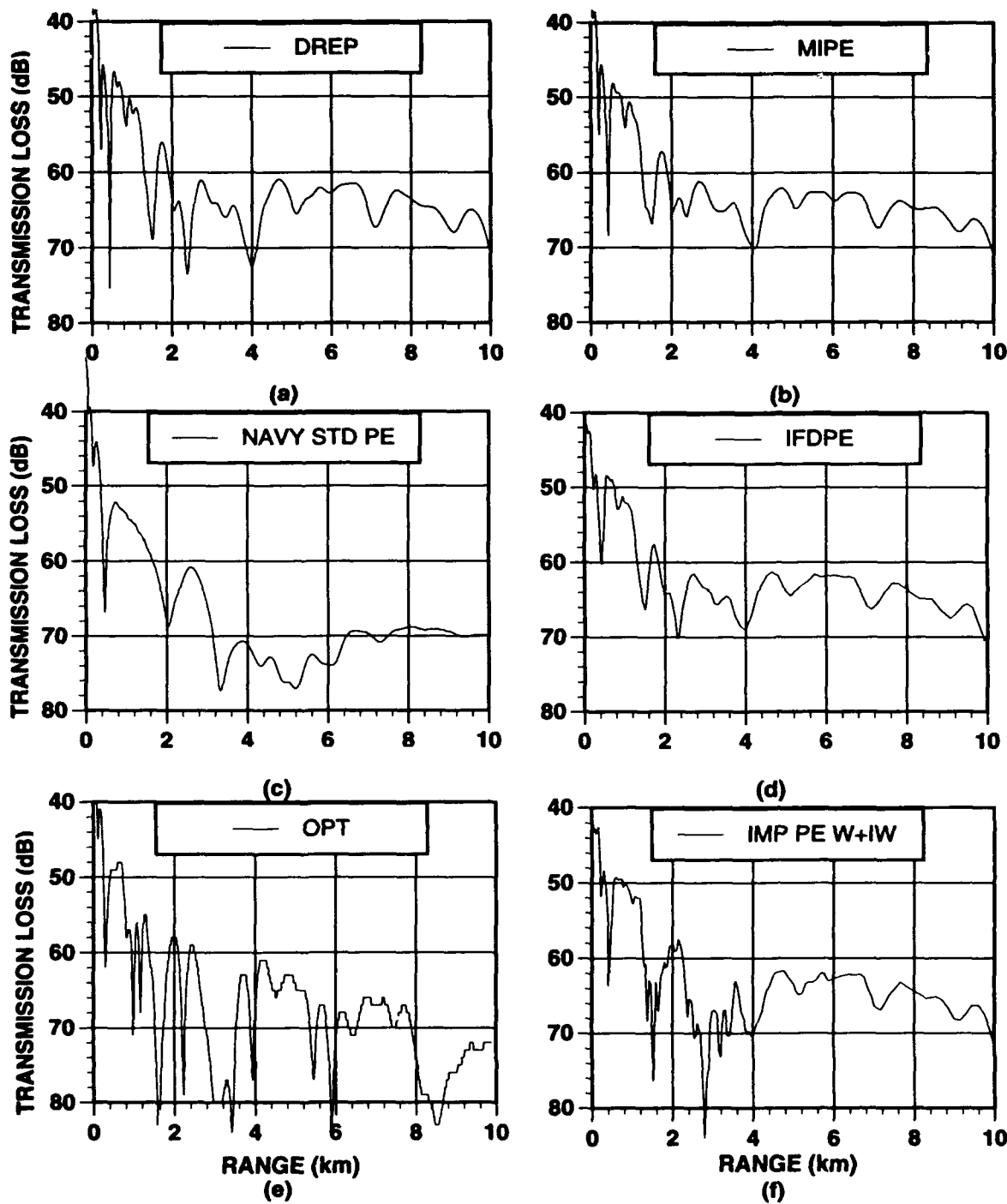


Fig. 2-5.2. Test Case 5B Results

PE Workshop II: Part 2 — Test Case Results

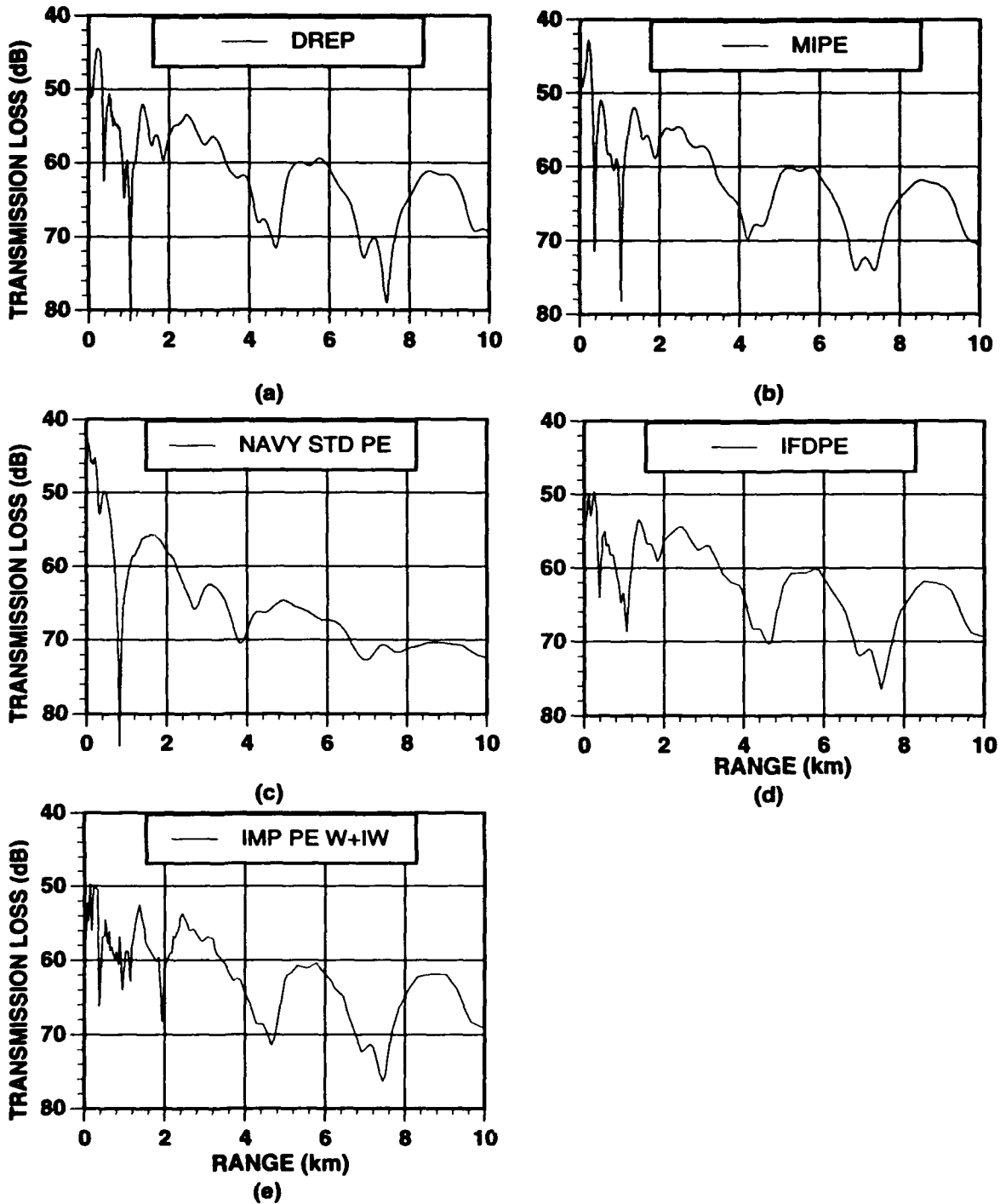


Fig. 2–5.3. Test Case 5C Results

TEST CASE 6

Underwater Acoustic Model Predictions vs. Measured Field Data

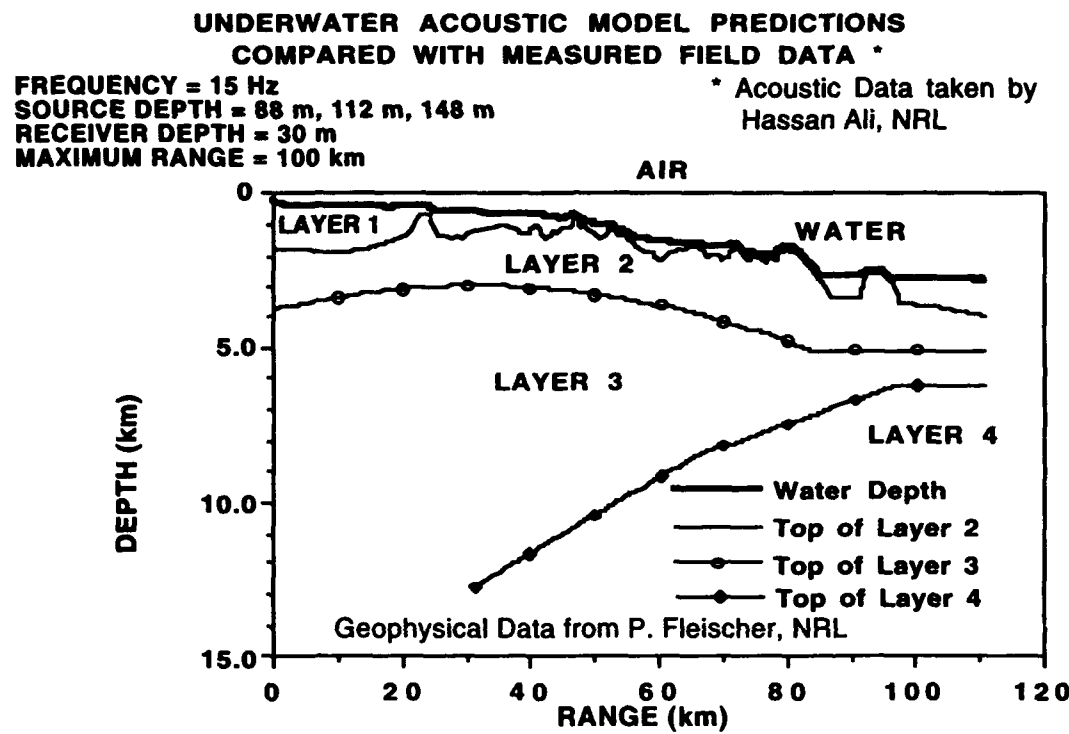
OBJECTIVE Compare PE model predictions to measured ocean acoustic data, given that a detailed and accurate set of environmental and geoacoustic parameters are known along the experiment track.

BACKGROUND In many ocean acoustics experiments, excellent acoustic data is taken but the knowledge of the ocean environment at the time the data is taken may be inadequate. The acoustic model user must then resort to historical data bases to obtain the ocean environmental parameters (sound speed profiles as a function of depth and range) and ocean-bottom environmental parameters (compressional wave speed and attenuation, shear wave speed and attenuation, density, all as a function of depth and range). The historical data bases can provide sound speed profiles in the water column that are, at best, only typical of that region of the worlds oceans. Ocean bottom properties obtained from historical data bases are usually less typical of the region, representing only an interpolation (or guess) based on sparse measurements made "nearby" the area of interest. Thus, the PE Workshop II was fortunate to have a comprehensive acoustic-environmental data set to present to the contributors.

THE TEST CASE PROBLEM Test Case 6 consists of a set of experimental acoustic measurements taken by Hassan Ali of NRL (Fisher et al. 1988; 1989) off the coast of Oregon. The experiment track ran from the shallow coastal waters (~200 m in depth) outward (100 km in range) into much deeper water (~4 km in depth). An accompanying set of environmental data in the experiment site was compiled by Pete Fleischer of NRL. Several information sources were used in obtaining the environmental data including data bases compiled by the ONR Acoustic Reverberation Special Research Program. Fortuitously, a seismic survey had been made along a track parallel to and within 30 miles of the acoustic experiment track. Thus, these complimentary sets of acoustic and environmental data represent a most comprehensive acoustic-environmental data set.

A tabular set of the environmental inputs used for this test case is included in Part 1, Appendix A. Figure 2-6.0 shows the depth-varying, range-varying bathymetry and ocean bottom strata. The acoustic experimental parameters were as follows: frequency = 15 Hz; fixed point receiver depths = 88 m, 112 m, and 148 m; moving point source depth = 30 m; range of calculation = 0 km to 100 km. This test case is most efficiently

PE Workshop II: Part 2 — Test Case Results



Expanded view of the first 5 km, showing the rough ocean-bottom interface and the rough interface between layer 1 and layer 2.

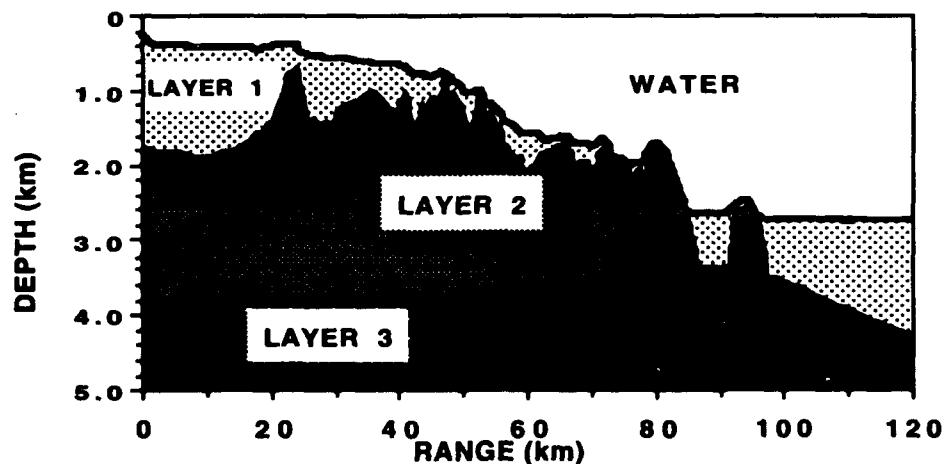


Fig. 2-60 Environment for Test Case 6.

modeled by employing reciprocity and treating the fixed point as the "source" position and the moving point as the "receiver" position.

THE REFERENCE SOLUTION The reference solution used for this test case was measured acoustic data taken along a track perpendicular to the coast line and extending from a shallow-water region (~200 m) to a deep-water region (>2,000 m). In this ocean acoustic experiment a vertical hydrophone array was bottom-moored in the shallow-water region. A tow ship sailed toward the deep-water region while dragging a 15-Hz cw acoustic source at a depth of 30 m below the sea surface. Acoustic signals received at the hydrophone array were processed for the hydrophones located at depths of 88 m, 112 m, and 148 m.

RESULTS AND DISCUSSION Figures 2-6.1, 2-6.2, and 2-6.3 give the comparisons between the acoustic experiment data and the various PE models' predictions. Test Cases 6A, 6B, and 6C refer to reciprocity source depths of 88 m, 112 m, and 148 m, respectively. In the comparisons made during the workshop, all of the models' predictions for each case were too high, i.e., the predictions gave higher transmission loss than the measured data.

An immediate observation by the workshop contributors was that the poor comparison between data and model predictions was due to either an error in the data (or its processing) or an error in the environmental data. Jensen provided a parameter study of how an error in the compressional wave attenuation could account for the poor comparisons. This is shown in Figs. 2-6.2(f) through 2-6.2(i).

The preponderance of evidence (up to this test case, the PE models had shown remarkable ability to include all pertinent physical mechanisms; the acoustic-environmental data was comprehensive, leaving little or no room for guessing at parameters; all of the PE models gave approximately the same predictions, and these predictions were uniformly too high) convinced Hassan Ali to have the data reprocessed. It is important to point out that this was the third processing of some of this data. A year earlier, poor comparisons between the data and model predictions had led the experimenters to have selected data processed a second time. The second processing produced no significant change in the values of the selected data. This third processing revealed an error in the processing parameters. Comparisons between the PE models' predictions and the thrice-processed experimental data are shown in Figs. 2-6.1, 2-6.2, and 2-6.3 with the reference data labeled as "Corrected Data."

SUMMARY Test Case 6 illustrates a recent trend in ocean data-model comparisons. The PE models have become so accurate that a poor comparison between model

PE Workshop II: Part 2 — Test Case Results

prediction and experimental data led to the questioning of the accuracy of the data. A decade ago, when the first PE Workshop was held, no model's prediction would have been seriously believed if it disagreed with the data.

FURTHER READINGS IN PART 3 Papers in Part 3 that discuss Test Case 6 are:

- Holmes, Eleanor S., and Laurie A. Gainey, "The Navy Standard Parabolic Equation Model, Broadband PE, and PE Workshop II."
- Jensen, Finn B., "PE Workshop II: Test Problem Solutions."
- Nghiem-Phu, Lan, Kevin B. Smith, and Fred D. Tappert, "FastPE, SlowPE, YourPE, MiPE: What are the Real Issues?"

PE Workshop II: Part 2 — Test Case Results

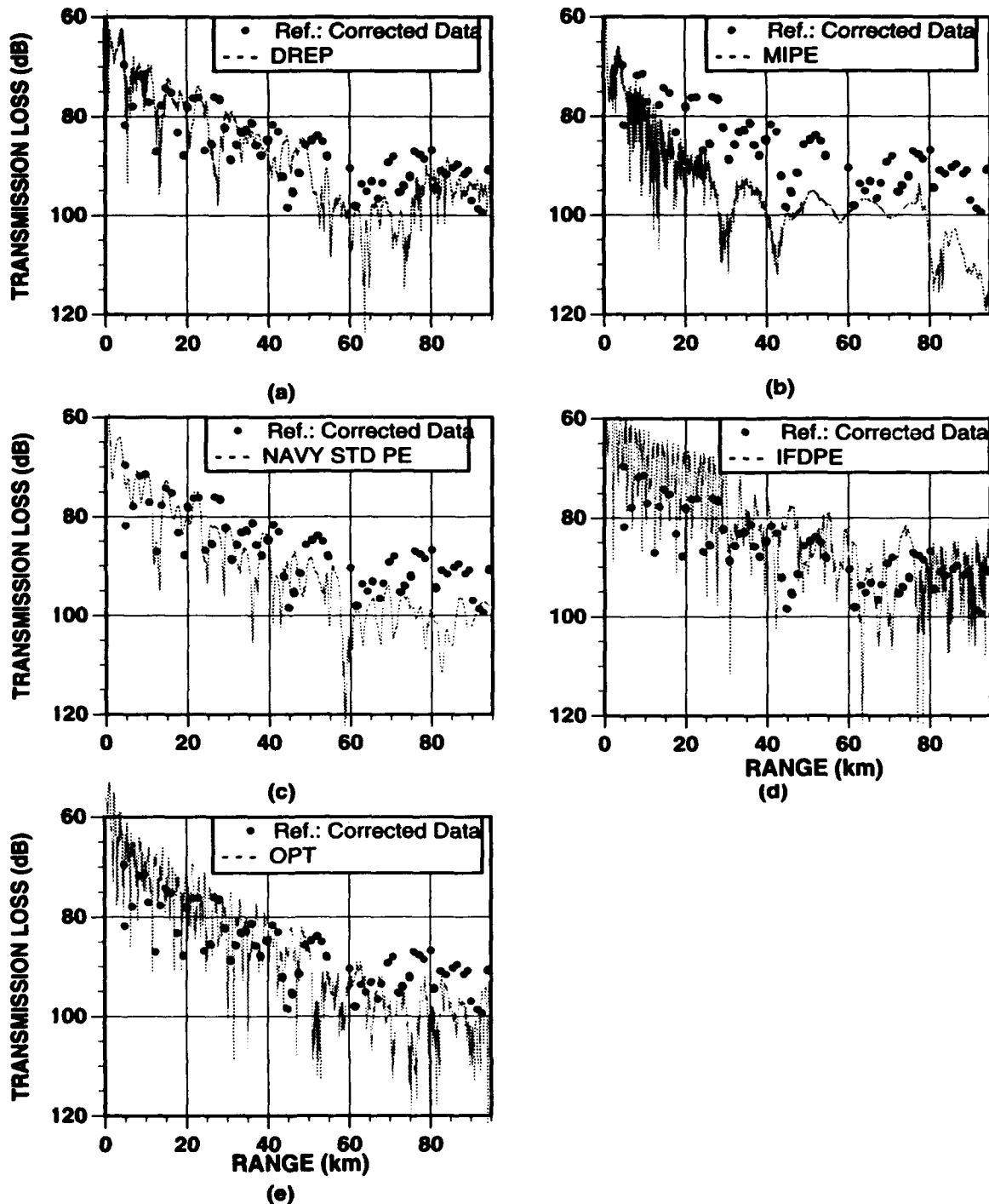


Fig. 2–6.1. Test Case 6A Results

PE Workshop II: Part 2 — Test Case Results

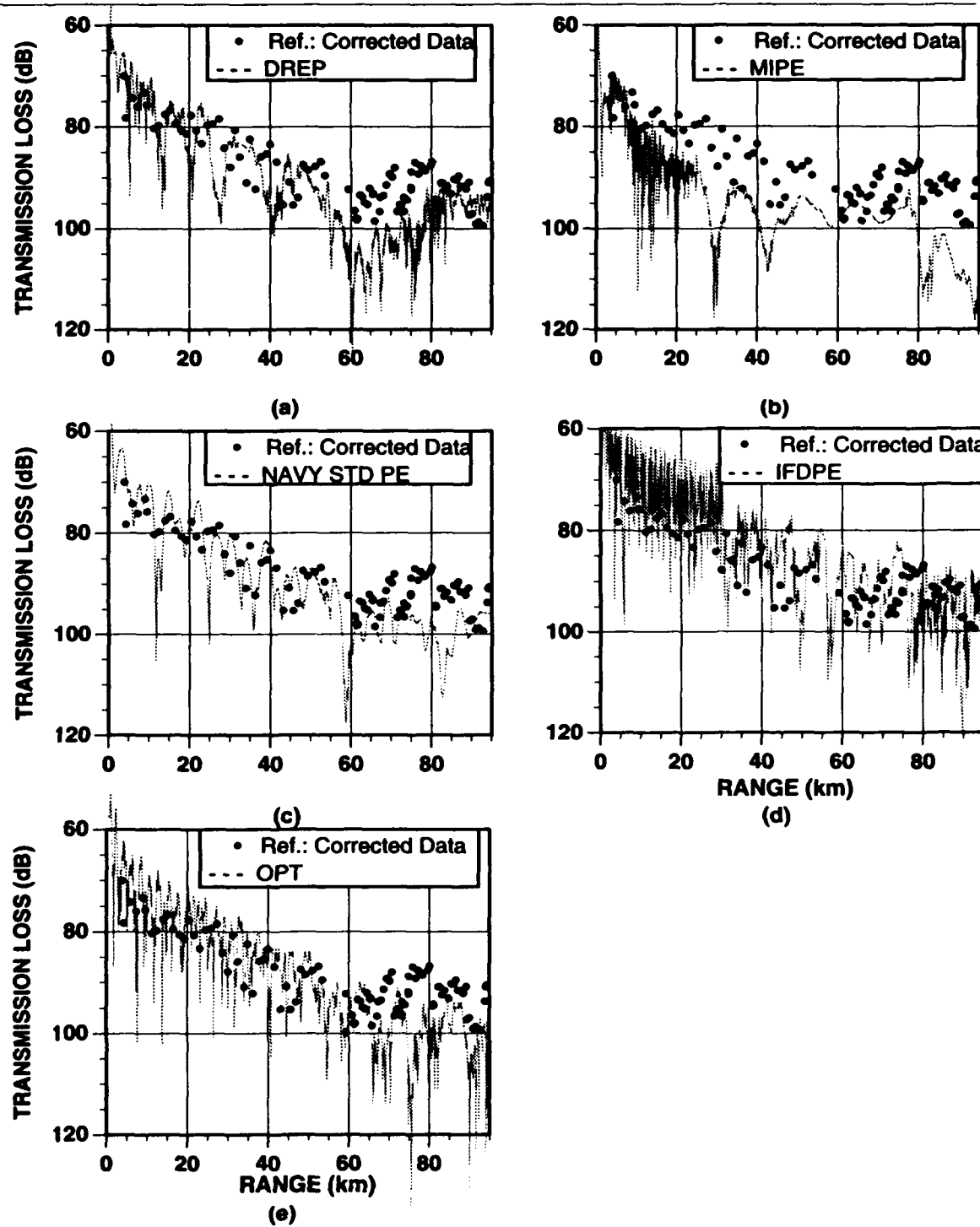


Fig. 2-6.2. Test Case 6B Results

PE Workshop II: Part 2 — Test Case Results

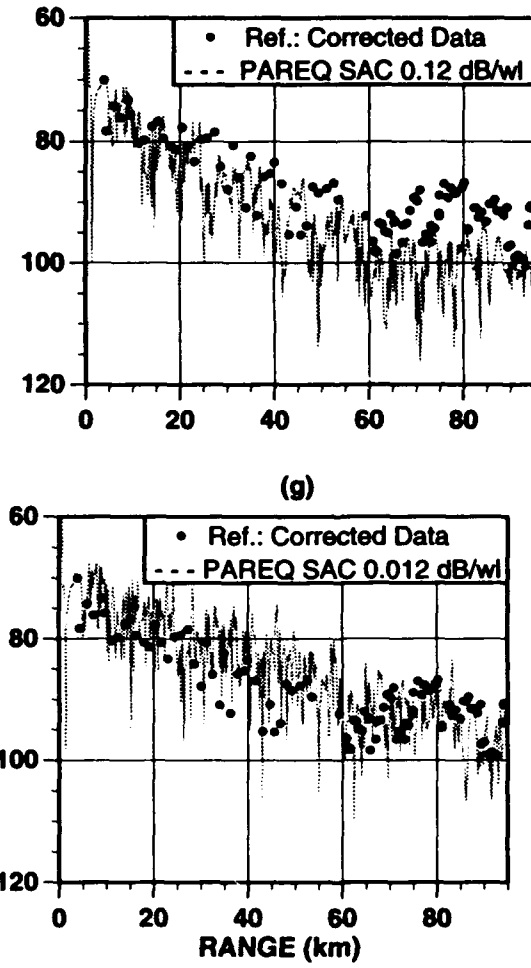
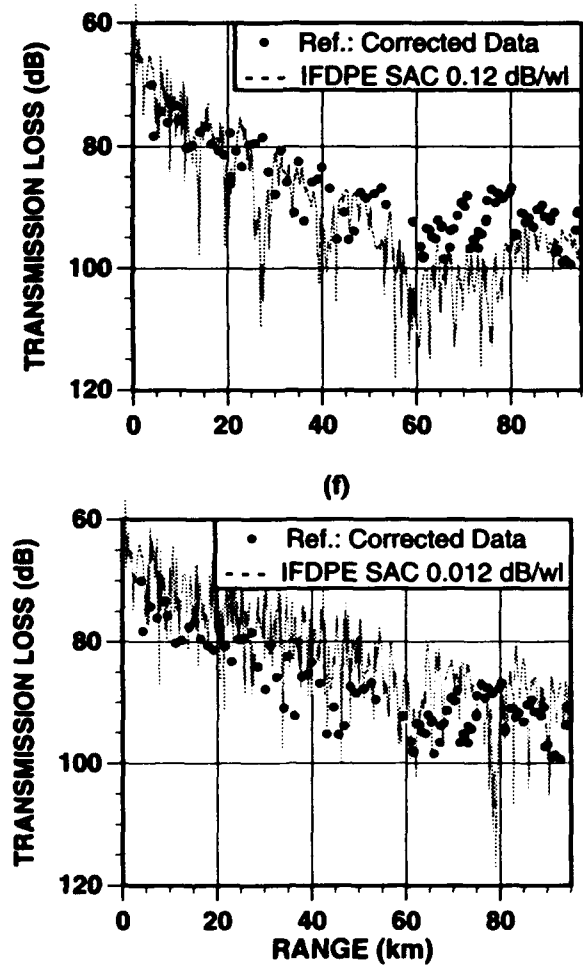


Fig. 2–6.2. Test Case 6B Results (Continued)

PE Workshop II: Part 2 — Test Case Results

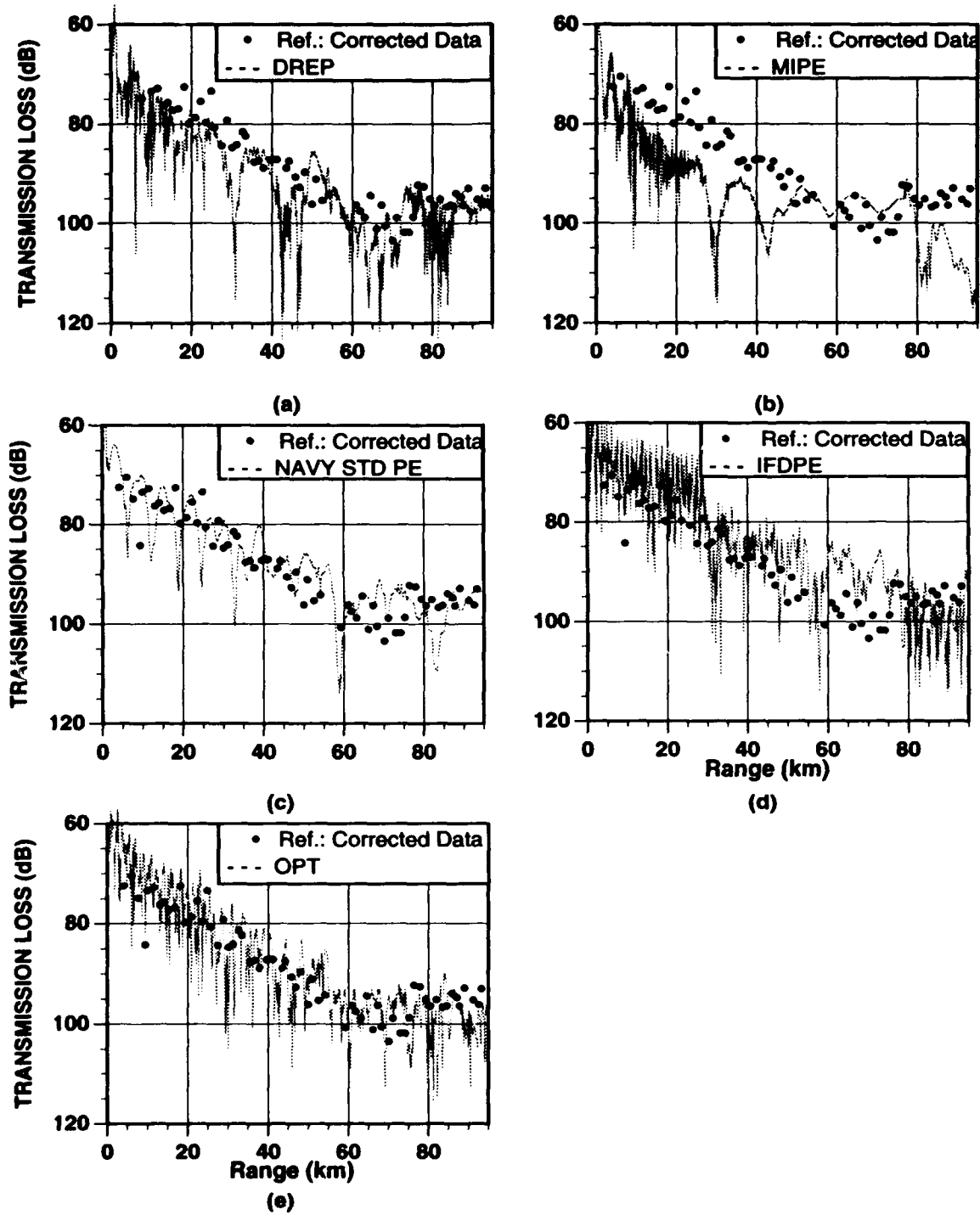


Fig. 2-6.3. Test Case 6C Results

TEST CASE 7

Long-Range Propagation in a Leaky Surface Duct

OBJECTIVE Explain why some wide-angle split-step PE models, when applied to long-range propagation in a leaky surface duct, overestimate the TL.

BACKGROUND This test case problem was submitted by Finn Jensen. He had observed that some (but not all) wide-angle split-step PE models using the Thomson–Chapman wide-angle approach will overestimate transmission loss (TL) by as much as 20 dB. This overestimation occurs when the PE model is applied to long-range propagation in a leaky surface duct overlying a strong upward refracting sound speed profile, such as the one shown in Fig. 2–7.0.

The error in TL is not present when the standard narrow-angle approximation is used in the split-step PE model. And, the difficulty has not been observed in wide-angle PE models that use finite-difference or finite-element solution techniques; these PE models use either a series expansion or a higher-order Padé approximation to the square root operator, i.e., they do not use the Thomson–Chapman approximation.

THE TEST CASE PROBLEM The environmental parameters of the problem are given in Fig. 2–7.0. The source frequency is 80 Hz, the source depth is 25 m, and the receiver depth is 100 m. Thus, both the source and the receiver are located in the 250-m-deep surface duct. The bottom is a range-independent, lossy fluid half-space, beginning at a depth of 4 km.

There are 78 propagating modes in the water waveguide, one of which is trapped in the surface duct. The first convergence zone (CZ) occurs at ~50 km in range.

THE REFERENCE SOLUTION The SNAP normal mode model (Jensen and Ferla 1979) was used by Jensen to obtain a reference solution. Since the environment in this test case is range independent, and over a long range (>100 km), a normal mode model should provide an accurate reference solution. In Fig. 2–7.1 the results from the SNAP model are labeled “SNAP SAC.”

RESULTS AND DISCUSSION The results for Test Case 7 are shown in the 12 plots comprising Fig. 2–7.1. Plots (a) through (e) were provided by Finn Jensen. They clearly illustrate the difficulty. In plot (a) the Thomson–Chapman (T–C) wide-angle

PE Workshop II: Part 2 — Test Case Results

option is used in the split-step PE model (PAREQ) and labeled as "T-C PE SAC." It disagrees with the reference solution by as much as 20 dB at ranges between 60 km and 100 km. The same PE model, PAREQ, using the Standard PE (std PE) narrow-angle option and labeled as "PAREQ SAC std PE" in plot (c) does not show any difference from the reference solution. The only difference between plots (a) and (c) are in the choices of the T-C wide-angle option vs. the std PE narrow-angle option.

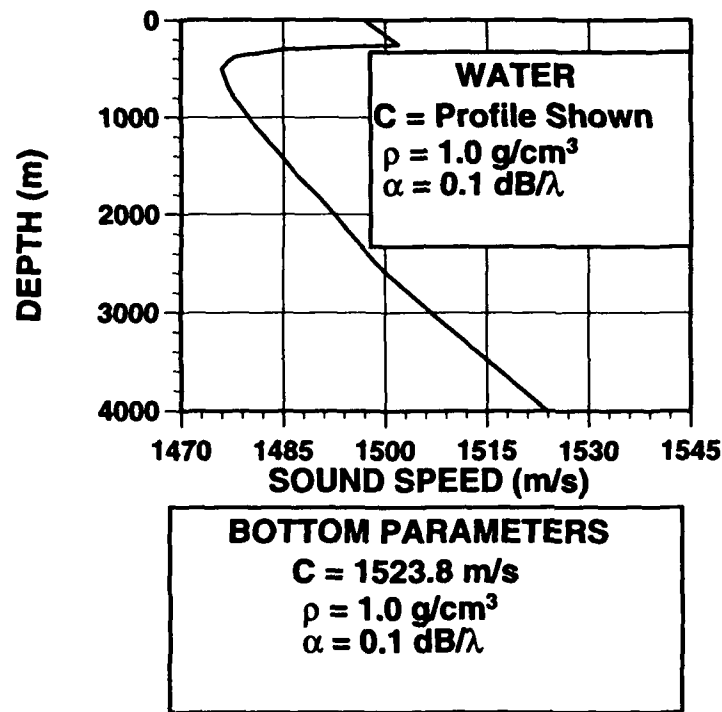


Fig. 2-7.0 Environment for Test Case 7.

Jensen also used the T-C wide-angle option with another split-step PE model, LOG PE (Berman et al. 1989), labeled as "LOG PE SAC" in plot (d) of Fig. 2-7.1. For range-independent environments, the "rays" associated with LOG PE are identical to those of the Helmholtz equation; thus, in this range-independent problem, the results from LOG PE should be the same as the normal mode reference solution. Plot (d) shows that the LOG PE does give a result closer to the reference solution, but still in disagreement by as much as 10 dB.

Jensen established that the disagreement was due to a phasing error associated with the surface ducted propagation and the leaky deep-diving propagation. He was able to show that the same disagreement can be obtained with the SNAP model if the surface duct sound speed is varied by just 0.5 m/s. This slight variation in the surface duct sound speed produced the results labeled "SNAP SAC mod surf SVP" in plot (b) of Fig. 2-7.1.

Finally, Jensen showed that the problem does not occur in some of the other well-known wide-angle approximations. Results from using the Claerbout wide-angle approximation in the implicit finite-difference PE model, IFD PE, (labeled as "IFD PE SAC Claerbout" in plot (e)) does not show any difference from the reference solution.

The Navy Standard PE model uses both the T-C wide-angle approximation and the split-step method. And, it is also susceptible to this problem as is shown in plot (f) of Fig. 2-7.1. In plot (f), the NRL version of the Navy Standard PE model was used with the T-C wide-angle option. Its results show too little loss in transmission in the 60 km to 100 km range as compared with the reference solution. This is in contrast with results shown by the other split-step PE models in plots (a) and (d), where the loss in transmission was too great when compared with the reference solution.

Plots (g), (h), and (i) of Fig. 2-7.1 are from the results of Lan Nghiem-Phu, Smith, and Tappert using the University of Miami's version of split-step PE, labeled "MIPE" in the plots. They show, in plot (h), the difference between the reference solution and the T-C wide-angle approximation using the MIPE model; and, in plot (i), the agreement between the reference solution and the standard PE narrow-angle approximation using the MIPE model. In each case they used the same reference sound speed, $C_0 = 1500$ m/s. By changing to a slightly different sound speed, $C_0 = 1482$ m/s, they are able to use the T-C wide-angle approximation in the MIPE model and get the same result as the reference solution. This is shown in plot (g).

The results presented by Lan Nghiem-Phu, Smith, and Tappert are highly significant, in that their investigations show that the correct solution can be obtained with the T-C wide-angle approximation for only a "very narrow spectrum of reference sound speed, C_0 ." They suggest that the problem be solved by using a PE derived from a " C_0 insensitive equation." Such a formulation exists in their UMPE model. Results from the UMPE model for this test case are given in their paper in Part 3 of these proceedings. Its result is identical to that shown in plot (g) of Fig. 2-7.1, and thus allows the T-C wide-angle approximation to produce correct results without having to select a "perfect" C_0 .

PE Workshop II: Part 2 — Test Case Results

Plots (j), (k), and (l) of Fig. 2–7.1 are the results from Thomson and Brooke. They confirm the findings previously discussed:

- PE models that do not use the T–C wide-angle approximation apparently avoid the difficulties illustrated by Test Case 7. This is shown in plot (j) where the finite-difference PE model labeled “DREPS” shows agreement with the reference solution.
- Split-step PE models that use the standard PE narrow-angle approximation also avoid the difficulties illustrated by Test Case 7. This is shown in plot (k) where the Thomson split-step PE model using the standard PE narrow-angle approximation gives the same result (labeled “DREP std PE” in plot (k)) as the reference solution.
- With the correct choice of C_o the split-step PE models using the T–C wide-angle approximation can get the correct results. This is shown in plot (l) for the Thomson split-step PE model with the T–C wide-angle approximation (i.e., the curve labeled “DREP T–C PE”). In this plot the correct C_o has been used.

SUMMARY This seemingly benign long-range, range-independent problem presented a supreme challenge to the Thomson–Chapman wide-angle approximation. The difficulty occurs in the choice of the reference sound speed, which in turn determines the phase calculated by the split-step PE model. In Test Case 7 the single trapped mode that is propagating in the surface duct is a leaky mode, which continually loses energy into the region below the duct. The strong upward refracting sound speed profile of this lower region refracts this energy back into the surface duct, thus causing interferences. A small error in the phase calculation by the PE model can result in a large (~20 dB) error downrange (beyond the first CZ, i.e., at ranges greater than 50 km). That this large disagreement is due to phase errors can be inferred from plot (a) of Fig. 2–7.1: the split-step PE model with the Thomson–Chapman wide-angle approximation greatly disagrees with the reference solution between the first and second CZ, but “miraculously” recovers so that it is in good agreement with the reference solution at the third CZ. Such recovery would not likely occur if there were errors in the magnitude of the propagated field.

The range of values for a correct choice of C_o is disturbingly small and the selection criterion essentially one of trial-and-error, i.e., the only rationale for the choice of a correct C_o is that it works. This gives strong impetus in the split-step PE modeling community to further the development of a C_o insensitive split-step PE model.

Presumably there are some terms in other wide-angle approximations (e.g., Claerbout’s approximation or higher order Padé approximations) that are missing in

the Thomson-Chapman approximation. This would explain why only the Thomson-Chapman approximation has the difficulty illustrated by Test Case 7. The precise reason is as yet unknown. Perhaps a decade from now this explanation will be just another successful step taken as PE model development marches forward, and documented by the PE Workshop III in the year 2002.

FURTHER READINGS IN PART 3 Two papers in Part 3 of these proceedings contain a very detailed discussion of the problems associated with the Thomson-Chapman wide-angle approximation in the split-step PE model. To fully grasp the subtle difficulties that this test case presents, the following two papers must be read:

- Jensen, Finn B., "PE Workshop II: Test Problem Solutions."
- Nghiem-Phu, Lan, Kevin B. Smith, and Fred D. Tappert, "FastPE, SlowPE, YourPE, MiPE: What are the Real Issues?"

PE Workshop II: Part 2 — Test Case Results

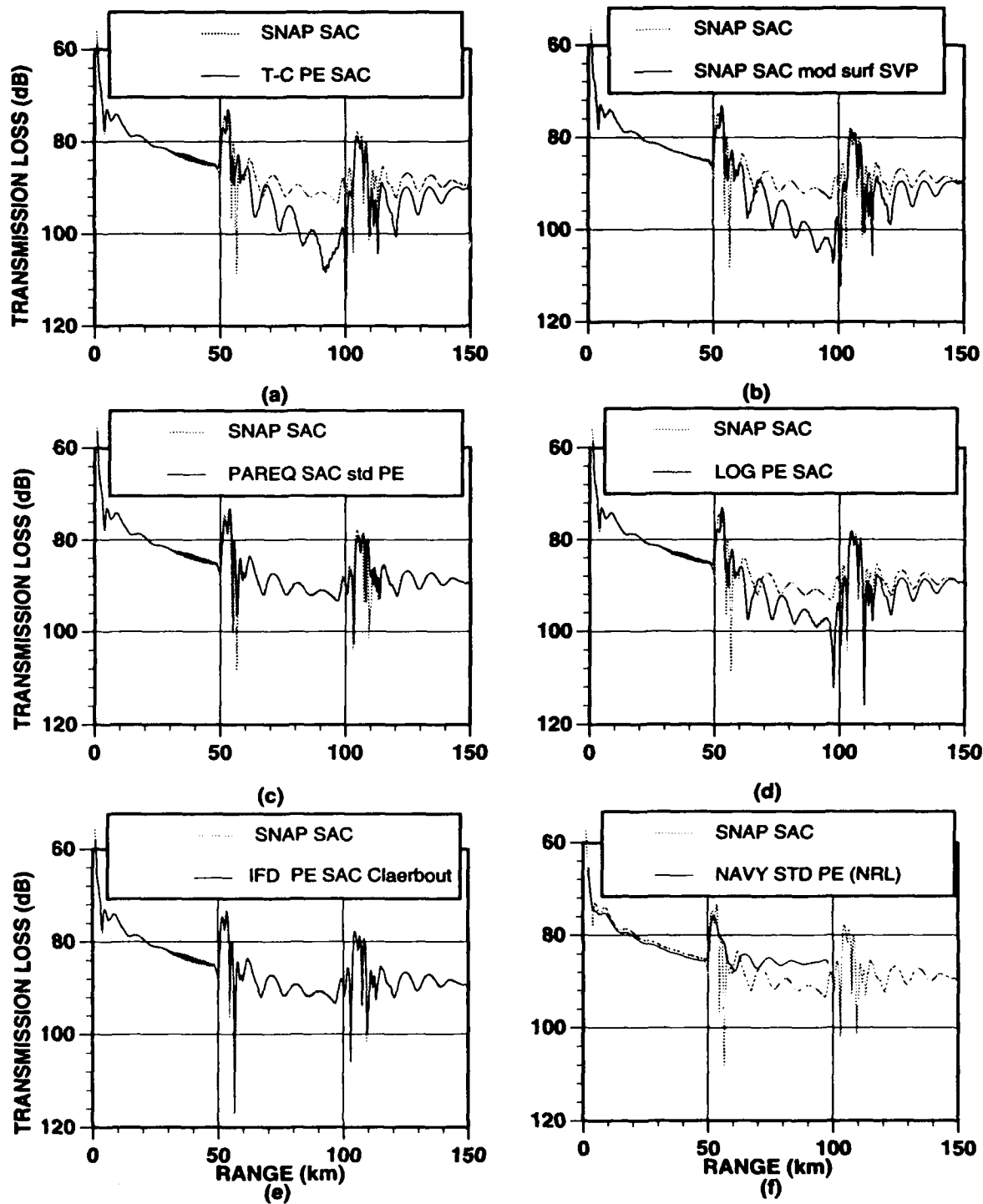


Fig. 2-7.1. Test Case 7 Results

PE Workshop II: Part 2 — Test Case Results

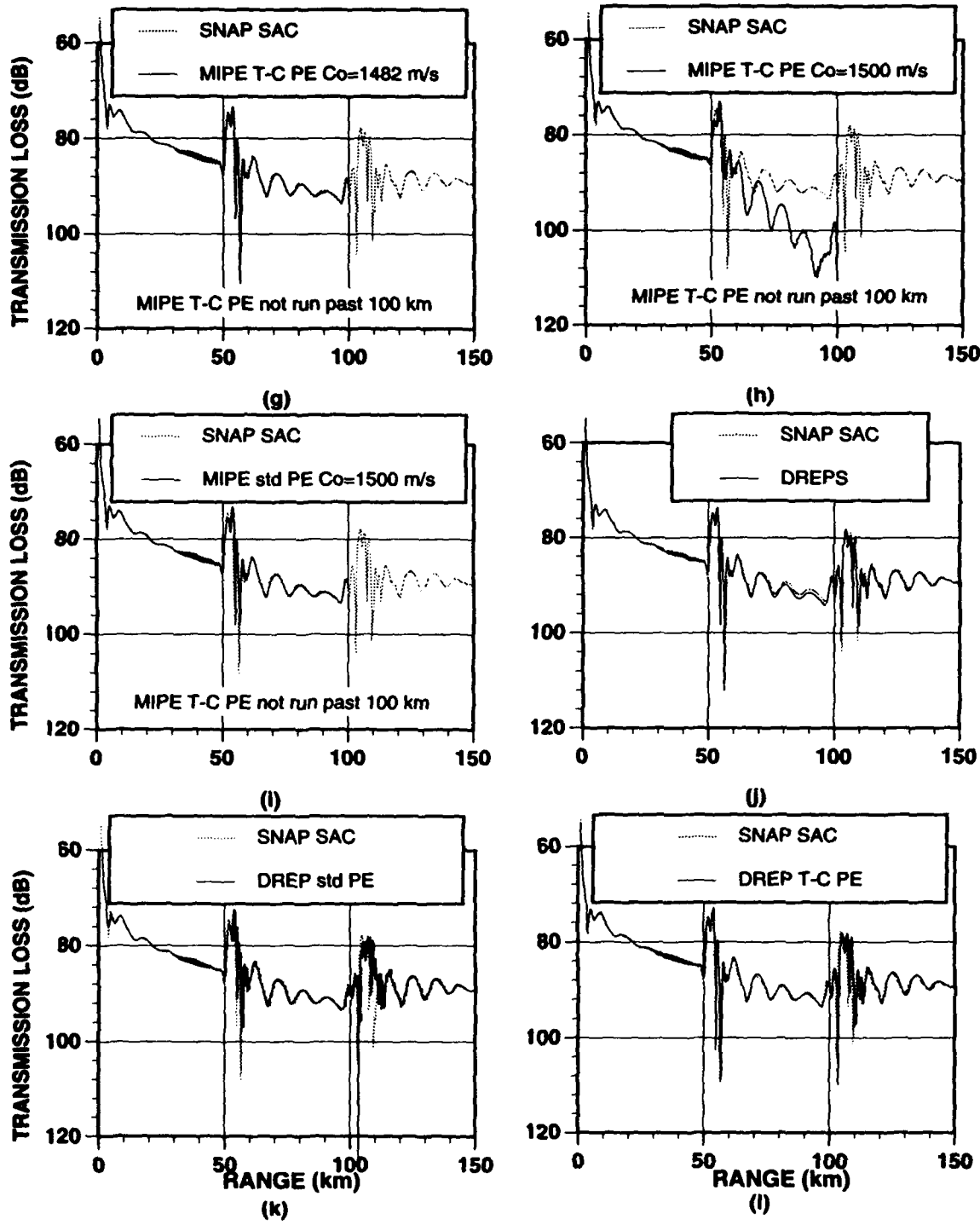


Fig. 2-7.1. Test Case 7 Results (Continued)

Bibliography

- Abrahamsson, L., and H.O. Kreiss (1990). "Boundary conditions for the parabolic equation in a range-dependent duct," *J. Acoust. Soc. Am.* **87**, 2438–2441.
- Baer R. N. (1981). "Propagation Through a Three Dimensional Eddy Including Effect on an Array," *J. Acoust. Soc. Am.* **69**, 70–75.
- Bamberger, A., B. Engquist, L. Halpern, and P. Joly (1988a). "Parabolic wave equation approximations in heterogeneous media," *SIAM J. Appl. Math.* **48**, 99–128.
- Bamberger, A., B. Engquist, L. Halpern, and P. Joly (1988b). "Higher order paraxial wave equation approximations in heterogeneous media," *SIAM J. Appl. Math.* **48**, 129–154.
- Berman, D. H., E. B. Wright, and R. N. Baer (1989). "An optimal PE-type wave equation," *J. Acoust. Soc. Am.* **86**, 228–233.
- Botseas, G., D. Lee, and K. E. Gilbert (1983). "IFD: Wide Angle Capability," Naval Underwater Systems Center, New London, CT, U.S.A., NUSC TR 6905.
- Botseas, G., D. Lee, and D. King (1987). "FOR3D: A Computer Model for Solving the LSS Three-Dimensional, Wide Angle Wave Equation," Naval Underwater Systems Center, New London, CT, U.S.A., NUSC TR 7943.
- Bremmer, H. (1951). "The W.K.B. approximation as the first term of a geometric-optical series," *Comm. Pure and Appl. Math.* **4**, 105–115.
- Brock, H. K. (1975). "The AESD parabolic equation model," AESD TN-75-07, Office of Naval Research, Arlington, VA, U.S.A.
- Chin-Bing, S. A., and J. E. Murphy (1993a). "Shear effects on ocean acoustic propagation due to step-periodic roughness along the ocean bottom interface," *Mathematical Modelling and Scientific Computing*, **2**, 780-785.
- Chin-Bing, S. A., and J. E. Murphy (1993b). "Long-Range Ocean Acoustic-Seismic Propagation Modeling Using Hybrid Finite Element and Parabolic Equation Models," in *Computational Acoustics: Scattering, Supercomputing and Propagation, Vol. 1*, R. L. Lau, D. Lee, and A. R. Robinson (eds.), (Elsevier Publishers (North-Holland), Amsterdam), 105–121.

- Claerbout, J. F. (1970). "Course grid calculations of waves in inhomogeneous media with application to delineation of complicated seismic structure," *Geophysics* **35**, 20–21.
- Claerbout, J. F. (1976). *Fundamentals of Geophysical Data Processing* (McGraw-Hill, New York), 206–207.
- Clayton, R. W., and B. Engquist (1980). "Absorbing boundary conditions for wave-equation migration," *Geophysics* **45**, 895–904.
- Collins, M. D. (1988a). "Low-frequency, bottom-interacting pulse propagation in range-dependent oceans," *IEEE J. Ocean. Eng.* **13**, 222–228.
- Collins, M. D. (1988b). "The time-domain solution of the wide-angle parabolic equation including the effects of sediment dispersion," *J. Acoust. Soc. Am.* **84**, 2114–2125.
- Collins, M. D. (1988c). "FEPE User's Guide," Naval Research Laboratory, Stennis Space Center, MS, U.S.A., NORDA Technical Note 365.
- Collins, M. D. (1989a). "A nearfield asymptotic analysis for underwater acoustics," *J. Acoust. Soc. Am.* **85**, 1107–1114.
- Collins, M. D. (1989b). "Applications and time-domain solution of higher-order parabolic equations in underwater acoustics," *J. Acoust. Soc. Am.* **86**, 1097–1102.
- Collins, M. D. (1989c). "A higher-order parabolic equation for wave propagation in an ocean overlying an elastic bottom," *J. Acoust. Soc. Am.* **86**, 1459–1464.
- Collins, M. D. (1990a). "The rotated parabolic equation and sloping ocean bottoms," *J. Acoust. Soc. Am.* **87**, 1035–1037.
- Collins, M. D. (1990b). "Benchmark calculations for higher-order parabolic equations," *J. Acoust. Soc. Am.* **87**, 1535–1538.
- Collins, M. D., and S. A. Chin-Bing (1990). "A three-dimensional parabolic equation model that includes the effects of rough boundaries," *J. Acoust. Soc. Am.* **87**, 1104–1109.
- Collins, M. D. (1991). "Higher-order Padé approximations for accurate and stable elastic parabolic equations with application to interface wave propagation," *J. Acoust. Soc. Am.* **89**, 1050–1057.
- Collins, M. D., and E. K. Westwood (1991). "A higher-order energy-conserving parabolic equation for range-dependent ocean depth, sound speed, and density," *J. Acoust. Soc. Am.* **89**, 1068–1075.

PE Workshop II: Part 2 — Test Case Results

- Collins, M. D., and R. B. Evans (1992). "A two-way parabolic equation for acoustic back scattering in the ocean," *J. Acoust. Soc. Am.* **91**, 1357–1368.
- Corones, J. P., B. DeFacio, and R. J. Krueger (1982). "Parabolic approximations to the time-independent elastic wave equation," *J. Math. Phys.* **23**, 577–586.
- Davis, J. A., D. White, and R. C. Cavanagh (1982), "NORDA Parabolic Equation Workshop, 31 March – 3 April 1981," Naval Research Laboratory, Stennis Space Center, MS, U.S.A., NORDA Technical Note 143.
- DeSanto, J. A. (1977). "Relation between the solutions of the Helmholtz and parabolic equations for sound propagation," *J. Acoust. Soc. Am.* **62**, 295–297.
- Douglas, J., Jr. (1956). "The Solution of Diffusion Equation by a High Order Correct Difference Equation," *J. Math. Phys.* **35**, 145–151.
- Evans, R. B. (1983). "A coupled mode solution for acoustic propagation in a waveguide with stepwise depth variations of a penetrable bottom," *J. Acoust. Soc. Am.* **74**, 188–195.
- Evans, R. B. (1986). "COUPLE: A user's manual," Naval Research Laboratory, Stennis Space Center, MS, U.S.A., NORDA Technical Note 332.
- Felsen, L. B. (1990). "Benchmarks: An option for quality assessment," *J. Acoust. Soc. Am.* **87**, 1497–1498.
- Fisher, C. A., H. B. Ali, and M. J. Authement (1988). "A VLF propagation experiment off the coast of Oregon: Measurements and numerical predictions," *J. Acoust. Soc. Am. Suppl. 1*, **84**, S91.
- Fisher, C. A., H. B. Ali, and M. J. Authement (1989), "A VLF Propagation Experiment off the Coast of Oregon Measurements and Numerical Predictions," Naval Research Laboratory, Stennis Space Center, MS, U.S.A., NORDA Technical Note 418.
- Fishman, L., and J. J. McCoy (1984). "Derivation and application of extended parabolic wave theories. Part 1. The factorized Helmholtz equation," *J. Math. Phys.* **25**, 285.
- Gilbert, K. E., X. Di, and D. Huang (1989). "Spectral decomposition of parabolic equation fields," *J. Acoust. Soc. Am. Suppl. 1* **85**, S70.
- Greene, R. R. (1984). "The rational approximation to the acoustic wave equation with bottom interaction," *J. Acoust. Soc. Am.* **76**, 1764–1773.
- Greene, R. R. (1985). "A high-angle one-way wave equation for seismic wave propagation along rough and sloping interfaces," *J. Acoust. Soc. Am.* **77**, 1991–1998.

Hardin, R. H., and F. D. Tappert (1973). "Application of the Split-Step Fourier Method to the Numerical Solution of Nonlinear and Variable Coefficient Wave Equations," *SIAM Rev.* **15**, 423.

Holmes, E. S., and L. A. Gainey (1991). "Software product specification for the parabolic equation model version 3.2," OAML-SPS-22, Naval Oceanographic Office, Bay St. Louis, MS, U.S.A.

Hudson, J. A. (1980). "A parabolic approximation for elastic waves," *Wave Motion* **2**, 207–214.

Jensen, F. B., and H. Krol (1975). "The use of the parabolic equation method in sound propagation modeling," SACLANTCEN Memo. SM-72, SACLANT Undersea Research Centre, La Spezia, Italy.

Jensen, F. B., and C. M. Ferla (1979). "SNAP: the SACLANTCEN normal-mode acoustic propagation model," SACLANTCEN Memo. SM-121, SACLANT Undersea Research Centre, La Spezia, Italy. (NTIS No. AD-A067 256).

Jensen, F. B., and W. A. Kuperman (1980). "Sound propagation in a wedge-shaped ocean with a penetrable bottom," *J. Acoust. Soc. Am.* **57**, 1564–1566.

Jensen, F. B., and M. G. Martinelli (1985). "The SACLANTCEN parabolic equation model (PAREQ)," SACLANT Undersea Research Centre, La Spezia, Italy.

Jensen, F. B., and H. Schmidt (1987). "Spectral decomposition of PE fields in a wedge-shaped ocean," in *Progress in Underwater Acoustics*, H. Merklinger (ed.), (Plenum, New York), 557–564.

Jensen, F. B., and C. M. Ferla (1990). "Numerical solutions of range-dependent benchmark problems in ocean acoustics," *J. Acoust. Soc. Am.* **87**, 1499–1510.

Knightly, G. H., D. Lee, and D.F. St. Mary (1987). "A higher-order parabolic wave equation," *J. Acoust. Soc. Am.* **82**, 580–587.

Knightly, G.H., G.Q. Li, D.F. St. Mary, and D. Lee (1989). "A Numerical Treatment of the Fluid/Elastic Interface for the Potential Equations," *J. Acoust. Soc. Am., Suppl. 1* **86**, S65.

Knightly, G. H., G. Q. Li, D. F. St. Mary, and D. Lee (1990). "Elastic Parabolic Equation and the Fluid/Elastic Interface," *J. Acoust. Soc. Am., Suppl. 1* **88**, S59.

Kriegsmann, G. A. (1985). "A multiscale derivation of a new parabolic equation which includes density variations," *Comp. Maths. Appl.* **11**, 817–821.

PE Workshop II: Part 2 — Test Case Results

- Kriegsmann, G. A., A. Taflove, and K. R. Umashankar (1987). "A new formulation of electromagnetic wave scattering using an on-surface radiation boundary condition approach," *IEEE Trans. Ant. and Prop.* **35**, 153–161.
- Landers, T., and J. F. Claerbout (1972). "Numerical calculations of elastic waves in laterally inhomogeneous media," *J. Geophys. Res.* **77**, 1476–1483.
- Lee, D., and J. S. Papadakis (1980). "Numerical Solutions of the Parabolic Wave Equation: An Ordinary-Differential-Equation Approach," *J. Acoust. Soc. Am.* **68**, 1482–1488.
- Lee, D., G. Botseas, and J. S. Papadakis (1981). "Finite-Difference Solution to the Parabolic Wave Equation," *J. Acoust. Soc. Am.* **70**, 795–800.
- Lee, D., and G. Botseas (1982). "IFD: An Implicit Finite-Difference Computer Model for Solving the Parabolic Equation," Naval Underwater Systems Center, New London, CT, U.S.A., NUSC Tech. Rep. 6659 (NTIS No. AD-A117 701).
- Lee, D., and S. T. McDaniel (1983). "A finite-difference treatment of interface conditions for the parabolic wave equation: The irregular interface," *J. Acoust. Soc. Am.* **73**, 1441–1447.
- Lee, D., Y. Saad, and M.H. Schultz (1986). "An efficient method for solving the three-dimensional wide angle wave equation," Yale University, New Haven, CT, U.S.A., Yale Univ. Res. Rep. YALEU/DCS/RR-463.
- Lee, D., and S. T. McDaniel (1988). *Ocean Acoustic Propagation by Finite Difference Methods*, (Pergamon Press, Oxford).
- Lee, D., Y. Saad, M. H. Schultz (1988). "An Efficient Method for Solving the Three-Dimensional Wide Angle wave Equation," in *Computational Acoustics: Wave Propagation*, D. Lee, R.L. Sternberg, and M.H. Schultz (eds.), (Elsevier Publishers (North-Holland), Amsterdam), 75–90.
- Lee, D., and F. Saied (1990). "A Fourth Order Finite Difference Scheme to Improve the Computation Speed of Wide Angle Propagation," in *Computational Acoustics: Ocean-Acoustic Model and Supercomputing*, D. Lee, A. Cakmak, and R. Vichnevetsky (eds.), (Elsevier Publishers (North-Holland), Amsterdam), 27–36.
- Lee, D., D. F. St. Mary, M. H. Schultz, and W. L. Siegmann (1990). "A New Model for Marching Computation of Ocean Acoustic Backscattering," *J. Acoust. Soc. Am. Suppl. 1* **88**, S87.
- Lee, D., M. H. Schultz and W. L. Siegmann, (1994). *Numerical Ocean Acoustic Propagation in Three Dimensions* (in preparation).

- Leontovich, M. A., and V. A. Fock (1946). "Solution of the problem of propagation of electromagnetic waves along the earth's surface by the method of the parabolic equation," *J. Expt. and Theor. Phys.* **16**, 557–573.
- McCoy, J. J. (1977). "A parabolic theory of stress wave propagation through inhomogeneous linearly elastic solids," *J. Appl. Mech.* **44**, 462–468.
- McDaniel, S. T. (1975). "Propagation of normal mode in the parabolic approximation," *J. Acoust. Soc. Am.* **57**, 307–311.
- McDaniel, S. T., and D. Lee (1982). "A Finite-Difference Treatment of Interface Conditions for the Parabolic Wave Equation: The Horizontal Interface," *J. Acoust. Soc. Am.* **71**, 855–858.
- McDaniel, S. T., Y. Saad, and D. Lee (1985). "Numerical Solutions of Sound Scattering in the Ocean: An Ordinary-Differential-Equation-Approach," *Proc. 11th IMACS World Congress*, Oslo, Norway, 127–130.
- McDaniel, S. T. (1991). "Backscattering from rough interfaces and the parabolic approximation," Applied Research Laboratory, Penn State University, State College, Pennsylvania, U.S.A., ARL Tech. Mem. 91–104.
- McDonald, B. E., and W. A. Kuperman (1987). "Time domain formulation for pulse propagation including nonlinear behavior at a caustic," *J. Acoust. Soc. Am.* **81**, 1406–1417.
- Murphy, J. E., and S. A. Chin-Bing (1991). "A seismo-acoustic finite element model for underwater acoustic propagation," in *Shear Waves in Marine Sediments*, J. M. Hovem, M. D. Richardson, and R. D. Stoll (eds.), (Kluwer Press, Amsterdam), 463–470.
- Orchard, B. J., W. L. Siegmann, and M. J. Jacobson (1990). "A Three-Dimensional Time-Domain Paraxial Approximation for Underwater Acoustic Wave Propagation," *J. Acoust. Soc. Am. Suppl. 1*, **87**, S130.
- Perkins, J. S., and R. N. Baer (1982). "An Approximation to the Three-Dimensional Parabolic Equation Method for Acoustic Propagation," *J. Acoust. Soc. Am.* **72**, 515–522.
- Porter, M. B., F. B. Jensen, and C. M. Ferla (1991). "The problem of energy conservation in one-way models," *J. Acoust. Soc. Am.* **89**, 1058–1067.
- Robinson, E. R., and D. H. Wood (1988). "Generating direct starting fields for parabolic equations," *J. Acoust. Soc. Am.* **84**, 1794–1801.

PE Workshop II: Part 2 — Test Case Results

- Sayed, F. (1990). *Numerical Techniques for the Time-Dependent Schrodinger Equation and their Parallel Implementation*, Yale University, New Haven, CT, U.S.A., Ph.D. Dissertation.
- Shang, E. C., and D. Lee (1989). "A Numerical Treatment of the Fluid/Elastic Interface under Range-Dependent Environments," *J. Acoust. Soc. Am.* **85**, 654–660.
- Sluijter, F. W. (1970). "Arbitrariness of dividing the total field in a optically inhomogeneous medium into direct and reversed waves," *J. Opt. Soc. Am.* **60**, 8-10.
- Spofford, C. W. (1973). "A Synopsis of the AESD Workshop on Acoustic-Propagation Modeling by Non-Ray Tracing Techniques," AESD TN-73-05, Arlington, VA, U.S.A.
- Tappert, F. D. (1977). "The parabolic approximation method," in *Wave Propagation and Underwater Acoustics*, J. B. Keller and J. S. Papadakis (eds.), Lecture Notes in Physics, Vol. 70 (Springer-Verlag, New York), Chap. V, 224–287.
- Tappert, F. D., and D. Lee (1984). "A range refraction parabolic equation," *J. Acoust. Soc. Am.* **76**, 1797–1803.
- Tappert, F. D. (1988). "Parabolic equation modeling of shear waves," *J. Acoust. Soc. Am.* **78**, 1905–1906.
- Tappert, F. D. (1990). "Full-wave three-dimensional modeling of long-range oceanic boundary reverberation," *J. Acoust. Soc. Am. Suppl. 1* **88**, S84.
- Thomson, D. J., and N. R Chapman (1983). "A wide-angle split-step algorithm for the parabolic equation," *J. Acoust. Soc. Am.* **74**, 1848–1854.
- Thomson, D. J., and D. H. Wood (1987). "A postprocessing method for removing phase errors in the parabolic equation," *J. Acoust. Soc. Am.* **82**, 224–232.
- Thomson, D. J., and C. S. Bohun (1988). "A wide-angle initial field for parabolic equation models," *J. Acoust. Soc. Am. Suppl. 1* **83**, S118.
- Thomson, D. J. (1989). "Modal decomposition of waves in range-varying waveguides," *J. Acoust. Soc. Am. Suppl. 1* **86**, S53–S54.
- Thomson, D. J. (1990). "Wide-angle parabolic equation solutions to two range-dependent benchmark problems," *J. Acoust. Soc. Am.* **87**, 1514–1520.
- Wetton, B. T. R., and G. H. Brooke (1990). "One-way wave equations for seismoacoustic propagation in elastic waveguides," *J. Acoust. Soc. Am.* **87**, 624–632.

PART 3

CONTRIBUTED PAPERS

Editors' Note: Part 3 of the proceedings contains, in first-author alphabetical order, the contributed papers from the workshop participants. It is a valuable adjunct to the results presented in Part 2. These papers contain the theoretical framework associated with a particular PE model, in-depth discussions of results, and the particulars of how the model was applied to a specific test case problem. In addition, the papers given in Part 3 provide the comprehensive list of references associated with a particular PE model. In some cases, the papers represent the initial results of a new model development or application, e.g., the backscatter capability of the PE model.

The PE Workshop II was organized with the philosophy that the participants have as much freedom as possible to present and discuss their results and ideas. In keeping with this spirit, the contributed papers that appear in Part 3 are unedited. They faithfully represent the contribution(s) by their author(s).

A Single-Scatter Formalism for Improving PE Calculations in Range-Dependent Media

Gary H. Brooke and David J. Thomson

*Defence Research Establishment Pacific
FMO Victoria, BC Canada V0S 1B0*

ABSTRACT

A single-scatter formalism for improving PE calculations in range-dependent acoustic media is described. The medium is sub-divided into range-independent sections in which the total field is expressed as forward and backward propagating components. At the vertical interfaces between sections, appropriate boundary conditions are applied that (i) approximate continuity of pressure and horizontal displacement and (ii) enable individual forward and backward scattered components to be computed. A single-scatter approximation, in conjunction with finite-difference PE approximations, allows the scattered field components in each section to be obtained by solving one or more tridiagonal systems of equations. Two different implementations for heterogeneous waveguides are described. The first algorithm, based on a wide angle PE algorithm for media with continuously varying material parameters, requires a single tridiagonal matrix system to be solved at each vertical interface. The second algorithm, based on an acoustic PE for media comprised of distinct horizontal homogeneous layers, requires at least two tridiagonal systems to be solved at each vertical interface. Numerical results are computed for the ASA Benchmark Wedge problem and demonstrate that the algorithms yield accuracies in the forward direction which compare favorably with that obtained using two-way coupled modes.

1. INTRODUCTION

Practical applications for acoustic propagation algorithms generally involve range-dependent media. The parabolic equation (PE) model has been used extensively in range-dependent problems because it maintains computational efficiency by incorporating a simple range updating procedure into its marching algorithm (i.e. the medium is allowed to change at each range step).

Recently, some PE models have been shown to be inaccurate when applied to configurations involving range dependent bathymetry. Specifically, comparisons with full spectrum (two-way) coupled mode results for the ASA Benchmark Wedge problem [1] have demonstrated that forward (one-way) modelling with the PE can be inaccurate even in cases where backscatter is considered to be negligible (i.e. the benchmark wedge angle is only 2.86°). Subsequently, an investigation by Porter, Jensen and Ferla [2] showed that forward modelling of the acoustic pressure field, in general, does not conserve energy for

lossless range dependent problems when range updating is used. In their study, the authors examined deficiencies associated with the range-updating procedure by examining an energy-conserving asymptotic (WKB) solution for weakly range-dependent media. Essentially, it was shown that a forward model, such as the PE, is not capable of satisfying totally the boundary conditions in the range direction (i.e. at the vertical interfaces introduced by range updating). A judicious choice of field variable in the analysis, however, was shown to improve the energy conservation capability of the one-way algorithms providing there was negligible backscatter. More importantly, the authors demonstrated that energy conserving and, hence, more accurate solutions were obtained by using a single-scatter version of two-way coupled modes in which all boundary conditions at each vertical interface were satisfied (within the context of single scattering).

This paper addresses the issue of energy conservation as it pertains to accurate PE model calculations for range-dependent media. It is demonstrated that PE models can be adapted to a two-way single-scatter formalism which incorporates backscattered fields and is, therefore, capable of preserving, approximately, continuity of both pressure and horizontal displacement in the range direction. As such, the two-way PE algorithms so derived are very similar in methodology to the single scatter coupled mode algorithm mentioned above. For example, both algorithms rely on the fact that the medium can be subdivided into range-independent sections separated by vertical interfaces. Moreover, at each vertical interface, where the medium changes abruptly, both algorithms allow coupling between forward and backward propagating energy. To date, this approach has been incorporated into two different finite-difference acoustic PE algorithms for heterogeneous media namely (i) the Thomson PE (DJTPE [3]) and (ii) the Brooke PE (GHBPE: an acoustic PE based on the Elastic-PE algorithm [4]). Two different PE algorithms were chosen for analysis because they differ fundamentally in the manner in which they discretize in the depth coordinate. DJTPE treats the medium as being continuous in depth, whereas, GHBPE treats the medium as being made up of distinct homogeneous layers. By comparing with solutions obtained by two-way coupled modes, both algorithms yield accurate results for the forward propagating energy in the ASA Benchmark Wedge problem. It should be noted that accurate solutions have also been obtained for this problem using an “energy-conserving” PE which propagates reduced pressure [5]. The latter PE algorithm, however, is only energy conserving when the backscatter is indeed negligible. The two-way PE models developed in this paper incorporate backscatter directly into the model and, therefore, are capable of conserving energy (in principle, at least) for a wider class of problems.

2. THEORY

The theory underlying two-way single-scatter PE propagation models for range-dependent media is outlined in this section. The approach taken here follows closely that used for coupled modes. That is, the range-dependent waveguide is subdivided into range-independent sections as illustrated for an idealized ocean in Figure 1. These sections are

separated by vertical interfaces where the medium changes abruptly. Within each range-independent section, the representation of forward and backward propagating fields for a uniform waveguide apply. At the vertical interfaces, scattering occurs which couples the forward and the backward propagating fields. Solution for scattered components is achieved by enforcing continuity of pressure and horizontal displacement at each vertical interface. A single-scatter approximation is made in which the multiple interaction of the backscattered fields between discontinuities is neglected.

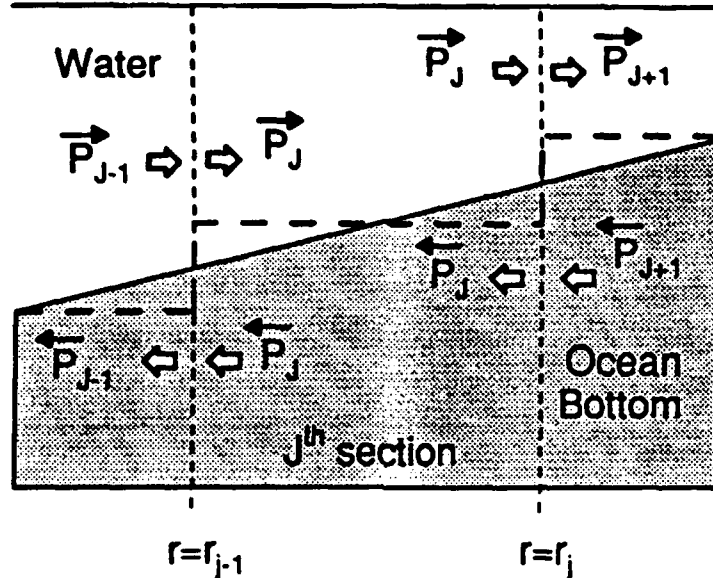


Figure 1. Range-dependent waveguide representation.

2.1 Range-Independent Waveguide Sections

Consider the range-independent waveguide shown in Figure 2. The medium is assumed to be continuously heterogeneous. That is, it consists of a single range-independent fluid layer with depth-dependent (but continuous) sound speed and density representative of an ideal ocean environment—a water column over a sediment bottom. It is further assumed that the sediment bottom is terminated at depth by a perfectly reflecting surface. This latter assumption is made based on a computational requirement associated with the PE method—the discretization grid is of finite extent. Of course, it is implied that an absorbing region deep within the sediment is included to minimize reflections from the fictitious boundary. The above representation of the waveguide (i.e. no sharp internal layer boundaries) allows a straightforward discretization scheme to be employed in the associated PE algorithm (DJTPe). A different PE algorithm with a less straightforward discretization scheme (GHBPE) is obtained by allowing both the sound speed and the density to be discontinuous at the water-sediment interface. For simplicity, the heterogeneous representation of the medium is used in the following derivation. The

corresponding analysis for layered media can be obtained simply by treating each layer to be homogeneous (with constant material parameters) and by satisfying the boundary conditions at all of the internal interfaces.

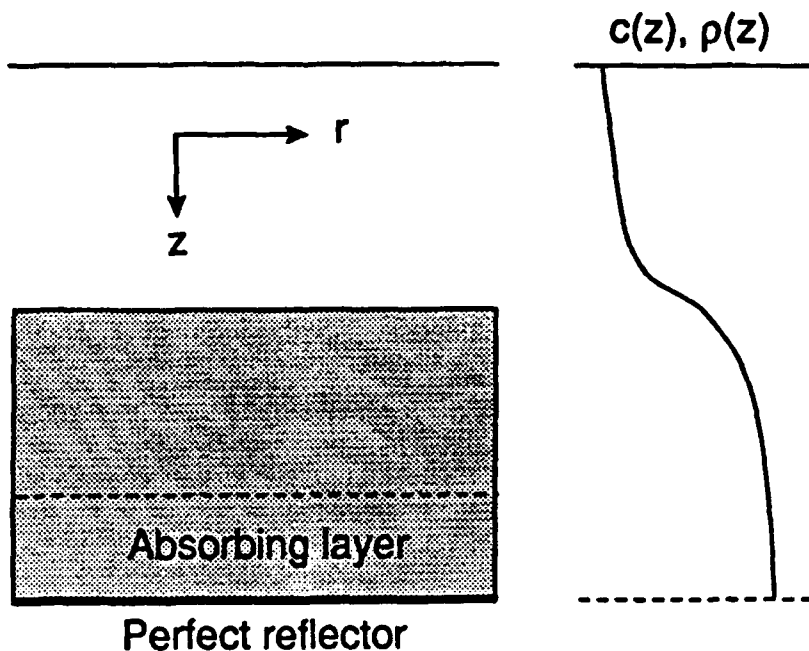


Figure 2. Range-independent heterogeneous waveguide section.

In the waveguide illustrated in Figure 2, the acoustic pressure, P , satisfies the following partial differential equation (with $e^{-i\omega t}$ time dependence and cylindrical symmetry)

$$\left\{ r^{-1} \partial_r (r \partial_r) + \rho(z) \partial_z (\rho^{-1}(z) \partial_z) + \frac{\omega^2}{c^2(z)} \right\} P(r, z) = 0 \quad (1)$$

where $c(z)$ and $\rho(z)$ represent, respectively, the depth dependent sound speed and density. In order to derive the PE equations, we first remove cylindrical spreading from the problem. That is, we define a reduced acoustic pressure, $p(r, z)$, such that

$$P(r, z) = \frac{1}{\sqrt{r}} p(r, z) . \quad (2)$$

Equation (1) can then be written (neglecting a term $O(r^{-2})$) as Helmholtz equation

$$\left\{ \partial_r^2 + \rho(z) \partial_z [\rho^{-1}(z) \partial_z] + \frac{\omega^2}{c^2(z)} \right\} p(r, z) = 0 \quad (3)$$

This equation can be factored into two first-order partial differential equations

$$\{\partial_r - ik_o Q^{1/2}(z)\} \tilde{p}(r, z) = 0 \quad (4)$$

and

$$\{\partial_r + ik_o Q^{1/2}(z)\} \tilde{p}(r, z) = 0 \quad (5)$$

where $k_o = \omega/c_o$ is a reference wavenumber, c_o is a reference speed and

$$Q^{1/2}(z) = \left\{ k_o^{-2} \rho(z) \partial_z [\rho^{-1}(z) \partial_z] + n^2(z) \right\}^{1/2} \quad (6)$$

is a pseudodifferential square root operator characteristic of parabolic equation methods. The refractive index, n , is defined as $n(z) = c_o/c(z)$ and the field quantities, $\tilde{p}(r, z)$ and $\tilde{p}(r, z)$, represent respectively, the forward and the backward propagating reduced pressure fields. The approximate solution of equations (4) and (5) can be obtained by approximating the square-root operator, by discretizing in range and depth and by marching in range. First, in anticipation of a marching solution, exponential phase factors are removed such that

$$\tilde{p}(r, z) = e^{+ik_o r} \tilde{\psi}(r, z) \quad (7)$$

and

$$\tilde{p}(r, z) = e^{-ik_o r} \tilde{\psi}(r, z) \quad (8)$$

which define PE field variables, $\tilde{\psi}(r, z)$ and $\tilde{\psi}(r, z)$. In this work, the operator $Q^{1/2}$ is approximated by a functional form, $F(Q)$, which will be specified in subsequent sections. Equations (4) and (5) can then be written as

$$\{\partial_r - ik_o [F(Q) - 1]\} \tilde{\psi}(r, z) = 0 \quad (9)$$

and

$$\{\partial_r + ik_o [F(Q) - 1]\} \tilde{\psi}(r, z) = 0 . \quad (10)$$

Solutions of equations (9) and (10) are required in order to describe the field within any range-independent section of the waveguide shown in Figure 1. Of course, the complete solution of the problem also requires that the fields satisfy boundary conditions at the vertical interfaces between these sections.

2.2 Vertical Interfaces

At each vertical interface of the range-dependent waveguide illustrated in Figure 1, the total field must satisfy continuity both of acoustic pressure and of horizontal displacement. A single scatter approximation is made whereby the interaction of backscattered fields

between vertical interfaces is ignored. Thus, for forward propagation (see Figure 1), we neglect the backscattered fields just to the right of all vertical interfaces. As an example, consider the interface at $r=r_j$ between the J^{th} and the $J+1^{\text{th}}$ section. In the single scatter approximation, the boundary conditions may be written as

$$\bar{P}_J(r_j, z) + \bar{P}_J(r_j, z) = \bar{P}_{J+1}(r_j, z) \quad (11)$$

and

$$\rho_J^{-1}(z) \partial_r [\bar{P}_J(r_j, z) + \bar{P}_J(r_j, z)] = \rho_{J+1}^{-1}(z) \partial_r [\bar{P}_{J+1}(r_j, z)] \quad (12)$$

where lower case subscripts refer to the range and the capitalized subscripts refer to the range section (i.e. the $J+1^{\text{th}}$ range section is defined between ranges r_j and r_{j+1}). In terms of the PE fields, equations (11) and (12) can be rewritten as follows

$$e_j \tilde{\psi}_J(r_j, z) + \tilde{\psi}_J(r_j, z) = e_j \tilde{\psi}_{J+1}(r_j, z) \quad (13)$$

and

$$\begin{aligned} e_j \rho_J^{-1}(z) \{ \partial_r \tilde{\psi}_J(r_j, z) + K_j^- \tilde{\psi}_J(r_j, z) \} + \{ \partial_r \tilde{\psi}_J(r_j, z) + K_j^+ \tilde{\psi}_J(r_j, z) \} \\ = e_j \rho_{J+1}^{-1}(z) \{ \partial_r \tilde{\psi}_{J+1}(r_j, z) + K_j^- \tilde{\psi}_{J+1}(r_j, z) \} \end{aligned} \quad (14)$$

where

$$e_j = e^{i2k_o r_j} \quad (15)$$

and

$$K_j^\pm = ik_o \left\{ 1 \pm [i2k_o r_j]^{-1} \right\} \quad (16)$$

The acoustic pressure in the range-dependent waveguide can be obtained by solving equations (9) and (10) in each section and requiring that those solutions also satisfy equations (13) and (14). The numerical solution of these equations forms the basis for a two-way PE algorithm.

3. TWO-WAY PE ALGORITHMS

In this section the two-way PE algorithms (DJTPE and GHBPE) are described. Within any range-independent waveguide section, the algorithms use a Crank-Nicolson discretization scheme in range and a finite-difference based discretization in the depth coordinate. The algorithms differ, however, in the manner in which the depth discretization is implemented, particularly for the continuity equations at the vertical interfaces.

The Crank-Nicolson scheme is straight range coordinate, equations (9) and (10) may be written as

$$\{1 - ik_o \Delta r [F(Q) - 1] / 2\} \bar{\psi}(r + \Delta r) = \{1 + ik_o \Delta r [F(Q) - 1] / 2\} \bar{\psi}(r) \quad (17)$$

and

$$\{1 - ik_o \Delta r [F(Q) - 1] / 2\} \bar{\psi}(r - \Delta r) = \{1 + ik_o \Delta r [F(Q) - 1] / 2\} \bar{\psi}(r) \quad (18)$$

Equations (17) and (18) state simply that forward (\rightarrow) and backward (\leftarrow) propagating fields satisfy the same equation, a requirement for isotropic media. It remains to perform the discretization in the depth coordinate.

3.1 DJTPE

The Thomson two-way PE algorithm (DJTPE) assumes that the medium is continuously heterogeneous within any range-independent section. This assumption implies that there is a continuous transition of material parameters at the interface between the water column and the ocean bottom which, in turn, directly affects the discretization scheme used in the depth coordinate. DJTPE employs a Claerbout [6] square-root approximation, $F_c(Q)$, defined as

$$F_c(Q) = 1 + 0.5Q / [1 + 0.25Q] \quad (19)$$

where

$$Q = 1 + \varepsilon + \mu \quad (20)$$

$$\varepsilon = n^2(z) - 1 + [i 2n(z)\alpha(z)] / k_o \quad (21)$$

$$\mu = \rho \partial_z (\rho^{-1} \partial_z) / k_o^2 \quad (22)$$

and where $\alpha(z)$ is the depth-dependent intrinsic absorption of the medium. Substitution of equation (19) into equation (17) leads to the following Crank-Nicolson finite-difference PE approximation for the forward propagation within the J^{th} range segment (superscript T refers to DJTPE)

$$L_{J,-}^T \bar{\psi}_{J+1}(r_j, z) = L_{J,+}^T \bar{\psi}_J(r_j, z) \quad (23)$$

where

$$L_{J,\pm}^T \triangleq 1 + 0.25[1 \pm ik_o \Delta r] [\varepsilon_J + \mu_J] \quad (24)$$

and where

$$[\varepsilon_J + \mu_J] \bar{\psi}_J(r_j, z) \sim \gamma p_{J,-} \bar{\psi}_J(r_j, z - \Delta z) + \gamma p_{J,+} \bar{\psi}_J(r_j, z + \Delta z) + \\ [\varepsilon_J + \rho_{J,o}] \bar{\psi}_J(r_j, z) \quad (25)$$

$$\gamma = [k_o \Delta z]^{-2} \quad (26)$$

$$\rho_{J,o} = \rho_{J,-} + \rho_{J,+} \quad (27)$$

$$\rho_{J,\pm} = 2\rho_J(z) / [\rho_J(z) + \rho_J(z \pm \Delta z)]. \quad (28)$$

In this discussion, z represents a depth vector whose components are the grid depths; the PE fields may now be interpreted as vectors over those depths. The Δ notation in equation (24) is used to define the matrices $L_{J,+}^T$ and $L_{J,-}^T$ in terms of the operators ε_J and μ_J (subscript J refers to the J^{th} range segment). Clearly, the modified centered-difference formula given by equation (25) results in a tridiagonal form for the matrices, $L_{J,+}^T$ and $L_{J,-}^T$. DJTPE, therefore, is marched through any range-independent waveguide section by solving a tridiagonal matrix system at each range step (as is the case in most acoustic PE algorithms).

The final task is to discretize the continuity equations at the vertical interfaces. The difficulty lies in equation (14) where there are terms involving $\partial_r \bar{\psi}$ and $\partial_r \bar{\psi}$. A direct substitution for these terms may be made from equations (8) and (9) with the result that (at the j^{th} interface)

$$\bar{\psi}_J(r_j, z) = e_j [\bar{\psi}_{J+1}(r_j, z) - \bar{\psi}_J(r_j, z)] \quad (29)$$

and

$$\begin{aligned} & \left\{ \rho_J^{-1} F(Q_J) + \rho_{J+1}^{-1} F(Q_{J+1}) + [i2k_o r_j]^{-1} [\rho_J^{-1} - \rho_{J+1}^{-1}] \right\} \bar{\psi}_{J+1}(r_j, z) \\ &= 2\rho_J^{-1} F(Q_J) \bar{\psi}_J(r_j, z) \end{aligned} \quad (30)$$

In deriving equation (30) from equation (14), we have used equation (29) to eliminate $\bar{\psi}_J(r_j, z)$. In any case, the continuity conditions now involve an approximate square root operator, $F(Q)$. Because DJTPE assumes the medium to be continuously heterogeneous, it is possible to use a standard (Tappert [7]) square-root approximation (i.e. $F(Q) = (1+Q)/2$) and then apply equation (25) directly. The result is a finite-difference approximation to the interface conditions which may be stated as

$$\bar{\psi}_J(z) = e_j \{ \bar{\psi}_{J+1}(r_j, z) - \bar{\psi}_J(r_j, z) \} \quad (31)$$

and

$$\{R_{J+1} M_{J+1,-}^T + R_J M_{J,+}^T\} \bar{\psi}_{J+1}(r_j, z) = \{R_j [M_{J,-}^T + M_{J,+}^T]\} \bar{\psi}_J(r_j, z) \quad (32)$$

where R_J and R_{J+1} are diagonal matrices with elements defined by the reciprocals of ρ_J and

ρ_{j+1} respectively. Once again using the Δ notation, the matrices $M_{J,+}^T$ and $M_{J,-}^T$ are defined in terms of the appropriate operators as

$$M_{J,\pm}^T \Delta \left\{ 1 \pm [i 2k_o r_j]^{-1} + 0.5[\epsilon_J + \mu_J] \right\} \quad (33)$$

It follows that the matrices $M_{J,+}^T$ and $M_{J,-}^T$ are tridiagonal and that equation (32) represents a tridiagonal matrix system for the forward scattered field at the j^{th} vertical interface. The solutions of this equation can then be substituted into equation (31) to obtain the backscattered field if desired.

In summary, DJTPE is a finite-difference two-way PE algorithm that uses a wide-angle Claerbout square-root approximation in marching the acoustic field through range-independent sections of the waveguide. It employs a Tappert square-root approximation in the solution for the scattered fields at the vertical interfaces. Computationally, the algorithm requires a tridiagonal matrix system to be solved not only at each range step but also at each vertical interface. Roughly speaking, the computational load for the DJTPE algorithm is twice that of a conventional one-way PE.

3.2 GHBPE

The Brooke two-way PE algorithm (GHBPE) assumes that the medium is made up of horizontally-stratified homogeneous layers; Thus, at the interface between the water column and the ocean bottom, the sound speed and the density are allowed to be discontinuous. The assumption of horizontal stratification is used directly in the discretization scheme for the depth coordinate. That is, the depth grid points are defined by the interfaces between horizontal layers (i.e. the waveguide is divided into many homogeneous horizontal layers).

GHBPE employs a rational linear square-root approximation (with complex coefficients) of the form

$$F_B(Q) = 1 + a_c Q / [1 + b_c Q] \quad (34)$$

where

$$Q = k_o^{-2} \partial_z^2 + n^2(z) + i 2n(z)\alpha(z) / k_o \quad (35)$$

The complex coefficients a_c and b_c are chosen according to a scheme detailed elsewhere [4]. In this work, their numerical values are given by $a_c = -0.4999976+i0$ and $b_c = 0.2500012-i0.0148130$. It suffices to say that they are close in magnitude to the corresponding Claerbout coefficients (see equation (19)) but have a small imaginary component. In an acoustic PE, complex square-root coefficients introduce an artificial absorption that serves to attenuate high-angle energy. Depending on the choice of c_o , it is

possible to attenuate artificially the low-angle energy as well. Care must be exercised, therefore, to ensure that the propagating energy of interest is not significantly attenuated.

In contrast to the DJTPE algorithm, substitution of equation (34) into equation (17) does not lead to an equation which can be discretized directly in the depth coordinate. Clearly, the horizontal interface between the water column and the ocean bottom precludes the use of a centered difference form for ∂_z^2 . This problem is alleviated by using a discretization scheme (devised by Greene [8]) in which the waveguide is divided purposely into many horizontal layers. Briefly, this scheme may be described as follows. At the interface between layers, equations which represent continuity of pressure and of vertical displacement are written in terms of second-order accurate forward (and backward) difference formulae. These forward and backward differences involve the operator ∂_z^2 . Equation (17), in conjunction with the square-root approximation in equation (34), is used to eliminate ∂_z^2 from these difference equations. Combining the resulting equations from all of the interfaces produces a tridiagonal matrix. Consequently a finite-difference PE algorithm can be derived which is marched in range by solving a tridiagonal matrix system in accordance with other acoustic PE algorithms. That is, for forward propagation (superscript B refers to GHBPE)

$$L_{J,-}^B \tilde{\psi}(r_j, z) = L_{J,+}^B \tilde{\psi}(r_{j-1}, z) \quad (36)$$

and for backward propagation

$$L_{J,-}^B \tilde{\psi}(r_{j-1}, z) = L_{J,+}^B \tilde{\psi}(r_j, z) \quad (37)$$

where the matrices $L_{J,+}^B$ and $L_{J,-}^B$ are tridiagonal and are obtained using the procedure outlined above. It is important to note that these matrices are not identical to the marching matrices defined by equation (23) in the DJTPE algorithm. A similar notation has been used only to be consistent.

The final step in defining the GHBPE algorithm is the discretization of the continuity equations at the vertical interfaces. As was stated previously, a direct substitution of equations (9) and (10) into equation (14) leads to an equation which involves ∂_z^2 (from the functional form of the square-root approximation). Once again, the horizontal layering of the waveguide does not allow this operator to be approximated by centered differences. Consequently, a different approach is required. Consider the first-order difference approximations given by

$$\partial_r \tilde{\psi}(r, z) \equiv [\tilde{\psi}(r + \Delta r, z) - \tilde{\psi}(r, z)] / \Delta r \quad (38)$$

and

$$\partial_r \tilde{\psi}(r, z) \equiv [\tilde{\psi}(r - \Delta r, z) - \tilde{\psi}(r, z)] / \Delta r \quad (39)$$

A comparison of equations (36-37) and equations (38-39) shows that in any range-independent section of waveguide (in particular, the J^{th} section) the following relationships hold

$$\partial_r \tilde{\psi}_J(r_j, z) \equiv \left\{ I - \left\{ L_{J,-}^B \right\}^{-1} L_{J,+}^B \right\} \tilde{\psi}_J(r_j, z) \quad (40)$$

and

$$\partial_r \tilde{\psi}_J(r_j, z) \equiv - \left\{ I - \left\{ L_{J,-}^B \right\}^{-1} L_{J,+}^B \right\} \tilde{\psi}_J(r_j, z). \quad (41)$$

Using equations (40) and (41), equations (13) and (14) may be discretized with the result that

$$\tilde{\psi}_J(r_j, z) = e_j \left\{ \tilde{\psi}_{J+1}(r_j, z) - \tilde{\psi}_J(r_j, z) \right\} \quad (42)$$

and

$$\left\{ R_{J+1} M_{J+1,-}^B + R_J M_{J,+}^B \right\} \tilde{\psi}_{J+1}(r_j, z) = \left\{ R_J \left[M_{J,-}^B + M_{J,+}^B \right] \right\} \tilde{\psi}_J(r_j, z) \quad (43)$$

where the matrices R_J and R_{J+1} have already been defined in terms of the densities and where the matrices $M_{J,+}^B$ and $M_{J,-}^B$ are given by

$$M_{J,\pm}^B = \left\{ 1 - ik_o \Delta r \left[1 \pm (2k_o r_j)^{-1} \right] \right\} I - \left\{ L_{J,-}^B \right\}^{-1} L_{J,+}^B \quad (44)$$

where I is the identity matrix. We note that although $L_{J,+}^B$ and $L_{J,-}^B$ are tridiagonal matrices, the matrix inverse involved in equation (44) implies that the matrices $M_{J,+}^B$ and $M_{J,-}^B$ are dense.

The above analysis indicates that a two-way finite-difference PE algorithm for horizontally layered media can be derived in which the fields are marched through range-independent sections by solving a tridiagonal matrix system at each range step and in which the scattering at each of the vertical interfaces is obtained from the solution of a dense matrix problem. Clearly, the computational load involved in such a procedure is prohibitively high. Fortunately, an alternative in the form of an iterative scheme is available.

Consider equation (43) premultiplied by the matrix product of $\left\{ L_{J,-}^B \right\}$ and $\left\{ R_J^{-1} \right\}$ and then rearranged to form

$$\begin{aligned} & L_{J,-}^B \left\{ \left[1 - ik_o \Delta r \left[1 - (2k_o r_j)^{-1} \right] \right] R_J^{-1} R_{J+1} + M_{J,+}^B \right\} \tilde{\psi}_{J+1}(r_j, z) \\ &= L_{J,-}^B \left\{ M_{J,-} + M_{J,+} \right\} \tilde{\psi}_J(r_j, z) + L_{J,-}^B \left\{ R_J^{-1} R_{J+1} \right\} \phi_{J+1}(r_j, z) \end{aligned} \quad (45)$$

where

$$\phi_{J+1}(r_j, z) = \left\{ L_{J+1,-}^B \right\}^{-1} L_{J+1,+}^B \vec{\psi}_{J+1}(r_j, z) \quad (46)$$

A comparison of equations (46) and (36) shows that the field quantity $\phi_{J+1}(r_j, z)$ is just the unknown forward scattered field marched ahead one range step in the $J+1^{\text{th}}$ range segment. Furthermore, if an approximation to $\phi_{J+1}(r_j, z)$ is obtained and substituted into equation (45), then the resulting matrix system involves only tridiagonal matrices and its solution yields the forward scattered field (premultiplying by the product of $\left\{ L_{J,-}^B \right\}$ and $\left\{ R_J^{-1} \right\}$ serves to tridiagonalize much of the original equation (44)). Thus, an iterative solution of equation (45) may be obtained as follows:

1. Approximate $\vec{\psi}_{J+1}(r_j, z)$ with $\vec{\psi}_J(r_j, z)$
2. Calculate the zeroth iterate $\phi_{J+1}^0(r_j, z)$ by marching $\vec{\psi}_{J+1}(r_j, z)$ ahead one range step in the $J+1^{\text{th}}$ range section.
3. Solve equation (46) for an improved estimate of $\vec{\psi}_{J+1}(r_j, z)$
4. Calculate the i^{th} iterate $\phi_{J+1}^i(r_j, z)$ by marching $\vec{\psi}_{J+1}(r_j, z)$ ahead one range step in the $J+1^{\text{th}}$ range section.
5. Repeat steps 3 and 4 until results converge.

In summary, GHBPE is a finite-difference two-way PE algorithm that uses a rational linear square-root approximation (with complex coefficients) in marching the acoustic field through range-independent sections of the waveguide. Also, it employs an iterative scheme to solve for the scattered fields at each of the vertical interfaces. Computationally, the algorithm requires one tridiagonal matrix system to be solved at each range step in the marching and $2N$ (N is the number of iterations) tridiagonal matrix systems to be solved at each vertical interface. Clearly, the computational load in GHBPE is significantly higher than in DJTPE and is a direct result of the initial assumption that the waveguide is horizontally stratified.

4. NUMERICAL RESULTS

In this section, numerical results are presented which illustrate the application of the two-way PE algorithms, DJTPE and GHBPE, to the ASA Benchmark Wedge problem [1]. The wedge configuration is illustrated in Figure 3. It represents a water layer ($\rho=1$, $c=1500$) over a sloping sediment layer ($\rho=1.5$, $c=1700$, $\alpha=0.5\text{dB}/\lambda$). The source frequency and depth for this problem are 25Hz and 100m respectively, and receivers are located at depths of 30m and 150m. Propagation loss as a function of range has been calculated using the two-way algorithms DJTPE and GHBPE for each receiver depth and compared to results obtained using the full spectrum coupled-mode model. For comparison purposes, the same results were generated using one-way versions of the algorithms (i.e. versions of DJTPE and GHBPE which do not include backscatter). All of the PE results presented here were

computed using a grid of 5m in range and 0.5m in depth. Also, for both algorithms, the perfect reflector was located at a depth of 1000m and an artificial absorbing region was located between depths of 500m and 1000m with absorption increasing from the intrinsic value at 500m to the intrinsic value plus $10\text{dB}/\lambda$ at 1000m.

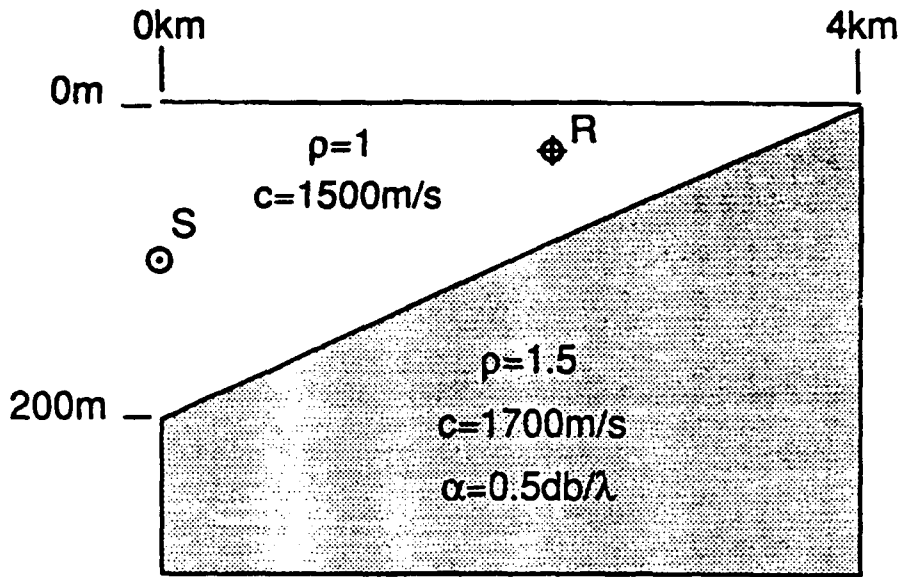


Figure 3. ASA Benchmark Wedge configuration

First consider the case involving the shallow receiver at 30m. A plot of transmission loss versus range for the one-way version of DJTPE without backscatter is shown as the solid curve in Figure 4(a). The reference solution obtained using two-way coupled modes is shown as the dashed curve in this figure.

There is an obvious discrepancy between the two curves indicating that a one-way PE (as is now well known) does not perform well in this problem. The results obtained using the two-way DJTPE algorithm are shown in Figure 4(b) as the solid curve. Once again, the reference coupled mode results are shown as the dashed curve. Clearly, the two-way PE algorithm is generating much more accurate results. Note that, at close ranges the PE is not able to represent accurately the higher angle energy—a better square-root approximation would alleviate this problem.

Corresponding results obtained for the deep receiver at 150m are shown in Figures 5(a) and (b), respectively. As was the case in the previous example, these figures show that the two-way DJTPE algorithm is required in order to generate accurate results for the ASA benchmark wedge.

The results obtained for the shallow receiver, using the one- and two-way GHBPE

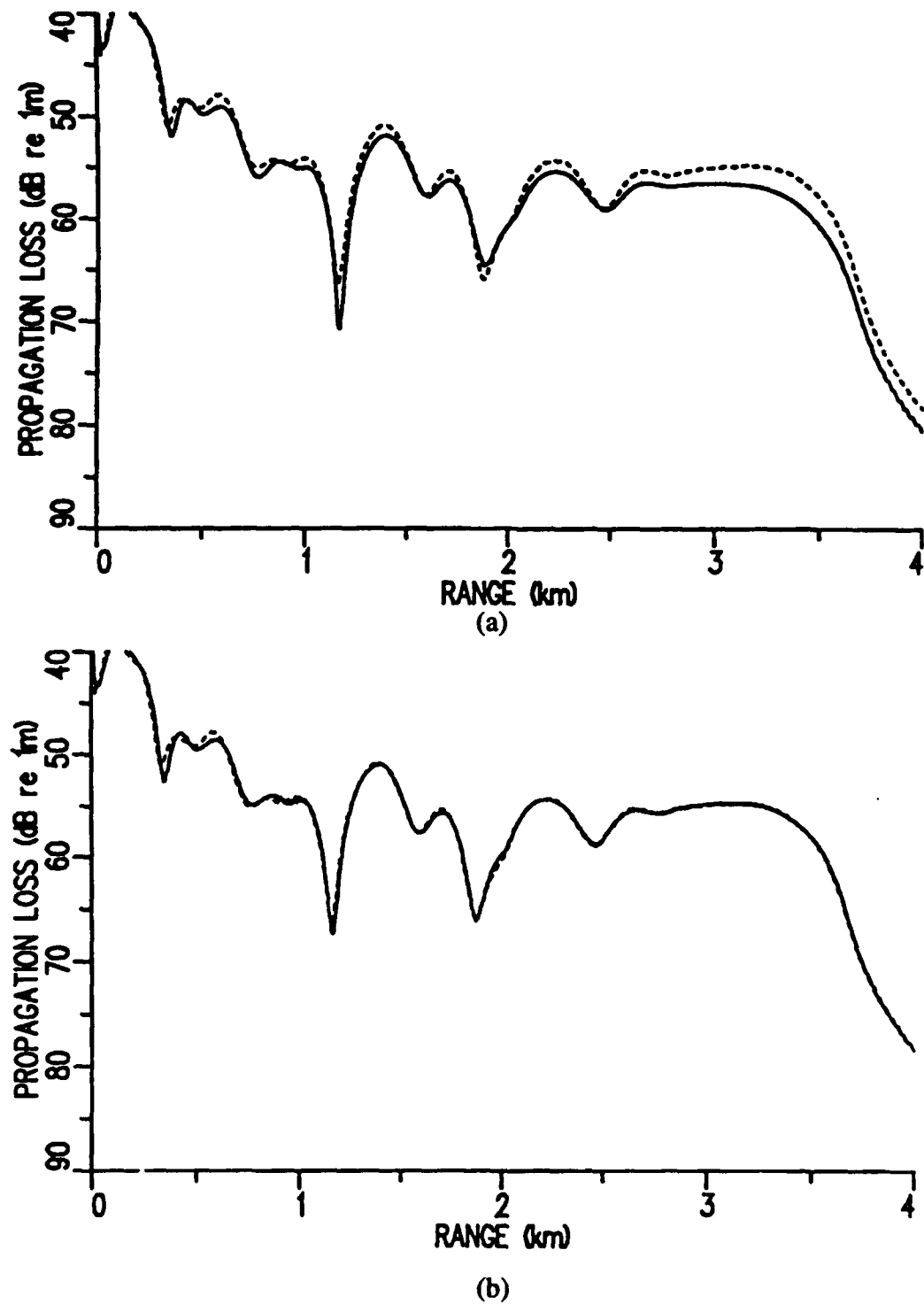


Figure 4. ASA Benchmark results (solid) for $R=30\text{m}$: a) one-way DJTPE and b) two-way DJTPE. Two-way coupled mode reference (dashed).

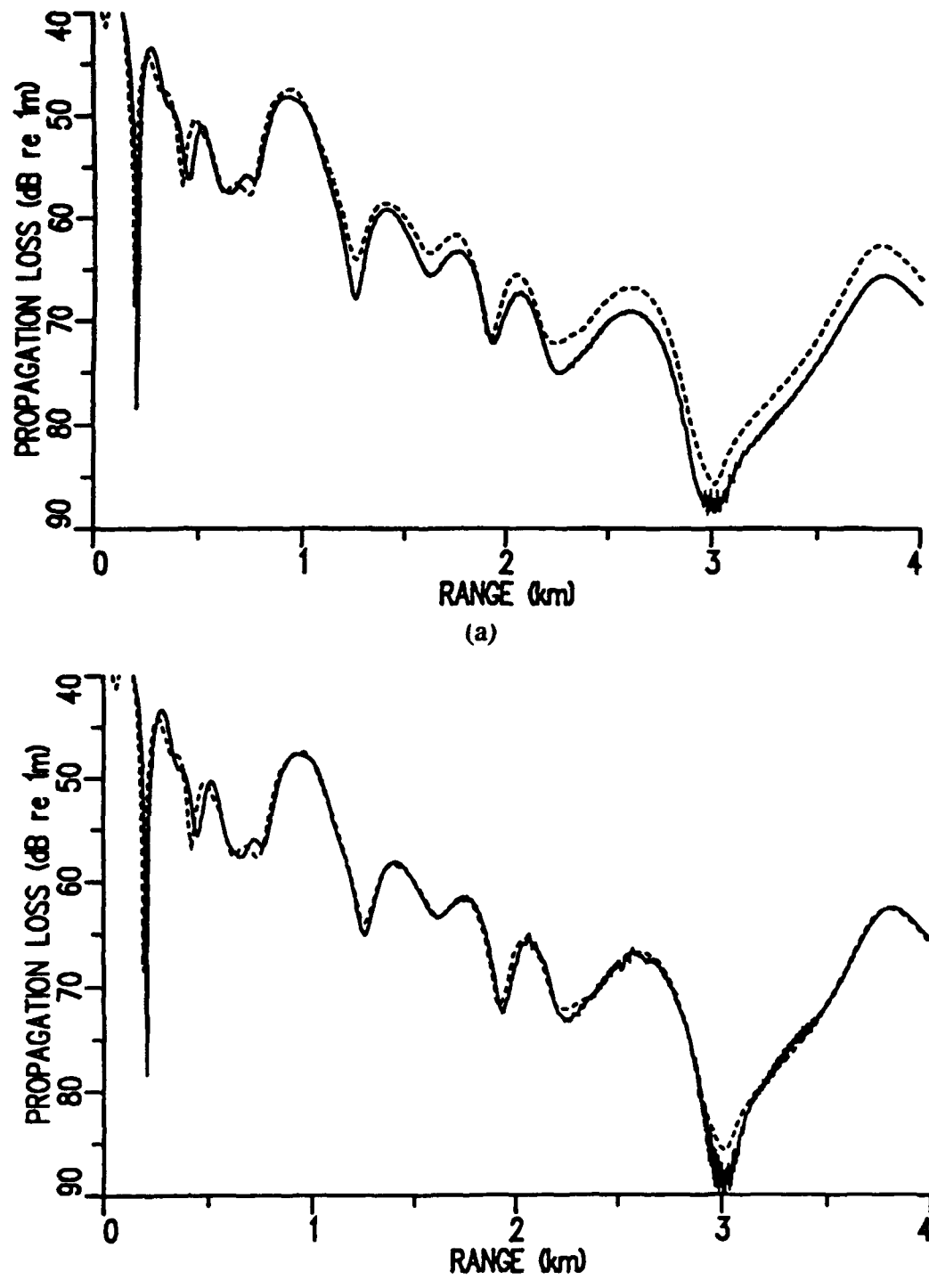


Figure 5. ASA Benchmark results (solid) for $R=150\text{m}$: a) one-way DJTPE and b) two-way DJTPE. Two-way coupled mode reference (dashed).

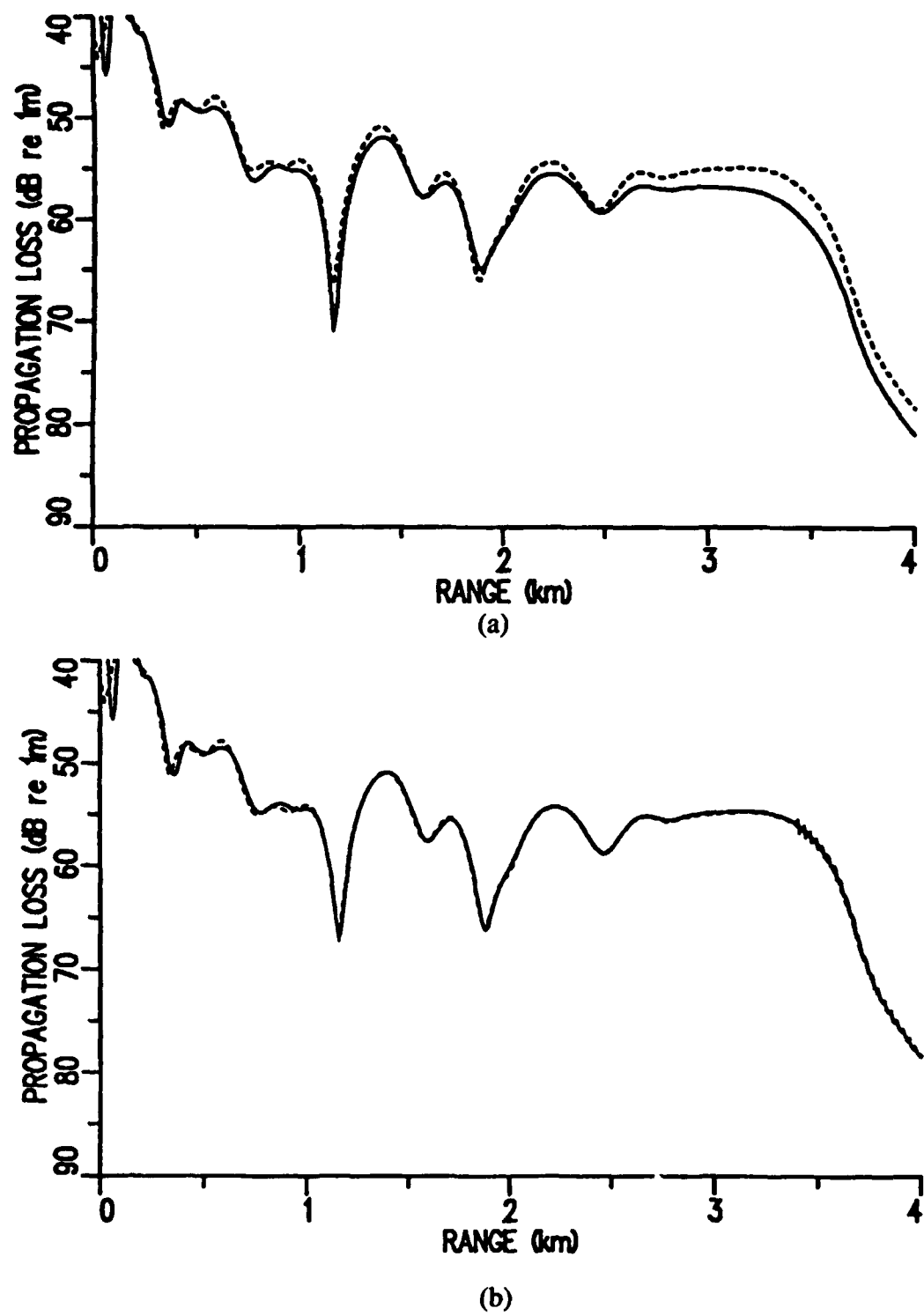


Figure 6. ASA Benchmark results (solid) for $R=30\text{m}$: a) one-way GHBPE and b) two-way GHBPE. Two-way coupled mode reference (dashed).

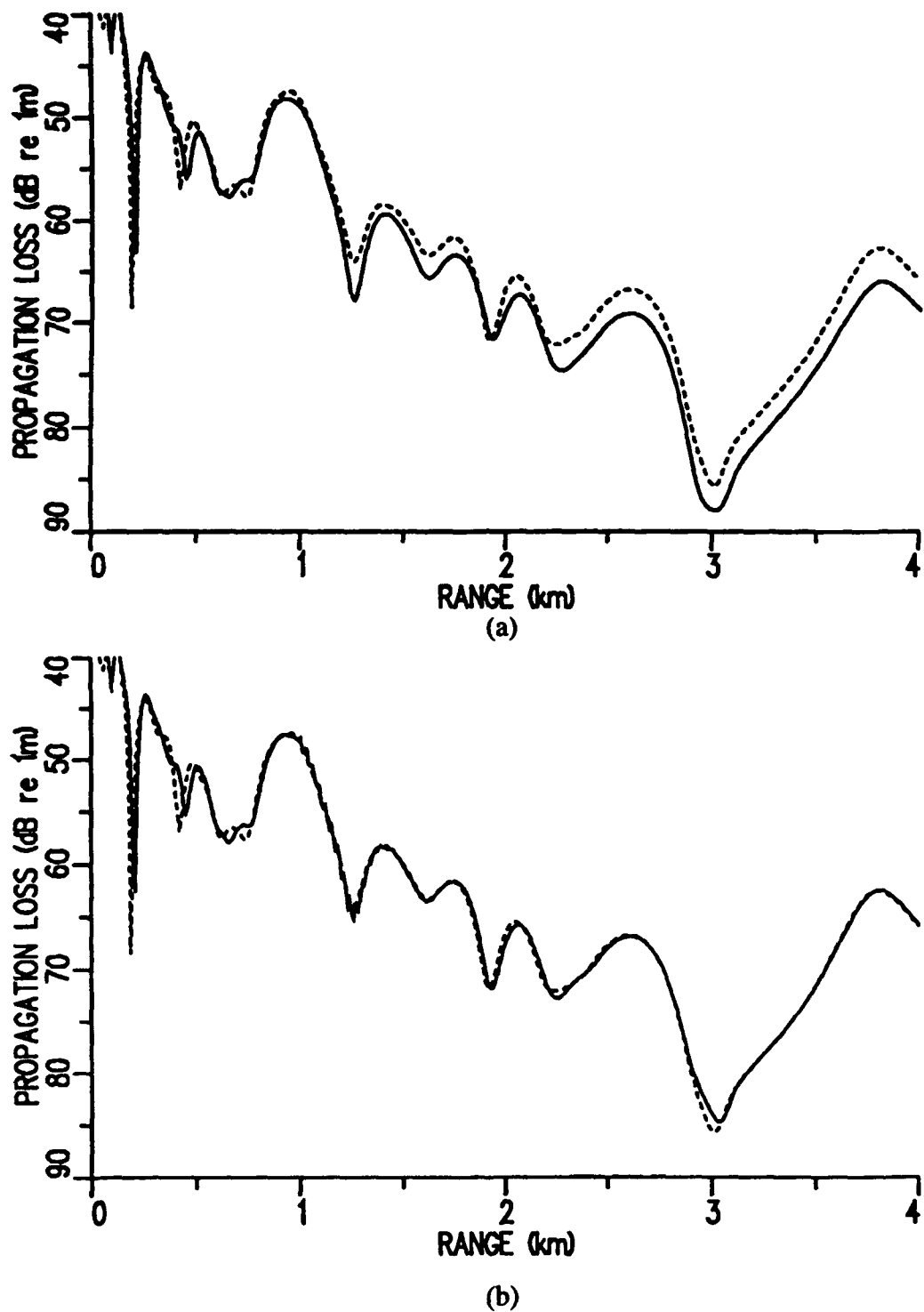


Figure 7. ASA Benchmark results (solid) for $R=150\text{m}$: a) one-way GHBPE and b) two-way GHBPE. Two-way coupled mode reference (dashed).

algorithms, are shown in Figures 6(a) and 6(b), respectively. The two-way GHBPE results were computed with ten iterations for the scattered field calculations. As with the DJTPE algorithm, a comparison with the reference solution indicates that the one-way GHBPE algorithm is unable to produce accurate solutions for the wedge problem, however, the two-way GHBPE algorithm performs very well in this case. The oscillations in the loss curve, as the receiver passes into the bottom layer at a range of 3400m (Figure 6(b)), seem to be characteristic of PE algorithms involving range-dependent layered media. Wide-angle propagating energy (artifact) is excited at the vertical faces. ASA Benchmark results(solid) for R=30m: a) one-way GHBPE and b) two-way GHBPE. Two-way coupled mode reference (dashed) vertical faces and interferes with the normal radiated energy into the bottom layer. A higher-order square root approximation helps to minimize this interference.

The final test case is that involving the deep receiver at 150m. The results corresponding to those shown in Figures 5(a) and (b) are shown in Figures 7(a) and 7(b), respectively. As before, the one-way GHBPE algorithm is not capable of producing accurate results for this receiver depth. The two-way GHBPE algorithm, however, performs very well. Note that the GHBPE results are slightly smoother than the DJTPE results, particularly in the deep null at a range of nearly 3km. This is a direct result of using the complex coefficients for the square-root approximation in GHBPE which attenuate the high angle energy causing the interference in the null.

5. SUMMARY

This paper represents a brief outline of a formalism which can be employed to improve the energy conserving capabilities, and hence accuracy, of PE algorithms when applied to range-dependent media. Essentially, two-way PE algorithms are devised which mimic closely the two-way coupled mode formulation. That is, the waveguide is segmented into range-independent sections separated by vertical interfaces at which the medium is allowed to change abruptly. The PE algorithms use a single scatter approximation to include backscatter at the vertical interfaces and, hence, allow the appropriate boundary conditions to be better satisfied. Two finite-difference PE algorithms are described (DJTPE and GHBPE) which differ only in the manner in which they are able to treat the discretization in the depth coordinate. DJTPE assumes the medium to be continuously heterogeneous and can therefore employ relatively straightforward centered differences in the discretization procedure. One important consequence of this fact is that DJTPE is able to solve a single tridiagonal matrix system for the scattered fields at the vertical interfaces directly. Alternatively, GHBPE treats the medium to be made up of distinct homogeneous horizontal layers. At the interfaces between layers, the material parameters are allowed to change discontinuously; the discretization procedure necessarily involves forward and backward differences. The disadvantage of this procedure is that GHBPE must employ an iterative

scheme (involving repeated tridiagonal matrix problems) to solve for the scattered fields at each vertical interface.

The two-way PE algorithms were tested by comparing with reference two-way coupled mode solutions for the ASA Benchmark Wedge problem. Both DJTPE and GHBPE yielded accurate results for this problem which confirms that conventional one-way PE algorithms can be adapted to include backscatter and, thereby, be energy conserving.

Computationally, DJTPE is the most efficient, roughly half as efficient as a conventional one-way algorithm. It requires the solution of a tridiagonal matrix system at each range step and at each vertical interface. GHBPE, by comparison, is relatively inefficient because although a single tridiagonal matrix must be solved at each range step, several such matrix systems must be solved at each vertical interface.

Finally, the rather limited tests done to date indicate that for acoustic problems involving heterogeneous media, the two-way DJTPE algorithm is the most promising approach. The two-way GHBPE algorithm, though relatively inefficient for acoustic problems, may provide the basis for applying the same approach to PE algorithms for horizontally stratified elastic media.

6. REFERENCES

1. F. Jensen and C.M. Ferla, "Numerical solutions of range-dependent benchmark problems in ocean acoustics," *J. Acoust. Soc. Am.* **87**, 1499-1510 (1990).
2. M.B. Porter, F. Jensen and C.M. Ferla, "The problem of energy conservation in one-way models," *J. Acoust. Soc. Am.* **89**, 1058-1067 (1991).
3. D.J. Thomson, "Wide-angle parabolic equation solutions to two range-dependent benchmark problems," *J. Acoust. Soc. Am.* **87**, 1514-1520 (1990).
4. B.T.R. Wetton and G.H. Brooke, "One-way wave equations for seismoacoustic propagation in elastic waveguides," *J. Acoust. Soc. Am.* **87**, 624-632 (1987).
5. M.D. Collins and E.K. Westwood, "A higher-order energy-conserving parabolic equation for range-dependent ocean depth, sound speed and density," *J. Acoust. Soc. Am.* **89**, 1068-1075 (1991).
6. J.F. Claerbout, "Coarse grid calculations of waves in inhomogeneous media with application to delineation of complicated seismic structure" *Geophysics* **35**, 20-21 (1970).
7. F.D. Tappert, "The parabolic approximation method," in: *Wave Propagation and Underwater Acoustics*, edited by J.B. Keller and J.S. Papadakis (Springer, New York, 1977), Chap. V, 224-287.
8. R.R. Greene, "A high-angle one-way wave equation for seismic wave propagation along rough and sloping interfaces," *J. Acoust. Soc. Am.* **77**, 1991-1998 (1985).

Higher-Order, Energy-Conserving, Two-Way, and Elastic Parabolic Equations

Michael D. Collins

*Naval Research Laboratory
Washington, D.C. 20375*

INTRODUCTION

The parabolic equation (PE) method was first applied to wave propagation problems in the 1940s [1]. After digital computers and the fast Fourier transform (FFT) became available, the PE method became an important computational method for range-dependent wave propagation. The introduction of an efficient numerical solution based on the FFT led to the widespread use of the PE method in underwater acoustics [2]. Improving the efficiency, accuracy, and capability of the PE method immediately became an active area of research. By the time of the first PE workshop [3], the first finite-difference [4] and wide-angle [5-7] PE models had appeared. This paper describes some of the improvements in the PE method that have occurred since the first PE workshop, including some recent work that has not been published elsewhere. The higher-order, energy-conserving, two-way, and elastic PEs are described in Sections 1-4. Some of the algorithms and computer codes used to obtain numerical solutions are discussed in Section 5. Solutions are presented for the second PE workshop test cases in Section 6. Some results that were obtained after the second PE workshop are discussed in Section 7.

Although phase errors were significantly reduced when the wide-angle PE was introduced, the accuracy of the PE method remained an issue of concern, and higher-order parabolic approximations were proposed [8,9]. In general, asymptotic solutions of differential equations are not guaranteed to converge even if the leading-order terms are accurate for some parameter values (e.g., the wide-angle PE is accurate for propagation angles less than about forty degrees from horizontal). Thus it was uncertain how much the aperture limitation of the PE could be reduced. The accuracy issue was resolved [10,11] when accurate solutions were obtained using the Padé approximations of [9] for problems involving propagation nearly orthogonal to the preferred direction and large piecewise-continuous depth variations in sound speed and density.

After phase errors were eliminated for range-independent problems (i.e., problems involving horizontally-stratified media), attention shifted to reducing amplitude errors for range-dependent problems (the most important application of the PE method), and range-dependent PEs (i.e., PEs designed for improved accuracy for range-dependent problems) were proposed [12-18]. Although it has been confirmed that the range-dependent PEs of [13] and [14] provide improved accuracy for some problems [18], the rotated PE was the first range-dependent PE confirmed to provide improved accuracy [16]. The energy-

conserving PE [18] is accurate for the outgoing component of most range-dependent problems, including problems involving steeply sloping ocean bottoms, very wide propagation angles, and large range and depth variations in the acoustic properties. The development of the energy-conserving PE involved the generalization of an energy-conserving normal-mode model [19] using a special numerical solution to avoid Gibbs oscillations.

After the PE method was improved to accurately handle outgoing energy, attention shifted to accounting for back-scattered energy. A PE that accounts for reverberation stochastically has been applied to model ocean-bottom back-scattering data [20]. It is more difficult to account for reverberation with the PE in a deterministic fashion. A pair of coupled PEs has been applied to model ocean-surface scattering [21]; however, accurate results were obtained only for the forward scattered field. The single-scattering approximation [22] has been incorporated into the PE to account for back-scattered energy and to further improve the accuracy of the outgoing component of the solution [23]. The two-way PE has been applied to solve reverberation problems that are too large and complicated to solve with other existing wave-based models and to simulate the localization of scatterers [23].

Extending the PE method to handle elastic ocean bottoms has been a topic of interest ever since the PE was first applied to underwater acoustics, and several elastic PE models were proposed prior to the first PE workshop [24-27]. The elastic PE requires a formulation that permits factorization [28], high accuracy for handling different waves speeds and nearly vertical propagation [29], and a special parabolic approximation to avoid instability [30]. The first successful elastic PE models [29,30] were combined and generalized [31] to obtain an elastic PE that is accurate and stable for range-independent problems, propagation nearly orthogonal to the preferred direction, propagation of all wave types including interface waves, and large depth and gradual range variations in the elastic properties. Although accuracy improvements are still being developed for range-dependent problems, accurate solutions have been obtained for problems involving sloping ocean bottoms with the rotated elastic PE [31] and the energy-conserving elastic PE.

1. THE HIGHER-ORDER PE

In this section, we describe the higher-order PE and its numerical solution. The acoustic pressure p is assumed to satisfy the pressure-release boundary condition $p = 0$ at the ocean surface and at an artificial boundary many wavelengths within the sediment. Since the sediment is lossy, the condition at the lower boundary accurately approximates the outgoing radiation condition at infinite depth. We work in cylindrical coordinates, where z is the depth below the ocean surface and r is the horizontal distance from a point source at $z = z_0$. We assume that $|kr| \gg 1$ and remove the spreading factor $r^{-1/2}$ from p . Range-dependent environments are approximated by a sequence of range-independent regions. In each range-independent region, the acoustic pressure satisfies the farfield equation,

$$\frac{\partial^2 p}{\partial r^2} + \rho \frac{\partial}{\partial z} \frac{1}{\rho} \frac{\partial p}{\partial z} + k^2 p = 0, \quad (1)$$

where ρ is the density, $k = (1 + i\eta\beta)\omega / c$ is the complex wavenumber, $\eta = (40\pi \log_{10} e)^{-1}$, β is the attenuation (in decibels per wavelength), c is the sound speed, and ω is the circular frequency.

Since the acoustic parameters c , ρ , and β depend only on z , Eq. (1) factors as follows:

$$\left(\frac{\partial}{\partial r} + ik_0 K \right) \left(\frac{\partial}{\partial r} - ik_0 K \right) p = 0, \quad (2)$$

$$K = \sqrt{1 + k_0^{-2} \left(\rho \frac{\partial}{\partial z} \frac{1}{\rho} \frac{\partial}{\partial z} + k^2 - k_0^2 \right)}, \quad (3)$$

where c_0 is the reference sound speed and $k_0 = \omega / c_0$ is the reference wavenumber. The following approximation is valid if the outgoing component of p dominates the incoming component:

$$\frac{\partial p}{\partial r} = ik_0 K p. \quad (4)$$

We apply a Padé approximation for the square-root function in Eq. (3) to obtain the higher-order PE,

$$\frac{\partial p}{\partial r} = ik_0 \left(1 + \sum_{j=1}^M \frac{a_{2j-1,M} x}{1 + a_{2j,M} x} \right) p, \quad (5)$$

$$x = k_0^{-2} \left(\rho \frac{\partial}{\partial z} \frac{1}{\rho} \frac{\partial}{\partial z} + k^2 - k_0^2 \right). \quad (6)$$

Since this Padé approximation involves only first powers of x , the numerical solution involves tridiagonal matrices, and multiple depth derivatives of the acoustic properties do not occur. There are different choices for the Padé coefficients that have different benefits. The following coefficients of [9] provide an approximation to K that is accurate to $O(x^{2M})$:

$$a_{2j-1,M} = \frac{2}{2M+1} \sin^2 \frac{j\pi}{2M+1}, \quad (7)$$

$$a_{2j,M} = \cos^2 \frac{j\pi}{2M+1}. \quad (8)$$

The case $M = 1$ corresponds to the original wide-angle PE [5]. The Padé coefficients described in Section 4 and tabulated in [31] are useful for suppressing Gibbs oscillations in the energy-conserving PE and instability in the elastic PE.

The numerical solution of the higher-order PE is based on the method of operator splitting [32]. The first term on the right side of Eq. (5) is handled by analytically removing the factor $\exp(ik_0r)$. The operator splitting solution of Eq. (5) requires a numerical solution for the following equation for $j = 1, \dots, M$:

$$(1 + a_{2j,M}x) \frac{\partial p}{\partial r} = (ik_0 a_{2j-1,M}x) p . \quad (9)$$

Finite differences based on Galerkin's method [29] are used to discretize Eq. (9) in z and Crank-Nicolson integration is used to integrate in r .

2. THE ENERGY-CONSERVING PE

The higher-order PE may be applied to solve range-dependent problems by allowing the acoustic parameters appearing in Eq. (5) to depend on r . Although this approach is accurate for many problems, large amplitude errors may arise for problems involving sloping ocean bottoms. The appropriate leading-order correction can be determined by considering the limit of arbitrarily small propagation angles, an approach that has been successful for accounting for the effects of nonlinearity [33], attenuation [34], dispersion [35], and three-dimensional variations [36,37] in outgoing solutions of the wave equation. We also present a complete energy-conservation correction in this section. Since the leading-order correction is robust, however, it is sufficient for most (if not all) ocean acoustic propagation problems.

For arbitrarily small propagation angles, p satisfies the following farfield equation in range-dependent media:

$$\frac{\partial^2 p}{\partial r^2} - \frac{1}{\rho} \frac{\partial \rho}{\partial r} \frac{\partial p}{\partial r} + k^2 p = 0 . \quad (10)$$

We assume that k has been rendered dimensionless with a length scale appropriate for the rate of range dependence. Substituting the WKBJ ansatz $p = A \exp(i\psi)$ into Eq. (10), we obtain

$$\frac{\partial^2 A}{\partial r^2} + 2i \frac{\partial A}{\partial r} \frac{\partial \psi}{\partial r} + iA \frac{\partial^2 \psi}{\partial r^2} - A \left(\frac{\partial \psi}{\partial r} \right)^2 - \frac{1}{\rho} \frac{\partial \rho}{\partial r} \frac{\partial A}{\partial r} - \frac{iA}{\rho} \frac{\partial \rho}{\partial r} \frac{\partial \psi}{\partial r} + k^2 A = 0 . \quad (11)$$

We assume that $|k| \gg 1$ and $\psi = O(k)$ and balance terms of $O(k^2)$ to obtain

$$\psi(r) = \int_0^r k(r') dr'. \quad (12)$$

Balancing terms of $O(k)$, we obtain the appropriate amplitude factor for range-dependent media,

$$2 \frac{\partial A}{\partial r} \frac{\partial \psi}{\partial r} + A \frac{\partial^2 \psi}{\partial r^2} - \frac{A}{\rho} \frac{\partial \rho}{\partial r} \frac{\partial \psi}{\partial r} = 0, \quad (13)$$

$$A(r) = \sqrt{\frac{\rho(r)c(r)}{\rho(0)c(0)}} A(0). \quad (14)$$

We define the new dependent variable $u = p / \alpha$, where $\alpha = \sqrt{\rho c}$, and Eq. (1) becomes

$$\frac{\partial^2 u}{\partial r^2} + \frac{\rho}{\alpha} \frac{\partial}{\partial z} \frac{1}{\rho} \frac{\partial}{\partial z} \alpha u + k^2 u = 0. \quad (15)$$

For range-independent environments, Eq. (15) reduces to the following outgoing wave equation:

$$\frac{\partial u}{\partial r} = ik_0 \tilde{K} u, \quad (16)$$

$$\tilde{K} = \sqrt{1 + k_0^{-2} \left(\frac{\rho}{\alpha} \frac{\partial}{\partial z} \frac{1}{\rho} \frac{\partial}{\partial z} \alpha + k^2 - k_0^2 \right)}. \quad (17)$$

In the limit of arbitrarily small propagation angles, Eq. (16) reduces to

$$\frac{\partial u}{\partial r} = iku, \quad (18)$$

which has the solution,

$$p(r) = p(0) \frac{\alpha(r)}{\alpha(0)} \exp \left[i \int_0^r k(r') dr' \right]. \quad (19)$$

We observe that Eq. (16) behaves properly in two important limits: it reduces to the WKBJ solution of Eq. (10) in the limit of small propagation angles; it reduces to the higher-order PE in the limit of gradual range dependence. We apply a Padé approximation for the square-root function in Eq. (17) to obtain the higher-order energy-conserving PE,

$$\frac{\partial u}{\partial r} = ik_0 \left(1 + \sum_{j=1}^M \frac{a_{2,j-1,M} \bar{x}}{1 + a_{2,j,M} \bar{x}} \right) u, \quad (20)$$

$$\bar{x} = k_0^{-2} \left(\frac{\rho}{\alpha} \frac{\partial}{\partial z} \frac{1}{\rho} \frac{\partial}{\partial z} \alpha + k^2 - k_0^2 \right). \quad (21)$$

To avoid Gibbs oscillations, Eq. (20) may be solved using either the special numerical solution described in [18] or the complex Padé coefficients tabulated in [31].

Although the energy-conserving PE of Eq. (20) is based on a small-angle assumption, it performs very well for most wide-angle problems. For some problems, however, a higher level of accuracy may be desirable. A range-dependent environment is approximated by a sequence of range-independent regions. If back scattering is negligible, a high level of accuracy may be achieved by conserving the energy flux,

$$E = \frac{1}{\rho} p \frac{\partial p}{\partial r}, \quad (22)$$

across the vertical boundaries between range-independent regions. The exact solution conserves E across boundaries because both p and E/p are conserved. We denote the incident and transmitted fields at the boundary between regions A and B by p_i and p_t . One approach for conserving energy is to substitute Eq. (4) into Eq. (22) and enforce the following point-wise boundary condition:

$$\frac{1}{\rho_B} p_t K_B p_t = \frac{1}{\rho_A} p_i K_A p_i, \quad (23)$$

where the subscripts A and B denote evaluation in the respective regions. Since this nonlinear boundary-value problem is difficult to solve, we apply the alternate condition,

$$\int \frac{1}{\rho_B} p_t K_B p_t dz = \int \frac{1}{\rho_A} p_i K_A p_i dz. \quad (24)$$

To derive a linear condition from Eq. (24), we apply the normal-mode representation,

$$p = \sum \chi_n \phi_n, \quad (25)$$

where ϕ_n and χ_n are the normal modes and modal coefficients. Using Eq. (25) and the inner product for the normal modes, we obtain

$$\int \frac{1}{\rho} p K p dz = \sum k_n \chi_n^2 , \quad (26)$$

where the k_n are the eigenvalues. Therefore, Eq. (24) is a point-wise boundary condition in mode space. Substituting Eq. (25) into Eq. (24) and rearranging, we obtain the linear condition,

$$\frac{1}{\sqrt{\rho_B}} K_B^{1/2} p_t = \frac{1}{\sqrt{\rho_A}} K_A^{1/2} p_i . \quad (27)$$

This energy-conservation approach requires slightly more work than Eq. (20) but less work than the two-way PE described in Section 3. The product representation (see Section 3) of a Padé approximation is used to implement the operator $K^{1/2}$ as described in [38].

3. THE TWO-WAY PE

In this section, we describe a single-scattering approach, which is related to the on-surface radiation condition method for scattering from compact objects [39]. In addition to handling back scattering, the two-way PE handles forward scattering more accurately than Eq. (20) for some problems. The following conditions must be satisfied at a vertical interface between range-independent regions A and B :

$$p_i + p_r = p_t , \quad (28)$$

$$\frac{1}{\rho_A} \frac{\partial}{\partial r} (p_i + p_r) = \frac{1}{\rho_B} \frac{\partial}{\partial r} p_t , \quad (29)$$

where p_r is the reflected field. Using Eq. (4), we replace the range derivatives in Eq. (29) with the depth operator K for the two regions (using the appropriate sign for the reflected field) to obtain

$$\frac{1}{\rho_A} K_A (p_i - p_r) = \frac{1}{\rho_B} K_B p_t . \quad (30)$$

Since K_A and K_B are depth operators, we may eliminate p_t from Eq. (30) using Eq. (28) to obtain

$$\left(\frac{1}{\rho_A} K_A + \frac{1}{\rho_B} K_B \right) p_r = \left(\frac{1}{\rho_A} K_A - \frac{1}{\rho_B} K_B \right) p_i . \quad (31)$$

One approach for computing the reflected field is to solve Eq. (31) directly. This inefficient approach involves a large non-banded matrix that requires a large amount of computer

memory space and a large amount of effort to invert. The reflected field can be computed efficiently with the following rearrangement of Eq. (31):

$$p_r = \frac{1}{2} \left(1 - K_A^{-1} \frac{\rho_A}{\rho_B} K_B \right) (p_i - p_r). \quad (32)$$

With this iteration formula, the current p_r iterate is substituted on the right side of Eq. (32) to compute the new iterate. This iteration scheme requires the solution of tridiagonal systems. If the initial iterate is taken to be $p_r = 0$, the iteration scheme is equivalent to the Neumann series [40],

$$p_r = (\Lambda - \Lambda^2 + \Lambda^3 - \dots) p_i, \quad (33)$$

$$\Lambda = \frac{1}{2} \left(1 - K_A^{-1} \frac{\rho_A}{\rho_B} K_B \right). \quad (34)$$

The Neumann series converges if the difference between the operators in the two regions is sufficiently small.

If the variation in the environment across a vertical interface is large, the Neumann series may diverge. For improved convergence, we use the following rearrangement of Eq. (31):

$$p_r = \frac{\gamma - 2}{\gamma} p_r + \frac{1}{\gamma} \left(1 - K_A^{-1} \frac{\rho_A}{\rho_B} K_B \right) (p_i - p_r), \quad (35)$$

where $\gamma \geq 2$ is a convergence factor. For $\gamma = 2$, Eq. (35) reduces to Eq. (32). For $\gamma > 2$, Eq. (35) converges for larger Λ than Eq. (32).

We have implemented the iteration schemes using the following Padé approximations:

$$K = \sqrt{1+x} \approx \prod_{j=1}^M \frac{1+b_{2j-1,M}x}{1+b_{2j,M}x}, \quad (36)$$

$$K^{-1} = \frac{1}{\sqrt{1+x}} \approx \prod_{j=1}^M \frac{1+b_{2j,M}x}{1+b_{2j-1,M}x}. \quad (37)$$

The product approximations defined by the coefficients tabulated in [23] are identical to the sum approximations defined by the Padé coefficients tabulated in [31].

There exists a direct solution of Eq. (31) that is based on banded matrices. The numerators and denominators in Eq. (36) are denoted by N and D , where $K = ND^{-1} = D^{-1}N$. Substituting this notation into Eq. (31) and rearranging, we obtain

$$\left(N_A D_B + D_A \frac{\rho_A}{\rho_B} N_B \right) D_B^{-1} p_r = \left(N_A D_B - D_A \frac{\rho_A}{\rho_B} N_B \right) D_B^{-1} p_i . \quad (38)$$

In contrast to the iteration scheme, this approach involves matrices with more than three diagonals.

4. THE ELASTIC PE

The derivation of the elastic PE begins with the following farfield equations of motion [41]:

$$\mu \frac{\partial^2 w}{\partial r^2} + \mu \frac{\partial^2 w}{\partial z^2} + \rho \omega^2 w + (\lambda + \mu) \frac{\partial \Delta}{\partial z} + \frac{\partial \lambda}{\partial z} \Delta + 2 \frac{\partial \mu}{\partial z} \frac{\partial w}{\partial z} = 0 , \quad (39)$$

$$(\lambda + 2\mu) \frac{\partial^2 \Delta}{\partial r^2} + (\lambda + 2\mu) \frac{\partial^2 \Delta}{\partial z^2} + \rho \omega^2 \Delta + 2 \frac{\partial \mu}{\partial z} \frac{\partial^2 w}{\partial r^2} + \omega^2 \frac{\partial \rho}{\partial z} w + \\ \left(\frac{\partial \lambda}{\partial z} + 2 \frac{\partial \mu}{\partial z} \right) \frac{\partial \Delta}{\partial z} + \frac{\partial}{\partial z} \left(\frac{\partial \lambda}{\partial z} \Delta \right) + 2 \frac{\partial}{\partial z} \left(\frac{\partial \mu}{\partial z} \frac{\partial w}{\partial z} \right) = 0 . \quad (40)$$

This formulation is convenient for problems involving continuous depth variations in the elastic properties. Loss is handled by using the complex compressional and shear speeds $C_p = c_p / (1 + i\eta\beta_p)$ and $C_s = c_s / (1 + i\eta\beta_s)$, where c_p and c_s are the real wave speeds and β_p and β_s are the compressional and shear attenuations. The Lamé constants λ and μ are defined by $\lambda = \rho(C_p^2 - 2C_s^2)$ and $\mu = \rho C_s^2$.

Equations (39) and (40) provide a coupled system of the form

$$F \frac{\partial^2}{\partial r^2} \begin{pmatrix} \Delta \\ w \end{pmatrix} + G \begin{pmatrix} \Delta \\ w \end{pmatrix} = \begin{pmatrix} 0 \\ 0 \end{pmatrix} , \quad (41)$$

where the matrices F and G contain depth operators. In contrast to other formulations of elasticity, Eq. (41) does not contain a term involving $\partial / \partial r$. Furthermore, the depth operators F and G commute with $\partial / \partial r$. Thus we may factor Eq. (41) to obtain the outgoing elastic wave equation,

$$\frac{\partial}{\partial r} \begin{pmatrix} \Delta \\ w \end{pmatrix} = ik_0 \sqrt{1 + \frac{F^{-1}(G - k_0^2 F)}{k_0^2}} \begin{pmatrix} \Delta \\ w \end{pmatrix} . \quad (42)$$

To derive an elastic PE from Eq. (42), an approximation for the function,

$$f(\zeta) = \sqrt{1 + \zeta}, \quad (43)$$

is used to evaluate the depth operator appearing in Eq. (42) as a differential operator, where the square-root function is defined in terms of the branch lying in the upper half of the complex plane. The following approximation is a generalization of the Padé series of [9]:

$$f(\zeta) \equiv g(\zeta) = 1 + \sum_{j=1}^M \frac{a_{2j-1,M} \zeta}{1 + a_{2j,M} \zeta}, \quad (44)$$

where the coefficients depend on M and may be complex. Applying the Padé series to Eq. (42), we obtain the higher-order elastic PE,

$$\frac{\partial}{\partial r} \begin{pmatrix} \Delta \\ w \end{pmatrix} = ik_0 \left[1 + \sum_{j=1}^M \frac{a_{2j-1,M} F^{-1}(G - k_0^2 F)}{k_0^2 + a_{2j,M} F^{-1}(G - k_0^2 F)} \right] \begin{pmatrix} \Delta \\ w \end{pmatrix}. \quad (45)$$

Equation (45) is valid in layers in which the elastic parameters vary continuously. For problems involving piecewise-continuous depth variations, discontinuities at boundaries are handled by applying the appropriate conditions for the displacements and stresses. We use generalizations of the interface conditions of [28]. To allow the factorization of Eq. (41) for problems involving multiple layers, these interface conditions (which are incorporated into the operators F and G) are formulated so that they involve only depth derivatives of the solution. Vertical displacement and both stress components are continuous across an interface between fluid layer A and solid layer B , and the following conditions are applied:

$$\frac{\partial}{\partial z} (\lambda_A \Delta_A) + \rho_A \omega^2 w_B = 0, \quad (46)$$

$$\lambda_A \Delta_A = \lambda_B \Delta_B + 2\mu_B \frac{\partial w_B}{\partial z}, \quad (47)$$

$$\frac{\partial}{\partial z} (\lambda_B \Delta_B) + 2 \frac{\partial}{\partial z} \left(\mu_B \frac{\partial w_B}{\partial z} \right) + \rho_B \omega^2 w_B = 0. \quad (48)$$

Conditions for other types of interfaces, which have been implemented and tested, are given in [31]. A numerical method for solving Eq. (45) with these interface conditions is described in [29].

To obtain an elastic PE that is both accurate and stable, we derive Padé approximations that have the capabilities but not the limitations of the Padé approximations of [9] and [30]. As

discussed in [30], approximations that map the lower half of the complex plane into itself can have stability problems. We refer to the Padé approximation of [9] as $g_0(\zeta)$, which corresponds to $g(\zeta)$ for the Padé coefficients given by Eqs. (7) and (8). These coefficients are obtained by requiring that the first $2M$ derivatives of f and g agree at $\zeta = 0$. Although this approximation is accurate, it does not have the stability properties of the approximation of [30].

To obtain a stable higher-order elastic PE, we require that the function,

$$\Gamma_j(\zeta) = \frac{d^j}{d\zeta^j} (f - g), \quad (49)$$

vanish at $\zeta = 0$ for $1 \leq j \leq 2M - m$. To determine the $2M$ coefficients of g , m additional constraints are required. Growing solutions can be eliminated by mapping points slightly below the real line for $\text{Re}(\zeta) < -1$ into the upper half of the complex plane [30]. Thus we require that the functions,

$$\Gamma_{2M-m+j}(\zeta) = g(\zeta_j - \zeta) - v_j, \quad (50)$$

vanish at $\zeta = 0$ for $j = 1, \dots, m$, where $\text{Im}(\zeta_j) \leq 0$, $\text{Re}(\zeta_j) \leq -1$, and $\text{Im}(v_j) \geq 0$. Other types of constraints, involving derivatives for example, might also be useful. As described in [23], Newton's method may be used to determine the Padé coefficients for which $\Gamma_j(0) = 0$ for $j = 1, \dots, 2M$.

For problems that involve thin elastic layers such as ice cover, it may be necessary to take $m > 1$ for stability. For problems that do not involve thin elastic layers, the eigenvalues in the lower half of the complex plane are very close to the real line; and stability can be achieved by perturbing the g_0 coefficients by taking $m = 1$, $\text{Im}(\zeta_1) = 0$, and $v_1 = g_0(\zeta_1) + i\varepsilon_1$, where ε_1 is a positive real number. This Padé series is slightly less accurate than the Padé series of [9] because one less derivative is required to match. This trade-off of accuracy for stability is an excellent bargain. For the case $\varepsilon_1 = 0$, the coefficients given by Eqs. (7) and (8) are recovered. The coefficients for the first seven Padé series are tabulated in [31] for $\varepsilon_1 = 1$ and $\zeta_1 = -3$. The complex Padé coefficients are also useful for filtering out Gibbs oscillations in the energy-conserving PE solution [18].

The two-way PE has been generalized to elastic media. In a solid medium, the following conditions must be satisfied at a vertical interface between range-independent regions A and B :

$$R_A S_A \left[\binom{\Delta_i}{w_i} - \binom{\Delta_r}{w_r} \right] = R_B S_B \binom{\Delta_r}{w_r}, \quad (51)$$

$$T_A \left[\begin{pmatrix} \Delta_i \\ w_i \end{pmatrix} + \begin{pmatrix} \Delta_r \\ w_r \end{pmatrix} \right] = T_B \begin{pmatrix} \Delta_r \\ w_r \end{pmatrix}, \quad (52)$$

where

$$R = \begin{pmatrix} 1 & -\frac{\partial}{\partial z} \\ \frac{\partial}{\partial z} \lambda & \rho \omega^2 + 2 \frac{\partial}{\partial z} \mu \frac{\partial}{\partial z} \end{pmatrix}, \quad (53)$$

$$S = \frac{\partial^{-1}}{\partial r^{-1}} \approx \frac{1}{ik_0} \prod_{j=1}^M \frac{k_0^2 + b_{2j,M} F^{-1}(G - k_0^2 F)}{k_0^2 + b_{2j-1,M} F^{-1}(G - k_0^2 F)}, \quad (54)$$

$$T = \begin{pmatrix} \lambda + 2\mu & -2\mu \frac{\partial}{\partial z} \\ 0 & 1 \end{pmatrix}. \quad (55)$$

The subscript notation in Eqs. (51) and (52) is analogous to the notation used in Section 3. Conservation of normal displacement u and tangential stress σ_{rz} is given by Eq. (51). Conservation of vertical displacement w and normal stress σ_{rr} is given by Eq. (52). The operators R , S , and T have been implemented (and tested for accuracy) for computing basic quantities (such as u , σ_{rr} , and σ_{rz}) from the dependent variables Δ and w . From Eqs. (51) and (52), we obtain the iteration formula,

$$\begin{pmatrix} \Delta_r \\ w_r \end{pmatrix} = \frac{\gamma - 2}{\gamma} \begin{pmatrix} \Delta_r \\ w_r \end{pmatrix} + \frac{1}{\gamma} (I - S_A^{-1} R_A^{-1} R_B S_B T_B^{-1} T_A) \left[\begin{pmatrix} \Delta_i \\ w_i \end{pmatrix} - \begin{pmatrix} \Delta_r \\ w_r \end{pmatrix} \right], \quad (56)$$

which is analogous to Eq. (32). The two-way elastic PE is implemented only for solid media at this time.

The energy-conserving PE has also been generalized to elastic media. The compressional and shear energy fluxes E_p and E_s [42] are defined by

$$\begin{pmatrix} E_p \\ E_s \end{pmatrix} = \begin{pmatrix} u \sigma_{rr} \\ w \sigma_{rz} \end{pmatrix}. \quad (57)$$

The energy fluxes are conserved across a vertical interface for the exact solution because all four quantities on the right side of Eq. (57) are conserved. We derive a leading-order

correction for the small-angle limit. As in the acoustic case, the approximation is not actually restricted to small angles. We consider the case of a sloping fluid-solid interface, which is approximated by a sequence of stair steps. Since σ_{rz} vanishes on the runs of the stair steps, this quantity and E_s go to zero on the rises of the stair steps as the lengths of the rises goes to zero (the accuracy of the rotated acoustic PE is due to a similar limit involving the ocean surface [16]). Therefore, it is only necessary to correct E_p . As in the acoustic case, we define the new dependent variable $U = \Delta / \alpha$. In the small-angle limit, E_p is conserved for the case

$$\alpha = (\rho c_p^3)^{-1/2}. \quad (58)$$

This correction, which is larger than and in the opposite direction of the correction for the acoustic PE, is accurate for a large class of problems. Since it is not as robust as the leading-order correction for the acoustic case, however, a complete energy-conservation correction would be useful for the elastic case.

5. COMPUTER IMPLEMENTATION

The PE models we have described have been implemented as FORTRAN computer programs. The codes have been used as subroutines for applications such as inversion for sediment properties [43], Fourier synthesis of time-domain solutions [23], and modeling three-dimensional back scattering [44]. Since the codes contain efficient algorithms, they have been applied to large-scale problems such as modeling global-scale propagation [45].

The code FEPE solves the higher-order energy-conserving PE. A user's guide exists for this code [46]. Some recent improvements to FEPE are not described in the user's guide, including the energy-conservation correction, a radiation boundary condition (RBC) at the lower boundary [43], a special tridiagonal system solver [11], the self-starter [38], and the capability to handle three-dimensional problems and problems involving rough boundaries [37]. To reduce the maximum required depth, we have installed an RBC as an option at the lower boundary of the computational grid, which is a generalization of the RBC of [47]. The RBC approach is more efficient than using an artificial absorbing layer for eliminating non-physical reflections.

A special tridiagonal solver has been designed to minimize run times for problems involving sloping ocean bottoms. As ocean depth varies, it is necessary to modify the entries of the tridiagonal matrices involved in the numerical solution of the PE and repeat the decomposition of the tridiagonal system. If the decomposition is done with Gaussian elimination, it is necessary to repeat a significant portion of the elimination process. The decomposition algorithm implemented in FEPE involves sweeping downward to the ocean bottom to eliminate entries below the main diagonal and sweeping upward to the ocean bottom to eliminate entries above the main diagonal. With this algorithm, the run time is

not affected by bathymetry variations. Due to this and other algorithm improvements, FEPE is several times faster than other finite-difference PE codes (e.g., compare the run times reported in [11,48]). A version of FEPE that uses a new solution technique discussed in Section 7 is two to three orders of magnitude faster than other finite-difference PE codes.

The code FEPES solves the higher-order energy-conserving elastic PE. An efficient solver for banded systems, analogous to the efficient tridiagonal solver in FEPE, has been installed in FEPES. The self-starter, which properly excites interface waves, has also been installed in FEPES. Both two-way and energy-conserving versions of FEPES have been developed and are discussed in Section 7.

6. THE TEST CASES

We have generated solutions for Test Cases 1-4, which are described elsewhere in this proceedings. These problems are well suited for illustrating the four basic PE models we have discussed. Our main goal was to maximize accuracy rather than minimize run time. However, we performed tests for Test Case 2 to illustrate the trade-off between run time and accuracy. We took $c_0 = 1500 \text{ m/s}$ for each of the problems. All stated run times are for a Digital VAX-8650 computer.

Test Case 1 was solved with FEPE using the computational depth spacing $\Delta z = 0.5 \text{ m}$ and range-dependent choices for M and the computational range step Δr . For $r < 2 \text{ km}$, we took $M = 12$ and $\Delta r = 1 \text{ m}$. For $r > 2 \text{ km}$, we took $M = 4$ and $\Delta r = 5 \text{ m}$. The lower RBC implemented at $z = 7.5 \text{ km}$ was constructed by optimizing a set of coefficients for energy incident at 30 deg from normal using Newton's method. The half-space PE starter [49] was used to initialize the PE at $r = 200 \text{ m}$. The run time was 3 hr. The FEPE solution appearing in Figure 1 is in excellent agreement with the exact solution. This illustrates the ability of the higher-order PE to handle very wide propagation angles. Since the medium is homogeneous, an accurate solution may also be obtained for this problem using the split-step Fourier algorithm [2]. However, the higher-order PE is the only existing PE that is accurate for problems involving both very wide propagation angles and variations in the parameters of the medium.

Test Case 2 was solved for a high level of accuracy with FEPE using a PE starter based on the normal modes for a homogeneous waveguide [46], truncating the grid at $z = 2 \text{ km}$, and taking $\Delta r = 5 \text{ m}$, $\Delta z = 0.5 \text{ m}$, and $M = 3$. This solution, which required 7 min of run time and appears in Figures 2A and 2B, is in excellent agreement with the two-way COUPLE solution [50,51]. We also solved this problem with FEPE using Greene's PE starter [7], truncating the grid at $z = 700 \text{ m}$, taking $M = 2$, and using larger values of the computational grid spacings. By taking $\Delta r = 10 \text{ m}$ and $\Delta z = 2 \text{ m}$, the run time was reduced to 12 s with only a slight sacrifice in accuracy. The solution generated using $\Delta r = 20 \text{ m}$ and $\Delta z = 4 \text{ m}$ required only 3 s of run time and is in good agreement with the two-way COUPLE solution. For $\Delta r = 40 \text{ m}$ and $\Delta z = 8 \text{ m}$, the run time was 0.8 s and the accuracy

is fairly good. For $\Delta r = 80$ m and $\Delta z = 16$ m, the run time was 0.2 s and the solution is undersampled but qualitatively accurate. These results appear in Figure 2c.

Test Case 3 was solved with the non-energy-conserving elastic PE (i.e., the implementation of [28-31]), the energy-conserving elastic PE, and the rotated elastic PE using a truncation depth of 1 km, $\Delta r = 5$ m, $\Delta z = 0.25$ m, and $M = 3$. These solutions appear in Figure 3. The rotated and energy-conserving solutions are in agreement. The amplitude error in the non-energy-conserving solution is in the opposite direction of the error in the non-energy-conserving acoustic PE solution for the related fluid problem [48]. The run time was 20 min for this problem.

Test Case 4 was solved with a two-way version of FEPE using a truncation depth of 1 km and $\Delta r = 5$ m, $\Delta z = 0.25$ m, and $M = 4$. Since multiple reflections are important for this problem for a point source in cylindrical geometry [23], we assumed a line source in plane geometry. The outgoing and back-scattered components of the two-way PE solution appearing in Figure 4 are in excellent agreement with the components of the two-way COUPLE solution. The run time was 20 min.

We did not solve Test Case 5 because it does not test any capability of the PE method that is not tested by the other test cases. Due to the uncertainties in acoustic and environmental data, we did not solve Test Case 6, which is essentially an under-determined inverse problem. We have applied the PE models described above to other sets of data, however, and have obtained excellent agreement between PE solutions and the data [43]. We did not solve Test Case 7 because it is relevant only to split-step Fourier solutions. This is an interesting test case, however, because it illustrates that unexpected results can occur, even with a model that has been thoroughly tested and widely used.

7. POST-WORKSHOP RESULTS

There are still many open issues in PE modeling that might one day justify a third PE workshop. In this section, we discuss some results that were obtained after the second PE workshop. Both the energy-conserving [52] and two-way [53] elastic PEs, which are described in Section 4, have been implemented and tested. The energy-conserving elastic PE has been applied to solve a problem involving mode cutoff and coupling into shear wave beams in the ocean bottom [52], a generalization of an interesting acoustic problem that was first solved with the PE method [54]. A conversion formula that is local in range and is useful for displaying solutions has been derived for computing the shear potential from the variables of the non-standard formulation of elasticity that is used with the elastic PE [53]. The self-starter, which is described in a separate paper in this proceedings, has been extended to the case of a source in a solid layer [53]. The split-step Padé solution is orders of magnitude faster than other finite-difference solutions [55]. This efficiency gain is achieved by exploiting the robustness of Padé approximations to reduce both asymptotic and numerical errors. The split-step Padé solution offers the accuracy of the higher-order

PE and the efficiency of the split-step Fourier solution. An efficient approach for solving three-dimensional problems has been developed [56]. The direct solution of the three-dimensional PE is practical only for relatively small problems [37] (only very small problems are practical for non-PE approaches). Under the adiabatic normal mode approximation [57], one obtains a set of two-dimensional (range-azimuth) PEs to solve [56]. Interesting and useful information can be obtained by solving for a small number (one, for example) of mode coefficients. With this reduction in dimension, it is practical to solve large-scale (even global-scale) problems.

REFERENCES

- [1] M.A. Leontovich and V.A. Fock, "Solution of the problem of propagation of electromagnetic waves along the earth's surface by the method of the parabolic equation," *J. Expt. and Theor. Phys.* **16**, 557-573 (1946).
- [2] F.D. Tappert, "Numerical solutions of a canonical nonlinear dispersive wave equation," *SIAM Rev.* **16**, 140 (1974).
- [3] "NORDA parabolic equation workshop," edited by J.A. Davis, D. White, and R.C. Cavanagh, NORDA Tech. Note 143, Naval Ocean Research and Development Activity, Stennis Space Center, Mississippi (1982).
- [4] D. Lee, G. Botseas, and J.S. Papadakis, "Finite-difference solution to the parabolic wave equation," *J. Acoust. Soc. Am.* **70**, 795-800 (1981).
- [5] J.F. Claerbout, *Fundamentals of Geophysical Data Processing* (McGraw-Hill, New York, 1976), pp. 206-207.
- [6] G. Botseas, D. Lee, and K.E. Gilbert, "IFD: Wide-angle capability," NUSC TR-6905, Naval Underwater Systems Center, New London, Connecticut (1983).
- [7] R.R. Greene, "The rational approximation to the acoustic wave equation with bottom interaction," *J. Acoust. Soc. Am.* **76**, 1764-1773 (1984).
- [8] G.H. Knightly, D. Lee, and D.F. St. Mary, "A higher-order parabolic wave equation," *J. Acoust. Soc. Am.* **82**, 580-587 (1987).
- [9] A. Bamberger, B. Engquist, L. Halpern, and P. Joly, "Higher order paraxial wave equation approximations in heterogeneous media," *SIAM J. Appl. Math.* **48**, 129-154 (1988).
- [10] M.D. Collins, "Applications and time-domain solution of higher-order parabolic equations in underwater acoustics," *J. Acoust. Soc. Am.* **86**, 1097-1102 (1989).

The PE Workshop II: Part 3 — Contributed Papers

- [11] M.D. Collins, "Benchmark calculations for higher-order parabolic equations," *J. Acoust. Soc. Am.* **87**, 1535-1538 (1990).
- [12] D. Lee and S.T. McDaniel, "A finite-difference treatment of interface conditions for the parabolic wave equation: The irregular interface," *J. Acoust. Soc. Am.* **73**, 1441-1447 (1983).
- [13] F.D. Tappert and D. Lee, "A range refraction parabolic equation," *J. Acoust. Soc. Am.* **76**, 1797-1803 (1984).
- [14] G.A. Kriegsmann, "A multiscale derivation of a new parabolic equation which includes density variations," *Comp. Maths. Appl.* **11**, 817-821 (1985).
- [15] A. Bamberger, B. Engquist, L. Halpern, and P. Joly, "Parabolic wave equation approximations in heterogeneous media," *SIAM J. Appl. Math.* **48**, 99-128 (1988).
- [16] M.D. Collins, "The rotated parabolic equation and sloping ocean bottoms," *J. Acoust. Soc. Am.* **87**, 1035-1037 (1990).
- [17] L. Abrahamsson and H.O. Kreiss, "Boundary conditions for the parabolic equation in a range-dependent duct," *J. Acoust. Soc. Am.* **87**, 2438-2441 (1990).
- [18] M.D. Collins and E.K. Westwood, "A higher-order energy-conserving parabolic equation for range-dependent ocean depth, sound speed, and density," *J. Acoust. Soc. Am.* **89**, 1068-1075 (1991).
- [19] M.B. Porter, F.B. Jensen, and C.M. Ferla, "The problem of energy conservation in one-way models," *J. Acoust. Soc. Am.* **89**, 1058-1067 (1991).
- [20] F. Tappert, "Full-wave three-dimensional modeling of long-range oceanic boundary reverberation," *J. Acoust. Soc. Am. Suppl. I* **88**, S84 (1990).
- [21] S.T. McDaniel, "Backscattering from rough interfaces and the parabolic approximation," ARL Tech. Mem. 91-104, Applied Research Laboratory, Penn State University, State College, Pennsylvania (1991).
- [22] H. Bremmer, "The W.K.B. approximation as the first term of a geometric-optical series," *Comm. Pure and Appl. Math.* **4**, 105-115 (1951).
- [23] M.D. Collins and R.B. Evans, "A two-way parabolic equation for acoustic back scattering in the ocean," *J. Acoust. Soc. Am.* **91**, 1357-1368 (1992).
- [24] T. Landers and J.F. Claerbout, "Numerical calculations of elastic waves in laterally inhomogeneous media," *J. Geophys. Res.* **77**, 1476-1483 (1972).

- [25] J.J. McCoy, "A parabolic theory of stress wave propagation through inhomogeneous linearly elastic solids," *J. Appl. Mech.* **44**, 462-468 (1977).
- [26] J.A. Hudson, "A parabolic approximation for elastic waves," *Wave Motion* **2**, 207-214 (1980).
- [27] J.P. Coronis, B. DeFacio, and R.J. Krueger, "Parabolic approximations to the time-independent elastic wave equation," *J. Math. Phys.* **23**, 577-586 (1982).
- [28] R.R. Greene, "A high-angle one-way wave equation for seismic wave propagation along rough and sloping interfaces," *J. Acoust. Soc. Am.* **77**, 1991-1998 (1985).
- [29] M.D. Collins, "A higher-order parabolic equation for wave propagation in an ocean overlying an elastic bottom," *J. Acoust. Soc. Am.* **86**, 1459-1464 (1989).
- [30] B.T.R. Wetton and G.H. Brooke, "One-way wave equations for seismoacoustic propagation in elastic waveguides," *J. Acoust. Soc. Am.* **87**, 624-632 (1990).
- [31] M.D. Collins, "Higher-order Padé approximations for accurate and stable elastic parabolic equations with application to interface wave propagation," *J. Acoust. Soc. Am.* **89**, 1050-1057 (1991).
- [32] W.H. Press, B.P. Flannery, S.A. Teukolsky, and W.T. Vetterling, *Numerical Recipes* (Cambridge University Press, Cambridge, 1986), pp. 660-667.
- [33] B.E. McDonald and W.A. Kuperman, "Time domain formulation for pulse propagation including nonlinear behavior at a caustic," *J. Acoust. Soc. Am.* **81**, 1406-1417 (1987).
- [34] M.D. Collins, "Low-frequency, bottom-interacting pulse propagation in range-dependent oceans," *IEEE J. Ocean. Eng.* **13**, 222-228 (1988).
- [35] M.D. Collins, "The time-domain solution of the wide-angle parabolic equation including the effects of sediment dispersion," *J. Acoust. Soc. Am.* **84**, 2114-2125 (1988).
- [36] D. Lee, Y. Saad, and M.H. Schultz, "An efficient method for solving the three-dimensional wide angle wave equation," Yale Univ. Res. Rep. YALEU/DCS/RR-463 (1986).
- [37] M.D. Collins and S.A. Chin-Bing, "A three-dimensional parabolic equation model that includes the effects of rough boundaries," *J. Acoust. Soc. Am.* **87**, 1104-1109 (1990).
- [38] M.D. Collins, "A self-starter for the parabolic equation method," *J. Acoust. Soc. Am.* **92**, 2069-2074 (1992). Also see self-starter paper appearing in this proceedings.

- [39] G.A. Kriegsmann, A. Taflove, and K.R. Umashankar, "A new formulation of electro-magnetic wave scattering using an on-surface radiation boundary condition approach," *IEEE Trans. Ant. and Prop.* **35**, 153-161 (1987).
- [40] R. Courant and D. Hilbert, *Methods of Mathematical Physics, Volume I* (Wiley, New York, 1953).
- [41] H. Kolsky, *Stress Waves in Solids* (Dover, New York, 1963), p. 11.
- [42] A. Ben-Menahem and S.J. Singh, *Seismic Waves and Sources* (Springer-Verlag, New York, 1981), p. 26.
- [43] M.D. Collins, W.A. Kuperman, and H. Schmidt, "Nonlinear inversion for ocean-bottom properties," *J. Acoust. Soc. Am.* **92**, 2770-2783 (1992).
- [44] M.D. Collins, G.J. Orris, and W.A. Kuperman, "Reverberation modeling with the two-way parabolic equation," in *Proceedings of the Ocean Reverberation Symposium*, edited by H. Urban, J. Preston, and D. Ellis (Kluwer, Dordrecht, in press).
- [45] B.E. McDonald, M.D. Collins, W.A. Kuperman, and K.D. Heaney, "Comparison of data and model predictions for Heard Island acoustic transmissions," *J. Acoust. Soc. Am.* (submitted).
- [46] M.D. Collins, "FEPE user's guide," NORDA TN-365, Naval Ocean Research and Development Activity, Stennis Space Center, Mississippi (1988).
- [47] R.W. Clayton and B. Engquist, "Absorbing boundary conditions for wave-equation migration," *Geophysics* **45**, 895-904 (1980).
- [48] F.B. Jensen and C.M. Ferla, "Numerical solutions of range-dependent benchmark problems," *J. Acoust. Soc. Am.* **87**, 1499-1510 (1990).
- [49] M.D. Collins, "A nearfield asymptotic analysis for underwater acoustics," *J. Acoust. Soc. Am.* **85**, 1107-1114 (1989).
- [50] R.B. Evans, "A coupled mode solution for acoustic propagation in a waveguide with stepwise depth variations of a penetrable bottom," *J. Acoust. Soc. Am.* **74**, 188-195 (1983).
- [51] R.B. Evans, "COUPLE: A user's guide," NORDA TN-332, Naval Ocean Research and Development Activity, Stennis Space Center, Mississippi (1986).
- [52] M.D. Collins, "An energy-conserving parabolic equation for elastic media," *J. Acoust. Soc. Am.* (submitted).

- [53] M.D. Collins, "A two-way parabolic equation for elastic media," *J. Acoust. Soc. Am.* **93**, (1993).
- [54] F.B. Jensen and W.A. Kuperman, "Sound propagation in a wedge-shaped ocean with a penetrable bottom," *J. Acoust. Soc. Am.* **67**, 1564-1566 (1980).
- [55] M.D. Collins, "A split-step Padé solution for the parabolic equation method," *J. Acoust. Soc. Am.* **93**, (1993).
- [56] M.D. Collins, "Three-dimensional solution of large-scale ocean acoustics problems," *J. Acoust. Soc. Am.* (submitted).
- [57] W.A. Kuperman, M.B. Porter, J.S. Perkins, and R.B. Evans, "Rapid Computation of Acoustic Fields in Three-Dimensional Ocean Environments," *J. Acoust. Soc. Am.* **89**, 125-133 (1991).

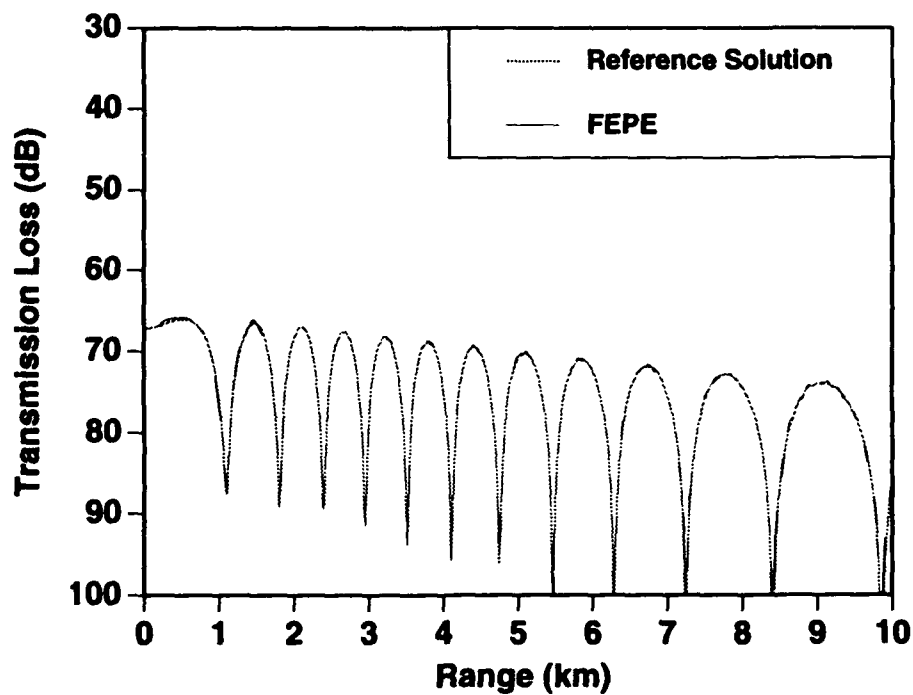


Figure 1. Test Case 1; FEPE compared to the reference solution.

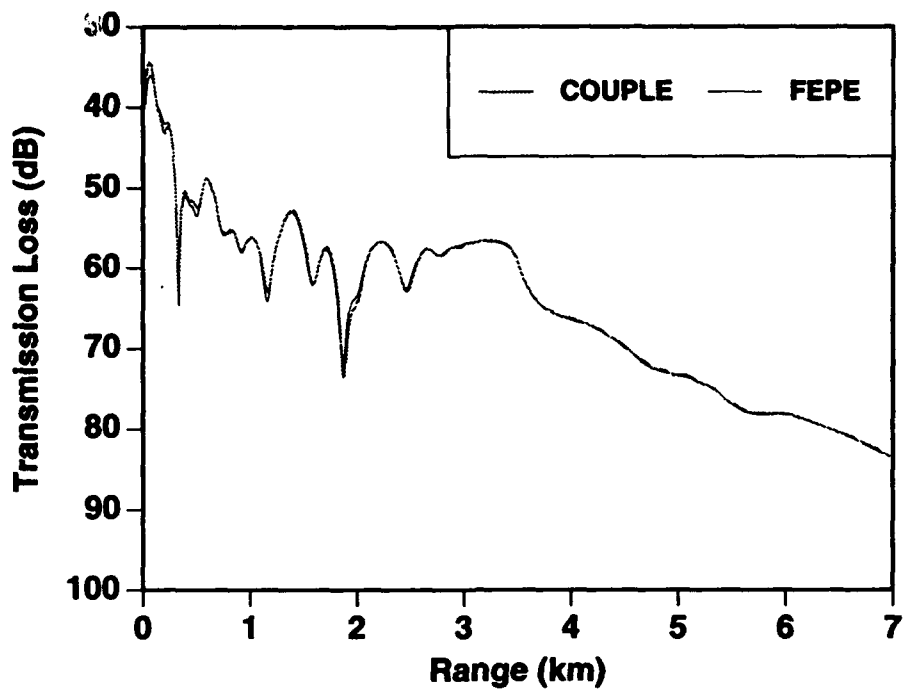


Figure 2a. Test Case 2A; FEPE results compared to results from COUPLE.

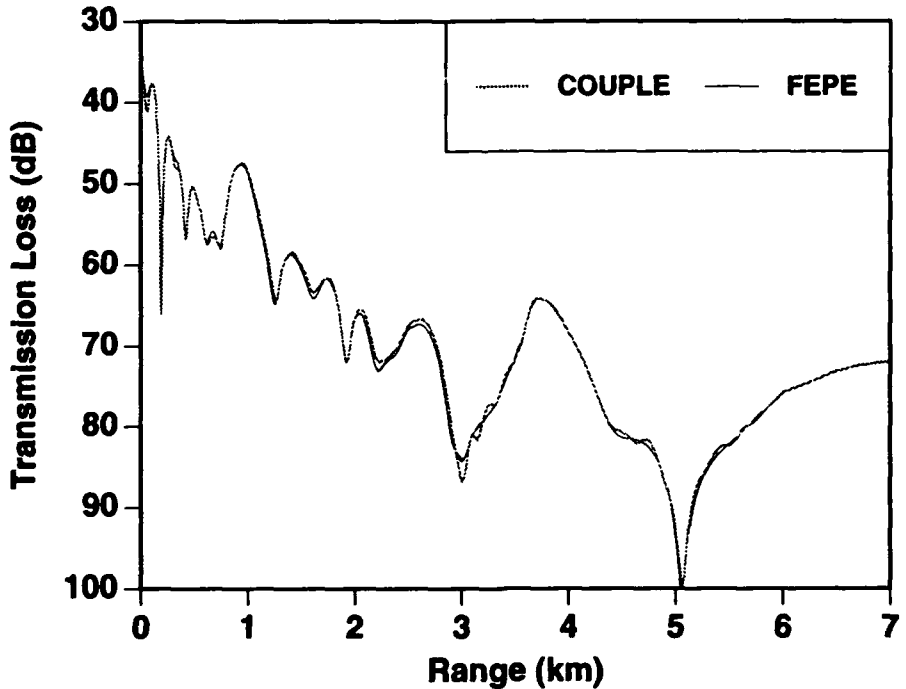


Figure 2b. Test Case 2B; FEPE results compared to results from COUPLE.

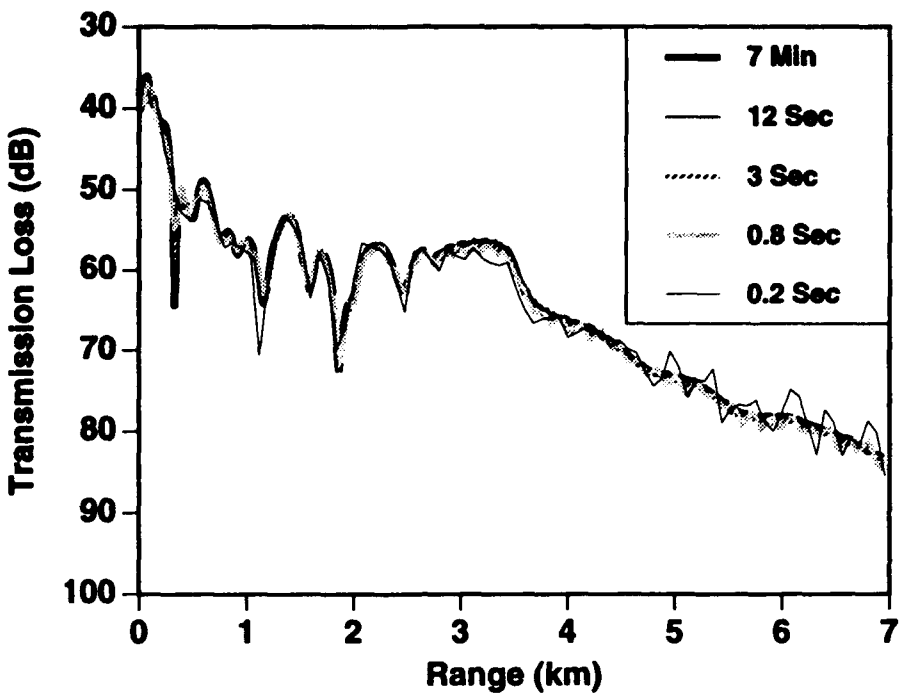


Figure 2c. Test Case 2A; Accuracy of FEPE results compared to computer runtimes.

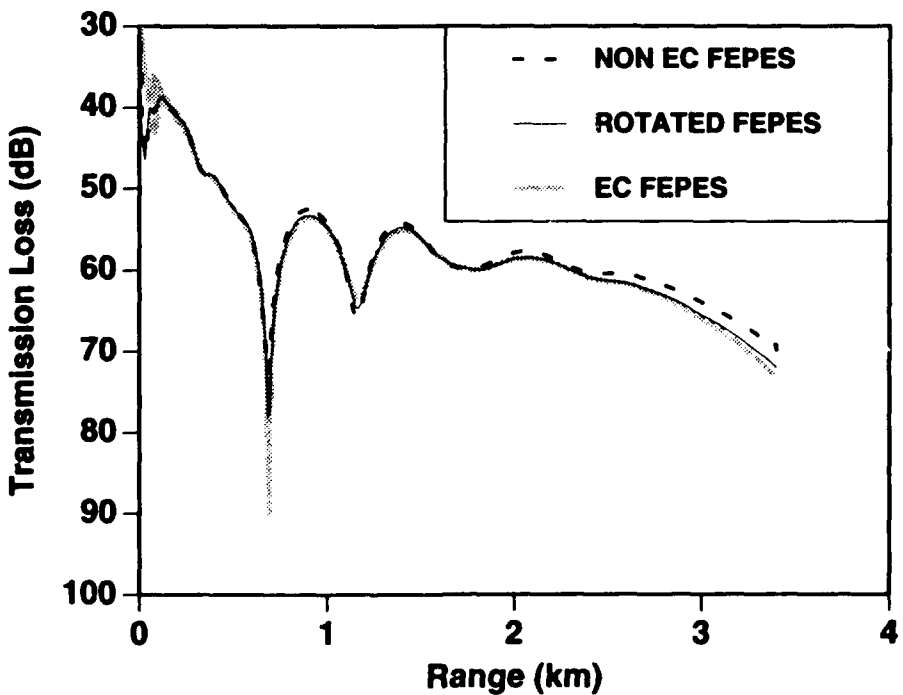


Figure 3. Test Case 3A; FEPES results: energy conserving, non-energy conserving, and rotated coordinates.

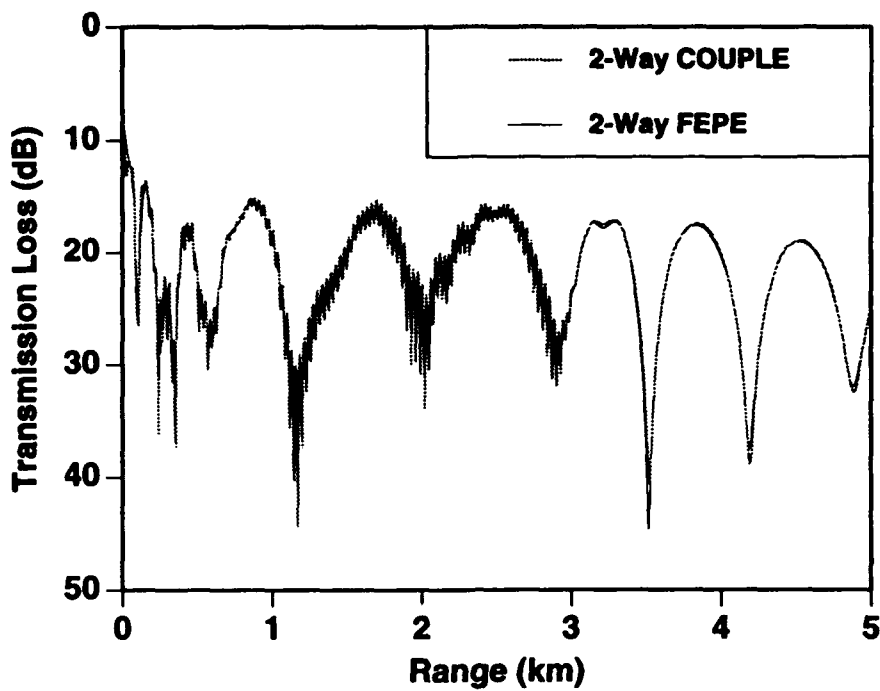


Figure 4a. Test Case 4A; Outgoing 2-way FEPE compared to total 2-way COUPLE.

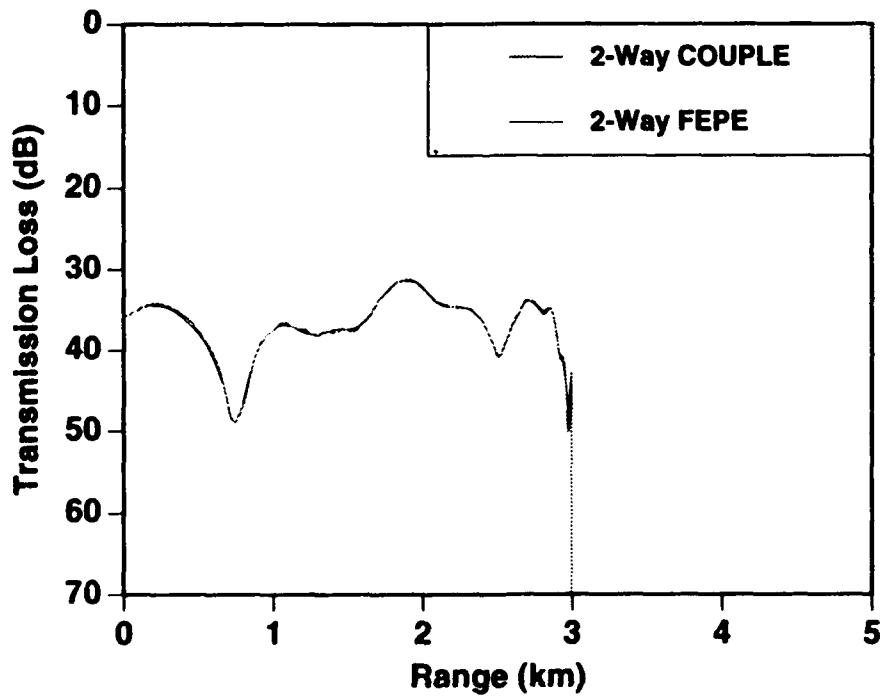


Figure 4b. Test Case 4A; Comparison of FEPE backscatter results.

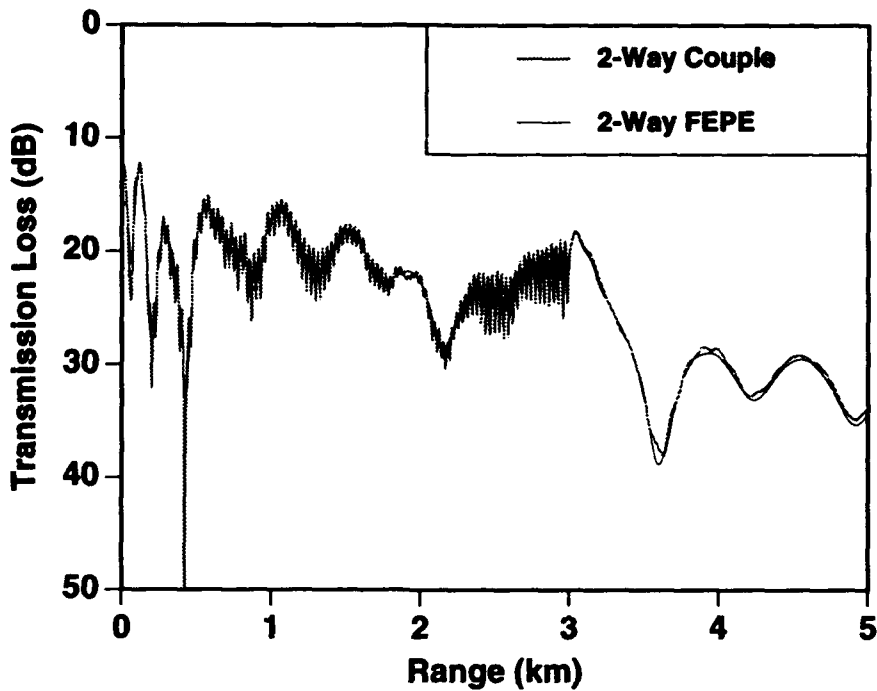


Figure 4c. Test Case 4B; Outgoing 2-way FEPE compared to total 2-way COUPLE.

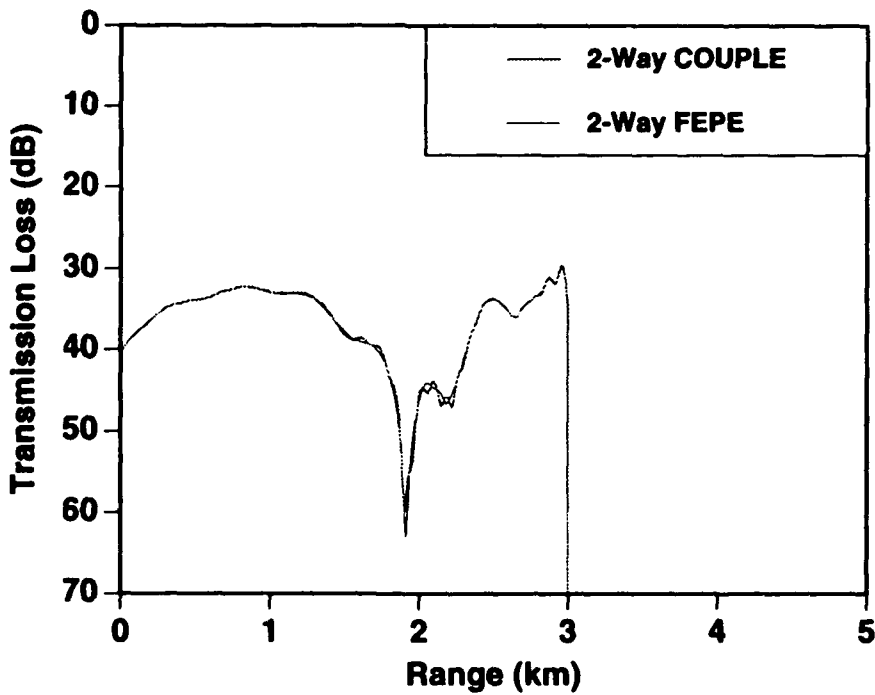


Figure 4d. Test Case 4B; Comparison of FEPE backscatter results.

The Self-Starter

Michael D. Collins
Naval Research Laboratory
Washington, DC 20375

INTRODUCTION

The problem of improving the initial condition for the parabolic equation (PE) method [1] has not received as much attention as other PE-related problems. This problem may be solved exactly with the method of normal modes [2]. Although efficient methods have been developed for determining the normal modes [3], this computational task may require a significant effort, especially when the eigenvalues are complex or the continuous spectrum is desired [4]. Several approximate PE starting fields have been developed to avoid solving the eigenvalue problem [1,5-7]. Although these efficient starters are accurate for many problems, they are based on asymptotic assumptions and break down for some problems.

The self-starter [8] is an efficient PE starter that is as accurate as the normal-mode starter. The self-starter is obtained by solving a one-dimensional boundary-value problem (BVP) with the PE method. Since the BVP is similar to the type of BVP that must be solved a large number of times to find the normal modes, the self starter is more efficient than the normal-mode starter. The self starter, which is constructed with a direct solution of a differential equation, is also less prone to trouble than the normal-mode starter, which requires a search for eigenvalues. The self starter depends on the depth dependence of the ocean and sediment and satisfies all boundary and interface conditions. The self-starter is accurate for problems involving wide propagation angles, large depth variations of the properties of the medium, low frequencies, interface waves, and the continuous spectrum.

1. THE ACOUSTIC CASE

For the problem of a line source in a range-independent fluid medium, the complex pressure p satisfies

$$\frac{\partial^2 p}{\partial x^2} + \rho \frac{\partial}{\partial z} \left(\frac{1}{\rho} \frac{\partial p}{\partial z} \right) + k^2 p = \delta(x) \delta(z - z_0), \quad (1)$$

where k is the complex wavenumber, ρ is the density, x is the range from the source, z is the depth below the ocean surface, and z_0 is the source depth. The application of the self-starter to range-dependent problems is described in [8]. Factoring Eq. (1) for $x > 0$, we obtain the outgoing wave equation,

$$\frac{\partial p}{\partial x} = ik_0(1+s)^{1/2} p, \quad (2)$$

where k_0 is a representative wavenumber and

$$s = k_0^{-2} \left(\rho \frac{\partial}{\partial z} \frac{1}{\rho} \frac{\partial}{\partial z} + k^2 - k_0^2 \right). \quad (3)$$

Integrating Eq. (1) over an arbitrarily small range interval about the origin, we obtain

$$\lim_{x \rightarrow 0^+} \frac{\partial p}{\partial x} = \frac{1}{2} \delta(z - z_0). \quad (4)$$

Substituting Eq. (2) into Eq. (4), we obtain

$$(1+s)^{1/2} p = -\frac{i}{2k_0} \delta(z - z_0). \quad (5)$$

To obtain a differential equation from Eq. (5), we apply the following approximation:

$$(1+s)^{1/2} \approx \prod_{j=1}^N \frac{1+a_{2j-1,N}s}{1+a_{2j,N}s}. \quad (6)$$

Values for the Padé coefficients are tabulated in [9] for $N \leq 7$. Substituting Eq. (6) into Eq. (5), we obtain the following BVP for the self-starter:

$$\prod_{j=1}^N \frac{1+a_{2j-1,N}s}{1+a_{2j,N}s} p = -\frac{i}{2k_0} \delta(z - z_0). \quad (7)$$

We have attempted to solve Eq. (7) directly and found that this approach is difficult due to the singularity of p at $z = z_0$.

We have developed an indirect numerical solution of Eq. (7) that is robust and involves three steps. The first step requires the solution of the BVP,

$$(1+s) q = -\frac{i}{2k_0^2} \delta(z - z_0), \quad (8)$$

which is related to the BVP for the wavenumber spectrum [10]. Although Eq. (8) may be

solved with normal modes, we apply instead the numerical approach described in [11] to avoid the eigenvalue problem. The second step is to march q in range with the PE a short distance to $x = x_0$ to obtain

$$q = \sum k_n^{-2} \phi_n(z_0) \phi_n(z) \exp(ik_n x_0), \quad (9)$$

where $\phi_n(z)$ and k_n are the eigenfunctions and eigenvalues. The normal-mode solution for q differs from the normal-mode solution for p only by the power of k_n appearing as a factor. As the final step, the power of k_n appearing in Eq. (9) is corrected by applying the PE operator to obtain

$$p = k_0 \prod_{j=1}^N \frac{1 + a_{2j-1,N}s}{1 + a_{2j,N}s} q = \sum k_n^{-1} \phi_n(z_0) \phi_n(z) \exp(ik_n x_0). \quad (10)$$

If x_0 is sufficiently large (on the order of a wavelength or even less), this approach is robust because the contribution of the evanescent modes (which compose the singularity) decays rapidly with range.

The self-starter is easily generalized to the case of a point source. The spreading factor $r^{-1/2}$ is removed from p in this case, and the exact (in the farfield limit $k_0 r \gg 1$) starting field is proportional to

$$p = \sum k_n^{-1/2} \phi_n(z_0) \phi_n(z). \quad (11)$$

The field is marched out to $r = r_0$, and the power of k_n appearing in Eq. (9) is corrected as follows:

$$p = k_0^{3/2} \prod_{j=1}^N \frac{1 + b_{2j-1,N}s}{1 + b_{2j,N}s} q = \sum k_n^{-1/2} \phi_n(z_0) \phi_n(z) \exp(ik_n r_0), \quad (12)$$

where

$$(1+s)^{3/4} \equiv \prod_{j=1}^N \frac{1 + b_{2j-1,N}s}{1 + b_{2j,N}s}. \quad (13)$$

The values for the Padé coefficients tabulated in [8] were generated using the same accuracy and stability constraints used to generate the Padé coefficients tabulated in [9,11].

2. THE ELASTIC CASE

The following equations of motion for an elastic waveguide are derived from [12]:

$$(\lambda + 2\mu) \frac{\partial^2 \Delta}{\partial x^2} + (\lambda + 2\mu) \frac{\partial^2 \Delta}{\partial z^2} + \rho \omega^2 \Delta + 2 \frac{\partial \mu}{\partial z} \frac{\partial^2 w}{\partial x^2} + \omega^2 \frac{\partial \rho}{\partial z} w + \\ \left(\frac{\partial \lambda}{\partial z} + 2 \frac{\partial \mu}{\partial z} \right) \frac{\partial \Delta}{\partial z} + \frac{\partial}{\partial z} \left(\frac{\partial \lambda}{\partial z} \Delta \right) + 2 \frac{\partial}{\partial z} \left(\frac{\partial \mu}{\partial z} \frac{\partial w}{\partial z} \right) = \delta(x) \delta(z - z_0), \quad (14)$$

$$\mu \frac{\partial^2 w}{\partial x^2} + \mu \frac{\partial^2 w}{\partial z^2} + \rho \omega^2 w + (\lambda + \mu) \frac{\partial \Delta}{\partial z} + \frac{\partial \lambda}{\partial z} \Delta + 2 \frac{\partial \mu}{\partial z} \frac{\partial w}{\partial z} = 0, \quad (15)$$

where the dilatation Δ is the divergence of the displacement vector, w is the vertical displacement, and λ and μ are the complex Lamé constants. Equations (14) and (15) form a coupled system of equations of the form

$$L \frac{\partial^2}{\partial x^2} \begin{pmatrix} \Delta \\ w \end{pmatrix} + M \begin{pmatrix} \Delta \\ w \end{pmatrix} = \begin{pmatrix} \delta(x) \delta(z - z_0) \\ 0 \end{pmatrix}, \quad (16)$$

where L and M are depth operators. The elastic PE is obtained by factoring Eq. (16) for $x > 0$ to obtain

$$\frac{\partial}{\partial x} \begin{pmatrix} \Delta \\ w \end{pmatrix} = i (L^{-1} M)^{1/2} \begin{pmatrix} \Delta \\ w \end{pmatrix}. \quad (17)$$

Integrating Eq. (16) over an arbitrarily small range interval about the origin, we obtain

$$\lim_{x \rightarrow 0^+} L \frac{\partial}{\partial x} \begin{pmatrix} \Delta \\ w \end{pmatrix} = \begin{pmatrix} \frac{1}{2} \delta(z - z_0) \\ 0 \end{pmatrix}. \quad (18)$$

Substituting Eq. (17) into Eq. (18), we obtain the following generalization of Eq. (5):

$$L (L^{-1} M)^{1/2} \begin{pmatrix} \Delta \\ w \end{pmatrix} = \begin{pmatrix} -\frac{1}{2} i \delta(z - z_0) \\ 0 \end{pmatrix}. \quad (19)$$

The operator square root in Eq. (19) is approximated using Eq. (6) to obtain the following generalization of Eq. (7):

$$L \prod_{j=1}^N \frac{k_0^2 + a_{2j-1,N}(L^{-1} M - k_0^2)}{k_0^2 + a_{2j,N}(L^{-1} M - k_0^2)} \begin{pmatrix} \Delta \\ w \end{pmatrix} = \begin{pmatrix} -\frac{1}{2} i k_0^{-1} \delta(z - z_0) \\ 0 \end{pmatrix}. \quad (20)$$

Although Eq. (20) is difficult to solve directly due to the singularity of the solution at $z = z_0$, the indirect method used to solve Eq. (7) generalizes to the elastic case. The first step involves solving

$$L(L^{-1}M) \begin{pmatrix} \Delta \\ w \end{pmatrix} = M \begin{pmatrix} \Delta \\ w \end{pmatrix} = \begin{pmatrix} -\frac{1}{2}ik_0^{-1}\delta(z - z_0) \\ 0 \end{pmatrix}. \quad (21)$$

The second step, which reduces the contribution of the evanescent modes, involves propagating Δ and w out a short distance in range using the elastic PE. In analogy to the acoustic case, the solution of Eq. (20) is completed by operating on the field with the rational-linear approximation for $(L^{-1}M)^{1/2}$. The self-starter for the elastic PE is easily generalized to the case of a point source. Since the normal-mode representations for the line-source and point-source solutions differ in the farfield by the power of k_n that appears as a factor, the final step for the point-source case involves operating on the field with $(L^{-1}M)^{3/4}$ rather than $(L^{-1}M)^{1/2}$.

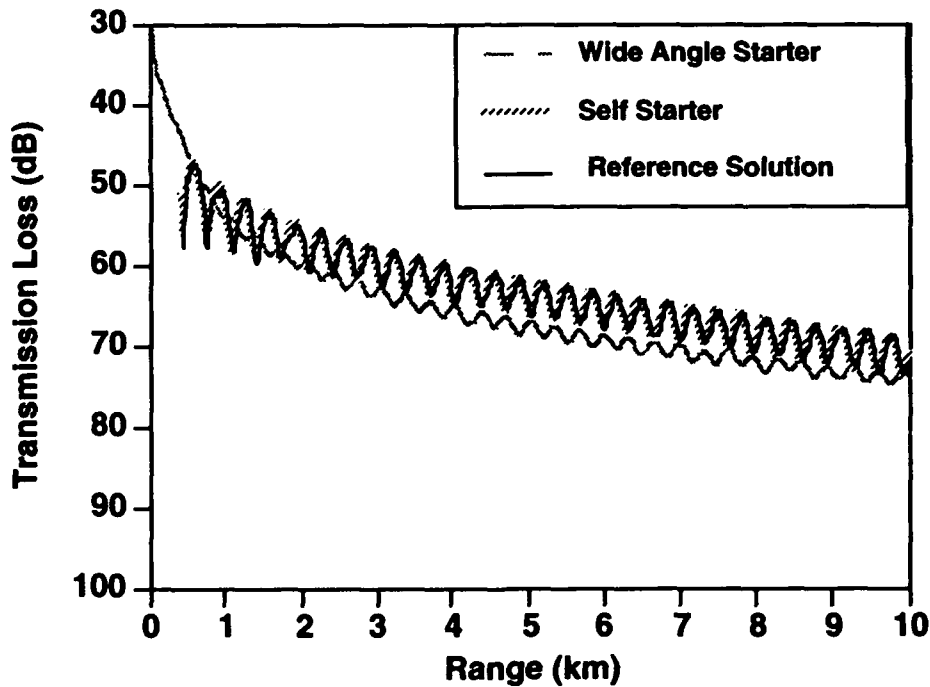


Figure 1. Illustration of the accuracy of the elastic PE self-starter.

To demonstrate the accuracy of the elastic PE self-starter, we consider a problem from [11] that involves an interface wave and a trapped mode near cutoff. A 5 Hz source is placed at $z = 85$ m in an ocean of depth 100 m. In the water column, $c = 1500$ m / s, $\rho = 1$ g / cm³, and $\beta = 0$. In the ocean bottom, $c_p = 2400$ m / s, $c_s = 1200$ m / s, $\beta_p = 0.1$, $\beta_s = 0.2$, and $\rho = 1.5$ g / cm³. We take $N = 5$ and $r_0 = 400$ m. Figure 1 contains solutions at $z = 85$ m

generated with the elastic PE using the self-starter and using the wide-angle PE starter of [5]. The solution generated using the self-starter is in agreement with the reference solution, which was generated using the spectral approach of [10]. The solution generated using the wide-angle PE starter has a large error.

REFERENCES

- [1] F.D. Tappert, "The parabolic approximation method," in *Wave Propagation and Underwater Acoustics*, edited by J.B. Keller and J.S. Papadakis, Lecture Notes in Physics, Volume 70 (Springer, New York, 1977).
 - [2] S.T. McDaniel, "Propagation of normal mode in the parabolic approximation," *J. Acoust. Soc. Am.* **57**, 307-311 (1975).
 - [3] M. Porter and E.L. Reiss, "A numerical method for ocean-acoustic normal modes," *J. Acoust. Soc. Am.* **76**, 244-252 (1984).
 - [4] R.B. Evans, "A coupled mode solution for acoustic propagation in a waveguide with stepwise depth variations of a penetrable bottom," *J. Acoust. Soc. Am.* **74**, 188-195 (1983).
 - [5] R.R. Greene, "The rational approximation to the acoustic wave equation with bottom interaction," *J. Acoust. Soc. Am.* **76**, 1764-1773 (1984).
 - [6] E.R. Robinson and D.H. Wood, "Generating direct starting fields for parabolic equations," *J. Acoust. Soc. Am.* **84**, 174-1801 (1988).
 - [7] M.D. Collins, "A nearfield asymptotic analysis for underwater acoustics," *J. Acoust. Soc. Am.* **85**, 1107-1114 (1989).
 - [8] M.D. Collins, "A self-starter for the parabolic equation method," *J. Acoust. Soc. Am.* **92**, 2069-2074 (1992).
 - [9] M.D. Collins and R.B. Evans, "A two-way parabolic equation for acoustic back scattering in the ocean," *J. Acoust. Soc. Am.* **91**, 1357-1368 (1992).
 - [10] H. Schmidt and F.B. Jensen, "A full wave solution for propagation in multilayered viscoelastic media with application to Gaussian beam reflection at fluid-solid interfaces," *J. Acoust. Soc. Am.* **77**, 813-825 (1985).
 - [11] M.D. Collins, "Higher-order parabolic approximations for accurate and stable elastic parabolic equations with application to interface wave propagation," *J. Acoust. Soc. Am.* **89**, 1050-1057 (1991).
 - [12] H. Kolsky, *Stress Waves in Solids* (Dover, New York, 1963), p. 11.
-

The Navy Standard Parabolic Equation Model, Broadband PE, and PE Workshop II

Eleanor S. Holmes

*Integrated Performance Decisions
Arlington, VA 22202*

Laurie A. Gainey

*Science Applications International Corp.
Mashpee, MA 02649*

INTRODUCTION

This report describes the Navy Standard Parabolic Equation (PE) propagation loss model and its use in predicting broadband transmission loss and time arrival structure of arriving signals. It also describes and discusses the PE WORKSHOP II test cases.

Section 1 derives the Parabolic Equation, beginning in this case with a broadband wave equation rather than the cw Helmholtz Equation. Section 2 defines procedures used to predict broadband transmission loss and time arrival structure with PE.

Section 3 describes the prediction of time arrival structure with the Navy Standard PE Broadband Post-Processor. Several example test cases are given, including an isovelocity environment, a CZ environment and a ducted precursor environment.

Section 4 describes the 6 PE Workshop II Test Cases, and PE performance on these test cases. Recommendations for upgrades to future versions of the Navy Standard PE are made.

The authors of this report are grateful to Ruth Keenan for supplying Sections 1.2 to 1.4, and for general advice and editing assistance.

SECTION 1: PARABOLIC EQUATION DERIVATION

In this section, we show the derivation of the Helmholtz equation from Maxwell's equations. Where many PE derivations begin with the Helmholtz equation, we will begin with a wave equation derived from Maxwell's equations which does not restrict propagation to narrow band (cw - continuous wave), as an introduction to the broadband discussion.

1.1 Maxwell's Equations to Helmholtz Equation

We begin with a general wave equation for electromagnetic propagation¹ derived from Maxwell's equations,

$$\frac{\partial^2 \Psi}{\partial r^2} + \frac{\partial^2 \Psi}{\partial y^2} + \frac{\partial^2 \Psi}{\partial z^2} - \frac{1}{c^2} \frac{\partial^2 \Psi}{\partial t^2} = \frac{-\rho}{4\pi r^2} \quad (\text{Maxwell 18.26})$$

where

- Ψ is the pressure field in (r, y, z, t)
- r is range (the x-direction) along a radial,
- y is the direction perpendicular to the track,
- z is depth,
- c is the speed of sound,
- t is time,

and

- ρ is the density of the medium.

The first approximation made is the far field approximation. In the far-field the term $\rho/4 \pi r^2$ is small enough to ignore, so we will set the right side of this equation to zero:

$$\frac{\partial^2 \Psi}{\partial r^2} + \frac{\partial^2 \Psi}{\partial y^2} + \frac{\partial^2 \Psi}{\partial z^2} - \frac{1}{c^2} \frac{\partial^2 \Psi}{\partial t^2} = 0 \quad (1)$$

This equation now shows another property of far field propagation. The energy now propagates as plane waves, not spherical waves, since the second derivative of the components of the field is zero. Now, if we can assume that energy is at a single frequency, then we can let

$$\Psi = \Psi e^{i\omega t}, \text{ and}$$

$$\frac{\partial^2 \Psi}{\partial t^2} = i^2 \omega^2 \Psi e^{i\omega t} = -\omega^2 \Psi e^{i\omega t}$$

where

$$\omega = 2\pi f = c_0 k,$$

$$-\omega^2 \Psi e^{i\omega t} = -c_0^2 k^2 \Psi e^{i\omega t}$$

Clearly,

$$\frac{\partial^2 \Psi}{\partial r^2} = \frac{\partial^2 \Psi}{\partial r^2} e^{i\omega t}, \quad \frac{\partial^2 \Psi}{\partial y^2} = \frac{\partial^2 \Psi}{\partial y^2} e^{i\omega t}, \quad \frac{\partial^2 \Psi}{\partial z^2} = \frac{\partial^2 \Psi}{\partial z^2} e^{i\omega t}$$

so dividing both sides of Equation (1) by $e^{i\omega t}$, we have

$$\frac{\partial^2 \psi}{\partial r^2} + \frac{\partial^2 \psi}{\partial y^2} + \frac{\partial^2 \psi}{\partial z^2} + k^2 n^2 \psi = 0$$

where n is the index of refraction, $\frac{c_0}{c(z)}$. Assuming no out of plane scatter, $\frac{\partial^2 \psi}{\partial y^2} = 0$, and

$$\frac{\partial^2 \psi}{\partial r^2} + \frac{\partial^2 \psi}{\partial z^2} + k^2 n^2 \psi = 0$$

which is the Helmholtz equation.

1.2 Helmholtz Equation to Parabolic Equation

This section and Sections 1.3 and 1.4 were adapted from a document prepared by Ruth Keenan of SAIC, and are part of her ICECAP documentation².

This very simplistic and abbreviated introduction to the parabolic equation, Fourier split-step method is intended to give the reader an appreciation for its mathematical foundations. This discussion is based on Ruth Keenan's notes from a "bag-lunch" presentation Rob Greene gave many years ago, possibly around 1979, at SAIC. For more detailed treatments the reader is referred to Tappert³, Lee and McDaniel⁴, Jensen and Krol⁵ and McDaniel⁶.

We first rearrange the Helmholtz equation, equation (2) as:

$$\left\{ \frac{\partial^2}{\partial r^2} + \left[\frac{\partial^2}{\partial z^2} + k^2 n^2 \right] \right\} \psi(r, z) = 0 . \quad (2)$$

The solution to the Helmholtz equation represents a complete, full wave solution to the wave equation for harmonic solutions. We want to rewrite the Helmholtz equation in a form conducive to the derivation of the parabolic equation, so consider the identity

$$(a^2 + b^2) = (a + ib)(a - ib).$$

If we let $a = \frac{\partial}{\partial r}$, and $b = \left[\frac{\partial^2}{\partial z^2} + k^2 n^2 \right]^{1/2}$, then equation (2) can be rewritten in the form of equation (3):

$$\left[\frac{\partial}{\partial r} + i \left(\frac{\partial^2}{\partial z^2} + k^2 n^2 \right)^{1/2} \right] \left[\frac{\partial}{\partial r} - i \left(\frac{\partial^2}{\partial z^2} + k^2 n^2 \right)^{1/2} \right] \psi = 0 . \quad (3)$$

The first term represents the backward propagating energy and the second term represents the forward propagating energy. The first limitation we impose on this solution to the wave equation is that only forward propagating energy is considered.

$$\left[\frac{\partial}{\partial r} - i \left(\frac{\partial^2}{\partial z^2} + k^2 n^2 \right)^{1/2} \right] \psi = 0 . \quad (4)$$

The key to solving equation (4) is to approximate the square root operator. First, simply rewrite this operator in the form of (5)

$$\begin{aligned} \left(\frac{\partial^2}{\partial z^2} + k^2 n^2 \right)^{1/2} &= \left[\frac{\partial^2}{\partial z^2} + k^2(n^2 - 1) + k^2 \right]^{1/2} \\ &= k \left[1 + \frac{1}{k^2} \frac{\partial^2}{\partial z^2} + (n^2 - 1) \right]^{1/2} \end{aligned} \quad (5)$$

so that we can easily apply a Taylor series expansion ($(1 + x)^{1/2} \approx 1 + x/2$), so that

$$\left(\frac{\partial^2}{\partial z^2} + k^2 n^2 \right)^{1/2} \approx k \left[1 + \frac{1}{2k^2} \frac{\partial^2}{\partial z^2} + \frac{1}{2} (n^2 - 1) \right]. \quad (6)$$

Substituting the right side of equation (6) into equation (4) results in the expression

$$\frac{\partial \psi}{\partial r} = i \left[k + \frac{1}{2k} \frac{\partial^2}{\partial z^2} + \frac{k}{2} (n^2 - 1) \right] \psi \quad (7)$$

Now, if we let ψ be modulated by a slowly varying envelope function

$$\psi = \phi e^{ikr} \quad (8)$$

and substitute this expression in equation (7), we have

$$\frac{\partial \phi}{\partial r} + ik\phi - i \left[k + \frac{1}{2k} \frac{\partial^2}{\partial z^2} + \frac{k}{2} (n^2 - 1) \right] \phi = 0. \quad (9)$$

the $k\phi$ terms drop out to yield the standard form of the parabolic equation,

$$\frac{\partial \phi}{\partial r} = i \left[\frac{1}{2k} \frac{\partial^2}{\partial z^2} + \frac{k}{2} (n^2 - 1) \right] \phi = 0. \quad (10)$$

1.3 Example of PE Angle Limitations

The Taylor series expansion of the operator in equation (6) limits the accuracy of the solution to a narrow aperture. Consider the simple solution

$$\psi = e^{i(\alpha r + \beta z)} \quad (11)$$

for an isovelocity ($n=1$) environment. The Helmholtz equation, equation (1), reduces to the familiar equation for a circle (which is why it is called the elliptic wave equation),

$$\begin{aligned} \frac{\partial^2 \psi}{\partial r^2} + \frac{\partial^2 \psi}{\partial z^2} + k^2 \psi &= 0 \\ -\alpha^2 - \beta^2 + k^2 &= 0 \\ k^2 &= (\alpha^2 + \beta^2). \end{aligned} \quad (12)$$

On the other hand, before the slowly varying envelope is removed from the parabolic equation, Equation (7), reduces to an expression for a parabola;

$$i\alpha \psi = i \left[k\psi + \frac{-\beta^2}{2k} \psi \right] \quad (13)$$

$$\alpha = k - \frac{\beta^2}{2k}; \quad k = \alpha + \frac{\beta^2}{2k}.$$

To evaluate the effect of this difference, consider the case $k=1$ ($k = \omega/c_o = 1$ implies evaluating this expression at about 238 Hz given a 1500 m/sec sound speed). Then

$$\alpha_{\text{elliptic}} = \sqrt{(1-\beta^2)}; \quad \alpha_{\text{parabolic}} = \left(1 - \frac{\beta^2}{2}\right). \quad (14)$$

The propagation angle, θ , is defined as, $\tan\theta = \beta/\alpha$. The following table (Figure 1-1) examines this discrepancy with angle of the parabolic approximation for this case if we take the elliptic expression as ground truth.

b	α Elliptic	α PE	θ Elliptic	θ PE	Error
0.0	1.00	1.00	0.00	0.00	0.00
0.1	0.99	1.00	5.74	5.74	0.00
0.2	0.98	0.98	11.45	11.54	-0.02
0.3	0.95	0.96	17.46	17.44	-0.11
0.4	0.92	0.92	23.58	23.50	-0.38
0.5	0.87	0.88	30.00	29.75	-1.04
0.6	0.80	0.82	36.87	36.20	-2.50
0.7	0.71	0.76	44.43	42.84	-5.72
0.8	0.60	0.68	53.13	49.64	-13.33
0.9	0.44	0.60	64.16	56.54	-36.50
1.0	0.00	0.50	90.01	63.44	Can't Compute
1.1	N/A for Elliptic	0.40	Imaginary Angles	70.25	Can't Compute
1.2	N/A for Elliptic	0.28	Imaginary Angles	76.87	Can't Compute
1.3	N/A for Elliptic	0.16	Imaginary Angles	83.21	Can't Compute
1.4	N/A for Elliptic	0.02	Imaginary Angles	89.19	Can't Compute

Figure 1-1. Parabolic approximation error.

1.4 Fourier Split-Step Solution to PE

For simplicity in notation, rewrite the standard form of the parabolic equation as

$$\frac{\partial \phi}{\partial r} = i [A(r, z) + B(z)]\phi \quad (15)$$

$$A = \frac{k}{2} [n^2 - 1], \quad B = \frac{1}{2k} \frac{\partial^2}{\partial z^2}.$$

Rewrite equation (15) as

$$\frac{\partial \phi}{\phi} = i [A + B] dr \quad (16)$$

and take the integral of both sides

$$\int \frac{d\phi}{\phi} = i \int [A + B] dr \quad (17)$$

$$\begin{aligned} \ln \phi|_r^{r+\Delta r} &= i \int_r^{r+\Delta r} (A + B) dr \\ \ln \phi(r + \Delta r) &= i \int_r^{r+\Delta r} (A + B) dr + \ln \phi(r). \end{aligned}$$

To remove the natural logarithm, exponentiate both sides of equation (17)

$$\phi(r + \Delta r) = \exp[i \int (A + B) dr] \phi(r). \quad (18)$$

Assume the integral varies slowly enough so that the approximation

$$\int_r^{r+\Delta r} C dr \approx C \Delta r \quad (19)$$

is valid, and

$$\phi(r + \Delta r) \approx \exp[i(A + B)\Delta r] \phi(r). \quad (20)$$

Now, assume we commute the operator

$$e^{i(A+B)} \approx e^{iA/2} e^{iB} e^{iA/2}$$

This introduces errors that depend upon Δr , frequency and the index of refraction, n . The error can be kept small if Δr is decreased.

$$\phi(r + \Delta r) \approx \exp(iA\Delta r/2) \exp(iB\Delta r) \exp(iA\Delta r/2) \phi(r) \quad (21)$$

PE Workshop II: Part 2 — Test Case Results

The solution to equation (21) is conveniently found by Fourier transform methods, which start with a known pressure field at the source and march forward with a range step Δr .

A property of Fourier transforms is that the Fourier transform of the depth derivative is the same as a wavenumber multiplication of the Fourier transform⁷.

$$f(x) = \frac{1}{2\pi} \int g(y) e^{ixy} dy \quad (22)$$

$$g(y) = \frac{1}{2\pi} \int f(x) e^{-ixy} dx$$

$$\mathcal{F}[f(x)] = g(y)$$

$$\begin{aligned} \mathcal{F}\left[\frac{df(x)}{dx}\right] &= \frac{1}{2\pi} \int \frac{d}{dx} g(y) e^{ixy} dy \\ &= iy \mathcal{F}[f(x)] \end{aligned}$$

It follows that the second derivative can be expressed as,

$$\mathcal{F}\left[\frac{d^2 f(x)}{dx^2}\right] = -y^2 \mathcal{F}[f(x)] \quad (23)$$

The application of this property to the parabolic equation is a bit more complicated because the second derivative is part of the exponential operator,

$$V = e^{i\Delta r B} \phi(z) \quad (24)$$

$$V = e^{i\left[\frac{\Delta r}{2k} \frac{\partial^2}{\partial z^2}\right]} \phi(z)$$

If the exponential term is broken up into its power series expression,

$$[e^x = 1 + x + x^2/2! + \dots]$$

then we see that equation (25) is a direct application of the Fourier transform property expressed in equation (24)

$$\int e^{i\left[\frac{\Delta r}{2k} \frac{\partial^2}{\partial z^2}\right]} \phi(l) e^{-izl} dl = e^{i\left[\frac{\Delta r^2}{2k}\right]} \mathcal{F}[\phi(z)] \quad (25)$$

Using this property

$$\phi(r + \Delta r, z) = e^{i\omega r/2} \mathcal{F}^{-1} \left[e^{-i\left[\frac{\Delta r^2}{2k}\right]} \mathcal{F} \left\{ e^{i\Delta r/2} \phi(r, z) \right\} \right]; \quad (26)$$

thus, the solution is conveniently found by Fourier transform methods, which start with a known pressure field at the source and march forward with a range step Δr following algorithm (26). A by-product of the Fourier split-step solution is that the pressure field is computed at each depth mesh point, thus the full field transmission loss displays do not require an extra computation time.

SECTION 2: BROADBAND TRANSMISSION LOSS

We define cw propagation as energy traveling at a single frequency. That is, the frequency spectrum of the cw signal consists of a single delta-function. This is only an approximation if the length of the signal is finite. For example, the spectrum of a time-limited cosine-shaped signal is a $\sin x/x$ pattern (shown in the Figure 2-1). The longer the signal duration, the narrower the $\sin x/x$ pattern will be, and the shorter the signal, the broader the pattern. However, most PE models treat this signal as if it actually has zero bandwidth.

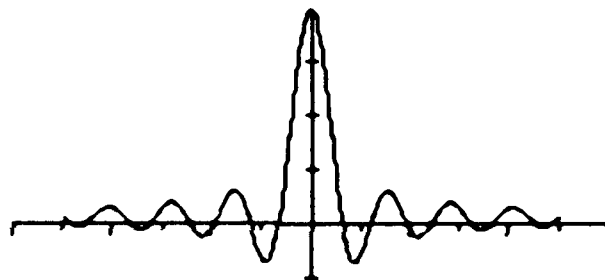


Figure 2-1. Spectrum of Time-Limited CW Signal

One way to model a real broadband signal is to integrate the Helmholtz Equation (2) over frequencies in a band:

$$\int_{k_1}^{k_2} \left[\frac{\partial^2 \psi}{\partial r^2} + \frac{\partial^2 \psi}{\partial z^2} + k_0^2 n^2 \psi \right] dk_0 = 0$$

It can be shown that the integral carries through to the Split Step Algorithm (Equation 26), and therefore the output from PE can be integrated to simulate a broadband signal. Some methods of processing broadband information are shown in the following diagram, Figure 2-2.

The leftmost branch of Figure 2-2, travel time computations, is the subject of Section 3.

Hanna and Rost⁸ suggested a method in which a single PE run is made at the center frequency of the band and the results are averaged in range and depth. The amount of range and depth averaging needed depends on the center frequency and the bandwidth of the signal. For this method, the range and depth averages are given by:

$$\Delta r > 100\lambda$$

and

$$\frac{\Delta z}{Z} = \frac{\Delta f}{F}$$

where

- Δr is the length of the range average window,
- Δz is the thickness of the depth averaging layer,
- λ is the acoustic wavelength,
- Z is the depth at which transmission loss is needed,
- Δf is the bandwidth
- and
- F is the center frequency of the band.

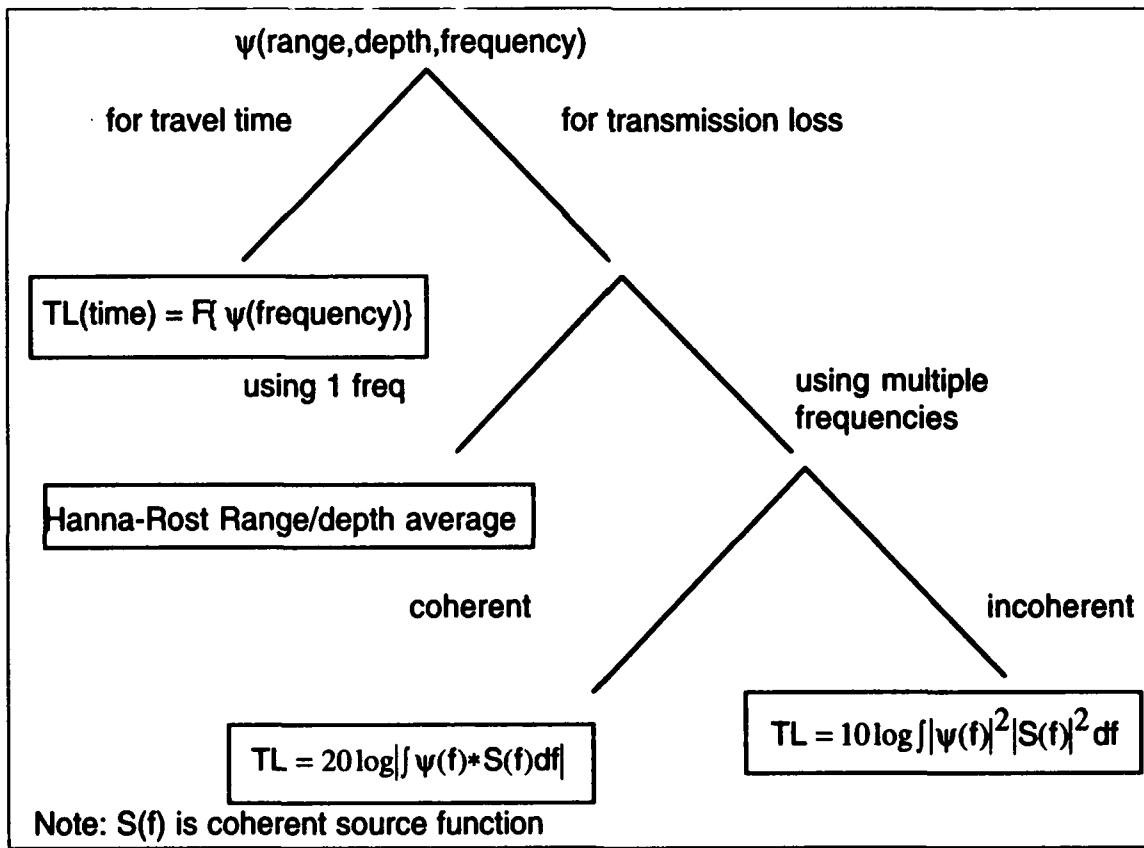


Figure 2-2. Broadband Processing Methods

The second approach, recently implemented as a post processor to the Navy Standard PE Model, is an incoherent average across the frequency band, in which the PE pressures at each frequency can be weighted by the source level $S(f)$:

$$\int_{f_2}^{f_1} (\text{PE Intensity}(f)) * |S(f)|^2 df \quad (27)$$

A coherent broadband calculation is similar to the incoherent method, but PE complex pressure is integrated against the source complex pressure.

SECTION 3: BROADBAND PE FOR TIME-ARRIVAL STRUCTURE

3.1 Theory of Fourier Synthesis

The output from the Parabolic Equation can also be used to predict time arrival structure. This is made possible by the Fourier identity:

$$P(t) = \mathcal{F}^{-1}\{\tilde{P}(f)\}$$

where

t is time (seconds)

f is frequency (Hertz)

$P(t)$ is complex pressure as a function of arrival time,

and

$\tilde{P}(f)$ is complex pressure as a function of frequency.

Intensity vs. time is then computed simply as the magnitude squared of the complex pressure. The approach to computing time arrival structure is to run PE at a dense set of frequencies across the frequency band of interest, saving complex pressures at discrete ranges and depths. Complex pressure is then used to produce pressure as a function of frequency for a given range/depth pair. Since this algorithm provides relative travel time and not absolute travel time, there is always some ambiguity due to the FFT wrap-around property. Absolute travel time, then, must be defined as:

$$t_{abs} = t_o + t + nT \text{ for } n = 0, 1, 2, \dots$$

where

$t_o = R/c_o$

R is range

c_o is the reference sound speed

t is relative travel time and

T is the length of the signal.

Note that t_o can easily be added into the results of the frequency-to-time Fourier transform. In order to sample the frequency band adequately, a frequency increment no greater than $1/T$ must be used. If the total length of the arrival is unknown, T can be estimated in a conservative fashion by computing the minimum and maximum time needed to cover the range from source to receiver. The conservative maximum travel time is computed using the

PE Workshop II: Part 2 — Test Case Results

steepest “ray” (θ_{max}) propagating at the minimum sound speed C_o , and the minimum time is computed using a 0° ray travelling at the maximum sound speed C_{max} :

$$T_{\min} = \frac{R}{C_{\min}}, \text{ where } C_{\min} = C_o \cos(\theta_{max}) \text{ and } T_{\min} = \frac{R}{C_{\max}}.$$

3.2 Simple 2-Ray Test Case

This test case involves a flat bottom, isovelocity environment. The fixed point depth for this case is 4000 ft and the beamwidth is 20° . In order to examine the direct ray and the 20° surface reflected ray, a quick calculation with simple geometry was performed to show that the rays should intersect again at 3.6 nmi at 4000 ft. In the following equation, r_1 is range to the surface in feet for the 20° ray, so total range to the 4000 ft depth is $2 * r_1$.

$$r_1 = \frac{4000}{\tan(20^\circ)}$$

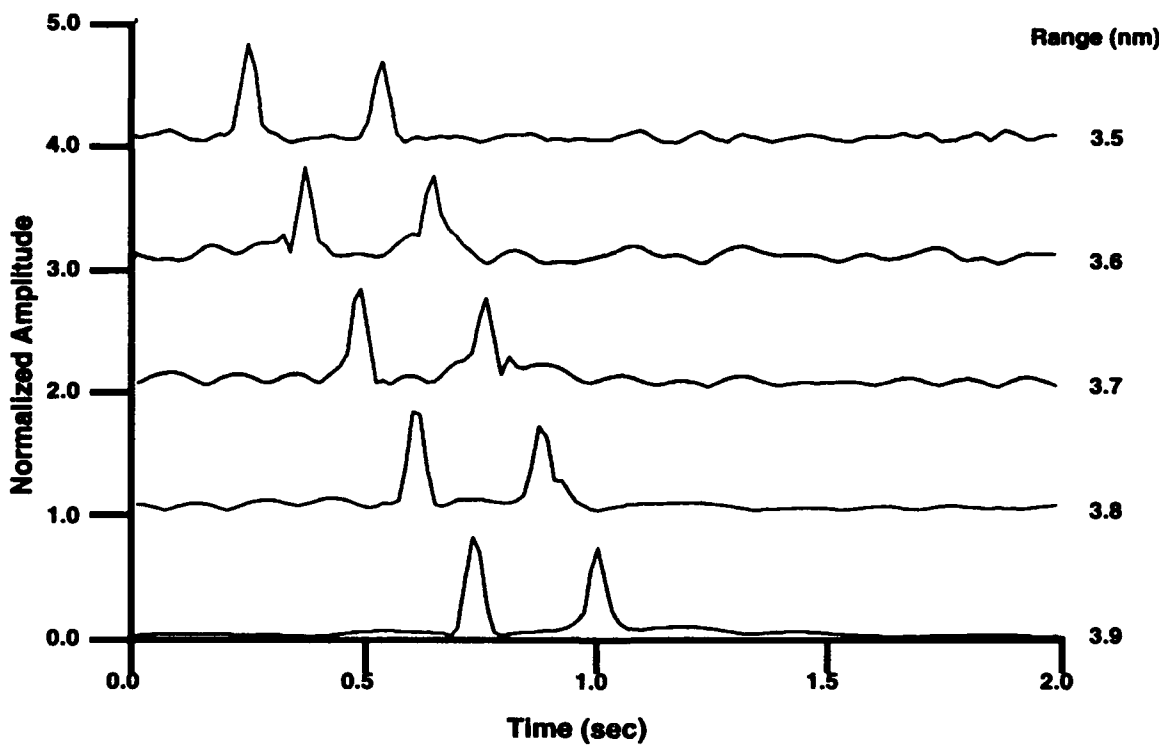


Figure 3-1. Broadband output for 2-ray case.

With a 5000 ft/sec sound speed, the arrival times of the two rays should differ by 0.28 seconds. PE was run over a 100 Hz band with 0.5 Hz resolution. This provided 2 seconds

of arrivals with a 0.02 second time resolution, which is more than sufficient for this case. Figure 3-1 shows the broadband output at 3.5, 3.6, 3.7, 3.8 and 3.9 nmi. Note that the time spread between the two arrivals at 4000 ft is indeed 0.28 seconds.

3.3 CZ Time-Arrival Structure

The next test case was a CZ environment with a flat bottom, as illustrated in Figure 3-2. To evaluate the arrivals for this case, the broadband computation was carried out at several ranges and depths along the track. Figure 3-3 shows arrival time vs. range for the 5000 ft depth. This type of output is instrumental in examining the moveout in time of the arrivals.

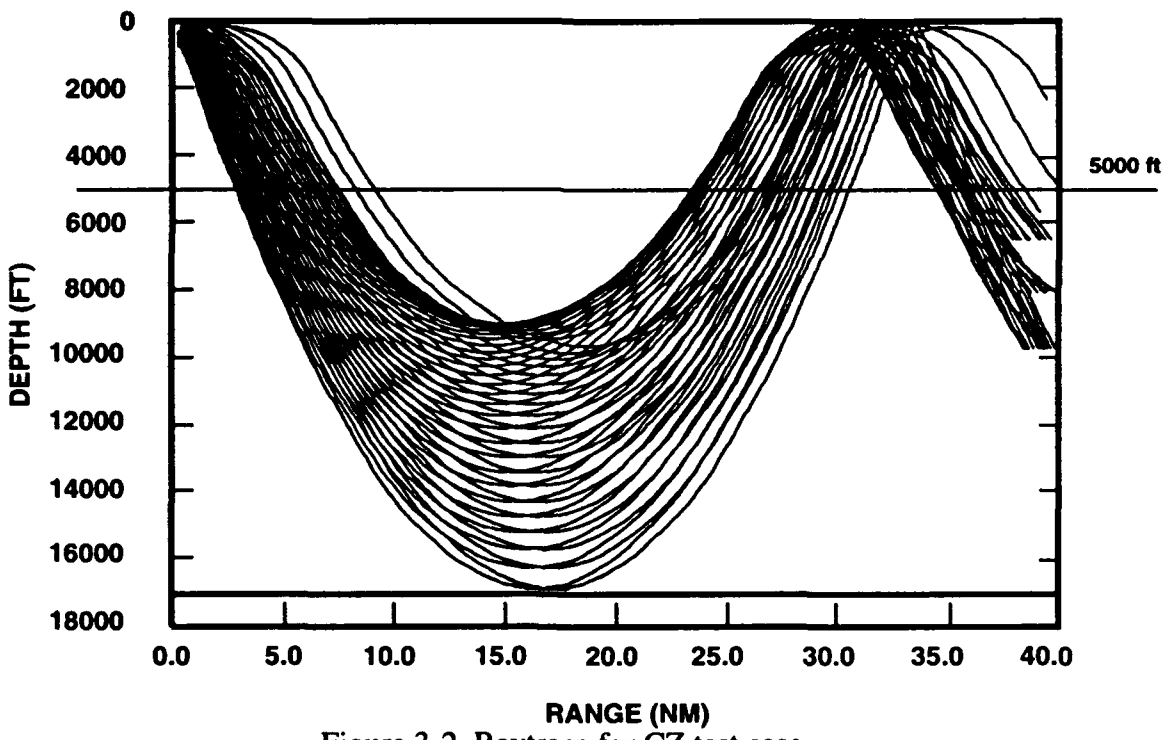


Figure 3-2. Raytrace for CZ test case.

The time arrival structure is shown on the left hand side of the plot. The next graph plots the time arrival of strongest TL peak. This graph is used to illustrate the FFT wraparound property of the broadband computation. Note that the arrival times have been adjusted to show absolute travel time. The time of maximum arrival graph is useful in tracking arrivals. When arrivals move out (as a function of range) to the maximum time and then quickly transition to the minimum time, this is indicative of the effects of the FFT wraparound property on the arrival and does not generally indicate a new arrival type.

PE Workshop II: Part 2 — Test Case Results

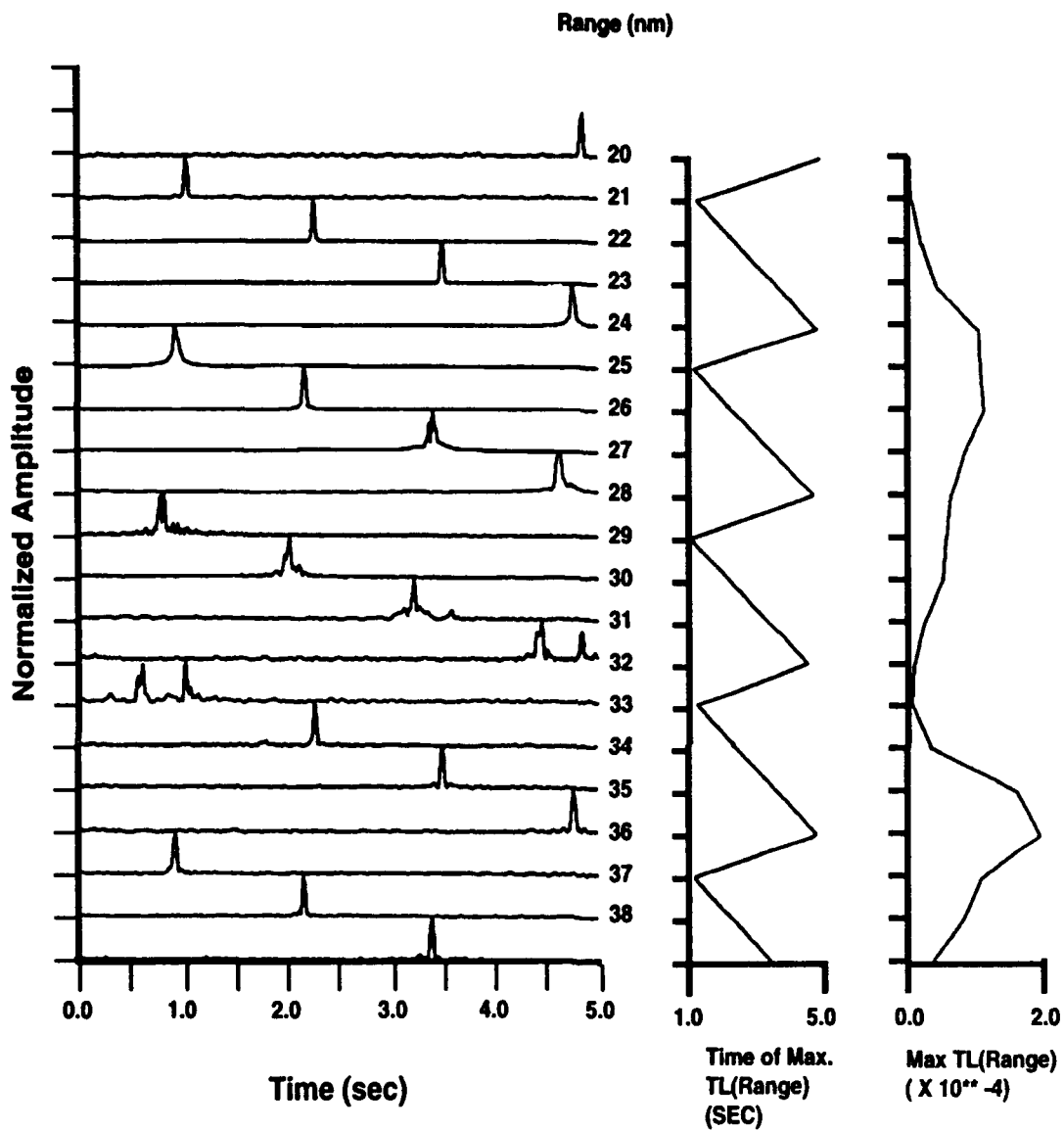


Figure 3-3. Broadband arrival structure for CZ test case.

The amplitudes of the time arrival structure are normalized to the maximum amplitude at each range. Thus, the peak amplitude vs. range graph shown on the right hand side of the plot is necessary to compare amplitudes at different ranges.

The time arrival plot for this environment is very informative in evaluating the arrival structure. At 20 nmi, the 5000 ft depth is within the shadow zone. Note that an arrival is

shown early in time and as range increases moves out in travel time. This arrival relates to upgoing rays. Looking across to the maximum amplitude plot, we can see that this arrival is very weak, consistent with diffracted energy. This illustrates the usefulness of a full field model broadband computation, as ray traces traditionally cannot model diffracted energy.

The energy of this peak slowly increases as the edge of the caustic is approached. The arrival at 24 nmi represents the intensity of one upgoing ray. The maximum energy increases sharply at 25 nmi, just at the edge of the caustic. This arrival represents two or more rays (the caustic) which have travel times very close to each other.

At 26 nmi, the maximum intensity falls back down as the range from the caustic increases. Note that the maximum energy decreases slowly until 30 nmi is reached. At 30 nmi, the 5000 ft depth is again within a shadow zone and the arrivals seen represent diffracted energy. Note that from 30 to 33 nmi there is a double peaked arrival. It is difficult to ascertain what causes this, but it is most likely energy diffracted from rays with slightly different travel times. The variation of intensity outside of the peak at 30 to 33 nmi, is due to the fact that the intensity of the peaks is so low, that we are in the realm of computational noise. Note that this is also true of the previous shadow zone at 20-21 nmi.

At 32 nmi we are beginning to see a new arrival, which is diffracted energy from the downgoing rays. This energy will reach the 5000 ft depth sooner than the upgoing rays which travel deeper in depth and thus take longer to reach that depth. At 33 nmi, the energy from the upgoing ray completely disappears from the problem, a fact that is verified by the ray trace.

The intensity of the downgoing rays increases sharply at 35 nmi, the edge of a caustic, and the increase is again due to two or more rays with the same travel time. Note that the intensity levels (as illustrated on the right-hand plot) are higher than they were at 24 to 25 nmi. From the ray trace, shown in Figure 3-2, the energy from the downgoing rays is more focused than the energy from the upgoing rays at 24-25 nmi.

As the energy decreases from 37 to 39 nmi, we can see from the ray trace that we are again entering a one downgoing ray region.

3.4 Ducted Precursors

Ducted precursors have been observed in data and modeled by Spofford and Keenan^{9,10}. Ducted precursors are generated from modes trapped within a surface duct. Each mode trapped in the surface duct leaks energy below the duct which travels as a CZ and/or bottom bounce path which couples back into the duct.

If the ducted energy has a group velocity greater than the CZ energy, the first ducted precursor arrival will be from energy which has leaked out of the surface duct, traveled as

a CZ or bottom bounce path for exactly one deep cycle, and then leaked back into the duct. The energy is coupled below the duct at a 0° grazing angle at a depth where the sound speed equals the phase velocity of the mode trapped in the duct, and the deep cycling energy may be either CZ or bottom bounce. If the range between the source and receiver is great enough to accommodate multiple CZ or bottom bounce cycles below the duct, then higher order precursor arrivals will be observed. This third test case was designed to model ducted precursors.

Our SVP was designed with high-sound-speed, strong, 250 m duct, as illustrated in Figure 3-4. By running MPP, we saw that the predicted travel time difference between the ducted paths and the CZ paths was about 1 second. The ray trace in Figure 3-5 shows the ducted and CZ arrivals, but a ray trace cannot predict the leaky ducted precursor energy. PE was run with a center frequency of 58 Hz and a 90 Hz bandwidth, with 0.3 Hz frequency resolution to yield about 3 seconds worth of arrival data.

The broad band post-processor was then run for a source at 300 ft, which is well within the duct (Figure 3-6). The first arrival in the 76-80 nmi range is the ducted energy and the CZ energy arrives about 1 second later. The two arrivals in between represent the ducted precursors of orders 1 and 2.

Although a ray model does not predict ducted precursors, it can be used to estimate ducted precursor arrival times and to validate a broadband model such as PE. In this case the arrival time of the first CZ-type ducted precursor at 78 nmi is:

$$T_{dp}(n) = T_d - n*T_{rd} + n*T_{dc}$$

where:

$T_{dp}(n)$	= arrival time of ducted precursor of order n
T_d	= arrival time of ducted only path
T_{rd}	= time the ducted only path would require to cover the horizontal range of the deep cycling path
T_{dc}	= arrival time of the deep cycling path (either CZ or bottom bounce) path

The intensities of the arrivals are relatively low from 70-75 nmi, with the ducted precursor arrival stronger than the CZ arrival. Within this range window, the CZ energy is within the shadow zone and the CZ arrival is due to energy that has been diffracted into the shadow zone. At 76 nmi, the CZ energy is dominant over the ducted and precursor arrivals.

The relative amplitudes of the ducted path and ducted precursor paths are dependent on the range, geometry, and reflection coefficients of the trapped modes. In this case the amplitude of the ducted arrival is less than that of the ducted precursors and the CZ arrival. The amplitude of the first order precursor is greater than that of the second order one in this case, but this is not a generalization for ducted precursors.

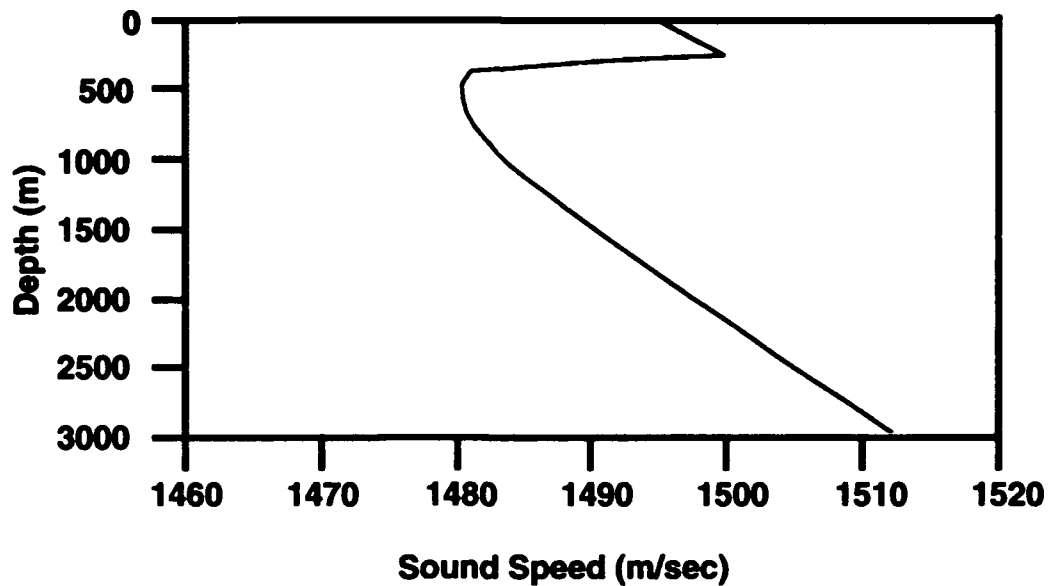


Figure 3-4. SVP for ducted precursor test case.

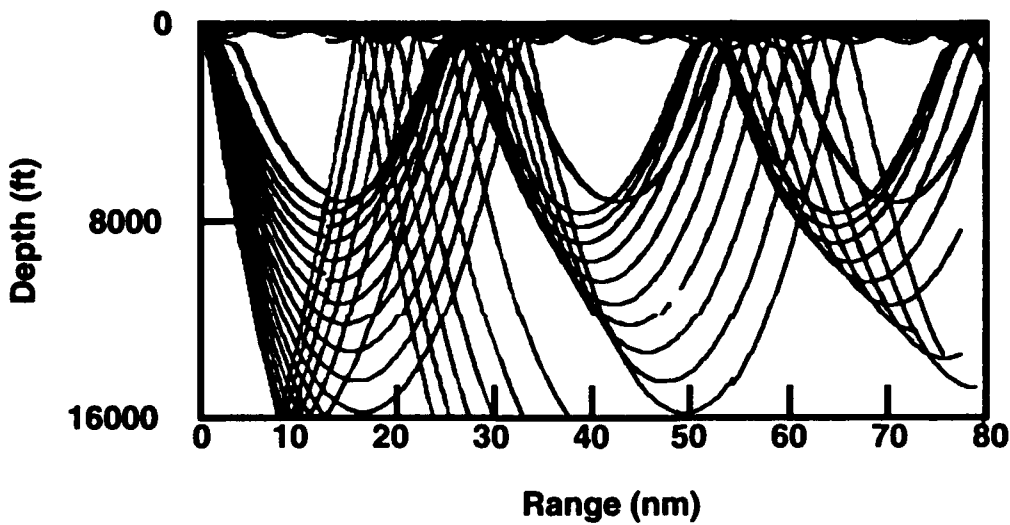


Figure 3-5. MPP raytrace for ducted precursor test case.

The arrival time structure was computed below the duct at the 1000 ft depth (Figure 3-7). It is interesting to note that the second ducted precursor is still in evidence in the CZ shadow zone ranges with the same time lag behind the CZ energy. This represents energy that has

PE Workshop II: Part 2 — Test Case Results

leaked out of the duct and contributed to the below duct field. Again the relative amplitude for the whole arrival is low with the shadow zone and at 75 nmi, where the direct CZ energy comes into play, the ducted precursor arrival is masked out by the amplitude of the CZ arrival. At 77 nmi, the presence of two CZ "rays" with similar travel times is indicated by the double peaked arrival.

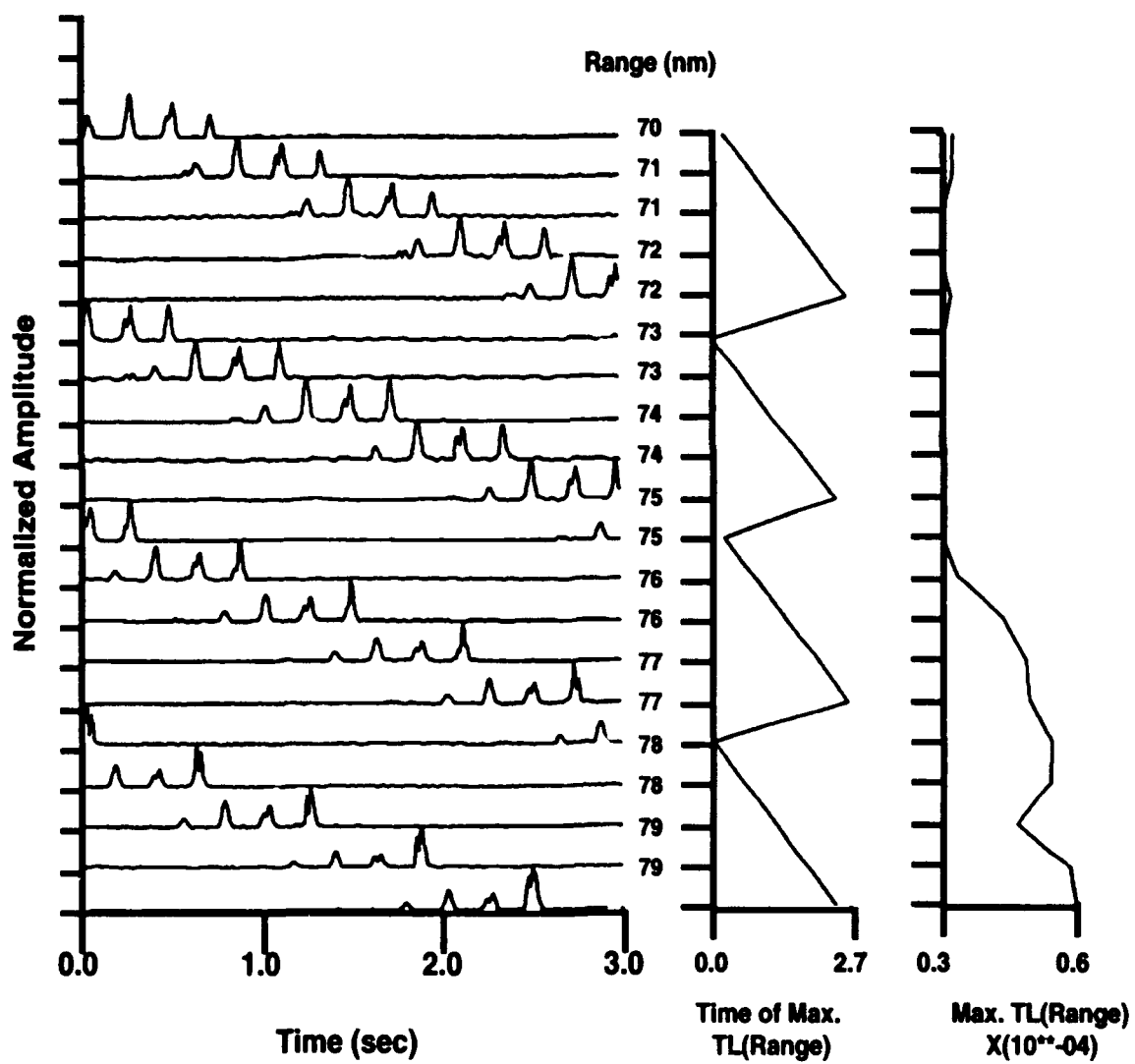


Figure 3-6. Broadband arrival structure for in-duct receivers. Depth = 333.337 ft.

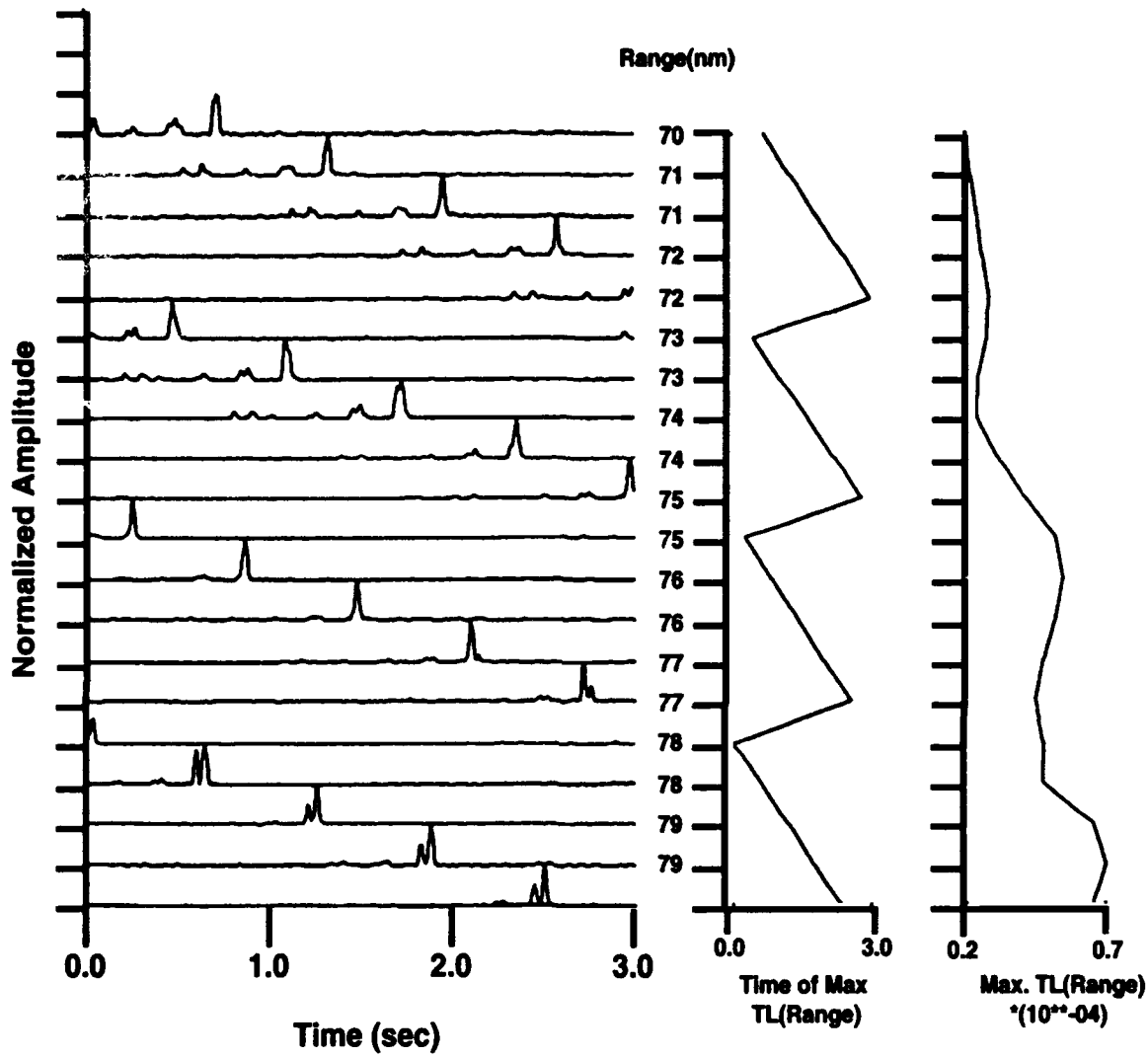


Figure 3-7. Broadband time arrival structure for out-of-duct receivers.

SECTION 4: WORKSHOP II TEST CASES

4.1 Introduction

All 6 of the test cases supplied for the ONR PE Workshop II were run using either the Navy Standard PE, Version 3.2¹¹, or a developmental copy of PE Version 3.3. Version 3.3 was chosen for some test cases because the presence of several upgrades in Version 3.3 facilitated creation of input files, and made evaluation of the test cases easier:

- input of absolute sound speed in the sediment, rather than sound speed relative to the sound speed at the bottom of the water column.
- input of attenuation in units of dB/λ instead of dB/foot .
- semi-coherence in the short-range, steep angle TL supplement, STEEP.

For each case, plots of the required transmission loss output are supplied. Runtimes are included for each case, and are relative to a 386-PC computer with a math coprocessor chip. All runtimes include I/O time as well as computational time.

Additionally, special problems and opportunities for improvement are noted.

4.2 Test Case Results

4.2.1 Test Case 1

A high angle Lloyd's mirror test case should pose serious problems for a split step PE model. The Navy Standard version of PE uses the Thomson-Chapman high angle phase error correction, which provides second-order accuracy in the approximation of the "square root operator" in the parabolic equation. Nevertheless, we still do not expect accuracy at the very high angles present in this test case.

This test case lends itself well to two of the upgrades to PE Version 3.3. Figure 4-1 shows a full field PE plot, illustrating the Lloyd's mirror effect. Figure 4-2 shows the PE transmission loss and an exact solution for Test Case 1. The Thomson source^{12,13} correction, suggested to us by Dr. Fred Tappert and currently implemented in PE Version 3.3 and the OPTAMAS PE model, was used to run this test case. The point of convergence shown in Figure 4-2 corresponds to 79°, the high angle cutoff for the Thomson source correction. We expected PE Version 3.3 to have phase problems at the high angles, but were surprised that the phase information from PE was so good! A plot to a larger range (Figure 4-3) shows continued good agreement.

The second upgrade to PE was an improvement to the STEEP algorithm which supplements high-angle transmission with a short-range ray trace. Whereas the current PE Version 3.2 provides an incoherent addition of all "steep" rays, and adds the result incoherently to the PE intensity, PE Version 3.3 sums rays coherently within a single order of bottom bounce, or between a direct path and a surface reflected path. The sum is still added incoherently to the PE energy. This test case happens to be ideal for testing and demonstrating this upgrade.

Figure 4-4 shows PE output from a run using a 10° vertical beamwidth for PE energy and the STEEP post-processor for energy between 10° and 90° Out to the 10 km range shown on this plot, there is excellent agreement, as we would expect. However, a longer-range plot, Figure 4-5, shows 1) too much energy at the "edge" of the PE beam, 2) too much

contribution from STEEP during the STEEP-to-PE transition, and 3) some wavering in the transmission loss after 40 km.

Figure 4-6 shows the PE solution using a 90° beamwidth, the Thomson source and no STEEP angle correction applied. The mesh spacing for this case was 46.14 ft, with a variable range step, and the total run time was 134 seconds on a 386 based machine.

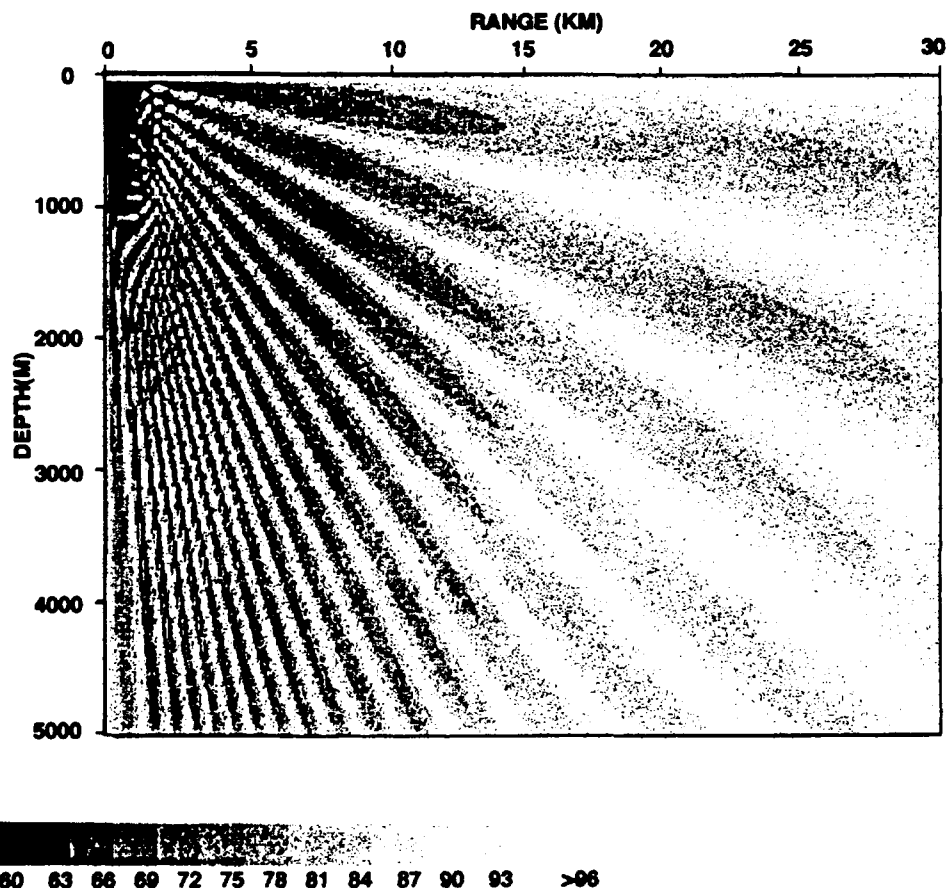


Figure 4-1. Test Case 1 full field plot.

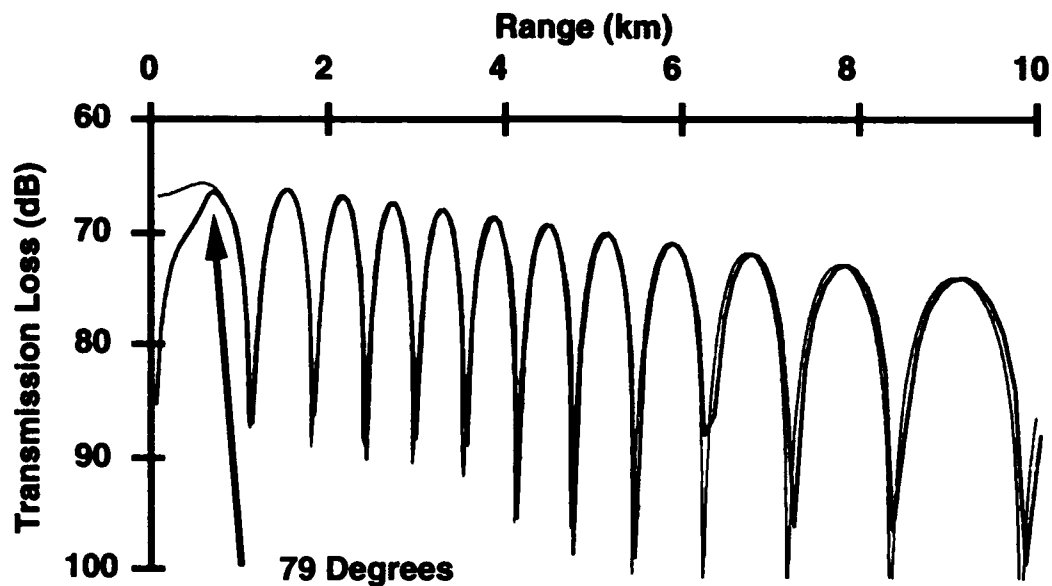


Figure 4-2. Results for Test Case 1 (over range 0 to 10 km) using Thomson source correction.

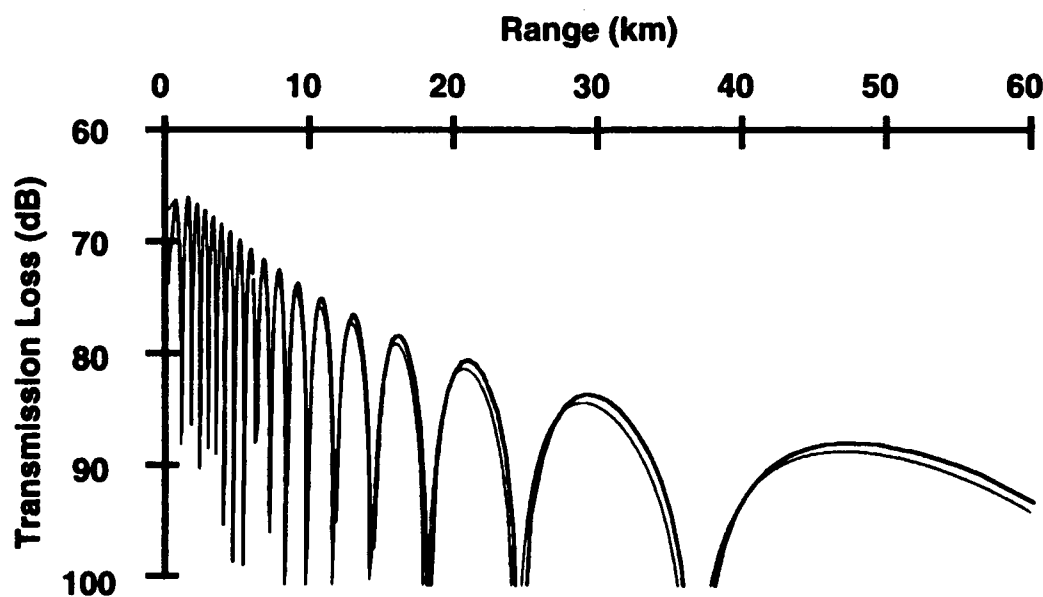


Figure 4-3. Results for Test Case 1 (over range 0 to 60 km) using Thomson source correction.

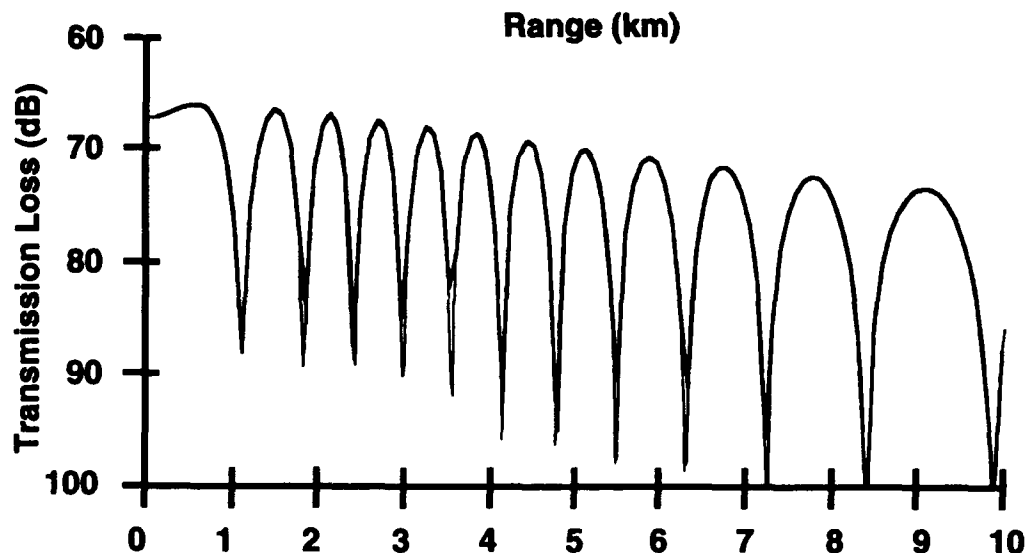


Figure 4-4. Results for Test Case 1 (over range 0 to 10 km) using STEEP post-processor.

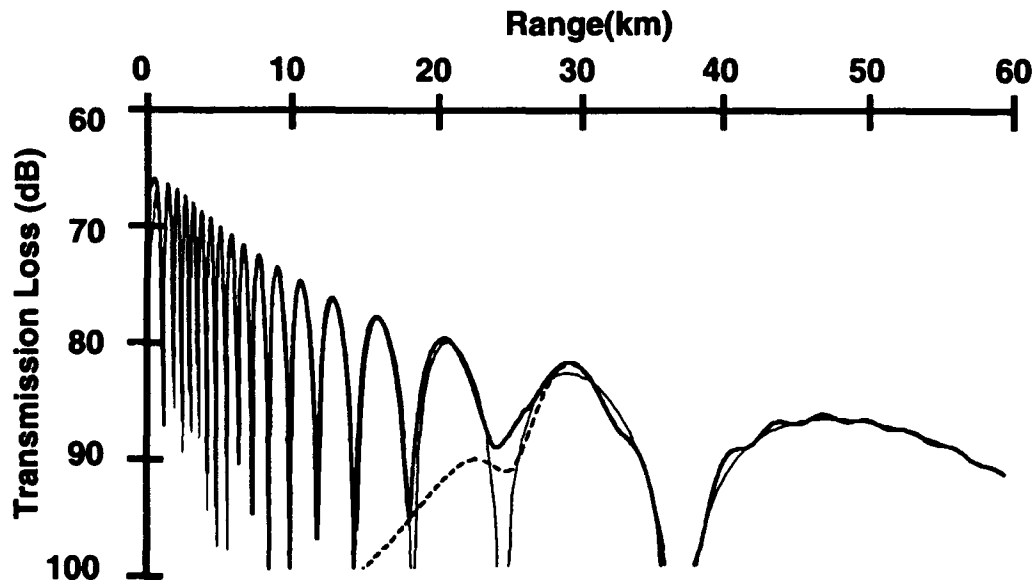


Figure 4-5. Results for Test Case 1 (over range 0 to 60 km) using STEEP post-processor.

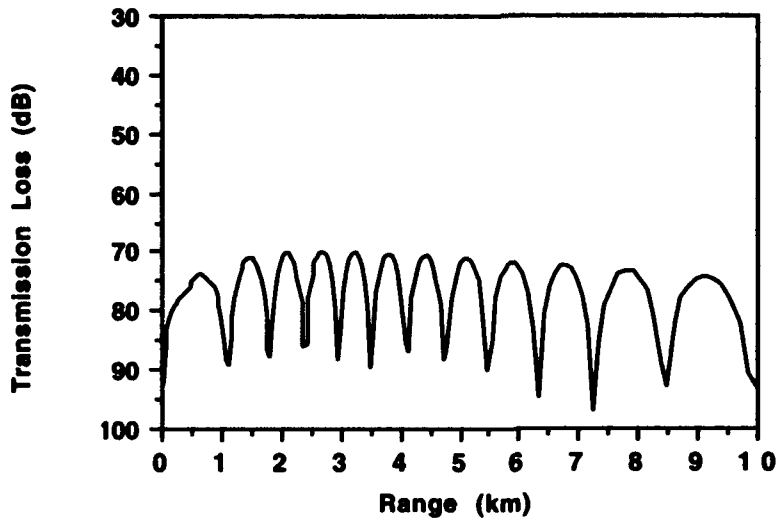


Figure 4-6. Case 1 results using 90° beam with no STEEP contribution.

4.2.2 Test Case 2

Test Case 2 is the upslope-downslope problem which was adapted from the “Wedge” benchmark. Figures 4-7 and 4-8 show the transmission loss vs. range at the 20 meter and 150 meter moving point depths.

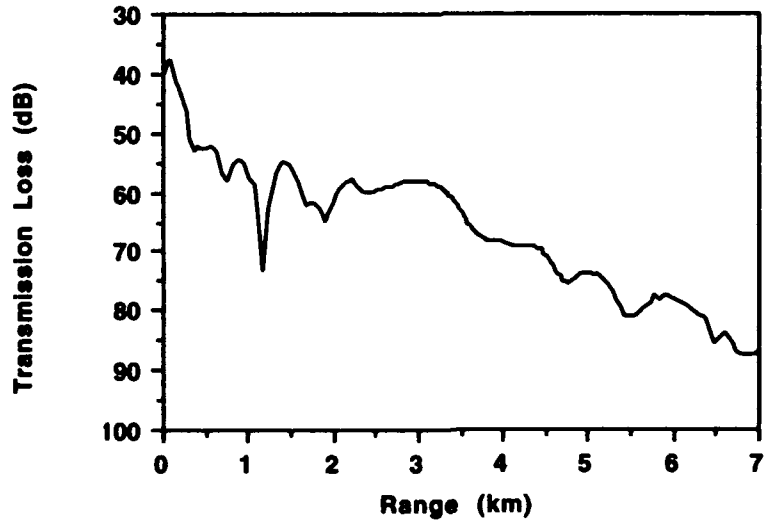


Figure 4-7 Case 2A: F = 25 Hz, ZS = 100m, ZR = 20 m.

The inputs for this case were tuned, to some extent, using the results from Test Case 3. Specifically, the thickness of the density transition region was artificially set to 30 feet, where PE would have chosen a transition region 60 feet thick. However, while this transition region modification made a significant difference in Test Case 3, it made no noticeable difference in this test case. The other input which was set to a non-default value was NTRANS, which was set to 1 to inhibit mesh space “stretching” which occurs normally for smaller vertical beam widths. A vertical beam width of $\pm 90^\circ$ was used for this case, so setting NTRANS to 1 did not distort the vertical beam, but did allow a denser depth mesh (since the mesh space was not “stretched”) for the same 2^8 transform.

The mesh spacing for this case was 5.5 feet with a variable range step. The total runtime was 73 seconds on a 386-based computer.

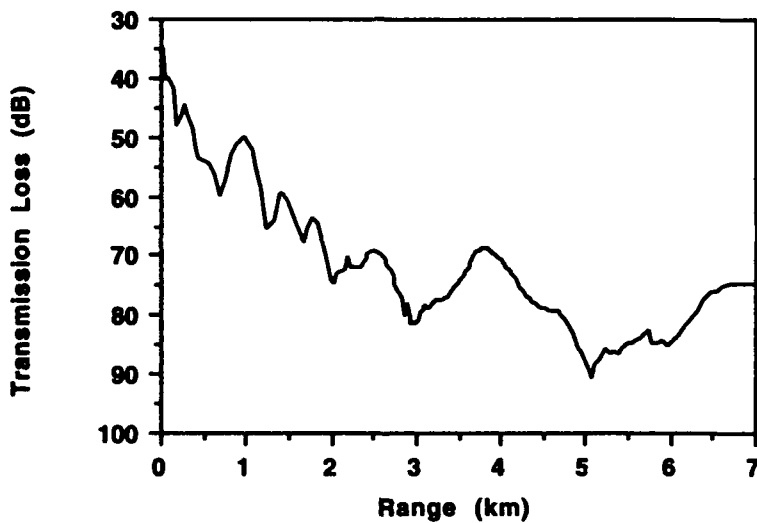


Figure 4-8. Case 2B: F=25 Hz, ZS = 100 m, ZR = 150 m.

4.2.3 Test Case 3

This test case was modified from an ASA benchmark test case by adding a shear speed of 800 m/s in the sediment. The upslope propagation is shown as a gray scale contour plot in Figure 4-9, and the transmission loss vs. range plots for 30 m and 150 m are presented in Figures 4-10 and 4-11.

While the Navy Standard PE was used for these test cases, the default inputs for the Navy Standard PE were not. The non-default input is DENSL, the length of the density transition region. While the Navy Standard PE produces a default value of about 60 feet for this test

case, we have input 30 feet for DENSL. This value was chosen to match the original ASA paper transmission loss. Figure 4-12 shows significant differences in transmission loss for the two values of DENSL, 30 and 60 ft, and supports Fred Tappert's suggestion that the Navy Standard PE default for DENSL be reduced by a factor of 2 or 3.

Validation for this test case is limited to running PE for the ASA benchmark case (without shear), and comparing PE outputs with the ASA benchmark outputs. Except for transmission loss to points deep in the sediment, the Navy Standard PE outputs match the benchmark case outputs. When shear was added, only about 1 dB of difference was observed.

The total run time for this case was 183 seconds. The mesh spacing was 5.5 ft and the PE variable range step was employed.

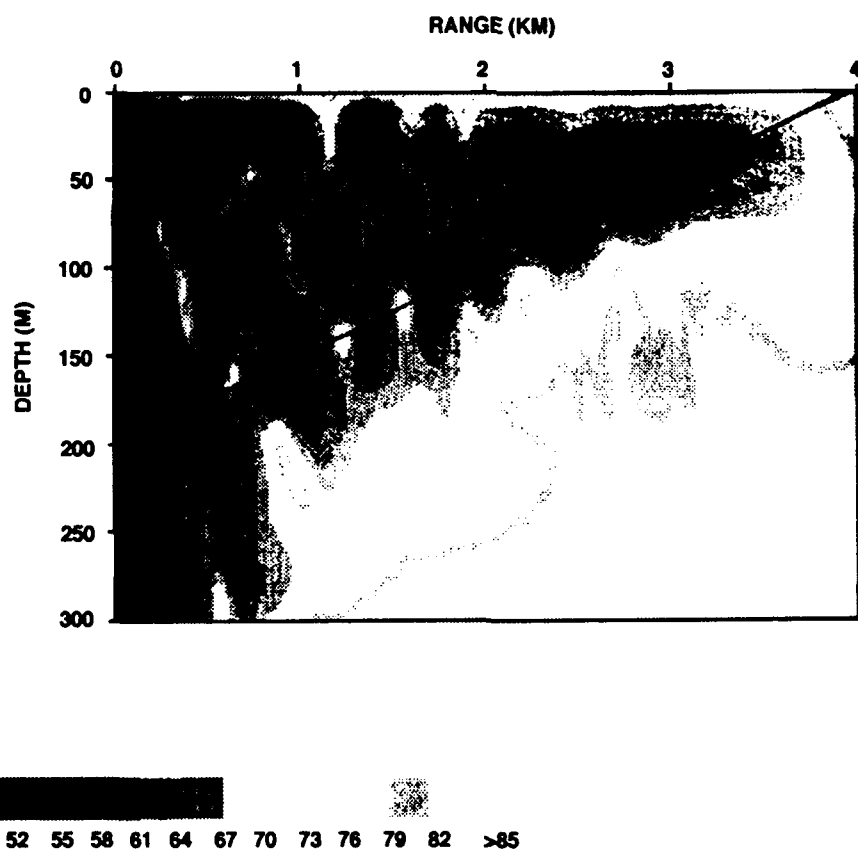


Figure 4-9 Contour plot for Test Case 3.

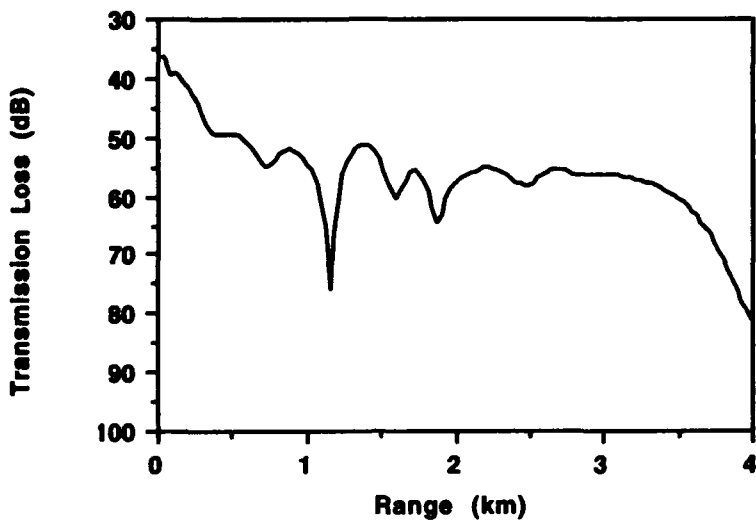


Figure 4-10. Case 3A: $F = 25$ Hz, $ZS = 100$ m, $ZR = 30$ m.

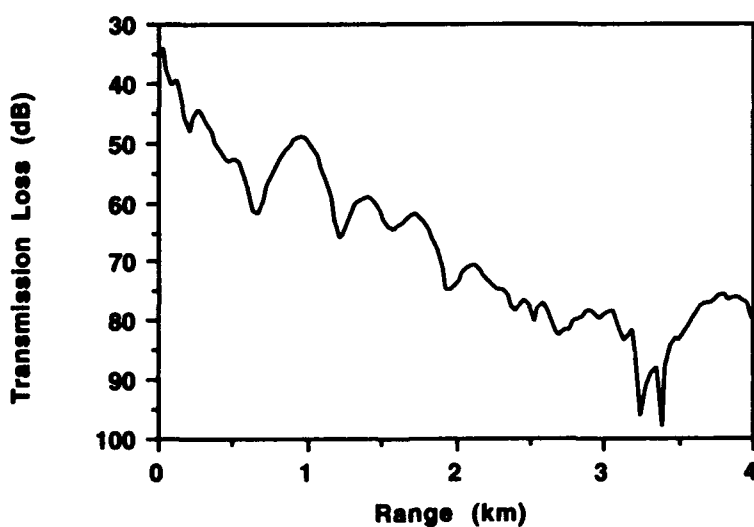


Figure 4-11. Case 3B: $F = 25$ Hz, $ZS = 150$ m, $ZR = 30$ m.

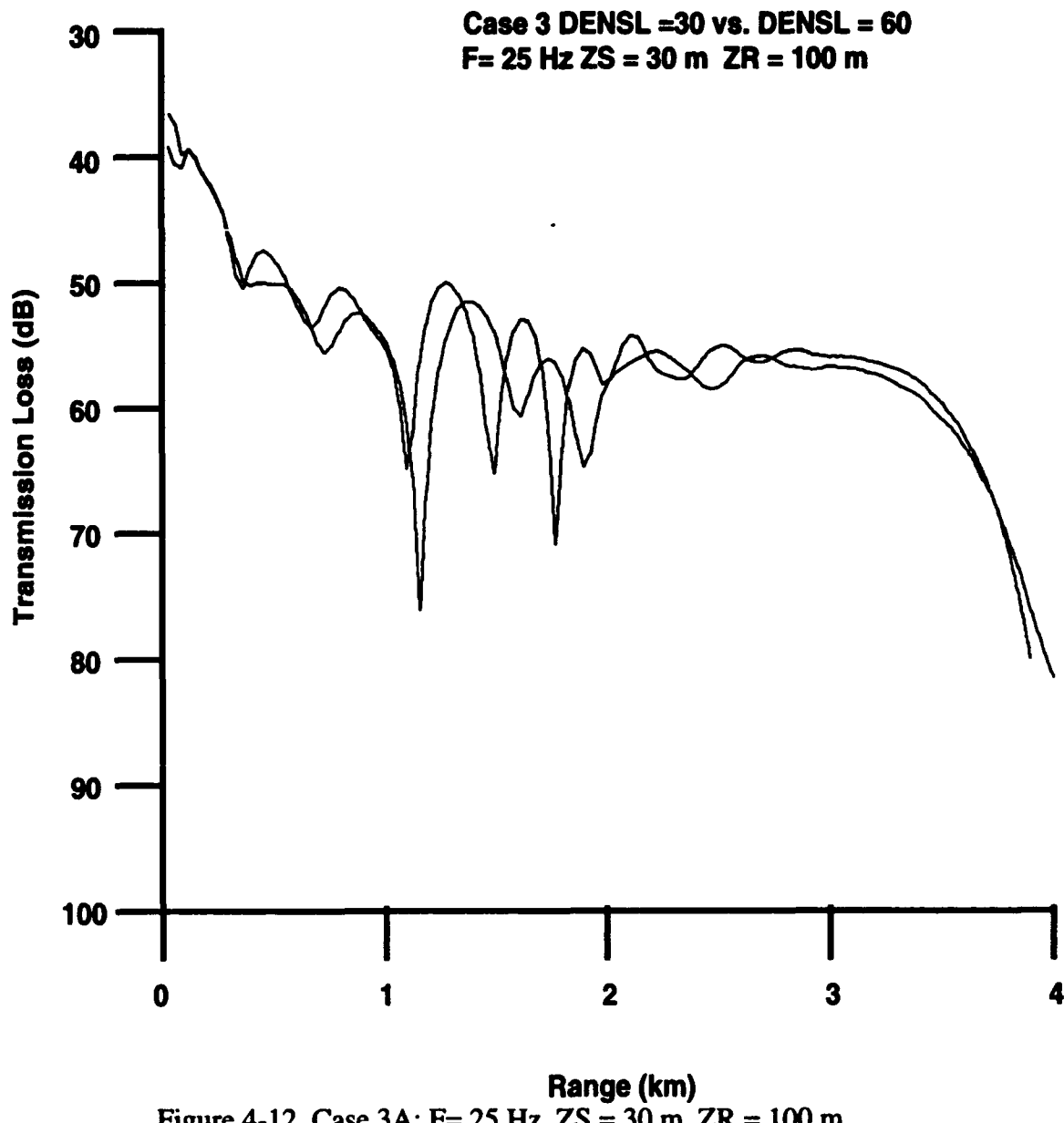


Figure 4-12. Case 3A: F= 25 Hz, ZS = 30 m, ZR = 100 m.

4.2.4 Test Case 4

This test case was designed to show the backscattering effects of a seawall. Since the Navy Standard PE does not operate in a two-way mode, several steps were taken to simulate the backscattered energy. First PE was run with the IWRMST=1 option turned on to save the

PE Workshop II: Part 2 — Test Case Results

complex pressure field at 3.0 km, the range at which the wall appears, and the computed complex pressure was saved at range increments of 0.01 km and at all PE depth mesh points; this accounted for the one-way portion of the problem.

The Rayleigh coefficient was calculated to estimate the backscattering loss of the wall. As Figure 4-13 shows, the maximum backscattering loss is 11 dB for incident angles on the wall steeper than 45°. Incident angles on the wall greater than 45° translate to PE propagating angles of less than 45°. For this test case, 11 dB was chosen as the angle-independent backscattering “coefficient”.

The next step was to run PE “backwards” with the field at the wall plus the backscattering effects as the “starting field”. This was accomplished by setting the IWRMST=2 option in the PE input file and reversing the environment. Subroutine PXTMOD was modified to read in the complex pressures field from the “forward” PE run, attenuate the energy by 11 dB on the wall and ∞ in the water column. Subroutine PXTMOD is a non-configuration managed routine designed to let the PE user inspect and/or modify the acoustic pressure field at any set of ranges and depths, so it lent itself well to this application.

The modified field output from PXTMOD was then used as the starting field for the PE run. Again, the complex pressures were saved at range increments of 0.01 km at all depths for the backward run. Figure 4-14 shows the TL curves of the backscattered energy (the “backward” part of the runs only) for the two “moving points.”

A small program was written which incoherently combined the complex pressure outputs from the “forward” and “backward” PE runs. Figures 4-15 and 4-16 show the two-way transmission loss vs. the one-way transmission loss (“forward”) for the two moving point depths. The solid curve is the two-way TL and the dashed line is the one-way TL. Note that the backscattered energy tends to fill in the nulls but only raises the peaks by about 1 dB. This is a reasonable amount of enhancement to the one-way TL, given that the backscattered field has been properly computed.

The range step was set to 30 ft only to facilitate the combination of the forward and backwards fields. The mesh spacing was set to 9.23 ft which was a factor of 4 less than the PE default mesh spacing. The density transition length was set to 30 ft, a factor of 2 less than the PE default transition length.

The run time for the forward part of the problem was 713 seconds on a 386-based machine, the high run time due in part to the small range step that was forced for this run. The run time for the backward part of the problem was 236 seconds, making the total run time on the order of 16 minutes.

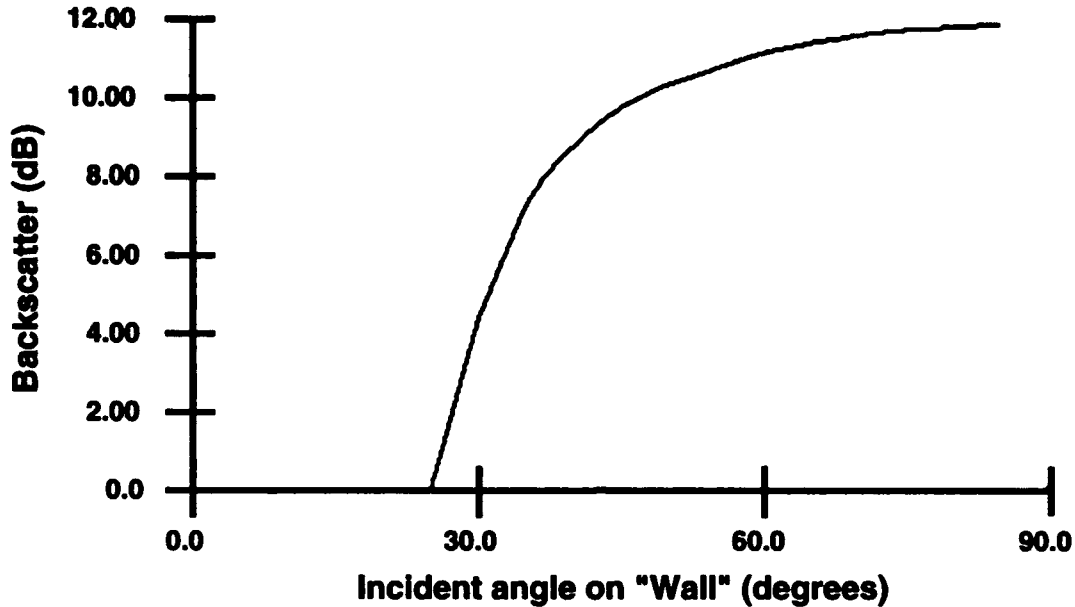


Figure 4-13. Case 4: Rayleigh coefficient for backscatter.

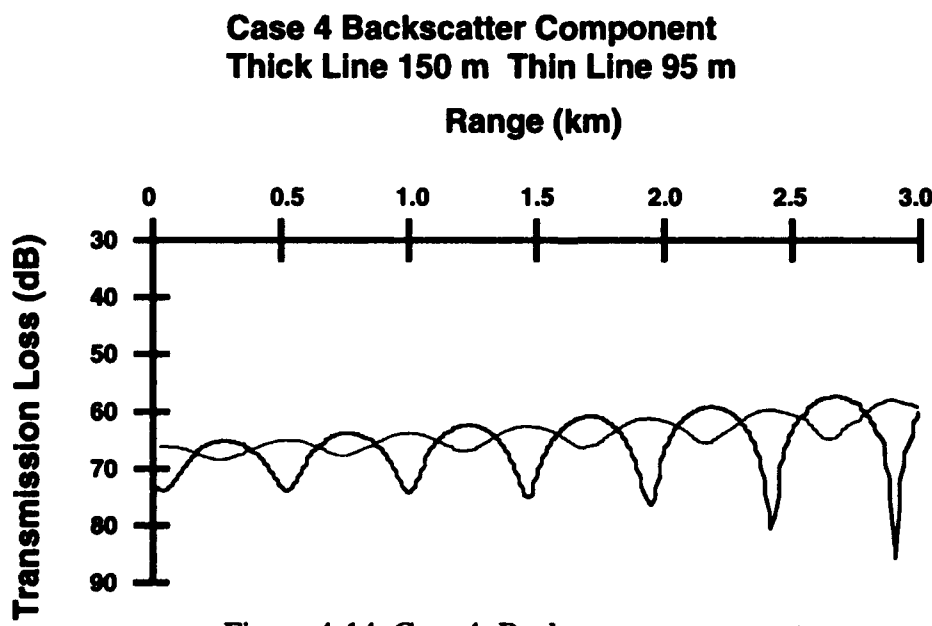


Figure 4-14. Case 4: Backscatter components.

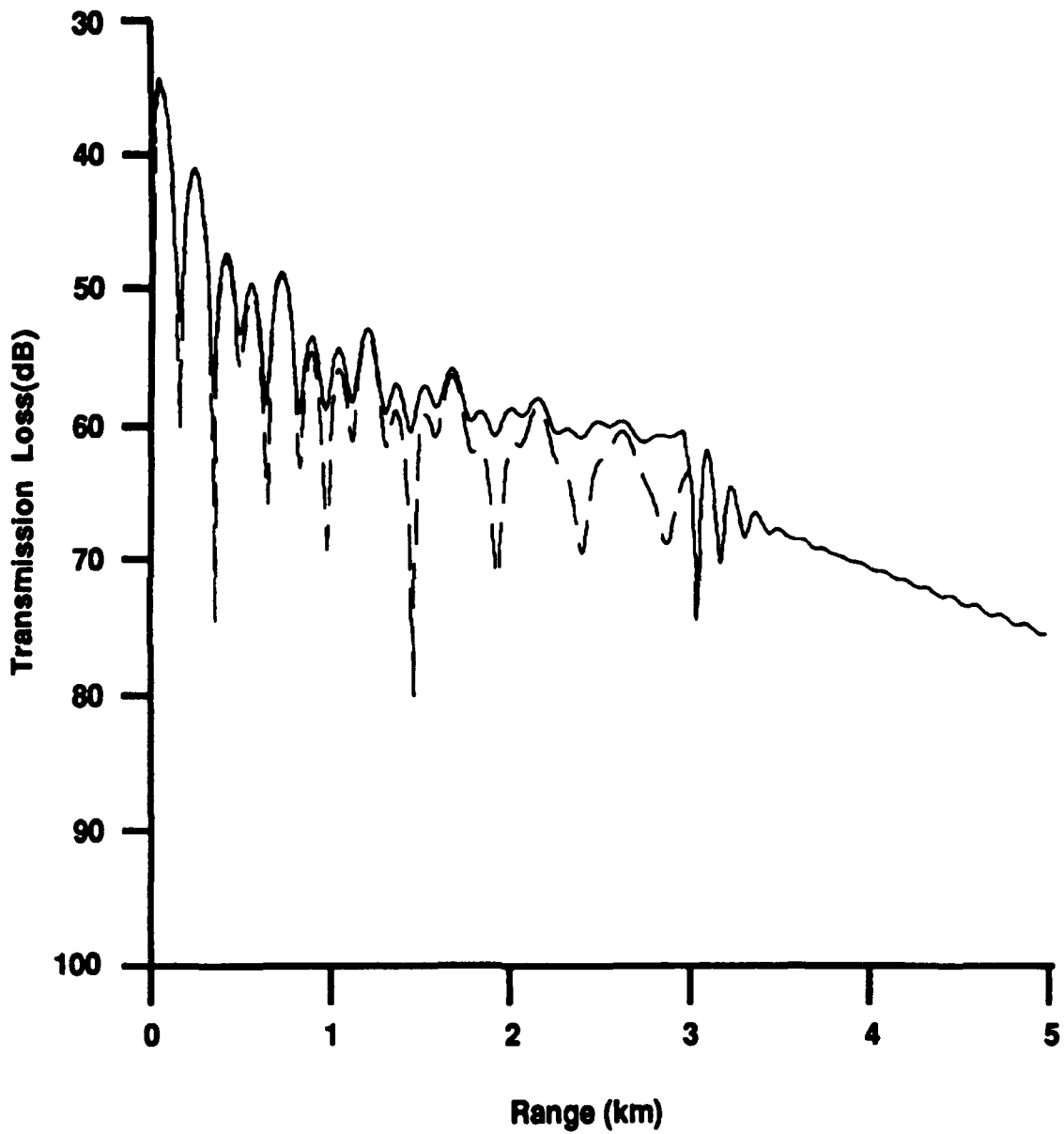


Figure 4-15. Test Case 4A.

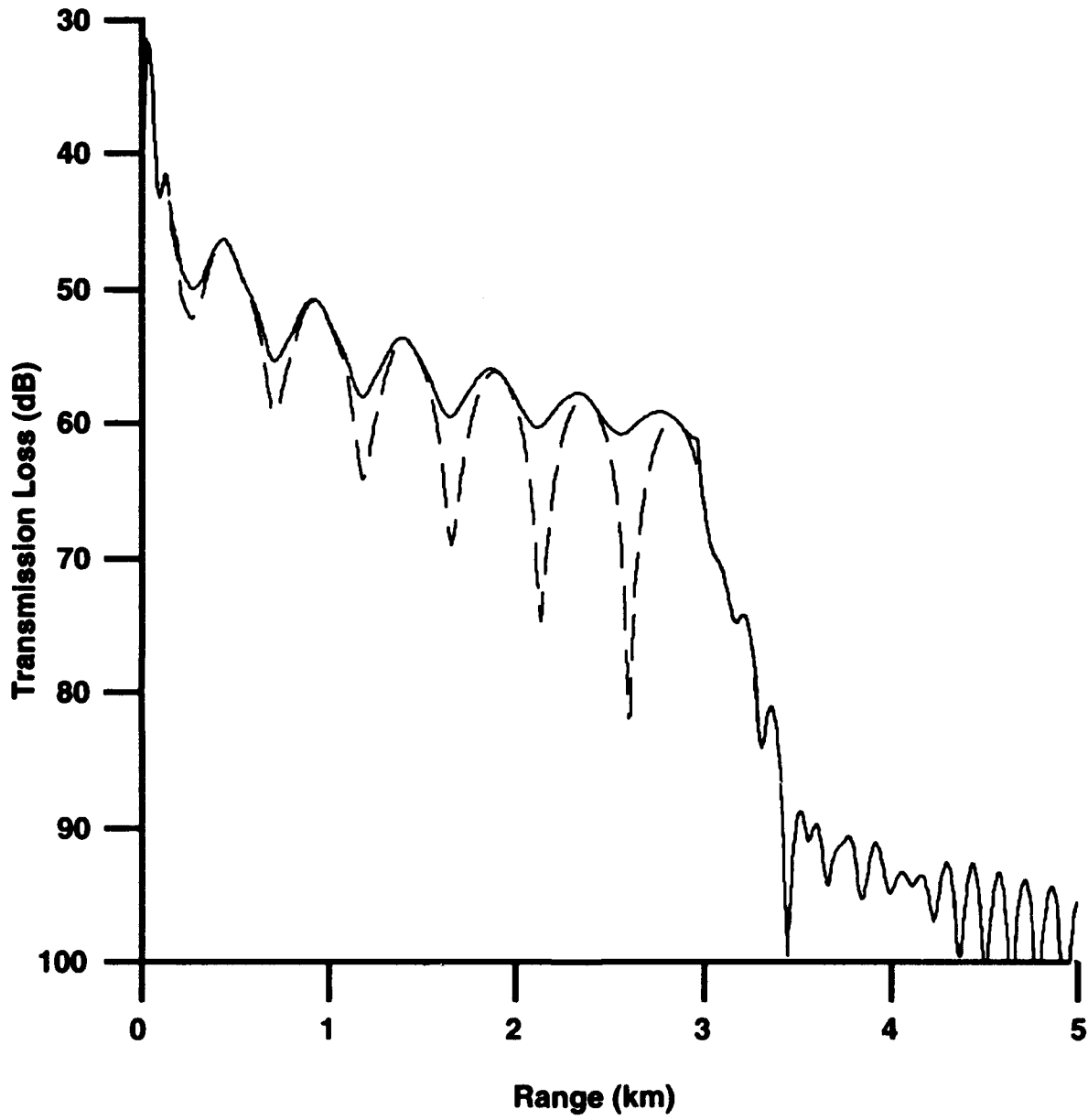


Figure 4-16. Test Case 4B.

4.2.5 Test Case 5

One common difference between range-dependent acoustic models is the way in which sound speed profiles are interpolated in range. Generally, sound speed as a function of depth is input to the model at a discrete set of ranges. What models do with this information varies. At least three interpolation schemes are worth discussing here:

- **No Interpolation.** The Navy Standard version of PE performs no sound speed interpolation in range. The sound speed input at one range is used until the next profile is input. Because of this, discontinuities occur at profile region boundaries, and energy can be “scattered” and wiped out by the bottom.
- **Linear Interpolation in Range and Depth.** This method is used by some other versions of Split Step PE including OPTAMAS PE. Its advantage is that there are no sound speed discontinuities in range. However, straight linear interpolation in range and depth does not always provide reasonable intermediate profiles.
- **Triangular Interpolation.** This method is employed by the MPP (Multiple Profile Program) ray trace model. It provides for smooth transition between profiles, and reasonable interpolated profiles. However, it is not completely automated, and the user must check and possibly adjust the interpolation. For this reason, triangular interpolation has not been implemented within the Navy Standard PE, but has been used as a pre-processor which can feed a set of interpolated profiles to PE. A program called CFIELD performs triangular interpolation and writes measured and interpolated profiles to the PE Alternate Sound Speed file.

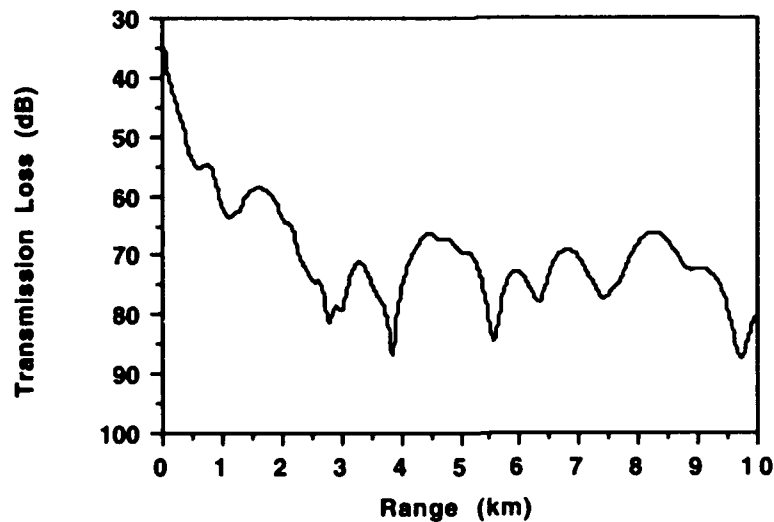


Figure 4-17. Case 5A: F= 25 Hz, ZS =100 m, ZR = 30 m.

The ability of PE to accept this alternate sound speed file allowed us to run this test case with interpolated profiles at every range step. CFIELD was supplied with the three isovelocity profiles at 0., 0.5, and 2.5 km, and provided hundreds of interpolated profiles between 0.5 and 2.5 km. PE then read the output file from CFIELD, and used this for its sound speed field.

PE Workshop II: Part 2 — Test Case Results

The PE results for this test case are shown in Figures 4-17, 4-18, and 4-19. A ray trace from MPP and a PE contour plot are also shown in Figures 4-20 and 4-21. While the ray trace shows the reflections from the water-sediment and sediment-basement interfaces, the PE run is at too low a frequency to see ray-like behavior without imagination.

The depth mesh spacing for this case was 36.91 feet and the range step was set to 0.005 nmi. The total run time for this case was 191 seconds on a 386-based machine.

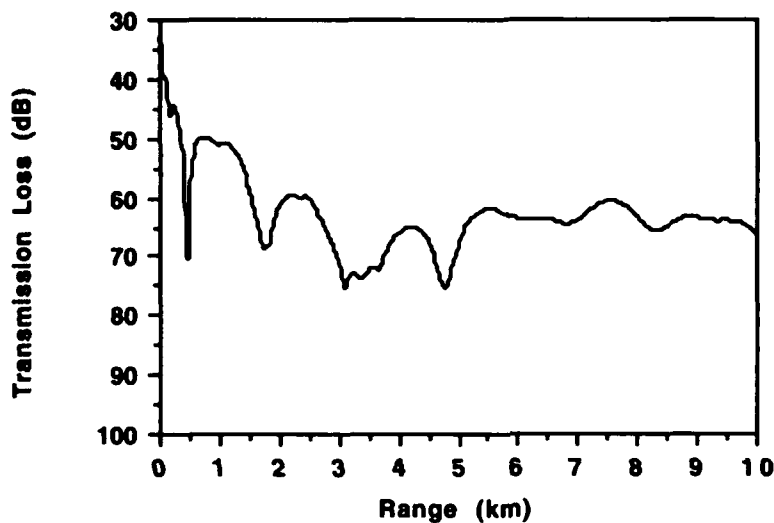


Figure 4-18. Case 5B: F= 25 Hz, ZS =100 m, ZR = 150 m.

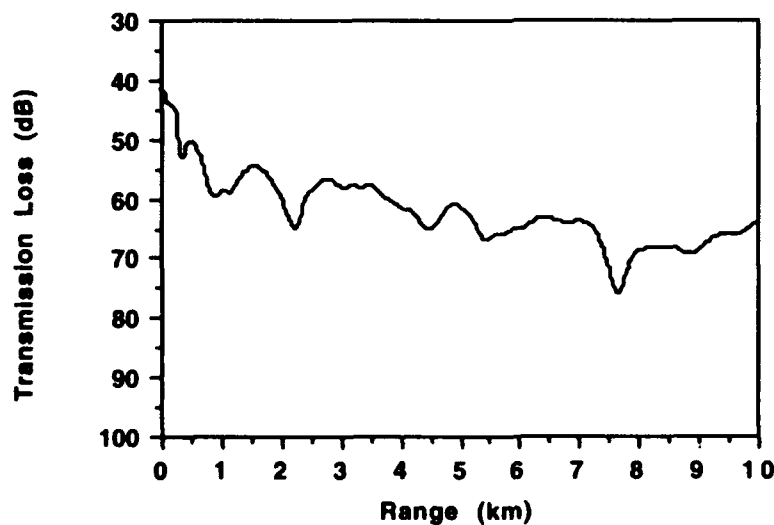


Figure 4-19. Case 5C: F= 25 Hz, ZS =100 m, ZR = 250 m.

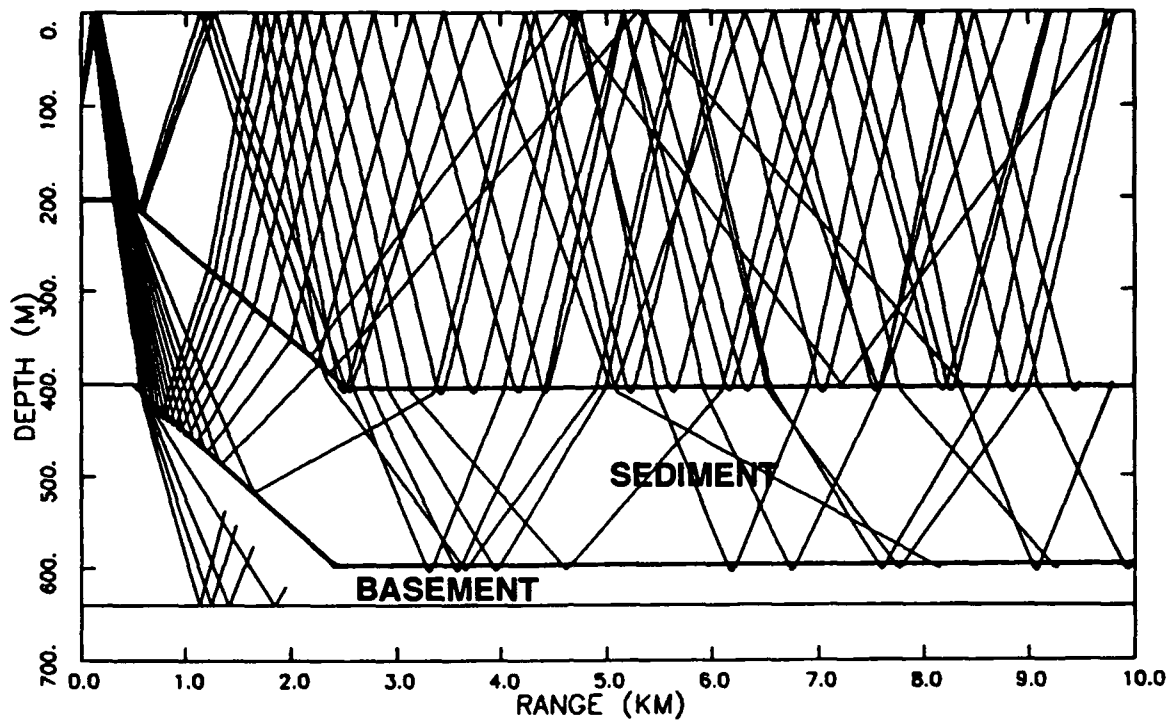


Figure 4-20. Ray trace for Test Case 5.

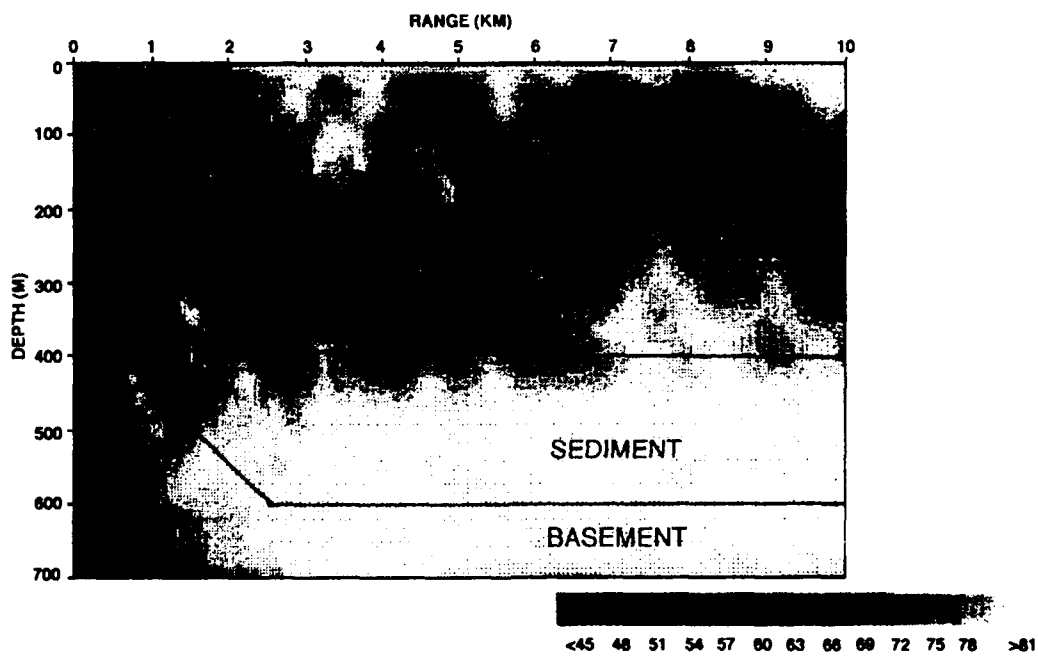


Figure 4-21 Contour plot for Test Case 5.

4.2.6 Test Case 6

This test case was designed to compare model results with measured field data. A complete description of the environment was supplied for this case. Figure 4-22 shows the bathymetry and sound velocity profiles for this environment. In addition, 32 bottom profiles were supplied.

Navy Standard PE was used with a user-forced 2^{10} transform size and a 90° beamwidth. Upon examination of the TL curves produced by using various transform sizes, it was noted that the curves converged at 2^{10} . The acoustic frequency of this case is 15 Hz and at the 0 range the water depth is only 200 meters. PE calculates the depth mesh spacing based on the maximum water depth, which in this case is 2650 m (at 97 km). Therefore the default 2^8 transform size, with a depth mesh spacing of 336 ft, would supply only two mesh points at the beginning of the track. A depth mesh spacing of 84 feet seemed to be as much was needed for this case. Further investigation of the computation of the transform size for VLF cases is warranted and has been an ongoing task.

Despite the complex description of the sediment, PE did not exhibit as much energy returned from the bottom as the measured data shows. Figure 4-23 shows a field intensity plot of the energy in the water column and the first 2000 ft of sediment for the first 10 km. While some energy does appear to be returning from the bottom at short ranges, this apparently is not enough to predict the levels of the measured data. Figures 4-24, 4-25 and 4-26 show the TL for the three moving points.

The run time for this case was 538 seconds on a 386-based computer.

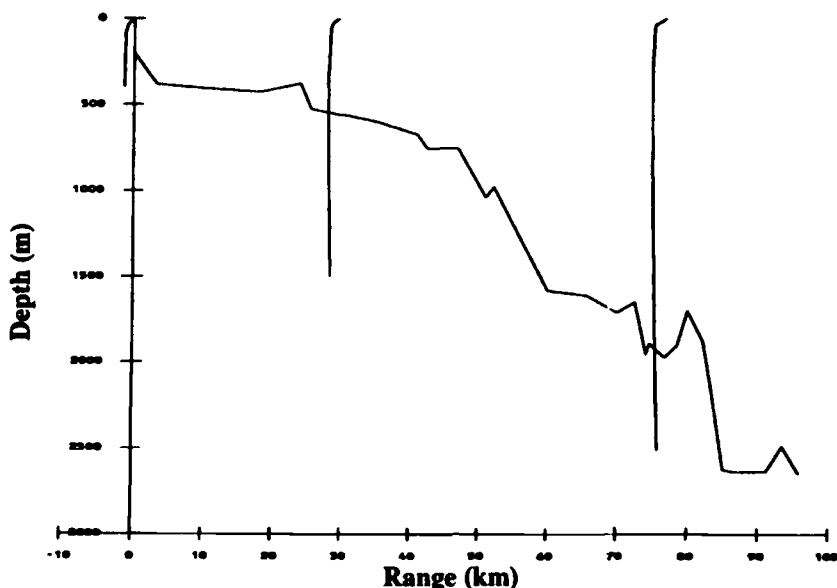


Figure 4-22. Environment for Test Case 6.

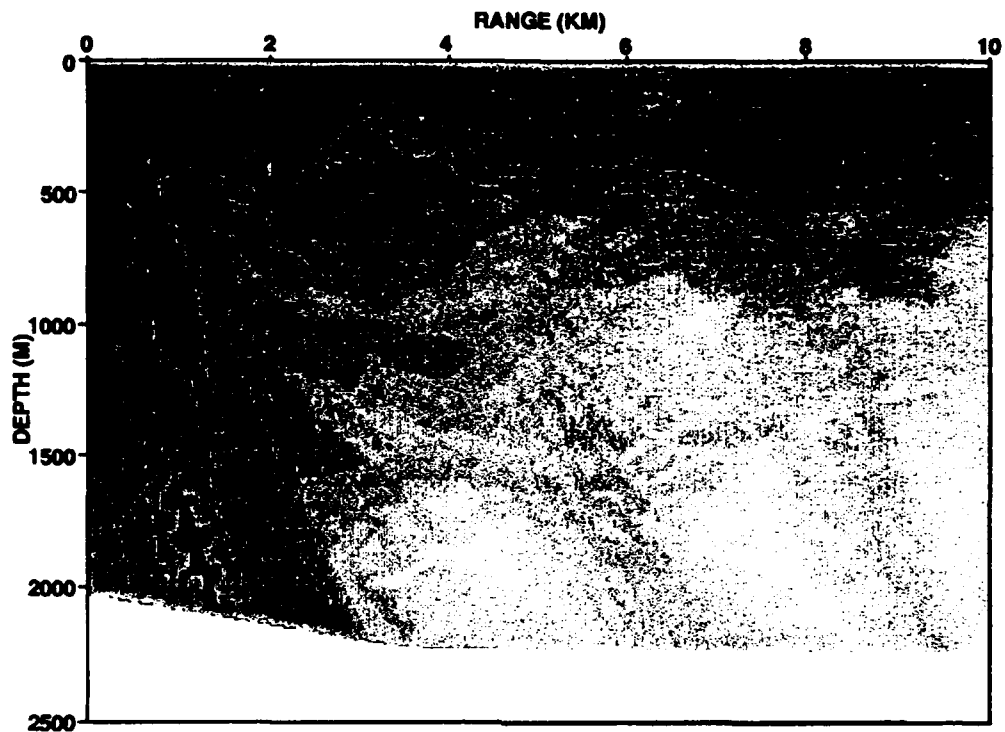


Figure 4-23. Contour plot Test Case 6.

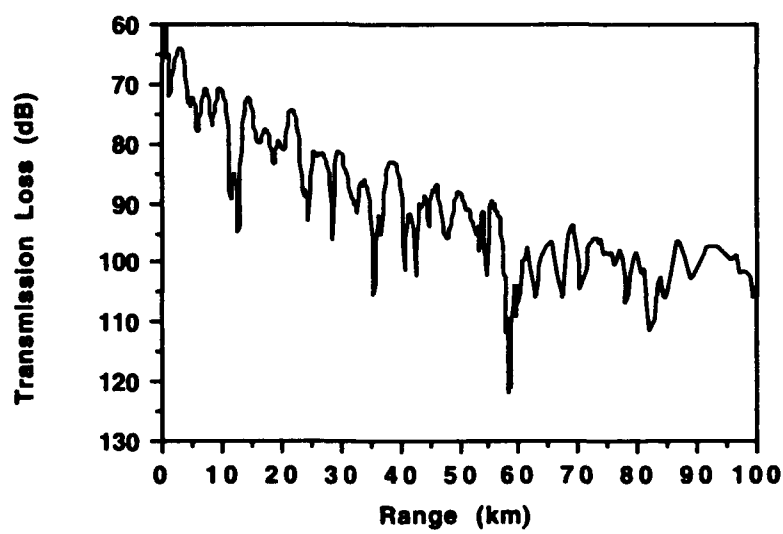


Figure 4-24. Case 6A: $F = 15$ Hz, $ZS = 30$ m, $ZR = 88$ m.

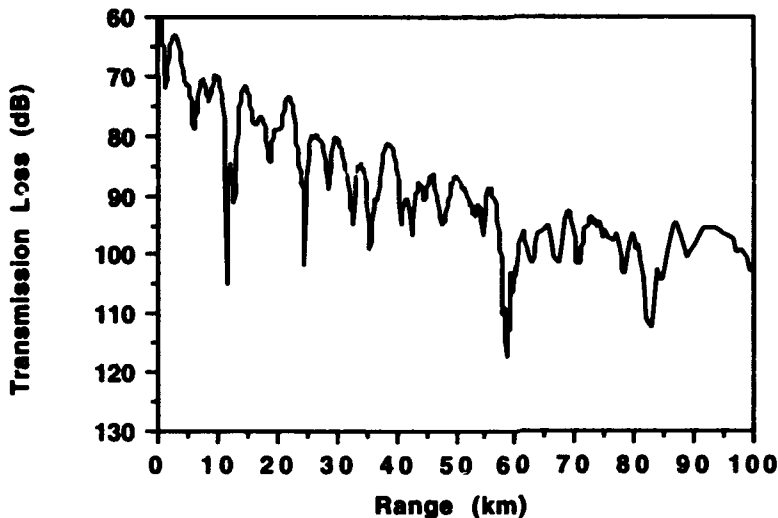


Figure 4-25. Case 6B: $F = 15$ Hz, $ZS = 30$ m, $ZR = 112$ m.

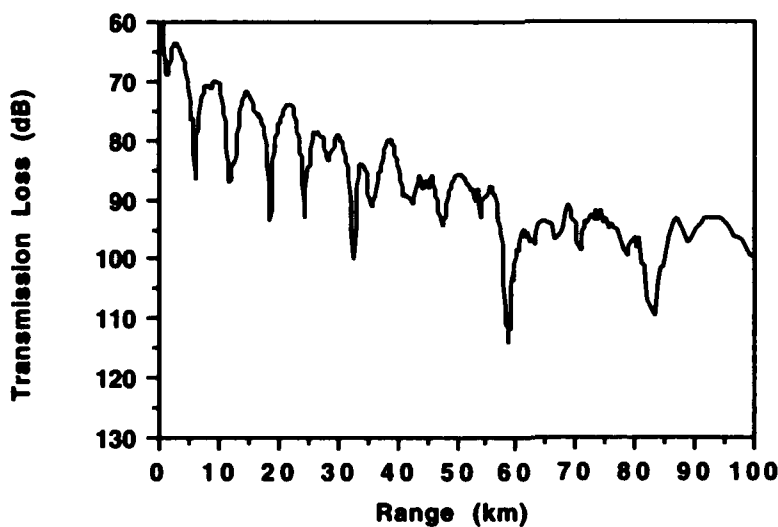


Figure 4-26. Case 6C: $F = 15$ Hz, $ZS = 30$ m, $ZR = 148$ m.

4.3 Conclusions

This set of test cases differs drastically in nature from the 32 “bake-off” test cases which were used to choose the Navy Standard Range-Dependent transmission loss models. Where the ASTRAL (ASEPS TRAnsmission Loss) model agrees well with the PE model for most

of the 32 measured transmission loss test cases, the PE Workshop II tests require *at least* a split step PE model, and sometimes more. From this, a question might arise: Can a PE model which has been tuned to be as fast as possible for operational use, possibly model high fidelity, heavily detailed environments, and does it matter?

The first part of the question will be answered at the workshop. This report was generated without benefit of the test case results, but our guess is that for many of the test cases, the Navy standard PE performed fairly well. Part of this is due to the fact that, while this PE is used as an operational model, it has been allowed to keep all of its development inputs. For example, we were able to turn off spherical earth correction and volume attenuation in the water column, control the PE range step and depth mesh, and extract and modify complex pressures from the PE field. In this sense, the Navy Standard PE is not *just* an operational model.

The second part of the question can be answered with a definite YES. Test Case 1 was a perfect testing ground for the semi-coherent steep angle TL supplement, and was also used to test the Thomson source. Both of these upgrades will improve PE performance in short range situations, and that is very operationally important.

All of the test cases are important to correctly modeling VLF propagation, and Test Case 6, the only measured data case, was impossible for us to model. We learned much about PE mesh spacing requirements through the test cases, all of which will be used in future PE upgrades. On the other hand, what we learned about the thickness of the density transition region may be more academic. In operational situations, it is probable that our knowledge of details of the environment (such as the exact sediment density, thickness, and sound speed gradients) will be vague enough so that the thickness of the density transition layer will not matter. However, as long as run time is not increased significantly, it does not hurt to implement an upgrade which is known to improve predictions when there is environmental information to support that prediction.

There are several areas in which the Navy Standard Parabolic Equation model can be improved without losing its operational usefulness. Since these test cases are all in the VLF region, run time is thankfully not a large consideration. The major upgrades have to do with mesh spacing. The following lists upgrades, including the first two which have already been implemented in the developmental copy of PE Version 3.3, which are indicated by this set of test cases.

- PE Range Step Restrictions require PE energy traveling at high angles to spend a minimum number of range steps in each of the water column, the sediment, and the basement. This avoids energy traveling through important features.
- For high frequencies and very high angles, a large vertical beam width is not practical for the operational PE model. Therefore, STEEP is modified have the

same number of bottom bounces, and for the surface-reflected and direct paths.

- The Thomson source should be implemented and compared with the Test Case 1 exact solution. This is expected to improve high angle predictions.
- PE Mesh Spacing Requirements include a minimum number of points in the water column at short range (in the PE near field)

REFERENCES

1. Feynman, R.P., R.B. Leighton, and M. Sands, *The Feynman Lectures on Physics, Vol. II*, Addison-Wesley, 1964 p. 18-11
2. Keenan, R. E., "PC ICECAP Physics Documentation," AEAS Report 91-006, July, 1991
3. Tappert, F.D., "The Parabolic Approximation Method," in *Lecture Notes in Physics*, (eds. J.B. Keller and J.S. Papadakis), No 70, Springer, New York, 1977
4. Lee, D. and S.T. McDaniel, chapter 7 in *Ocean Acoustic Propagation by Finite Difference Methods*, (ed. E.Y. Rodin), Pergamon Press, United Kingdom, 1988
5. Jensen, F. and H. Krol, "The Use of the Parabolic Equation Method in Sound Propagation Modeling," SM-72, 15 August 1975, SACLANT Centre
6. McDaniel, S.T., "Propagation of normal mode in the parabolic approximation," *J. Acous. Soc. Am.*, Vol. 57(2), 1975, pp.307-311
7. Mathews, J. and R.L. Walker, *Mathematical Methods of Physics*, W.A. Benjamin, Inc, New York, 1970, p.110
8. Hanna, J.S. and P.V. Rost, "Relationships among frequency, depth, and range averages for propagation.," SAIC internal memorandum
9. Spofford, C.W., and R.E. Keenan, "Summary of Status of Ducted Precursor Modeling," SAI-83-841-WA, June 1982
10. Keenan, R.E., and C.W. Spofford, "A Model for Ducted Precursors (Leakage Arrivals)," SAI-82-468-WA, May 1981
11. Holmes, E.S., and L.A. Gainey, "Software Product Specification for the Parabolic Equation Model Version 3.2," to be distributed by NAVO, February 2, 1991
12. Thomson, D.J., "Wide-angle parabolic equation solutions to two range-dependent benchmark problems," *J. Acoust. Soc. Am.* 87, 1514-1520 (1990)
13. Thomson, D.J. and C.S. Bohun, "A wide-angle initial field for parabolic equation models," *J. Acoust. Soc. Am. Suppl. 1* 83, S118 (1988)

PE Workshop II: Test Problem Solutions

Finn B. Jensen

*SACLANT Undersea Research Centre
19026 La Spezia, Italy*

ABSTRACT

This document presents solutions to five out of seven test problems discussed at the PE Workshop II held in Slidell, LA on 6–10 May 1991. The workshop was organized by the Naval Oceanographic and Atmospheric Research Laboratory (NOARL) as a follow-up meeting to the first PE workshop held in March 1981, with emphasis this time on range-dependent test problems. The original call for contributions (NOARL Memo Ser 124A-035, dated 18 Jan 1991), defined six test problems, each of which was designed to address a particular aspect of the general modeling problem: (i) Source beamwidth and angle-dependent phase errors; (ii) Energy conservation in sloping bottom environments; (iii) Effects of bottom elasticity; (iv) Modeling of backscattered energy; (v) Propagation through both range-varying sound speed and bathymetry; (vi) Comparison with measured field data. These six test problems are described in detail in the above-mentioned NOARL memorandum. An additional test problem involving propagation in a leaky surface duct was discussed on the last day of the workshop. The solution to this problem is presented here as Test Case 7.

1 TEST CASE 1

A point source placed near a reflecting boundary in a homogeneous medium gives rise to the well-known Lloyd-mirror interference pattern (Fig.1.1) for which an exact field solution is available. The Lloyd-mirror pattern is ideal for checking both the angular distribution of energy associated with a given starting field and the high-angle capability of various PE models.

The problem considered here is a fluid halfspace with a constant speed of 1500 m/s. The frequency is 40 Hz and the source/receiver depths are 350 m and 3990 m. The image reference solution is shown as the solid line in Fig.1.2. The dashed PE result was generated by the Thomson-Chapman PE, which is known to be exact (no phase errors) for a homogeneous medium. In fact, beyond 1.5 km the PE result is in perfect agreement with the reference solution. The lower PE amplitude at short ranges is due to an automatic truncation of the Thomson halfspace source at the first interference null. Numerically stable results were obtained with a computational grid of $\Delta z = 10$ m and $\Delta r = 10$ m.

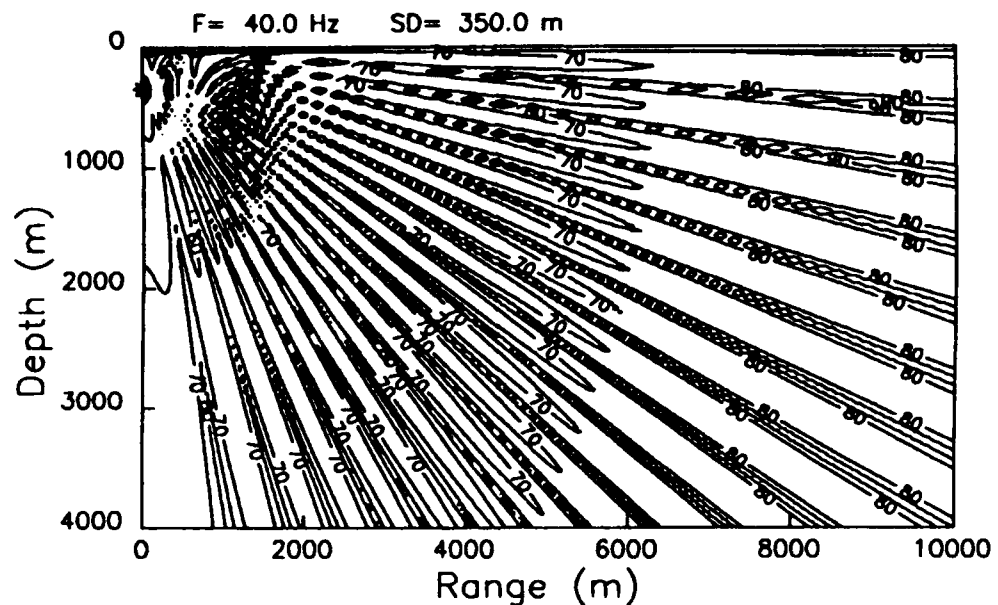


Figure 1.1 Contoured field solution for Lloyd-mirror problem.

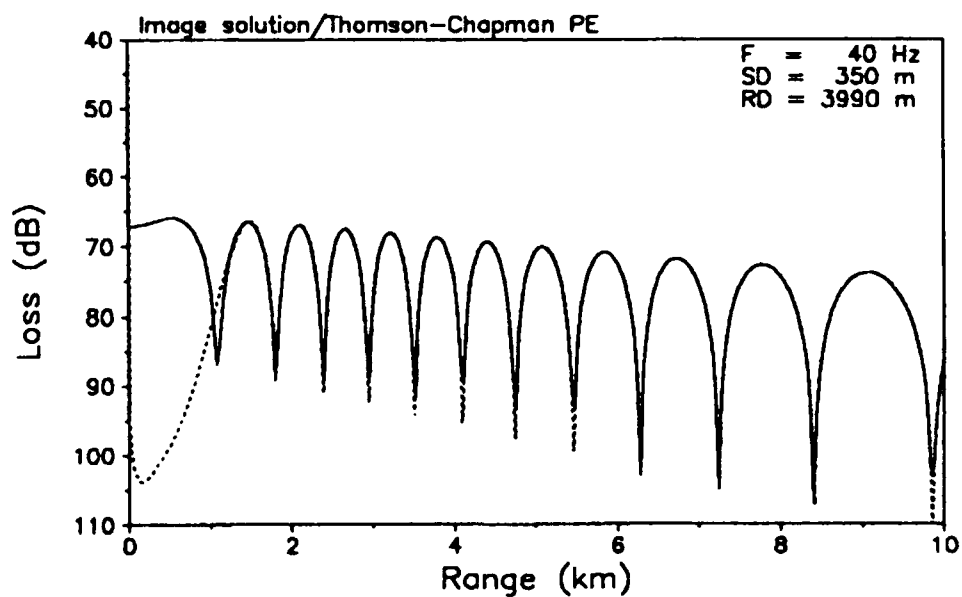


Figure 1.2 Comparison of image reference solution (solid line) with Thomson-Chapman PE result (dotted line).

2 TEST CASE 2

The problem of energy conservation in one-way models was dealt with in considerable detail in two recent journal articles [JASA **89**, 1058–1067 (1991); JASA **89**, 1068–1075 (1991)]. This test problem reiterates the issue by considering upslope-downslope propagation for a 25-Hz source placed at 100 m depth in a homogeneous water column with a sound speed of 1500 m/s. The water depth is 200 m at range zero, 25 m at 3.5 km, and 200 m at 7.0 km. The bottom is homogeneous with a sound speed of 1700 m/s, a density of 1.5 g/cm³ and an attenuation of 0.5 dB/λ.

We use the COUPLE normal-mode code to generate a reference solution. Numerically stable results were obtained with a false bottom depth of 3000 m and with 400 stair steps in range. A total of 90 modes were included in the calculations. The energy-conserving two-way COUPLE results are shown as the solid lines in Figs. 2.1 and 2.2 for receivers at 20 m and 150 m, respectively. Also shown as the dotted lines are the one-way pressure-matched COUPLE results, which do not conserve energy. In fact, we see that the one-way results lose energy during upslope propagation (0–3.5 km) and gain energy during downslope propagation (3.5–7.0 km). For this symmetric problem, where the up and downslope effects entirely balance one another, the one-way result is seen to give the correct answer at range 7 km. The maximum level error is 2–3 dB at mid-range.

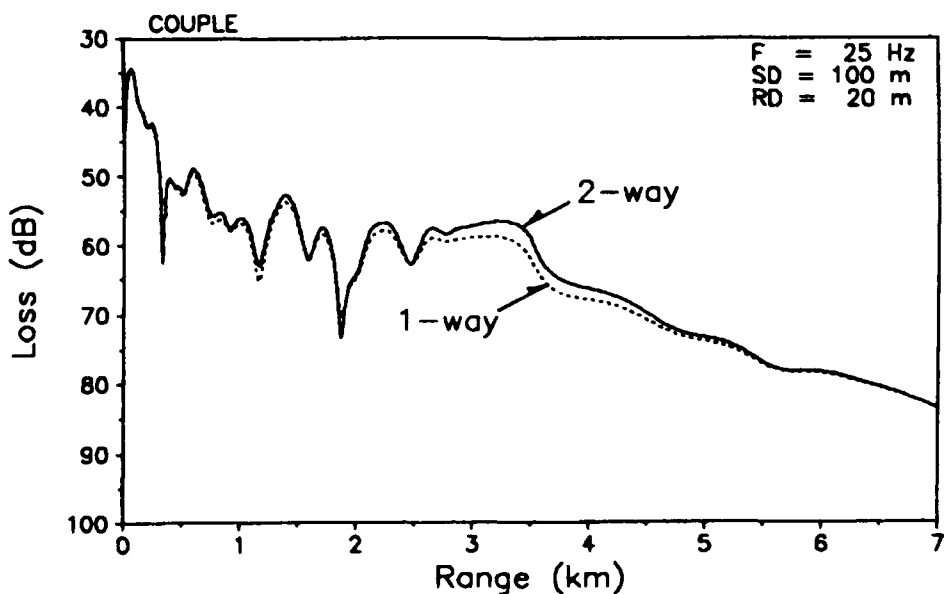


Figure 2.1 Comparison of energy-conserving two-way COUPLE result with one-way pressure-matched solution for a receiver at 20 m.

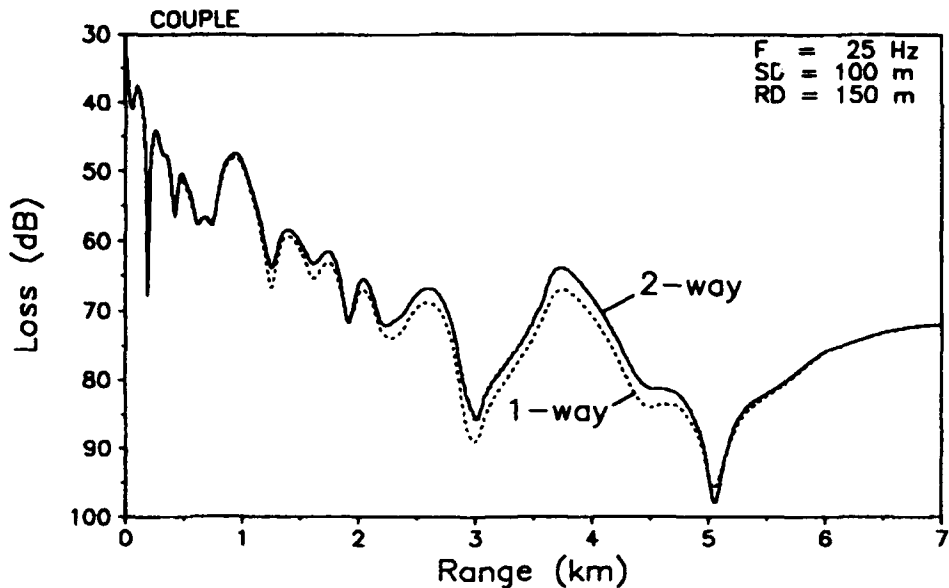


Figure 2.2 Comparison of energy-conserving two-way COUPLE result with one-way pressured-matched solution for a receiver at 150 m.

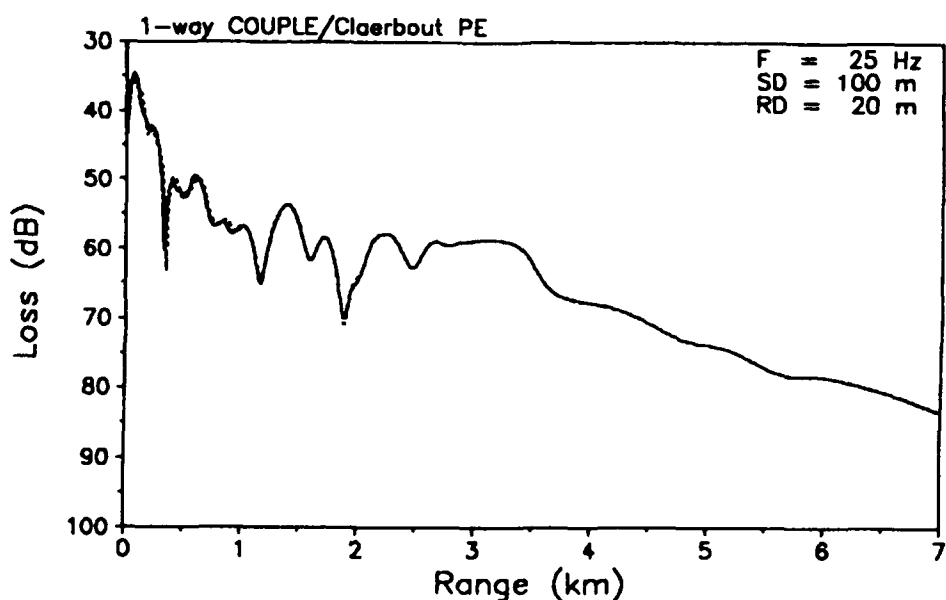


Figure 2.3 Comparison of one-way results from COUPLE (solid line) and Claerbout PE (dotted line) for a receiver at 20 m.

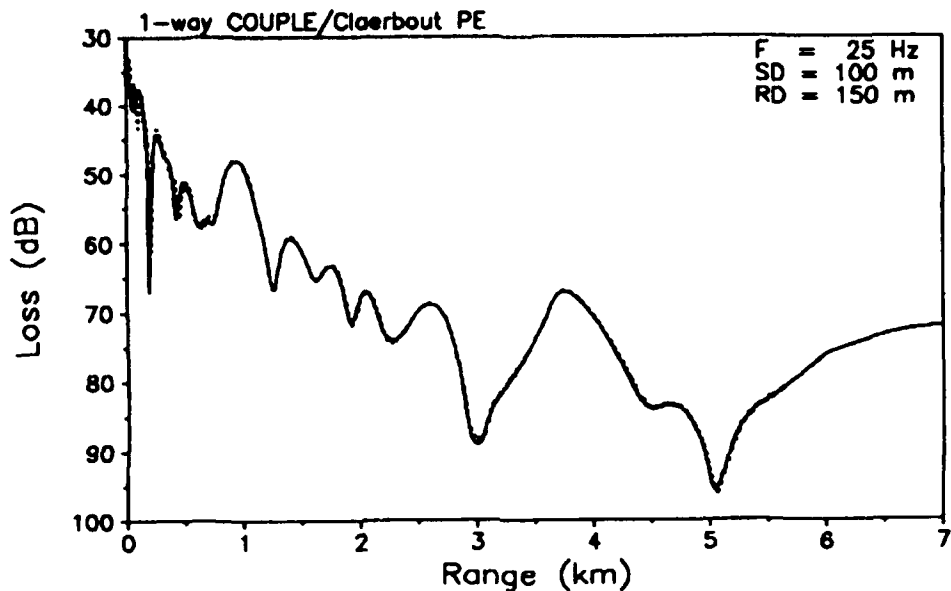


Figure 2.4 Comparison of one-way results from COUPLE (solid line) and Claerbout PE (dotted line) for a receiver at 150 m.

As an example of a non-energy-conserving PE, we present results from the Claerbout PE as implemented in the IFD code. This is again a pressure-matched forward solution, which should agree closely with the one-way COUPLE results; this is confirmed by the comparisons shown in Figs. 2.3 and 2.4. Numerically stable PE results were obtained with a computational grid of $\Delta z = 0.5$ m and $\Delta r = 2.0$ m. Clearly, the recently developed energy-conserving PE's [JASA 89 1068–1075 (1991)] should produce answers in close agreement with the *two-way* COUPLE solutions.

3 TEST CASE 3

No solutions were generated for this test problem.

4 TEST CASE 4

Most of the existing PE implementations are one-way models, which only solve for the forward propagating field. Test problem 4 was included to look at backscattering from a single stair step in a homogeneous shallow-water duct. The water depth is 200 m out to a range of 3 km, and 100 m beyond. Water and bottom properties are identical to those in Test Case 2, and we again consider a 25-Hz source at a depth of 100 m.

We use the COUPLE normal-mode code to generate a reference solution. Numerically stable results were obtained by including 90 modes with a false bottom depth of 3000 m. Figure 4.1 displays the COUPLE result for a receiver depth of 95 m, assuming a reflecting

boundary condition at the source range. The vertical line at range 3 km indicates the position of the stair step. Note the “noisy” structure on the initial 3 km caused by interference between outgoing and backscattered field components. These components are displayed separately in Fig. 4.2, showing that on average, the backscattered component is 10–15 dB lower than the forward propagating field component. Similar results for a receiver depth of 150 m are given in Figs. 4.3 and 4.4. No PE solutions were generated for this test problem.

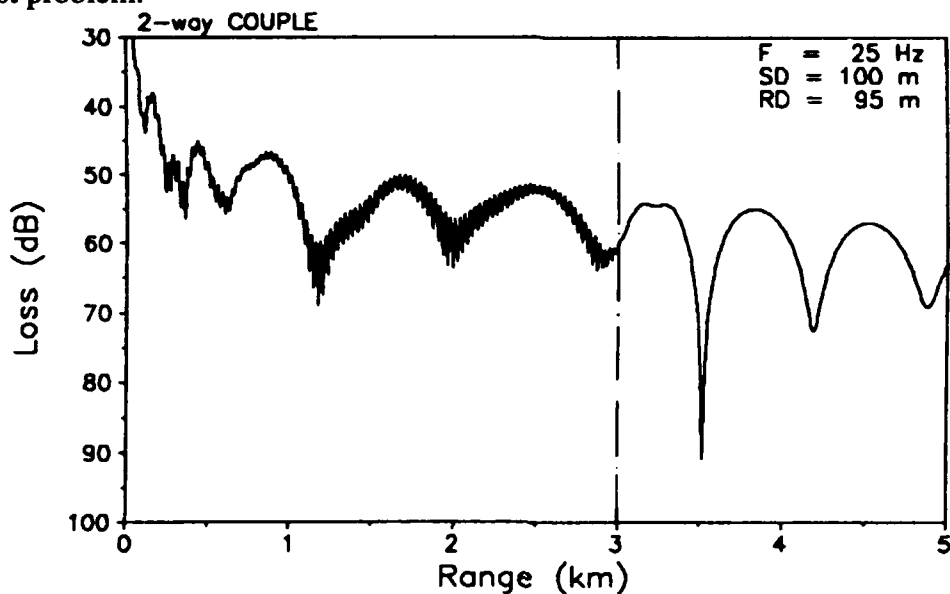


Figure 4.1 Two-way COUPLE solution for a receiver depth of 95 m.

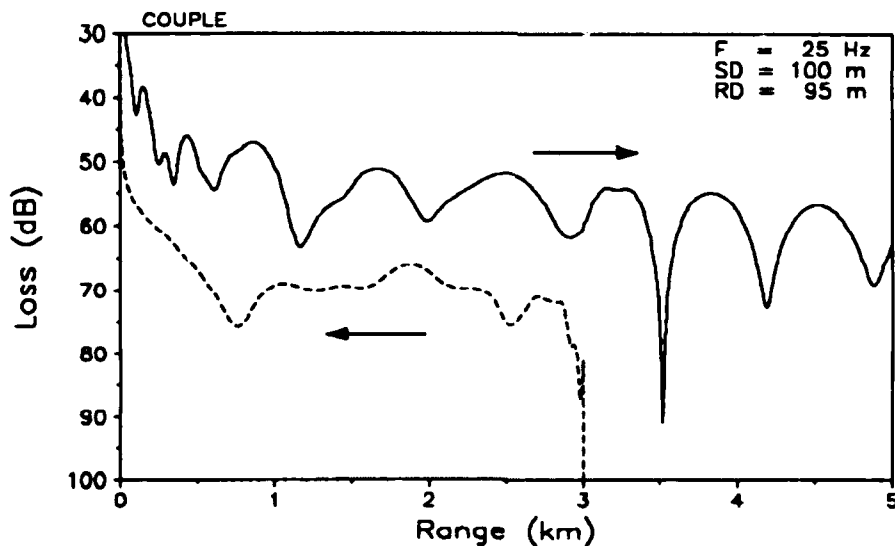


Figure 4.3 Display of the outgoing (solid) and the backscattered (dashed) components of the two-way COUPLE solution.

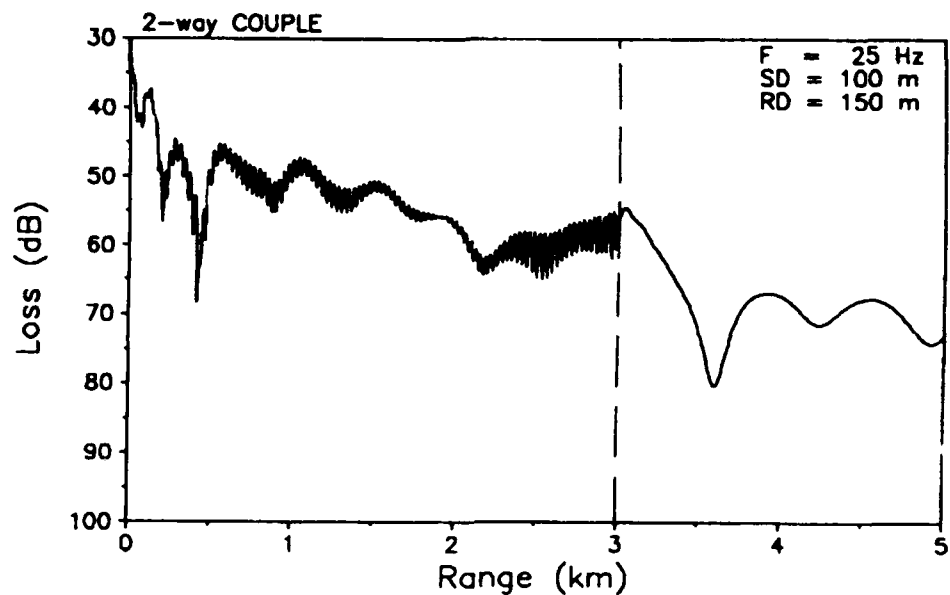


Figure 4.3 Two-way COUPLE solution for a receiver depth of 150 m.

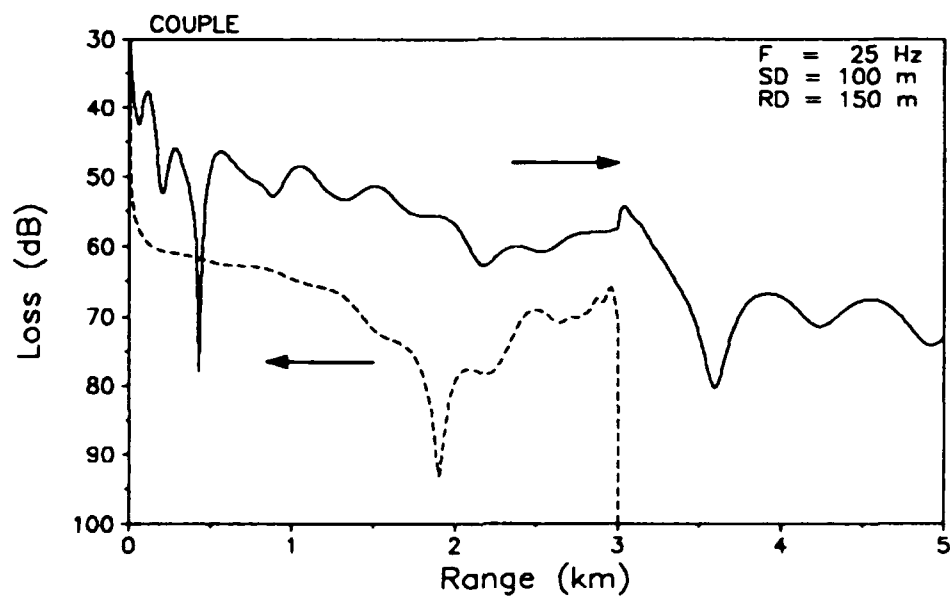


Figure 4.4 Display of the outgoing (solid) and the backscattered (dashed) components of the two-way COUPLE solution.

5 TEST CASE 5

No solutions were generated for test problem 5.

6 TEST CASE 6

The modeling of experimental data is quite a different problem than the detailed point-by-point comparisons with accepted reference solutions discussed in the previous examples. Thus, a test problem involving real data generally reveals more about the accuracy of the environmental information than about the acoustic model itself. In test case 6 an overly detailed environmental description was provided both for the water column (three profiles with 60–100 depth points and with sound speeds given with an accuracy of 0.001 m/s!!) and for the bottom with 32 geoacoustic profiles along the 100 km propagation track. This kind of detail easily leaves the (false) impression of being also a highly accurate representation of the acoustic environment.

The 15-Hz acoustic data were collected for three different source depths (88, 112, and 148 m) and for a receiver at 30 m. Since the source depth dependence in the data was found to be negligible, we decided to carry out the modeling for just the 112-m source. Two PE approximations were tested: the standard narrow-angle PE (Tappert-Hardin) implemented in the PAREQ code, and the wide-angle Claerbout PE implemented in the IFD code. Numerically stable results for PAREQ were obtained with a computational grid of $\Delta z = 10$ m and $\Delta r = 20$ m, while IFD required $\Delta z = 5$ m and $\Delta r = 10$ m.

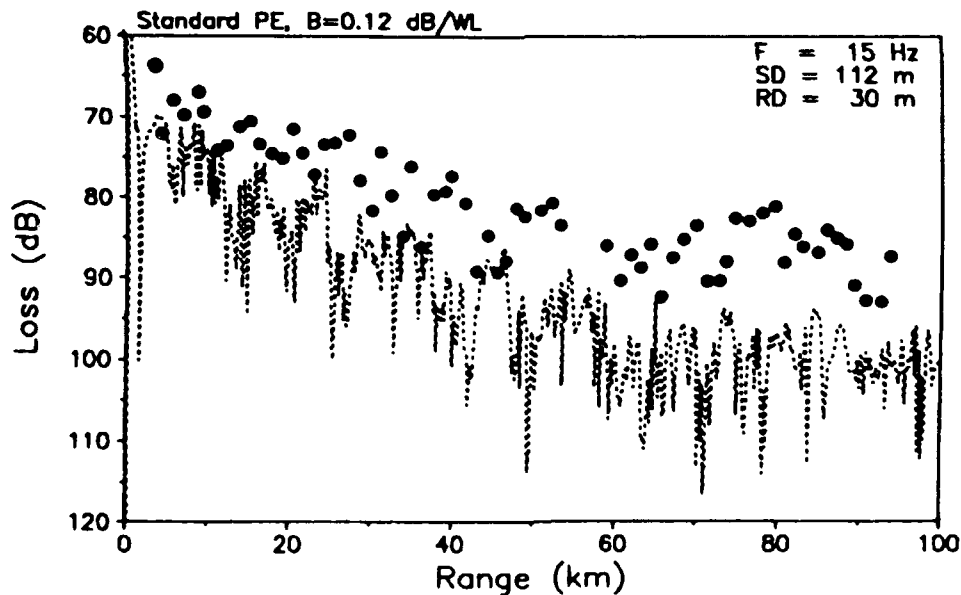


Figure 6.1 Comparison of measured propagation losses with PE predictions (Tappert-Hardin) for a sediment attenuation of $0.12 \text{ dB}/\lambda$.

The model results in Figs. 6.1 and 6.2 both show levels which are 10–15 dB too low at longer ranges. Other PE results presented at the Workshop showed the same trend, confirming the earlier statement that the issue for this test problem is not the accuracy of the PE model (narrow-angle/wide-angle, energy-conserving/non-energy-conserving), but rather the accuracy of the environmental model.

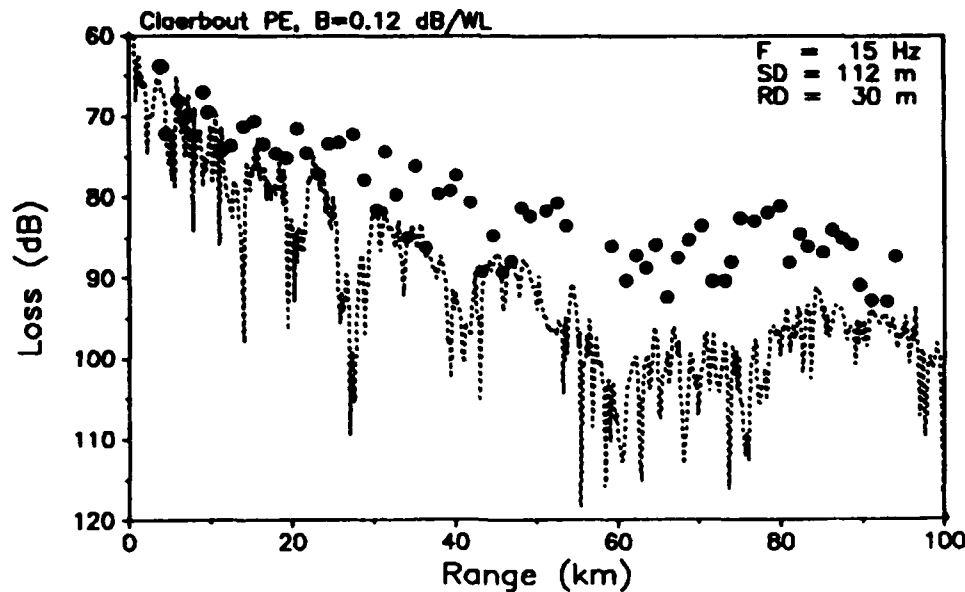


Figure 6.2 Comparison of measured propagation losses with PE predictions (Claerbout), for a sediment attenuation of $0.12 \text{ dB}/\lambda$.

What then is the most likely reason for the poor agreement between data and model predictions in Figs. 6.1 and 6.2? Assuming the data to be well-calibrated and to represent “ground truth”, we will have to reconsider the geoacoustic model. Clearly there is too much loss in the PE results, which points to the sediment attenuation as being in error. In fact, the predicted levels are very sensitive to the attenuation in the upper bottom layer (current values: $0.12 \text{ dB}/\lambda$ at the seafloor and $0.27 \text{ dB}/\lambda$ at 1.5 km depth). We have tried to reduce the attenuation by an order of magnitude to $0.012 \text{ dB}/\lambda$ and obtained the results shown in Figs 6.3 and 6.4 for the standard PE and the Claerbout PE, respectively. Here the model/data agreement is much better, almost perfect for the wide-angle PE in Fig. 6.4.

In conclusion, the model/data comparison indicates that the super-detailed geoacoustic model is inaccurate. Thus the wave attenuation in the upper bottom layer at 15 Hz has been estimated to be $0.12 \text{ dB}/\lambda$ (presumably extrapolated from high-frequency data) whereas the modeling result shows that a much smaller value of $0.012 \text{ dB}/\lambda$ is more likely. Of course, a lower attenuation of the waterborne sound can also be achieved by increasing the speed contrast at the seafloor in order to enhance the critical-angle effect. In that case the sediment attenuation is less important for long-range propagation. In any event, the various ways to obtain better agreement between model predictions and measured data all relate to the *environmental model*, while the accuracy of the acoustic model is less important. This, of course, just reflects the standing difficulties in actual prediction work: How do we provide the acoustic model with meaningful environmental inputs? This issue is sufficiently complex to deserve the undivided attention of a full workshop by itself.

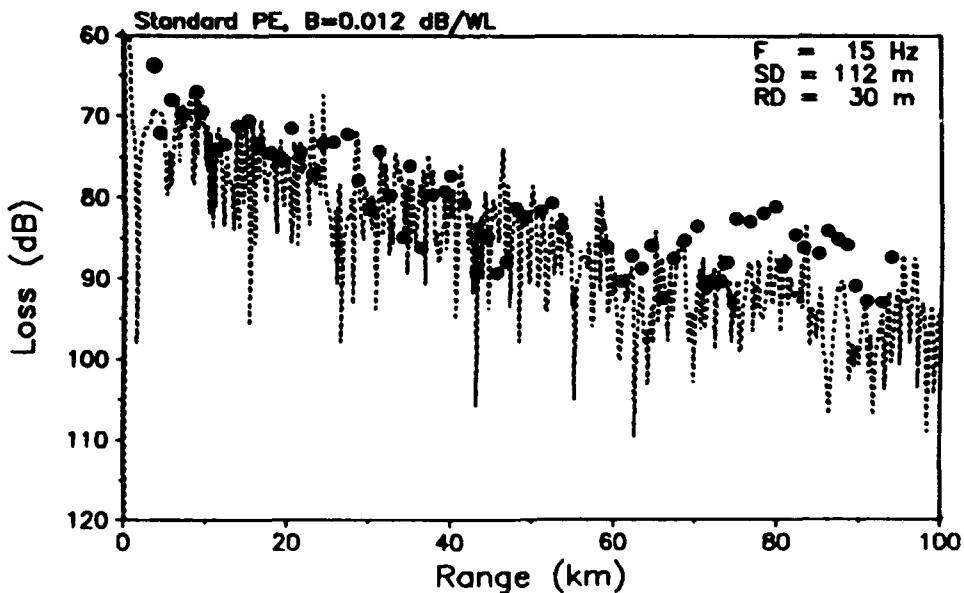


Figure 6.3 Comparison of measured propagation losses with PE predictions (Tappert-Hardin) for a sediment attenuation of $0.12 \text{ dB}/\lambda$.

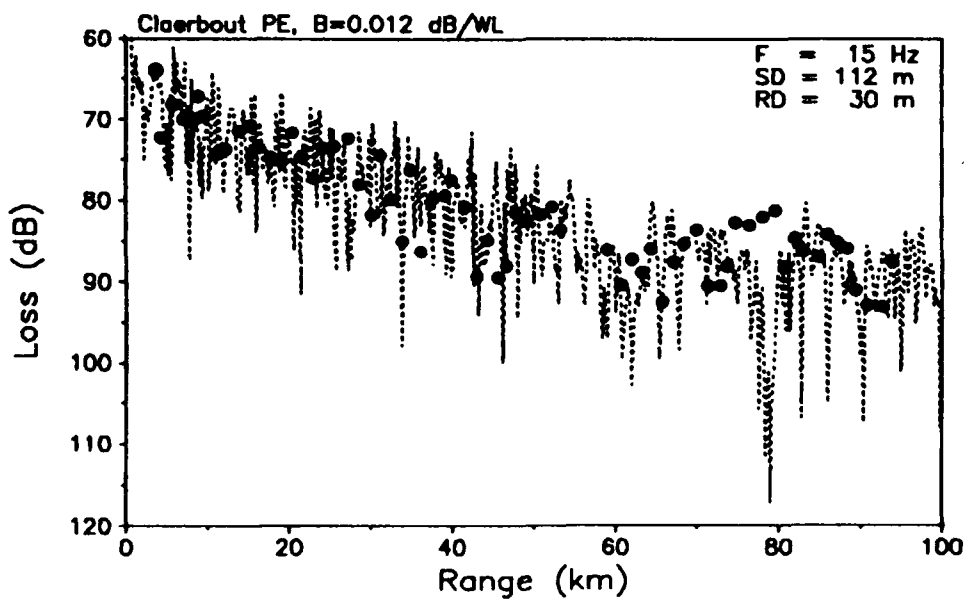


Figure 6.4 Comparison of measured propagation losses with PE predictions (Claerbout) for a sediment attenuation of $0.012 \text{ dB}/\lambda$.

7 Test Case 7

This test problem was introduced on the last day of the workshop, and even though it is a range-independent acoustic problem, it does reveal serious deficiencies in some PE approximations. As shown in Fig.7.1, the test problem deals with long-range propagation in a surface duct. The source frequency is 80 Hz, which results in only one mode being guided in the 250-m deep duct. This mode is a leaky (virtual) mode, which continuously sheds energy into the lower medium, as indicated by the dashed arrows. Also shown in Fig.7.1 is one example of a leaky energy path through the deep ocean (turning depth ~2700 m), which returns to the surface duct approximately 50 km down-range, in between the first and the second convergence zone. Hence, assuming the leakage to be significant, propagation for both source and receiver in the surface duct will consist of purely ducted energy out to the first CZ, and by interference between the ducted mode and the leaky energy beyond the first CZ. In fact, the problem gets increasingly complicated as we move out in range, with an additional leaky arrival appearing after each passing of a convergence zone.

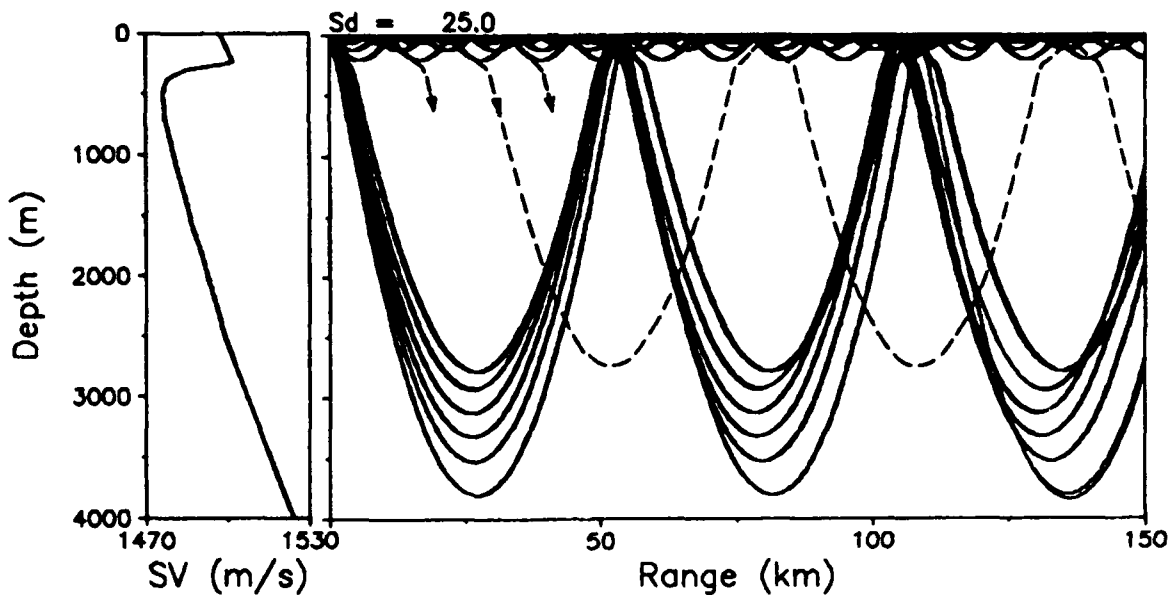


Figure 7.1 Sound-speed profile and associated ray diagram for leaky surface duct problem. The leaky paths are indicated by dashed lines.

The critical aspect of this test problem is that a small phase error for the refracted leaky path compared to the ducted path can result in large changes in sound level in the duct beyond the first CZ. Thus, in the case where the two arrivals (the ducted and the leaky arrival) have similar amplitudes, we may observe level changes of several tens of dB's between constructive and destructive path interference.

The reference solution to this problem for a source at 25 m and a receiver at 100 m was generated by the SNAP normal-mode code. At 80 Hz there are a total of 78 modes, of which one is guided in the surface duct. The SNAP reference solution is shown as the full line in the remaining figures of this section. Note that the transmission loss curve in Fig. 7.2 shows all the characteristic features of this test problem: Single-mode propagation out to the first CZ (~50 km) followed by a two-mode pattern arising from the interference between the ducted mode and a leaky arrival.

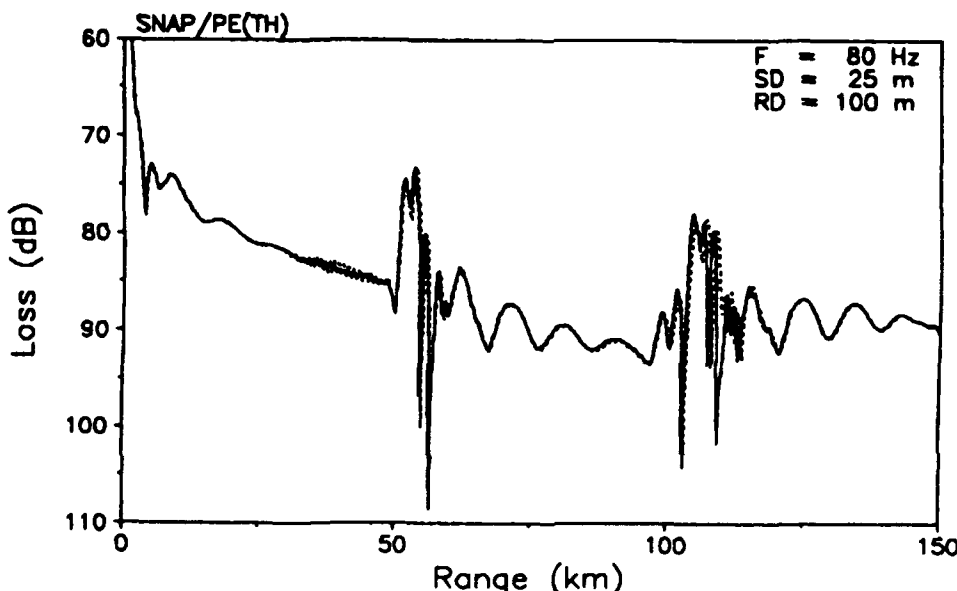


Figure 7.2 Comparison of normal-mode reference solution (SNAP) with standard narrow-angle PE solution (Tappert-Hardin).

Four PE approximations were tested on this problem. Three of these (Tappert-Hardin, LOGPE, Thomson-Chapman) are implemented in the PAREQ split-step code, for which numerically stable results were obtained with a computational grid of $\Delta z = 3$ m and $\Delta r = 50$ m. The last PE approximation (Claerbout) was run with the IFD code, which required a computational grid of $\Delta z = 1.5$ m and $\Delta r = 10$ m.

The results given in Figs. 7.2–7.5 show that only the standard PE and the wide-angle Claerbout PE handle this problem accurately. Both the LOGPE (Fig. 7.4) and the Thomson-Chapman PE (Fig. 7.5) predict too low levels beyond the first CZ due to a small relative phase error between the ducted and the leaky path, which in this case leads to destructive interference between the two arrivals. We can explicitly show that the prediction error is due to an incorrect phasing of one of the two arrivals. By changing the sound speed in the surface duct by just 0.5 m/s and hence altering the phase of the ducted arrival, we obtain the dotted SNAP result shown in Fig. 7.6, which is very similar to the erroneous PE result of Fig. 7.5.

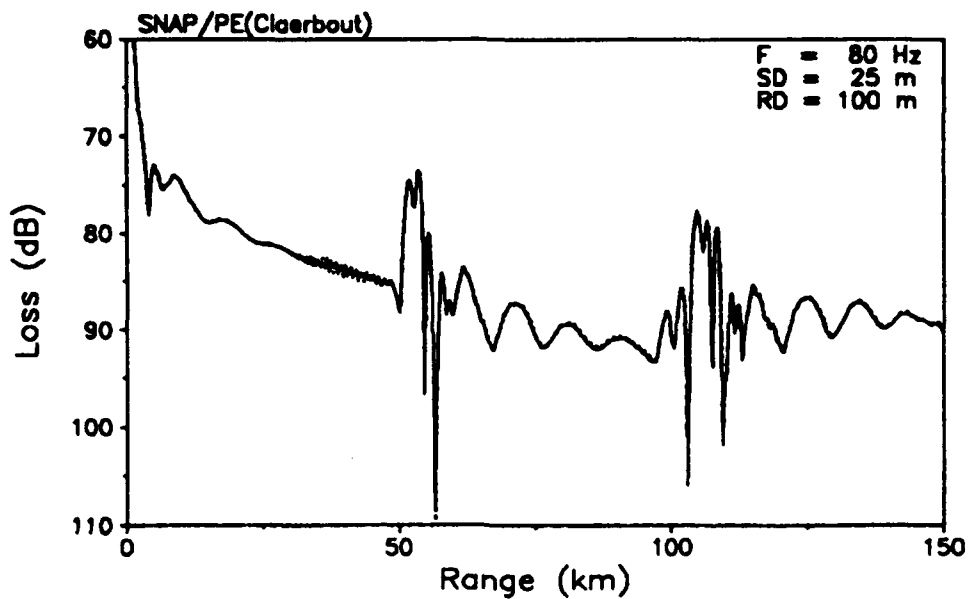


Figure 7.3 Comparison of normal-mode reference solution (SNAP) with angle-angle PE solution (Claerbout).

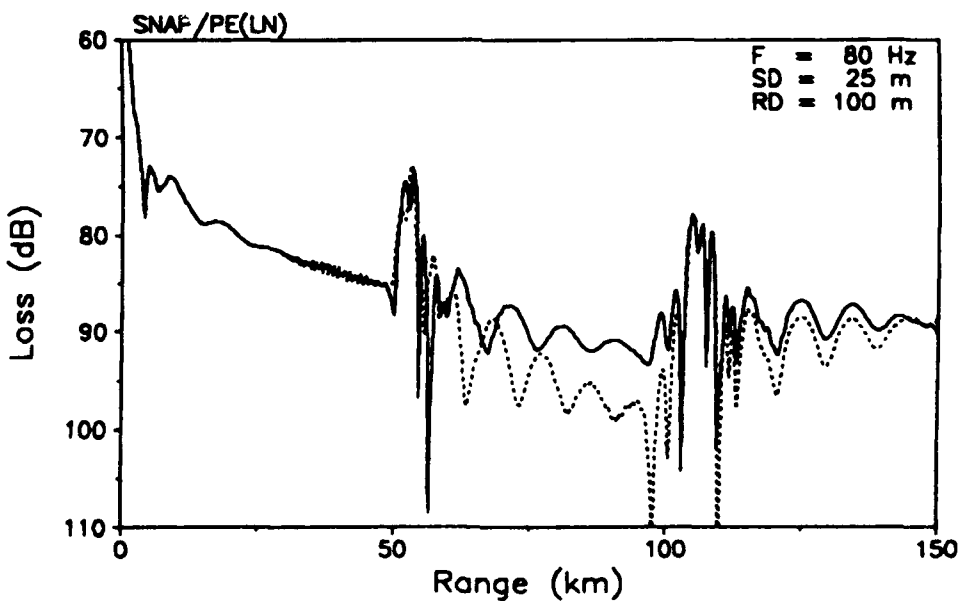


Figure 7.4 Comparison of normal-mode reference solution (SNAP) with LOGPE solution (Berman-Wright-Baer).

In summary, it has been shown that one family of PE approximations perform well on this test problem, while other PE's show severe deficiencies. Specifically, all PE approximations based on a *series expansion* of the square-root operator (Tappert-Hardin,

Claerbout, higher-order Pade' forms) give accurate results, because phase errors relate directly to the angle of propagation. The other PE's considered here (LOGPE, Thomson-Chapman) are based on different approximation techniques for the square-root operator, with the result that phase errors have a complicated relationship to environmental properties along a given sound path. Clearly, in this case a significant phase error occurs between the ducted path and the leaky refracted path to cause prediction errors of more than 10 dB in the Thomson-Chapman PE (US Navy Standard Model) and somewhat less in the LOGPE.

Applications of the IFD Model

Ding Lee

*Naval Undersea Warfare Center
New London CT 06320*

Martin H. Shultz

*Yale University
New Haven CT 06520*

Donald St. Mary

*University of Massachusetts
Troy, NY 12180*

William L. Siegmann

*Rensselaer Polytechnic Institute
Amherst, MA 01003*

George Botseas

*Naval Undersea Warfare Center
New London CT 06320*

ABSTRACT

The acoustic wave propagation prediction model IFD (Implicit Finite Difference), developed in the early 1980's, is based on the solution of a pseudo-partial differential equation, of which the Parabolic Equation (PE) is a special case. The model is applied to solve a set of six problems distributed by the PE Workshop Committee. A number of these problems fall within the capability of this model, while others do not. Nevertheless, the model will be applied to all of the problems in order to observe its responses. The results can be used to appraise the influence of the actual ocean physics.

1. INTRODUCTION

Before the First PE Workshop [1], Lee and Papadakis successfully applied numerical Ordinary Differential Equation (ODE) methods [2] to solve the standard Parabolic Equation(PE) that had been introduced by Tappert [3]. Even though the numerical results from the method are accurate, the ODE method is explicit and its stability is conditional. To relax these restrictions, Lee et al. developed an Implicit Finite Difference (IFD) scheme [4] to solve the standard PE. This method was implemented into a computer code, labeled IFD [5], thereby creating a basic model to accurately solve acoustic wave propagation problems. Later, Gilbert, Lee, and Botseas [6] introduced the wide-angle PE and modified the IFD code to include the capability to handle wide-angle propagation. An important feature of the IFD model is its accurate treatment of the bottom boundary condition whenever this is supplied precisely. To widen the capability of treating boundaries, Lee and McDaniel [7,8] applied the same implicit difference scheme to specify the conditions for interfacial boundaries. The increasing uses of the IFD model in the mid 1980's suggested the need for a clear and detailed documentation of the model. Lee and McDaniel wrote a book, *OCEAN ACOUSTIC PROPAGATION BY FINITE DIFFERENCE METHODS* [9], published in 1988 by Pergamon Press, Oxford, England. This book presents the

detailed development and properties of the finite difference schemes for the solution of acoustic propagation problems in realistic ocean environments. The basic properties, including “problems of consideration”, “development of the finite difference scheme”, “treatment of interface and boundary conditions”, “step-size analysis”, “wide-angle capability”, “selected examples”, and a “listing of the computer program”, can be found in Ref. 9.

Since the early development of the IFD model until recently, there have been no changes in the IFD code. The code has maintained its originality and has continued to provide accurate computational results within its range of validity. Nevertheless, other desirable and useful capabilities have been proposed and developed theoretically but are not yet incorporated into this code.

In this paper we briefly highlight the development of the IFD model in order to indicate its capabilities in Section 2. Then, Section 3 is devoted to summarize useful enhancements. Some of these useful enhancements have been expanded and recognized as separate independent research projects. In particular, two of these research topics are numerical modeling of three-dimensional wave propagation problems and backscattering. Included in Section 4 are computational IFD results for a set of six problems distributed by the PE Workshop Committee. Some of these problems fall within the capability of the IFD model, and some do not. Nevertheless, the IFD model was applied to numerically solve all of the six problems so that we can observe its responses. We feel that these results can be used to examine the influence of actual ocean physics.

2. THE IFD MODEL

The Implicit Finite Difference (IFD) model solves a representative ocean acoustic wave propagation, pseudo-partial differential equation in two dimensions (depth and range). In this paper, we summarize the development of this model so that the readers can sense its capabilities. For comprehensive details of the entire development, one can consult Ref. 9.

2.1 The Mathematical Model

The IFD model solves the following representative wave equation:

$$U_r = ik_0 \left(-1 + \frac{1+px}{1+qx} \right) U \quad (1)$$

where $U(r,z)$ is the wave field,

k_0 = reference number

$$x = n^2(r, z) - 1 + \frac{1}{k_0^2} \frac{\partial^2}{\partial z^2}$$

and $n(r, z)$ defines the index of refraction, the ratio of the reference sound speed c_0 and the sound speed $c(r, z)$.

The parameters p and q are arbitrary, having specific values according to the different rational function approximations to the square-root operator. If one chooses $p=1/2$, $q=0$, Eq.(1) reduces to

$$U_r = \frac{ik_0}{2} (n^2(r, z) - 1) U + \frac{i}{2k_0} \frac{\partial^2 U}{\partial z^2} \quad (2)$$

which is the standard PE introduced into underwater acoustics by Tappert.

Another choice of p and q is $p=3/4$, $q=1/4$, which is the choice suggested by Claerbout [10].

Equation (1), our representative 2-dimensional wide-angle wave equation (Claerbout coefficients), is a pseudo-partial differential equation. Equation (1) is valid for the prediction of one-way wave propagation in the fluid medium and in the far-field without backscattering.

2.2 The Numerical Solution

To develop a numerical finite difference solution for Eq. (1), we express Eq.(1) in an operator form, i.e.

$$U_r = LU \quad (3)$$

where

$$L = ik_0 \left(-1 + \frac{1+px}{1+qx} \right) \quad (4)$$

A finite difference approximation of Crank-Nicolson type gives the analog of Eq.(3) as follows:

$$\left(1 - \frac{1}{2} \Delta r L \right) U^{n+1} = \left(1 + \frac{1}{2} \Delta r L \right) U^n \quad (5)$$

where Δr is the range increment. The numerical scheme, Eq.(5), is implemented by a marching procedure. The discretization of Eq.(5) by a finite difference scheme results in a

symmetric, tri-diagonal system of equations which is inexpensive to solve. In addition, the numerical scheme, Eq.(5), applied to solve Eq.(4) is unconditionally stable.

2.3 The Computer Code

The original code [5] that implements the numerical solution, Eq.(5), was developed for a VAX 11/780 computer at the Naval Underwater System Center (NUSC), New London Laboratory. The code was written in the FORTRAN language. In 1989 the IFD code was installed on a CRAY X-MP computer at NUSC. In view of the increased use of the code nationwide and worldwide, it is believed that IFD is installed on computers other than the two mentioned above.

The code is designed to be relatively easy to use and to modify. The code allows users to supply their own input subroutines, so that their environmental information may be processed realistically and accurately. Sound speed profiles, initial values, surface and bottom boundary conditions, plus other factors such as attenuation and density variations can be user-supplied as inputs. A default value is built-in for the choice of depth increments in case a user has no other knowledge by which to make a proper choice. Users can request the use of the narrow or wide-angle formula by supplying the coefficients p and q . Insufficient bottom information can be accounted for by the code with the application of an artificial bottom to remove bottom-interacting energy and to make the problem solvable. References 5 and 9 provide a comprehensive documentation of the computer code.

3. ENHANCEMENTS

A few desirable capabilities have been developed theoretically but are not incorporated into the IFD code at this stage. Each enhancement can be classified as an independent research topic. One of these is the extension of the 2-dimensional model to 3 dimensions. Significant progress has been made in this topic, for which the 3-dimensional model FOR3D [11] has been developed. One extension of FOR3D is to develop a model for handling backscattering by means of a marching procedure. Also, not incorporated into the IFD model is the numerical treatment of the interface between fluid and elastic media, as introduced by Shang and Lee [12]. Another enhancement is the development of a forth-order finite difference scheme [13] which allows the use of a larger depth step size, so that computation speed can be improved. Related to the PE development is an enhancement to pulse propagation.

3.1 A Three-Dimensional Model (FOR3D)

In Eq. (1), the rational function expression comes from an approximation of a square-root operator, i.e.

$$\sqrt{1+x} \cong \frac{1+px}{1+qx}. \quad (6)$$

Lee, et al. [14] applied a different rational approximation to the three-dimensional square-root operator, to develop a counterpart representative equation of Eq.(1) in 3 dimensions that accounts for variations in the azimuth (θ) variable. Their rational function approximation to the square-root operator is:

$$\sqrt{1+X+Y} = 1 + \frac{1}{2}X - \frac{1}{8}X^2 + \frac{1}{2}Y \quad (7)$$

where $X = n^2(r, \theta, z) - 1 + \frac{1}{k_0^2} \frac{\partial^2}{\partial z^2}$ (8)

and

$$Y = \frac{1}{k_0^2 r^2} \frac{\partial^2}{\partial \theta^2} \quad (9)$$

The 3-dimensional wide-angle wave equation that results for Eq.(7) - (9) is labeled LSS (Lee-Saad-Schultz) equation. The LSS equation has the form

$$U_r = ik_0 \left(-1 + \left(1 + \frac{1}{2}X - \frac{1}{8}X^2 + \frac{1}{2}Y \right) \right) U \quad (10)$$

Had the square -root operator $\sqrt{1+X+Y}$ been approximated by a linear polynomial in X and Y , Eq. (7) would become

$$\sqrt{1+X+Y} = 1 + \frac{1}{2}X + \frac{1}{2}Y \quad (11)$$

in this case, Eq. (10) would become

$$U_r = ik_0 \left(-1 + \left(1 + \frac{1}{2}X + \frac{1}{2}Y \right) \right) U \quad (12)$$

This 3- dimensional PE has been introduce previously [3,15,16]

Lee, et al. treated Eq. (10) locally as a first order ordinary differential equation, solving it symbolically by

$$U(r + \Delta r, \theta, z) = e^{-ik_0 \left(-1 + \left[1 + \frac{1}{2}X - \frac{1}{8}X^2 + \frac{1}{2}Y \right] \right) \Delta r} U(r, \theta, z) \quad (13)$$

to obtain the acoustic envelope U in the closed interval $[r, r+\Delta r]$. A splitting of the

exponential operator, together with rational function approximations, gives the solution of Eq. (13) by

$$U^{n+1} = \left(1 + \left[\frac{1}{4} - \frac{\delta}{4}\right]X\right)^{-1} \left(1 + \left[\frac{1}{4} + \frac{\delta}{4}\right]X\right) \left(1 - \frac{\delta}{4}Y\right)^{-1} \left(1 + \frac{\delta}{4}Y\right) U^n \quad (14)$$

where $\delta = -ik_0\Delta r$. A comprehensive description of the development of the LSS equation and its numerical solution can be found in [14].

A computer code was developed to implement the approximation of Eq. (14). Since the compete solution of the LSS equation involves a Finite difference scheme, an Ordinary differential equation method, and a Rational function approximation for 3- Dimensional problems, the code is labeled FOR3D. This code is fully operational on a CRAY X-MP at NUSC. A detailed description of his 3-dimensional development is in preparation, to be published as a book entitled NUMERICAL OCEAN ACOUSTIC PROPAGATION IN THREE DIMENSIONS [17]

3.2 Backscattering

In 1985 a numerical treatment of backscattering by a marching procedure was introduced by McDaniel, et al. [18]. The approach involves applying an ordinary differential equation method to solve the far field elliptic equation locally. This idea led to the development of solving two PE's in both incoming and outgoing directions. An experimental computer code was constructed but not finalized for real applications.

Recently Lee, et al. [19] extended the prior formulation to three dimensions. A new implementation has been developed, whose initial consideration is directed toward 2 dimensions (depth and range) for two purposes: (1) to check the validity of the model against a known 2-dimensional exact solution, and (2) to investigate physical scattering effects in a simpler context. The marching procedure based on the PE approach is now under development for the treatment of both forward and backward scattering [19].

The development to date is aimed at solving a scattering equation

$$U_{rr} + 2ik_0U_r + U_{zz} + k_0^2(n^2(r,z) - 1)U = 0 \quad (15)$$

by first factoring Eq. (15) into an operator expression

$$\begin{aligned} & \left(\frac{\partial}{\partial r} + ik_0(1 + \sqrt{1+X})\right) \left(\frac{\partial}{\partial r} + ik_0(1 - \sqrt{1+X})\right) U = \\ & -ik_0 \left(\frac{\partial}{\partial r} \sqrt{1+X} - \sqrt{1+X} \frac{\partial}{\partial r}\right) U \end{aligned} \quad (16)$$

Then, a numerical marching procedure is developed to solve the operator equation in 2 steps. Symbolically the right-hand-side of Eq.(16) is labeled $g(k_0 r, z, u)$.

$$L_2 v = g \quad (17)$$

and

$$L_1 u = v \quad (18)$$

where

$$L_1 = \frac{\partial}{\partial r} + ik_0(1 - \sqrt{1 + X}) \quad (19)$$

and

$$L_2 = \frac{\partial}{\partial r} + ik_0(1 + \sqrt{1 + X}) \quad (20)$$

Equations (17) and (18) are equivalent to Eq.(16), which in turn is identical to Eq.(15). The functional $g(k_0 r, z)$ is one type of scattering indicator because $g(k_0 r, z)$ is zero if and only if $n(r, z)$ is range independent.

A marching procedure based on a PE approach is under development for handling both forward and backward scattering. We have outlined the development of our mathematical model, the solution approach, the numerical solution and progress in the development of the research code. To date, the marching procedure has been successfully carried out to handle both weak and strong scattering in the forward direction. The research code has been tested by application to a problem whose solution is known (WAVES IN LAYERED MEDIA, second edition, Chapter VIII, by L.M. Brekhovskikh [20]). Results compare favorably with the exact solution. Research and development of the model will continue in order to achieve a full capability for backscattering with numerical efficiency.

3.3 Shear Waves

In 1989 Shang and Lee [12] took advantage of the IFD model in order to introduce a numerical technique that matches compressional and shear waves on the fluid/elastic interface boundary. A system of parabolic equations was used to represent wave propagation in the elastic medium, so that the complete development is based on a PE approach. In the fluid medium, the solution is obtained by the IFD code. In the elastic medium, the two elastic fields satisfy a system of two parabolic equations. The compressional and elastic wave fields are related by a system of three equations which were derived to satisfy the fluid/elastic interface conditions. Research code for this development was constructed and used to test the validity of the Shang-Lee model by comparing against a known solution [21]. To improve the code for actual application, an elastic equation solver must be incorporated; Knightly, et al. [22,23] are engaging in this development. One

advantage of this approach is the coupling between the fluid and elastic systems, thereby allowing the combined model to handle range-dependent shear speed in the elastic medium.

3.4 A Fourth-Order Finite Difference Scheme

One of the high-order finite difference methods, developed by Saied [24] for solving the partial differential equation of the Schrodinger type, is particularly useful for ocean acoustics. The Schrodinger equation is a parabolic equation of complex coefficients. The scheme of interest, extracted from a family of methods is the fourth-order method introduced by Douglas in early 1965 [25].

Recall that the numerical scheme of Eq.(5) involves the operator L and $\frac{\partial^2}{\partial z^2}$. In the IFD solution, the operator is treated in the following manner:

$$\frac{\partial^2}{\partial z^2} U = \frac{1}{h^2} \delta_z^2 U = \frac{1}{h^2} (U_{j+1} - 2U_j + U_{j-1}) \quad (21)$$

where h = depth increment. The Douglas operator treats this operator in such a way that

$$\frac{\partial^2}{\partial z^2} = \frac{1}{h^2} \frac{\delta_z^2}{1 + \frac{1}{12} \delta_z^2}. \quad (22)$$

Lee and Saied [13] substituted the operator expression, Eq.(22), into the scheme of Eq.(5) and derived another tri-diagonal system. Experimental computations show that the IFD code can produce the same results using both the Crank-Nicolson and Douglas approximations. However, using the Douglas operator, the computation speed is 5 times faster than using the Crank-Nicolson operator. This enhancement is not incorporated currently into the IFD code, but it is incorporated into the FOR3D code, because the IFD solution falls into a special case of FOR3D.

3.5 Pulse Propagation PE

Orchard, et al. [26] developed narrow and wide-angle 3-dimensional time-domain paraxial approximations to the wave equation for modeling acoustic propagation. The approximate representative equations are designed to be appropriate for ocean applications that include pulse propagation with dissipative volume attenuation and variable density. Further work should be done to connect such results with numerical implementations.

4. TEST CASES FOR PE WORKSHOP II

4.1 TEST CASE 1

The selection of a starting field can play an important role in the results produced by a PE model. In addition to testing the starting field the geometry of this problem will also test

the high angle capability of a model.

The environment is a Lloyd's mirror problem. The fluid is a half-space with a pressure release surface and a constant sound speed of 1500 m/sec. The density is 1.0 gm/cc with no attenuation. The fixed point depth (source depth) is 350 m with a moving point depth (receiver depth) of 3990 m. The frequency is 40 Hz.

4.1.1 IFD Results

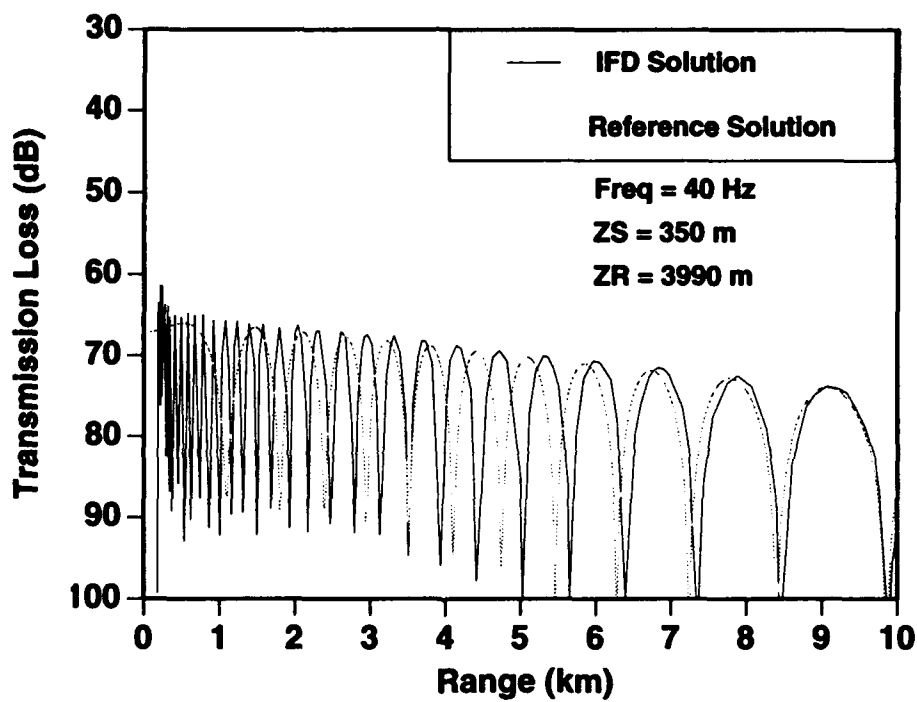


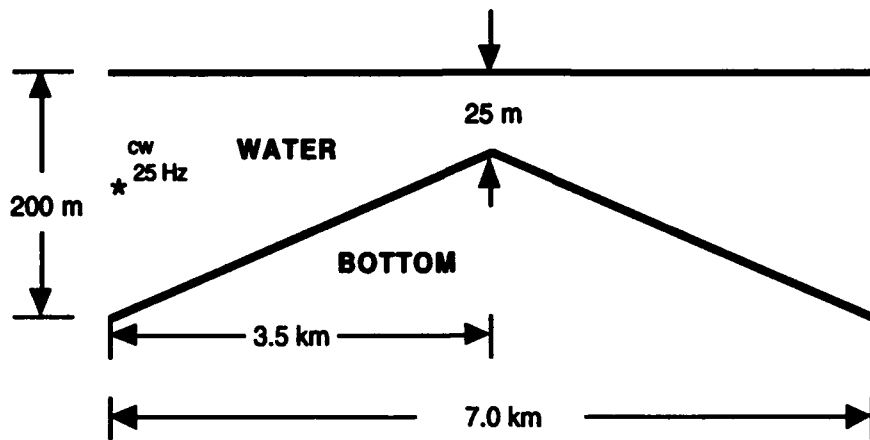
Figure 1: Propagation Loss Comparison for Case 1.

4.1.2 Remark

The accurate solution of this problem requires a starter with very wide-angle capability; moreover, the propagation prediction model must have the capability of handling very wide angles also. The difference in the figure is due to the inaccurate (40°-angle) starter plus the fact that the IFD model was not yet improved to have the very wide angle capability.

4.2 TEST CASE 2

This test case is an upslope-downslope problem that is an extension to the Acoustical Society of America (ASA) benchmark problem. This case is designed to test how well the models conserve energy in a strongly range-dependent environment. The following figure defines the geometry and physical parameters of the problem.



In the water the sound speed is 1500 m/s, the density is 1 gm/cc, and there is no attenuation. In the fluid bottom the sound speed is 1700 m/s, the density is 1.5 gm/cc, and there is an attenuation of $0.5 \text{ dB}/\lambda$. The frequency is 25 Hz, the fixed point depth (source depth) is 100 m, and the moving point depths (receiver depths) are 20 m and 150 m.

4.2.1 IFD Results

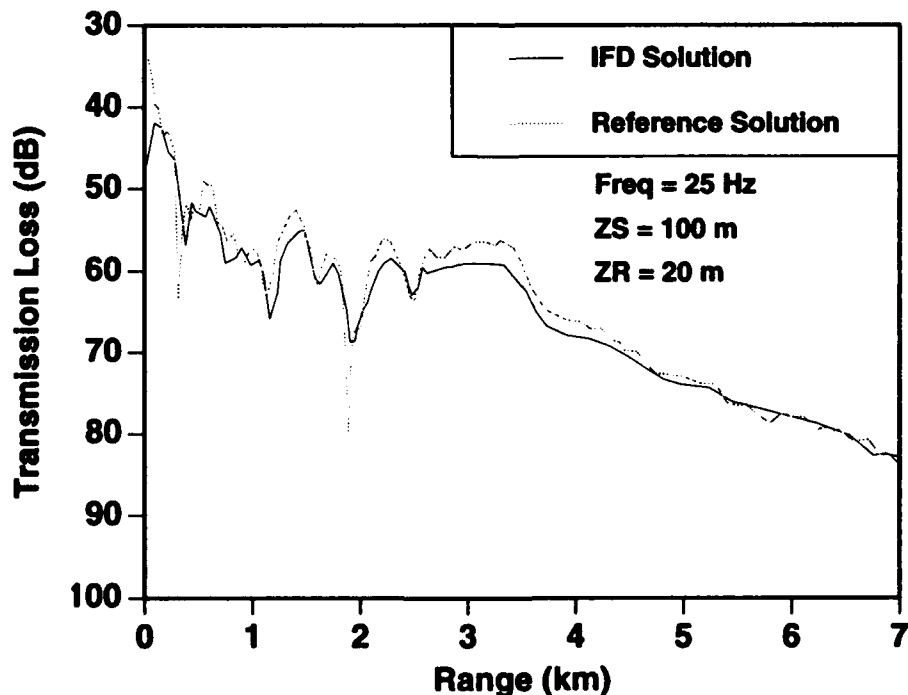


Figure 2: Propagation Loss comparison for Case 2 (Receiver depth = 20 m).

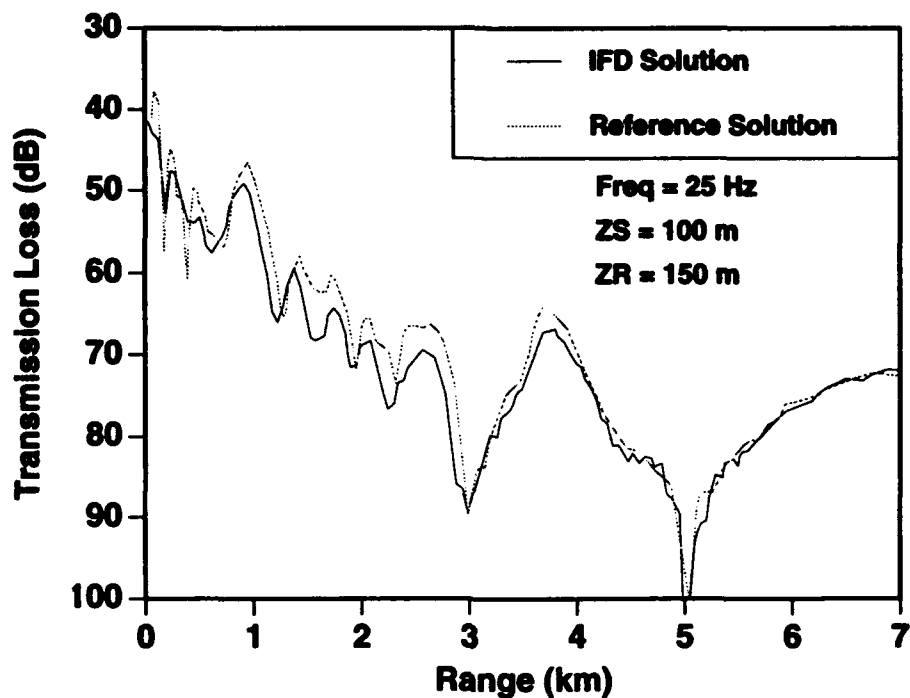
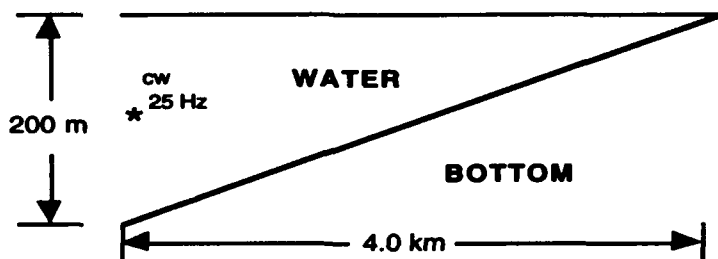


Figure 3: Propagation Loss comparison for Case 2 (Receiver depth = 150 m).

4.3 TEST CASE 3

Recently there has been great interest in extending the underwater acoustic problem to more realistic treatments of the bottom, including elastic media. This case is an adaptation of the ASA Benchmark problem to include an elastic bottom.



In the water the sound speed is 1500 m/s, the density is 1 gm/cc, and there is no attenuation. In the elastic bottom the compressional speed is 1700 m/s, the shear speed is 800 m/s, the density is 1.5 gm/cc, and both the compressional and shear attenuations are 0.5 dB/λ. The frequency is 25 Hz, the fixed point depth (source depth) is 100 m, and the moving point depths (receiver depths) are 30 m and 150 m.

4.3.1 IFD Results

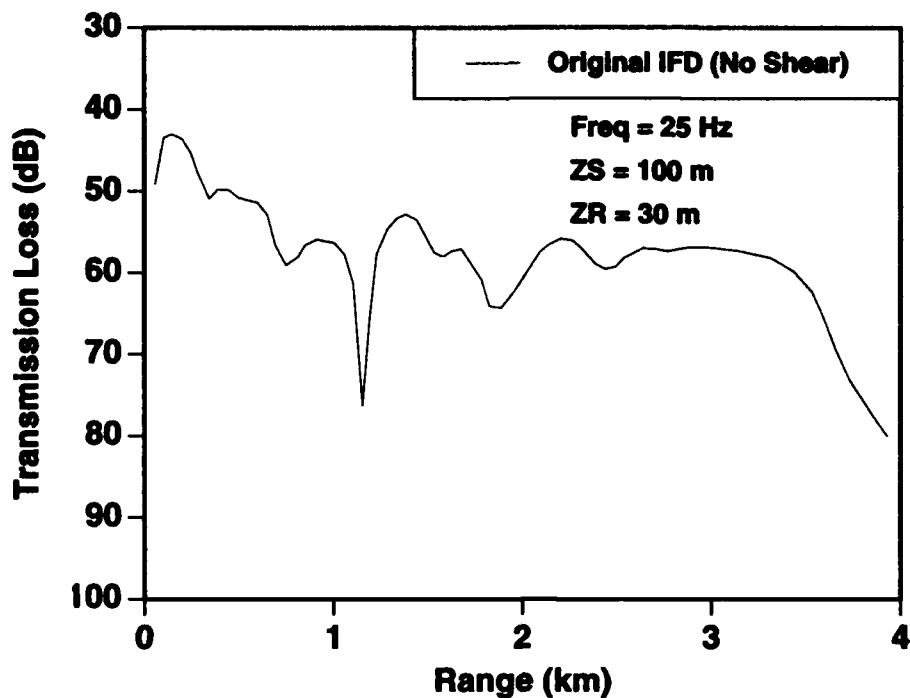


Figure 4: Propagation Loss vs. Range for Case 3 (Receiver depth = 30 m).

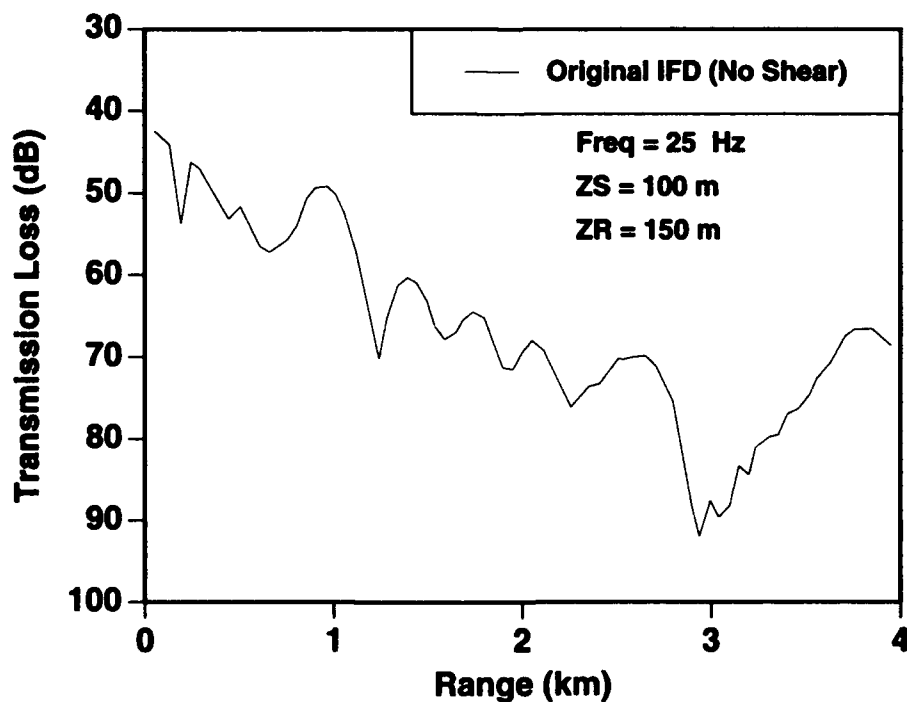
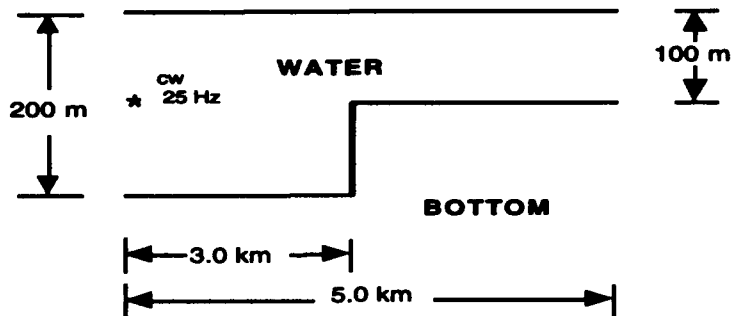


Figure 5: Propagation Loss vs. Range for Case 3 (Receiver depth = 150 m).

4.4 TEST CASE 4

This test case is presented to test the ability of different models to handle the problem of backscattered energy.

In the water the sound speed is 1500 m/s, the density is 1 gm/cc, and there is no attenuation. In the fluid bottom the sound speed is 1700 m/s, the density is 1.5 gm/cc, and there is an attenuation of $0.5 \text{ dB}/\lambda$. The frequency is 25 Hz, the fixed point depth (source depth) is 100 m, and the moving point depths (receiver depths) are 95 m and 150 m.



4.4.1 Remark

The IFD model, at this stage, was not fully developed to have the capability of handling backscatter.

4.4.2 IFD Results

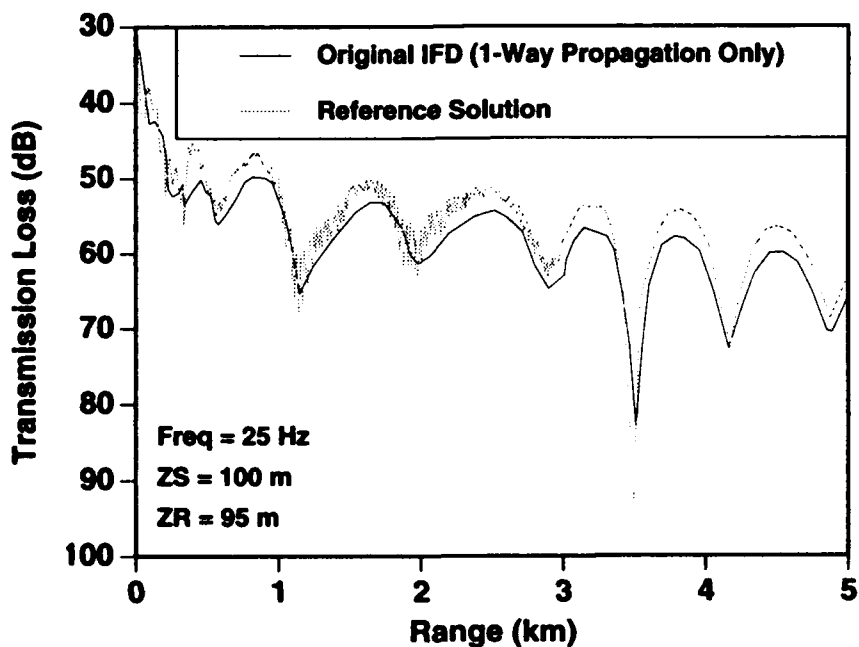


Figure 6: Propagation Loss vs. Range for Case 4 (Receiver depth = 95 m).

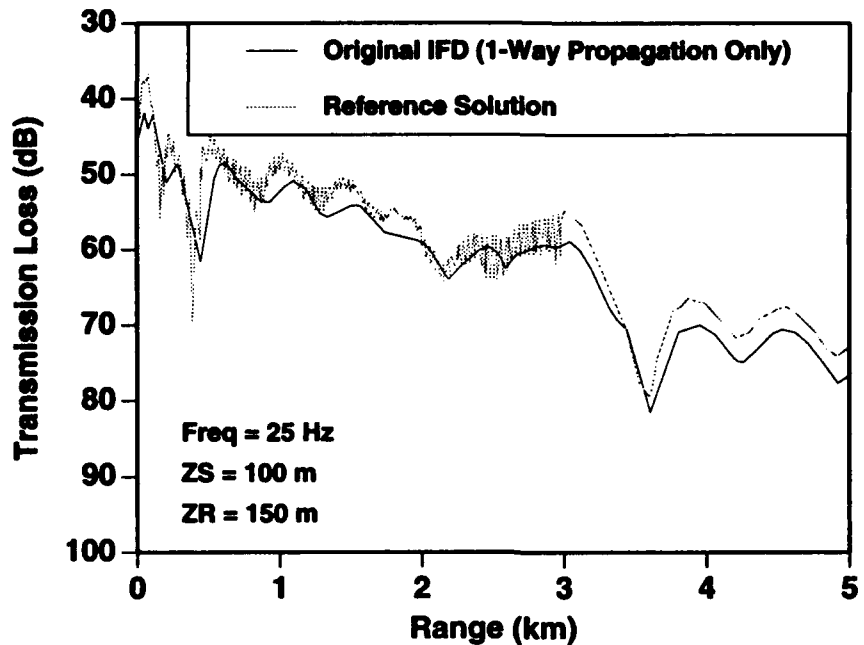
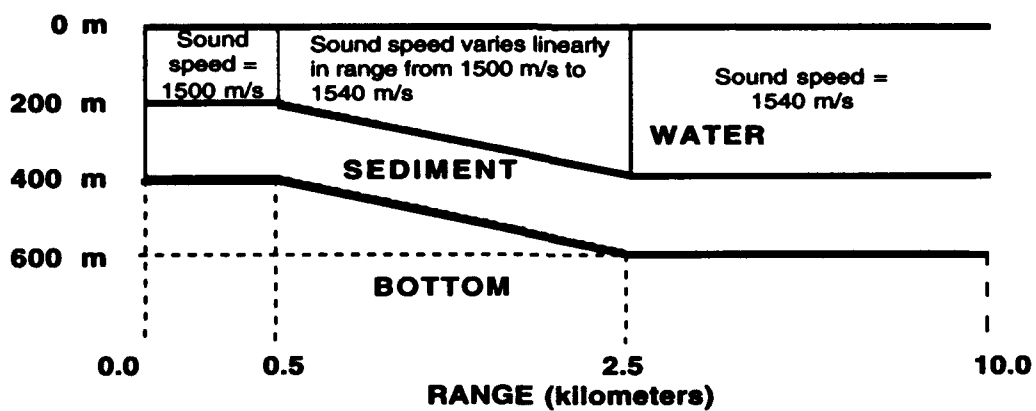


Figure 7: Propagation Loss vs. Range for Case 4 (Receiver depth = 150 m).

4.5 TEST CASE 5

This case is designed to test the ability of underwater propagation and scattering codes to handle range variations in the sound speeds in a range-dependent situation.



The bathymetry of this test case can be looked at as a flat bottom of 200 m depth out to a range of 0.5 km. At that range a downslope section is encountered that drops off 200 m over the next 2,000 m. The bottom then remains flat at 400 m out to the final range of 10,000 m.

The sound speed structure in the *water* is not a function of depth but does have a dependence on the range. It is a constant 1500 m/sec out to a range of 0.5 km. Over the downslope portion of the bathymetry the sound speed varies linearly in range from 1500 m/s to 1540 m/s. At a range of 2.5 km the sound speed remains a constant 1540 m/s out to a range of 10.0 km. The density of the water is 1 gm/cc and there is no attenuation.

The fluid bottom consists of two layers: the first bottom layer (i.e., the *sediment*) is a constant 200 m thick and follows the contour of the water/sediment interface; the second bottom layer (i.e., the *bottom*) is a homogeneous layer of infinite depth. The pertinent physical parameters of these two bottom layers are as follows: The *sediment* sound speed is 1700 m/s, the density is 1.5 gm/cc, and the attenuation is 0.5 dB/λ. The *bottom* sound speed is 1900 m/s, the density is 3.0 gm/cc, and the attenuation is 0.1 dB/λ.

The frequency is 25 Hz, the fixed point depth (source depth) is 100 m, and the moving point depths (receiver depths) are 30 m, 150 m and 250 m.

4.5.1 IFD Results

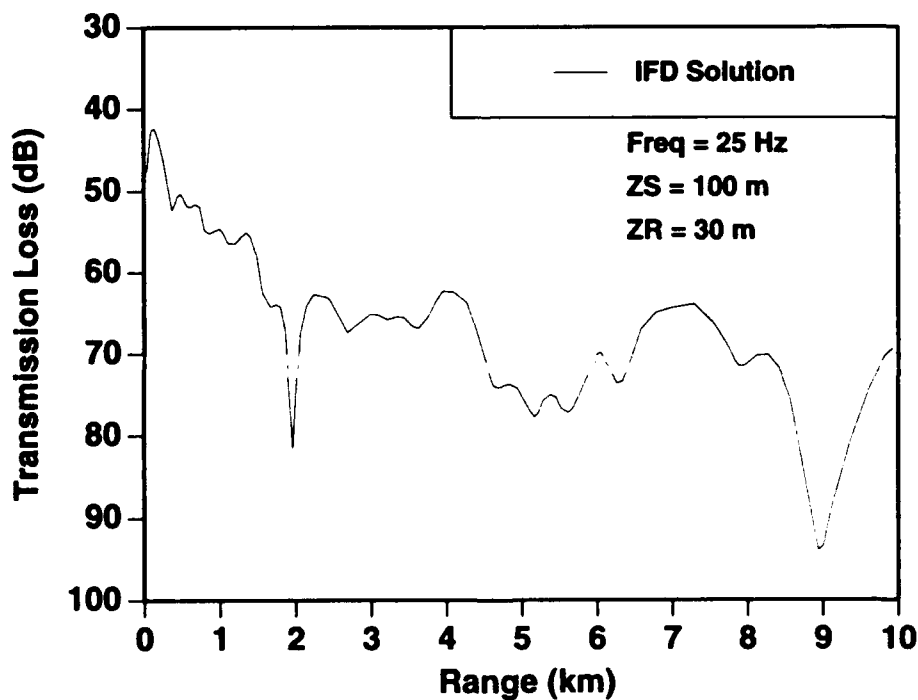


Figure 8: Propagation Loss vs. Range for Case 5 (Receiver depth = 30 m).

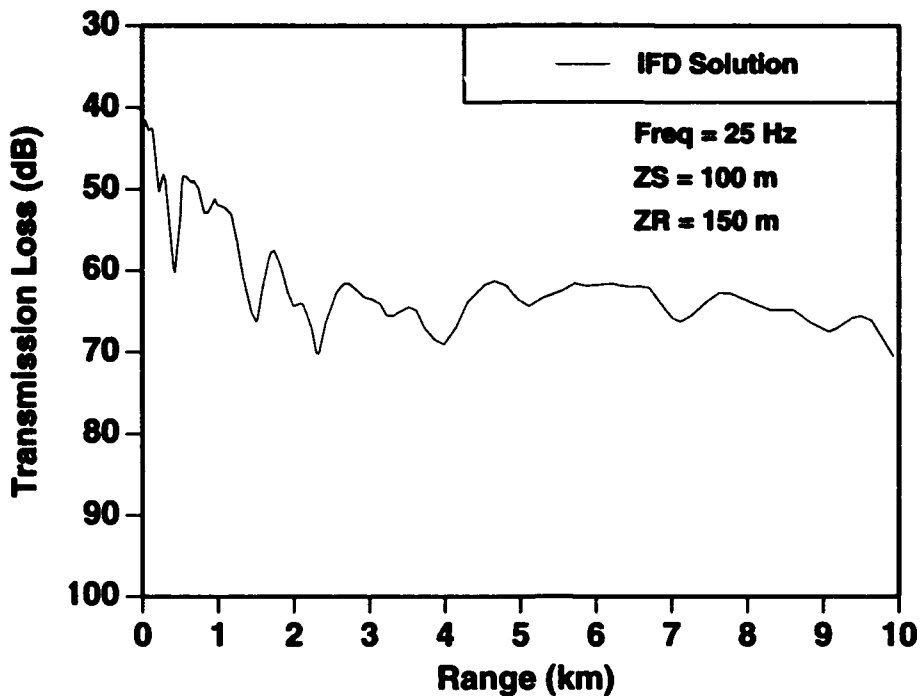


Figure 9: Propagation Loss vs. Range of Case 5 (Receiver depth = 150 m).

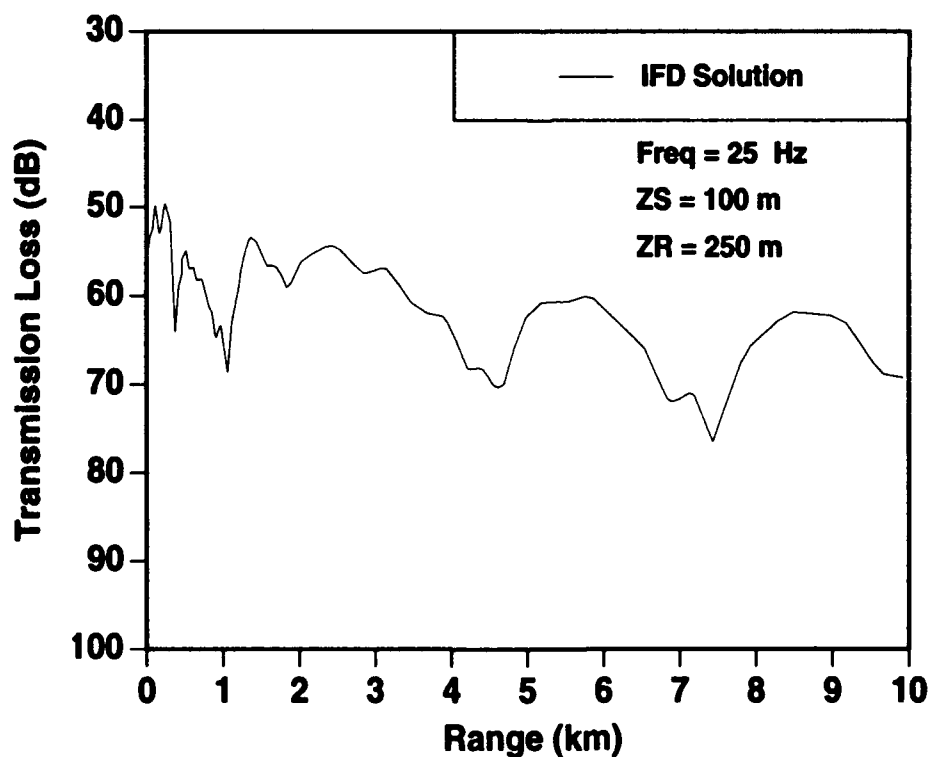


Figure 10: Propagation Loss vs. Range of Case 5 (Receiver depth = 250 m).

4.6 TEST CASE 6

This test case will test the different models against measured field data. The necessary environmental information is listed in the Department of the Navy, ONR Code 124 (AEAS) and ONR Code 1125A memorandum Ser 124A-35 dated 18 January 1991. There were three sound speed profiles measured along the track. The bathymetry is also supplied with the range in km and the depth in meters. A series of range-dependent geoacoustic descriptions are also supplied, where the depths are measured relative to the water sediment interface.

4.6.1 IFD Results

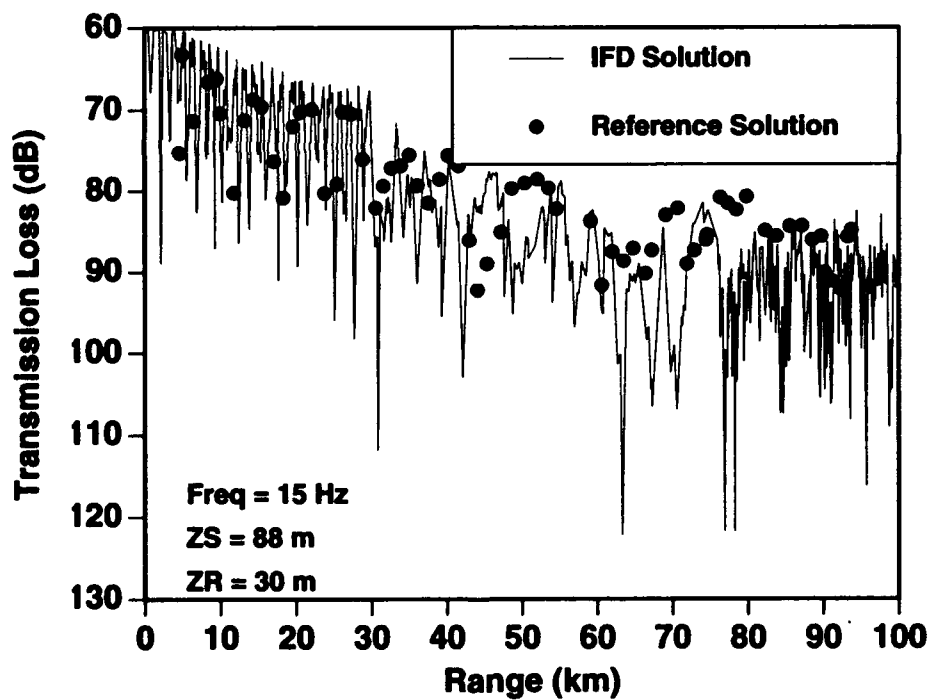


Figure 11: Propagation Loss vs. Range of Case 6 (Source depth = 88 m).

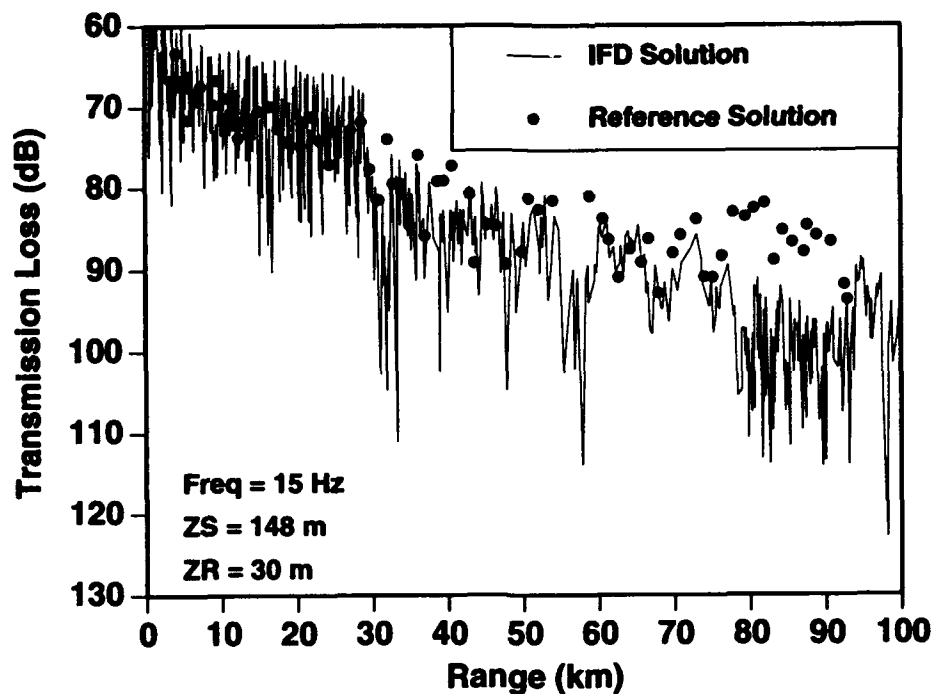


Figure 13: Propagation Loss vs. Range of Case 6 (Source depth = 148 m)

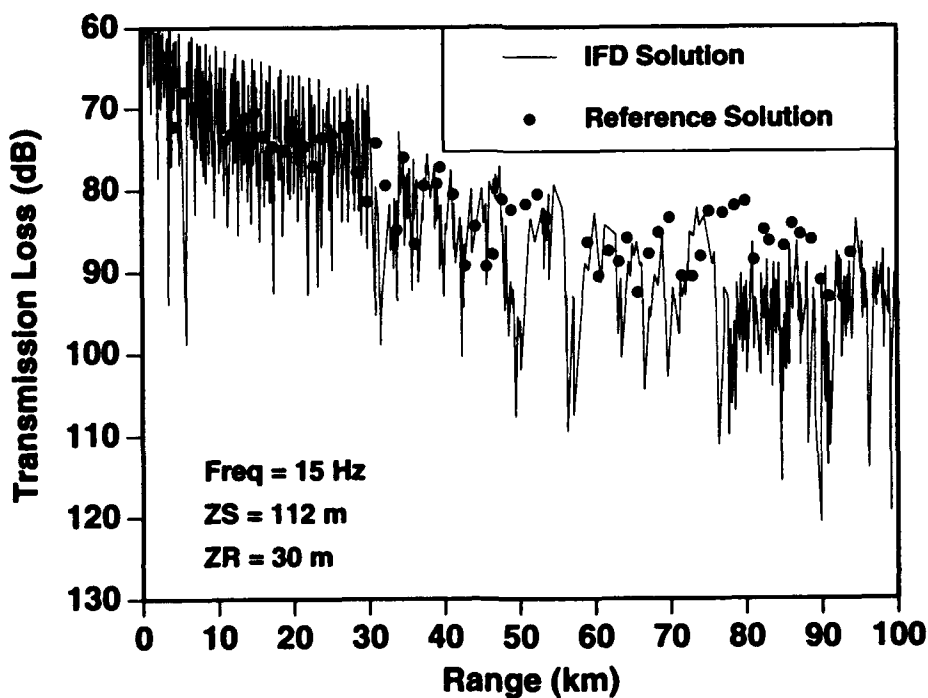


Figure 12: Propagation Loss vs. Range of Case 6 (Source depth = 112 m)

5. CONCLUSIONS

In recent years it is encouraging and interesting to see so much progress related to PE. Some developments reported here represent progress in current implementations. Future enhancements indicate useful capabilities to come. If these enhancements can be incorporated into the IFD model, certainly the model could benefit more users.

ACKNOWLEDGMENTS

This research was continuously and jointly supported by the Office of Naval Research(ONR) and the Naval Underwater System Center (NUSC). Recent work was performed under ONR Grant N00014-91-WX-24038 to NUSC, NUSC Independent Research Projects A65025 and A65027, ONR Grant N00014-91-J-1033 to Rensselaer, ONR Grant N00014-89-J-1671 to Yale, and ONR Grant N00014-91-J-1119 to University of Massachusetts.

REFERENCES

1. Davis, J.A., D. White, and R.C. Cavanaugh (eds.), "NORDA Parabolic Equation Workshop," TN-143, Naval Ocean Research and Development Activity, Bay St. Louis, MS 1982.
2. Lee, D., and J.S. Papadakis, "Numerical Solutions of the Parabolic Wave Equation: An Ordinary-Differential-Equation Approach," *J. Acoust. Soc. Am.*, **68**(5), 1980, 1482-1488.
3. Tappert F.D., "The Parabolic Approximation Method," In *WAVE PROPAGATION & UNDERWATER ACOUSTICS*, J.B.Keller and J.S. Papadakis (eds.), Vol **70**. Springer-Verlag, Heidelberg, 1977.
4. Lee, D., G. Botseas, and J. S. Papadakis, "Finite-Difference Solution to the Parabolic Wave Equation," *J. Acoust. Soc. Am.*, Vol. **70** No.3 1981, 795-800.
5. Lee, D., G. Botseas, "IFD: An Implicit Finite Difference Computer Model for Solving the Parabolic Equation," Naval Underwater Systems Center TR#6659, 1982.
6. Botseas, G., D. Lee, and K. E. Gilbert, "IFD: Wide Angle Capability," Naval Underwater Systems Center TR#6905, 1983.
7. McDaniel, S.T., and D. Lee, "A Finite-Difference Treatment of Interface Conditions for the Parabolic Wave Equation: The Horizontal Interface," *J. Acoust. Soc. Am.*, Vol.**71**, No. 4, 1982, 855-858.
8. Lee, D., and S.T. McDaniel, "A Finite-Difference Treatment of Interface Conditions for the Parabolic Wave Equation: The Irregular Interface," *J. Acoust. Soc. Am.*, Vol. **73**, No. 5, 1983, 1441-1447.

PE Workshop II: Part 3 -- Contributed Papers

9. Lee, D., and S.T. McDaniel, *OCEAN ACOUSTIC PROPAGATION BY FINITE DIFFERENCE METHODS*, Pergamon Press, Oxford 1988.
10. Claerbout, J.F., *FUNDAMENTALS OF GEOPHYSICAL DATA PROCESSING WITH APPLICATIONS TO PETROLEUM PROSPECTING*, McGraw-Hill Book Co. Inc., New York, 1976.
11. Botseas, G., D. Lee, and D. King, "FOR3D: A Computer Model for Solving the LSS Three-Dimensional, Wide Angle Wave Equation," Naval Underwater Systems Center TR#7943, 1987.
12. Shang, E.C. and D. Lee, "A Numerical Treatment of the Fluid/Elastic Interface under Range-Dependent Environments," *J. Acoust. Soc. Am.* Vol. **85**, No. 2, 1989, 654-660.
13. Lee, D. and F. Saied, "A Fourth Order Finite Difference Scheme to Improve the Computation Speed of Wide Angle Propagation," In *COMPUTATIONAL ACOUSTICS: Ocean-Acoustic Model and Supercomputing*, D. Lee, A. Cakmak, and R. Vichnevetsky (eds.) North-Holland, Amsterdam, 1990, 27-36.
14. Lee, D., Y. Saad, M.H. Schultz, "An Efficient Method for Solving the Three-Dimensional Wide Angle wave Equation," In *COMPUTATIONAL ACOUSTICS: Wave Propagation*, D. Lee, R.L. Sternberg, and M.H. Schultz (eds.), North-Holland, Amsterdam, 1988, 75-90.
15. Baer R. N. "Propagation Through a Three Dimensional Eddy Including Effect on an Array," *J. Acoust. Soc. Am.*, Vol. **69**, 1981, 70-75.
16. Perkins, J.S., and R.N. Baer, "An Approximation to the Three-Dimensional Parabolic Equation Method for Acoustic Propagation," *J Acoust. Soc. Am.* Vol. **72**, 1982, 515-522.
17. Lee, D., M.H. Schultz and W. L. Siegmann, *NUMERICAL OCEAN ACOUSTIC PROPAGATION IN THREE DIMENSIONS*, (In preparation) 1994.
18. McDaniel, S.T., Y. Saad, and D.Lee, "Numerical Solutions of Sound Scattering in the Ocean: An Ordinary-Differential-Equation-Approach," *Proc 11th IMACS World Congress*, Oslo, Norway, 1985, 127-130.
19. Lee, D., D.F. St. Mary M.H. Schultz, and W.L. Siegmann, "A New Model for Marching Computation of Ocean Acoustic Backscattering," *J. Acoust. Soc. Am. Supplement 1*, Vol. **88**, 1990, S87.
20. Brekhovskikh, L.M., *WAVES IN LAYERED MEDIA*, Second Edition, Academic Press, 1980.

PE Workshop II: Part 3 — Contributed Papers

21. Ewing, W.M., W.S. Jardetzky, and F. Press, *ELASTIC WAVES IN LAYERED MEDIA*, McGraw-Hill, New York, 1957.
22. Knightly, G.H., G.Q.Li, D.F. St. Mary, and D. Lee, "A Numerical Treatment of the Fluid/Elastic Interface for the Potential Equations," *J. Acoust. Soc. Am., Supplement 1*, Vol. **86**, 1989, S65.
23. Knightly, G.H., G.Q.Li, D.F. St. Mary, and D. Lee, "Elastic Parabolic Equation and the Fluid/Elastic Interface", *Acoust. Soc. Am., Supplement 1*, Vol. **88**, 1990, S59.
24. Saied, F., *NUMERICAL TECHNIQUES FOR THE TIME-DEPENDENT SCHRODINGER EQUATION AND THEIR PARALLEL IMPLEMENTATION*, Ph.D. Dissertation, Yale University, New Haven, USA, 1990.
25. Douglas, J., Jr., "The Solution of Diffusion Equation by a High Order Correct Difference Equation," *J. Math.Phys.*, Vol. **35**, 1956, 145-151.
26. Orchard, B.J., W.L. Siegmann, and M.J. Jacobson, "A Three-Dimensional Time-Domain Paraxial Approximation for Underwater Acoustic Wave Propagation," *J. Acoust. Soc. Am., Supplement 1*, Vol **87**, 1990, S130.

FastPE, SlowPE, YourPE, MiPE: What are the Real Issues?

Lan Nghiem-Phu

MAC Systems & University of Miami/RSMAS

Kevin B. Smith & Fred D. Tappert,

University of Miami/RSMAS/AMP

Miami, Florida

1. Introduction

Since its introduction to the underwater acoustics community, the PE model has been used extensively for modeling the acoustic pressure field in real ocean environments. Over the years, many improvements in physics, equations, algorithms and databases have been achieved. The result has been a proliferation of PE models. However, serious issues remain with regard to what these models represent. Can they be trusted? If so, to what extent, and for what applications?

Of course, this is an enormously complex and therefore difficult problem that will linger for years to come. There are no simple answers. Nonetheless, these issues cannot be discarded since acoustic modeling can significantly contribute to our understanding of acoustic propagation, leading to improved sonar system performance.

Among classes of PE models, one can identify two broad categories: one devoted to pure academic research, and another oriented to operational sonar systems. In the following discussion, both categories will be touched upon in a general way. Finally, in the spirit of the PE Workshop II, we present the results from a particular PE model, the Miami PE model (MIPE), together with pertinent discussions of the various test cases.

2. The MIPE Model

During the course of the PE Workshop II, Tappert¹ reminisced about the history of PE, mentioning in passing the “PE model baby book”². The MIPE model is a direct descendent of this now famous split-step PE algorithm (a.k.a. “the dusty old deck”). In fact, in the earlier years in Miami, the dusty old deck was chosen over another descendent of this PE model, the AESD version, to become the foundation of what is now the MIPE model. It is worth noting that the AESD version later became the Navy standard PE model. The dusty old deck has since been revamped, embellished and vectorized to improve the speed of execution. A by-product of this effort has been the high-visibility PESOGEN systems.

The name MIPE itself is not precise enough to pinpoint any particular version of the many Miami PE models that exist at any moment because the Miami models are constantly

improving in physics and in algorithms toward better efficiency and accuracy at the same time. Yet another Miami PE model, called the UMPE (University of Miami PE) is presented here for the first time, introducing a C_0 insensitive PE model. It suffices to say that all MIPE models share a common start from the dusty old deck.

The MIPE model presented here is a version derived from the PESOGEN system. It requires the SKY Warrior II array processor and can run in either a PESOGEN or Sun system. The results reported here have been obtained from a Sun3/160 equipped with a SKY Warrior II array processor.

The most prominent features of this MIPE model are:

- Split-Step Fourier algorithm
- Thomson-Chapman wide angle formulation
- Smoothed density and sound speed between water/sediment (sediment/basement) interface(s)
- Wide angle source with wave number domain filter
- Full FFT transform so that rough surfaces can be treated with the generalized method of images.

The many other features of this MIPE model, such as the broadband mode, the matched field mode, the multiple forward scattering mode, the full-wave reverberation mode and the directional source and receiver mode will not be discussed since the PE II test cases only address smooth boundaries with single frequency, single omnidirectional source and receiver.

3. The Real Issues

A pure objective is the mathematical endeavor of solving the acoustic wave equation as accurately as possible. In the science of ocean acoustics, it is pointless to achieve this objective without taking into account the ocean itself. Therein lie the complications that render necessary the various approximations being invoked so that acceptable solutions can be obtained within existing means. Because of the presence of the surrounding environments, ocean acoustics must be treated with the inclusion of accurate descriptions of the ocean as it actually is at any time and place. This is no small task.

On the one hand, it would be nice to verify that, indeed, one could mathematically and numerically obtain an accurate solution to a well posed problem. However, this is merely a necessary condition because, on the other hand, the solution also needs to be accurate in more difficult realistic cases. A success of a well tuned model, for a well posed problem is by no means a guarantee that reliable predictions can be obtained in more trying situations.

This point is well illustrated in Test Case 6, where it appears that no model, no matter how well tuned, can predict the measured data.

The point above raises the question of what accuracy should be required of a solution. Should more terms or more environmental data be added to improve the solution? And if indeed the solution is improved somewhat, is it worth the cost? More importantly, will the improvement be stable or will it become completely chaotic due to uncontrollable uncertainties in the environment? These, among other issues, indicate that serious thought needs to be given to this complex problem and that the book is certainly not closed on the modeling of sound propagation in the real ocean.

By solving the wave equation, one important component of the sonar equation, the transmission loss (TL) can be obtained. This TL is precisely what is being sought so that the science of sound propagation in the ocean finds an application in sonar systems. This important application helps to justify the ongoing research in PE modeling. It is in operational sonar systems that PE models may prove themselves most useful.

In order for the PE model to be useful in sonar applications, what then is the accuracy to be required? The answer is well hidden in the difficult task of finding the balance in which the description of the environment is well matched with the limitations of the physics underlying a particular PE model and the speed of a particular computer. This assertion must of course be qualified by the specification of a particular acoustic frequency regime. For higher frequency applications, oceanic features of the same scale length as the acoustic wave length will not be available. In this regime, it is wise to seek predictions of statistics. In lower frequency regimes, sparse descriptions of the ocean environment may well be adequate as long as one can be satisfied with equally sparse predictions. In neither case will pointwise accuracy be achievable.

For the above reasons, the MIPE model is not expected to provide TL predictions with pointwise accuracy, especially in real ocean environments. There are other PE models with higher order accuracy that might include extra physics such as the propagation of shear waves. These higher order terms and/or more physical parameters might show improvements in pointwise predictions in some examples.

This is not to say that the MIPE model cannot provide pointwise accuracy. To within its limitations, it will provide pointwise accuracy for cases for which the algorithm and equation have been designed. An example is test case 1, where the Thomson-Chapman approximation is exact. To within the limitation of the implementation of very high angles, close to 90 degrees, the MIPE model is shown to have pointwise accuracy. This test case is a welcome exercise for the verification of various implementation issues. For example, special care is needed while implementing the k-space symmetry in MIPE because it has retained the traditional “half-integer” mesh in depth.

In view of the above discussion, one goal of MIPE is that predictions should have small uniform errors for all ocean environments. Whether this goal is achievable is debatable, but certainly pointwise accurate predictions would be far more difficult. Small uniform errors could be quantified as a “few” dB’s. “Few” will vary depending on the applications. Rather, the emphasis will be placed upon the timeliness of the predictions for it to be operationally useful.

4. The Test Cases

In all of the test cases that follow, the MIPE model was used with fixed range step Δr and depth mesh Δz . The Δr and Δz are obtained by refining the computational mesh until the solution converges.

There are only a few parameters that need to be adjusted (or computed). First, the mixing lengths are computed to obtain smooth transitions in the index of refraction and in the density discontinuities. Smooth transition between layers are crucial in obtaining accurate and fast solution for bottom limited applications. Second, the bottom boundary condition needs to be implemented so that numerical artifacts are not introduced and thus contaminate the solution. Third and last, the wave number filter has to be designed with care to prevent artificial reflections.

The solutions are presented in forms of plots of TL as a function of range for given source/receiver depths. Figures 1 through 7 correspond to Test Cases 1 through 7 respectively.

4.1 Test Case 1 - Figure 1

MIPE has pointwise accuracy with the exception of angles close to 90 degrees.

4.2 Test Case 2 - Figures 2a & 2b

The difficulty here (to approach pointwise accuracy) is that the requirement of a mixing length at the apex has altered sufficiently the environment to affect the solution. The net result is that pointwise accuracy is not possible.

4.3 Test Case 3 - Figures 3a & 3b

MIPE does not propagate shear waves, but rather treats them as a loss mechanism³. The additional loss due to shear wave conversion is 4.82 dB/nmi-Hz. Since shear waves are treated as a loss, only reflections from the sediment layer are treated adequately. As a consequence, the prediction of TL can be trusted only when the receiver is in the water column and when shear propagation is unimportant. When the receiver is in the sediment layer, the loss prediction is too high.

4.4 Test case 4 - Figures 4a & 4b

This test case is treated such that the underwater sea cliff is a linear (rather than circular) feature in a small angular sector in azimuth. We stress that MIPE and its ancestors have never made the physically unrealistic assumption of cylindrical symmetry. Therefore, there is no reason to consider a circular wall. The computed field is a coherent sum of two fields. The forward propagating field obeys the usual PE wave equation, while the incoming field is coupled with the outgoing field via the effective reflection coefficient computed from both sound speed and density discontinuities across the cliff. By using the linear model of the cliff, the rapid oscillations due to the interference between outgoing and incoming waves are not amplified as the origin is approached and have lesser magnitude than if a circular feature were assumed.

4.5 Test case 5 - Figures 5a, 5b & 5c

Special code needed to be written for the MIPE model to handle cases 5 and 6 because of the extra layers. By adding one extra layer, an additional mixing length is required.

4.6 Test case 6 - Figures 6a, 6b, 6c & 6AF (Full field 6a)

By a straightforward extension, a multi-layer capability has been added to the MIPE model. All three TL predictions are high compared with measured data. There are many possible explanations. This issue is being addressed by other contributions in the workshop and it is not being addressed here. The central issue here is clearly the necessary data bases to support any acoustic model. This creates a sense of urgency for an answer to the balance between super accuracy in the model output versus the imprecise state of the art of the available data bases.

4.7 Test case 7 - Figures 7a, 7b, 7c & 7d

Ironically, this test case was believed to be discarded because “it is too easy”. It turns out that Test Case 7 now casts a large shadow in what has been accepted as a standard for improved solution to PE wide angle modeling. The new “discovery” is not that the Thomson-Chapman (T-C) equation cannot produce the correct solution, but that it can only produce the correct solution within a very narrow spectrum of reference sound speed C_o . In other words, T-C is highly sensitive to the choice of the reference sound speed. The disturbing fact is that the predicted level is highly C_o dependent. While Figure 7a shows that T-C yields the correct solution with the value of $C_o = 1482$ m/s, Figure 7b shows that errors as large as tens of dB’s are introduced when $C_o = 1500$ m/s. Figure 7c displays the correct solution obtained from the standard PE (SPE) approximation with $C_o = 1500$ m/s. We have investigated the reason for this anomaly without being able to pinpoint the causes for such behavior. Our investigation included mixing various “propagators” (standard and wide angle) with various index of refraction “potentials” (also standard and wide angle).

The rational behind this investigation was the search for a regime where the derivative of the split-step operator with respect to C_o is stable. This unfruitful search prompted us to believe that a C_o insensitive equation is now urgently needed. Such an equation has been described previously¹. Figure 7d (courtesy of Dr. Jacob Roginsky/RSMAS-AMP) shows the preliminary results of the wide angle UMPE model where the C_o insensitive equation has been implemented. Indeed, the three TL curves for widely different C_o 's are almost indistinguishable from one another, except at ranges in the neighborhood of about 80km. However, upon closer examination, the absolute level is about 1 dB higher than the reference. The reason for this systematic shift in level has not yet been found. Also, extension to range dependent environments needs to be worked out.

5. Discussions

The above section presents results for all 7 test cases where the MIPE model was used in a semi-research mode. The user is a sophisticated split-step PE modeler with years of experience. It can be stated that for a given problem, a convergent solution is always obtainable because the split-step Fourier algorithm is unconditionally stable. Due to practical considerations, and also due to limitations imposed by the physics, the solution might not possess pointwise accuracy. The limitations are well known, however, and mostly environmentally related. The “few” dB's of deviation can be reduced by sacrificing run time but this “improvement” must be well warranted to justify the increase in costs.

A far more difficult task is to remove the requirement of an experienced operator while simultaneously keeping the uniform error small with a small execution time. This requires an adaptive scheme that will be dependent upon the environment in a complicated way. More than ever, the requirement for a better understanding of how the environmental data bases influence a particular acoustic model must be addressed so that the latter can be improved to achieve the goal of fast, reliable predictions of TL's.

Test cases 6 and 7 pose challenges to be addressed by the entire modeling community. Although the C_o insensitivity of the UMPE model holds much promise, work needs to be carried forward to address the mysteries of the sensitivity to C_o of the Thomson-Chapman equation and to determine what should be done so that reliable TL predictions can become reality.

References

1. F.D. Tappert, “The parabolic equation approximation method,” in *Wave Propagation and Underwater Acoustics*, ed.,.. by J.B. Keller and J.S. Papadakis, Lecture notes in Physics, Vol.70 (Springer Verlag, 1977).
2. F.D. Tappert, “The PE Model Baby Book”, unpublished document, April 1986.
3. F. D. Tappert, “Parabolic Equation Modeling of Shear Waves,” *J. Acoust. Soc. Am.* **78**(5), Nov. 1988, 1905-1906

Figure 1: Case 1 - MIPE

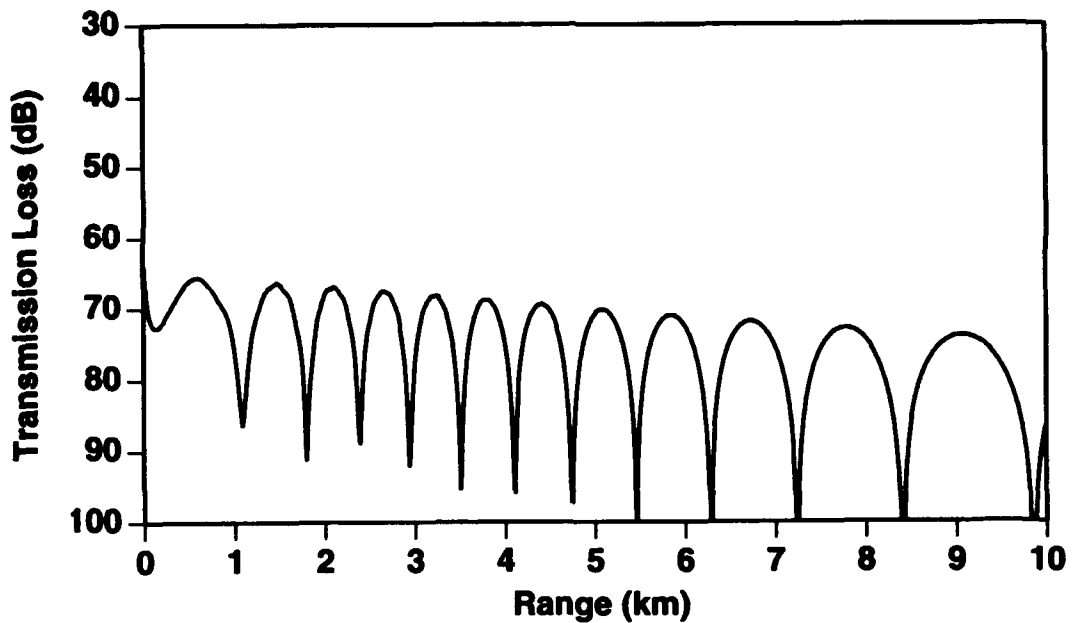


Figure 2a: Case 2a - MIPE

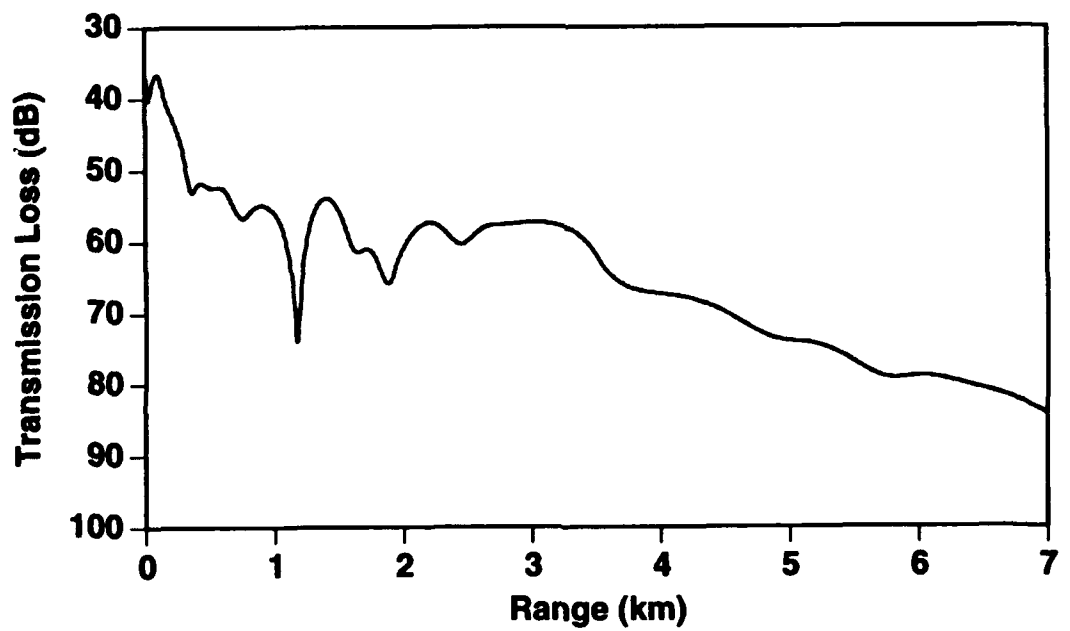


Figure 2b: Case 2b - MIPE

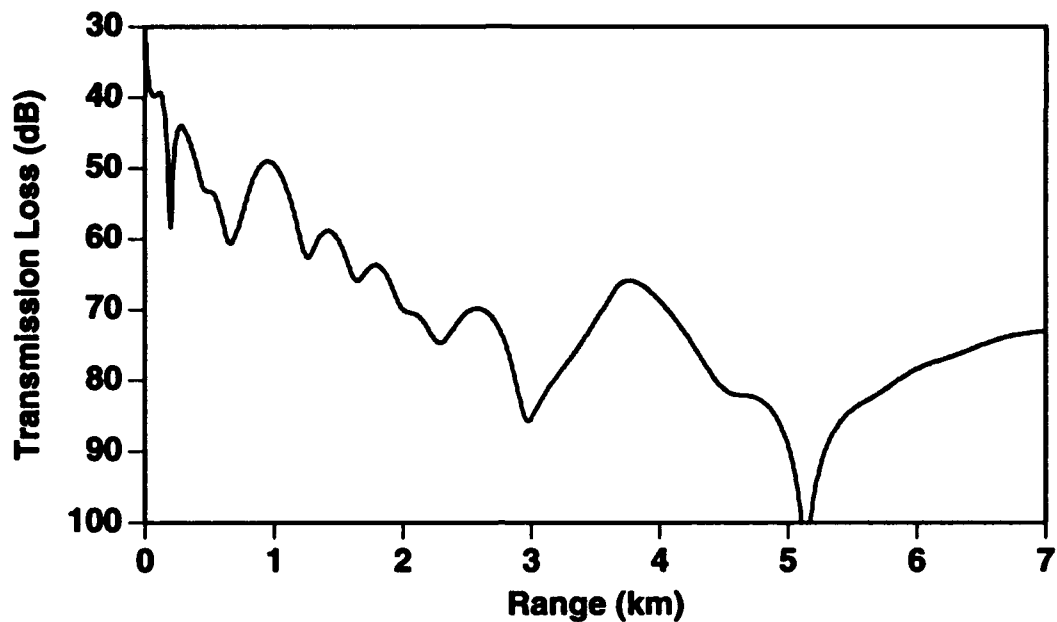


Figure 3a: Case 3a - MIPE

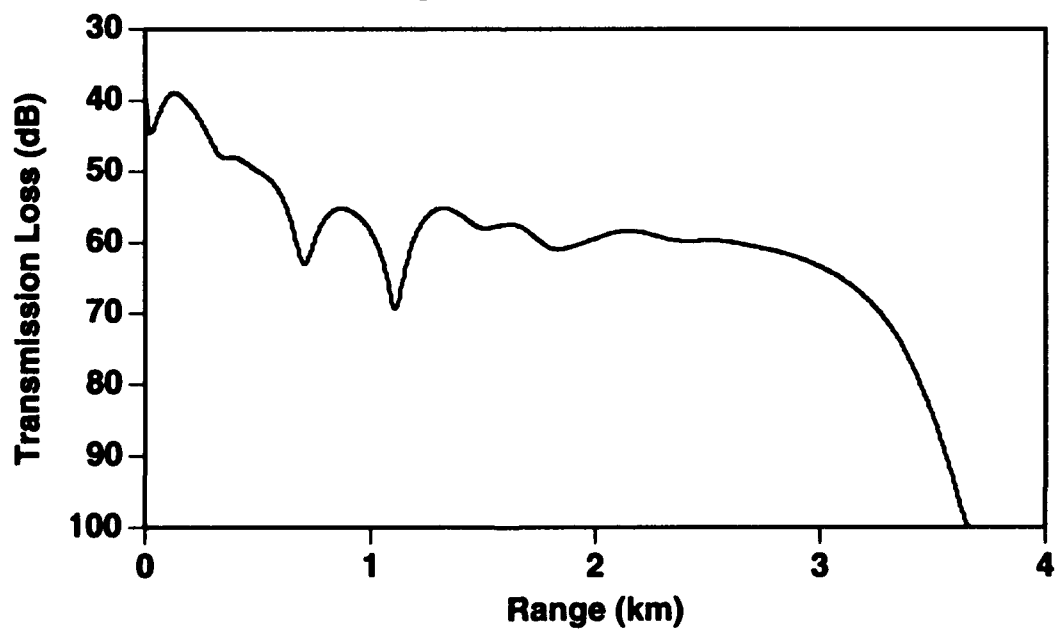


Figure 3b: Case3b - MIPE

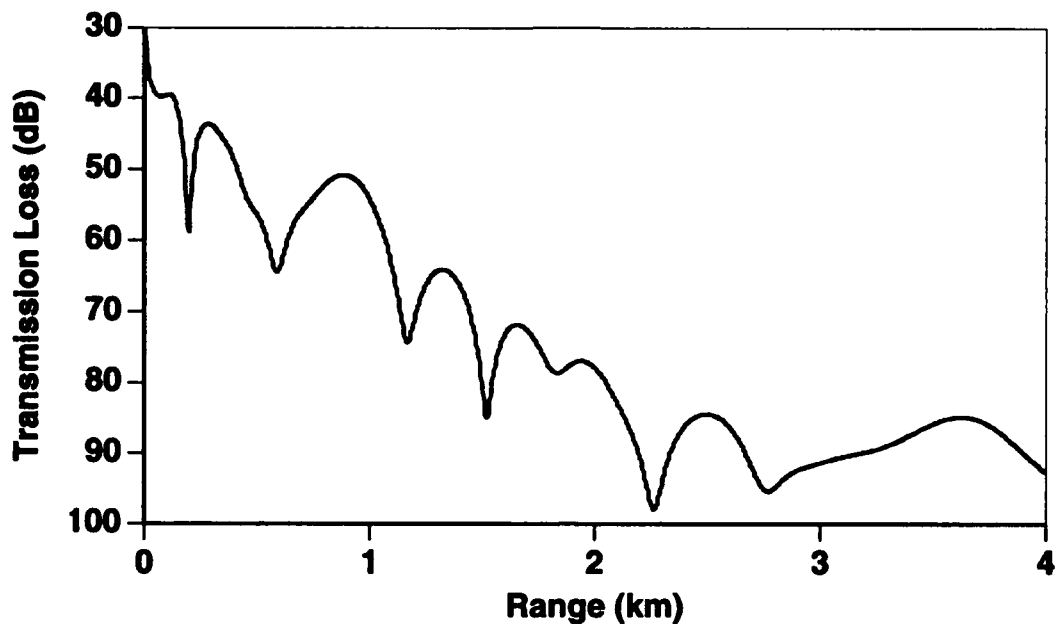


Figure 4a: Case 4a - MIPE

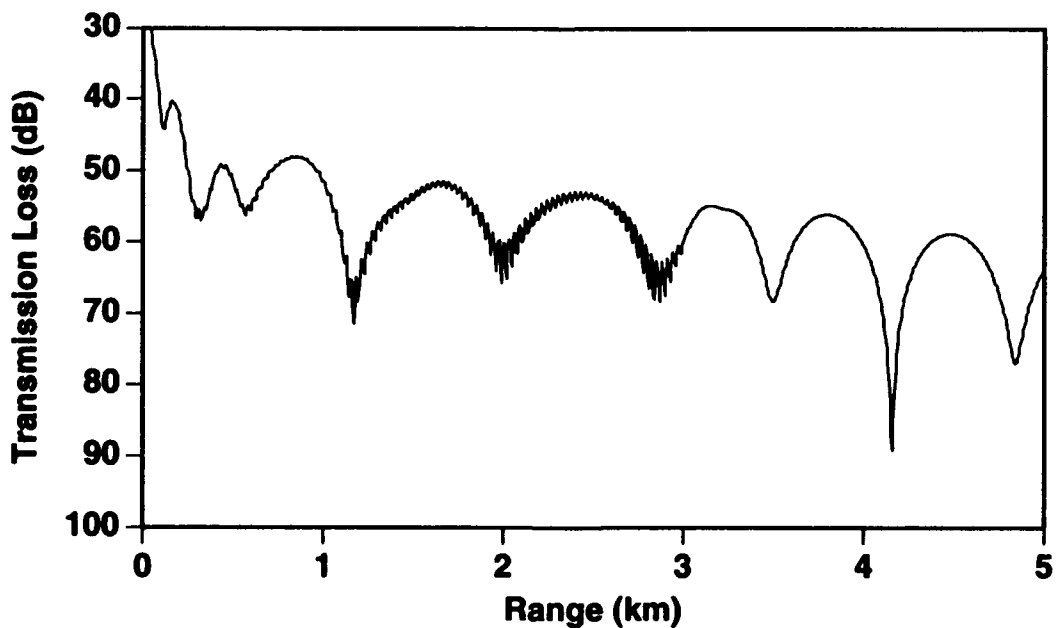


Figure 4b: Case 4b - MIPE

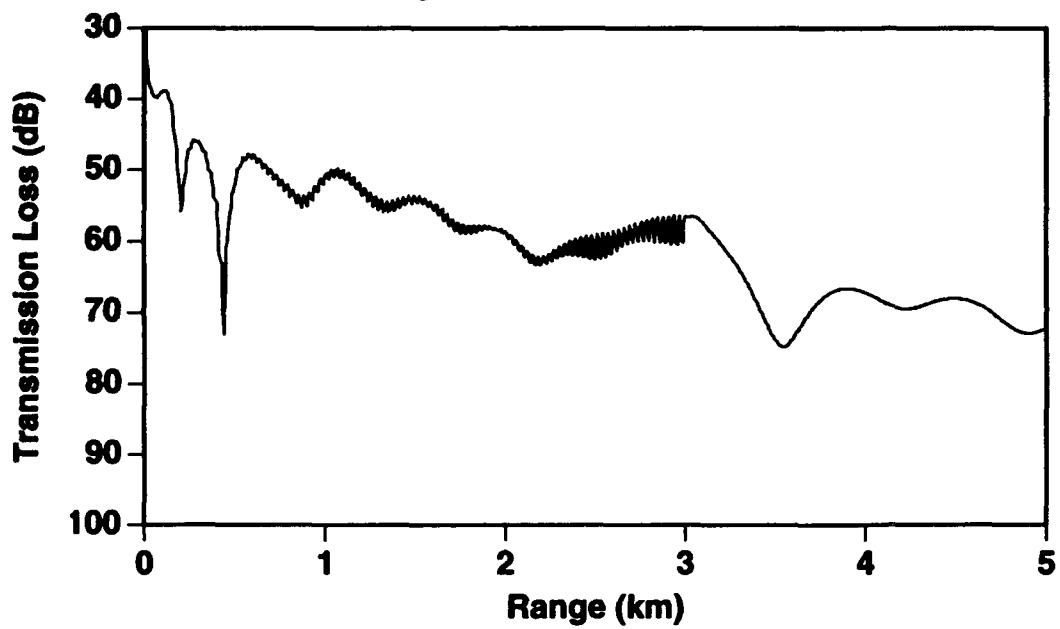


Figure 5a: Case 5a - MIPE

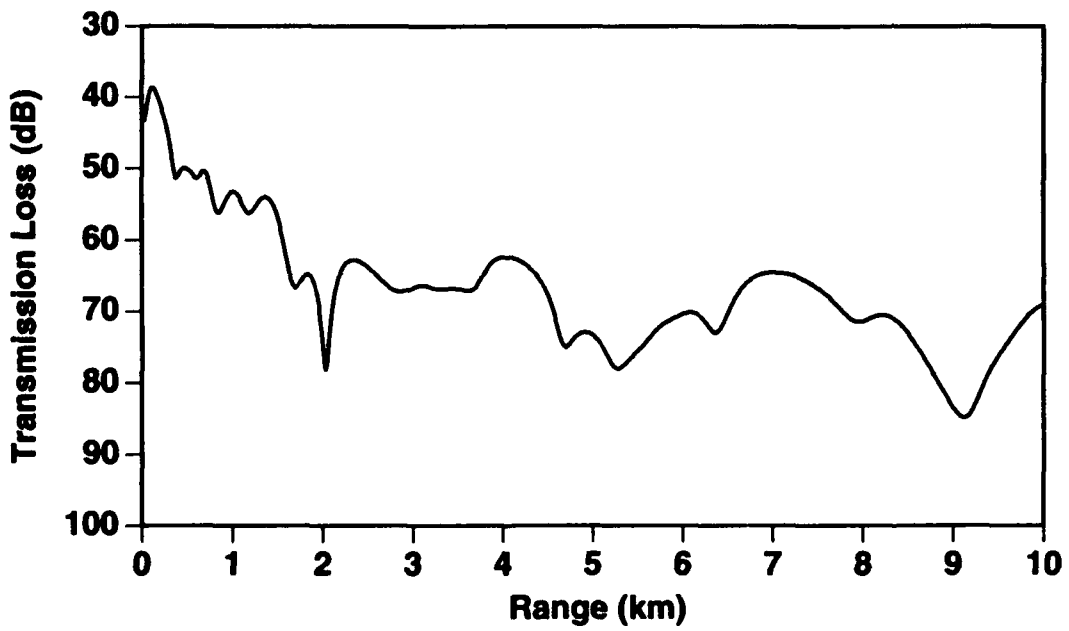


Figure 5b: Case 5b - MIPE

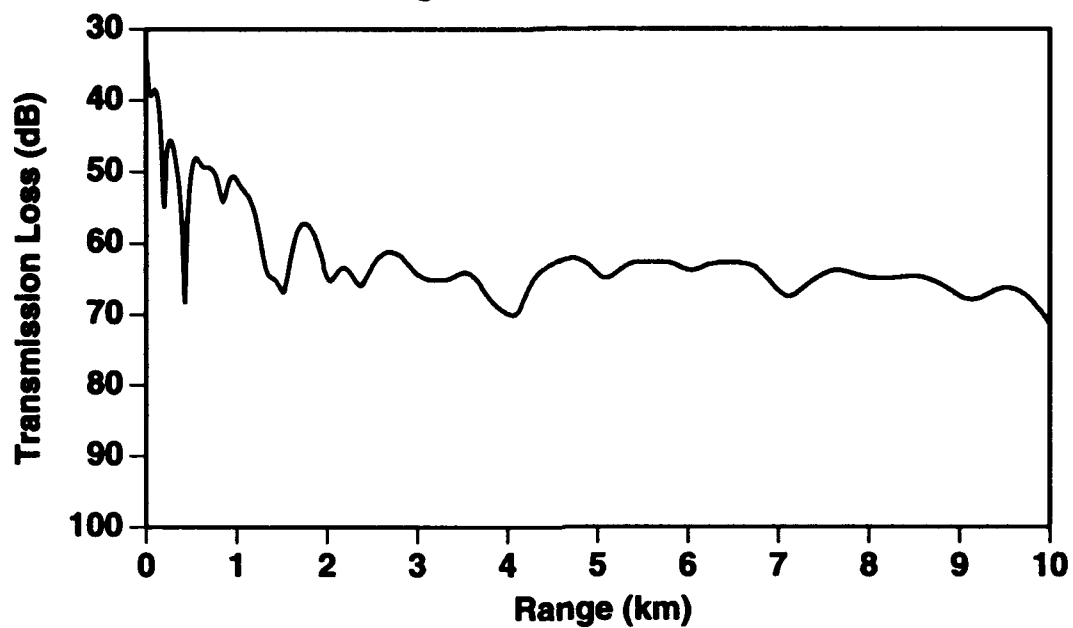
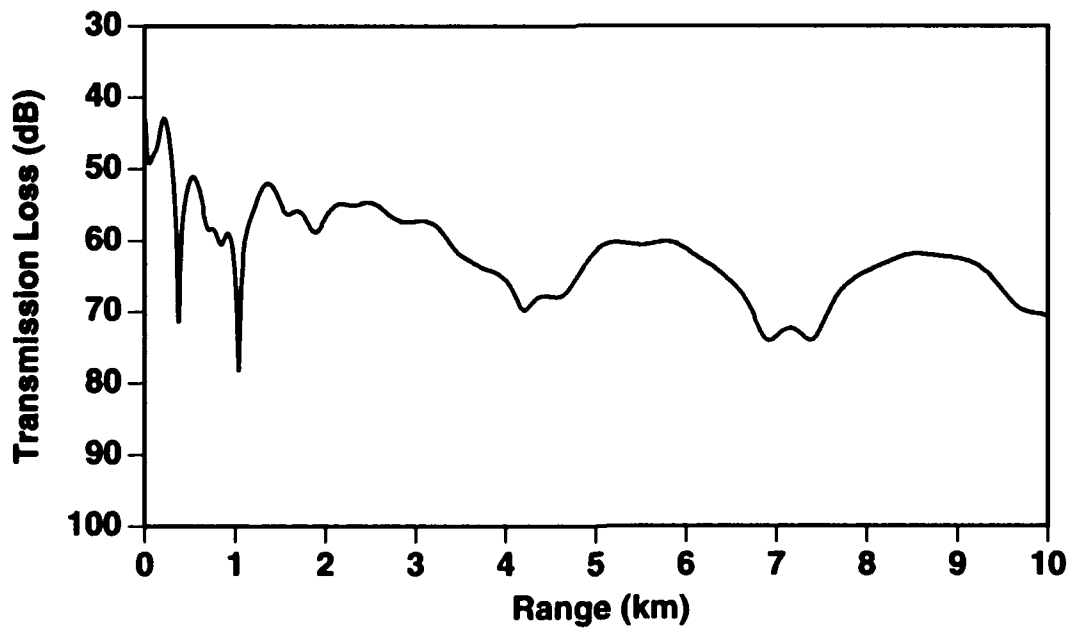
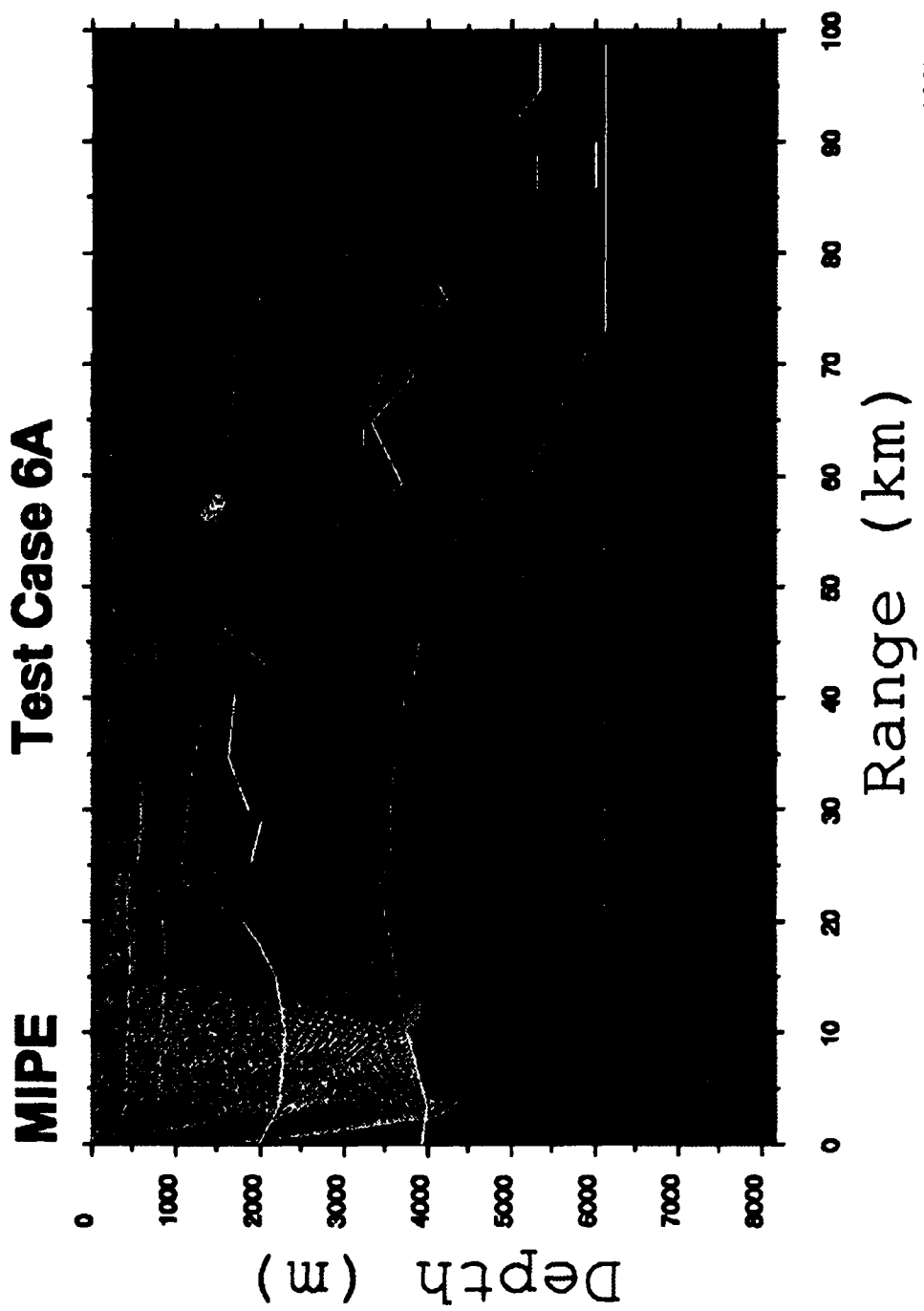


Figure 5c: Case 5c - MIPE





LNP/DSC
KBS & FDT/UM-RSMAS-AMP
Miami, Florida

Figure 6AF

Figure 6a: Case 6a - MIPE

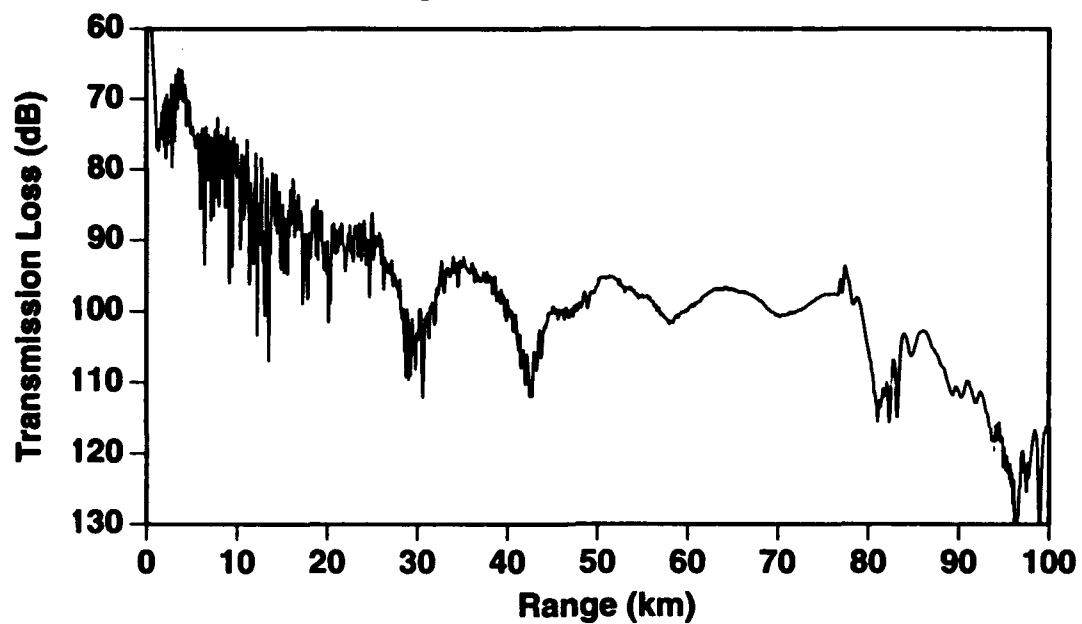


Figure 6b: Case 6b - MIPE

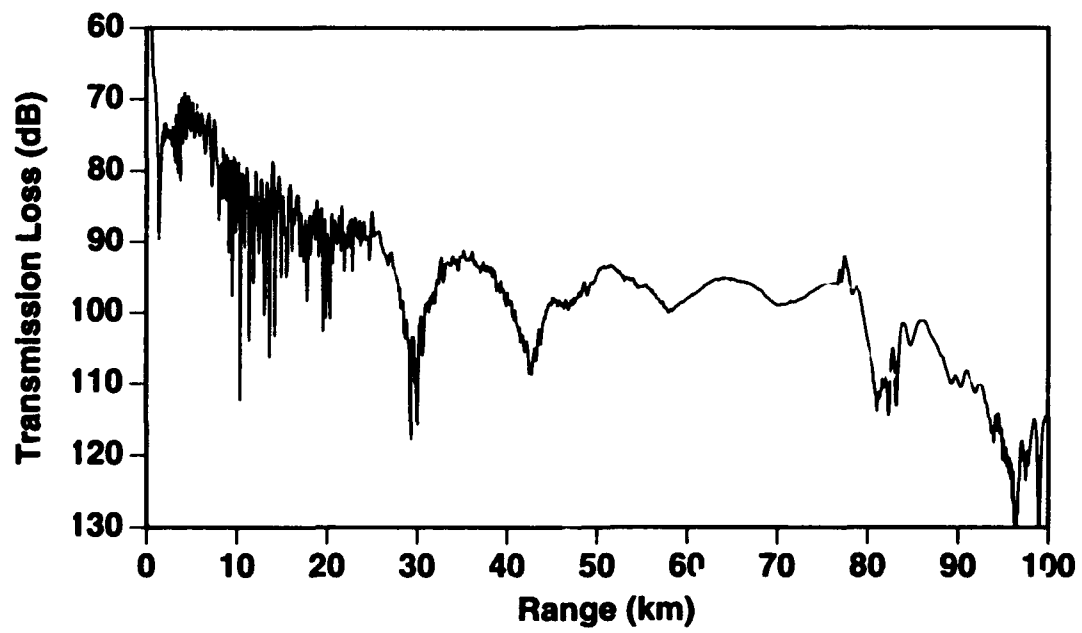


Figure 6c: Case 6c - MIPE

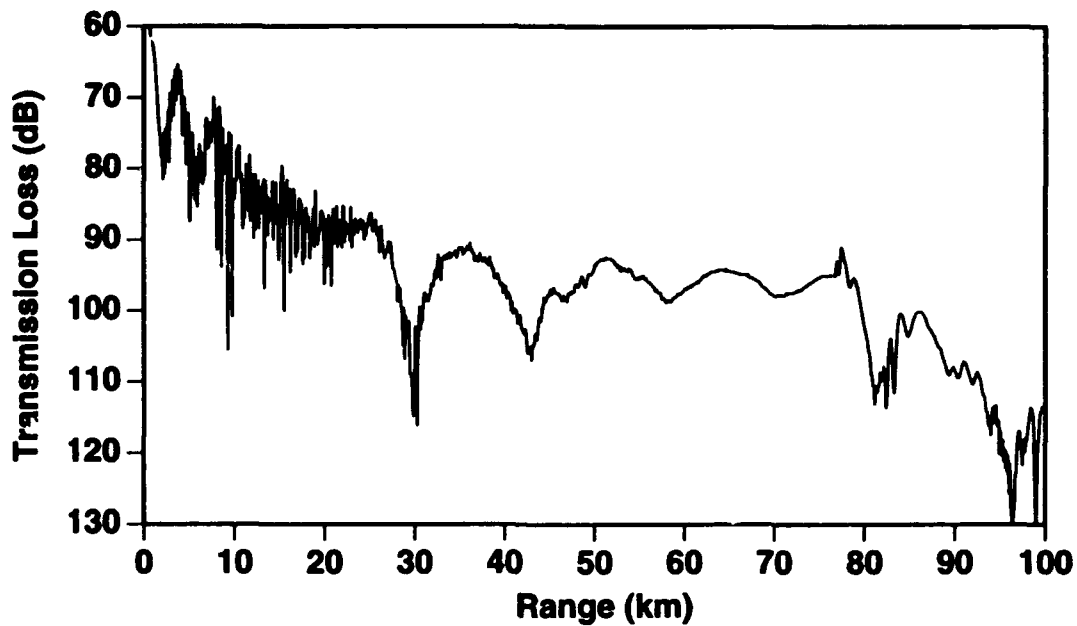


Figure 7a: Case 7 - MIPE

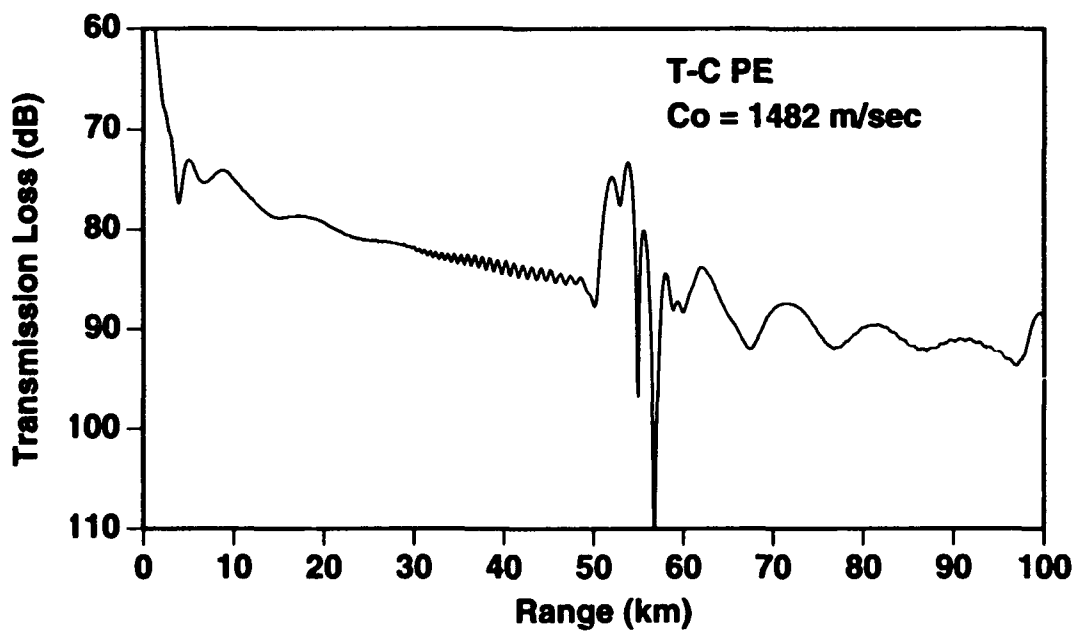


Figure 7b: Case 7 - MIPE

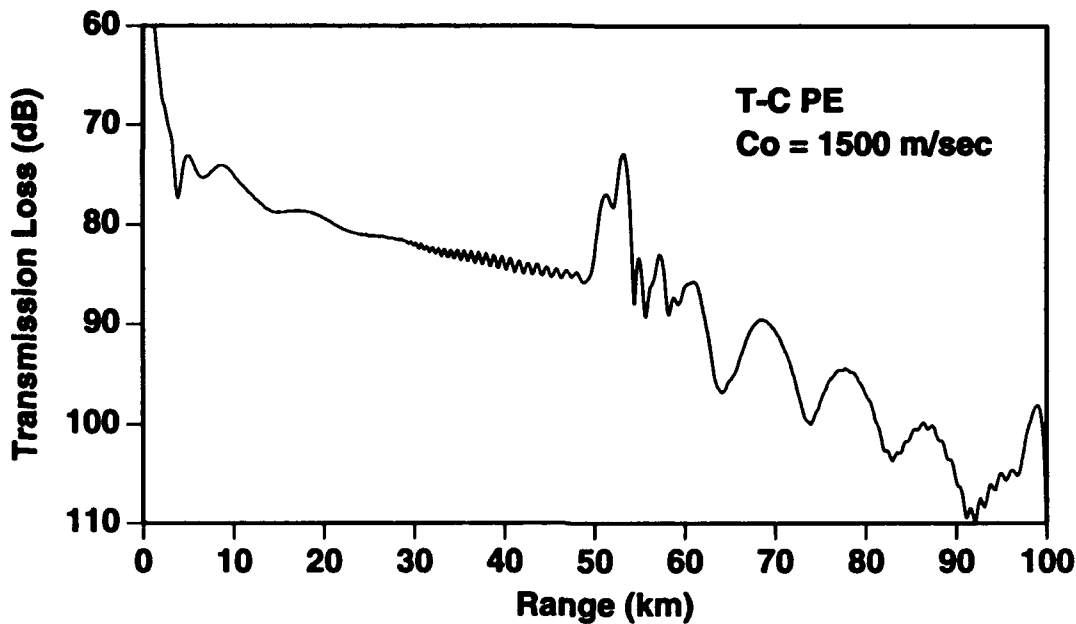


Figure 7c: Case 7 - MIPE

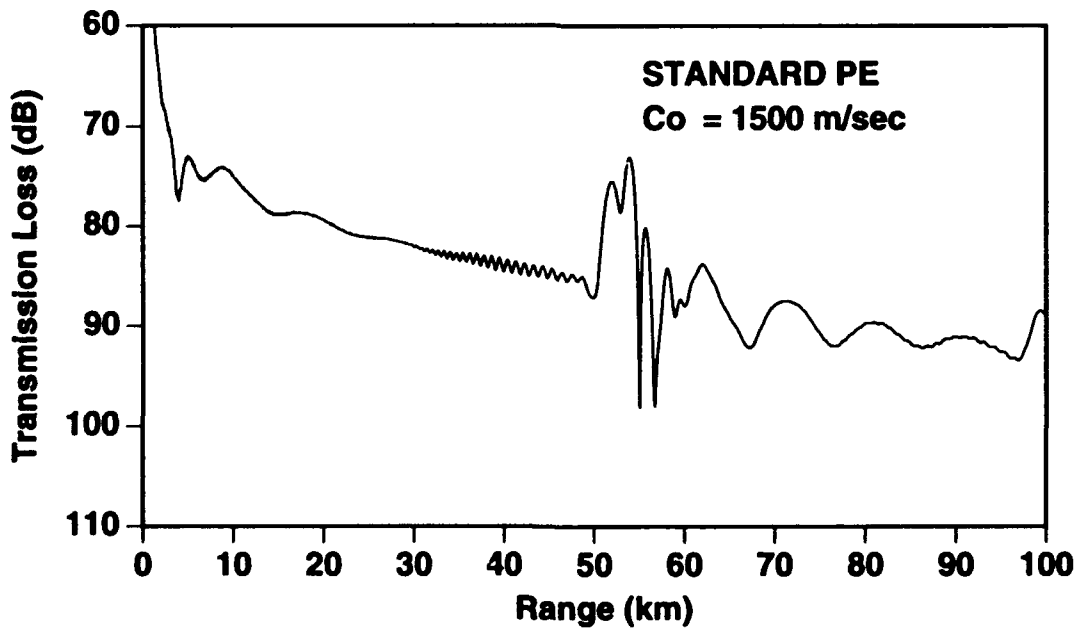
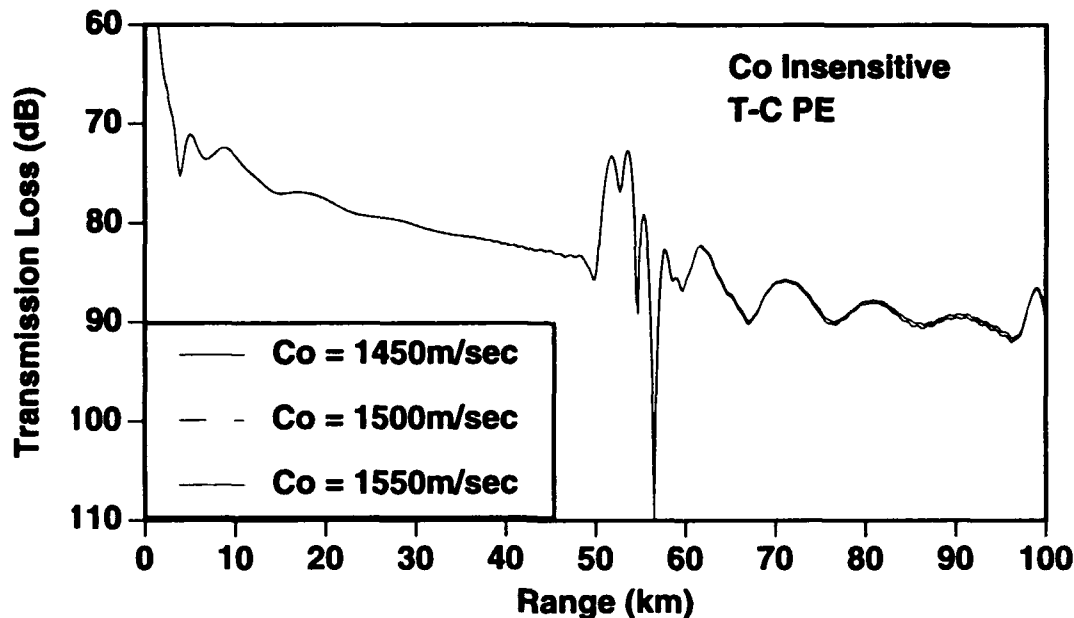


Figure 7d: Case 7 - MIPE



Impedance Bottom Boundary Conditions for the Parabolic-Type Approximations in Underwater Acoustics

J.S. Papadakis

*University of Crete and Institute of Applied
and Computational Mathematics FORTH
P.O.Box 1527,
Heraklion 711 10 Crete, Greece*

1. ABSTRACT

The different parabolic approximations to the reduced wave equation which model acoustic propagation in the ocean usually treat the bottom as an interface and the domain of propagation includes an absorbing layer below the bottom interface. Thus, the boundary problem to be solved has zero boundary conditions at the surface as well as at the bottom boundary. In this paper exact boundary conditions are derived for the physical horizontal bottom boundary. These boundary conditions are non-local but integrable and can be incorporated in finite difference schemes for the parabolic equations [Ref 1,2,3].

2. PARABOLIC APPROXIMATIONS

By factoring the Helmholtz operator and using a linear rational approximation to the square root operator we derive the general wide angle parabolic approximation.

$$\frac{\partial u}{\partial r} = -ik_0 \left(1 - \frac{1 + \left[(n^2(r,z) - 1) + \frac{1}{k_0^2} \frac{\partial^2}{\partial z^2} \right] p}{1 + \left[(n^2(r,z) - 1) + \frac{1}{k_0^2} \frac{\partial^2}{\partial z^2} \right] q} u \right) \quad (\text{GW})$$

where

$u=u(r,z)$ is the acoustic pressure,

$k_0 = \frac{2\pi f}{c_0}$ is the reference wave number,

f is the source frequency,

c_0 is a reference sound speed

$n=n(r,z)$ the index of refraction,

p,q constants.

With $p=1, q=0$ we arrive at the standard parabolic equation

$$2ik_0u_r + u_{zz} + k_0^2[n^2(r,z) - 1]u = 0 \quad (\text{S})$$

which we call S-equation and with $p = \frac{3}{4}$ and $q = \frac{1}{4}$ we arrive at the wide angle Claerbout equation

$$(4k_0^2 + k_0^2(n^2 - 1) + \partial_z^2)u_r = i(2k_0^2(n^2 - 1) + 2k_0\partial_z^2)u \quad (\text{W})$$

which we call the W-equation.

3. BOTTOM-BOUNDARY CONDITIONS

Assuming a horizontal bottom boundary and homogeneous sub-bottom region we derive, from an impedance formulation, the bottom boundary condition for the S-equation.

$$u(r, z_B) = -\frac{\sqrt{i\rho_B}}{\sqrt{2\pi k_0\rho_w}} \int_0^r e^{ik_0(n_B^2 - 1)(r-s)/2} (r-s)^{-1} u_z(s, z_B) ds \quad (\text{IS})$$

where

- $z = z_B$ is the horizontal bottom interface and
- $n_B =$ constant, is the index of refraction for $z \geq z_B$
- $\rho_w =$ the density in the water ($z \leq z_B$)
- $\rho_B =$ the density in the bottom ($z \geq z_B$)

The bottom boundary condition for the IW-equation under the same assumptions is

$$u(r, z_B) = -i\alpha \frac{\rho_B}{\rho_w} u_z(r, z_B) - \alpha\gamma \frac{\rho_B}{\rho_w} \frac{k_0}{2}(p-q) \int_0^r u_z(r-s, z_B) e^{ik_0(p-q)\delta s/2} \cdot \left\{ -iJ_1\left(\frac{k_0}{2}(p-q)\gamma s\right) + J_0\left(\frac{k_0}{2}(p-q)\gamma s\right) \right\} ds \quad (\text{IW})$$

Where

$$\alpha = \left(\frac{q}{k_0^2[1+q(n_B^2 - 1)]} \right)^{1/2} \quad \gamma = \frac{1}{q[1+q(n_B^2 - 1)]} \quad \delta = \frac{2q(n^2 - 1) + 1}{q[1+q(n_B^2 - 1)]}$$

Finally, if we assume that the subbottom region supports shear waves the bottom boundary condition for the S-equation with elastic bottom becomes

$$u(r, z_B) = \frac{k_0}{4\pi} \int_0^r u_z(s, z_B) \int_{-\infty}^{\infty} e^{ik_0(\lambda-1)(r-s)/2} f(n_B^2 - \lambda) d\lambda ds \quad (\text{IFEL})$$

where

$$f(n_B^2 - \lambda) = -\frac{i}{k_0} \frac{\rho_B}{\rho_w} (n_B^2 - \lambda)^{-1/2} \cdot \left\{ \frac{k_0^4}{k_s^4} (n_s^2 - 2\lambda)^2 + 4 \frac{k_0^4}{k_s^4} \lambda (n_B^2 - \lambda)^{-1/2} (n_s^2 - \lambda)^{1/2} \right\}$$

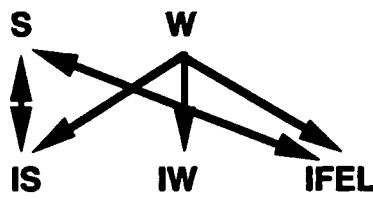
where $k_s = 2\pi f / c_s$, $n_s = c_o/c_s$ where c_s = the shear speed in the bottom. For a brief derivation of the above formulas see Appendix A.

4. NUMERICAL ALGORITHMS AND COMPUTER CODE

We apply an implicit finite difference scheme to march the field in the r-direction for both S and W-equations. We use the same Δr , Δz in numerically representing IS, IW, and IFEL boundary conditions and obtain a computer code which uses either the S or W-equations combined in the following diagram with the boundary conditions to calculate the outgoing wave for the Helmholtz's equation.

Equations

Boundary Conditions



Thus we have the choice of the following codes, S+IS, S+IFEL in the case of narrow angle propagation and the codes W+IS, W+IW, and W+IFEL in the case of wide angle propagation.

It should be pointed out that the IFEL bottom boundary condition the analytic transform of the function can not be calculated and a Fast Fourier Transform was implemented. However, the function $f(n_B^2 - \lambda)$ to be transformed is singular at 0 and ∞ . For this reason at zero a careful analysis has to be applied in order for the singularity to be integrated correctly (see[3]). At infinity a Hanning window is used to amend the problem.

5. APPLICATIONS

Here some typical examples of sound propagation in the ocean will be presented where an implicit finite difference code to the parabolic equations S and W will be combined with numerical codes for the non-local boundary conditions IS, IW, and IFEL.

Example I This is a well known example suggested by Dr. H. Bucker. The parameters of the problem are: Water depth 240 m, Frequency 100 Hz, Source depth 30 m, Receiver depth 90 m, the water density is 1 gm/cm³, bottom density is 2.1 gm/cm³, with no attenuation. The sound speed profile in the water consists of linear segments as follows: at 0 depth 1500 m/sec, at 120 m depth 1498 m/sec and at the bottom interface (240 m) 1500 m/sec. In the subbottom regions the sound speed is 1550 m/sec.

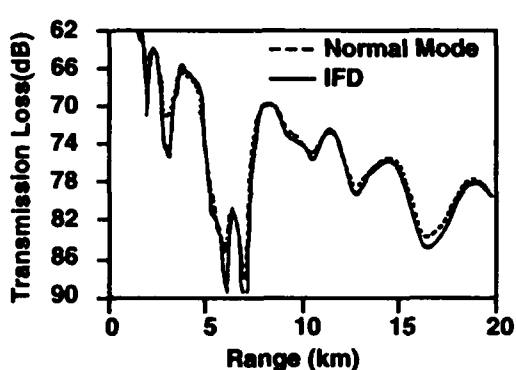


Figure 1: The solutions are given by normal mode theory and the IFD code by Lee and Botseas.

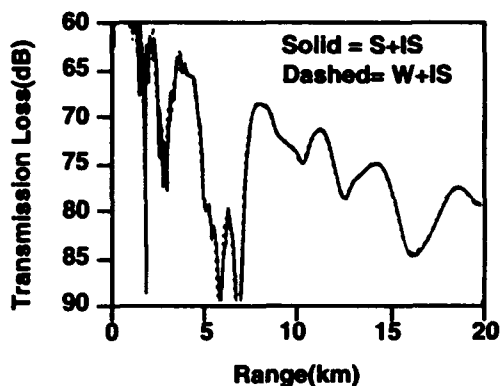


Figure 2: The solutions are given by implementation of the codes W+IS and S+IS

Example II. This example is a case of a range independent environment consisting of an isovelocity water column. The parameters of the problem are: frequency 250 Hz, water depth 100 m sound speed in the water 1500 m/sec, density in the water 1.0 gm/cm³, density in the bottom 1.2 gm/cm³, sound speed in the bottom 1590 m/sec, source depth 99.5 m and a receiver depth of 99.5 m, the attenuation in the bottom is 0.5 dB/wavelength.

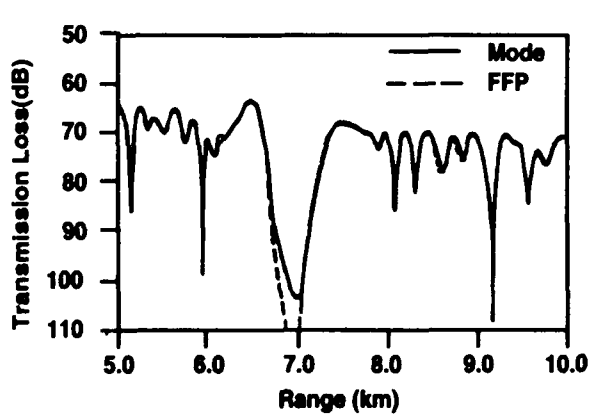


Figure 3: Normal mode (SNAP) and Fast Field Program solutions.

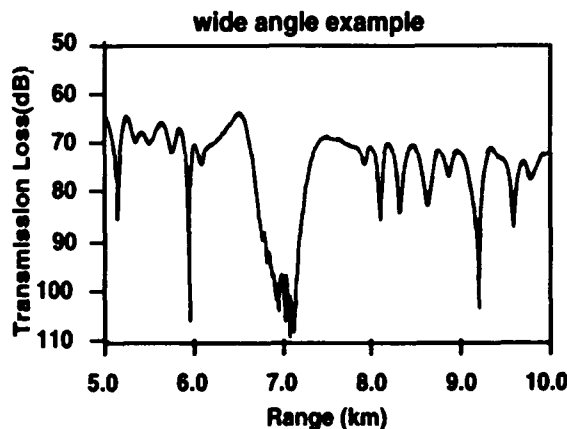


Figure 4: The solution is given by W+IS.

Example III. In this example an elastic bottom is assumed. The parameters are: Frequency 500 Hz, water depth 100 m, source depth 50 m, receiver depth 50 m, sound speed in the water 1500 m/sec sound speed in the bottom 1550 m/sec, water density 1.0 gm/cm³, bottom density 1.2 gm/cm³, bottom attenuation 1 dB/wavelength, shear speed in the bottom 600 m/sec, shear attenuation 0.5 dB/wavelength.

Figure 5 has the propagation loss versus range from the SAFARI [Ref. 9] program and S+IS code without shear. Figure 6 has the results from SAFARI and S+SI with shear at the bottom.

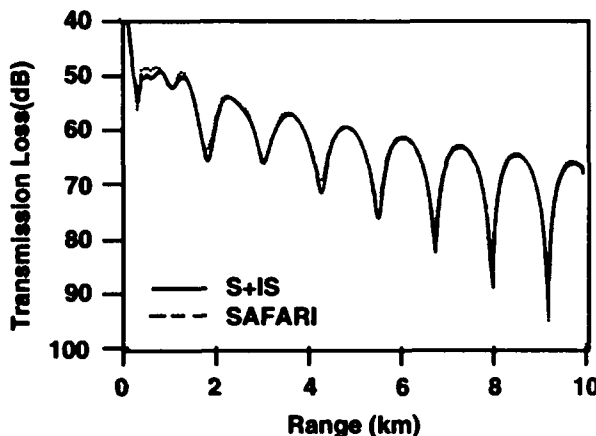


Figure 5. Fluid case.

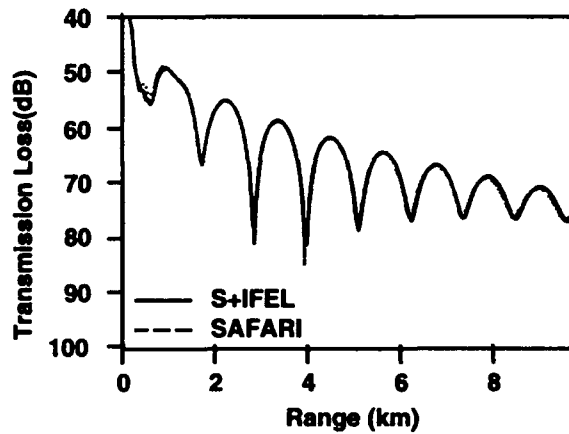


Figure 6. Elastic case.

REFERENCES

1. Lee, D., and McDaniel, S.T., *Ocean Acoustic Propagation by Finite Difference Methods*, Pergamon Press, 1987.
2. Papadakis, J.S., "Impedance Formulation of the Bottom Boundary Condition for the Parabolic Equation Model in Underwater Acoustics", NORDA Parabolic Equation Workshop 31 March -3 April 1981.
3. Papadakis, J.S., et al, "A New method for a Realistic Treatment of the Sea Bottom in the Parabolic Approximation" (to appear in JASA)
4. Campbell, G. A. and Foster, R. M., *Fourier Integrals for Practical Applications*, (d. Van Nostrand Company, 1951), p 53.
5. Collins, M.D., "A high-order parabolic equation for wave propagation in an ocean overlying an elastic bottom", *J. Acoust. Soc. Am.* **86** (1989) 1459-1464.
6. Collins M.D., "Applications and time-domain solution of high-order parabolic equations in underwater acoustics", *J. Acoust. Soc. Am.* **86** (1989) 1099-1103.

7. Wetton, B.T. and Brooke, G.H., "One-way wave equations for seismoacoustic propagation in elastic waveguides", *J. Acoust. Soc. Am.* **87** (1989) 624-632.
8. Tolstoy, I., Clay, C.S. *Ocean Acoustics* (McGraw-Hill, New York, 1966), p25.
9. Schmidt, H., "SAFARI, Seismo-Acoustic Fast field Algorithm for Range Independent Environments, User's Guide", SACLANTCEN SR-113 SACLANTCEN, La Spezia, Italy.

APPENDIX A. Derivation of the impedance conditions for the Parabolic Equation.

We derive the impedance boundary condition for the (GW) equation. The continuity conditions at the water-bottom interface are

$$u^w(r, z_B) = u^B(r, z_B) \quad (1)$$

$$u_z^w(r, z_B) = \frac{\rho_w}{\rho_B} u_z^B(r, z_B) \quad (2)$$

where u^w and u^B are the function u at the water layer and the bottom layer respectively.

Applying a Fourier transform [Ref. 4] with respect to r to equations (1) and (2) we get the impedance condition

$$\frac{U^w(\lambda, z_B)}{U_z^w(\lambda, z_B)} = \frac{\rho_B}{\rho_w} \frac{U^B(\lambda, z_B)}{U_z^B(\lambda, z_B)}$$

where U is the Fourier transform of u . Applying the same Fourier transform to equation (GW) for $z \geq z_B$ we have

$$2\pi i \lambda \left[k_0^2 + qk_0^2(n_B^2 - 1) + q\partial_z^2 \right] U^B = i \left[k_0^3(p - q)(n_B^2 - 1) + k_0(p - q)\partial_z^2 \right] U^B$$

which is a second order linear differential equation in the depth function $U^B(\lambda, z_B)$. Assuming only an outgoing wave as $z \rightarrow \infty$ we arrive at the equation

$$\frac{U^w(\lambda, z_B)}{U_z^w(\lambda, z_B)} = -i\alpha \frac{\rho_B}{\rho_w} \left(\frac{2\pi i \lambda - i \frac{k_0(p - q)}{q}}{2\pi i \lambda - i \frac{k_0(p - q)(n_B^2 - 1)}{1 + q(n_B^2 - 1)}} \right)^{1/2}$$

Applying the inverse Fourier transform and after some manipulations we derive the (IW) equation. With the same process the (IS) and (IFEL) equations are derived.

Coupled Modes for Rapid Range-Dependent Modeling

Michael B. Porter, Carlo M. Ferla and Finn B. Jensen

SACLANT Undersea Research Centre
I-19026 La Spezia, Italy

Abstract

Normal mode models are widely used for solving range-*independent* ocean acoustic problems. The approach generalizes to range-*dependent* problems by dividing the problem into a sequence of range-independent segments and using normal modes to represent the solution in each segment. While this coupled-mode approach has proven extremely useful for checking other models, it has generally been considered uncompetitive with parabolic equation (PE) algorithms in terms of run time.

We show that an optimized coupled-mode algorithm is practical and in fact competitive with the parabolic equation. To develop an efficient algorithm we take advantage of a widely used finite-difference algorithm for solving the range-independent normal mode problems. As in PE models, we make the *a priori* assumption that the field is dominated by the outgoing component. We also bypass the calculation of mode coupling matrices, and compute the mode amplitudes in a new segment directly by projecting the pressure field onto the new mode set. This allows the solution to be constructed by a simple marching. We illustrate the algorithm using several oceanic scenarios involving range-dependent oceanographic and bathymetric features.

1 Introduction

A common starting point for ocean acoustics problems is the Helmholtz equation in two-dimensions:

$$\frac{1}{r} \frac{\partial}{\partial r} \left(r \frac{\partial p}{\partial r} \right) + \rho(z) \frac{\partial}{\partial z} \left(\frac{1}{\rho(z)} \frac{\partial p}{\partial z} \right) + \frac{\omega^2}{c^2(r,z)} p = \frac{-\delta(z - z_s)\delta(r)}{2\pi r}. \quad (1)$$

where ρ is the density $c(r, z)$ the sound speed and ω is the circular frequency of the source. This equation must also be augmented with appropriate boundary conditions.

One way of solving the Helmholtz equation is to divide the problem into a sequence of N range-independent segments in range [1] as illustrated in Fig.1. Then, within each range-segment the exact solution can be constructed using normal modes as a sum of right- and left-traveling waves. Neglecting contributions from higher-order modes or from the continuous spectrum, the general solution in the jth segment can be written as follows:

$$p^j(r, z) = \sum_{m=1}^M [a_m^j H1_m^j(r) + b_m^j H2_m^j(r)] Z_m^j(z), \quad (2)$$

where $H1,2(r) = H_0^{(1,2)}(r)$ are Hankel functions, and k_m^j and $Z_m^j(z)$ are solutions of the depth-separated equation:

$$\left. \begin{aligned} \rho(z) \frac{d}{dz} \left(\frac{1}{\rho(z)} \frac{dZ(z)}{dz} \right) + \left(\frac{\omega^2}{c^2(z)} - k^2 \right) Z(z) &= 0 \\ Z(0) &= 0 \\ \frac{dZ}{dz}(D) &= 0 \end{aligned} \right\}. \quad (3)$$

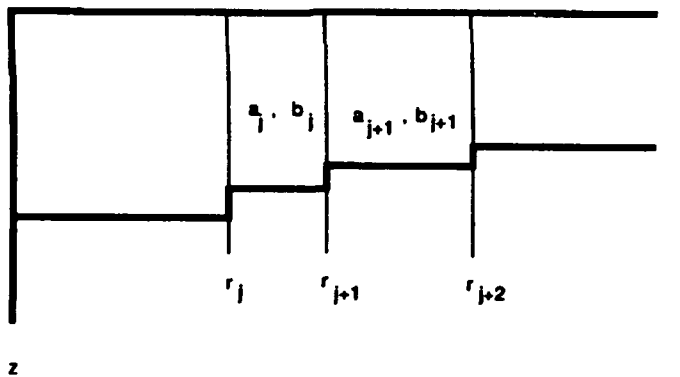


Fig. 1 Segmentation for the coupled mode formulation

The boundary conditions imposed imply a pressure release surface located at $z=0$ and a perfectly rigid bottom located at $z=D$. Then, imposing continuity of pressure and particle velocity along each of the vertical interfaces leads to a large block-banded matrix for the mode coefficients a_m^j and b_m^j in each segment. The pressure field is then computed by summing up the modes in each segment as given in Eq.2.

This type of approach has been used in the COUPLE model [1] and successfully applied to a number of benchmark problems [2,3]. While extremely useful for providing benchmark

solutions the direct solution of the Helmholtz equation in this manner is usually not practical for ocean acoustics problems because of the execution time.

Instead, for range-dependent problems the method of choice is often a PE type solution. This approach takes advantage of the fact that ocean acoustics problems are often dominated by just the right-traveling component of the solution, leading to equations which can be rapidly solved by marching forward in range.

Our objective in this paper is to examine the alternative of using coupled-modes in a similar one-way fashion. The key question is whether or not an optimized marching solution based on normal modes is competitive in terms of run-time with existing PE models.

2. One-way coupled normal modes

To obtain the one-way formulation in each segment we seek a solution in the form of just a right-traveling wave:

$$p^j(r, z) = \sum_{m=1}^M a_m^j Z_m^j(z) H1_m^j(r). \quad (4)$$

With the range of possible solutions restricted to just the right-traveling component we must relax the continuity conditions on vertical interfaces. For the sake of comparison with existing models we have implemented the one-way coupled mode solution using pressure-matching at interfaces discarding the condition of continuity of particle velocity. However, as discussed in Ref.[3] this informal step can have important implications for solution accuracy. A single-scatter type condition yields much improved results and is normally our method of choice.

The condition of continuity at each interface can therefore be written:

$$\frac{1}{\sqrt{\rho_{j+1}}} \sum_{m=1}^M a_m^{j+1} Z_m^{j+1}(z) = \frac{1}{\sqrt{\rho_j}} \sum_{m=1}^M a_m^j H1_m^j(r_j) Z_m^j(z). \quad (5)$$

Taking advantage of the mode orthogonality we apply the operator:

$$\int (\bullet) \frac{Z_l^{j+1}(z)}{\sqrt{\rho_{j+1}(z)}} dz, \quad (6)$$

yielding:

$$a_l^{j+1} = \sum_{m=1}^M a_m^j H1_m^j(r_j) \bar{c}_{lm}, \quad l = 1, \dots, M, \quad (7)$$

where,

$$\bar{c}_{lm} = \int \frac{Z_l^{j+1}(z) Z_m^j(z)}{\sqrt{\rho_j(z) \rho_{j+1}(z)}} dz. \quad (8)$$

The denominator in this coupling term is a geometric mean of the analogous terms obtained using pressure-matching and velocity matching.

In matrix form, Eq. (7) can be written:

$$\mathbf{a}^{j+1} = \mathbf{CH}_1^j \mathbf{a}^j. \quad (9)$$

Well-polished codes exist for solving for the normal modes in quite complicated multilayered environments. A popular technique uses a standard centered finite-difference approximation combined with Richardson extrapolation [4]. The resulting tridiagonal algebraic eigenvalue problem is solved using roughly $30 M N_z$ floating-point operations where N_z is the number of grid points in depth and M is the number of modes calculated. Typically, $M \approx N_z / 10$ so that we obtain an operation count of $3 N_z^2$. An algorithm for doing the one-way mode coupling has been incorporated in two popular implementations of the modal algorithm (KRAKEN [5] and SNAP [6]. We refer to the one-way version of SNAP as C-SNAP and will be showing results obtained with that model. Timings and results are similar for the coupled-mode version of KRAKEN.

The modes calculated by these models are provided on a finely tabulated grid of depth points. The m th vector is then used to define the m th column of a matrix \mathbf{U}^j . For an isodensity problem, we can then approximate the coupling matrix by the discrete form:

$$\mathbf{C}^j \approx (\mathbf{U}^{j+1})' \mathbf{U}^j, \quad (10)$$

which is equivalent to evaluating the coupling integral by the trapezoidal rule. (For a variable-density problem this equation is slightly modified.) Substituting in Eq. (9) we obtain:

$$\mathbf{a}^{j+1} \approx \left\{ (\mathbf{U}^{j+1})' [\mathbf{U}^j (\mathbf{H}_1^j \mathbf{a}^j)] \right\}. \quad (11)$$

We can describe the steps in this equation as follows: one advances the phase of the coefficients to the next segment, then one sums up the modes to compute the field just to

the left of the interface and finally, one projects the pressure field onto the mode set in the next segment. Computing the coupling matrix would involve the calculation of the matrix-matrix product $(U^{j+1})' U^j$ but when the operations are done in the order indicated by Eq. (11), one performs only the operation of a matrix times a vector and therefore obtains a significant savings in execution time.

Let us consider the alternative PE approach. The pressure field is represented in terms of an envelope function as:

$$p(x, z) = \psi(x, z)e^{ik_0 x} \quad (12)$$

where the envelope function then satisfies

$$\frac{\partial \psi}{\partial r} = \frac{ik_0}{2} \left(n^2 - 1 + \frac{1}{k_0^2} \frac{\partial^2}{\partial z^2} \right) \psi. \quad (13)$$

This is the standard parabolic equation originally considered by Tappert [7]. In fact, we shall be presenting comparisons with a popular implicit finite-difference PE (IFDPE)[8] which uses a higher-order approximation to the square root operator. The PE equation is then discretized using a simple centered-finite difference operator. A single range-step then requires solving a linear system and doing a matrix-vector multiply. The matrices involved are all tridiagonal so that about $10 N_z$ floating-point operations per range step are required, where N_z is the number of points in the depth grid. The complete solution is thus calculated in $10 N_z N_r$ operations where N_r is the number of range steps.

When the normal mode problem is solved using the same centered finite-difference approximation the cost of computing the modes at a single range is roughly $3N_z^2$ operations. Thus, if N_{prof} stairsteps are required to define the environment, the total cost is $3N_z^2 N_{prof}$ operations. (The final mode synthesis typically uses a small percentage of additional time, although in cases where many source/receiver combinations are involved it can dominate.)

Thus we have

$10 N_z N_r$	IFDPE
$3N_z^2 N_{prof}$	Normal Mode.

For range-independent environments ($N_{prof} = 1$) where the field is desired beyond a few water depths $N_r > N_z$ the normal mode solution is faster. For this reason normal mode solutions have generally been favored for range-independent environments.

However, for range-dependent environments the normal mode calculation must be done in each segment where the environment is updated. For gradually varying environments a few updates suffice and the normal mode approach is significantly faster. For strongly varying environments it may be necessary to use a new profile every wavelength in range. In this case, the standard PE approach is significantly faster.

The question then is, do typical ocean environments vary enough to favor PE solutions or coupled normal mode solutions? We can give a partial answer by considering some example problems.

3 Propagation over a seamount

The environment is illustrated schematically in Fig. 2. The sound speed profile is a canonical deep water profile. Range-dependence in the problem comes from an idealized seamount that is symmetric and extends from 80 km to 120 km and is 1000 m high. The transmission loss calculated using C-SNAP is shown in Fig. 3 for a source depth of 100 m and a source frequency of 50 Hz. In order to obtain a solution which is sufficiently narrow-angled that the PE solution is valid, we have used a modal starting field retaining only those modes which are waterborne; that is, turned before hitting the bottom. The field shows a convergence zone type pattern involving a beam of energy cycling up and down the water column. At a range of about 90 km the beam hits the seamount and reflects at steeper angles.

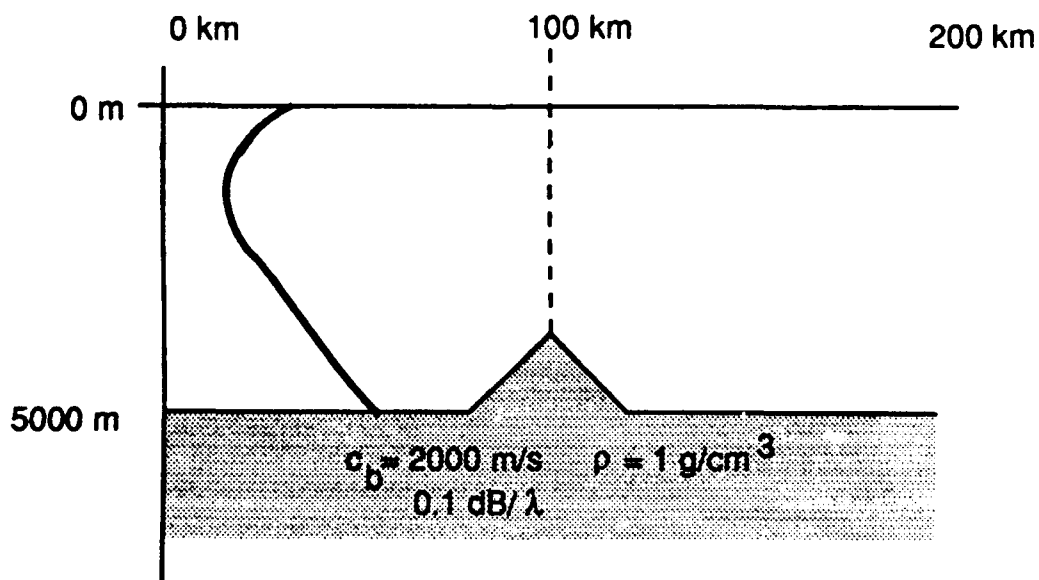


Fig. 2 Schematic of the seamount problem

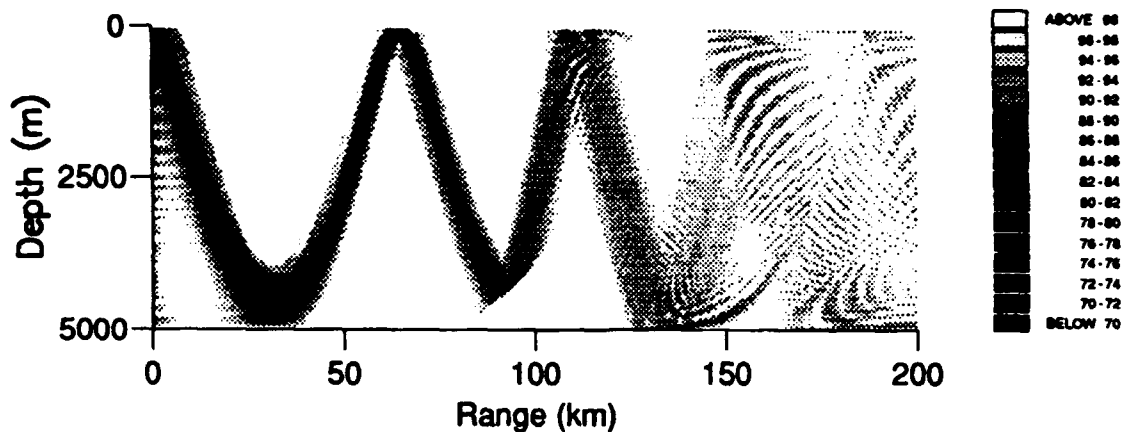


Fig. 3 Coupled mode transmission loss for the seamount problem

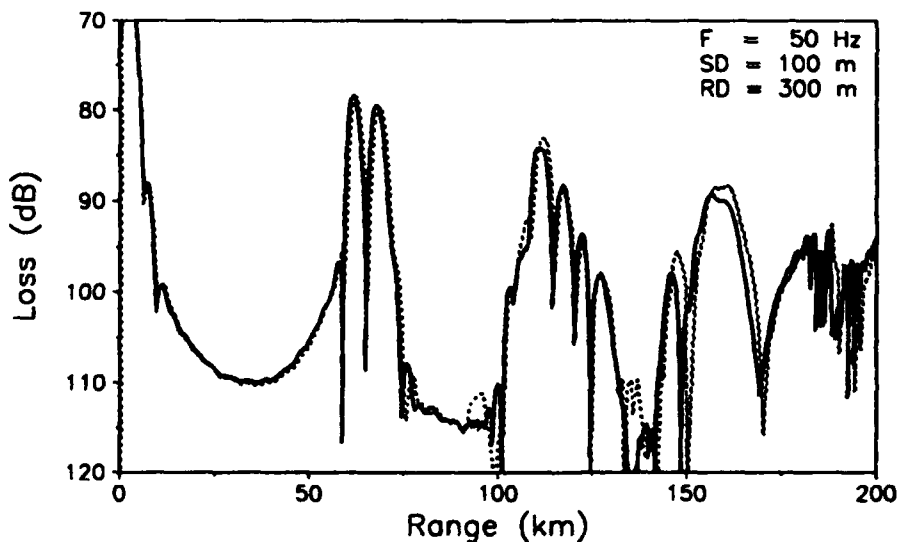


Fig. 4 Transmission loss for the seamount problem at a receiver depth of 300 m (C-SNAP (—), IFDPE (---)).

We have also solved this problem using the IFDPE model and obtained a plot that is visually indistinguishable from the coupled-mode result in Fig. 3. A more quantitative sense of the error is seen by comparing a slice from the transmission loss plot taken at a receiver depth of 300 m as shown in Fig. 4. We observe that there is excellent agreement between

the IFDPE and one-way coupled-mode solutions. The execution time for both models is approximately half an hour on a roughly 1 megaflop machine (VAX 8600).

4 Propagation over a continental slope

A schematic of the environment is shown in Fig. 5. This type of environment is a prototype of continental slope propagation where the initial 500 m in range represents a continental shelf. (This problem is a modified version of benchmark problem 5 from the PE Workshop II [9] with the sediment layer removed to obtain a problem solvable by the COUPLE program.)

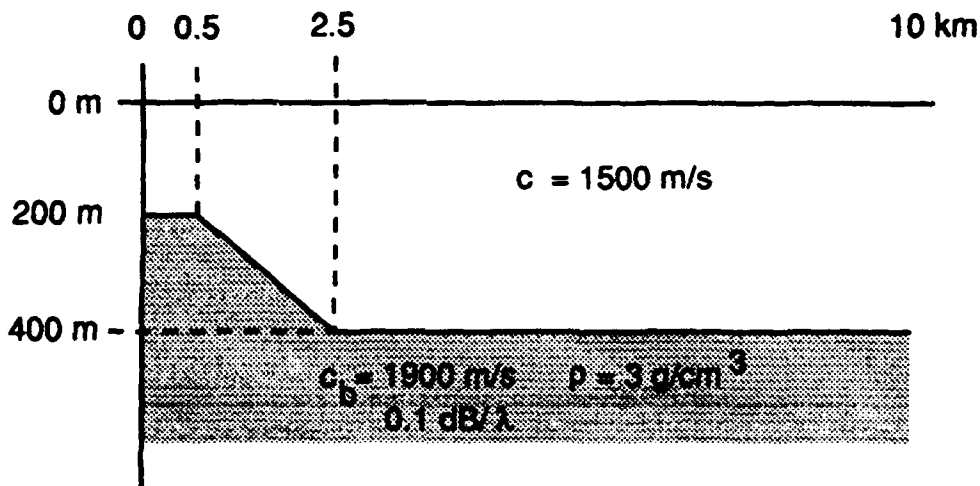


Fig. 5 Schematic of the continental slope problem.

Taking a source depth of 100 m and the source frequency of 25 Hz we obtain with C-SNAP the transmission loss shown in Fig. 6. Again, in order to accommodate the angle limitations of the PE we have chosen to use a narrow-angle source generated using just the discrete modes at the origin. The field shows a somewhat complicated 4-8 mode interference pattern. Once again, the IFDPE results (not shown) were indistinguishable in terms of the grey shade plot

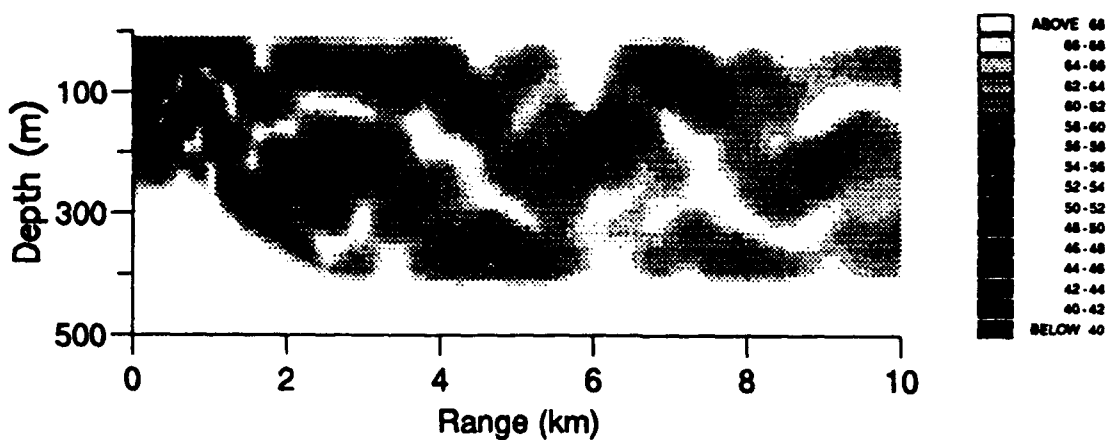


Fig. 6 Transmission loss for the continental slope problem.

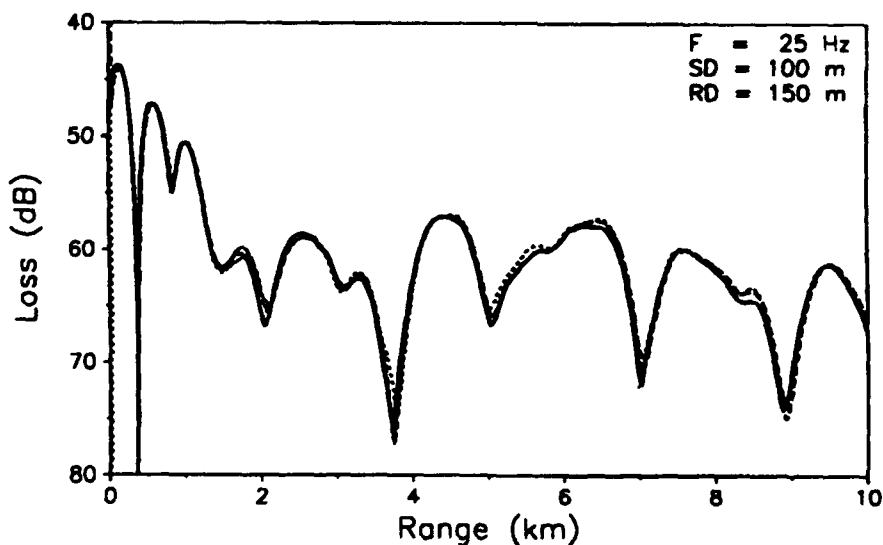


Fig. 7 Transmission loss for the continental slope problem at a receiver depth of 150 m (C-SNAP (—), IFDPE (---), COUPLE (- · - ·) }

Again to be precise about the level of agreement between the models we turn to a line plot taken at a fixed receiver depth of 150 m. This problem involves few modes so that we can also provide an independent check using the full two-way coupled-mode solution (COUPLE). The comparison of C-SNAP, IFDPE and COUPLE is shown in Fig. 7 showing

excellent agreement among all three models. As in the previous test problem, the one-way coupled-mode (C-SNAP) and IFDPE solutions required comparable times (approximately 1 minute).

5 Summary and Conclusions

We have shown that the normal mode approach offers a viable alternative to PE modeling for range-dependent environments with run-times which, in our test problems, are roughly comparable. A precise comparison of execution time is complicated by the fact that it is difficult to define an error criterion which all would agree is meaningful to the user. Which is more important: accuracy in the convergence zone position or in its level? Furthermore, there are a number of parameters in each model which can be tuned to optimize execution time (e.g., source spectrum, range and depth grids, angular width of the PE or modal spectrum).

In favor of the coupled normal mode approach we note that while much work has been done to improve PE's little work has been done on optimizing coupled normal modes and, indeed, there seem to be numerous possibilities for further improvement. For instance, generalized 'wedge-modes' [10] may allow for much larger range-steps.

Furthermore, the normal mode approach allows multiple source depths to be handled with negligible additional effort since execution time is dominated by the time required to compute the modes, a calculation which does not need to be repeated for additional depths. This benefit is particularly important when matched-field processing is used to localize sources by scanning over source position (see Ref. [11] and references therein).

It seems probable that there will always be a place for PE models. Circumstances favoring their use are 1) problems with range-dependence along the entire track and 2) problems where the field is desired on a fine range-depth grid. However, we feel that one-way coupled mode algorithms offer many possibilities, and suitably optimized may well prove a more desirable alternative for typical ocean acoustic problems.

References

- [1] R. B. Evans, "A coupled mode solution for acoustic propagation in a waveguide with stepwise depth variations of a penetrable bottom," *J. Acoust. Soc. Am.* **74**, 188--195 (1983).
- [2] F. B. Jensen and C. M. Ferla, "Numerical solutions of range-dependent benchmark problems in ocean acoustics," *J. Acoust. Soc. Am.* **87**, 1499--1510 (1990).
- [3] M. B. Porter, Carlo M. Ferla and F. Jensen, "The Problem of Energy Conservation in One-Way Equations", *J. Acoust. Soc. Amer.* **89**(3), 1058--1067 (1991)

PE Workshop II: Part 3 — Contributed Papers

- [4] M. B. Porter and E. L. Reiss, "A numerical method for bottom interacting ocean acoustic normal modes", *J. Acoust. Soc. Am.* **77**, 1760--1767 (1985).
- [5] M. B. Porter, *The KRAKEN Normal Mode Program*, SACLANT Undersea Research Center Technical Report, (1992).
- [6] F. B. Jensen and M. C. Ferla, "SNAP: the SACLANTCEN normal mode acoustic propagation model", SACLANTCEN SM-121, La Spezia, Italy, SACLANT Undersea Research Centre, 1979.
- [7] F. D. Tappert, "The parabolic approximation method," in *Wave Propagation in Underwater Acoustics*, edited by J. B. Keller and J. S. Papadakis (Springer-Verlag, New York, 1977), pp. 224--287.
- [8] D. Lee, G. Botseas and J. S. Papadakis, "Finite difference solution of the parabolic equation," *J. Acoust. Soc. Am.* **70**, 795--800 (1981).
- [9] S. A. Chin-Bing, D. B. King, J. A. Davis and R. B. Evans (eds), *PE Workshop II: Proceedings of the Second Parabolic Equation Workshop May 6-9, 1991*, (Naval Research Laboratory NRL /BE/7181-93-0001, Stennis Space Center, MS, 1993).
- [10] H. Primack and K. E. Gilbert, "A two-dimensional downslope propagation model based on coupled wedge modes" *J. Acoust. Soc. Amer., Suppl. 1*, **88** (1990).
- [11] Michael B. Porter, Ronald L. Dicus and Richard Fizell, "Simulations of Matched Field Processing in a Deep-water Pacific Environment", *IEEE J. of Oceanic Engineering* (special issue on Underwater Acoustic Signal Processing), Vol. OE-12(1), 173--181 (1987).

Windowed Transformations and Marching Algorithms for Localized Phase-Space Representations

B.Z. Steinberg

J.J. McCoy

*The Catholic University of America,
Washington DC 20064*

Abstract

We consider a wedding of the marching methodology and the phase-space localization. The result is a new framework in which the propagation process appears as an *ordered sequence of local events*. The framework requires a description of that portion of the environment that effects the localized event only during the "time" of occurrence of that event. Thus, for example, the events of the interaction with the ocean surface and bottom can be isolated from the propagation through the water column. The properties of the new scheme are discussed and demonstrated via test case 1.

1. Introduction

This paper presents a new and different framework to the description of sound propagation in underwater environments. The framework can be described as a wedding of two approaches. The first is the sequential ordering of events, governed by the methodology of marching the acoustic field. This procedure is well known to the community of underwater sound propagation. The second approach is the description of the field in localized phase-space formats, governed by windowed transformations. The strength of the wedded methodology is that it explicitly incorporates the interpretation of sound propagation as an *ordered sequence of local events*, thus placing our intuitive perception of the propagation process in a systematic framework. We anticipate that the framework is of fundamental importance since it requires a description of that portion of the environment that effects the localized event and only at the occurrence of that event. Thus, for example, the interaction of the acoustic field with the ocean surface and bottom can be isolated from the propagation through the water column. Also, processing of wave data like simultaneous spatial and directional filtering (imposing local radiation conditions) may be systematically performed in a local fashion. These properties further suggest that this is a natural framework to march fields in range dependent environments since certain "turning around" events are confined within regions in phase space that are known *a priori*.

2. Range and Cross Range Localization

First, short comment regarding terminology. Many of the methods for tackling wave problems are based, in one way or another, on either spatial or spectral description of the

field. Spatial being a description of the field as a spatial superposition of Green's functions and spectral being a description of the field as a superposition of plane-waves or modes. Both representations are global: point sources radiate to all directions, plane waves or modes occupy the entire domain. Accordingly, The entire domain of the problem must be incorporated into each propagator before applying the synthesizing integrals. There is no way to assign *a priori* specific wave events in the medium to specific propagators and vice versa.

One-way wave theory and the methodology of marching the radiation field offer an alternative route to the global approaches [1,2]. Clearly, it is the explicit sequential ordering that makes the marching methodology a tool of vital importance. Events in one cross range plane are completely determined by the events in the plane preceding it, and the separation between the planes may be made as small as one wishes. The range direction, therefore, is treated locally. The implementations of this approach, however, are global in the cross range direction exactly in the sense discussed above.

Phase-space beam representations are new techniques that naturally lend themselves to an inherent simultaneous spatial and spectral (or directional) localization in the transverse direction. The techniques have been investigated and discussed thoroughly in [3]. We shall briefly summarize the approach. A scalar time-harmonic acoustic field $u(x,z)$ satisfies the Helmholtz equation in a two dimensional medium (x,z) with z being the range coordinate. An initial acoustic field $u_o(x)=u(x,0)$ is assumed to radiate into the $z>0$ half plane. The local properties of $u_o(x)$ can be measured by the windowed Fourier transform (WFT), defined as,

$$U_o(\bar{x}, \bar{\xi}) = \int u_o(x) w^*(x - \bar{x}) e^{-i\omega \bar{\xi} \cdot dx} \quad (1)$$

where ω is the radial frequency and $w(x)$ is a square integrable window function centered around the origin. The two variables function $U_o(\bar{x}, \bar{\xi})$ describes the local spectral (directional) properties of the field in the neighborhood of \bar{x} . The field may be reconstructed from its local spectrum via,

$$u_o(x) = \frac{\omega}{2\pi N^2} \iint U_o(\bar{x}, \bar{\xi}) w(x - \bar{x}) e^{-i\omega \bar{\xi} \cdot dx} d\bar{x} d\bar{\xi} \quad (2)$$

where N^2 is the L^2 norm of the window function. Equation 2 describes the field as a superposition of shifted (by \bar{x}) and modulated (by $\bar{\xi}$) windows. We may consider the propagation of the field via Eq. (2). This is done by propagating the shifted and modulated windows that, evidently, give rise to shifted and tilted beams. The field is therefore described by a superposition of beams, $b(x,z;\bar{x},\bar{\xi})$, tagged by their initial location and direction variables,

$$u(x, z) = \frac{\omega}{2\pi N^2} \iint U_O(\bar{x}, \bar{\xi}) b(x, z; \bar{x}, \bar{\xi}) d\bar{x} d\bar{\xi} \quad (3)$$

The summation is done simultaneously over locations and directions, hence the term *phase space representation*. With properly chosen windows, the windowed transformation favors *a priori* the beams propagating along the local preferred direction of radiation of the initial field, thereby establishing effective localization around skeletal lines in phase-space that coincide with the geometrical acoustic description of the field [3,4]. Unlike geometrical theories, this localization is not due to high frequency asymptotics and is uniformly valid. Unlike plane waves and point sources, a beam-type propagator, when properly chosen, is localized in direction and location. It stays confined within a propagation distance related to its parameters—the Rayleigh distance. Wave events occurring within this range can be treated locally. Moreover, the specific portion of the local spectra that participate in a wave event is well confined in phase-space within regions that can be identified *a priori*. However, every beam type propagator is bound to diverge beyond its Rayleigh distance and eventually loose its localization properties [3].

3. The Combined Methodology

By combining the two approaches together, that is: by marching localized beam-type spectrum over steps that are shorter than the typical diffraction length of the propagator, one may describe the field as an ordered sequence of localized events over arbitrary propagation distances [4]. This is obtained by operating with Eq. (2) on Eq. (3) after a short propagation distance, say Δz (not necessary with the same window!). One obtains for the local spectrum at Δz ,

$$U(\bar{x}, \bar{\xi}, \Delta z) = \iint U_o(\bar{x}_o, \bar{\xi}_o) B(\bar{x}, \bar{\xi}; \bar{x}_o, \bar{\xi}_o, \Delta z) d\bar{x}_o d\bar{\xi}_o \quad (4)$$

where the phase-space propagator $B(\bar{x}, \bar{\xi}; \bar{x}_o, \bar{\xi}_o, \Delta z)$ is obtained by the WFT of the propagating beam [4]. It measures the degree of coupling between a phase-space constituent at the initial plane and a phase-space constituent at the next plane. In ray theory, this coupling is different from zero if and only if the two points in phase-space, $(\bar{x}_o, \bar{\xi}_o)$ and $(\bar{x}, \bar{\xi})$, belong to the same ray trajectory. However, the coupling measured by $B(\bar{x}, \bar{\xi}; \bar{x}_o, \bar{\xi}_o, \Delta z)$ is strong for phase-space points that belong to the same ray, and it decreases exponentially (Gaussian) in the regions of phase-space that do not form together a ray trajectory. Moreover, since each phase-space constituent occupies a well-confined region, its propagation and its coupling to the constituents at the next plane are governed by the medium properties in its close neighborhood. Finally, each phase-space constituent in a give plane can be treated independently of the others at that plane.

3.1 The Propagator

A general expression for B in nonhomogeneous media is not available but as we shall see much can be learned by evaluating it for a homogeneous medium using the Gaussian window,

$$w(x) = e^{-\frac{\omega^2}{2\beta}} = e^{-\frac{(x/\lambda)^2}{2\Delta^2}}; \Delta^2 = \beta / (2\pi\lambda\nu) \quad (5)$$

where β is a parameter that determines the window width, λ is the wavelength, ν is the wave velocity and Δ is the window width in units of a wavelength. Reference [4] provides an explicit expression for B in a homogeneous medium in terms of a single Fourier integral and an asymptotic analysis of its properties. We shall summarize the important results. The propagator is essentially a Gaussian in phase-space, centered around,

$$\bar{x}_o = \bar{x} - \Delta z \tan \bar{\theta}_c; \bar{\theta}_c = \sin^{-1} \nu \bar{\xi}_c, \bar{\xi}_c = \frac{\Delta_o^2 \bar{\xi}_o + \Delta_1^2 \bar{\xi}}{\Delta_o^2 + \Delta_1^2}, \quad (6)$$

$$\bar{\xi}_o = \bar{\xi} \quad (7)$$

with typical widths along the \bar{x} and $\bar{\xi}$ directions,

given by,

$$\Delta_{\bar{x}} = \lambda(\Delta_o^2 + \Delta_1^2)^{1/2} \left[1 + (\Delta z / Z_R)^2 \right]^{1/2} \quad (8)$$

$$\Delta_{\bar{\xi}} = (\Delta_o^2 + \Delta_1^2)^{1/2} / (\sqrt{8}\pi\nu\Delta_o\Delta_1) \quad (9)$$

where $Z_R = 2\pi\lambda(\Delta_o^2 + \Delta_1^2)\cos^3 \bar{\theta}_c$, and where Δ_o and Δ_1 are the normalized window widths in the first (initial) and second plane, respectively. Equations (6) and (7) describe localization around a ray trajectory. From Eq. (8) it is seen that the propagator stays confined if the step size is short relative to Z_R which can be interpreted as a diffraction distance in phase-space. Figures 1a and 1b show a plot of $|B|$ in the dimensionless $(\bar{x}_o / \lambda, \nu \bar{\xi}_o)$ plane for the point $(0, 0.4)$ in the $(\bar{x} / \lambda, \nu \bar{\xi})$ plane. We have used identical windows with $\Delta_o = \Delta_1 = 2\lambda$, thus the diffraction length is 48λ . Figure 1a shows the propagator for $\Delta z = 2\lambda$. The outer contour shows 5% of the maximal magnitude. Localization around the “skeletal point” defined by Eqs. (6a) and (7a) is in evidence. In Fig. 1b the step size has been increased to 24λ . As a result localization has been degraded. The area of integration in the $(\bar{x}_o, \bar{\xi}_o)$ plane in Eq. (4) may be confined *a priori* to the

effectively contributing domains depicted in Fig. 1. These domains are readily obtained by simple geometrical consideration and by the use of the algebraic expressions in Eqs. (8) and (9). The consequences are of fundamental importance: only a small neighborhood (around the skeletal point) of the phase-space in the initial plane has to be considered for the treatment of each phase-space point of the next plane.

3.2 Pressure Release Surface

The use of the homogeneous medium propagator in the presence of a pressure release surface is facilitated by a simple local mirroring operation. If the surface is located at $x=0$, then one may show that $\bar{U}(\bar{x}, \bar{\xi}) = -U(-\bar{x}, -\bar{\xi})$. Thus, the presence of the surface can be augmented in Eq. (4) by integrating only for $\bar{x} \geq 0$ and performing a mirroring about $\bar{x} = 0$. Due to locality, only a narrow strip of the order of $\Delta_{\bar{x}}$ has to be mirrored.

3.3 Phase-Space Filtering

In the context of wave propagation, phase-space filtering can be interpreted as a process by which we impose *local radiation conditions*. Perhaps the simplest example is the modeling of an infinitely extended bottom (or artificial computational boundary) where one would like to suppress all the wave constituents that propagate near the bottom and facing down, without effecting the upward or downward propagation in the water column. The nature of the problem requires an explicit simultaneous control of both directional and spatial structures of the field. This clearly does not conform well with global approaches. As a result, spurious reflections from the artificial boundary that decay like an inverse polynomial are unavoidable. Local phase-space formats are the natural framework for imposing local radiation conditions since they assign local directions to each small neighborhood in the problem. The filtering operation in phase-space is manifested by restricting the region of integration in Eq. (4) to a subdomain D of the $(\bar{x}_o, \bar{\xi}_o)$ plane,

$$T_D U(\bar{x}, \bar{\xi}, \Delta z) = \iint_{(\bar{x}_o, \bar{\xi}_o) \in D} B(\bar{x}, \bar{\xi}; \bar{x}_o, \bar{\xi}_o, \Delta z) U_o(\bar{x}_o, \bar{\xi}_o) d\bar{x}_o d\bar{\xi}_o. \quad (10)$$

A measure of how well this operation imposes local radiation conditions is the value of the filtered local spectrum for $(\bar{x}, \bar{\xi}) \in \bar{D}$ where \bar{D} is the complement of D in the $(\bar{x}, \bar{\xi})$ plane. This may serve also as a measure for the degree of spurious reflections. It can be shown that (see [4] for details),

$$\begin{aligned} |T_D U(\bar{x}, \bar{\xi}, \Delta z)|^2 &\leq 2 \left(\frac{\pi \beta}{\omega \epsilon} \right)^{1/2} \|u\| \max_{(\bar{x}_o, \bar{\xi}_o) \in D} e^{-2(1-\epsilon)L^2} \\ L^2 &= (\bar{\xi} - \bar{\xi}_o)^2 / 2\Delta_{\bar{\xi}}^2 + (\bar{x} - \bar{x}_o - \Delta z \tan \bar{\theta}_c)^2 / 2\Delta_{\bar{x}}^2 \end{aligned} \quad (11)$$

for every $0 \leq \epsilon \leq 1$ and $(\bar{x}, \bar{\xi}) \in \bar{D}$, where $\|u\|$ is the L^2 norm of the field. The filtering operation results in an exponentially (Gaussian) decaying tails (spurious reflections) in phase-space. The filtered region is mapped from the initial plane along ray trajectories and the rate of decay of the spurious effects depends on the widths $\Delta_{\bar{x}}$ and $\Delta_{\bar{\xi}}$. This operation influence wave events only when they "arrive" to the relevant region and practically does not penetrate to the region of interest.

3.4 Point Source in Phase-Space

In our model, a point source is characterized by a collection of beams, emanating from a confined spatial neighborhood and radiating to all directions. In phase-space, this is manifested by a strip centered around the line $\bar{x} = x'$ where x' is the coordinate of the source. The phase-space distribution of a point source with $x' = 0$ using Gaussian window of width 3λ is shown in Fig. (2). The distribution is exponentially (Gaussian) decreasing in the \bar{x} direction away from $\bar{x} = x'$ (see [4]).

4. Numerical Example

The properties of the new scheme are demonstrated here via test case No. 1. An initial distribution of a point source in phase-space has been propagated from the source plane down to range of 266λ , using the asymptotic propagator with Gaussian windows of width λ and step size of 2λ . Three typical distributions, at ranges of 10λ , 60λ and 266λ are depicted in Fig. (3). Local mirroring has been performed in the strip $-20\lambda \leq \bar{x} \leq 0$ (approximately $3\Delta_{\bar{x}}$). The computational boundaries in Eq. (4) are those shown in the figures. Nevertheless, spurious reflections were practically zero (note that the receiver depth is 106.4λ). At short range ($z=10\lambda$, Fig. 3a), two distinct phase-space distributions, centered around the skeletal lines $\bar{x} = \pm 9.33\lambda + z \tan \bar{\theta}$ ($\bar{\theta} = \sin^{-1} v \xi$) are easily identified. These lines represent, respectively, the direct and reflected ray families. With increasing range, the distribution evolves by a clockwise rotation and the skeletal lines become closer (Fig. 3b). The ray families interfere in the region between the skeletal lines. Finally, at $z=266\lambda$, the skeletal lines almost overlap and the phase-space representation, still concentrated around these lines, describes essentially the interference pattern of the two ray families. The field at the receiver has been computed from $U(\bar{x}, \bar{\xi}, \Delta z)$ via Eq. (2) and the transmission loss curve is shown and compared to the analytic solution in Fig. 3d (dashed and solid lines, respectively). The curves agree very well for ranges that are larger than 60λ , that corresponds to radiation angles of about 60° . The discrepancy at short ranges is due to the use of the asymptotic propagator.

The localization and filtering philosophy has been employed in all computations. We first computed the location of the skeleton, then, computation of Eq. (4) was performed only for the $(\bar{x}, \bar{\xi})$ that lie close to the skeleton (see [4] for details). Moreover, the integration in the $(\bar{x}_o, \bar{\xi}_o)$ plane was confined *a priori* to the regions of dominant contribution of the propagator (see Fig. 1 and Eqs. (6)-(9)). Test computations of the same problem, but

without any prior confinement or filtering were also performed. The results were, of course, the same.

References

- [1] F. D. Tappert, "The Parabolic Approximation Method", in *Wave Propagation in Underwater Acoustics*, edited by J. B. Keller and J. S. Papadakis (Springer, New York, 1977), p. 224.
- [2] L. Fishman and J. J. McCoy, "Derivation and Application of Extended Parabolic Wave Theories. Part I. The Factorized Helmholtz Equation", *J. Math. Phys.* **25**, 285 (1984).
- [3] B. Z. Steinberg, E. Heyman and L. B. Felsen, "Phase Space Beam Summation for Time Harmonic Radiation from Large Apertures", *J. Opt. Soc. Am. A8*, 41 (1991).
- [4] B. Z. Steinberg and J. J. McCoy, "Marching Acoustic Fields in Phase Space", *J. Acoust. Soc. Am.* **93**, 188-204 (1993).

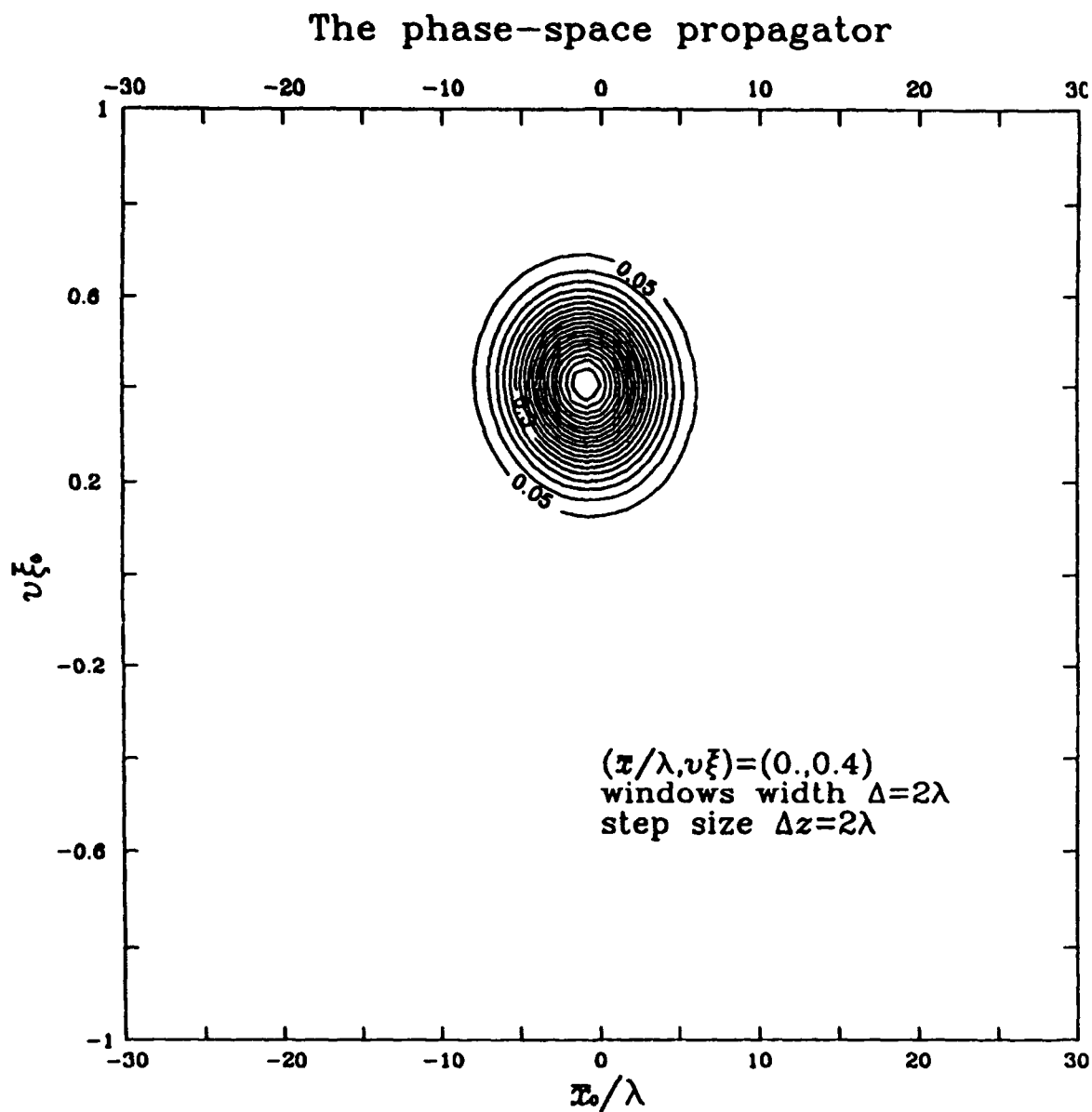


FIGURE 1A:

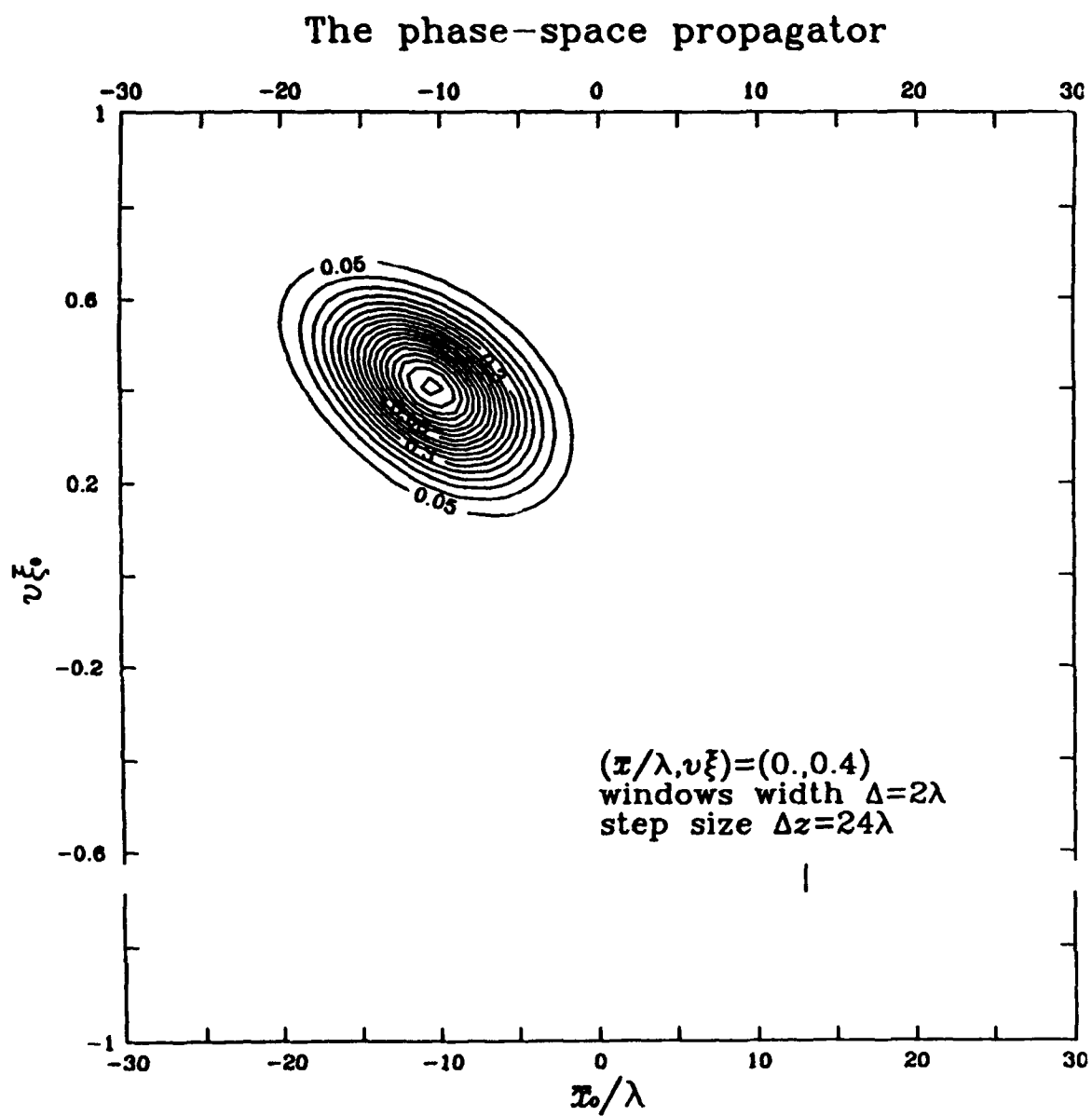


FIGURE 1B:

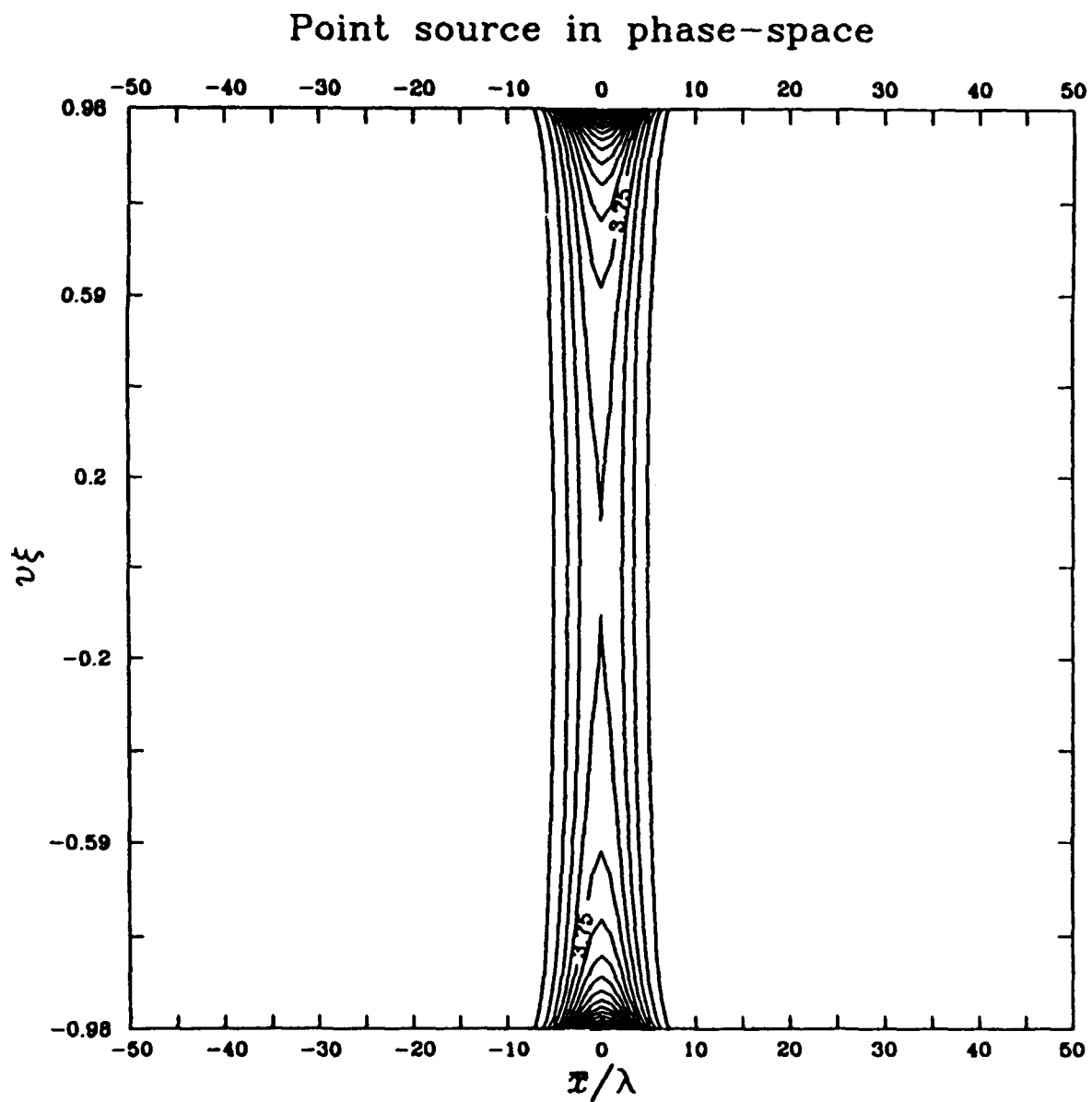


FIGURE 2:

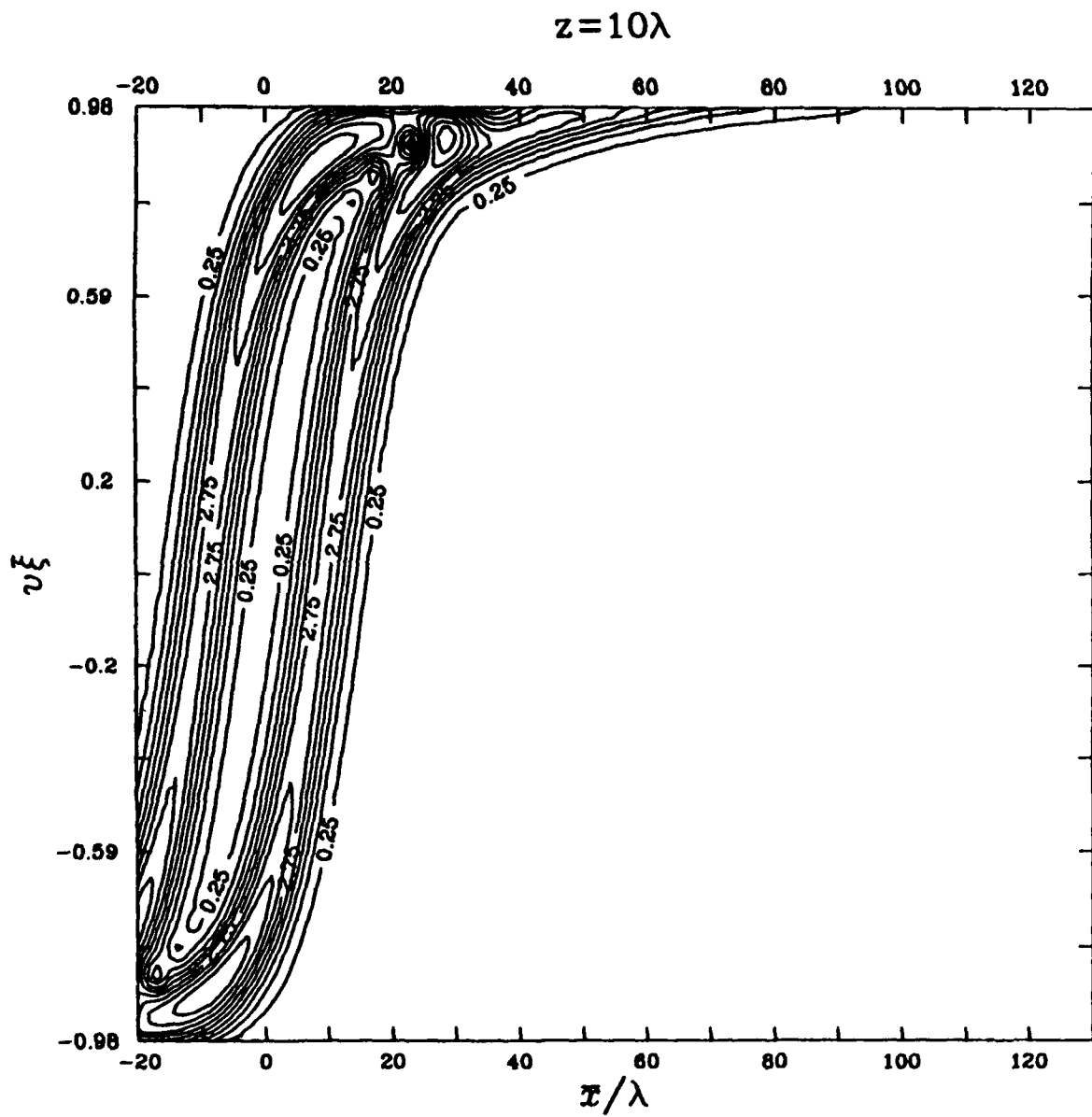


FIGURE 3A:

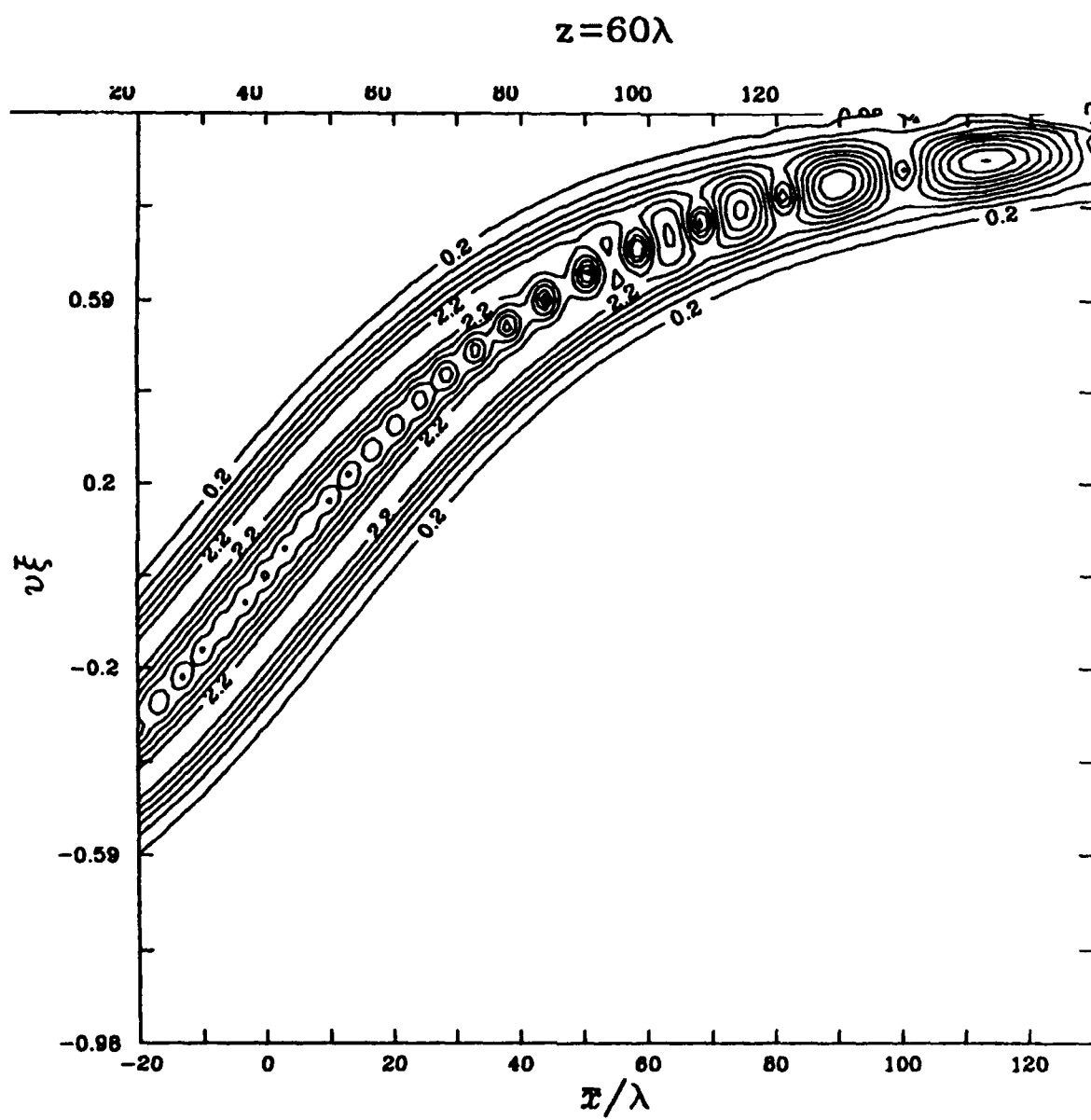


FIGURE 3B:

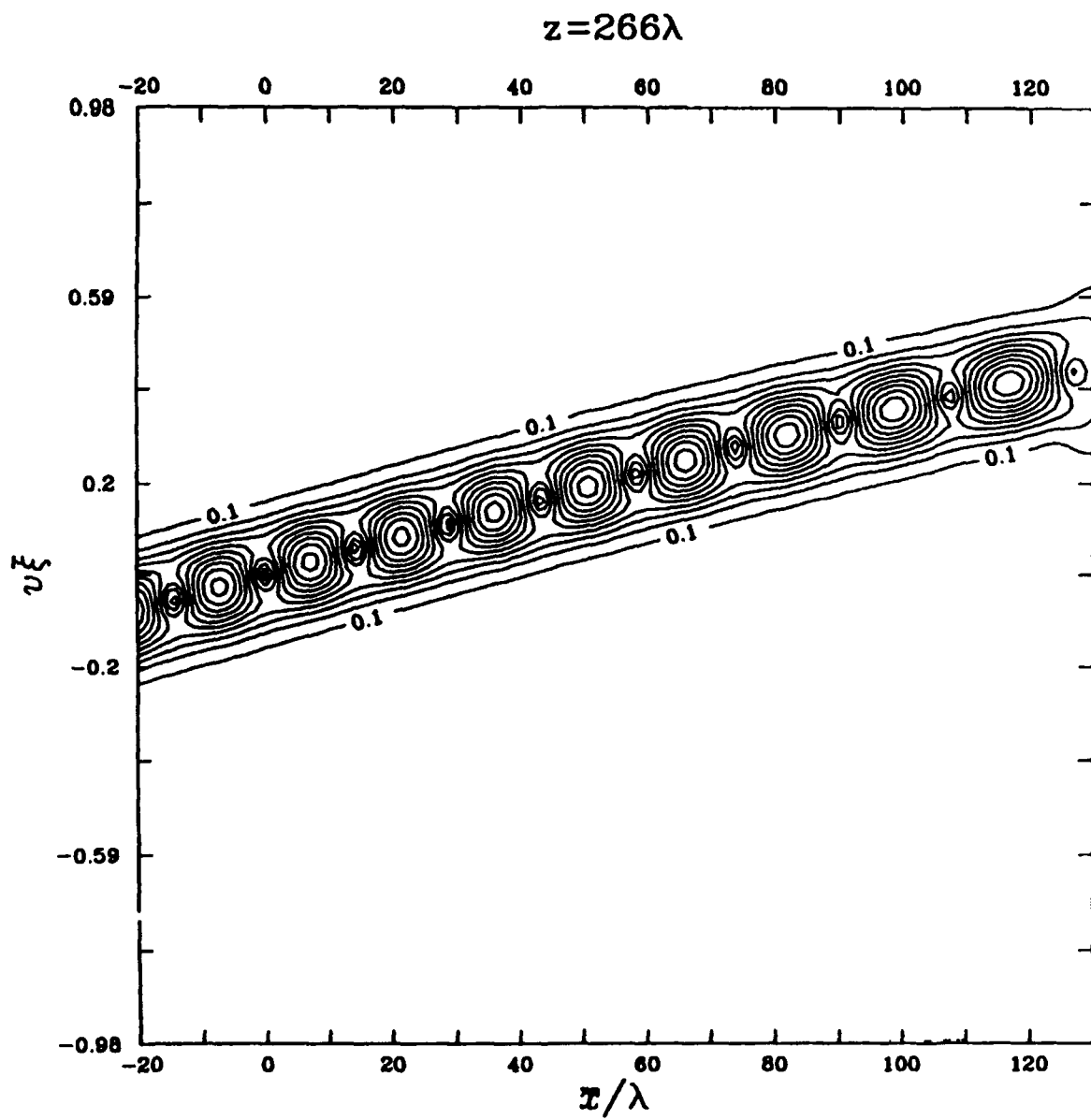


FIGURE 3C:

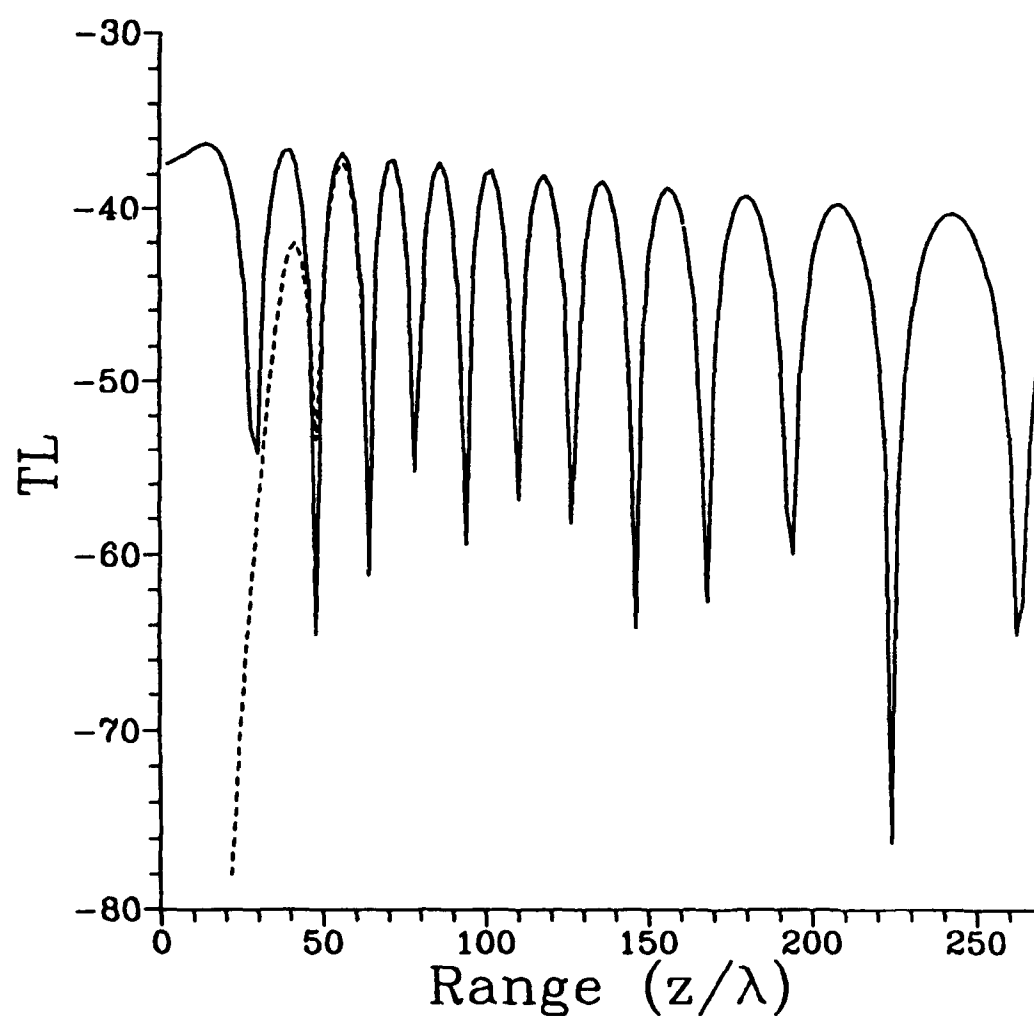


FIGURE 3D:

PE-Based Spectral Decomposition

David J. Thomson

*Defence Research Establishment Pacific
FMO Victoria, British Columbia
Canada V0S 1BO*

ABSTRACT

In a layered waveguide, the field p satisfying the acoustic wave equation is exactly related to the field ψ satisfying the standard parabolic equation (PE) by an integral transform. The non-local relationship between p and ψ maps into a local one in the spectral (horizontal wavenumber) domain. This unique spectral relationship forms the basis of an efficient and accurate method of postprocessing PE solutions into solutions of the wave equation. Because this method of obtaining p from ψ is exact, it is not restricted to low-angle propagation, small changes in the refractive index, or judicious choice of reference wavenumber, conditions usually associated with the standard parabolic approximation. PE-based spectral decomposition can also be a useful tool for analyzing fields propagating in range-dependent waveguides. In this case, the modal amplitudes and horizontal wavenumbers of ψ can be determined exactly by spectral analysis of a suitable ψ -field correlation function. The amplitudes and wavenumbers of the normal modes of p are then obtained by simple mapping rules.

1 INTRODUCTION

Predictions of low-frequency sound propagation in range-dependent environments are routinely carried out using models based on the parabolic equation (PE) approximation [1,2]. This is mainly due to the fact that the PE can be solved numerically using efficient marching algorithms. Other full-wave approaches capable of treating propagation in range-varying media, such as coupled-modes, are more computationally intensive [3]. One disadvantage of using PE methods is that because they provide numerical solutions to the total acoustic field at each point on a computational grid, information on the propagation of individual spectral components (modes) is not readily available. Such information can facilitate the interpretation of the acoustic field behaviour in complex propagation situations.

The present paper describes a PE-based spectral method suitable for analyzing fields propagating in waveguides. The method is based on an exact relationship between the solution p of the wave equation and the solution ψ of the standard parabolic equation. This relationship between fields takes the form of a non-local integral transform [4]. In contrast, the horizontal wavenumber spectra of these fields are related locally. This unique spectral relationship forms the basis of an *a posteriori* method of mapping ψ -fields into p -fields [5]. It is also possible to determine the modal amplitudes of p by spectral analysis of a certain ψ -field correlation function. Although this connection between p and ψ fields is restricted to propagation in range-independent environments, the spectral approach can be used to determine the modal properties of fields propagating in range-dependent environments.

Previously, Jensen and Schmidt [6] presented a hybrid scheme for numerically decomposing the PE field at a given range into its spectral components versus horizontal wavenumber. The decomposition was accomplished by treating the PE field versus depth as a source field in the SAFARI code [7,8]. This code constructs the “local” (range-independent) Green’s function corresponding to the PE source field excitation. This “local” Green’s function is precisely the spectral decomposition in horizontal wavenumbers of the PE field versus depth at the given range in the waveguide. By carrying out this decomposition at different ranges in a wedge-shaped ocean, they were able to identify and study the propagation of individual modes in both adiabatic and coupled-mode situations. A similar method has recently been proposed by Gilbert *et al.* [9] based on an operator formalism [10].

In contrast to this hybrid approach, Feit and Fleck [11] developed a modal decomposition scheme based directly on the “propagating beam method” to study the propagation of light in optical fiber waveguides. The propagating beam method in optics is equivalent to the PE method in underwater acoustics. Their PE-based modal decomposition scheme is based on three related concepts: (1) an exact relationship between PE modes and normal modes; (2) an efficient split-step marching algorithm for solving the PE; and (3) spectral analysis of a suitably-defined PE correlation function. Items (1) and (2) are well-known in the underwater acoustics literature [4,5,12]. Although items (1) and (3) assume propagation in range-independent waveguides, the PE-based scheme can be applied in a range-varying environment [13,14]. Moreover, this method of modal decomposition does not depend on the split-step algorithm of item (2) to solve the parabolic equation.

In the next section, we provide a brief development of the theory underlying the PE based spectral decomposition method. Three related postprocessing topics are treated: (1) converting numerical PE solutions into solutions of the wave equation for range-independent media; (2) decomposing pressure fields versus depth into their normal mode components for range-independent media; and (3) extending the PE-based modal decomposition scheme in (2) for use in range-dependent environments. Each topic is illustrated with numerical examples.

2 THEORETICAL BACKGROUND

2.1 Parabolic Approximation

Let the region $z > 0$ (z positive downward) of a cylindrical coordinate system (r, θ, z) be occupied by an oceanic waveguide, and let $p(r, z) \exp(-i\omega t)$ represent the azimuthally symmetric, time-harmonic acoustic field due to a point harmonic source located at $r = 0$, $z=z_o$. For $r > 0$, the acoustic pressure $p(r, z)$ is assumed to satisfy the scalar wave equation

$$\frac{1}{r} \frac{\partial}{\partial r} \left(r \frac{\partial p}{\partial r} \right) + \frac{\partial^2 p}{\partial z^2} + k_o^2 n^2 p = 0 , \quad (1)$$

where $n(r, z) = c_o/c(r, z)$ is the refractive index, $c(r, z)$ is the sound speed, and $k_o = \omega/c_o$ is an arbitrary reference wavenumber. Equation 1, which underlies all of the standard linear propagation models of ocean acoustics (multipath expansion, fast field, normal mode, parabolic equation) [15,16], can be generalized to accommodate the effects of nonzero

absorption α and variable density ρ . In addition, the physically meaningful solutions to Eq. 1 must satisfy appropriate boundary conditions.

It is well known [1,2] that instead of solving Eq. 1 for p the outgoing pressure in the far-field ($k_o r \gg 1$) can be determined by solving the “one-way” evolution equation

$$\frac{\partial \psi}{\partial r} = ik_o(Q - 1)\psi , \quad (2)$$

where

$$p(r, z) = (k_o r)^{-1/2} \psi(r, z) \exp(ik_o r) \quad (3)$$

and Q denotes the pseudo-differential operator

$$Q = \sqrt{n^2 + \frac{1}{k_o^2} \frac{\partial^2}{\partial z^2}} . \quad (4)$$

While strictly only valid for horizontally stratified media, $n = n(z)$, Eq. 2 forms the basis for obtaining PE predictions of underwater sound propagation in waveguides that are range-dependent. This is accomplished by treating the environment at each range to be locally independent of r over a small interval Δr so that Eq. 2 can be integrated to obtain the formal result

$$\psi(r + \Delta r, z) = \exp\{ik_o \Delta r (Q - 1)\} \psi(r, z) . \quad (5)$$

Since the backscattered field is neglected in this “one-way” equation, the environment can be updated at each range step to accommodate range-varying media (for a recent discussion on this procedure, however, see [17] [18]).

Although Eq. 5 can be marched outward in range, it is computationally demanding to make use of the full matrix representation of the exact square-root operator Q [19,20]. The numerical efficiency of the PE is achieved by approximating Q with an operator that can be represented by a matrix that is diagonally banded. Different approximations to Q lead to different parabolic equations. In particular, the truncated binomial series expansion of Q due to Tappert [1,2]

$$Q - 1 = \frac{1}{2}(Q^2 - 1) = \frac{1}{2}(n^2 - 1) + \frac{1}{2k_o^2} \frac{\partial^2}{\partial z^2} \quad (6)$$

leads to the standard parabolic equation of underwater acoustics,

$$\frac{\partial \psi}{\partial r} = \frac{ik_o}{2}(n^2 - 1)\psi + \frac{i}{2k_o} \frac{\partial^2 \psi}{\partial z^2} \quad (7)$$

The usual justification for the approximation in Eq. 6 relies on the interpretation that for small propagation angles and small variations in the refractive index, $(1/2)(Q^2 - 1)$ is, in some sense, small. It should be noted that for *any* approximation to Q , Eq. 3 only approximately relates the PE field variable ψ to the acoustic pressure p . Even the recent “wide-angle” approximations to Q based on a Pade series representation [21] will give rise to phase errors beyond some range.

2.2 Exact Relation between ψ and p

For range-independent media, DeSanto [4] has shown that Eq. 3 can be regarded as the first term in a stationary phase expansion of an exact integral transform relating p to ψ . This exact integral relationship is given by

$$p(r, z) = (2\pi i)^{-1/2} \int_0^\infty \psi(r, t) \exp\left(\frac{ik_o}{2t}(r^2 + t^2)\right) \frac{dt}{t}. \quad (8)$$

It is worthwhile noting that Eq. 8 does not require $(1/2)(Q^2 - 1)$ to be small. Hence, accurate numerical solutions to the standard parabolic equation can, in principle, be mapped into accurate numerical solutions to the wave equation. Moreover, since Eq. 1 is independent of reference wavenumber, it is evident that any value of k_o can be used to solve Eq. 7 for ψ and used in Eq. 8. That is, although ψ depends strongly on k_o , the integral transformation described by Eq. 8 maps every k_o -dependent ψ -field into the same p -field.

Thomson and Wood [5] have shown that the non-local relationship expressed by Eq. 8 becomes a local one after transformation into the appropriate horizontal wavenumber domains of p and ψ . This spectral connection is given by

$$g(k, z) = \frac{1}{k_o} \sqrt{\frac{i}{2\pi}} f(s, z), \quad (9)$$

where g , the Hankel transform of p , and f , the half-range Fourier transform of ψ , are defined respectively by

$$g(k, z) = \int_0^\infty p(r, z) J_o(kr) r dr \quad (10)$$

$$f(s, z) = \int_0^\infty \psi(t, z) \exp(-ist) dt. \quad (11)$$

The horizontal wavenumbers k and s are related by the nonlinear (but local) mapping

$$k = k_o \sqrt{1 + \frac{2s}{k_o}}. \quad (12)$$

This local relationship can be exploited to develop an efficient and accurate method of postprocessing solutions of the standard PE into solutions of the acoustic wave equation [5]. This postprocessing approach is shown schematically as the clockwise route in Fig. 1.

Instead of applying Eq. 8 directly to process $\psi(t,z)$ into $p(r,z)$, as indicated in the counterclockwise route in Fig. 1, we first use Eq. 11 to determine the PE kernel $f(s,z)$ as a function of horizontal wavenumbers. This PE kernel function can then be mapped into the Green's function kernel $g(k,z)$ for the wave equation using the local relations in Eq. 9 and Eq. 12. Finally, the solution p is recovered from a knowledge of its Green's function by applying an inverse Hankel transform, namely

$$p(r,z) = \int_0^{\infty} g(k,z) J_o(kr) k dk . \quad (13)$$

In practice, both the half-range Fourier transform in Eq. 11 and the inverse Hankel transform in Eq. 13 are carried out on equispaced data using the fast Fourier transform (FFT) algorithm. Because the mapping in Eq. 12 from s to k is nonlinear, interpolation between wavenumbers is necessary prior to applying the inverse Hankel transform.

2.3 Modal Decomposition of ψ - and p -Fields

For range-independent waveguides, the sound speed c , density ρ and absorption α are functions of depth z only and Eq. 7 can be solved by separation of variables. In this case, it is straightforward to use Eq. 8 to establish the spectral connection relating the PE modes of Eq. 7 to the normal modes of Eq. 1. The resulting expansion into PE modes can easily be verified to be [4]

$$\psi(r,z) = \sum_j a_j u_j(z) \exp(is_j r), \quad (14)$$

where the depth-dependent mode functions u_j satisfy the eigenvalue equation

$$\frac{d^2 u_j}{dz^2} + (k_o^2 n^2(z) - k_j^2) u_j = 0, \quad (15)$$

and the a_j are the mode amplitudes. The PE modal wavenumbers s_j are given by

$$s_j = \frac{k_j^2 - k_o^2}{2k_o}. \quad (16)$$

Equation 15 is recognized [4,15,16] as the depth-dependent equation associated with the normal mode eigenfunctions of the acoustic wave equation. The horizontal wavenumbers k_j are the corresponding normal mode eigenvalues. The u_j 's can be normalized to form a complete orthonormal set. In ocean acoustics, the usual boundary conditions imposed on the fields satisfying Eq. 15 require each u_j to vanish at $z = 0$ and remain bounded as $z \rightarrow \infty$.

As a result, Eq. 14 admits only a finite number of propagating modes. It can be shown [15,16] that each mode amplitude a_j is proportional to $u_j(z_\rho)$. Thus, if a point source is located at a null of the j th mode, mode j will not be excited. Similarly, if a point receiver is placed at a null of the j th mode, mode j will not contribute to the total field there.

Substituting Eq. 14 into Eq. 8 and using Eq. 16 yields

$$\begin{aligned} p(r, z) &= \frac{1}{\sqrt{2\pi i}} \sum_j a_j u_j(z) \int_0^\infty \exp\left(\frac{ik_o^2 t}{2k_o} + \frac{ik_o r^2}{2t}\right) \frac{dt}{t} \\ &= \sqrt{\frac{\pi i}{2}} \sum_j a_j u_j(z) H_o^{(1)}(k_j r) \\ &\approx \frac{1}{\sqrt{k_o r}} \sum_j \left(a_j \sqrt{k_o / k_j}\right) u_j(z) \exp(ik_j r) \end{aligned} \quad (17)$$

In the sequence leading to Eq. 17, both the integral representation of the Hankel function $H_o^{(1)}(k_j r)$ [22, page 956, entry 8] and the first term of its asymptotic expansion [22, page 962, entry 3] were used. Equation 17 is the well-known modal solution for the field p in a layered waveguide. It is evident from this result that the amplitudes a'_j and wavenumbers k_j of these normal modes can be obtained *a posteriori* from the amplitudes a_j and wavenumbers s_j of the PE modes by the mappings

$$a'_j = a_j \sqrt{k_o / k_j}, \quad (18)$$

and

$$k_j = k_o \sqrt{1 + \frac{2s_j}{k_o}}. \quad (19)$$

2.4 ψ -Field Correlation Function

From the preceding analysis, it is clear that the modal properties of ψ lead directly to the modal properties of p . An efficient algorithm for modally analyzing ψ has been developed by Feit and Fleck [11] for the case of propagation in optical waveguides. Their method can easily be adapted to analyze the modal properties of fields propagating in range-dependent waveguides [13,14].

Consider the PE field correlation function Φ defined by

$$\Phi(R, t) = \int_0^\infty \psi^*(R, z) \psi(R + t, z) dz \quad (20)$$

Here $\psi^*(R, z)$ is the complex conjugate of the field at range R used to initiate the PE

solution. The sequence of values $\Phi(R, t_l)$ for $t_l = l\Delta r$, $l = 0, \dots, L-1$ is readily computed during the step-by-step numerical solution of Eq. 7. Substituting the modal representation for ψ given in Eq. 14 into the defining integral for Φ given in Eq. 20 and noting that the u_j 's are orthonormal, it is readily shown that the PE correlation function assumes the analytical form

$$\Phi(R, t) = \sum_j |a_j|^2 \exp(is_j(t - R)). \quad (21)$$

On taking the Fourier transform of Eq. 21 it follows at once that

$$\begin{aligned} \mathcal{F}\{\Phi\} &= \int_0^\infty \Phi(R, t) \exp(-isr) dr \\ &= \sum_j |a_j|^2 \exp(-is_j R) \delta(s - s_j) \end{aligned} \quad (22)$$

Thus it is observed that spectral analysis of the PE amplitude correlation function Φ should produce peaks in the spectrum at the wavenumbers s_j of the PE modes. The magnitude of the peak corresponding to the j th mode is proportional to the power $|a_j|^2$ contained in that mode. The amplitudes $|a_j|^2$ and horizontal wavenumbers k_j of the corresponding normal modes of p are recovered using Eq. 18 and Eq. 19 respectively. If a fast Fourier transform (FFT) routine is used to estimate the spectrum of Φ , the resolution of the PE modal wavenumbers is determined by the range interval $L\Delta r$ over which the numerical solution of Eq. 7 is performed, i.e., $\Delta s = 2\pi / L\Delta r$. For a given number of steps L , this resolution may be improved by using line-shape fitting techniques [11] (i.e., windowing) or zero-pad interpolation.

2.5 Application to Range-Varying Media

The application of the PE-based modal decomposition method to propagation in range-varying media is straightforward. Suppose Eq. 7 has been solved for $\psi(r, z)$ in the range-dependent waveguide shown schematically in the upper part of Fig. 2. Here the range-dependence is manifested in the variable-depth bathymetry. The subbottom region is taken to be lossy ($\alpha \neq 0$).

Because the waveguide properties vary with range, the modal amplitudes and wavenumbers also vary with range. The modal structure of the field at a given range R , say, can be found by using the complex field $\psi(R, z)$ to initialize a range-independent PE calculation for an environment characterized by the "local" waveguide properties at the range R . This is illustrated at the bottom of Fig. 2. For this range-independent calculation, the numerical PE solution is marched out to a range determined by the required spectral resolution. The correlation function Φ for this new PE field can then be analyzed spectrally to determine the mode properties of the initial data $\psi(R, z)$. There is one technical detail that should be mentioned. For a lossy waveguide, the field $\psi(R, z)$ will have been affected by attenuation in the region $0 < r < R$. In order to obtain a meaningful spectral decomposition of $\psi(R, z)$, it is necessary to set $\alpha = 0$ during the range-independent PE calculation while

forming the data Φ for $r = R$. Otherwise, the magnitudes of the modal peaks will be underestimated. This detail is illustrated in the bottom of Fig. 2.

2.6 Remarks on Decomposing VLA Data

The numerical solution of Eq. 7 is undertaken on a fine computational grid of spacing Δr in range and Δz in depth that spans the entire cross-section of the oceanic waveguide. For modeling propagation from a point source, simple starting fields $\psi(0,z)$ can be used [1,23]. Since Eq. 2 is solved recursively, it is evident that the field at a given range R , $\psi(R,z)$, contains all the spectral information necessary to continue propagating the field for $r > R$. For a range-independent waveguide, the horizontal wavenumber spectrum associated with this given field is invariant with range. It is precisely this property of the field in the waveguide that allows the PE-based modal decomposition to be carried out.

Accurate PE transmission loss calculations usually involve a trial-and-error procedure to determine suitable values of k_0 , Δr and Δz [24]. As seen in the mappings of Eq. 18 and Eq. 19, however, the choice of k_0 is taken into account in the spectral analysis of the field. On the other hand, the computational grid spacings used to solve PE are determined mainly by two factors: (a) the number of propagating modes, which depends on the acoustic frequency and the environmental properties of the waveguide, and (b) the algorithm used to solve Eq. 7. For shallow-water environments, where the low-frequency propagating fields are usually bottom-limited, it is typical to use Δz , $\Delta r \ll \lambda$ where λ is the acoustic wavelength in water.

The above observations suggest that a measured pressure field versus depth, obtained using data from a vertical line array (VLA) for example, can be used to initiate a PE-based modal decomposition. Such mode filtering is a necessary first step in applying matched-mode processing to localize a source in an oceanic waveguide [25]–[28]. In general, it is not practical to build VLA's that have hydrophone spacings that are as small as the depth grid spacings required by the PE model. Also, with any VLA, it is not possible to sample the pressure field outside of the water column, i.e., in the bottom. However, accurate results with the PE-based modal decomposition method can still be achieved if the measured VLA field is first interpolated between hydrophones and extrapolated into the bottom on a depth grid that meets the requirements of the PE model. Numerical evidence supporting this claim as well as a description of suitable interpolation and extrapolation algorithms is given in [29,30].

3 NUMERICAL EXAMPLES

In this section, three numerical examples are used to illustrate the above postprocessing methods. The first two examples deal with propagation in a range-independent environment. The third example considers range-dependent propagation in a waveguide with a variable-depth bottom.

3.1 Example 1

The first example demonstrates the capability of the postprocessing method for transforming numerical solutions of the standard PE into solutions of the wave equation for a standard benchmark problem. This example was introduced as test case 2b in the first PE

Workshop held in 1981 [2]. Figure 3 shows the environmental configuration for this range-independent test case.

A 25-Hz point source is located at a depth of 500 m in the upper layer of a bilinear sound speed profile. This upward refracting ocean overlays a uniform half-space whose properties match those at the water/bottom interface. For the PE calculations, an absorbing layer was inserted below $z = 1750$ m to suppress unwanted reflections from the bottom of the computational grid. With this profile, all acoustic rays with grazing angles $|\theta| < 30^\circ$ are confined to the water column.

Figure 4 shows a set of transmission losses, $-10\log_{10} |p|^2$, computed as a function of range for a receiver located at a depth of 500 m. The reference curve (dashed line) was computed using the SAFARI [8] code. In the upper panel, the solid curve was computed by solving Eq. 7 using the split-step Fourier algorithm [23] on a computational grid with horizontal step-size $\Delta r = 25$ m and vertical step-size $\Delta z = 4$ m. The reference sound speed $c_0 = 1300$ m s $^{-1}$ used in this calculation lies well below the phase velocities of the propagating modes. It is evident that the standard PE does not provide a good approximation to the wave equation in this case. In the lower panel, the solid curve shows the result of postprocessing the standard PE curve using the clockwise $\psi \rightarrow p$ route depicted in Fig. 1. It is apparent that this method of computing the solution to the wave equation is in excellent agreement with the reference solution.

Similar transmission loss comparisons are shown in Figs. 5 and 6 using values of c_0 equal to 1500 m s $^{-1}$ and 1700 m s $^{-1}$ respectively to solve Eq. 7. It is clear that the unprocessed standard PE solutions are very dependent on the value of c_0 used. On the other hand, the postprocessed PE solutions are in excellent agreement with the reference solution, which is independent of the parameter c_0 . These calculations support the claim that the postprocessing algorithm gives results which are independent of angle of propagation, size of the index of refraction, and value of reference sound speed used.

The above results consider propagation losses out to a maximum range of 333 wavelengths. The accuracy of the reconstructed fields is evident and confirms the accuracy with which the PE was solved using the split-step algorithm. Since any “wide-angle” evolution equation will give rise to phase errors beyond some range, it is interesting to examine the accuracy of the postprocessing method at greater ranges. In Fig. 7, comparisons are shown for the range interval 60 to 80 km, or 1333 wavelengths for this example. A value of $c_0 = 1500$ m s $^{-1}$ was used in the PE calculations. It is seen that the postprocessed PE method continues to provide accurate reconstructions at these ranges.

3.2 Example 2

Environmental parameters for the second example were chosen to represent the shallow waters of the Canadian Arctic continental slope [31]. These data were used previously to study PE-based decomposition of VLA data [29,30]. The environmental and physical parameters for this example are given in Fig. 8. Although the sound speed profile in the water is upward-refracting, at 25 Hz most of the energy interacts with the high-speed bottom. Note that because c , ρ , and α are all discontinuous across the ocean-bottom boundary, the operator $(1/2)(Q^2 - 1)$ in Eqs. 6 and 7 needs to be modified accordingly near the ocean/bottom interface.

Figure 9 shows a plot of transmission loss versus depth produced using the SNAP normal mode model [32] at a distance of 50 km from the source. This curve represents the coherent sum of the twelve propagating modes that are supported in the waveguide at this frequency. The SNAP calculations were carried out using 512 equispaced receivers depths spaced $\Delta z = 1.953125$ m apart. It is evident that most of the energy in these modes is confined to the water column at this range.

Using $c_0 = 1500$ m s⁻¹ and Eq. 3, the data in Fig. 9 were used to provide an initial field to the standard PE model. The PE solution was propagated to a range of 40.96 km using a finite-difference Crank-Nicolson algorithm [23] and a range grid step $\Delta r = 5$ m. The resulting 8192 points of the correlation function Φ were processed with a hanning window and then zero padded to 2¹⁵ points before taking an FFT to produce the horizontal wavenumber spectrum. This spectrum is shown in Fig. 10. For comparison, the modal amplitudes and wavenumbers computed using the SNAP model are indicated by dots (The SNAP code was modified in order to remove the dependence of the spectral results on receiver depth. This was done by removing the normalized modal eigenfunction $u_n(z)$ from Eq. (25) in [32]). It is clear from the results in Fig. 10 that the PE-based modal decomposition method is able to recover the modal amplitudes and wavenumbers from the SNAP pressure field. For this example, the equivalent angle of mode 12 is 43° and the acoustic impedance increases by a factor of 2.75 across the water/bottom interface.

3.3 Example 3

The third example illustrates the effect of a common range-dependent feature of ocean environments, namely, the variation of water depth with range. In recent years, sound propagation over a constant slope has received considerable attention [3,6,33]. The particular model environment used here was introduced by Jensen and Kuperman [33] to demonstrate the capability of the PE method for studying upslope propagation in a wedge-shaped environment. Since this example features a penetrable bottom, the upslope propagation is associated with non-adiabatic conversion of energy from the discrete to the continuous mode spectrum. Figure 11 depicts the environmental and physical parameters for the wedge example.

A 25-Hz source is located at $r = 0$, $z = 112$ m in a water layer of depth 200 m. This waveguide is range-independent for the interval $0 < r < 5$ km. Beyond $r = 5$ km, the bottom slope changes to the constant value of 1.55° to form a wedge whose apex is at a range of 12.391 km. The computational grid sizes $\Delta r = 5$ m and $\Delta z = 0.5$ m were used for the finite-difference PE calculations. Normal mode analysis [33] indicates that three propagating modes can be supported in the 200-m depth part of the waveguide. By placing the source near the null of the second mode, only modes 1 and 3 are excited.

Figure 12 displays contours of transmission loss for this wedge-shaped environment. The contour levels were chosen to illustrate the main features of the field behaviour in this situation and vary from 63 dB to 90 dB in 3-dB intervals. The uncontoured regions in the water indicate losses less than 63 dB whereas the uncontoured regions in the bottom indicate losses greater than 90 dB. The prominent downward beam in the vicinity of the source corresponds to the radiation of the “continuous source modes” into the bottom. Within the region $0 < r < 5$ km, the field in the water exhibits an interference pattern associated with the two propagating modes. As the sound propagates up the slope, two

more well-defined beams are seen to penetrate the water-bottom interface. The upslope ranges to these beams correspond to the cutoff depths of the two propagating modes. As pointed out by Jensen and Kuperman [33], the cutoff of each mode is not abrupt. In this sloping-bottom environment, the finite distance over which cutoff takes place provides an aperture for radiation of a beam into the bottom.

Figure 13 shows the PE-based modal decomposition results for the range-independent portion of the waveguide. The upper panel shows the contoured levels of transmission loss for this region while the lower panel shows the spectral decompositions of the field at the specific ranges $r = 0, 1, \dots, 5$ km. Because this portion of the waveguide has a flat bottom, the wavenumbers of the two propagating modes do not vary with range. The peak at the higher wavenumber corresponds to mode 1. The other peak in the spectrum corresponds to mode 3. At $r = 0$, the power is nearly equally distributed between the two modes. For $r > 0$, the spectral power has been normalized to the power at zero range. It is evident that both modes lose power as they propagate down the waveguide, with mode 3 losing energy at a greater rate than mode 1. This loss of power in the propagating modes is due to the presence of absorption ($\alpha \neq 0$) in the bottom half-space. Since the decaying "tail" of mode 3 extends deeper into the bottom than the "tail" associated with mode 1, the power in mode 3 is affected more by this absorption. This larger modal attenuation coefficient can also be understood by appealing to the well-known ray-mode analogy [34] whereby the equivalent ray associated with mode 3 propagates at a steeper grazing angle than the ray associated with mode 1.

The PE modal decomposition results for the range-dependent portion of the waveguide are shown in Fig. 14. The main features in this case are the variation in modal wavenumbers with range and the conversion of mode energy from the discrete to the continuous spectrum at cutoff. Mode 3 reaches the cutoff depth between $r = 6$ and $r = 7$ km where its spectral energy is radiated into the continuous spectrum and is removed from the waveguide. Moreover, as mode 1 propagates upslope, it is seen that its wavenumber shifts to lower values. Because the modal attenuation increases as the horizontal wavenumber decreases, the amplitude of this mode is observed to decay with range until it reaches cutoff between $r = 11$ and $r = 12$ km.

4 SUMMARY

A novel method was presented for carrying out the spectral decomposition of fields propagating in range-dependent waveguides. The method makes use of an exact, nonlocal relationship connecting the solution p of the wave equation to the solution ψ of the standard parabolic equation for range-independent waveguides. In the spectral domain, this relationship is a local one and forms the basis of an algorithm for generating a solution to p from a numerical solution to ψ . In addition, it was demonstrated how the spectral properties of a suitably-defined PE field correlation function can be used to find the horizontal wavenumbers and mode amplitudes associated with the normal modes propagating in both range-independent and range-dependent waveguides. Comparisons with reference solutions for layered media demonstrated the accuracy of the PE-based spectral method. In particular, it was shown that the postprocessed PE results were not limited to low-angle propagation, small changes in the refractive index, or to a judicious choice of reference sound speed. Although the upslope wedge example represents essentially adiabatic propagation conditions, the PE-based decomposition method is applicable to situations where mode coupling is important.

References

- [1] F. D. Tappert, "The parabolic approximation method," in *Wave Propagation and Underwater Acoustics*, edited by J. B. Keller and J. S. Papadakis (Springer, New York, 1977), Chap. V, pp. 224–287.
- [2] J. A. Davis, D. White and R. C. Cavanagh, "NORDA Parabolic Equation Workshop, 31 March–3 April 1981," NORDA Tech. Note 143 (1982).
- [3] F. B. Jensen and C. M. Ferla, "Numerical solutions of range-dependent benchmark problems in ocean acoustics," *J. Acoust. Soc. Am.* **87**, 1499–1510 (1990).
- [4] J. A. DeSanto, "Relation between the solutions of the Helmholtz and parabolic equations for sound propagation," *J. Acoust. Soc. Am.* **62**, 295–297 (1977).
- [5] D. J. Thomson and D. H. Wood, "A postprocessing method for removing phase errors in the parabolic equation," *J. Acoust. Soc. Am.* **82**, 224–232 (1987).
- [6] F. B. Jensen and H. Schmidt, "Spectral decomposition of PE fields in a wedge-shaped ocean," in *Progress in Underwater Acoustics*, edited by H. Merklinger (Plenum, New York, 1987), pp. 557–564.
- [7] F. B. Jensen and H. Schmidt, "Efficient numerical solution technique for wave propagation in horizontally stratified environments," *Comp. & Maths. with Appl.* **11**, 699–715 (1985).
- [8] H. Schmidt, "SAFARI Seismo-Acoustic Fast field Algorithm for Range-Independent environments," SACLANTCEN Report SR-113 (1988).
- [9] K. E. Gilbert, X. Di and D. Huang, "Spectral decomposition of parabolic equation fields," *J. Acoust. Soc. Am. Suppl. 1* **85**, S70 (1989).
- [10] K. E. Gilbert and R.B. Evans, "A Green's function method for one-way wave propagation in a range-dependent ocean environment," in *Ocean Seismo-Acoustics*, edited by T. Akal and J. M. Berkson (Plenum, New York, 1986), pp. 21–28.
- [11] M. D. Feit and J. A. Fleck, Jr., "Computation of mode properties in optical fiber waveguides by a propagating beam method," *Appl. Optics* **19**, 1154–1164 (1980).
- [12] D. J. Thomson and N. R. Chapman, "A wide-angle split-step algorithm for the parabolic equation," *J. Acoust. Soc. Am.* **74**, 1848–1854 (1983).
- [13] D. J. Thomson, "Modal decomposition of waves in range-varying waveguides," *J. Acoust. Soc. Am. Suppl. 1* **86**, S53–S54 (1989).
- [14] D.J. Thomson, "Modal decomposition of PE fields in a range-dependent environment," Defence Research Establishment Pacific, Victoria, B.C., Canada, Preprint 90-08, 1990.

- [15] D.S. Ahluwalia and J.B. Keller, "Exact and asymptotic representations of the sound field in a stratified ocean," in *Wave Propagation and Underwater Acoustics*, edited by J. B. Keller and J. S. Papadakis (Springer, New York, 1977), Chap. II, pp. 14–85.
- [16] F.B. Jensen, "Numerical models in underwater acoustics," in *Hybrid Formulation of Wave Propagation and Scattering*, edited by L.B. Felsen (Nijhoff, Dordrecht, 1984), pp. 295–335.
- [17] M.B. Porter, F. B. Jensen and C. M. Ferla, "The problem of energy-conservation in one-way models," *J. Acoust. Soc. Am.* **89**, 1058–1067 (1991).
- [18] G.H. Brooke and D.J. Thomson, "A single-scatter formalism for improving PE calculations in range-dependent media," in *Proceedings of the Second Parabolic Equation Workshop May 6–9, 1991*, edited by S.A. Chin-Bing, D.B. King, J.A. Davis and R.B. Evans (Naval Research Laboratory NRL/BE/7181-93-0001, Stennis Space Center, MS, 1993), pp. 126–144.
- [19] L. Fishman and J. J. McCoy, "A new class of propagation models based on a factorization of the Helmholtz equation," *Geophys. J. R. Astron. Soc.* **80**, 439–461 (1985).
- [20] L. Fishmar and S.C. Wales, "Phase space methods and path integration: the analysis and computation of scalar wave equations," *J. Comput. and Appl. Math.* **20**, 219238 (1987).
- [21] M.D. Collins, "Benchmark calculations for higher-order parabolic equations," *J. Acoust. Soc. Am.* **87**, 1535–1538 (1990).
- [22] I. S. Gradshteyn and I. M. Ryzhik, *Table of Integrals, Series, and Products*, edited by A. Jeffrey (Academic, New York, 1980).
- [23] D.J. Thomson, "Wide-angle parabolic equation solutions to two range-dependent benchmark problems," *J. Acoust. Soc. Am.* **87**, 1514–1520 (1990).
- [24] F.B. Jensen, "The art of generating meaningful results with numerical codes," *J. Acoust. Soc. Am. Suppl. 1* **80**, S20 (1986).
- [25] T.C. Yang, "A method of range and depth estimation by modal decomposition," *J. Acoust. Soc. Am.* **82**, 1736–1745 (1987).
- [26] G.R. Wilson, R.A. Koch and P.J. Vidmar, "Matched mode localization," *J. Acoust. Soc. Am.* **84**, 310–320 (1988).
- [27] E.C. Shang, "An efficient high-resolution method of source localization processing in mode space," *J. Acoust. Soc. Am.* **86**, 1960–1964 (1989).
- [28] T.C. Yang, "Effectiveness of mode filtering: A comparison of matched-field and matched-mode processing," *J. Acoust. Soc. Am.* **87**, 2072–2084 (1990).
- [29] D.J. Thomson, G.R. Ebbeson and B.H. Maranda, "Modal decomposition of the pressure field on a vertical line array," *J. Acoust. Soc. Am.* **89**, 2000 (1991).

- [30] G.R. Ebbeson, D.J. Thomson and B.H. Maranda, "Spectral decomposition of underwater sound received on a vertical line array," in *Oceans' 91 Proceedings*, Vol. 3 (IEEE, Piscataway, 1991), 1336–1343 (1991).
- [31] G.R. Ebbeson, "Mode-stripping by the continental slope in an Arctic environment," Defence Research Establishment Pacific, Victoria, B.C., Canada, Preprint 90-07, 1990.
- [32] F.B. Jensen and M.C. Ferla, "SNAP: The SACLANTCEN Normal-Mode Acoustic Propagation Loss Model," SACLANTCEN ASW Research Centre, San Bartolomeo, Italy, Memorandum SM-121, 1979.
- [33] F. B. Jensen and W.A. Kuperman, "Sound propagation in a wedge-shaped ocean with a penetrable bottom," *J. Acoust. Soc. Am.* **57**, 1564–1566 (1980).
- [34] C.T. Tindle and K.M. Guthrie, "Rays as interfering modes in underwater acoustics," *J. Sound Vib.* **34**, 291–295 (1974)

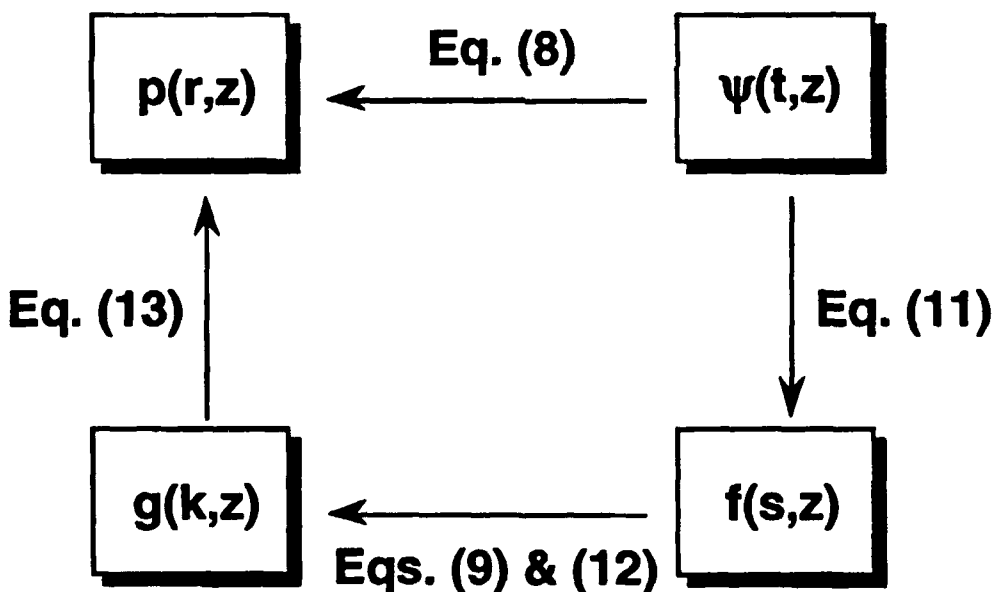


Figure 1. Postprocessing algorithm for numerically computing p from ψ .

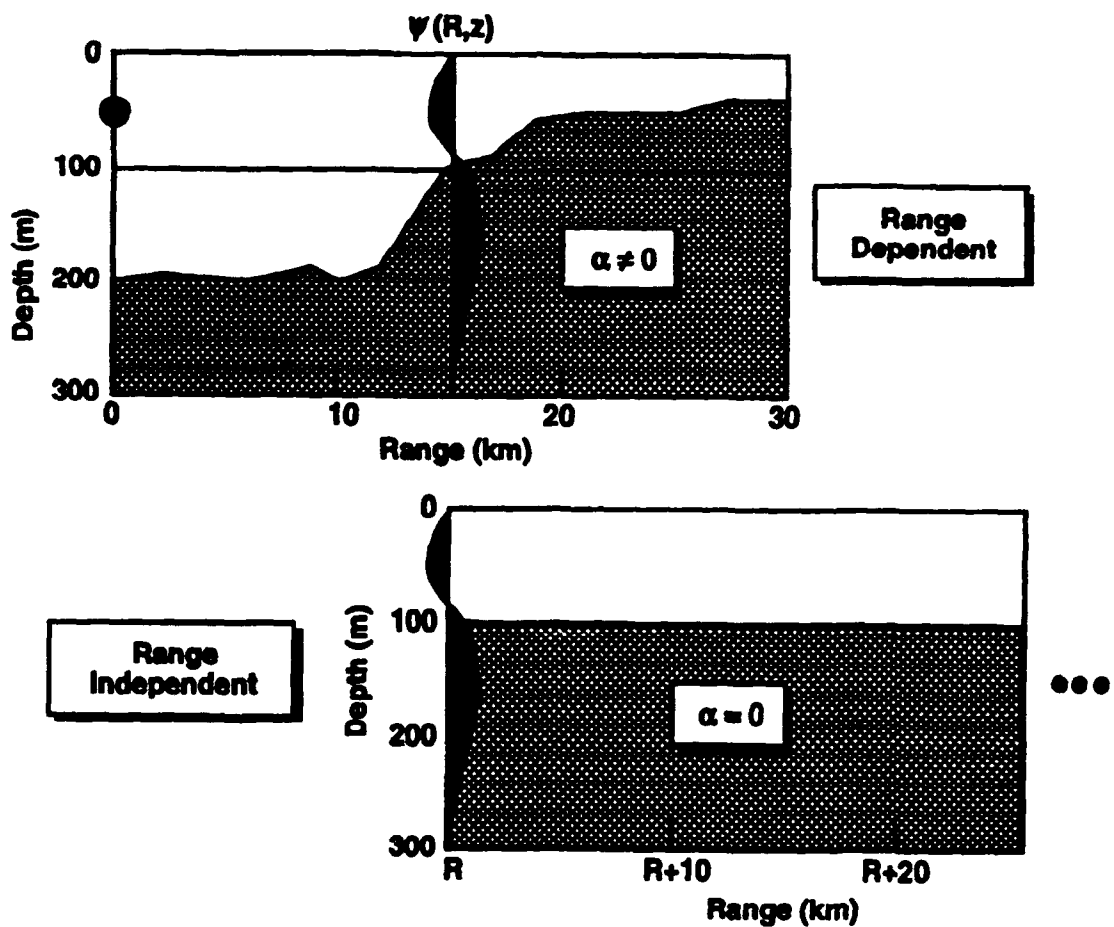


Figure 2. Application of the PE-based modal decomposition method to the field $\psi(R, z)$ in a range-dependent waveguide.

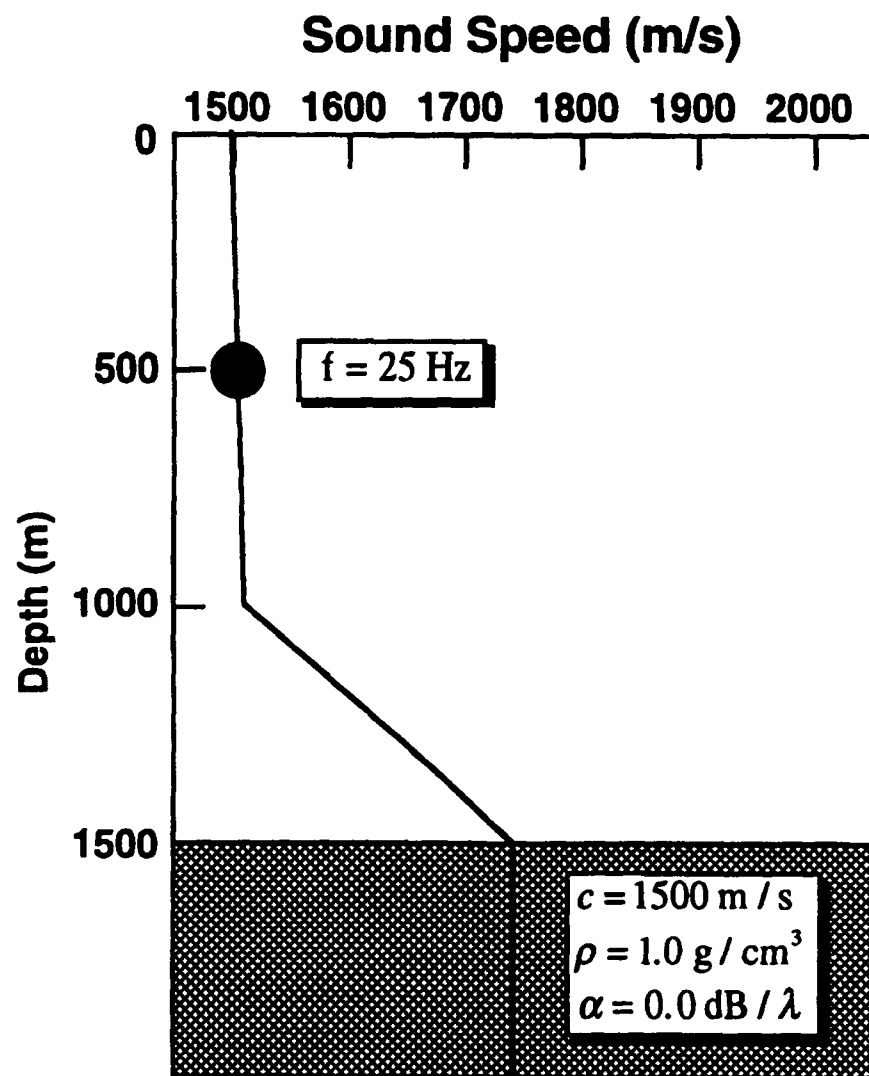


Figure 3. Physical and environmental parameters for example 1.

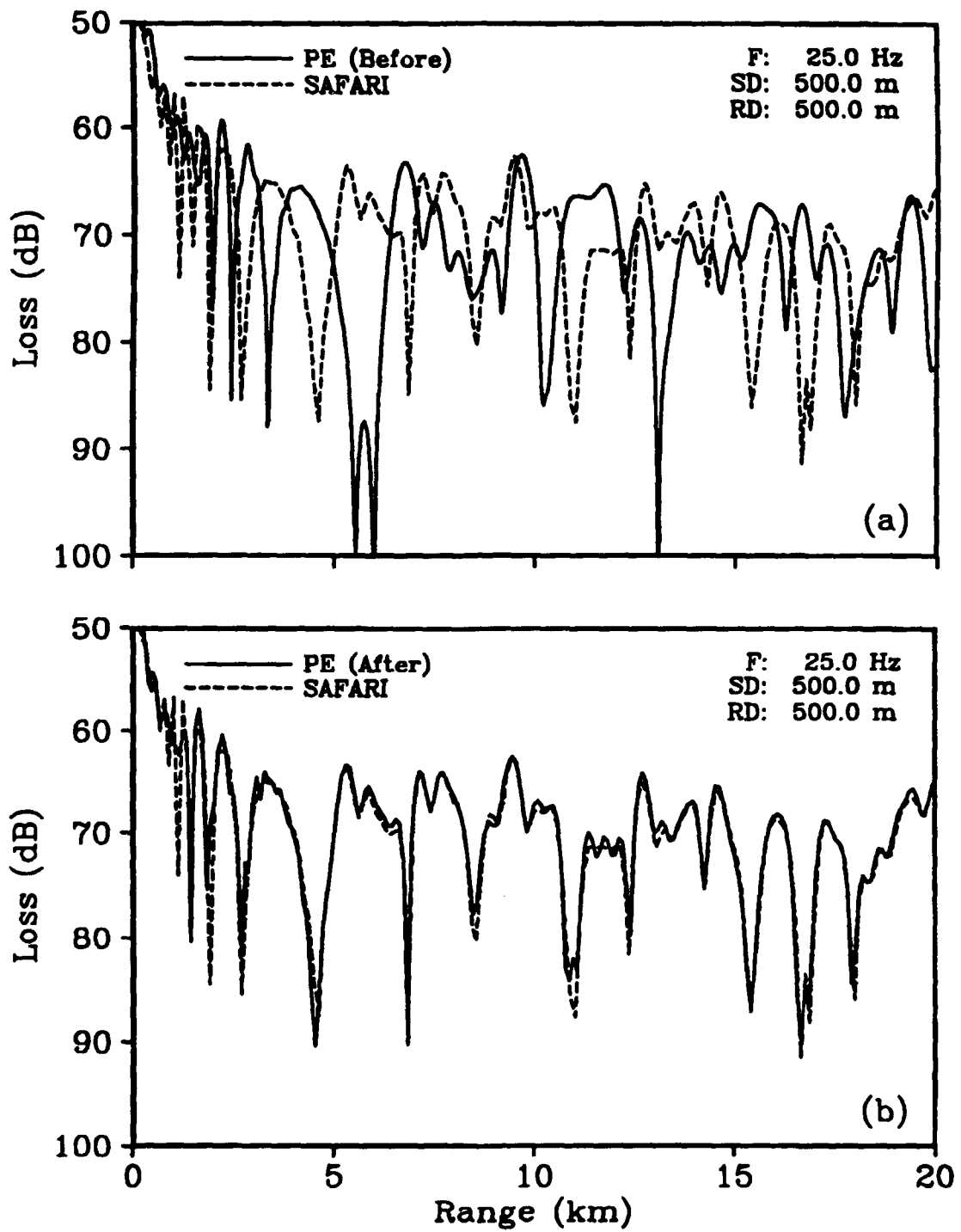


Figure 4. PE and SAFARI transmission loss comparisons for example 1 showing (a) standard PE (before) and (b) postprocessed PE (after); $c_0 = 1300 \text{ ms}^{-1}$.

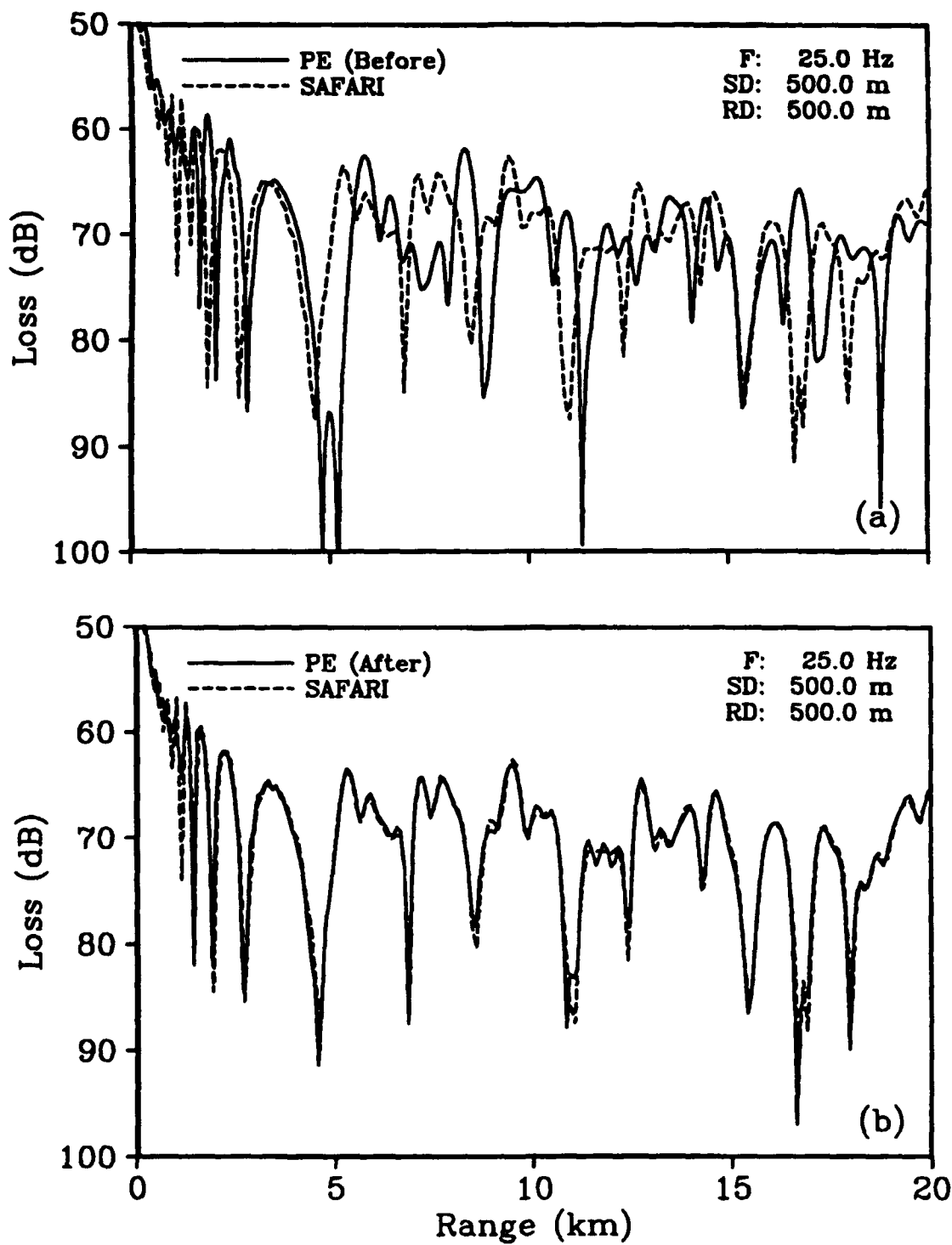


Figure 5. PE and SAFARI transmission loss comparisons for example 1 showing (a) standard PE (before) and (b) postprocessed PE (after); $c_0 = 1500 \text{ m s}^{-1}$

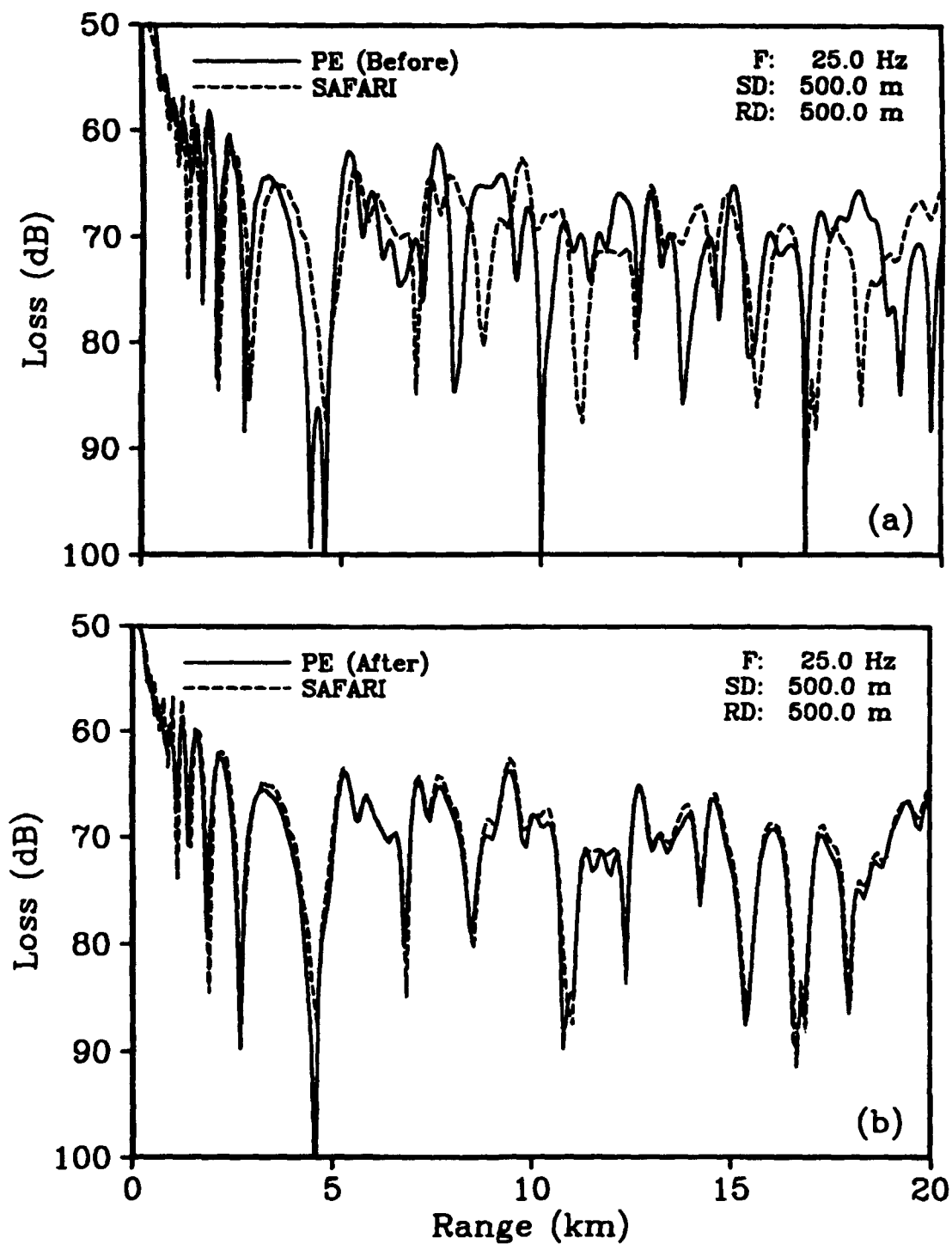


Figure 6. PE and SAFARI transmission loss comparisons for example 1 showing (a) standard PE (before) and (b) postprocessed PE (after); $c_0 = 1700 \text{ m s}^{-1}$.

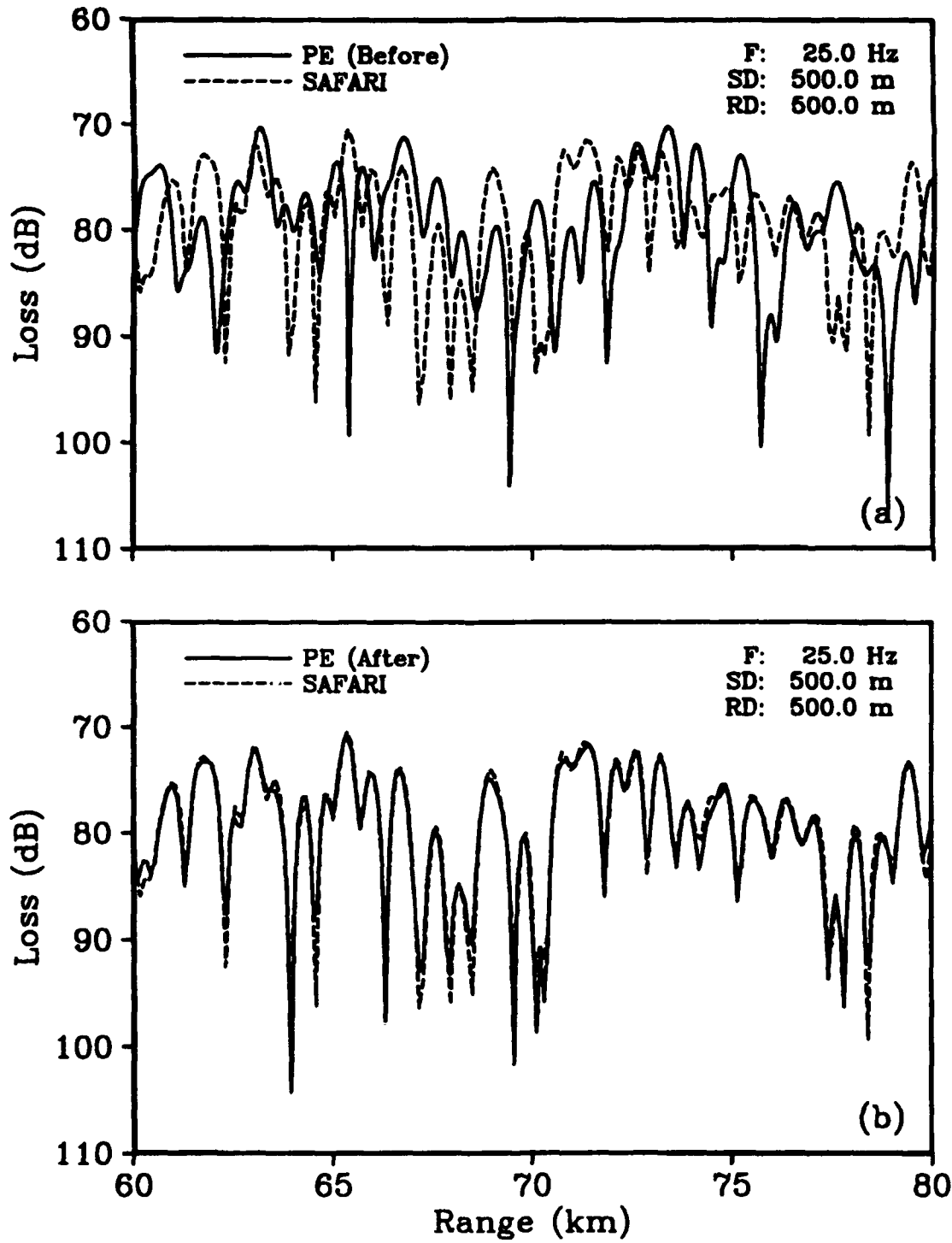


Figure 7. PE and SAFARI long-range transmission loss comparisons for example 1 showing (a) standard PE (before) and (b) postprocessed PE (after). $c_0 = 1500 \text{ m s}^{-1}$.

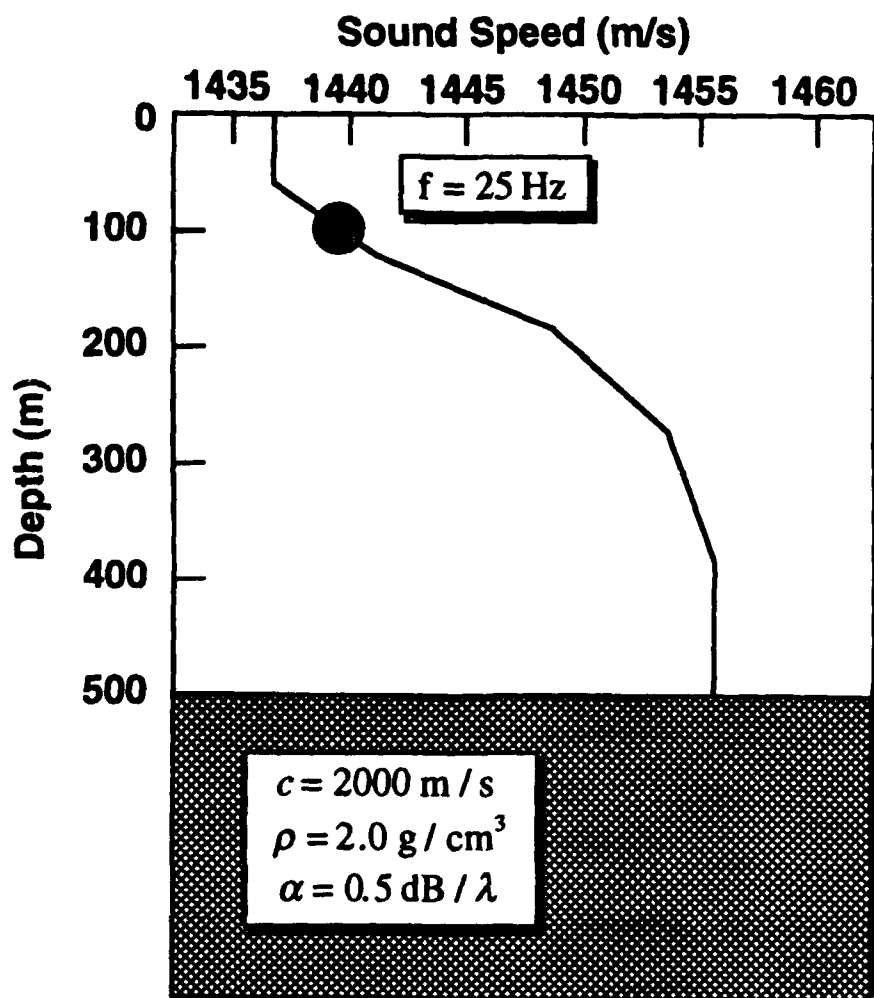


Figure 8. Physical and environmental parameters for example 2.

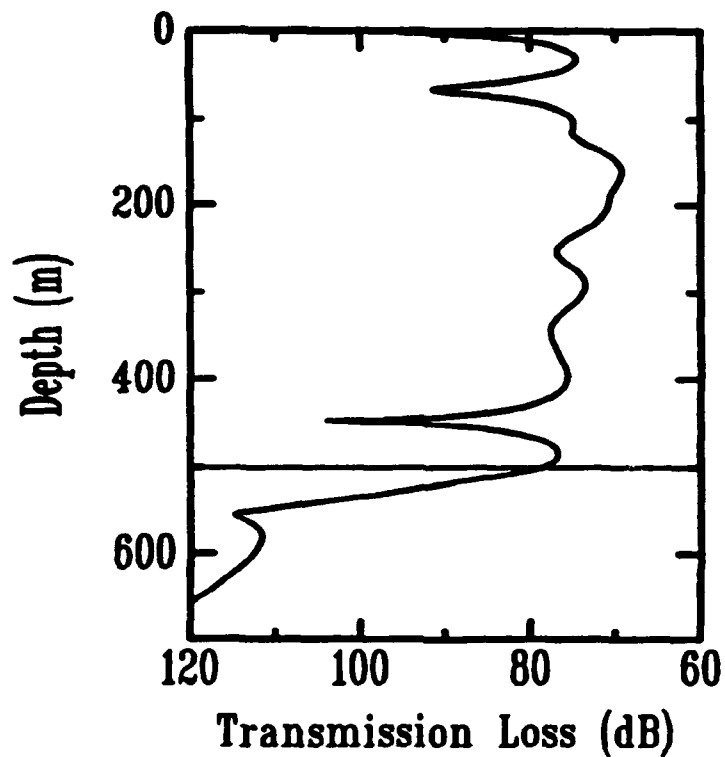


Figure 9. Transmission loss versus depth at a range of 50 km for example 2.

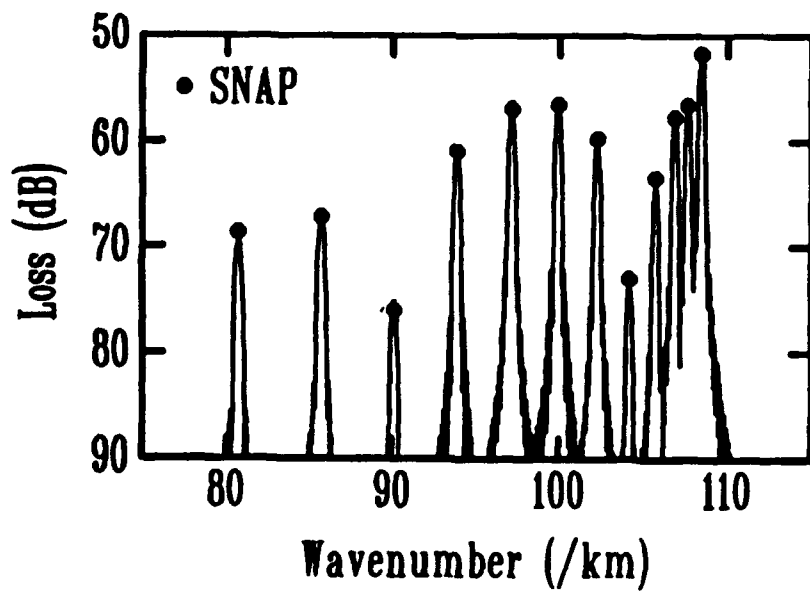


Figure 10. PE and SNAP modal decomposition comparison for example 2.

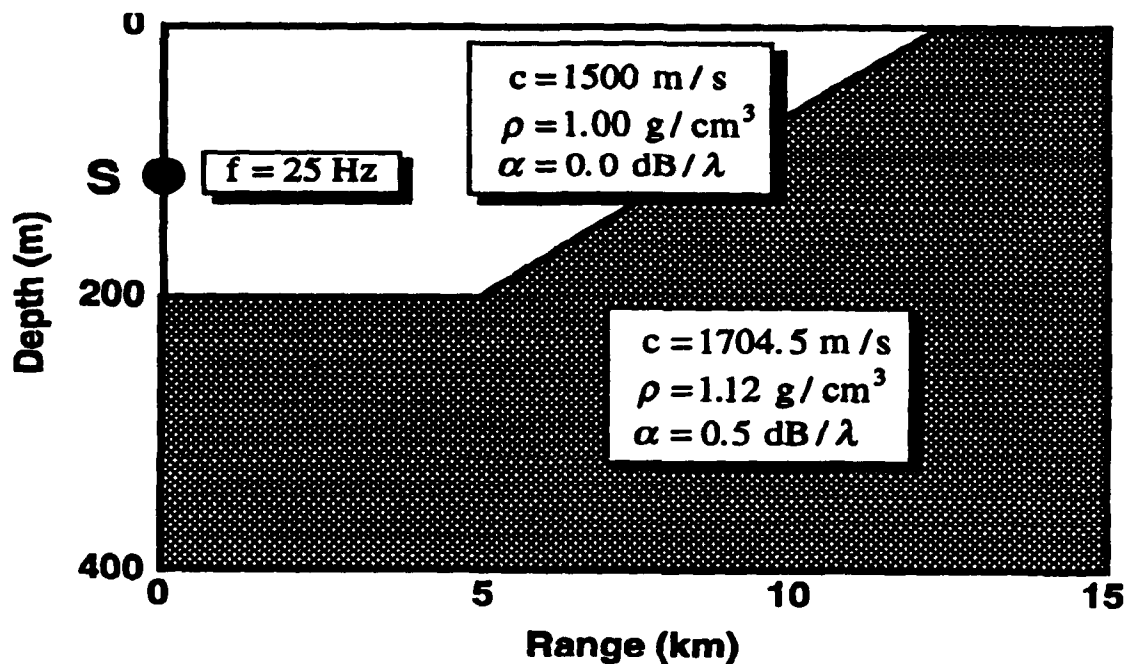


Figure 11. Physical and environmental parameters for example 3

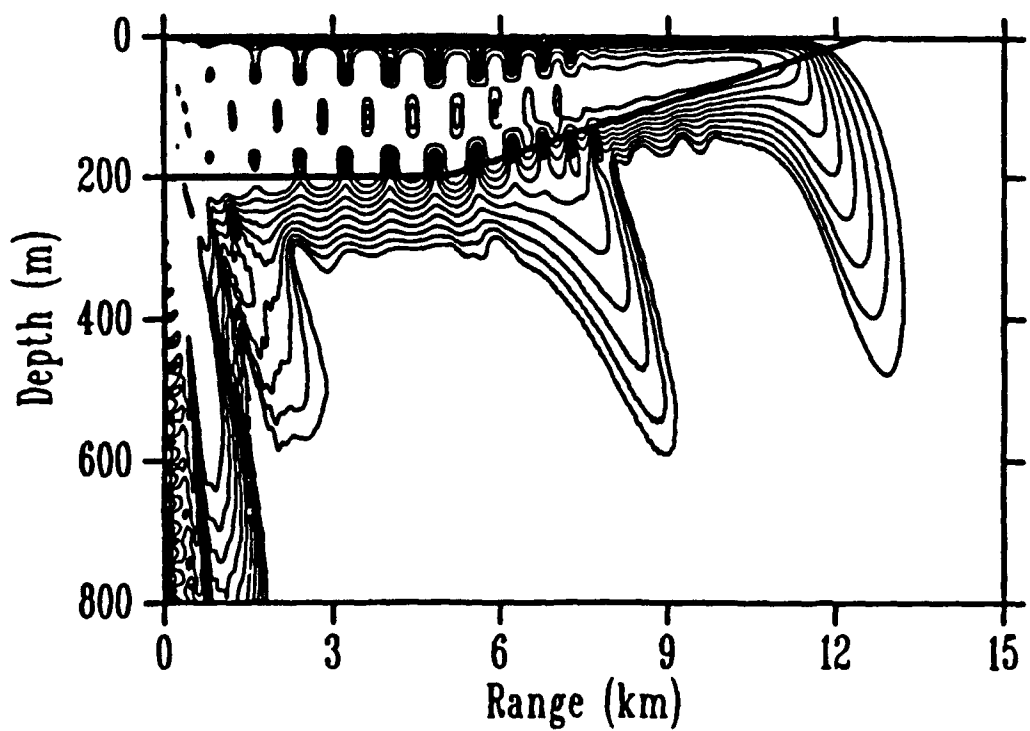


Figure 12. PE transmission loss contours for example 3.

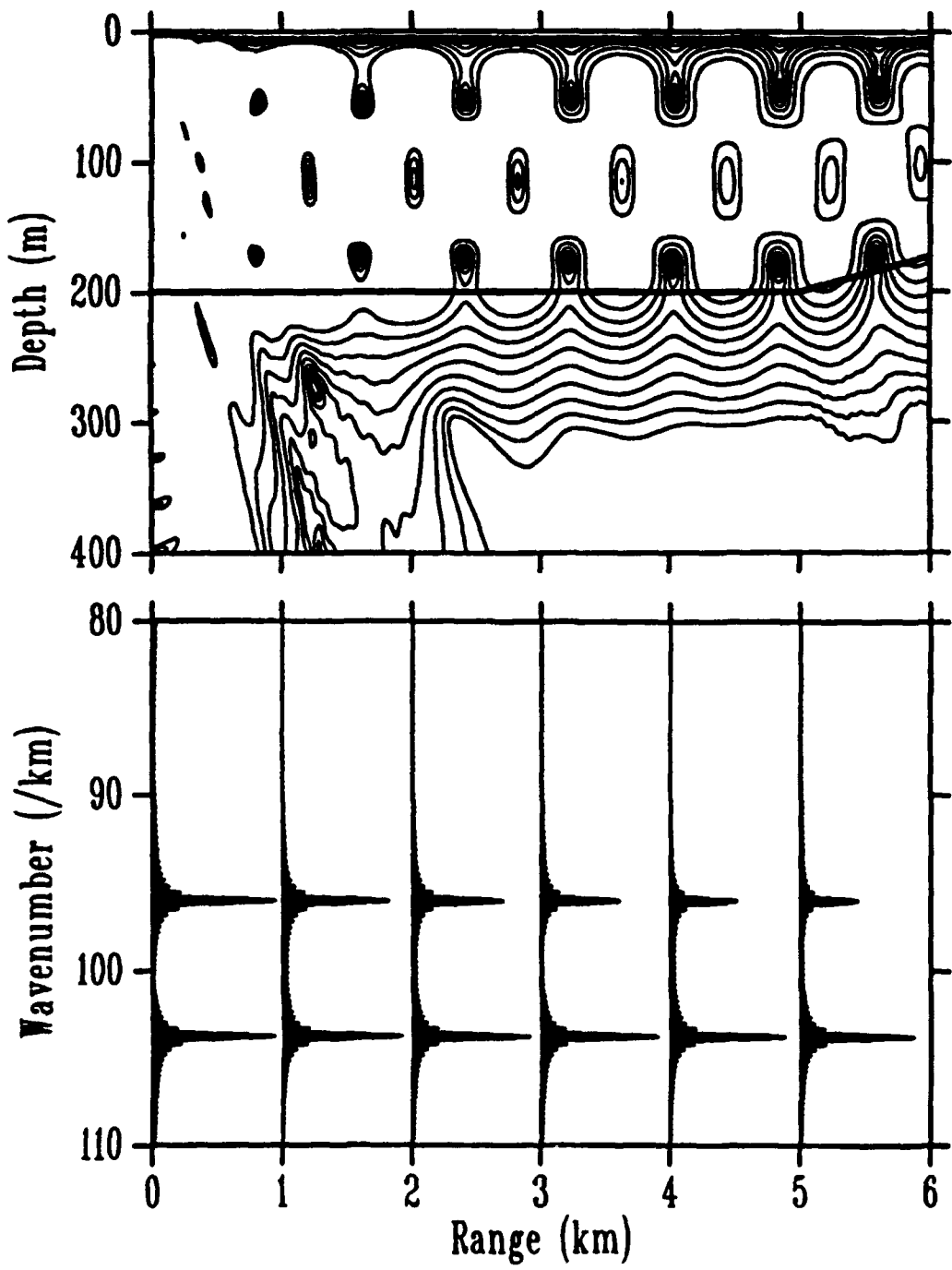


Figure 13. PE modal decomposition (lower panel) and corresponding loss contours (upper panel) in the flat-bottom region of example 3.

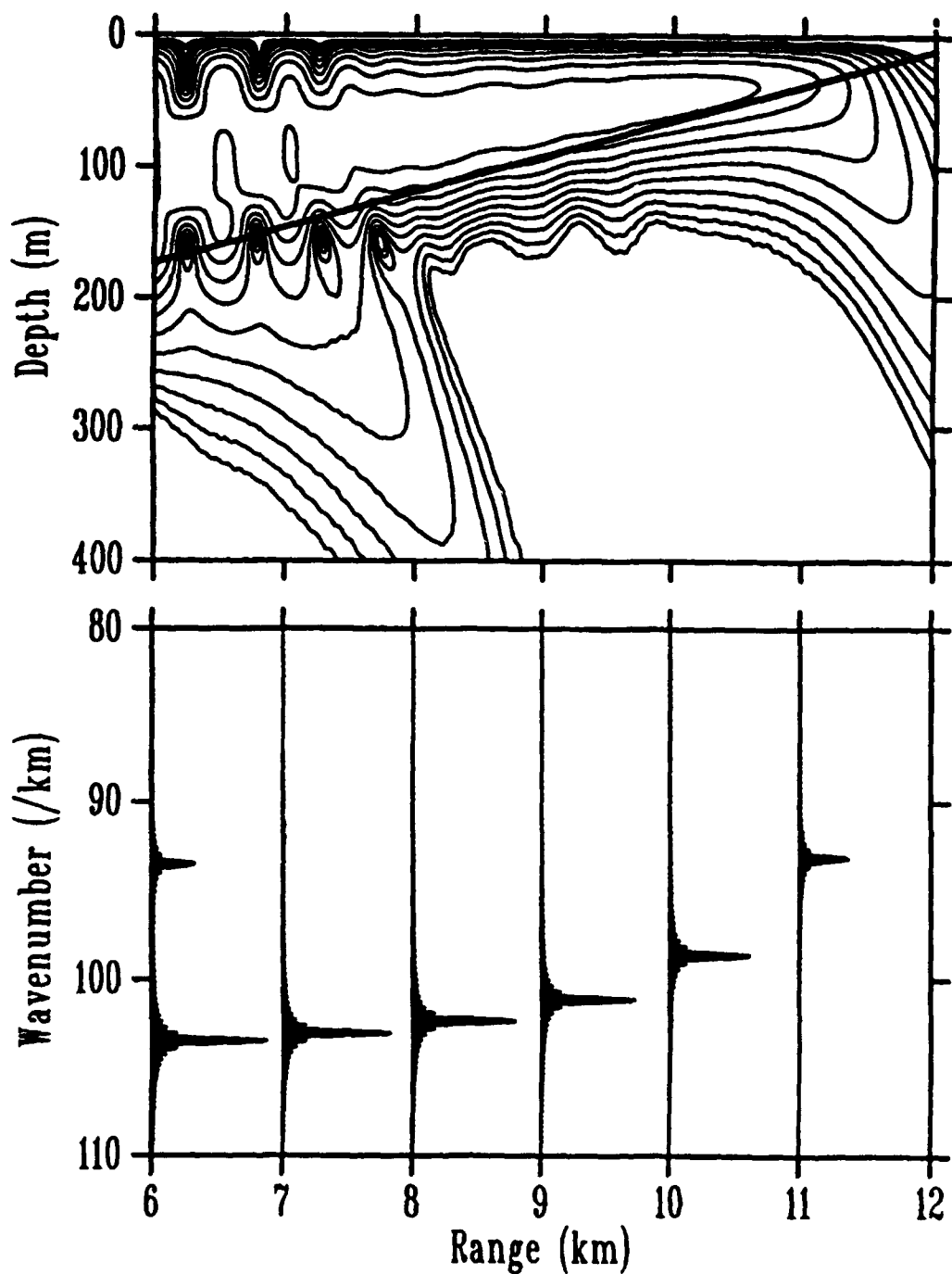


Figure 14. PE modal decomposition (lower panel) and corresponding loss contours (upper panel) in the sloping-bottom region of example 3.

The OPTAMAS System

[Editors' Notes]

The transmission loss model in the OPTAMAS system was used to supply some of the results contained in the PE Workshop II proceedings. (No representative of the OPTAMAS system was able to attend the workshop; these results were supplied by Nils Paz [Systems Integrated] after the workshop had concluded.) Since some members of the underwater acoustic research community may not be familiar with the OPTAMAS system and its design criteria, it was felt that a short discussion of the system would be in order. The following information was obtained from the OPTAMAS User's Guide (1990).

OPTAMAS is an acronym for the Optimization of the Performance of Theater ASW Mobile Acoustic Sensors. The OPTAMAS system was originally developed in 1988 to provide acoustic performance predictions, to manage contacts of acoustic targets, and to aid decisions that involve asset-allocation in searches over a large ocean area. It also combined environmental data, sensor data, and target data that cover a large ocean area.

The OPTAMAS system was developed by integrating several existing software and database products to provide a system consisting of an acoustic propagation model, a beam noise processor, an analyzer for in situ BT measurements to produce a 3-D grid of the sound speed field based upon environmental data bases, and an optical scanner and color copier—all of this operating on a low-cost, high-performance workstation. With the OPTAMAS system, the ASW commander could easily and effectively determine the optimum employment of towed arrays and sonobuoy fields for surveillance and tactical missions. The OPTAMAS system provides accurate and fast determination of signal excess, probability of detection, target position estimation, and search tactics for a variety of sensors and targets.

Some of the key features of the OPTAMAS system are as follows:

- On-Site collected water column temperature profiles can be used to update the historical sound speed data supplied via the standard Navy Generalized Digital Environmental Model (GDEM) by using the Tactical Thermal Analysis Program (TTAP).
- The acoustic propagation module of OPTAMAS is a vectorized version of the Navy Standard Parabolic Equation model (Brock 1975) and based on the approach described in the PESOGEN-II User's Manual Supplement (1990).

PE Workshop II: Part 3 — Contributed Papers

- The Wagstaff Iterative Technique (WIT) is used to provide estimates of the directional ambient noise field from historical or near real-time collected data. This module will produce a “noise heading rose” and an “array heading surface” which permit optimal array-deployment-decisions to be made by the ASW operator.
- The OPTAMAS computer-assisted search module uses the environmental acoustic data provided by TTAP, the PE model, and WIT to provide search planning and target localization information, and individual sensor system performance estimates.

The only part of the OPTAMAS system that is relevant to the PE Workshop II is the acoustic propagation model that was used to provide solutions to the test cases. As noted, this propagation model is a vectorized computer code of an earlier version of the Navy Standard PE model. It is based on the approach used in the PE Solution Generator (PESOGEN) system. Thus, it uses the split-step solution algorithm and obtains wide-angle capability via the Thomson-Chapman formulation.

It is important to note that, as in the case of the Navy Standard PE model, the OPTAMAS system also uses parameters that are preselected for implementation in the operational Navy. The custodian of OPTAMAS did not change its operational parameters for the PE Workshop II test case results nor did he change its reference distance to the distance of 1 m as was used by all other workshop modelers. The custodian of OPTAMAS estimates that the results from OPTAMAS will be approximately 2 dB different from the results of the other models in the PE Workshop II.

An exception was made in the size of the range steps used by OPTAMAS; the range steps were decreased by 20 in order to minimize the choppy looking results. The choppy “steps” in the transmission loss curves are a consequence of the OPTAMAS system’s requirement to write the results in integer format rather than floating point format. This is done to reduce the amount of computer storage required.

REFERENCES

H. K. Brock, “The AESD parabolic equation model,” AESD TN-75-07, Office of Naval Research, Arlington, VA (1975).

“OPTAMAS 2.1 User’s Guide”, Systems Integrated, 8080 Dagget Street, San Diego, CA, Sept. 1990.

“PESOGEN-II User’s Manual Supplement, Version V2.8”, Technical Manual TM 03-90, Daubin Systems Corp., Key Biscayne, FL, Feb. 1990.

Bibliography

- Abrahamsson, L., and H.O. Kreiss (1990). "Boundary conditions for the parabolic equation in a range-dependent duct," *J. Acoust. Soc. Am.* **87**, 2438–2441.
- Baer R. N. (1981). "Propagation Through a Three Dimensional Eddy Including Effect on an Array," *J. Acoust. Soc. Am.* **69**, 70–75.
- Bamberger, A., B. Engquist, L. Halpern, and P. Joly (1988a). "Parabolic wave equation approximations in heterogeneous media," *SIAM J. Appl. Math.* **48**, 99–128.
- Bamberger, A., B. Engquist, L. Halpern, and P. Joly (1988b). "Higher order paraxial wave equation approximations in heterogeneous media," *SIAM J. Appl. Math.* **48**, 129–154.
- Berman, D. H., E. B. Wright, and R. N. Baer (1989). "An optimal PE-type wave equation," *J. Acoust. Soc. Am.* **86**, 228–233.
- Botseas, G., D. Lee, and K. E. Gilbert (1983). "IFD: Wide Angle Capability," Naval Underwater Systems Center, New London, CT, U.S.A., NUSC TR 6905.
- Botseas, G., D. Lee, and D. King (1987). "FOR3D: A Computer Model for Solving the LSS Three-Dimensional, Wide Angle Wave Equation," Naval Underwater Systems Center, New London, CT, U.S.A., NUSC TR 7943.
- Bremmer, H. (1951). "The W.K.B. approximation as the first term of a geometric-optical series," *Comm. Pure and Appl. Math.* **4**, 105–115.
- Brock, H. K. (1975). "The AESD parabolic equation model," AESD TN-75-07, Office of Naval Research, Arlington, VA, U.S.A.
- Chin-Bing, S. A., and J. E. Murphy (1993a). "Shear effects on ocean acoustic propagation due to step-periodic roughness along the ocean bottom interface," *Mathematical Modelling and Scientific Computing* **2**, 780–785.
- Chin-Bing, S. A., and J. E. Murphy (1993b). "Long-Range Ocean Acoustic-Seismic Propagation Modeling Using Hybrid Finite Element and Parabolic Equation Models," in *Computational Acoustics: Scattering, Supercomputing and Propagation, Vol. 1*, R. L. Lau, D. Lee, and A. R. Robinson (eds.), (Elsevier Publishers (North-Holland), Amsterdam), 105–121.

PE Workshop II: Part 3 — Contributed Papers

- Claerbout, J. F. (1970). "Course grid calculations of waves in inhomogeneous media with application to delineation of complicated seismic structure," *Geophysics* **35**, 20–21.
- Claerbout, J. F. (1976). *Fundamentals of Geophysical Data Processing* (McGraw-Hill, New York), 206–207.
- Clayton, R. W., and B. Engquist (1980). "Absorbing boundary conditions for wave-equation migration," *Geophysics* **45**, 895–904.
- Collins, M. D. (1988a). "Low-frequency, bottom-interacting pulse propagation in range-dependent oceans," *IEEE J. Ocean. Eng.* **13**, 222–228.
- Collins, M. D. (1988b). "The time-domain solution of the wide-angle parabolic equation including the effects of sediment dispersion," *J. Acoust. Soc. Am.* **84**, 2114–2125.
- Collins, M. D. (1988c). "FEPE User's Guide," Naval Research Laboratory, Stennis Space Center, MS, U.S.A., NORDA Technical Note 365.
- Collins, M. D. (1989a). "A nearfield asymptotic analysis for underwater acoustics," *J. Acoust. Soc. Am.* **85**, 1107–1114.
- Collins, M. D. (1989b). "Applications and time-domain solution of higher-order parabolic equations in underwater acoustics," *J. Acoust. Soc. Am.* **86**, 1097–1102.
- Collins, M. D. (1989c). "A higher-order parabolic equation for wave propagation in an ocean overlying an elastic bottom," *J. Acoust. Soc. Am.* **86**, 1459–1464.
- Collins, M. D. (1990a). "The rotated parabolic equation and sloping ocean bottoms," *J. Acoust. Soc. Am.* **87**, 1035–1037.
- Collins, M. D. (1990b). "Benchmark calculations for higher-order parabolic equations," *J. Acoust. Soc. Am.* **87**, 1535–1538.
- Collins, M. D., and S. A. Chin-Bing (1990). "A three-dimensional parabolic equation model that includes the effects of rough boundaries," *J. Acoust. Soc. Am.* **87**, 1104–1109.
- Collins, M. D. (1991). "Higher-order Padé approximations for accurate and stable elastic parabolic equations with application to interface wave propagation," *J. Acoust. Soc. Am.* **89**, 1050–1057.
- Collins, M. D., and E. K. Westwood (1991). "A higher-order energy-conserving parabolic equation for range-dependent ocean depth, sound speed, and density," *J. Acoust. Soc. Am.* **89**, 1068–1075.

PE Workshop II: Part 3 — Contributed Papers

- Collins, M. D., and R. B. Evans (1992). "A two-way parabolic equation for acoustic back scattering in the ocean," *J. Acoust. Soc. Am.* **91**, 1357–1368.
- Corones, J. P., B. DeFacio, and R. J. Krueger (1982). "Parabolic approximations to the time-independent elastic wave equation," *J. Math. Phys.* **23**, 577–586.
- Davis, J. A., D. White, and R. C. Cavanagh (1982), "NORDA Parabolic Equation Workshop, 31 March – 3 April 1981," Naval Research Laboratory, Stennis Space Center, MS, U.S.A., NORDA Technical Note 143.
- DeSanto, J. A. (1977). "Relation between the solutions of the Helmholtz and parabolic equations for sound propagation," *J. Acoust. Soc. Am.* **62**, 295–297.
- Douglas, J., Jr. (1956). "The Solution of Diffusion Equation by a High Order Correct Difference Equation," *J. Math. Phys.*, **35**, 145–151.
- Evans, R. B. (1983). "A coupled mode solution for acoustic propagation in a waveguide with stepwise depth variations of a penetrable bottom," *J. Acoust. Soc. Am.* **74**, 188–195.
- Evans, R. B. (1986). "COUPLE: A user's manual," Naval Research Laboratory, Stennis Space Center, MS, U.S.A., NORDA Technical Note 332.
- Felsen, L. B. (1990). "Benchmarks: An option for quality assessment," *J. Acoust. Soc. Am.* **87**, 1497–1498.
- Fisher, C. A., H. B. Ali, and M. J. Authement (1988). "A VLF propagation experiment off the coast of Oregon: Measurements and numerical predictions," *J. Acoust. Soc. Am. Suppl. 1*, **84**, S91.
- Fisher, C. A., H. B. Ali, and M. J. Authement (1989), "A VLF Propagation Experiment off the Coast of Oregon Measurements and Numerical Predictions," Naval Research Laboratory, Stennis Space Center, MS, U.S.A., NORDA Technical Note 418.
- Fishman, L., and J. J. McCoy (1984). "Derivation and application of extended parabolic wave theories. Part 1. The factorized Helmholtz equation," *J. Math. Phys.* **25**, 285.
- Gilbert, K. E., X. Di, and D. Huang (1989). "Spectral decomposition of parabolic equation fields," *J. Acoust. Soc. Am. Suppl. 1* **85**, S70.
- Greene, R. R. (1984). "The rational approximation to the acoustic wave equation with bottom interaction," *J. Acoust. Soc. Am.* **76**, 1764–1773.
- Greene, R. R. (1985). "A high-angle one-way wave equation for seismic wave propagation along rough and sloping interfaces," *J. Acoust. Soc. Am.* **77**, 1991–1998.

PE Workshop II: Part 3 — Contributed Papers

- Hardin, R. H., and F. D. Tappert (1973). "Application of the Split-Step Fourier Method to the Numerical Solution of Nonlinear and Variable Coefficient Wave Equations," *SIAM Rev.* **15**, 423.
- Holmes, E. S., and L. A. Gainey (1991). "Software product specification for the parabolic equation model version 3.2," OAML-SPS-22, Naval Oceanographic Office, Bay St. Louis, MS, U.S.A.
- Hudson, J. A. (1980). "A parabolic approximation for elastic waves," *Wave Motion* **2**, 207-214.
- Jensen, F. B., and H. Krol (1975). "The use of the parabolic equation method in sound propagation modeling," SACLANTCEN Memo. SM-72, SACLANT Undersea Research Centre, La Spezia, Italy.
- Jensen, F. B., and C. M. Ferla (1979). "SNAP: the SACLANTCEN normal-mode acoustic propagation model," SACLANTCEN Memo. SM-121, SACLANT Undersea Research Centre, La Spezia, Italy. (NTIS No. AD-A067 256).
- Jensen, F. B., and W. A. Kuperman (1980). "Sound propagation in a wedge-shaped ocean with a penetrable bottom," *J. Acoust. Soc. Am.* **57**, 1564-1566.
- Jensen, F. B., and M. G. Martinelli (1985). "The SACLANTCEN parabolic equation model (PAREQ)," SACLANT Undersea Research Centre, La Spezia, Italy.
- Jensen, F. B., and H. Schmidt (1987). "Spectral decomposition of PE fields in a wedge-shaped ocean," in *Progress in Underwater Acoustics*, H. Merklinger (ed.), (Plenum, New York), 557-564.
- Jensen, F. B., and C. M. Ferla (1990). "Numerical solutions of range-dependent benchmark problems in ocean acoustics," *J. Acoust. Soc. Am.* **87**, 1499-1510.
- Knightly, G. H., D. Lee, and D.F. St. Mary (1987). "A higher-order parabolic wave equation," *J. Acoust. Soc. Am.* **82**, 580-587.
- Knightly, G.H., G.Q. Li, D.F. St. Mary, and D. Lee (1989). "A Numerical Treatment of the Fluid/Elastic Interface for the Potential Equations," *J. Acoust. Soc. Am., Suppl. 1* **86**, S65.
- Knightly, G. H., G. Q. Li, D. F. St. Mary, and D. Lee (1990). "Elastic Parabolic Equation and the Fluid/Elastic Interface," *J. Acoust. Soc. Am., Suppl. 1* **88**, S59.
- Kriegsmann, G. A. (1985). "A multiscale derivation of a new parabolic equation which includes density variations," *Comp. Maths. Appl.* **11**, 817-821.
- Kriegsmann, G. A., A. Taflove, and K. R. Umashankar (1987). "A new formulation of

electromagnetic wave scattering using an on-surface radiation boundary condition approach," *IEEE Trans. Ant. and Prop.* **35**, 153–161.

Landers, T., and J. F. Claerbout (1972). "Numerical calculations of elastic waves in laterally inhomogeneous media," *J. Geophys. Res.* **77**, 1476–1483.

Lee, D., and J. S. Papadakis (1980). "Numerical Solutions of the Parabolic Wave Equation: An Ordinary-Differential-Equation Approach," *J. Acoust. Soc. Am.* **68**, 1482–1488.

Lee, D., G. Botseas, and J. S. Papadakis (1981). "Finite-Difference Solution to the Parabolic Wave Equation," *J. Acoust. Soc. Am.* **70**, 795–800.

Lee, D., and G. Botseas (1982). "IFD: An Implicit Finite-Difference Computer Model for Solving the Parabolic Equation," Naval Underwater Systems Center, New London, CT, U.S.A., NUSC Tech. Rep. 6659 (NTIS No. AD-A117 701).

Lee, D., and S. T. McDaniel (1983). "A finite-difference treatment of interface conditions for the parabolic wave equation: The irregular interface," *J. Acoust. Soc. Am.* **73**, 1441–1447.

Lee, D., Y. Saad, and M.H. Schultz (1986). "An efficient method for solving the three-dimensional wide angle wave equation," Yale University, New Haven, CT, U.S.A., Yale Univ. Res. Rep. YALEU/DCS/RR-463.

Lee, D., and S. T. McDaniel (1988). *Ocean Acoustic Propagation by Finite Difference Methods*, (Pergamon Press, Oxford).

Lee, D., Y. Saad, M. H. Schultz (1988). "An Efficient Method for Solving the Three-Dimensional Wide Angle wave Equation," in *Computational Acoustics: Wave Propagation*, D. Lee, R.L. Sternberg, and M.H. Schultz (eds.), (Elsevier Publishers (North-Holland), Amsterdam), 75–90.

Lee, D., and F. Saied (1990). "A Fourth Order Finite Difference Scheme to Improve the Computation Speed of Wide Angle Propagation," in *Computational Acoustics: Ocean-Acoustic Model and Supercomputing*, D. Lee, A. Cakmak, and R. Vichnevetsky (eds.), (Elsevier Publishers (North-Holland), Amsterdam), 27–36.

Lee, D., D. F. St. Mary, M. H. Schultz, and W. L. Siegmann (1990). "A New Model for Marching Computation of Ocean Acoustic Backscattering," *J. Acoust. Soc. Am. Suppl. 1* **88**, S87.

Lee, D., M. H. Schultz and W. L. Siegmann, (1994). *Numerical Ocean Acoustic Propagation in Three Dimensions*, (In preparation).

PE Workshop II: Part 3 — Contributed Papers

- Leontovich, M. A., and V. A. Fock (1946). "Solution of the problem of propagation of electromagnetic waves along the earth's surface by the method of the parabolic equation," *J. Expt. and Theor. Phys.* **16**, 557–573.
- McCoy, J. J. (1977). "A parabolic theory of stress wave propagation through inhomogeneous linearly elastic solids," *J. Appl. Mech.* **44**, 462–468.
- McDaniel, S. T. (1975). "Propagation of normal mode in the parabolic approximation," *J. Acoust. Soc. Am.* **57**, 307–311.
- McDaniel, S. T., and D. Lee (1982). "A Finite-Difference Treatment of Interface Conditions for the Parabolic Wave Equation: The Horizontal Interface," *J. Acoust. Soc. Am.* **71**, 855–858.
- McDaniel, S. T., Y. Saad, and D. Lee (1985). "Numerical Solutions of Sound Scattering in the Ocean: An Ordinary-Differential-Equation-Approach," *Proc. 11th IMACS World Congress*, Oslo, Norway, 127–130.
- McDaniel, S. T. (1991). "Backscattering from rough interfaces and the parabolic approximation," Applied Research Laboratory, Penn State University, State College, Pennsylvania, U.S.A., ARL Tech. Mem. 91–104.
- McDonald, B. E., and W. A. Kuperman (1987). "Time domain formulation for pulse propagation including nonlinear behavior at a caustic," *J. Acoust. Soc. Am.* **81**, 1406–1417.
- Murphy, J. E., and S. A. Chin-Bing (1991). "A seismo-acoustic finite element model for underwater acoustic propagation," in *Shear Waves in Marine Sediments*, J. M. Hovem, M. D. Richardson, and R. D. Stoll (eds.), (Kluwer Press, Amsterdam), 463–470.
- Orchard, B. J., W. L. Siegmann, and M. J. Jacobson (1990). "A Three-Dimensional Time-Domain Paraxial Approximation for Underwater Acoustic Wave Propagation," *J. Acoust. Soc. Am. Suppl. I* **87**, S130.
- Perkins, J. S., and R. N. Baer (1982). "An Approximation to the Three-Dimensional Parabolic Equation Method for Acoustic Propagation," *J. Acoust. Soc. Am.* **72**, 515–522.
- Porter, M. B., F. B. Jensen, and C. M. Ferla (1991). "The problem of energy conservation in one-way models," *J. Acoust. Soc. Am.* **89**, 1058–1067.
- Robinson, E. R., and D. H. Wood (1988). "Generating direct starting fields for parabolic equations," *J. Acoust. Soc. Am.* **84**, 1794–1801.

- Saied, F. (1990). *Numerical Techniques for the Time-Dependent Schrodinger Equation and their Parallel Implementation*, Yale University, New Haven, CT, U.S.A., Ph.D. Dissertation.
- Shang, E. C., and D. Lee (1989). "A Numerical Treatment of the Fluid/Elastic Interface under Range-Dependent Environments," *J. Acoust. Soc. Am.* **85**, 654–660.
- Sluijter, F. W. (1970). "Arbitrariness of dividing the total field in a optically inhomogeneous medium into direct and reversed waves," *J. Opt. Soc. Am.* **60**, 8-10.
- Spofford, C. W. (1973). "A Synopsis of the AESD Workshop on Acoustic-Propagation Modeling by Non-Ray Tracing Techniques," AESD TN-73-05, Arlington, VA, U.S.A.
- Tappert, F. D. (1977). "The parabolic approximation method," in *Wave Propagation and Underwater Acoustics*, J. B. Keller and J. S. Papadakis (eds.), Lecture Notes in Physics, Vol. 70 (Springer-Verlag, New York), Chap. V, 224–287.
- Tappert, F. D., and D. Lee (1984). "A range refraction parabolic equation," *J. Acoust. Soc. Am.* **76**, 1797–1803.
- Tappert, F. D. (1988). "Parabolic equation modeling of shear waves," *J. Acoust. Soc. Am.* **78**, 1905–1906.
- Tappert, F. D. (1990). "Full-wave three-dimensional modeling of long-range oceanic boundary reverberation," *J. Acoust. Soc. Am. Suppl. I* **88**, S84.
- Thomson, D. J., and N. R Chapman (1983). "A wide-angle split-step algorithm for the parabolic equation," *J. Acoust. Soc. Am.* **74**, 1848–1854.
- Thomson, D. J., and D. H. Wood (1987). "A postprocessing method for removing phase errors in the parabolic equation," *J. Acoust. Soc. Am.* **82**, 224–232.
- Thomson, D. J., and C. S. Bohun (1988). "A wide-angle initial field for parabolic equation models," *J. Acoust. Soc. Am. Suppl. I* **83**, S118.
- Thomson, D. J. (1989). "Modal decomposition of waves in range-varying waveguides," *J. Acoust. Soc. Am. Suppl. I* **86**, S53–S54.
- Thomson, D. J. (1990). "Wide-angle parabolic equation solutions to two range-dependent benchmark problems," *J. Acoust. Soc. Am.* **87**, 1514–1520.
- Wetton, B. T. R., and G. H. Brooke (1990). "One-way wave equations for seismoacoustic propagation in elastic waveguides," *J. Acoust. Soc. Am.* **87**, 624–632.